ЖУРНАЛ
ЭКСПЕРИМЕНТАЛЬНОЙ И ТЕОРЕТИЧЕСКОЙ
ФИЗИКИ
АКАДЕМИЯ НАУК СССР

SOVIET PHYSICS

JETP

VOLUME 8 (35) NUMBER 1

A Translation

of the

Journal of Experimental and Theoretical Physics

of the

Academy of Sciences of the USSR

Volume 35

JANUARY, 1959

Published by the

AMERICAN INSTITUTE OF PHYSICS
INCORPORATED

SOVIET PHYSICS
JETP

A translation of the Journal of Experimental and Theoretical Physics of the USSR.

SOVIET PHYSICS is a monthly journal published by the American Institute of Physics for the purpose of making available in English reports of current Soviet research in physics as contained in the Journal of Experimental and Theoretical Physics of the Academy of Sciences of the USSR. The page size of SOVIET PHYSICS will be 8½" x 11", the same as other Institute journals.

Transliteration of the names of Russian authors follows the system employed by the Library of Congress.

This translating and publishing project was undertaken by the Institute in the conviction that dissemination of the results of researches everywhere in the world is invaluable to the advancement of science. The National Science Foundation of the United States encouraged the project initially and is supporting it in large part by a grant.

The American Institute of Physics and its translators propose to translate faithfully all the material in the Journal of EXPERIMENTAL AND THEORETICAL PHYSICS OF THE USSR appearing after January 1, 1955. The views expressed in the translated material, therefore, are intended to be those expressed by the original authors, and not those of the translators nor of the American Institute of Physics.

Two volumes are published annually, each of six issues. Each volume contains the translation of one volume of the Journal of EXPERIMENTAL AND THEORETICAL PHYSICS OF THE USSR.

Subscription Prices:

Per year (12 issues)	
United States and Canada	$75.00*
Elsewhere	79.00*
Back Numbers	
Single copies	$ 8.00

*$35 and $39, respectively, to libraries of non-profit degree-granting institutions.

Subscriptions should be addressed to the American Institute of Physics, 335 East 45th Street, New York 17, New York.

SOVIET PHYSICS

JETP

A translation of the Journal of Experimental and Theoretical Physics of the USSR.

SOVIET PHYSICS JETP VOL. 35 (8), NO. 1, pp 1-216 JANUARY, 1959

INTERACTION OF COSMIC RAY PARTICLES WITH VARIOUS NUCLEI

N. L. GRIGOROV, A. V. PODGURSKAIA, A. I. SAVEL' EVA, and L. M. POPEREKOVA

Submitted to JETP editor September 27, 1956; resubmitted March 25, 1958

J. Exptl. Theoret. Phys. (U.S.S.R.) **35**, 3-15 (July, 1958)

The transition effect of stars and single heavily ionizing particles was studied by means of nuclear emulsions exposed at the altitudes of 20 and 9 km under various absorbers. The results indicate that the multiplicity and mean disintegration energy of the stars are proportional to $A^{1/3}$. Data on the flux and spectrum of heavily ionizing particles in air and under lead absorbers make it possible to analyze earlier results[1] on the production of π^0 mesons in lead and air. It is shown that the mean energy carried away by π^0 mesons produced in interactions of $\sim 10^{10}$ ev cosmic ray primaries with nuclei is proportional to the radius of the target nucleus.

INTRODUCTION

We have determined the average characteristics of the interaction between primary cosmic ray particles of $\sim 10^{10}$ ev energy and light nuclei through the study of the various secondary components of cosmic radiation observed in the atmosphere.[2]

We have studied the dependence of star energy and multiplicity on the atomic number of the disintegrating nucleus, in order to find out to which extent these characteristics depend on the size of the target nucleus. Moreover, having investigated the variaion of the flux of heavily-ionizing particles and the ionization due to these in air and under lead absorbers of various thickness, we found it possible to determine the energy carried away by π^0 mesons produced in lead, and, comparing its value with the energy of π^0 mesons produced in air, to draw conclusions regarding meson production in light and heavy nuclei; this could be done by a more correct method than that used earlier.[1]

Our method of determining the energy of a nuclear disintegration is based on the following considerations: As the result of disintegration, the nucleus emits heavy charged particles that carry away an average energy E_C. The major portion of these particles have a range considerably smaller than the absorption mean free path of the star-producing component. Under a sufficiently thick layer x of matter ($x < R$, where R is the range of secondary particles produced in nuclear disintegrations), an equilibrium is reached between the secondary and primary particles. Then the charged products of nuclear disintegrations lose in one gram of matter, an amount of energy equal to that gained, in one gram, from all nuclear disintegrations. To determine E_C, it is therefore necessary to measure the total ionization produced per unit volume by all heavily-ionizing particles. Let $N(I, \theta)\,dI\,d\Omega$ represent the number of particles with specific ionization I to $I + dI$, traveling at zenith angle θ in a solid angle $d\Omega$. The ionization energy loss in one gram of matter, suffered by all particles, is then

$$\frac{\Delta E}{\Delta x} = \beta_{\text{rel}} \int_{\Omega} d\Omega \int_{I_{\min}}^{\infty} \frac{I}{I_{\text{rel}}} N(I, \theta)\, dI, \qquad (1)$$

where β_{rel} is the relativistic ionization loss per gram of the given substance for relativistic particles with ionization I_{rel}. For the equilibrium conditions

$$E_c = (\Delta E/\Delta x)\, L_i /S,$$

where S is the flux of the star-producing component and L_i is the interaction mean free path for the given substance.

If the energy E_c transferred to charged products of nuclear disintegration is known, the total energy of disintegration E_t can be found under the assumption that the neutrons carry away an amount of energy $(A - Z)/Z$ times larger than that carried away by the protons. Since, according to reference 3, the main fraction of energy is carried away by protons, we have

$$E_t = AE_c /Z. \qquad (2)$$

1. EXPERIMENTAL RESULTS

Emulsions were chosen for the measurement of the ionization due to heavily-ionizing particles, in view of good identification of particles through their specific ionization.

As stated in the Introduction, to determine E_t we had to measure the particle spectrum $N(I, \theta)\, dI\, d\Omega$ under absorbers of sufficient thickness, made of materials with different atomic number. The experiments were carried out at the geomagnetic latitude 51°, using graphite and lead absorbers of various thickness at an altitude of 20 km, and using lead and paraffin absorbers at 9 km altitude.

Electron-sensitive emulsions 400 μ thick were used in the stratospheric experiments. One part of the plates, 4×4 cm, was placed under flat lead absorbers I, II and III (cf. Fig. 1a), 5, 15, and 33 mm in thickness respectively. Another part of the plates, also 4×4 cm in size, was placed between flat graphite absorbers IV, V, and XI, 13, 39, and 86 mm in thickness. Lead and graphite absorbers were placed together with the plates in hermetic copper cassettes with walls 0.5 mm thick (cf. Fig. 1a). A pair of plates wrapped in a single layer of paper was placed back to back under each filter. The plates were placed in a vertical plane. Two hermetic brass cassettes VII and VIII, with walls 0.3 mm thick and containing a pair of 6×9 cm plates without absorbers, were used in addition. One of these cassettes was placed in the array, at a distance of ~40 cm from the cassettes containing the lead and graphite absorbers. The other was hung 4 m above the array. All cassettes were filled with pure argon at atmospheric pressure.

A diagram of the flight and position of the cassettes in the array are shown in Fig. 1, b and c.

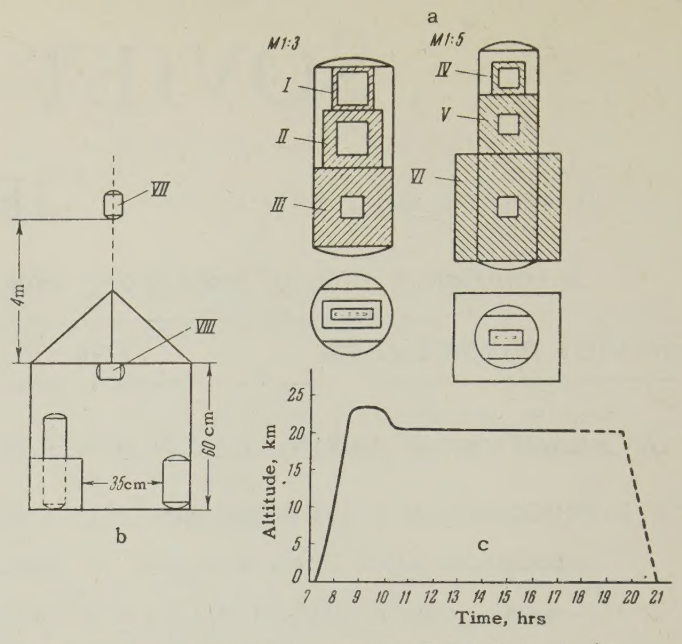

FIG. 1. a – position of nuclear emulsion plates in the cassettes under graphite and lead absorbers in the stratospheric experiment, b – position of the cassettes in the array, c – flight diagram.

The altitude was monitored by radio during the flight. The radio communication stopped 11 hrs after the start. This happened at the altitude of 20 km. The apparatus landed after 21 hours. Assuming that the apparatus descended with the same velocity as it ascended (which is true in most cases), then the array spent about 11 hours at altitude ≥ 20 km (cf. flight diagram, Fig. 1c; the inferred part of the flight is indicated by the dotted line). In the following, the time of flight at 20 km is taken as ~11 hours.

Electron-sensitive emulsions 600 μ in thickness were used in the experiments at 9 km altitude. Eight 5×10 cm plates (4 in each cassette) were placed in two hermetic brass cassettes with walls 0.3 mm thick, filled with argon at atmospheric pressure. One cassette was placed in a lead cylinder, with side walls 3.5 cm thick. The other cassette was placed in a paraffin vessel of the same form with walls 17 cm thick. The plates in both cassettes were exposed in a vertical position.

The emulsions were exposed in an airplane during a month. The total time spent at 9 km altitude amounted to 25 hours.

In scanning, we measured (a) the total number of stars with $N_h \geq 3$ under various absorbers, (b) the number of single heavily-ionizing particles stopping in the emulsion, and (c) the number of single heavily-ionizing particles traversing the emulsion, and their angular as well as specific ionization distribution.

2. STARS UNDER VARIOUS ABSORBERS

The data on the number of stars under various absorbers, given in Table I, represent the mean of two scannings of each plate by several observers. The standard deviation of the measurements of the number of stars by different observers was found to be 5 to 6% (two times larger than the statistical error).

TABLE I

Altitude, km	Material and thickness of the absorber, mm	Number of stars cm^{-3} day^{-1}
20	Air	2350
	Graphite 13	1910
	" 39	2520
	" 86	2190
	Lead 5	2130
	" 15	2360
	" 33	2430
9	Paraffin 170	402
	Lead 35	417

It can be seen from Table I that, within the limits of experimental errors, amounting to 6%, the number of stars found in the plates exposed at 9 and 20 km altitude is independent of the material of the absorber surrounding the emulsion.

3. HEAVILY IONIZING PARTICLES UNDER VARIOUS ABSORBERS

The plates were scanned for stopping heavily-ionizing particles at 450× magnification. Each field of view was scanned in the whole depth of the emulsion. We measured the angle θ between the projection of the track on the plane of the plate and the vertical, the dip of the track, and its length (from the point of entrance into the emulsion to the point where the particle stopped).

The plates were scanned for particles traversing the emulsion at 2020× magnification. The scanning was carried out along the surface (at the depth of a few microns). All tracks with grain density $g \gtrsim 2g_{min}$ and a length of projection on the emulsion plane $l \geq 800\mu$ were noted in the scanning. For tracks traversing the emulsion and satisfying these above conditions, we measured the length l of projection on the emulsion-plane, the grain density g, and the angle θ between the projection and the vertical.

It was not possible to determine the direction of motion of the particle along the track when the particle did not stop in the emulsion. The angular distribution of these particles about the vertical was therefore measured in the range from 0 to 90°. The number of inspected fields of view and the number of particles found in them were noted in the scanning for stopping and traversing particles.

The angular distribution of the traversing particles at 20 and 9 km altitude is shown in Fig. 2.

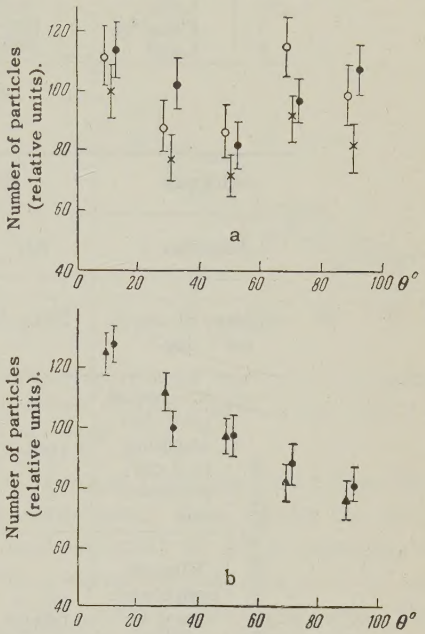

FIG. 2. Angular distribution of heavily ionizing particles, non-stopping in the emulsion, under various absorbers: a – at 20 km altitude, b – at 9 km altitude. The x axis represents the angle between the projection of the track on the plane of emulsion and the vertical, and the y axis the number of particles between 0 and 20°. Absorbers: × – graphite, o – air, ● – lead, ▲ – paraffin.

The angular distribution of particles, recorded in emulsions exposed at 20 km altitude in air, has been plotted from 549 tracks, that under 86 mm of graphite from 549 tracks, and that under 33 mm of lead from 670 tracks. These distributions are normalized in Fig. 2 to the same number of detected particles. The angular distribution of traversing particles in plates exposed at 9 km altitude under 170 mm of paraffin has been plotted from 1240 tracks, and that under 35 mm of lead from 1212 trakcs.

It can be seen from Fig. 2 that the angular distributions of traversing particles are practically identical under absorbers of small or large atomic number (air, graphite, and lead at 20 km altitude, paraffin and lead at 9 km). At 20 km, the angular distribution of tracks traversing the emulsion is practically isotropic. At 9 km, the angular distribution of the particles is slightly anisotropic, evidently owing to the greater anisotropy of the star-producing component.

TABLE II

Altitude, km	Absorber	Range of angles								
		0–20°	20–40°	40–60°	60–80°	80–100°	100–120°	120–140°	140–160°	160–180°
20	Air	79±5	59±4	63±5	61±5	64±5	53±4	45±4	48±4	44±4
20	Graphite	76±5	69±6	69±6	63±6	69±6	51±5	36±4	30±4	37±4
20	Lead	65±6	57±5	57±5	61±6	61±6	52±5	46±5	45±5	50±5
9	Paraffin	78±11	70±11	70±11	70±11	47±8	50±9	44±8	45±9	27±6
9	Lead	103±9	74±8	66±7	66±7	47±6	41±6	44±6	35±5	33±5

TABLE III

Altitude		20 km (400 μ emulsion)			9 km (600 μ emulsion)	
Absorber		Air	Graphite, 86 mm	Lead, 33 mm	Paraffin, 170 mm	Lead, 35 mm
Number of stars, cm^{-3} day^{-1}		2350±120*	2190±120*	2430±120*	402±8	417±12
Stopping particles	Number of particles stopping in 1 cm^2 per minute	0.110±0.005	0.141±0.007	0.162±0.009	0.075±0.004	0.0.5±0.004
	Flux of particles 6 Mev ≤ E ≤ 20 Mev, cm^{-2} $sterad^{-1}$	0.069±0.006	0.058±0.005	0.085±0.006	0.023±0.0015	0.024±0.0015
Flux of traversing particles 20 Mev ≤ E ≤ 180 Mev, cm^{-2} min^{-1} $sterad^{-1}$		2.5±0.1	2.5±0.1	2.8±0.3	0.34±0.01	0.38±0.01

*The error represents the standard deviation, amounting to 6% of the measured value.

Results of the measurements of the angular distribution of stopping particles are given in Table II. The distribution is normalized to the same total number of particles detected under various absorbers.

In certain cases, the mass of heavily ionizing particles traversing the emulsion was determined by multiple scattering and grain-density measurements. These non-systematic measurements have shown that, both in the atmosphere and under lead, the majority of traversing particles are protons. It was possible, therefore, to obtain the energy distribution of these particles from the measured grain density, assuming they were all protons.

It is evident that the energy spectrum of the detected particles traversing the emulsion will differ from the true spectrum since, for particles with different grain density g, the solid angle within which they are classified as having traversed the emulsion will be different.

In addition, the true value of grain density is different from that observed in its dependence on the angle of dip of the track with respect to the plane of emulsion. Corresponding corrections were applied to the energy spectrum of traversing particles. The spectra represented by the histograms in Fig. 3 (for 20 km altitude) and Fig. 4 (for 9 km) were obtained as the result. Experimental points are shown in the figures.

It can be seen from Fig. 3 and 4 that the energy spectrum of traversing particles is practically independent of the atomic number of the absorber, at both altitudes, 20 km and 9 km. The values of the flux of traversing particles, accounting for the corrections, are given in Table III (4th column).

The energy spectrum of stopping particles was determined from the measured range spectrum,

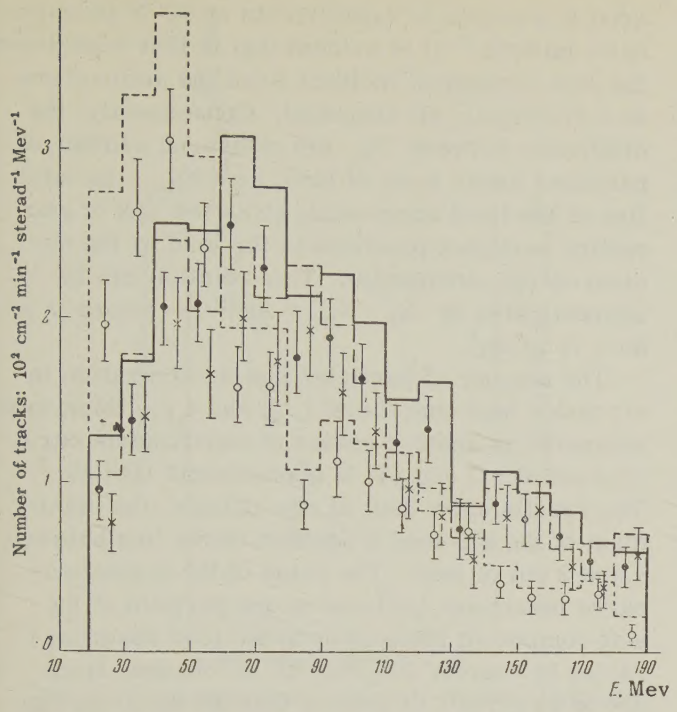

FIG. 3. Energy spectrum of heavily-ionizing particles traversing the emulsion (all particles are assumed to be protons) at 20 km altitude. The x axis represents the particle energy, and the y axis the flux of particles with a given energy under various absorbers: × – graphite, ○ – air, ● – lead.

under the assumption that all particles were protons. In constructing the spectrum, we took it into account that the finite thickness of the emulsion distorts considerably the true range distribution. After introducing a corresponding correction, the energy spectrum of stopping particles was found to be identical under all absorbers, within the limits of statistical errors of the measurements. In the energy range 6 Mev ≤ E ≤ 20 Mev, the spectrum is

$$N(E)\,dE = \text{const}\,dE.$$

The absolute intensity of the flux of stopping particles is given in Table III (3rd column). It can be seen that when the plates were surrounded by a layer of lead 3.3 to 3.5 cm thick (effective thickness 5 to 6 cm), the number of stars and of single particles remained practically constant at both elevations.

4. PRODUCTION OF π^0 MESONS IN SUBSTANCES WITH DIFFERENT ATOMIC NUMBER

Information can be gained on the production of π^0 mesons by cosmic ray particles in light (air) and heavy (lead) substances, comparing the energy ϵ_{π^0} carried away by π^0 mesons per second in one gram of air and lead at the same observation level, for equal intensity and properties of the producing component. If we denote the mean value of energy carried away by π^0 mesons in one interaction of the generating particle with air and lead nuclei by $E_{\pi^0}^{\text{Air}}$ and $E_{\pi^0}^{\text{Pb}}$ respectively, then we have the following relation between ϵ and E:

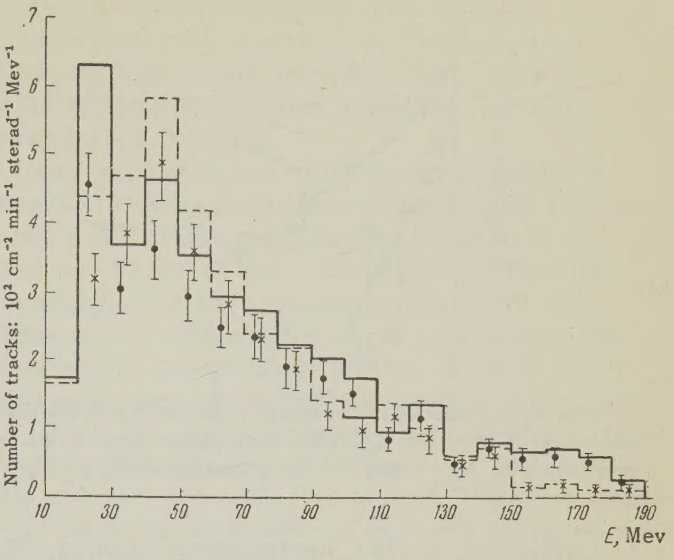

FIG. 4. Energy spectrum of heavily ionizing particles traversing the emulsion, at 9 km altitude, under various absorbers: × – paraffin, ● – lead.

$$\varepsilon_{\pi^0}^{\text{Air}} = E_{\pi^0}^{\text{Air}} P/L_{\text{Air}}\,,\quad \varepsilon_{\pi^0}^{\text{Pb}} = E_{\pi^0}^{\text{Pb}} P/L_{\text{Pb}},$$

where L_{Air} and L_{Pb} are the interactions mean free paths of the generating particles in air and lead, respectively, and P is the total flux of these particles. Eliminating P, we obtain

$$E_{\pi^0}^{\text{Pb}}/E_{\pi^0}^{\text{Air}} = \varepsilon_{\pi^0}^{\text{Pb}} L_{\text{Pb}}/\varepsilon_{\pi^0}^{\text{Air}} L_{\text{Air}}\,. \qquad (3)$$

The value of $\epsilon_{\pi^0}^{\text{Air}}$ can be determined in the following way: The energy $\epsilon_{\text{sc}}(x)$ transferred to the soft component per second and per gram at atmospheric depth x g/cm^2, is related to the energy flux $S^{\text{H}}(x)$ carried by the soft component through 1 cm^2 of horizontal surface and to the total flux of soft component $N_{\text{sc}}(x)$ by the expression[1]

$$\frac{dS^{\text{r}}(x)}{dx} + \beta N_{\text{sc}}\,(x) = \varepsilon_{\text{sc}}\,(x). \qquad (4)$$

where $\beta = \text{C} - \text{dE}\,(\text{dx})_{\text{ion}}$ is the ionization loss for relativistic electrons.

We determined $\epsilon_{\text{sc}}(x)$ using data of references 1, 2, and 4. The dependence of $\epsilon_{\text{sc}}(x)$ on the atmospheric depth x is shown in Fig. 5. Curve 1 refers to measurements at 31° geomagnetic latitude, where the energy of primary cosmic ray particles is $E_0 \geq 7$ Bev. Curve 2 represents the difference of measurements at 51° and 31° geomagnetic latitude (1.5 Bev ≤ E_0 < 7 Bev).

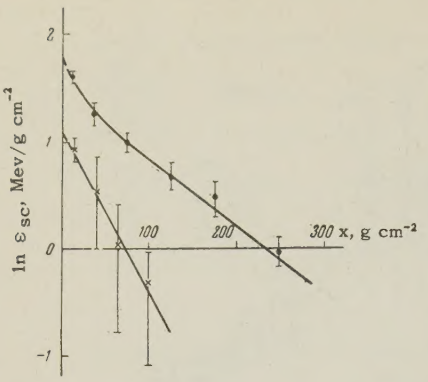

FIG. 5. Dependence of the energy transferred into the soft component in 1g of air, ε_{sc} on the atmospheric depth x: ● – for primaries with $E_0 \leq 7$ Bev, × – for primaries with $1.5 \leq E_0 \leq 7$ Bev.

Correcting $\epsilon_{sc}(x)$ for the contribution of electrons originating in the μ-meson decay, we obtain the energy carried away by π^0 mesons in one gram of atmosphere, i.e., $\epsilon_{\pi^0}^{Air}$. Corresponding values of $\epsilon_{\pi^0}^{Air}$ are given in the fifth column of Tables IV and V.

The energy $\epsilon_{\pi^0}^{Pb}$ carried away by π^0 mesons in one gram of lead per second can be determined from the following considerations. If $n(t)$ represents the number of electrons under a thickness of lead t, originating in the decay of π^0 mesons produced in it, then the energy transferred to π^0 mesons in one gram of lead can be found from the equation

$$n(t) = \varepsilon_{\pi^0}^{Pb} \exp\{-t/L_{Pb}\}\, \gamma(t)/\beta_{Pb}, \qquad (5)$$

where $L_{Pb} = 160$ g/cm^2 is the interaction mean free path of nuclear active particles in lead, $\beta_{Pb} = 1.2$ Mev-g^{-1}cm^2 is the ionization loss suffered by relativistic electrons in lead, and

$$\gamma(t) = \int_0^t N(\xi) \exp\{\xi/L_{Pb}\}\, d\xi / \int_0^\infty N(\xi)\, d\xi,$$

where $N(\xi)$ is the mean number of particles at the depth ξ in showers produced by π^0-decay photons.

From Eq. (5) we have

$$\varepsilon_{\pi^0}^{Pb} = n(t)\, \beta_{Pb}/\gamma(t) \exp\{-t/L_{Pb}\}. \qquad (6)$$

It can be seen from Eq. (6) that in order to find $\epsilon_{\pi^0}^{Pb}$, it is necessary to measure the total flux of particles $n(t)$ of the soft component under the lead absorber in which it is produced. The particles measured should not include any particles due to the electron-photon component incident upon the lead absorber.

The number of particles under a lead absorber 8 cm thick (effective thickness ~9 cm) was measured in a series of experiments at 51° N geomagnetic latitude.[2] It is evident that in that experiment the soft component incident from the atmosphere was practically all absorbed. Consequently, the difference between N_8, the measured number of particles under 8 cm of lead, and N_{hc}, the total flux of the hard component, gives the flux of secondary particles produced in the lead by the nuclear-active component. This relation can be approximated by $N_8 - N_{hc} = Ae^{-x/\lambda}$, where $\lambda = 80 \pm 17$ g/cm^2.

The number of particles and the ionization in air under lead absorbers 1, 2, and 4 cm thick were measured in another series of experiments carried out at 31° and 51° N geomagnetic latitude.[2] The results show that, at any altitude, the maximum of the air-lead transition curve lies between 1 and 2 cm of lead. The value of the transition-curve maximum (related to one particle of the soft component incident upon the lead absorber) varies by merely 20% only as x changes from 310 to 40 g/cm^2. It follows that the mean energy of the particles of the soft component in the atmosphere is practically independent of the depth of observation, and that the transition curves should be similar at all altitudes.

The value of the mean energy is such that the air-lead transition curve for 4 cm of lead (~4.7 cm effective thickness), has an ordinate equal to the flux of charged particles of the soft component (cf. the transition curve for x = 310 g/cm^2 in Fig. 6 of reference 2). At high altitudes, however, the air-lead transition curve becomes distorted: particles not present under the absorber at low altitudes begin to appear (cf. Fig. 6 of reference 2). These particles are due to the production of π^0 mesons in the absorber. The flux of the "additional" particles, equal to $N_4 - N_0$ (where N_4 is the flux of particles under an absorber in the atmosphere) determines the required value $n(t)$. Certain corrections, which will be discussed below, have to be applied to the calculation.

The y axis in Fig. 6 represents the difference $N_4 - N_0$ measured at various depths x in the atmosphere at two geomagnetic latitudes. It can be seen from Fig. 6 that the number of the "additional" particles under 4 cm of lead is, at all altitudes, the same as under 8 cm of lead ($N_8 - N_{hc}$). (The calculation shows that, in cascades initiated by 3×10^8 to 10^9 ev photons originating in the decay of π^0 mesons produced in lead, the number of particles under 8 cm Pb is only 20% higher than that under 4 cm Pb.) At high altitudes, the flux of the "additional" particles under 4 cm Pb equals ~ 1.5 cm^{-2}sec^{-1}. If we assume that the interac-

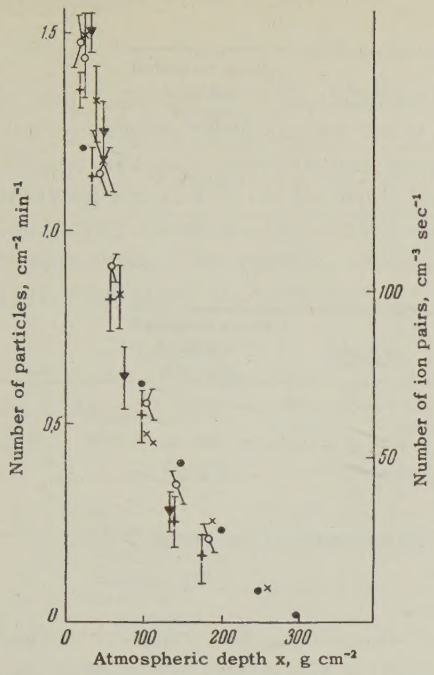

FIG. 6. Dependence of the number of electrons (left-hand scale) originating in the π^0 mesons produced, and the ionization due to them (right-hand scale), on the atmospheric depth x. Results of measurements at 51°N geomagnetic latitude: ▼: $N_8 - N_{hc}$, ○: $N_4 - N_0$, ●: $I_4 - I_0$; results of measurements at 31°N latitude: +: $N_4 - N_0$, ×: $I_4 - I_0$.

tion mean free path of the generating particles in lead equals 160 g/cm^2 and that the total flux of these particles decreases with the atmospheric depth as the mean free path $\lambda = 80 + 17$ g/cm^2, we find that, in the mean, 60 secondary particles are emitted from the 4 cm layer of lead in each interaction between a primary with energy ≥ 7 Bev ($\overline{E}_0 \approx 20$ Bev) and a lead nucleus. It is clear that the majority of these particles are electrons, produced in lead as the result of cascade multiplication.

If the air-lead transition effect is measured by means of an ionization chamber, then the difference between ionization I_4 measured under a lead absorber 4 cm thick, and that measured in the atmosphere, I_0, represents the ionization due to photons from the decay of π^0 mesons produced in the absorber. The dependence of $I_4 - I_0$ on x is shown in Fig. 6 (the scale for $I_4 - I_0$ is given on the right-hand-side).

The ratio $(I_4 - I_0)/(N_4 - N_0) = \overline{K}$ represents the mean specific ionization of the "additional" particles. It follows from Fig. 6, that, at all altitudes, $\overline{K} = 120$ ion pairs/cm, which is 1.7 times the specific ionization of fast electrons (70 ion pairs/cm).[5] This increase of the specific ionization is due to two causes: (a) errors in the number of particles measured under the lead absorber (owing to finite dimensions of the counter), and (b) the presence there of slow electrons, which undergo large scattering within the volume of the chamber and which suffer, therefore, a larger energy loss $(dE/dx)_{ion}$.

Our measurements of the transition effect of heavily-ionizing particles indicate that the flux and spectrum of these particles are identical in air and under 4 cm of lead. The total ionization due to heavily-ionizing particles is, therefore, also identical for both conditions. In consequence, the increase in the specific ionization under 4 cm Pb cannot be ascribed to the heavily-ionizing particles.

In Eq. (6), $n(t)$ is the true number of electrons under a lead absorber of thickness t, and β is the average ionization loss in lead. If we determine $\epsilon_{\pi^0}^{Pb}$ by using the number of particles observed and putting $\beta_{Pb} = 1.2$ Mev/g-cm^{-2} for relativistic particles, then, in order to obtain the correct value of $n(t)_{obs}\beta_{Pb}$, it is necessary to multiply it by the factor 1.7, which accounts automatically both for the error in the measurement of the number of particles in our arrangement and for the increased ionization loss for a certain fraction of the electrons.

Since the measurement of the number of particles has been carried out under sufficiently thick lead absorbers (4.7 and 9.0 cm mean thickness) then the electron flux observed under the absorbers (in the differences $N_4 - N_0$ and $N_8 - N_{hc}$) contains a contribution from secondary penetrating particles produced in the first interaction between the "primary" particle and a lead nucleus. According to our estimates, secondary interactions increase the number of electrons under the absorber by 10% for $t = 4.7$ cm and by 25% for $t = 9.0$ cm. In addition, about 10% of detected particles represent penetrating particles produced in lead.

The corrected values of $\epsilon_{\pi^0}^{Pb}$ are listed in Tables IV and V.

In Table IV (measurements at 51° geomagnetic latitude) and in Table V (at 31° geomagnetic latitude), the atmospheric depth in g/cm^2 of the observation level is given in column 1, the mean thickness t of the lead absorber (under which the electron flux was measured) in column 2, the corrected electron flux in column 3, the energy transferred to π^0 mesons per second in one gram of lead in column 4, the energy transferred to π^0 mesons per second in one gram of air in column 5, the ratio $E_{\pi^0}^{Pb}/E_{\pi^0}^{Air}$ (the energy transferred to π^0 mesons in one act of interaction with a lead nucleus to that with an air nucleus) in column 6, and the mean weighted value of $E_{\pi^0}^{Pb}/E_{\pi^0}^{Air}$ in column 7. All errors given are statistical.

TABLE IV

x, g/cm²	t, radiation units	n (t) cm⁻² sec⁻¹	$\varepsilon_{\pi^0}^{Pb}$, Mev g⁻¹ sec⁻¹	$\varepsilon_{\pi^0}^{Air}$ Mev g⁻¹ sec⁻¹	$E_{\pi^0}^{Pb}/E_{\pi^0}^{Air}$	Mean weighted value of $E_{\pi^0}^{Pb}/E_{\pi^0}^{Air}$
30	10	1.76±0.17	3.2±0.3	4.7±0.6	1.8±0.3	1.85±0.2
30	20	1.85±0.30	3.4±0.6	4.7±0.6	1.9±0.4	

TABLE V

x, g/cm²	t, radiation units	n (t) cm⁻² sec⁻¹	$\varepsilon_{\pi^0}^{Pb}$ Mev g⁻¹ sec⁻¹	$\varepsilon_{\pi^0}^{Air}$ Mev g⁻¹ sec⁻¹	$E_{\pi^0}^{Pb}/E_{\pi^0}^{Air}$	Mean weighted value of $E_{\pi^0}^{Pb}\ E_{\pi^0}^{Air}$
0*	10	2.5±0.3	4.6±0.6	5.5±0.3	2.2±0.3	
20	10	1.9±0.2	3.6±0.3	3.8±0.2	2.5±0.3	2.4±0.2
30	10	1.8±0.2	3.2±0.3	3.2±0.4	2.7±0.4	

*The values for x = 0 are obtained by means of extrapolation of the curves in Figs. 5 and 6.

It can be seen that $E_{\pi^0}^{Pb}/E_{\pi^0}^{Air} = 2.4 \pm 0.2$ at 31° geomagnetic latitude, where the primary particles have an energy $E_0 \geq 7$ Bev. At 51° geomagnetic latitude, where particles of lower energies down to 1.5 Bev are also present, the value of the ratio is 1.85 ± 0.2.

5. DISCUSSION OF RESULTS

1. Production of Heavily-Ionizing Particles in Air and in Light Substances

The range of most particles originating in stars is much smaller than the range of the star-producing component. It follows, therefore, that the number of particles stopping in one gram of the absorber should be equal to the number of particles produced in one gram of the absorber.

Let us denote by ν_i the mean number of heavily-ionizing particles produced in the disintegration of one nucleus with mass number A_i. We shall denote further by $N_{stop}(A_i)$ the number of particles stopping in one gram of the matter of an absorber of mass number A_i, and by $N_{stop}^{em}(A_i)$ — the number of particles stopping in one gram of emulsion surrounded by the absorber. It follows from the equilibrium condition that

$$N_{stop}(A_i) = \nu_i N_{star}(A_i),$$

where $N_{star}(A_i)$ is the number of stars produced in one gram of the matter of the absorber.

Heavily-ionizing particles are produced in the absorber, and stop in the emulsion. The power of the latter is β_{em}/β_i times larger than that of the absorber (β_{em} and β_i is the ionization loss in emulsion and in the absorber respectively) and we have, therefore

$$N_{stop}^{em}(A_i) = N_{stop}(A_i)\,\beta_{em}/\beta_i, \quad N_{stop}^{em}(A_i) = \nu_i \beta_{em} N_{star}(A_i)/\beta_i.$$

The number of stars produced in one gram of the matter of the absorber can be expressed in terms of the number of stars produced in one gram of the emulsion surrounded by it:

$$N_{star}(A_i) = N_{star}^{em}(A_i)\,\sigma_i A_{em}/\sigma_{em} A_i = N_{star}^{em}(A_i)\,(A_{em}/A_i)^{1/3},$$

since the effective cross-section for star production is $\sigma \sim A^{2/3}$ (reference 6). We have, therefore,

$$\nu_i = N_{stop}^{em}(A_i)\,\beta_i / N_{star}^{em}(A_i)\,\beta_{em}\left(\frac{A_i}{A_{em}}\right)^{1/3} \qquad (7)$$

Taking the ratios of such expressions for lead and air and for graphite and air, and making use of the experimental data (Table III), we obtain

$$\nu_{Pb}/\nu_{Air} = 2.0 \pm 0.24;$$

$$\nu_C/\nu_{Air} = 0.82 \pm 0.10, \text{ at 20 km altitude}$$

It can be seen that, within the limits of experimental errors $\nu \sim A^{1/3}$.

2. Disintegration Energy of Light and Heavy Nuclei

According to Eqs. (1) and (2), we have

$$E_t = \frac{A}{Z} E_c = \frac{A}{Z}\frac{L_i}{S}\beta \int_\Omega d\Omega \int_{I_{min}}^{\infty} \frac{I}{I_{rel}} N(I, \theta)\, dI \qquad (8)$$

$$= \frac{A}{Z}\frac{L_i}{S}\beta \bar{I} N_{hi},$$

where $\bar{I}$ is the mean specific ionization of the flux of heavily ionizing particles, and N_{hi} is their total flux.

In our experiments, $I_{min} = 2 I_{rel}$ (where I_{rel} is the specific ionization of a relativistic particle). For traversing particles, $I \leq 12 I_{rel}$. The remain-

ing particles stopped in the emulsion:

$$\bar{I}N_{hi} = \bar{I}_{tr} N_{tr} + \bar{I}_{stop} N_{stop},$$

where $\bar{I}_{tr}$ and $\bar{I}_{stop}$ are the mean specific ionization of traversing and stopping particles, and N_{tr} and N_{stop} are their total fluxes, respectively.

We calculated the values of $\bar{I}_{tr}$ and $\bar{I}_{stop}$, using the observed spectrum, corrected for geometry of the apparatus. The results, expressed in units of I_{rel}, are given in Table VI.

TABLE VI

Altitude, km	Absorber and its thickness, mm	$\bar{I}_{tr}$ (traversing particles)	$\bar{I}_{stop}$ (stopping particles)
20	Air	5.8±0.3	18.2±1.7
	Lead, 33	4.7±0.3	21.3±2.3
	Graphite, 86	4.9±0.2	19.2±1.9
9	Paraffin, 170	6.3±0.4	20.8±1.7
	Lead, 35	6.1±0.4	20.8±1.6

Using the data on the fluxes of the traversing and stopping particles (Table II) and the data of Table VI, we obtain the values of $\bar{I}N_{hi}$ for 20 km altitude.

In order to exclude the unknown flux of the generating component S, we form the ratios of Eq. (8) for the results of measurements under various absorbers. For the altitude of 20 km we find then that $E_d^{Pb}/E_d^{Air} = 2.1 + 0.3$, and $E_p^{C}/E_p^{Air} = 0.82 + 0.08$. Evidently, the disintegration energy E_d is proportional to $A^{1/3}$. We can conclude from the results on star production in substances with different atomic numbers that the mean number of particles in a star ν and the mean disintegration energy of the nucleus $\bar{E}_d$ are proportional to $A^{1/3}$, i.e., to the size of the nucleus.

3. Dependence of the Energy Carried Away by π^0 Mesons on the Mass Number of the Nucleus

A comparison of the energy carried away by π^0 mesons in interactions involving lead and air nuclei shows (cf. Tables IV and V) that, in collisions with lead nuclei, primary particles with energy $E_0 \geq 7$ Bev transfer to π^0 mesons twice the amount of energy transferred in collisions with air nuclei. This result can be explained by the assumption that a collision of the "primary" particle with a heavy nucleus represents a series of collisions with lighter nuclei. The mean number of such collisions in the lead nucleus is $n = (A_{Pb}/A_{Air})^{1/3} = 2.4$.

We showed earlier[2] that a nucleon with $E_0 \geq 7$ Bev colliding with air loses 28 ± 3% of its primary energy on π-meson production. The remaining 72% of the energy is carried away by a single nucleon. Assuming the above collision model, a nucleon with $E_0 \geq 7$ Bev should, in the mean, carry away an energy equal to $(0.72 \pm 0.03)^{2.4} E_0 = (0.45 \pm 0.06) E_0$ in an interaction with a lead nucleus. Consequently, $E_\pi^{Pb}/E_0 = 55 + 6\%$ of the primary energy will be spent on π-meson production in lead, and $E_\pi^{Air}/E_0 = 28 + 3\%$ in air.

It is natural to assume that the energy carried away by π^0 mesons is half the energy carried away by π^+ mesons, in collisions with both light and heavy nuclei. We should have then

$$E_{\pi^0}^{Pb}/E_{\pi^0}^{Air} = \frac{(55 \pm 6)\%}{(28 \pm 3)\%} = 2.0 \pm 0.3.$$

It can be concluded, therefore, that the energy carried away by π^0 mesons varies roughly in proportion to the size of the nucleus, i.e., $E_{\pi^0} \sim A^{1/3}$.

CONCLUSIONS

1. In interactions between ~10 Bev nucleons and atomic nuclei, the disintegration energy E_d and the energy carried away by the π^0 mesons are proportional to the size of the nucleus, i.e.,

$$E_d \sim A^{1/3}; \quad E_{\pi^0} \sim A^{1/3}.$$

2. The observed dependence of E_d and E_{π^0} on A is consistent with the assumption that an interaction between a primary particle and a heavy nucleus represents a succession of independent interactions of a similar type to that with a lighter nucleus, e.g., an air nucleus. The mean number of these independent interactions is proportional to $\sim A^{1/3}$.

[1] N. L. Grigorov and V. S. Murzin, Izv. Akad. Nauk, SSSR, Ser. Fiz. **17**, 21 (1953).

[2] N. L. Grigorov, Usp. Fiz. Nauk, **58**, 599 (1956).

[3] U. Camerini and C. F. Powell, Usp. Fiz. Nauk **40**, 76 (1950).

[4] S. I. Brikker and N. L. Grigorov, Dokl. Akad. Nauk SSSR **86**, 1089 (1952).

[5] Grigorov, Rapoport, and Shipulo, Dokl. Akad. Nauk SSSR **91**, 491 (1953).

[6] I. Barbour, Phys. Rev. **82**, 280 (1951).

Translated by H. Kasha

SELFCONSTRICTING DISCHARGES IN DEUTERIUM AT HIGH RATES OF CURRENT GROWTH

V. S. KOMEL'KOV

Submitted to JETP editor February 6, 1958

J. Exptl. Theoret. Phys. (U.S.S.R.) 35, 16-26 (July, 1958)

Results of investigation of selfconstricting discharges are described for rates of current rise in the range 7×10^{11} to 1.4×10^{12} amp/sec, and for current amplitudes up to 2×10^6 amp. The initial deuterium pressure in the chambers varied between 0.1 and 10 mm of Hg. The highest gas temperature that was possibly attained was about 200 ev.

1. INTRODUCTION

In earlier papers[1-3] a description was given of the development of a powerful electric discharge in deuterium at pressures between 10^{-3} and 1 mm of Hg. Basic quantitative relations which agreed in a satisfactory manner with the experimental data, were also given. All the investigations referred to above were carried out with the aid of apparatus which made it possible to attain an initial rate of current rise of 5×10^{10} to 1.5×10^{11} amp/sec. Since an increase in the initial rate of current rise was accompanied by an increase in the velocities and the temperature of the gas at the instant of complete contraction, it appeared to be of interest to investigate these processes at the highest attainable rates and amplitudes of the current.

With reference to the capacitor installation which was at our disposal, an increase in these parameters was possible only by decreasing the inductance of all the elements of the circuit (capacitors, current leads, discharge gap), and also by decreasing the inductance of the discharge column itself. The methods which were used to decrease the inductances of the circuit have been described by Komel'kov and Aretov.[4] In order to reduce the inductance of the discharge column it was necessary to reduce the height of the chamber to a few centimeters, and to limit the range of the initial gas pressure in the chamber from 0.1 to 10 mm of Hg. If the gas pressure is reduced further, the vapor of the metal of the electrodes fills the working volume of the chamber too rapidly and cools the gas.

To obtain photographic records, use was made of transparent glass chambers with flat metallic electrodes. The energy liberated by the circuit during the discharge was so great that the chamber was repeatedly completely destroyed. Under such conditions, probe measurements, which require averaging over many experiments, would have made the experiment very complicated. They had to be discarded, and we had to limit ourselves only to optical recording of the constriction, and to recording the current and the voltage across the chamber electrodes. The experiments described below have been carried out with the participation of D. S. Parfenov, G. N. Aretov, and B. P. Surnin.

2. THE TECHNIQUE AND THE EXPERIMENTAL METHOD

1. The discharge under investigation took place in glass chambers of 190 mm internal diameter. The height of the chamber, the form of the electrodes, the discharge gap, and the current lead connections are shown in the figures given below. In order to prevent the breakdown of the short chambers along the surface of the wall (in air) the rubber insulation of the circuit was introduced inside the chamber, and served at the same time as a vacuum seal. The mechanical strength of the conductors in the immediate vicinity of the chamber was increased by means of steel braces. Because of this, the conductors lasted through the whole series of experiments without undergoing any appreciable deformation. The air was pumped out of the chamber by an oil diffusion pump down to a pressure of 10^{-5} mm of Hg. The chamber was filled with 98.9% pure deuterium through an opening in the lower electrode.

2. The electric circuit diagram of the apparatus is given in Fig. 1. The capacitance C_1 of the main capacitor bank was 130 μf. An auxiliary capacitor $C_2 = 3$ μf was connected in parallel with it. Both capacitors were charged through a

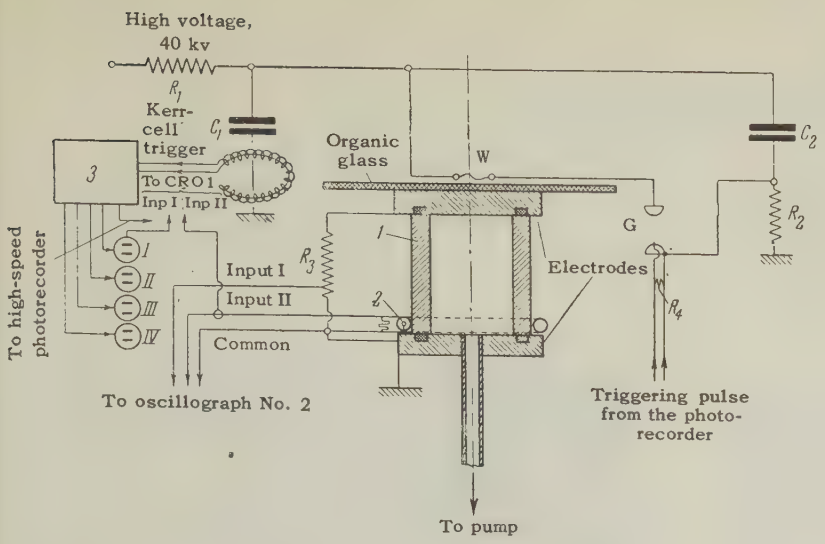

FIG. 1. Electrical circuit diagram of the apparatus. 1 – glass chamber; 2 – Rogovskii belt; 3 – control unit for the Kerr cells; I, II, III, IV – Kerr cells.

resistance $R_1 = 300\,k\Omega$ until they reached equal potential. Variations in the diameter of the discharge channel were recorded by means of a fast mirror photorecorder SFR-2M. When the mirror was in the working position, the photo-recorder sent a triggering pulse to the discharging air gap G. The capacitor C_2 was discharged into a grid of thin wires W which exploded as a result of this, and broke the thin (1 to 2 mm thickness) insulation made of organic glass. The discharge of the main capacitor C_1 into the chamber occurred from 2 to 10 μsec after the triggering pulse. The resistance $R_2 = 10^6\,\Omega$ is introduced into the circuit in order to limit the discharge current to ground after the breakdown of the discharge gap G. The ohmic potential divider was made of a bifilar wound resistor ($R_3 = 810\,\Omega$) connected to the chamber electrodes. The potential divider was situated outside the current conductors, where there were no magnetic fields. The connecting conductor leading to the upper electrode passed through the main conductors; the inductance of the loop formed by it was not larger than 2 cm. The voltage at the output of the potential divider amounted to 0.01 of the circuit voltage. The discharge current (measured by means of a Rogovskii belt) and the voltage on the potential divider were recorded by a double beam oscillograph OK-17M.

Simultaneously with the photo-scanning, the discharge was photographed by means of four Kerr cells which were fed with 15-kv pulses from a special unit which was switched on at the start of the discharge of capacitor C_1. This unit generated five pulses; four reached the Kerr cells, and one reached the spark gap of the photorecorder, producing a light marker on the film. This marker (cf. the "Synchr" marker in Figs. 3 to 5 and 10) enabled us to establish the correspondence between the current oscillograms and the photographic records. To reduce the background on the records given by the Kerr cells, explosive shutters were installed near the observation window of the chamber container.

3. EXPERIMENTAL RESULTS

(a) **Small Chamber.** The construction of the chamber is shown in Fig. 2. The chamber was situated inside a depression of the lower current conductor, covered by a reinforced top. The period of current oscillations during the discharge of the capacitor bank into the chamber was 12.2 μsec. The inductance of the whole circuit, calculated from the second and the third periods of the current, did not exceed 27.5 cm.* On the basis of measurements and calculations the inductances of the individual circuit elements have the following values: (1) The inductance of the capacitor bank is 6.5 cm; (2) the inductance of the current lead is 6.0 cm; (3) the inductance of the discharge gap (over one period) is 8.5 cm; (4) the inductance of the chamber together with the flanges is 6.5 cm. The maximum rate of current growth in the circuit with a working voltage of $U_0 = 40\,kv$ reached a value of 1.4×10^{12} amp/sec. The measured amplitude of the current in the circuit amounted to 1.8×10^6 amp. The current graph in the case of discharge through short chambers has rather insignificant variations during the contraction and the expansion of the discharge channel. This may be explained by the fact that the inductance of the constricted discharge channel amounts to not more than $\frac{1}{3}$ of the inductance of the whole circuit.

*1 cm = 10^{-9} henry – Transl. Ed.

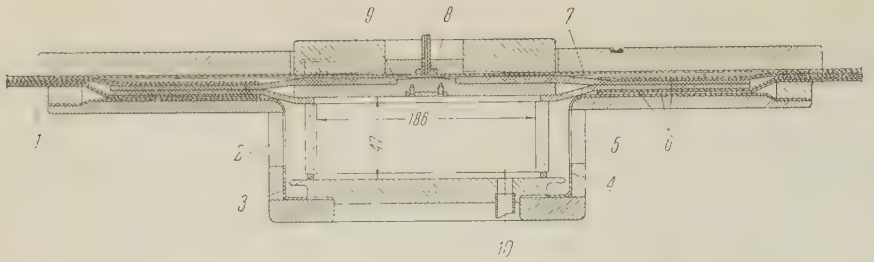

FIG. 2. Construction of the small chamber. 1 – grounded conductor; 2 – window for photographing the discharge by means of Kerr cells; 3 – rubber seal; 4 – glass chamber; 5 – window for photographing the discharge by means of the photorecorder; 6 – rubber insulation; 7 – high voltage conductor; 8 – explosive discharger; 9 – organic glass; 10 – to vacuum pump.

At a pressure of 10 mm of Hg the discharge and the luminescence of the gas at first take place over the whole volume, and then the luminescence becomes weaker. After a pause of 0.6 μ sec, it again becomes more intense near the chamber walls. As many as 30 narrow channels are formed which are relatively more luminous and which gradually expand. Their approach towards one another forms, in fact, the constriction of the discharge which proceeds at an ever increasing rate. During the initial period of constriction, the speed is not greater than 1.5×10^6 cm/sec, but at the instant of maximum constriction it amounts to 5.4×10^6 cm/sec. Figure 3 shows the photorecorder display, the Kerr-cell records, and the oscillograms of the current and of the voltage for this discharge. We see that a constriction has formed in the middle of the channel, just at the point where the photorecorder slit is situated. At this spot the maximum speed of the gas referred to earlier exceeds the average speed of contraction of the channel by a factor of 2.7. Complete contraction occurs near the maximum of the current which is equal to 1.38×10^6 amp. At this instant a characteristic break occurs in the current curve, called a "singularity" in the papers referred to earlier. The minimum radius of the constricted channel is equal to 1.7 cm. The expansion of the gas after the constriction occurs with an initial speed of 3.6×10^6 cm/sec. The speed of expansion gradually decreases. During the sixth microsecond a second constriction begins, but does not have time to be completed, since a part of the gas reaches the wall causing its evaporation and the formation of a new wave containing a large admixture of the material of the wall. Therefore repeated waves coming from the wall (not shown in the photograph) approach the center considerably more slowly. The boundaries of the channel are quite sharply pronounced during the first contraction, and the luminescence of the walls is not very noticeable at that time. As soon as the converging layers of the gas meet one another, the walls of the chamber begin to emit light, apparently owing to the

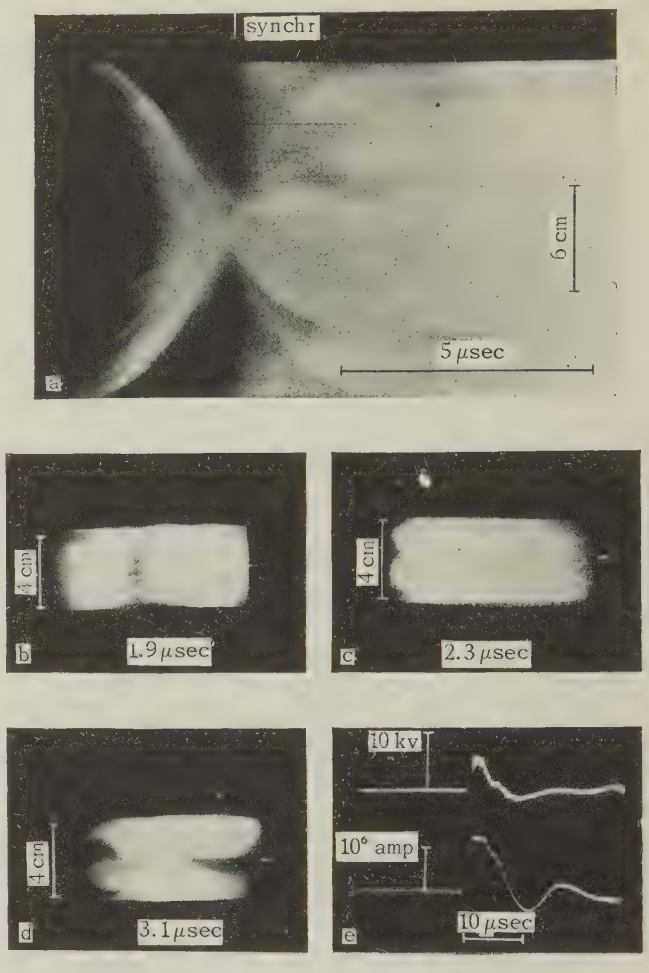

FIG. 3 a – photorecorder display, b, c, d – Kerr-cell records, e – current and voltage oscillograms for discharges in small chambers at a pressure of 10 mm of Hg.

short-wave radiation from the discharge channel. The luminescence of the walls is not accompanied by any breakdown or redistribution of current, since otherwise this would have been made evident by the photorecorder display.

During the initial contraction period, the current in the discharge is equal to 620 kiloamp. If this is evaluated for the individual channels that can be seen on the photorecorder display, then the average current in each channel is approximately 20 kiloamp. After a microsecond it reaches 440 to

550 kiloamp. Simultaneously with their movement towards the center, the channels expand with a speed of (0.8 to 1.0) $\times 10^6$ cm/sec. The channels merge into a continuous annular layer during the third microsecond. The thickness of this layer obtained as a result of measurements made on the photorecorder display is 3 cm.

The intensity of the field in the discharge was calculated from the oscillograms, using the relations:

$$E_R = \frac{U_R}{l}; \quad U_R = U_0 - L\frac{dI}{dt} - I\frac{dL}{dt},$$

where U_0 is the voltage recorded on the oscillogram, L the inductance of the loop formed by the measuring wire (leading to the upper electrode) and the discharge channel, l the distance between the electrodes, and I the current in the discharge.

At the beginning of the contraction (dL/dt = 0). E_R = 850 v/cm. Subsequent measurements of E_R become unreliable, owing to oscillations which make it difficult to determine the derivative of the current.

At a pressure of 1 mm of Hg, the discharge emits considerably less light. The constriction process has much in common with the one described earlier. Just as in the earlier case, the expansion of the gas differs appreciably from a simple motion of shock waves (cf. Fig. 4). The luminous layer of gas begins to move towards the center of the chamber after the discharge current has reached 550 kiloamp. This layer consists of 30 small channels whose brightness considerably exceeds the brightness of luminescence of the surrounding gas. As the channels move towards the center of the chamber, they practically do not expand. The internal boundaries of the layer undergoing contraction touch one another 1.5 μsec after the beginning of the discharge. The thickness of the layer at that instant amounts to 2.2 cm. The speed of contraction is initially equal to 4.5×10^6 cm/sec. By the time of complete contraction, it reaches a value of 8×10^6 cm/sec. The minimum radius of the column is 1.5 cm. The current at the "singularity" is 1.6×10^6 amp at the instant of constriction. The external regions of the gas being compressed approach the center 0.3 μsec later, and restrain the expansion of the gas whose speed at that time does not exceed 1.5×10^6 cm/sec. After the outer layers have approached, the speed of expansion increases to 9×10^6 cm/sec. Cylindrical symmetry of the column of the contracting gas is retained both before and after expansion. Soon after the beginning of the expansion the gas separates into layers. One part goes back

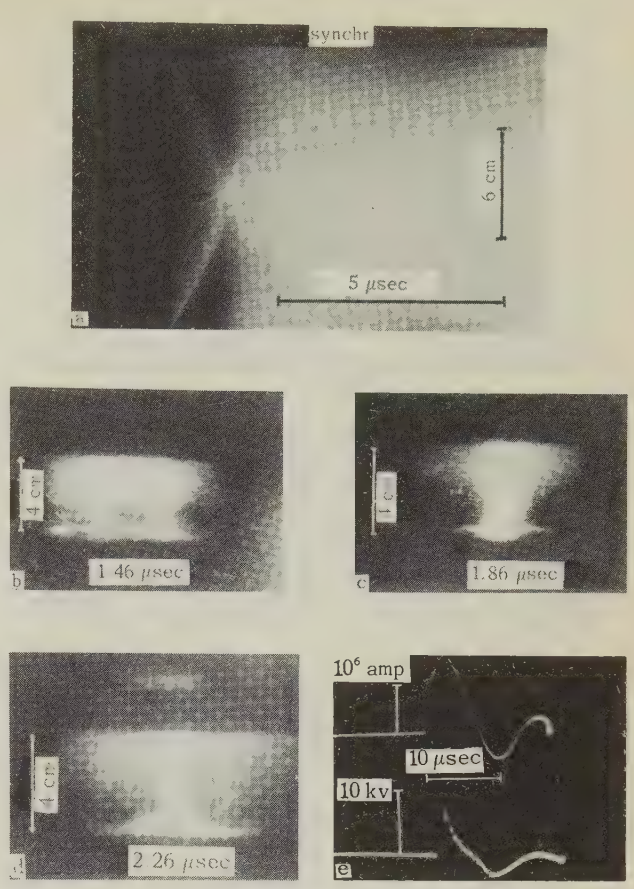

FIG. 4 a – photorecorder display, b, c, d – Kerr-cell records, e – current and voltage oscillograms for discharges in small chambers at a pressure of 1 mm of Hg.

towards the center of the chamber where the luminous channel remains, and another part of the gas goes towards the chamber walls.

The stratification occurs three times separated by intervals of 0.2 to 1 μsec and, apparently, is of a symmetric nature, as may be seen from the third Kerr-cell record. The internal column is more brightly luminous, and may be picked out in the photograph right up to the fourth microsecond. Small oscillations in the oscillograms of the current and the voltage, which last right up to the fifth microsecond, correspond to the fluctuations in the gas column.

At a pressure of 0.1 mm, the relative luminosity of the chamber walls increases, and this makes it more difficult to interpret the photograph. Nevertheless the principal features can still be seen (Fig. 5). A characteristic feature of the process is the occurrence not of one, but of three compression waves moving towards the center with constant velocity at times equal to 0.44, 0.85, and 1.46 μsec after the beginning of the compression. The velocities of the fronts amount respectively to 8.6×10^6, 1.1×10^7, and 1.4×10^7 cm/sec. The second and

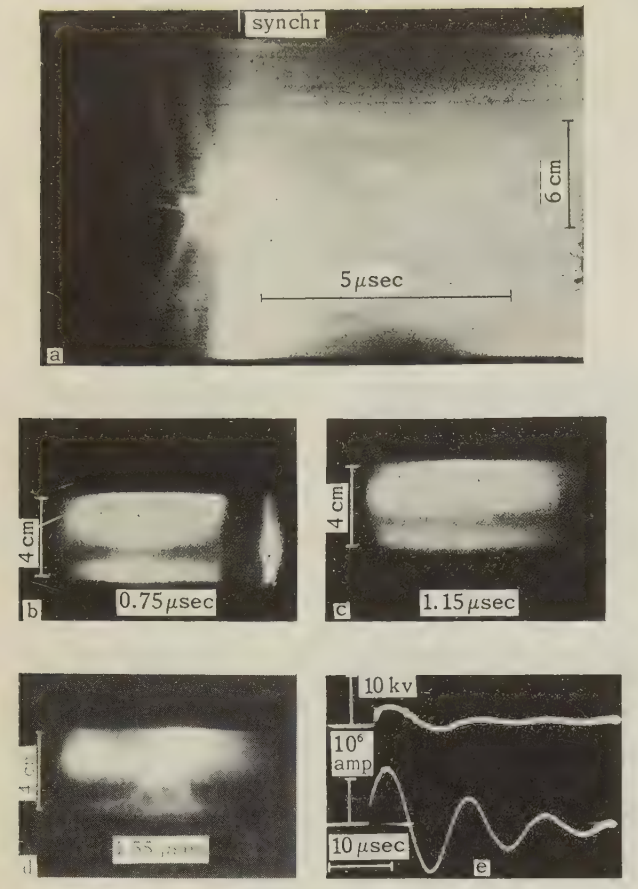

FIG. 5 a – photorecorder display, b, c, d – Ker-cell records, e – current and voltage oscillograms for discharges in small chambers at a pressure of 0.1 mm of Hg.

the third fronts begin to move even before the preceding front has reached the center of the chamber. The individual channels in these fronts appear not at the beginning, but almost at the time of complete contraction. The channels approach one another, forming constrictions of a certain kind, which shows that the currents flowing in them are parallel.

Both in the photorecorder displays and also in the Kerr-cell records (the two are in good agreement) it can be noted that the channels are surrounded by an atmosphere of luminous gas within which they approach one another. The separation begins after the first compression and slows down as each successive front approaches the center of the chamber. The minimum diameter of the channel is 1.5 cm during the first contraction, 3.7 cm during the second, and 5.6 cm during the third. The total current in the circuit, at the instant when the first wave starts, amounts to 350 kiloamp; for the second and third waves this current is respectively 900 and 1200 kiloamp. To each compression there correspond small oscillations in the oscillogram of the current whose maximum values for each of the waves are 1.1×10^6, 1.2×10^6 and 1.3×10^6 amp. In view of the fact that the compression waves are superimposed in time, the measured current can be related to the discharge column only for the third wave.

The voltage across the electrodes, as recorded by the oscillograph, at first falls and then rises; during the first microsecond it amounts to 4300 v, it then increases to 14.4 kv and remains at this level until the fourth microsecond. The gradient in the chamber when the current through it passes through its maximum (when there is no inductive component) is 3 kv/cm. At pressures of 10 and 1 mm of Hg, a falling off of the voltage was observed during the first and second microseconds.

(b) **Large Chamber.** Just as in the preceding case, in the case of experiments with the large chamber an explosive discharger was used, placed between the upper flat flange of the chamber and the high-voltage lead. The lower flange had a small convex portion which was made in order to introduce the head of a scintillation counter into the depression that is formed below. The height of the glass chamber was 155 mm. The distance between the projection in the lower electrode and the upper electrode was 123 mm, the inner radius of the chamber was 92 mm. The small convex projection of the lower electrode did not affect the process of constriction which proceeded in exactly the same manner as in the case of a flat lower electrode. The copper conductor surrounding the chamber had a flare in its lower part. On top, a steel ring was placed around the copper coaxial cable to increase its mechanical strength. The total inductance of the circuit together with the chamber and the discharger, as evaluated from the period of oscillations of the current, did not exceed 55 cm. The inductance of the measuring loop at the beginning of the process (when the current flows near the chamber walls) attained a value of 7 cm. The initial rate of rise of the current in the discharge was 0.73×10^{12} amp/sec.

At a pressure of 10 mm of Hg the contraction process begins already at a current of 500 to 600 kiloamp after a number of narrow channels (approximately 40) have been formed in the discharge. The contraction takes place with an average speed of 3×10^6 cm/sec (cf. Fig. 6). The converging layer of gas had a thickness of 2.5 to 3 cm. The inner boundaries of the layer met 3.2 μsec after the start, the outer ones met 0.6 μsec later. At the instant of complete contraction when the diameter of the channel was reduced to 3.6 cm the current in the discharge attained a value of 1.1×10^6 amp, and owing to the relative increase in the inductance of the discharge channel the current

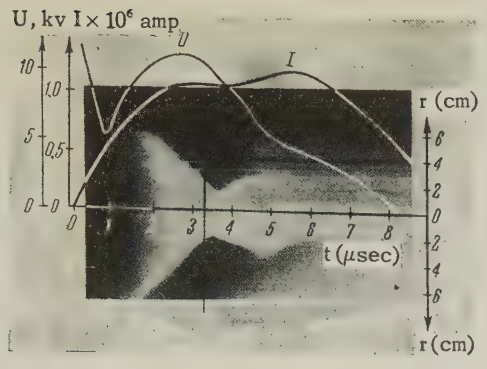

FIG. 6. Photorecorder display of a discharge at p = 10 mm. of Hg with the current and voltage oscillograms superimposed on it.

lost its sinusoidal form. The peak of the sinusoidal curve was flattened and showed dips characteristic of the so-called "singularities." The expansion of the gas occurs with speeds in the range (1.2 to 2.1) × 10^6 cm/sec. A second compression was observed 1.5 microsec after the first one; the diameter of the channel in this case was reduced to 7 cm. The current at the second "singularity" was larger than at the first by 100 kiloamp. Between the instant of breakdown and the beginning of the compression, the voltage across the electrodes fell from 40 to 5.5 kv, and then increased to 12 kv. The maximum of the voltage coincides with the beginning of the "singularity" on the current curve, and is delayed with respect to the moment of complete contraction which may be seen on the photorecorder display.

At a pressure of 1 mm of Hg, the contraction begins 1.16 μsec after breakdown. The speed of contraction varies between 4.8 × 10^6 and 6.1 × 10^6 cm/sec. In the photorecorder display (Fig. 7) one may see, just as in the preceding cases, a network of channels forming the contracting layer; the thickness of the latter is 2.2 cm. On the Kerr-cell records horizontal bands can be seen which are particularly noticeable at times immediately preceding a complete contraction. Their appearance indicates that the instability characteristic of the plasma manifests itself in the contracting layer even before complete contraction has taken place. Complete contraction occurs 2.7 μsec after breakdown and lasts 0.3 μsec. The minimum diameter of the constricted channel is 1.7 cm. The expansion of the gas occurs in an asymmetrical manner: the channel remains constricted at the electrodes for some time, while at other points the expansion occurs more rapidly. The speed of expansion attains values up to 3.7 × 10^6 cm/sec. A second compression begins 0.25 μsec later, and takes place with a speed of 4.5 × 10^6 cm/sec; then a small expansion occurs, and after that the diameter of the channel practically does not change until the sixth microsecond. Thus the channel remains constricted during 3 to 4 microsec.

The current in the discharge varied in the following way: at the moment when the gas separated from the walls its value was I_0 = 576 kiloamp. During the first compression it was 1.16 × 10^6 amp, and during the second compression it was 1.3 × 10^6 amp.

(c) **Chamber with conical electrodes.** The construction of the chamber is shown in Fig. 8. The upper convex electrode has the form of a truncated cone with its vertex directed into the chamber. The lower electrode is the same as in the preceding chamber. With this construction of the electrodes, in spite of the small gap at the center of the chamber, the discharge is formed at the chamber walls. To make it easier for the breakdown to occur at the center, in some of the experiments sharp points were placed on the flat summit of the upper elec-

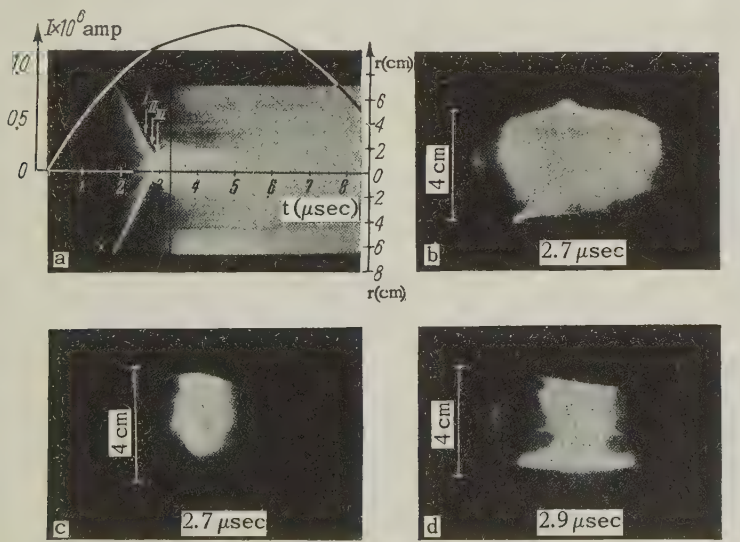

FIG. 7. a – photorecorder display with current oscillogram superimposed on it; b, c, d – Kerr-cell records of the discharge at a pressure of 1 mm of Hg.

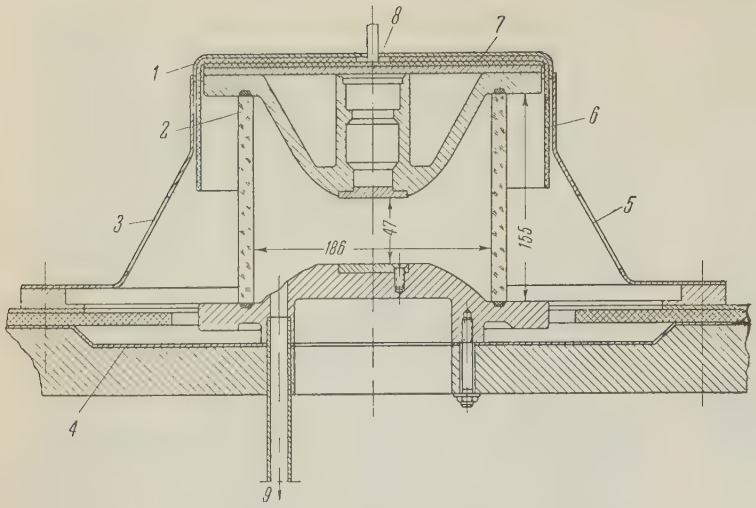

FIG. 8. Construction of chamber with conical electrodes. 1 – high voltage conductor, 2 – glass chamber, 3 – window for photographing the discharge by means of Kerr-cells, 4 – grounded conductor, 5 – window for photographing the discharge by means of photorecorders, 6 – rubber, 7 – organic glass, 8 – explosive discharger, 9 – to vacuum pump.

trode in such a way that the minimum gap between the electrodes was reduced to 17 mm.

At a pressure of 10 mm of Hg, the upper electrode was provided with a sharp point, but this did not prevent the formation of a skin-layer near the walls of the chamber. Although breakdowns were sometimes observed in the center of the chamber, nevertheless the main part of the current apparently flowed near the walls. The phenomenological aspects of the phenomena remained the same as in the preceding cases (Fig. 9). The start occurred 0.5 to 0.7 μsec after breakdown. The speed of contraction at the beginning amounted to 1.3×10^6 cm/sec, and then increased to 5.2×10^6 cm/sec. The diameter of the channel was reduced from 18.5 to 2.3 cm. The expansion of the channel occurs in a fairly symmetric manner with a speed of 5×10^6 cm/sec. Repeated contractions in these experiments are more sharply defined, they occur 1 μsec and 2.5 μsec after the first contraction.

At a pressure of 1 mm of Hg, the sharp point was removed from the upper electrode. The skin layer is formed at the wall and begins to contract 0.6 μsec after breakdown with the total current in the discharge having a value of 370 kiloamp (Fig. 10). The initial speed of contraction is 2.8×10^6 cm/sec, and the final speed is 7.8×10^6 cm/sec. Just as in the two preceding cases contraction proceeds at this pressure quite symmetrically. The photographs by means of the Kerr cells allow us to observe in the gas layer various forms of instability which manifests itself practically from the very beginning. At the moment of complete contraction they are transformed into the "constrictions" described above. The contraction of the skin layer lasts not longer than 0.3 μsec, after which expansion begins, followed by a second, third, and a not very pronounced fourth contraction. In this case no appreciable broadening of the channel is observed. The smallest diam-

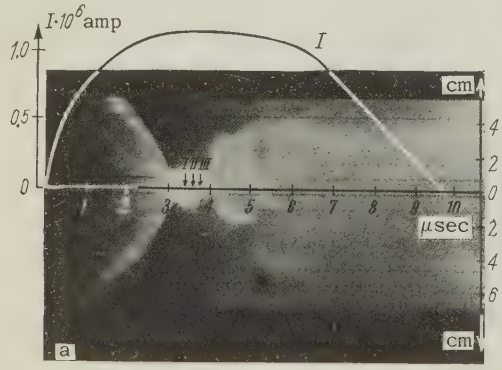

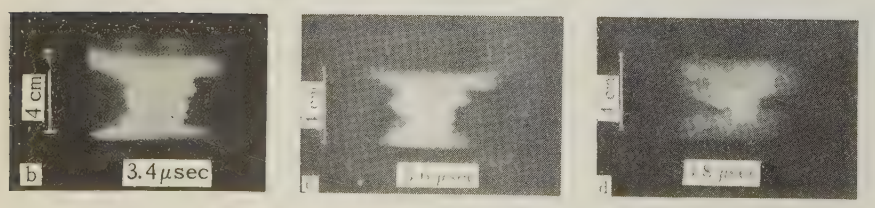

FIG. 9. a – photorecorder display with current oscillogram superimposed on it, b, c, d, – Kerr-cell records of the discharge. Pressure is 10 mm of Hg.

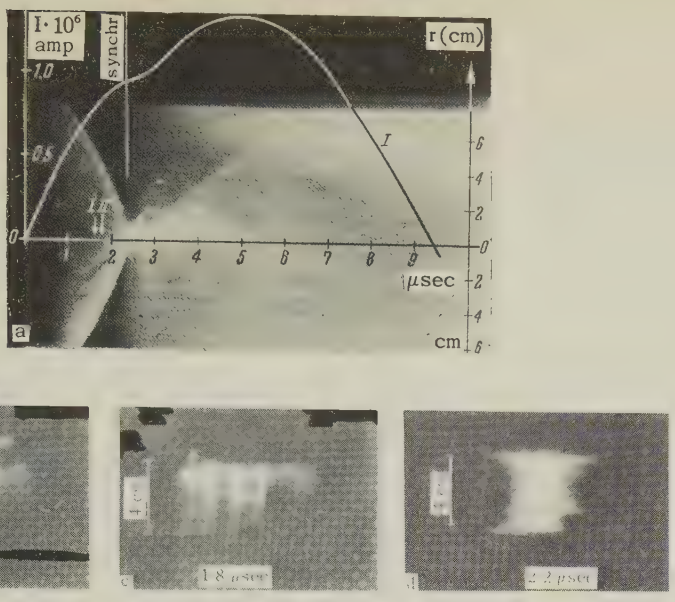

FIG. 10. a – photorecorder display with current oscillogram superimposed on it, b, c, d – Kerr-cell records of the discharge. Pressure is 1 mm of Hg.

eter of the "pinch" during the second and the third contraction is 2.0 cm, and the total length of time during which it lasts is 2.4 μsec. Just as in the case of the short chambers, the expansion of the gas is accompanied by the separation of the gas into layers. The first two contractions occur at the same value of the current equal to 1.04×10^6 amp, while the third and the fourth contractions correspond to currents of 1.1×10^6 and 1.3×10^6 amp.

(d) **Neutron measurements**. Neutron measurements were made by means of a counter and an apparatus of type B, and also by means of a scintillation counter. The thresholds of sensitivity of the apparatus were 10^6 and 10^4 neutrons respectively. The apparatus did not record any neutron emission.

4. DISCUSSION OF RESULTS

(a) **Initial processes**. The discharge in the chamber during the time when its conductivity is small (Townsend build-up) occupies the whole volume, or its greater part. When short voltage pulses of 0.1 μsec duration are applied to the chamber, diffuse streamers are observed which spread over the whole volume of the chamber. When the conductivity increases and the current in the discharge attains values of tens of kiloamperes, the skin effect becomes distinctly evident. The start occurs after the formation of the conducting layer situated along the periphery of the chamber. As we have seen, its thickness does not vary appreciably at pressures of 10 and 1 mm of Hg (Fig. 11), and only at a pressure of 0.1 mm of Hg does it become appreciably less. The variation in the current at which the break-away occurs is shown in Fig. 12 as a function of the pressure.

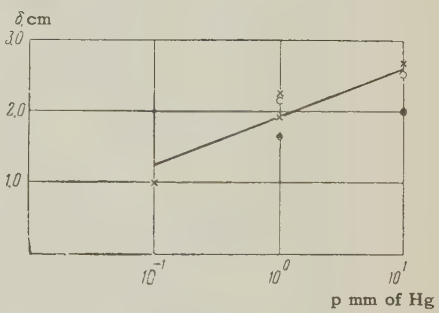

FIG. 11. Variation of the thickness of the conducting layer with pressure: o – large chamber, × – small chamber, • – chamber with conical electrodes.

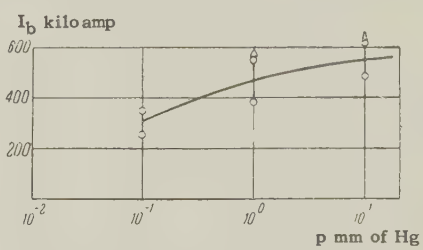

FIG. 12. Breakaway currents at different pressures. Measured values: o – for small chambers, Δ – for large chambers.

The average conductivity σ in the luminous layer at the moment of the start can be roughly estimated from the thickness δ of the layer (it may exceed the thickness of the skin-layer by a factor of 2 to 3). From the well known expression:

$$\sigma = c^2 t / 2\pi\delta^2 = (0.5 \div 1.4) \cdot 10^{14} \text{ CGS esu.}$$

The order of magnitude of this quantity may also be found from the longitudinal field strength E_R in the discharge at the instant of the start, on the assumption that the current in the layer is dis-

tributed uniformly:

$$\sigma = I_0/2\pi R^2 E_R,$$

where R is the radius of the chamber, and I_0 is the current at the time it breaks away from the wall. By utilizing the measured values of I_0 and E_R we obtain a conductivity of 0.3×10^{14}, which remains practically constant as the pressure is varied by two orders of magnitude. A gas which has such a conductivity has an electron temperature of 3 to 6 ev. The unavoidable evaporation of the walls leads to impurities in the deuterium which manifest themselves by the high luminosity of the gas after contraction, when the deuterium should be highly ionized and less luminous. As may be seen from photographs, there is no continuous conducting layer at pressures of 1 to 10 mm of Hg. Instead there is a network of channels which have a relatively higher luminosity and consequently a higher current density. Since the magnetic pressure is given by $P_M \approx iH$ (H is the magnetic field, i is the current density), the pressure experienced by these channels is greater, and they start first. A layer of ionized gas is left behind them. The current in it will grow as the gas moves in towards the center.

Efficient capture of neutral gas by means of the charge-exchange mechanism becomes possible from the moment when the converging channels coalesce into one continuous front. At a pressure of 10 mm of Hg, the formation of a continuous annular layer occurs at a radius of 45 mm. At smaller pressures the radius of capture is larger. However, complete capture does not occur even in the case of a continuous annular layer. This is particularly noticeable at a pressure of 0.1 mm of Hg, when there is observed a series of contraction waves, which are possible only in the presence of residual gas. Thus the number of particles which the conducting layer will "sweep" towards the center can in actual fact differ appreciably from the number of particles present in the chamber cross section.

(b) **Contraction and scattering.** The speed of contraction of plasma in the discharge varies from zero up to a certain maximum value. Its increase depends on the pressure, on the circuit parameters, on the shape of the electrodes, and on the instability of the contracting layer. It was noted earlier that at p = 10 mm of Hg the speed of the gas at the point where constrictions are formed may exceed the average speed (temperature) of the gas during contraction by a factor of 3 (and the temperature by an order of magnitude). At the instant of complete contraction, a longitudinal redistribution of the particle density may occur, owing to the existence of constrictions.

The maximum speeds in the three variants of chamber design described earlier differ from each other only very little. However, if one compares the maximum speeds of contraction obtained for chambers of equal diameter with flat electrodes used in various installations[2,5] the influence of such a parameter as U_0/L_{init} becomes noticeable. Figure 13 shows the curves of $v_{max} = f(p)$ for

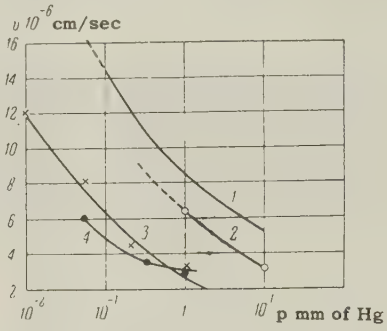

FIG. 13. Dependence of the maximum speed of contraction on the pressure for shock circuits with the parameter U_0/L_{init} having the values: $1 - 1.4 \times 10^{12}$; $2 - 0.7 \times 10^{12}$; $3 - 2 \times 10^{11}$; $4 - 5.7 \times 10^{10}$

apparatus with different values of U_0/L_{init}. The influence of the parameter U_0/L_{init}, on the speed of contraction may be seen best of all in the case of p = 1 mm of Hg. At this pressure the constrictions are least pronounced, and the errors in measuring the speeds of contraction are least. Even in the case of a relatively very rapid rate of rise of current, the converging layer of gas remains compact at a pressure of p = 1 mm of Hg. At smaller pressures this compact nature is not preserved. As may be seen from Fig. 14, v_{max} grows mono-

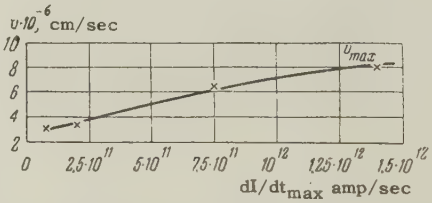

FIG. 14. Dependence of the maximum speed of contraction on the initial rate of current growth in the discharge; p = 1 mm of Hg.

tonically, increasing by factor of 2.5 as U_0/L_{init} increases by a factor 10 [$v_{max} \approx (U_0/L_{init})^{1/2.5}$].

At the instant of contraction, the current in the discharge depends significantly on the initial pressure. Figure 15 shows the measured and the calculated (cf. Leontovich and Osovets[3]) values of the current during the first contraction. The best agreement is observed at a pressure of 1 mm of Hg. At lower and, particularly, at higher pressures the discrepancies become appreciable. If one calculates the time of the first contraction by means of a formula given by Leontovich and Osovets[3] then the observed value always turns out to be higher then the calculated one. There are at least four reasons for such a discrepancy: (1) the

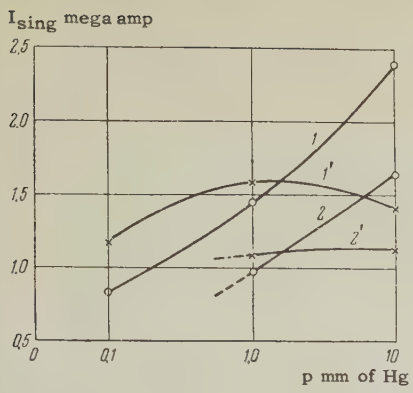

FIG. 15. Current in the discharge at the first contraction. 1, 1′ – small chamber, 2,2′ – large chamber, o – calculated values, × – experiment.

deviation of the current from a linear form at times close to τ_{sing} (which is important for large τ_{sing} and large p); (2) the smearing out of the current front and of the converging layer of gas; (3) the imperfect nature of the mechanism of "sweeping up" of the gas, owing to which only a portion and not the whole gas contained in the chamber is collected (this is more important at low pressures); (4) the capture of heavy particles from the chamber walls. A relatively satisfactory agreement between calculated and actual values is apparently explained by the fact that the various deviations compensate one another at least partially.

As we have seen, the contracting layer of gas, prior to colliding with the layers which it encounters, has a comparatively low ion and electron temperature, and therefore the degree of ionization in this layer must be relatively low (cf. also Lukianov and Sinitsyn[6]). The layer contains a large number of neutral particles. The principal part of the heating occurs during the short shock compression, when a part of the kinetic energy of directed motion of particles is transformed into heat. An evaluation of the temperature with the aid of formulas for the equilibrium state[7] $T = I^2/4Nk$ is hardly justified in this case. It is therefore best to estimate the maximum temperature by utilizing v_{max} ($v^2_{max} = 3kT/M_D$). Figure 16 shows the temperature determined in this manner for small chambers at various pressures. The limiting

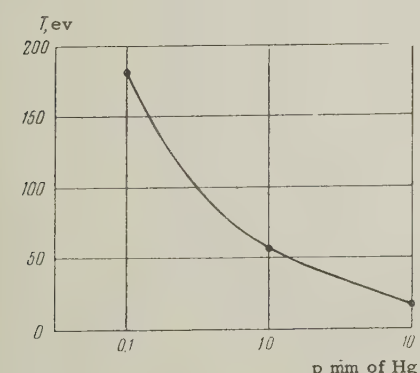

FIG. 16. Maximum gas temperature during contraction (small chamber).

temperature attained at a pressure of 0.1 mm of Hg amounts to 180 ev. One might think that under our conditions, neutrons of thermonuclear origin might be produced by the higher speed of contraction. However, a simple calculation shows that this is not the case. The neutron yield A may be estimated from the well-known relationship

$$A = {}^1/_2 nN \langle \delta V \rangle \tau l,$$

where n is the particle density in the column at the instant of compression, N is the initial number of particles in the cross section of the chamber, $\langle \sigma V \rangle$ is the cross section for the reaction, l is the length of the column in cm, τ is the time of contraction in sec. Calculations made on the basis of the following assumptions: (1) all the gas is captured during contraction, (2) the measured speed is the average speed for a Maxwellian distribution of particle velocities, (3) $\tau = 10^{-6}$ sec, give a neutron yield of approximately 10^3 at p = 0.1 mm of Hg. This value is below the threshold of sensitivity of the recording devices. At higher pressures the neutron yield is even less.

Thus in the case of small chambers, in spite of the higher speed of contraction compared with the large chambers described earlier by Artsimovich et al.,[2] the neutron yield is either entirely absent or is very small. This result confirms the point of view expressed at that time with respect to the non-thermonuclear origin of the neutron radiation then observed.

The figures quoted above for the limiting compression of the gas, calculated from the ratio of the cross sections of the chamber and of the pinch, are somewhat overestimated. At a pressure of 10 mm of Hg the radius of capture is in actual fact smaller than the diameter of the chamber. If the gas is collected in a column starting with the radius of capture, then the limiting compression amounts approximately to 10. If p = 0.1 mm of Hg, it is impossible to introduce corrections because we have not one, but three compression waves. The most accurate result, apparently, is obtained at a pressure of 1 mm when the symmetry of contraction is well preserved, when a satisfactory agreement with results of calculation is observed, and when, probably, there is no appreciable smearing of the current front, as is indicated by the sharp boundaries of the pinch. The limiting compression in this case attains a value of 140. This number may be regarded only as a rough approximation, since we have no reliable estimate of the amount of captured gas.

During a shock compression of short duration one can observe inside the pinch simultaneous

movement of waves of compression and decompression moving towards each other. However, this is the only point of similarity with elementary wave processes.

The expanding front of the gas has a structure that differs sharply from a simple shock wave. The front oscillates several times, and for quite different reasons than those given by Leontovich and Osovets.[3] Some of the gas is directed towards the center and some continues its movement towards the boundaries of the chamber at a reduced speed. A relatively more luminous narrow channel is preserved at the center. It may be observed on photographs during several microseconds, until the current passes its maximum value. In the case of a simple shock compression, the gas would have remained at the center not longer than 0.3μ sec. It is natural to assume that at the center of the pinch the current continues to flow even after contraction, as was observed by means of probe measurements and at lower pressures and speeds of contraction.[2,3] The luminosity in the front of the expanding gas is due to neutral particles which are not held by the field of the current. As the current builds up in the boundary portions of the gas column, which have a certain amount of conductivity, the column breaks up into layers. The hottest particles are carried towards the center and give rise to repeated compressions, while the cold particles are directed towards the walls. After the walls have been bombarded, a conducting layer of heavy particles is formed there. The contraction of this layer proceeds at considerably lower speeds. At this time the current at the center falls, while the current at the walls rises.

The influence of electrodes on the development of the discharge should naturally be more pronounced in short chambers, owing to the shorter time required for the metal vapor to penetrate deeply into the gap, and owing to the removal of heat by the electrodes. Both processes begin at the instant of onset of the discharge, but are most strongly pronounced after contraction. Before contraction, the temperature of the gas in the skin layer is not greater than 6 ev. The corresponding speed of neutral atoms of copper is equal to $v_{Cu} = v_D\sqrt{M_D/M_{Cu}} = 2.3 \times 10^5$ cm/sec. Thus, the copper vapor will advance not more than 5 mm during contraction. An appreciable removal of heat at such speeds would be observed only after 12μ sec. After contraction (if $p = 0.1$ mm of Hg) the time for the removal of heat would amount to 3.5μ sec, while v_{Cu} would increase to 2.8×10^6 cm/sec. It follows from these figures that it is not advantageous to conduct experiments with short chambers at lower pressures.

The author expresses his deep gratitude to Academician M. A. Leontovich and S. M. Osovets for valuable remarks.

[1] I. V. Kurchatov, Атомная энергия (Atomic Energy) **3**, 65 (1956).

[2] Artsimovich, Andrianov, Basilevskaia, Prokhorov, and Filippov, Атомная энергия (Atomic Energy) **3**, 84 (1956).

[3] M. A. Leontovich and S. M. Osovets, Атомная энергия (Atomic Energy) **3**, 81 (1956).

[4] V. S. Komel'kov and G. N. Aretov, Dokl. Akad. Nauk S.S.S.R. **110**, 559 (1956).

[5] Borzunov, Orlinskii and Osovets, Атомная энергия (Atomic Energy) **4**, 149 (1958).

[6] S. Iu. Lukianov and V. I. Sinitsyn, Атомная энергия (Atomic Energy) **3**, 88 (1956).

Translated by G. Volkoff
2

PHOTOPRODUCTION OF NEGATIVE PIONS FROM DEUTERIUM NEAR THE THRESHOLD

M. I. ADAMOVICH, G. V. KUZ'MICHEVA, V. G. LARIONOVA, and S. P. KHARLAMOV

P. N. Lebedev Physics Institute, Academy of Sciences, U.S.S.R.

Submitted to JETP editor February 10, 1958

J. Exptl. Theoret. Phys. (U.S.S.R.) **35**, 27-38 (July, 1958)

This investigation was performed with the Lebedev Physics Institute's 265-Mev synchrotron using photographic emulsions containing D_2O. Detailed information concerning the reaction $\gamma + d \rightarrow p + p + \pi^-$ was obtained for photon energies up to 200 Mev. Various experimental characteristics of the reaction are compared with the predictions of the impulse approximation theory. The experimental results are consistent with the theory which takes into account the interaction between nucleons in the final state. It is shown that the square of the matrix element for photoproduction of pions from neutrons near the meson threshold is constant and equals $(0.785 \pm 0.072) \times 10^{-27}$ cm^2. This value corresponds to $\sigma^-/\sigma^+ = 1.34$.

1. INTRODUCTION

A number of investigators[1-3] have measured the ratio between the cross sections for the reactions $\gamma + d \rightarrow p + p + \pi^-$ and $\gamma + d \rightarrow n + n + \pi^+$. This ratio is used to represent the ratio for the photoproduction of negative and positive pions from free nucleons. Watson[4] has indicated the following conditions under which the observed ratio σ^-/σ^+ for deuterium will be the same as for free nucleons: (1) correctness of the impulse approximation, (2) production of photomesons in the S state, and (3) negligibly small Coulomb interactions between mesons and nucleons. Fulfillment of the first two conditions has not been verified experimentally, although σ^-/σ^+ has been measured many times. Fulfillment of the third condition has been secured experimentally by the recording of high-energy mesons. The following fact must be taken into account in connection with the first condition. For photons up to 200 Mev (to insure fulfillment of the second condition) the relative kinetic energy of the two protons is small and, as we have shown experimentally,[5,6] an essential part is played by interaction of the nucleons in the final state. The nucleon interaction rules out the application of single-nucleon kinematics to the photoproduction of pions from deuterium.

In the experiments reported in references 1 and 2, the single-nucleon kinematics was used to determine σ^-/σ^+. The energy dependence obtained in this way and the value of σ^-/σ^+ at the meson threshold are in disagreement with theoretical predictions. This discrepancy may possibly be accounted for by the difference between the $\pi^- - p - p$ and $\pi^+ - n - n$ systems and the contribution of photons from the entire bremsstrahlung spectrum above threshold to the yield of pions with a definite energy. A certain arbitrariness in extrapolating σ^-/σ^+ to the pion photoproduction threshold is also involved.[2]

It was the purpose of the present work to obtain information concerning the reaction $\gamma + d \rightarrow p + p + \pi^-$ near the threshold of pion photoproduction, with principal attention being devoted to verification of the correctness of the impulse approximation. Furthermore, by using the impulse approximation and taking into account the Coulomb and nuclear interactions of the particles in the final state, conclusions are reached regarding pion photoproduction from free neutrons.

2. EXPERIMENTAL METHOD

We studied the photoproduction of negative mesons from deuterium by means of emulsions containing deuterium, which were exposed directly to the photon beam. Emulsions loaded with deuterium served as targets and detectors at the same time. This method provides a detailed picture of the interaction which leads to the production of negative pions from deuterium.

We used type-P 400 μ NIKFI emulsions, which are sensitive to relativistic particles. An amidol developer was used as recommended by the NIKFI (Motion Picture and Photography Scientific Research Institute). The uniformity of development as to depth was entirely satisfactory.

Before irradiation a batch of plates was impregnated with heavy water at 18 to 19°C. A plate

measuring 3.0×6.0 cm^2 absorbs an average of 0.770 g of heavy water in one hour. Such a loaded emulsion is 800μ thick during irradiation, and 1 cm^3 of the loaded emulsion contains 3.2×10^{22} deuterium nuclei.

The plates were bombarded by photon beams, with a maximum energy of 250 and 200 Mev at a distance of 5 m from the target, produced by the Lebedev Physics Institute synchrotron. The photon beam traversed the shielding and primary lead collimators, passed through the gap of the electromagnet, and reached a plate whose emulsion faced the beam. The 7000-oersted field of the electromagnet swept electrons from the photon beam. Carbon blocks shielded the plates from scattered radiation. Irradiation occurred at a glancing angle of 30°. A graphite ionization chamber was placed directly behind the plate to determine the photon beam through the emulsion.

The plates were scanned by MBI-2 microscopes with $20 \times 10 \times 1.5$ magnification. As a check of efficiency, some batches of plates were scanned twice by different persons. Stars were recorded with an efficiency not lower than 96% under the worst conditions. $60 \times 15 \times 1.5$ magnification was used in the measurements.

The energies of particles stopping in the emulsion were determined from the residual ranges. The dependence of the residual range on particle energy was calculated for different degrees of impregnation occurring experimentally. The energies of particles whose tracks did not terminate in the emulsion but were inclined at a small angle were determined from grain density by comparison with calibration curves of grain density versus residual range. The calibration was performed for each set of plates, using a few long-range mesons and protons stopping in the emulsion. The sensitivity of the plates was considerably reduced by impregnation; this made it possible to use grain counts to determine particle energies in a broad interval. However the reduced sensitivity of the plates permitted registration of pions only with energies not above 40 Mev.

The identification of particle tracks stopping in the emulsions presented no difficulty. Tracks which left the emulsion at a small dip angle were identified from grain density and multiple scattering. Multiple scattering was measured with a MBI-8 microscope using the coordinate method. Figure 1 shows the distribution of proton and pion tracks according to grain density and multiple scattering. The axes of the figure are the logarithms of the grain density in 500-micron cells and the coordinate second difference. Identification by means of grain density and multiple scattering can be used only within certain limits and is laborious; we therefore used it relatively infrequently.

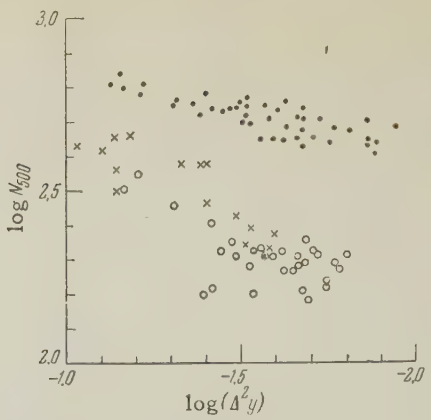

FIG. 1. Grain density vs multiple scattering for protons and mesons of one of the processed sets of plates. The dots represent protons; the crosses represent pions; the circles represent pions from the reaction $\gamma + d \to p + p + \pi^-$.

Three-prong stars found in the plates were analyzed in order to distinguish those associated with the reaction $\gamma + d \to p + p + \pi^-$. For this purpose we determined the energies and angles of emission of all particles in a star with respect to the photon beam direction, which was ascertained in each plate from the tracks of secondary electrons, the majority of which were parallel to the photon beam. Analysis of each star was based on conservation of photon energy and momentum in $\gamma + d \to p + p + \pi^-$. For brevity the following notation was used. The vector sum of the momenta of all three particles is called the star momentum $\mathbf{P}$. The sum of the particle energies, the meson rest mass, and the difference between the rest masses of the deuteron and the two protons is called the photon energy E_γ. The photon energy expressed in momentum units and directed along the photon beam is called the photon momentum $\mathbf{P}_\gamma$. When $\mathbf{P}$ agreed with $\mathbf{P}_\gamma$ the star was assigned to the reaction $\gamma + d \to p + p + \pi^-$. A natural measure of the deviation of the star momentum from the photon momentum is $\Delta P = |\mathbf{P} - \mathbf{P}_\gamma|$. This parameter includes the errors in measurements of both angles and energies. If the spread of ΔP results only from errors of measurement, its distribution must obey the Maxwellian law $\Phi(\Delta P) \sim (\Delta P)^2 \exp\{-h^2(\Delta P)^2\}$, where h is a measure of accuracy equal to $2/\pi(\Delta P)_{av}$. Figure 2 shows the distribution of stars with respect to ΔP. In the momentum measurements the proton rest mass is taken as unity. The same figure shows the Maxwellian distribution with the parameter h obtained experimentally. The distribution

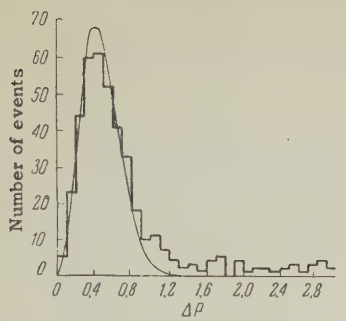

FIG. 2. Histogram of star distribution with respect to ΔP. The solid curve is the Maxwellian distribution.

has a maximum at $\Delta P = 0.45$ and drops sharply in the interval from 0.5 to 1.0. The experimental distribution also shows a "tail" for large values of ΔP. All stars with ΔP smaller than 1.1 are assigned to the reaction $\gamma + d \rightarrow p + p + \pi^-$.

It is necessary to determine the validity of ΔP as a criterion. The investigated reaction $\gamma + d \rightarrow p + p + \pi^-$ could contain an admixture of photoreactions in emulsion nuclei such as the following photoreactions for oxygen:

$$\gamma + O_8^{16} \rightarrow p + \pi^- + O_8^{15};\ O_8^{15} \rightarrow N_7^{15} + \beta^+;$$

$$\gamma + O_8^{16} \rightarrow p + p + \pi^- + N_7^{14};$$

$$\gamma + O_8^{16} \rightarrow p + p + n + \pi^- + N_7^{13},\ N_7^{13} \rightarrow C_6^{13} + \beta^+.$$

Similar reactions can be written for carbon, nitrogen and other nuclei. A control experiment was performed for the purpose of estimating the contribution of these secondary reactions to the number of recorded instances of the reaction under investigation. The control emulsions were loaded with light water and irradiated by a photon beam. Three-prong stars were analyzed by the previous method. The scanned area on plates loaded with light water was 64 cm^2. This same area on plates loaded with heavy water contains on the average 20 instances of the reaction $\gamma + d \rightarrow p + p + \pi^-$, represented by stars with the parameter $\Delta P < 1.1$. In the plates containing light water not a single three-prong star was found with ΔP smaller than 1.1. It might be assumed that all stars with $\Delta P < 1.1$ represent reactions with emulsion nuclei rather than with deuterium. Then the probability that an area of 64 cm^2 would contain not a single star with ΔP between 0 and 1.1 is of the order of 10^{-9}. The assumption is thus shown to be unfounded. We can thus consider that, within the limits of accuracy of the control experiment, no secondary reactions appear among assigned instances of $\gamma + d \rightarrow p + p + \pi^-$. The "tail" of the star distribution with respect to the parameter is, however, caused by secondary reactions with emulsion nuclei. Thus the analysis using the ΔP criterion unambiguously selects instances of negative-pion photoproduction from deuterium.

The following different cases were encountered during the analysis: (1) All three particles stopped in the emulsion. (2) One or two particles emerged from the emulsion but could be identified either visually or by grain density and multiple scattering. These were the two simplest cases where the ΔP criterion of $\gamma + d \rightarrow p + p + \pi^-$ could be applied. (3) A particle left the emulsion and could not be identified by multiple scattering. In this case we were able to arrive at an unambiguous conclusion regarding the nature of the particle. We had two unknown quantities (the energy of the particle and the energy of the photon) and four equations which described the conservation laws. Two equations were used to determine the energy of the particle and the total momentum of the star. The satisfying of the other two equations showed the correctness of the hypothesis that the star represented $\gamma + d \rightarrow p + p + \pi^-$. (4) Two particles left the emulsion, neither of which could be identified by the usual methods. As in the preceding cases, we knew the directions of all three particles and thus had three unknown quantities (the energies of the particles and of the photon) and four conservation equations. Three equations served to determine the unknowns, while the fourth equation verified fulfillment of the conservation laws. Different masses were successively assumed for the two particles, after which the ΔP criterion for conservation was checked. If the criterion was satisfied, then, as in the preceding case, the hypothesis concerning the nature of the particles was correct and the star represented $\gamma + d \rightarrow p + p + \pi^-$. If $\Delta P > 1$, so that the ΔP criterion was not satisfied, nothing could be said regarding the nature of the particles. It could only be affirmed that the star did not result from the reaction under investigation. The number of $\gamma + d \rightarrow p + p + \pi^-$ stars that were identified only by means of the conservation laws, comprised 8% of the instances of this reaction.

As an additional check of the correctness of pion identification in the $\gamma + d \rightarrow p + p + \pi^-$ reaction by the third and fourth methods described above, stars which included pion tracks with small dip angles were subjected to identification by these same methods. The same mesons were then identified by grain density and multiple scattering. Figure 1 shows to what extent these different methods were identical. Here the crosses denote the calibration pions and the circles denote pions in the reaction $\gamma + d \rightarrow p + p + \pi^-$ that were identified through the conservation laws.

For the investigated photon energy range, there were no cases in which all three particles left the

emulsion. This fact, as well as the small percentage of stars with two escaping and unidentified tracks, was favored by the following factors: the irradiation of the plates at a small glancing angle (30°) and the discarding of the lowest 100μ and uppermost 20μ of the impregnated emulsion.

3. EXPERIMENTAL RESULTS

Emulsions loaded with heavy water enabled us to register pions with energies up to 40 Mev. However, in view of the density fluctuations of the grain background, 30 Mev must be regarded as the effective limit. We were thus able to measure the total cross sections in all plates for photons up to 174 Mev. In an area of 2050 cm^2 of scanned emulsion containing deuterium nuclei, we found, in the entire photon spectrum, 720 stars belonging to the photoproduction of negative pions from deuterium. The method described in the preceding section enables us to determine for each instance of $\gamma + d \rightarrow p + p + \pi^-$ the photon energy, the particle energy, the energy of relative motion of the two protons, the direction of emission of the particles with respect to the photon beam, and other characteristics.

The complete results for photons from the threshold to 174 Mev are represented in Fig. 3. Each $\gamma + d \rightarrow p + p + \pi^-$ event is characterized in this diagram by the momentum of relative motion of the two protons $p = \frac{1}{2}|\mathbf{p}_1 - \mathbf{p}_2|$ on the vertical axis and the half-sum of the momenta $q = \frac{1}{2}|\mathbf{p}_1 + \mathbf{p}_2|$ on the horizontal axis. The proton momenta $\mathbf{p}_1$ and $\mathbf{p}_2$ are expressed in units of μc, where μ is the pion rest mass. The curve represents the limiting values of p and q determined by the conservation laws for 174-Mev photons. From similar diagrams for each photon

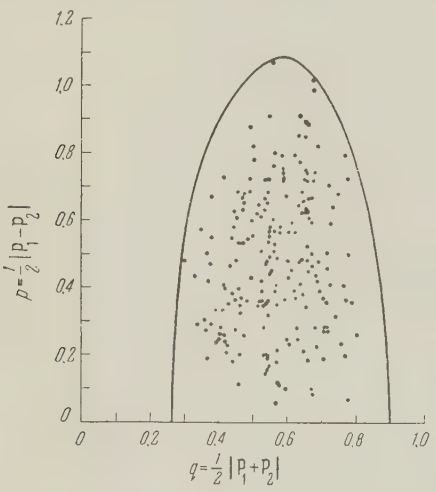

FIG. 3. Distribution of $\gamma + d \rightarrow p + p + \pi^-$ events with respect to p and q.

energy interval we obtain all the characteristics of the $\gamma + d \rightarrow p + p + \pi^-$ reaction, which are discussed below. A few sets of more sensitive plates made it possible to obtain total cross sections for photon energies from 174 to 202 Mev. All of these plates were used to determine the cross sections for the production of pions of less than 30 Mev for the photon range from 174 to 202 Mev. In order to obtain total cross sections for photons from the threshold to 202 Mev, we used 320 instances of pion photoproduction from deuterium.

Figure 4 shows the dependence of the total cross section for pion photoproduction on the photon energy. Schiff's spectrum[7] was used as

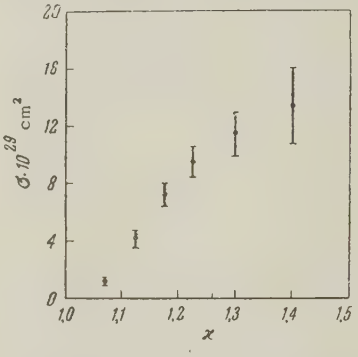

FIG. 4. Dependence of the total cross section for $\gamma + d \rightarrow p + p + \pi^-$ on the photon energy $\varkappa$.

the bremsstrahlung spectrum. The vertical lines represent statistical errors. The photon energy $\varkappa$ is expressed in units of μc^2. Errors in the determination of photon energies result from errors in measurement of the energies of particles that leave the emulsion. The error in the photon energy varies from event to event but is always smaller than the selected photon energy interval.

Figure 5 gives the experimental ratio of the cross section $\sigma_{2.5}$ for $\gamma + d \rightarrow p + p + \pi^-$ with $q/p \geq 2.5$ to the total cross section σ as a func-

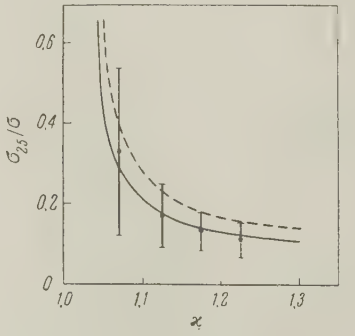

FIG. 5. Dependence of the ratio $\sigma_{2.5}/\sigma$ on the photon energy $\varkappa$.

tion of photon energy. Instances of the reaction with $q/p \geq 2.5$ are in the lower part of the $p-q$ diagram (Fig. 3).

The relative motion of two protons is characterized by the kinetic energy $T = p^2/M$, where

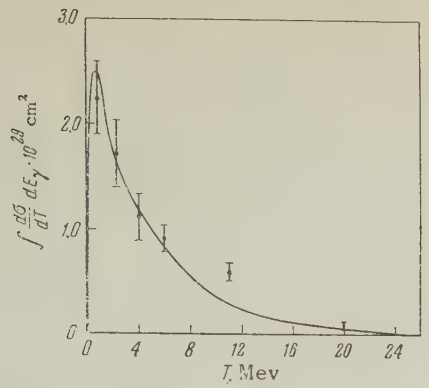

FIG. 6. Energy spectrum of the relative motion of the two protons.

M is the proton mass. Figure 6 shows the energy spectrum of this relative motion. T is plotted on the horizontal axis while the vertical axis gives the integral of $d\sigma/dT$ over the photon spectrum from the threshold to 174 Mev, i.e., $\int (d\sigma/dT)\, dE\gamma$. The error ΔT in the kinetic energy of relative proton motion is determined by the errors in measuring the energy of each proton and the angle between their directions of motion. The errors are smallest for low values of T. The intervals of T were selected to make ΔT smaller than the intervals themselves.

Figure 7 shows the experimental distribution of $\gamma + d \rightarrow p + p + \pi^-$ with respect to the parameter $\epsilon = p - q$ for photons up to 174 Mev. ϵ in-

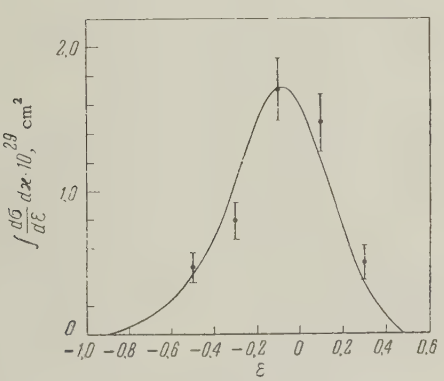

FIG. 7. Spectrum of ε.

directly describes the angle between the two proton directions The parameter ϵ is zero when the angle between the proton tracks is close to 90°; it becomes negative for angles smaller than 90° and positive for angles larger than 90°. The peak of the experimental distribution is on the side of negative values of ϵ, which is evidence that angles smaller than 90° predominate.

The table gives experimental cross sections for $\gamma + d \rightarrow p + p + \pi^-$ with the pion energy lying in the range $5 < E_\pi < 30$ Mev and the relative proton momentum $p < 0.7$. The cross sections, which were determined for all of the plates, are given for the photon energies $\kappa = 1.125$, 1.175, 1.225, and 1.30 in units of μc^2. The statistical errors are also indicated.

4. DISCUSSION OF RESULTS AND COMPARISON WITH THEORY

The p — q diagram of Fig. 3 shows that, for photon energies from the threshold to 174 Mev, reactions with a relative proton momentum below 0.3 comprise 21% of the total. This relative momentum corresponds to 2.0 Mev energy of relative proton motion. From this experimental fact we can derive qualitative information concerning a change of the spin of the nucleon system during the photoproduction of negative pions from deuterium. If the deuteron radius 4.3×10^{-13} cm represents the size of the nucleon system, then, roughly speaking, when the energy of relative proton motion is below 2.5 Mev, a triplet proton spin state is forbidden by the Pauli principle. Our large count of reactions with small relative kinetic energy of the two protons indicates that the spin of the nucleon system is changed during the photoproduction of negative pions. This means that an E1 transition occurs and leads to the production of S-state pions and of protons in the singlet spin state $^1S_0$. A detailed investigation of the final states of the $\gamma + d \rightarrow p + p + \pi^-$ reaction has been performed by one of the present authors and is presented in reference 8.

Let us now consider the influence of the initial nucleon state on the photoproduction of pions. The average distance between the nucleons in the deuteron is large. We can therefore assume that the

Dependence of cross section for meson production ($5 < E_\pi < 30$ Mev, $p < 0.7$) on photon energy κ

κ	1.125	1.175	1.225	1.30
$\sigma \cdot 10^{29}$, cm² (experimental)	2.98±0.50	5.90±0.70	5.91±0.91	3.66±0.52
$\sigma \cdot 10^{29}$, cm² (theoretical)	$4.09\,\lvert K_n\rvert^2 \cdot 10^{-2}$	$7.15\,\lvert K_n\rvert^2 \cdot 10^{-2}$	$7.44\,\lvert K_n\rvert^2 \cdot 10^{-2}$	$4.62\,\lvert K_n\rvert^2 \cdot 10^{-}$

photon interacts with one nucleon while the other nucleon remains in the state of motion which it possessed in the deuteron. This picture of the photon-deuteron interaction in pion production corresponds to the impulse approximation, which employs an initial-state wave function that takes into account the motion of the nucleons in the deuteron. This is usuallly the Hulthen wave function

$$\varphi(r) = \sqrt{7/9\pi}\,[e^{-\alpha r} - e^{-7\alpha r}]/r,$$

where $\alpha = \sqrt{M\epsilon_0/\hbar}$ and ϵ_0 is the deuteron binding energy. The nucleon states following the reaction appear in the final-state wave function.

A quantitative comparison of theory and experiment requires consideration of the particle interaction in the final state of the $\gamma + d \rightarrow p + p + \pi^-$ reaction. An exact calculation of the Coulomb and nuclear interactions of the nucleons in the impulse approximation has been performed by A. M. Baldin,* whose final expression for the photoproduction cross section of pions from deuterium is

$$d\sigma = \{A(p, q)\,|K_n|^2 + B(p, q)\,|L_n|^2\}\,dpdq,$$

where $A(p, q)$ and $B(p, q)$ are complicated functions of the absolute values of the relative proton momentum p and the half-sum q and depend only slightly on the photon energy; $|K_n|^2$ and $|L_n|^2$ are squared matrix elements of the operators in the interaction Hamiltonian $H = K_n\sigma + L_n$ usually used in the impulse approximation. Here σ is the Pauli spin matrix. Baldin kindly placed at our disposal his tables of values of $A(p, q)$ and $B(p, q)$. Integration of $d\sigma$ over p and q gives the total cross section for negative pion photoproduction from deuterium. The integration region for each photon energy is determined by energy and momentum conservation. For example, the integration region for 174-Mev photons is the portion of the plane bounded by the curve and the axis $p = 0$ in the $p - q$ diagram of Fig. 3. To perform the integration it is necessary to know the dependence of the operators K_n and L_n on q and on the pion momentum. In deriving his expression for $d\sigma$, Baldin neglected the dependence of K_n and L_n on the nucleon momentum. For $q < 1$ this is an accurate approximation, but for $q \sim 1$ it can cause an error on the order of 10%.[5] From experimental findings we can reach some conclusion regarding the magnitudes of $|K_n|^2$ and $|L_n|^2$ and their dependence on pion momentum. The analysis in reference 8 of the pion angular distributions and the energy dependence of the total cross section for $\gamma + d \rightarrow p + p + \pi^-$ showed that, close to threshold, the pions are produced in the S state as a result of electric dipole absorption of photons. This indicates that the matrix element of pion photoproduction is independent of pion momentum. It is known[4] that, from spin and parity conservation and from the hypothesis that S-state pions are produced near threshold, the transition matrix has the form $A\sigma e$, which is of the type $K\sigma$. It thus follows from experiment that, first, $|K_n|^2 \gg |L_n|^2$ (if, of course, the impulse approximation is valid) and second, the matrix element can be regarded as independent of pion momentum within the limits of statistical accuracy.

We shall now make a direct comparison of the impulse approximation and experiment. Let us consider the reaction $\gamma + d \rightarrow p + p + \pi^-$ when $q/p \gg 2.5$. In this region $B(p, q) \ll A(p, q)$, which is associated with the fact that $B(p, q)$ does not take into account the interaction of the nucleons in the final state. We shall assume $L_n \neq 0$ and $K_n = 0$. This leads to the following value for the ratio of the integral cross section over the photon spectrum with $q/p \geq 2.5$ to the total pion photoproduction cross section:

$$\int \sigma_{q/p \geqslant 2.5}\,d\varkappa \Big/ \int \sigma\,d\varkappa$$

$$= \iiint\limits_{q/p \geqslant 2.5} B(p, q)\,dp\,dq\,d\varkappa \Big/ \iiint B(p, q)\,dpdqd\varkappa = 0.003.$$

As could be expected, this value disagrees strongly with the experimental result $\int\sigma_{2.5}\,d\kappa/\int\sigma\,d\kappa = 0.146 \pm 0.036$. Thus the assumptions that the nucleons do not interact in the final state and that $K_n = 0$ are invalid. If $|L_n|^2/|K_n|^2$ is small, the ratio of the integral cross sections is 0.145, which is in very good agreement with the experimental result 0.146 ± 0.036. Figure 5 shows the dependence of $\sigma_{2.5}/\sigma$ on the photon energy κ. The solid curve represents the theoretical dependence of this ratio on photon energy. The dashed curve represents the theoretical ratio $\sigma_{2.5}/\sigma$, neglecting the Coulomb interaction of protons in the final state. Both curves were calculated for $L_n = 0$. The figure shows that the experimental points are close to the solid curve but all lie below the dashed curve. It follows that the Coulomb interaction of the protons plays an important part in addition to the nuclear interaction.

For a more detailed comparison of theory and experiment we must know the magnitude of the squared matrix element $|K_n|^2$. In our calcula-

*Presented at the 1957 Conference on Elementary Particle Physics in Venice and Padua.

tions we used $|K_n|^2 = 0.76 \times 10^{-27}$ cm^2, which corresponds to a theoretical value of 1.30[9] for σ^-/σ^+ near the pion photoproduction threshold. Figure 6 compares the theoretical distribution $f(T) = \int \frac{d\sigma}{dT} dE_\gamma$ with the experimental distribution with respect to the kinetic energy T of relative proton motion. Good agreement is shown both in absolute magnitude and in shape up to values of T of the order of 8 to 10 Mev. For higher energies the experimental points are above the theoretical curve; this will be accounted for hereinafter. Figure 7 compares the experimental distribution of $\gamma + d \rightarrow p + p + \pi^-$ with respect to ϵ and the theoretical distribution $\varphi(\epsilon) = \int \frac{d\sigma}{d\epsilon} d\kappa$, where $\epsilon = p - q$. The figure shows that the experimental values are in satisfactory agreement with theory regarding the absolute value and location of the maximum as well as the shape of the distribution, although for positive values of ϵ (large values of p) the experimental points lie somewhat above the theoretical curve. Distributions with respect to T and ϵ were chosen for the comparison with theory because the cross sections show sharpest dependence on these parameters. The lack of a large amount of data makes this very important. The differential cross sections $d\sigma/dT$ and $d\sigma/d\epsilon$ were obtained by numerical integration.

The agreement between experiment and the theoretical curves in Figs. 5 to 7 is evidence of the correctness of the impulse approximation, which takes account of nucleon interaction in the final state. We note that for p and $q \sim 1$ much significance must not be attached to the theoretical results because in this range of values the behavior of the wave function within the range of the nuclear forces is important and corrections that have been neglected in the theory are highly significant. Examples of such corrections are the dependence of K_n on nucleon momentum and the correction for the Coulomb interaction between the pion and protons. This may explain the discrepancy between experiment and theory for large T and positive ϵ, corresponding to $p > 0.7$. For other values of p the experimental distributions are in good agreement with theory. It must be especially emphasized that the impulse approximation furnishes a good description of the experimental results by using the theoretical value $\sigma^-/\sigma^+ = 1.3$ for the negative-to-positive ratio of pion photoproduction.

5. PHOTOPRODUCTION OF NEGATIVE PIONS FROM NEUTRONS

The analysis of experimental results which was given in the preceding section shows that the S matrix of negative pion photoproduction from neutrons is of the form $K\sigma$. The differential cross section for pion photoproduction from free neutrons in the center-of-mass system can, like that for protons,[2] be written as

$$\frac{d\sigma^-}{d\Omega} = \frac{1}{(2\pi)^2} |K_n|^2 \frac{\eta\omega}{(1 + (\nu/M))^2},$$

where η and ω are the momentum and total energy of the pion in the center-of-mass system, ν is the photon energy in the same system, and $\mu = \hbar = c = 1$. The magnitude of $|K_n|^2$ could be determined from the differential cross section $d\sigma = A(p, q)|K_n|^2 dp\, dq$ of negative pion photoproduction in deuterium. Unfortunately, we have insufficient data for the purpose. The squared matrix element $|K_n|^2$ must therefore be determined from the integral cross sections.

The weighted average $|K_n|^2_{av}$ obtained from five values of $|K_n|^2$ for different photon energies κ in the interval from 1.04 to 1.35 is $(0.84 \pm 0.04) \times 10^{-27}$ cm^2. However the integration of the differential cross section $\int d\sigma = |K_n|^2 \iint A(p, q)\, dp\, dq$ over the entire range of variation of p and q that is determined by the conservation laws artificially introduces some uncertainties into the value of $|K_n|^2$, which are ignored in the impulse approximation.

To obtain the most accurate value of $|K_n|^2$, the experimental and calculated cross sections must be compared in the region where the theory has greatest validity, i.e., for values of p and q which permit us to neglect effects that are not taken into account in the theory. The best region of applicability of the impulse approximation, when the Coulomb interaction between the pion and protons is neglected, is given by the conditions p, $q < 1$. The condition $q < 1$ is satisfied by photon energies from threshold ($\kappa_0 = 1.04$) to $\kappa = 1.30$. On the other hand, as we have seen from comparison of the experimental and theoretical distributions with respect to T, experiment and theory are in good agreement for $p < 0.7$. For the photon energies $\kappa = 1.07$ and 1.125, p and q are always smaller than 0.7, while for $\kappa = 1.175$ they are always smaller than 0.8. Therefore the total cross sections for $\gamma + d \rightarrow p + p + \pi^-$ at these energies does not depend essentially on the behavior of the

wave function within the range of nuclear forces. Multiple scattering is also unimportant, since the pion energy does not exceed 30 Mev. But in the photon energy range $\kappa = 1.04$ to 1.35 the total cross section can be affected by a Coulomb interaction between the pion and one of the protons. The Coulomb force between a pion and a proton can be neglected when the pion has energy of at least a few Mev.[4] We have chosen 5 Mev as a reasonable criterion. Then the cross sections for pion photoproduction with $E_\pi > 5$ Mev by photons with $\kappa = 1.125$ and 1.175, together with the cross sections for $p < 0.7$ and $5 < E_\pi < 30$ Mev at $\kappa = 1.225$ and 1.30, will provide a correct value for negative pion photoproduction from free neutrons near threshold. The table contains experimental values of $\gamma + d \rightarrow p + p + \pi^-$ cross sections for $5 < E_\pi < 30$ Mev and relative proton momentum $p < 0.7$.

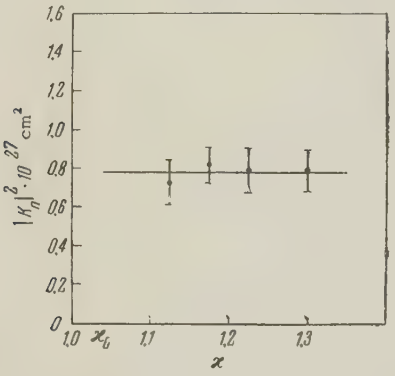

FIG. 8. The squared matrix element of pion photoproduction from neutrons as a function of photon energy.

The second line of the table gives the theoretical values of the same cross sections. Figure 8 represents the squared matrix element $|K_n|^2$ as a function of photon energy κ, the values being taken from the table. The vertical lines denote statistical errors. We see from the figure that within the limits of statistical error the squared matrix element of S-state pion photoproduction from neutrons is constant in the photon energy range from 1.125 to 1.30. The horizontal line represents the average value $|K_n|^2_{av} = (0.785 \pm 0.072) \times 10^{-27}$ cm^2. The integral cross section with respect to photon energy κ for $p < 0.5$ gives $|K_n|^2 = (0.755 \pm 0.081) \times 10^{-27}$ cm^2. The insensitivity of $|K_n|^2$ to p proves that $|K_n|^2$ has been determined accurately.

Thus a detailed investigation of the reaction $\gamma + d \rightarrow p + p + \pi^-$ shows that the squared matrix element of pion photoproduction from neutrons near threshold has the constant value $|K_n|^2 = (0.785 \pm 0.072) \times 10^{-27}$ cm^2. The data given in reference 2, unlike ours, indicate that this squared matrix increases as the threshold is approached. In our experiments $\gamma + d \rightarrow p + p + \pi^-$ was investigated by registering all three particles, whereas the authors of reference 2 registered only a single photon of definite energy out of the entire photon spectrum with a 300-Mev maximum. Since the single-nucleon kinematics, which serves as a basis for interpretation of the data in reference 2, is invalid for the $\gamma + d \rightarrow p + p + \pi^-$ reaction, we question the conclusion reached in that paper that $|K_n|^2$ increases as the threshold is approached.

Our value $|K_n|^2_{av} = (0.785 \pm 0.072) \times 10^{-27}$ cm^2 corresponds to the following value for the cross section ratio for photoproduction of S-state negative and positive pions from free nucleons near threshold:

$$\sigma^-/\sigma^+ = |K_n|^2/|K_p|^2 = 1.34 \pm 0.14.$$

The indicated errors include only the statistical errors of σ^- and σ^+; the value of σ^-/σ^+ depends strongly, of course, on the calibration of the photon beam. We have used the data of reference 2 on positive photomesons from hydrogen, which were obtained with the University of Illinois betatron. A number of effects (photodisintegration of deuterons, proton Compton effect etc), which were measured at both the Illinois betatron and the Lebedev Physics Institute synchrotron, given identical cross sections with 10% statistical accuracy. We can thus assume that the ratio $\sigma^-/\sigma^+ = 1.34 \pm 0.14$ does not contradict field theory.[9] We arrived at this conclusion in the preceding section in comparing the experimental and the theoretical distributions calculated by using the theoretical value $\sigma^-/\sigma^+ = 1.3$.

We are now engaged in measuring the cross section for positive pion photoproduction from hydrogen in order to obtain a more certain value of σ^-/σ^+.

In conclusion we wish to thank Professor V. I. Veksler for valuable suggestions and his continued interest, and A. M. Baldin for the use of his tables of functions and for a discussion of the results.

[1] Beneventano, Carlson-Lee, Stoppini, Bernardini, and Goldwasser, Nuovo cimento **12**, 156 (1954).

[2] Beneventano, Bernardini, Carlson-Lee, Stoppini, and Tau, Nuovo cimento **4**, 323 (1956).

[3] Sands, Teasdale, and Walker, Phys. Rev. **95**, 592 (1954).

[4] K. M. Watson, Phys. Rev. **95**, 228 (1954).

[5] A. M. Baldin, Proc. CERN Symposium, Geneva, **2**, 272 (1956).

[6] Adamovich, Veksler, Kuz'micheva, Larionova,

and Kharlamov, Proc. CERN Symposium, Geneva, **2**, 265 (1956).

[7] L. I. Schiff, Phys. Rev. **83**, 252 (1951).

[8] M. I. Adamovich, J. Exptl. Theoret. Phys. (U.S.S.R.) **35**, 39 (1958), JETP **8**, 29 (1959).

[9] Chew, Goldberger, Low, and Nambu, Phys. Rev. **106**, 1345 (1957).

Translated by I. Emin
3

SOVIET PHYSICS JETP VOLUME 35 (8), NUMBER 1 JANUARY, 1959

AN INVESTIGATION OF THE FINAL STATES IN THE PHOTOPRODUCTION OF NEGATIVE π MESONS ON DEUTERIUM

M. I. ADAMOVICH

P. N. Lebedev Physics Institute, Academy of Sciences, U.S.S.R.

Submitted to JETP editor February 10, 1958

J. Exptl. Theoret. Phys. (U.S.S.R.) **35**, 39-44 (July, 1958)

Photographic emulsions were used to study the $\gamma + d \rightarrow p + p + \pi^-$ reaction, giving the angular distributions and energy spectra of the mesons and the relative motion of the two protons close to the meson photoproduction threshold. Analysis shows that there is an electric dipole transition taking place, causing the spin of the nucleon system to change and the meson to be produced in the S state. The shape of the spectra and the energy dependence of the cross section are explained by the interaction of the nucleons in the final state.

1. INTRODUCTION

A detailed investigation of the photoproduction of negative π mesons on deuterium can be used to obtain information both on the elementary process of meson photoproduction on neutrons,[1] and on the process of meson production on the simplest nucleon system. In this two-nucleon system it is easy to study the effects of nuclear binding, the Pauli exclusion principle, and the Coulomb and nuclear interactions of the particles in the final state on the photoproduction of mesons. Such an investigation should be performed at photon energies up to 200 Mev, since at these energies the influence of multiple scattering of the meson is negligible. In this way we can investigate how the final state of the particles influences the properties of the meson production process and establish some of the properties of negative π-meson production on deuterium. A detailed investigation of this process gives information on the role of the spin interaction in photoproduction close to threshold.

The $\gamma + d \rightarrow p + p + \pi^-$ reaction was studied in nuclear emulsions containing deuterium. The emulsions were placed in the photon beam (maximum energy 250 Mev) of the synchrotron of the Academy of Sciences Physics Institute. The experimental procedure is described elsewhere.[1] The data were obtained for the photon energy range between threshold and 174 Mev. Figure 1 shows the angular distributions of the π mesons in the center-of-mass (c.m.) coordinate system for photons with energies of 153 to 167 and 167 to 174 Mev. The vertical line segments indicate the statistical uncertainties. Within the limits of statistical uncertainty, the angular distributions are isotropic.

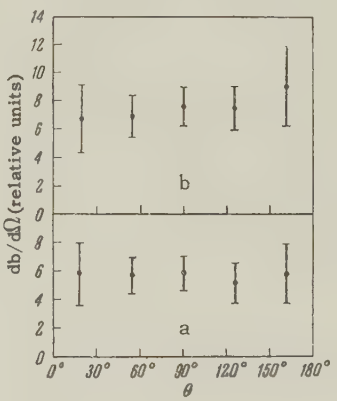

FIG. 1. Angular distribution of π mesons in the c.m. system for photon energies (a) 153 to 167 Mev, and (b) 167 to 174 Mev.

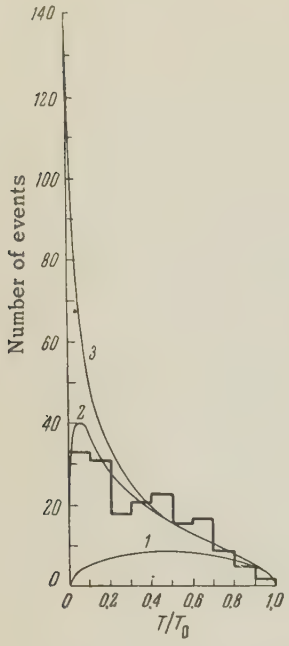

FIG. 2. The energy spectrum of relative motion of the two protons.

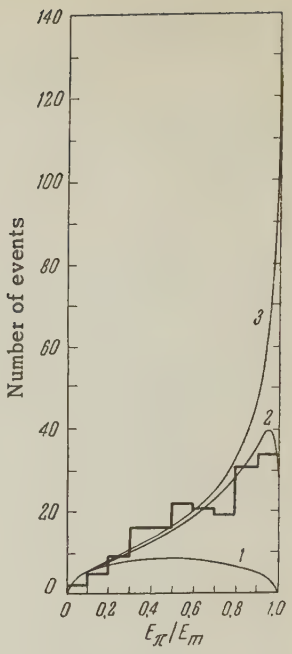

FIG. 3. The energy spectrum of the π mesons in the c.m. system.

Figure 2 shows a histogram of the kinetic energy of relative motion of the two protons in the 153 to 174 Mev interval. The abscissa is measured in units of T/T_0, where T_0 is the maximum possible energy of relative motion and is equal to the sum of the energies of all three particles in the c.m. system.

Figure 3 shows a histogram of the π-meson energy spectrum in the same photon-energy interval, in the c.m. system. The abscissa is measured in units of E_π/E_m, where E_m is the maximum possible kinetic energy of the π meson, which, in the nonrelativistic approximation, is $E_m = 2MT_0/(2M + \mu)$, where μ and M are the meson and proton masses, respectively.

2. ANALYSIS OF THE MESON ANGULAR DISTRIBUTIONS

For photon energies up to 174 Mev, the energy of relative motion of the two protons in the final state is always less than 25 Mev and tends to be small because the mesons carry away most of the momentum. Since the nucleons in deuterium are located far from each other, the protons emitted as a result of π-meson photoproduction can have large orbital angular momenta in spite of their relatively low energy. The protons may therefore be in final S, P, D, F, or higher angular-momentum states. In the photon energy range studied, the π-meson momentum in the c.m. system is always less than 0.62 (we express the momentum η in units of μc). If we assume the meson-nucleon interaction radius to be finite and of order of magnitude $\hbar/\mu c$, then in the c.m. system the π mesons will be in S and P states.

The table gives all the dipole transitions as a result of which the π mesons are produced in the S state, and some dipole transitions which lead to π mesons in the P state. The same table gives the total angular momentum and parity of the system in the intermediate state. The relative intensities to different final states for the transitions indicated in the tables depend both on the electromagnetic structure of the system and on the type of interaction which leads to meson production. For instance, one of the factors giving rise to the E1 ($^1S_0$, S) transition is the nucleon-spin dependence of the interaction leading to meson photoproduction (the first symbol in the brackets denotes the state of the protons, and the second the meson state). This transition

Electromagnetic transition	Intermediate state	Dependence of cross section on maximum meson momentum	Meson angular distribution
$E1\ (^1S_0, S)$	0^-	η_m^2	const
$E1\ (^3D_2, S)$	2^-	η_m^4	const
$M1\ (^3P_0, S)$	0^+	η_m^4	const
$M1\ (^3P_1, S)$	1^+	η_m^4	const
$M1\ (^3P_2, S)$	2^+	η_m^4	const
$M1\ (^3F_2, S)$	2^+	η_m^4	const
$E1\ (^3P_0, P)$	1^-	η_m^6	$1 + \cos^2\theta$
$E1\ (^3P_1, P)$	1^-	η_m^6	$3 - \cos^2\theta$
$M1\ (^1S_0, P)$	1^+	η_m^4	$1 + \cos^2\theta$
$M1\ (^3D_2, P)$	1^+	η_m^6	$13 + \cos^2\theta$

must involve a spin change in the nucleon system, which is possible only if the interaction Hamiltonian contains a term depending on the nucleon spin.

An attempt was made to discover which transitions actually take place by analyzing the angular distributions of the mesons. To do this, we calculated the angular distributions of the electromagnetic dipole transitions shown in the table, using the formula obtained by Morita and others[2] for the differential cross section of photonuclear reactions; this formula is found from quite general premises concerning the addition of angular momenta and parity conservation. Schematically, our reaction can be represented in the form

$$\text{photon + deuteron} \rightarrow \text{intermediate state} \rightarrow \text{nucleon system + meson}$$

We treat the nucleon system as the final nucleus, which contains the angular momentum of the system. The theoretical meson angular distributions for the dipole transitions are shown in the table. Mesons produced in the S state have isotropic angular distributions for all dipole transitions. From these calculations it follows also that transitions with the same proton states will interfere. For instance, the angular distribution of π mesons for the E1 ($^1S_0$, S) and M1 ($^1S_0$, P) transitions and their interference is of the form

$$d\sigma/d\Omega \sim |a|^2 - (3\sqrt{2}/2)(a^*b + ab^*)\cos\theta + {}^9/_4 |b|^2 (1 + \cos^2\theta),$$

where a and b are the amplitudes of these two transitions.

The fact that the experimental π-meson angular distributions are isotropic in the c.m. system indicates that in the photon energy interval between 153 and 174 Mev the transitions involve mostly meson production in the S state. Our analysis of the angular distributions of the π mesons cannot be used to choose any particular one of the transitions shown in the table.

3. ANALYSIS OF THE ENERGY SPECTRA

A finite meson-nucleon interaction radius implies[3] that at low meson energies the transition amplitude depends on the meson momentum as η^l, where l is the orbital angular momentum of the meson. The energy dependence of the cross section of the $\gamma + d \rightarrow p + p + \pi^-$ reaction is determined not only by that of the matrix element and the density of final meson states, but also by the density of the final states for the pair of nucleons, as well as by their interaction.

Let the total kinetic energy of the particles in the c.m. system after the reaction be T_0. This energy is divided between the π meson and both protons in such a way that the vector sum of the three momenta vanishes. The π mesons therefore have a continuous energy spectrum extending from zero to the maximum energy E_m, corresponding to a continuous kinetic energy spectrum for the relative motion of the two protons from T_0 to zero. When the π meson is produced in the S state and the particles do not interact, the shapes of these spectra are uniquely determined by the density of final states, and can be written

$$\frac{d\sigma}{dT} = A\sqrt{\frac{T}{T_0}}\sqrt{1-\frac{T}{T_0}}; \qquad \frac{d\sigma}{dE_\pi} = B\sqrt{1-\frac{E_\pi}{E_m}}\sqrt{\frac{E_\pi}{E_m}} \tag{1}$$

for the relative motion of the protons and for the mesons, respectively. In this equation A and B are normalizing constants. In Figs. 2 and 3 these spectra are indicated by the curves labeled 1. It is seen that the experimental spectrum is heavier in the region of low kinetic energy of relative motion of the two protons. One might expect that as a result of the attraction of the nucleons the energy spectra would have maxima in the neighborhood of E_m for the mesons and $T = 0$ for the protons.

Watson[4] has given a consistent theory of the effect of interaction between the particles in the final state. He showed that independent of the type of primary process, the forces of nuclear attraction not only increase the cross section, but also change the shape of the spectrum. The new expressions for the spectra given in Eq. (1) then become

$$\frac{d\sigma}{dT} = A\frac{\left[\frac{T}{T_0}\left(1-\frac{T}{T_0}\right)\right]^{1/2}}{[(\alpha^2/MT_0)+(T/T_0)]}; \qquad \frac{d\sigma}{dE_\pi} = B\frac{\left[\left(1-\frac{E_\pi}{E_m}\right)\frac{E_\pi}{E_m}\right]^{1/2}}{\{[2\alpha^2/(2M+\mu)E_m]+1-(E_\pi/E_m)\}}, \tag{2}$$

where α is the reciprocal of a, the nucleon-nucleon scattering length. The numerators of these expressions are proportional to the final-state densities of the three particles. The final-state interaction between the nucleons determines the denominators. Strictly speaking, the shape of the spectra given by (2) is correct only for relative proton momenta p for which $\hbar/p > r_0$, where r_0 is the range of the primary interaction. Since we have assumed from the start that $r_0 \sim \hbar/\mu c$,

Eqs. (2) are valid for small T/T_0 up to about 0.3 or 0.4. For large values of T/T_0 (greater, say, than 0.7), however, the interaction does not contribute strongly and Eqs. (2) automatically become (1). Since it is not particularly important in what follows to know the shape of the spectra for T/T_0 values lying between 0.4 and 0.7, we shall assume that Eqs. (2) are valid over the whole range of this variable. Curves 2 on Figs. 2 and 3 give the spectra according to this equation, where we have set $a = 7.7 \times 10^{-13}$ cm, as obtained by Jackson and Blatt from experiments on proton-proton scattering in the singlet $^1S_0$ state. The value of T_0 was obtained by averaging experimental results in our photon energy range. Curves 2 are normalized to the experimental spectra. The normalizing coefficients A and B found in this way are also used in normalizing other spectra (curves 1 and 3). Curves 3 on the figures are the spectra given by Eq. (2) if the scattering length of the singlet state is taken as $a = -2.43 \times 10^{-12}$ cm, obtained from experiments on neutron scattering by protons.

It is seen from the graphs that curves 2 are in good agreement with experiment. This means that the nuclear interaction between the protons in the $^1S_0$ state plays an important role in the $\gamma + d \to p + p + \pi^-$ reaction. The only transition which leads to the S state for the meson and the $^1S_0$ state for the protons is E1 ($^1S_0$, S). Therefore among the different possible transitions with photon energies up to 174 Mev, the controlling one is electric dipole absorption of the photons with formation of an S state meson and with a spin change in the nucleon system.

In addition to the nuclear interaction, there is a Coulomb interaction between the protons in the final state of this reaction. Comparison of curves 2 and 3 on Figs. 2 and 3 can be used to estimate the effect due to this Coulomb interaction. Estimating this effect on the principle of charge independence of nuclear forces, we see that the maximum in the $\gamma + d \to p + p + \pi^-$ reaction is much lower than that in the $\gamma + d \to n + n + \pi^+$ reaction.

4. ANALYSIS OF THE ENERGY DEPENDENCE OF THE TOTAL CROSS SECTION

How the total cross section depends on the maximum possible π-meson energy can be found by integrating the meson energy spectra. It is more convenient to express this dependence in terms of the square of the maximum π-meson momentum in the c.m. system. The maximum possible momentum η_m is uniquely related to the photon energy κ in the laboratory coordinate system. Integration of the spectra given by (1) indicates a relation of the form $\sigma \sim \eta_m^4$. According to Eq. (2) the total cross section is proportional to η_m^2. Thus the total cross section for the photoproduction of π mesons in the S state is proportional to η_m^2 for the E1 ($^1S_0$, S) transition, and proportional to η_m^4 for all the other dipole transitions. It can be shown similarly that the total cross section is proportional to η_m^4 for the M1 ($^1S_0$, P) transition, and to η_m^6 for all the other dipole transitions into the meson P state. The dependence of the total cross section on the maximum possible π-meson momentum for each transition is given in the third column of the table.

The total cross section for production of π-mesons in the S state should be related by an expression of the form $\sigma = (b\eta_m^2 + d\eta_m^4)/\nu$ to the maximum meson momentum, where b and d are constants, and ν is the photon momentum in the c.m. system in units of μc. The intermediate powers of η_m do not appear, since the interference terms do not contribute to the total cross section. The ν-dependence is taken from meson theory.[3] At energies sufficiently close to threshold, the ν-dependence is not important. Figure 4

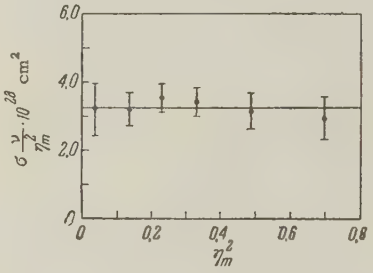

FIG. 4. The dependence of $\sigma\nu/\eta_m^2$ on the square of the maximum π-meson momentum.

gives $\sigma\nu/\eta_m^2$ as a function of η_m^2 for the photon energy interval from threshold to 202 Mev. The total cross sections for the $\gamma + d \to p + p + \pi^-$ reaction are taken from Adamovich et al.[1] The horizontal line through the experimental points on the graph gives $b = (3.25 \pm 0.22) \times 10^{-28}$ cm^2, and $d = 0$ within the limits of experimental error. At the meson photoproduction threshold, where the dependence on the photon energy is not important, the total cross section of this reaction is $\sigma = (3.25 \pm 0.22) \times 10^{-28} \eta_m^2$ cm^2. The proportionality between the cross section and η_m^2 is an indication that the reaction is caused primarily by the electric dipole E1 ($^1S_0$, S) transition. This, in turn, means that the interaction Hamiltonian describing the photoproduction of negative π mesons close to threshold depends on the spin variable of the nucleon. It follows from this that, in terms of the phenomenological impulse approxi-

mation theory, the interaction Hamiltonian is of the form $H = K\sigma$, where K is the transition operator, and σ is the Pauli spin matrix. In addition, the results presented in the last two sections show that the matrix element for the photoproduction of negative mesons on deuterium neutrons close to threshold is independent of the meson momentum. This last conclusion is in agreement with our previous results[1] obtained by a detailed comparison of experiment and the theory of the impulse approximation.

In conclusion, the author expresses his gratitude to Professor V. I. Veksler for his interest and for valuable advice, as well as to A. M. Baldin and V. N. Maikov for participating in discussions of the results.

[1] Adamovich, Kuz'micheva, Larionova, and Kharlamov, J. Exptl. Theoret. Phys. (U.S.S.R.) **35**, 27 (1958) JETP **8**, 21 (1959).

[2] Morita, Sugie, and Yoshida, Progr. Theoret. Phys., Japan, **12**, 713 (1954).

[3] M. Gell-Mann and K. M. Watson, Annual Review Nuclear Science (Annual Reviews, Inc., Stanford, 1954), Vol, 4, p. 238.

[4] K. M. Watson, Phys. Rev. **88**, 1163 (1952).

[5] J. D. Jackson and J. H. Blatt, Revs. Mod. Phys. **22**, 77 (1950).

Translated by E. J. Saletan
4

SOVIET PHYSICS JETP VOLUME 35 (8), NUMBER 1 JANUARY, 1959

OBSERVATIONS OF THE PINCH EFFECT AT DECREASING CURRENTS

V. P. GRANOVSKII, K. P. RIUMINA, V. I. SAVOSKIN, and G. G. TIMOFEEVA

All-Union Electrotechnic Institute

Submitted to JETP editor February 12, 1958

J. Exptl. Theoret. Phys. (U.S.S.R.) **35**, 45-49 (July, 1958)

Image-converter photographs have been taken of transient states of pulsed discharges in H_2 and Hg at pressures of 10^{-2} to 10^{-3} mm Hg. The peak pulse currents were 1.3 to 5.5 kiloamperes and the pulses were 300 μsec long. Electrodynamic deformations (contraction and kinking) are observed at negative values of di/dt. It is found that these deformation effects first disappear (as manifested by the straightening and expansion of the column) at points of high local gas density (anode or cathode, depending on the experimental conditions).

THE contraction of a high-current discharge due to its own magnetic field (pinch effect) has been observed by a number of investigators.[1-5] In some of these investigations, contraction of the column has been observed only at increasing currents.[4]

1. We have carried out a systematic investigation of pinches at increasing and decreasing currents in cylindrical tubes (internal diameter 10 and 32 mm) filled with hydrogen or mercury vapor at pressures of 10^{-2} to 10^{-3} mm Hg. The current pulses were approximately 300 μsec long with peak values i_p = 1.3 to 5.5 kiloamperes; these currents were obtained by discharging a 300-μf capacitor charged at 1 to 3 kv. Before the experiments the tubes and the electrodes were conditioned by operation at high pulsed currents (5 to 6 kiloamperes) for several hours, either with frequent replacement of the filler gas or with continuous pumping (if Hg vapor was used).

Pictures of the discharge were obtained with an image converter (IC)* operating as a high-speed one-shot shutter. Because of the low intensity, the exposure time could not be reduced below 1.5 μsec, although special film and exposure procedures were used. Simultaneous oscillograms were taken of the tube current i and the shutter gating pulse V_g, using a two-beam high-voltage oscilloscope. The particular stage of the discharge at which the photograph was taken was determined by the position of the gating pulse with respect to the initiation of current flow in the discharge.

*The tube used in the present work was the PIM-3 image converter developed by M. M. Butslov.

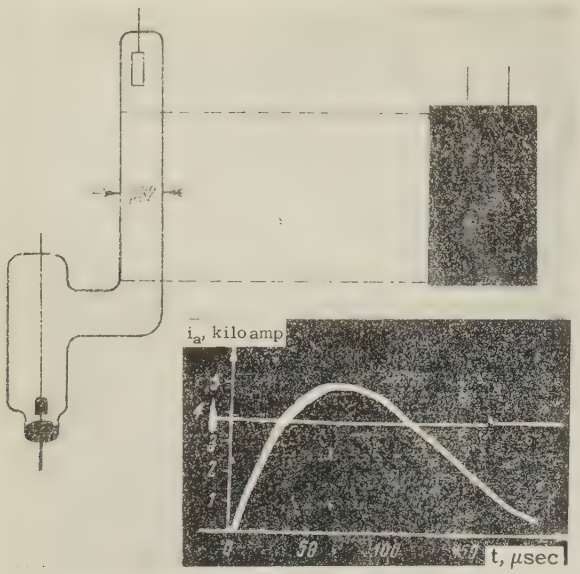

FIG. 1. Photograph of a discharge column in mercury vapor at a pressure $p = 0.3\mu$ Hg. The cooling temperature of the cathode $-15°C$, the exposure is 1.5μ sec. To the left there is a sketch of the tube, above which are shown the oscillograms for i_p and V_g. The lines above the photograph denote the walls of the tube.

Hereinafter the time between the initiation of current flow and the time at which the photograph is taken will be called the photo-delay time t_{ph} while the discharge current at the time the photograph is taken will be called the photo current i_{ph}.

Many photographs of the discharge were obtained under different current-flow conditions. It is apparent from these photographs that contraction of the column can occur at positive, zero, and negative values of di/dt. As an example, Fig. 1 shows a photograph of a discharge in mercury vapor together with the i and V_g oscillograms for a special tube for which the following parameters apply: working diameter 32 mm, mercury condensation temperature $T_c = -15°C$, peak current $i_p = 5.5$ kiloamperes, photo-delay time $t_{ph} = 160$ μ sec (i.e., exposure 80μ sec after the current reaches its maximum), and photo current $i_{ph} = 1.3$ kiloamperes. It will be noted that contraction of the column is observed even at long photo-delay times ($t_{ph} > t_p$).

In Fig. 2 are shown two series of photographs of discharges in a narrow hydrogen-filled tube (i.d. 10 mm) with solid electrodes at two pressures, $p = 2\mu$ Hg and $p = 10\mu$ Hg. The peak currents are approximately the same in both series of photographs. The arrows on the current oscillogram below the photographs indicate the time at which the photographs were taken. It is apparent that the discharge remains contracted at negative values of di/dt. On the other hand, an incipient change in the shape of the discharge is observed at the anode: first the kinking disappears and then expansion is observed. The higher the pressure of the filler gas, the greater the fraction of the column in which expansion has occurred at a given photo-delay time. The same effects are observed in a tube of the same diameter filled with mercury vapor. In wider tubes (32 mm), no expansion of the contracted column in the region of the cathode is observed under the same conditions.

In straight tubes 32 mm in diameter, with a liquid mercury cathode which is not separated from the working section of the tube by shields, the straightening and expansion of the contracted

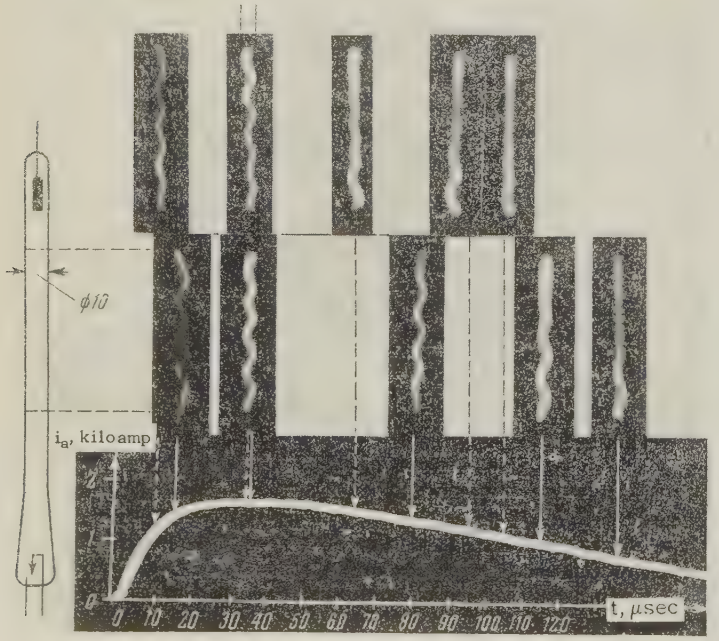

FIG. 2. Instantaneous photograph of the discharge column in hydrogen at $p = 10\mu$ HG (upper series) and $p = 2\mu$ Hg (lower series). The exposure is 1.5μ sec. To the left we have a sketch of the tube, above is the current oscillogram; the solid arrows denote the instant of $p = 2\mu$ Hg, the dotted arrows denote the instant of exposure at $p = 10\mu$ Hg.

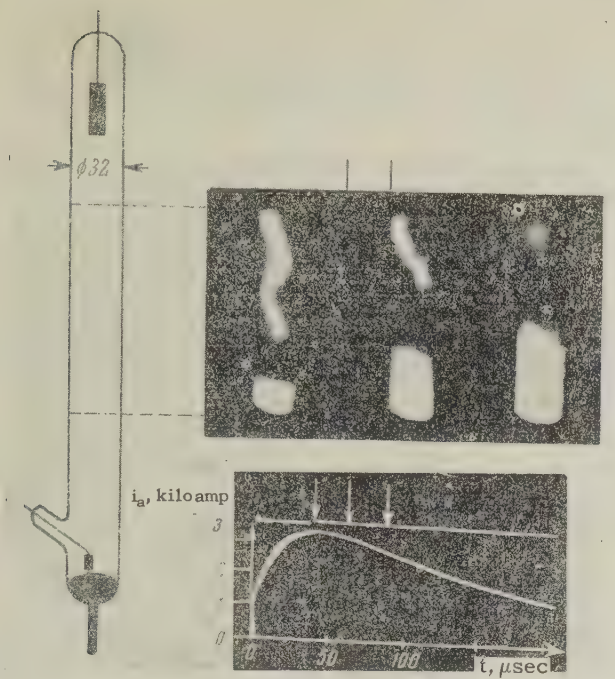

FIG. 3. Instantaneous photographs of the discharge column in mercury vapor at an intial pressure p = 1μ Hg. The exposure is 1.5 μsec. To the left is a sketch of the tube, above we have the oscillogram; the arrows indicate the time at which the exposure is made.

column starts at the cathode end. This effect is illustrated by the photographs and accompanying oscillograms shown in Fig. 3. These pictures show that longer values of the photo-delay time are to be associated with more uniform illumination of the cathode. However, if the working part of the tube consists of an inclined anode section joined to the cathode part, which is well cooled, (to prevent penetration of the mercury vapor from the cathode into the working part of the tube), no expansion of the column at the cathode is observed in the course of time (cf. Fig. 1). This effect is also absent when solid cathodes are used.

2. It is apparent from the results obtained that the electrodynamic contraction and expansion of the discharge column are not a function of the sign of the current derivative, but only the ratio of instantaneous current to mean gas density in a given section of the tube at a given instant of time. At high currents, a higher gas density (averaged over the cross section) is to be associated with earlier straightening and expansion of the column, i.e., the interval between the time at which the current reaches its peak and the time at which the deformation effects disappear becomes smaller (cf. Figs. 2 and 3). Apparently the pinch vanishes first in the anode region in narrow tubes because this is a point of high gas density. The localized density increase results from the transport of the single type of gas molecules to the anode by virtue of electron collisions; this phenomenon is of greater importance in narrow discharge tubes (cf. for example, reference 6). The expansion of the contracted column at the cathode in tubes with mercury cathodes is explained reasonably by the increase in the vapor density in the cathode region because of evaporation from the cathode. This interpretation is supported by observations made with a bent tube, in which the vapor from the cathode could not reach the working part of the tube; in this case no expansion of the contracted column was observed at the cathode.

These photographs can be used to estimate the velocity of propagation of vapor from the cathode by measuring the distance from the cathode at which expansion of the column occurs on photographs taken at different delay times t_{ph}. In the last column of the table we present data obtained by this means on the velocity of propagation of mercury vapor from the cathode in a tube with an internal diameter of 32 mm at peak currents i_p = 2.8 and 3.2 kiloamperes and an initial pressure p = 1μ Hg. The data in the table indicate that the displacement velocity of the gas increases with time. This increase is apparently a consequence of the heating of the vapor by the current which passes through it. A rough estimate indicates that the gas temperature reaches values of the order of 10^4 °K.

3. Image-converter observations of discharges in tubes with internal diameters of 10 and 32 mm filled with hydrogen or mercury vapor at a pressure of 10^{-2} to 10^{-3} mm Hg and currents of 1.3 to 5.5 kiloamperes lead to the following conclusions.

(a) The electrodynamic deformations of the mercury column (contraction and kinking) depend on the ratio of the instantaneous current to the mean gas density at a given instant of time and not on the sign of the current derivative.

(b) A changeover from contraction and kinking to expansion and straightening occurs first at points of high local gas density. This changeover

i_a, kiloamp	t_{photos}, μsec	v, cm/sec
2.8	40 55	$4 \cdot 10^4$
2.8	40 70	$12 \cdot 10^4$
3.2	35 42	$2.8 \cdot 10^4$
3.2	35 60	$8 \cdot 10^4$
3.2	42 60	$10 \cdot 10^4$

can occur under the following conditions: (1) in narrow tubes — at the anode, as a consequence of the transport of gas to the anode under the influence of electron collisions; (2) in wide tubes with mercury cathodes — at the cathode, as a consequence of cathode evaporation; (3) in cases of extended contact of the pinch with the walls of the tube — at points of contact, as a consequence of the evolution of absorbed gases from the walls. The last case would seem to explain the effect observed in reference 4.

[1] S. W. Cousins and A. A. Ware, Proc. Phys. Soc. **64B**, 159 (1951).

[2] J. E. Allen and J. D. Craggs, Brit. Journ. App. Phys. **5**, 446 (1954).

[3] V. L. Granovskii and G. G. Tiomfeeva, J. Exptl. Theoret. Phys. (U.S.S.R.) **28**, 378 (1955) and **30**, 477 (1956), Soviet Phys. JETP **1**, 381 (1955) and **3**, 437 (1956).

[4] Artsimovich et al., Атомная энергия (Atomic Energy) **3**, 76 (1955).

[5] R. Carruthers and P. A. Davenport, Proc. Phys. Soc. (London) **70B**, 49 (1957).

[6] A. Ruttenauer, Z. Physik **10**, 69 (1923); I. M. Druyvesteyn, Physica **2**, 255 (1935); B. N. Kliarfeld' and I. A. Poletaev, Dokl. Akad. Nauk SSSR **23**, 460 (1939).

Translated by H. Lashinsky
5

SOVIET PHYSICS JETP VOLUME 35 (8), NUMBER 1 JANUARY, 1959

PARAMAGNETIC RESONANCE OF FREE RADICALS IN WEAK FIELDS

A. K. CHIRKOV and A. A. KOKIN

Ural Polytechnic Institute

Submitted to JETP editor February 19, 1958

J. Exptl. Theoret. Phys. (U.S.S.R.) **35**, 50-55 (July, 1958)

The line shape and line width for paramagnetic absorption in crystalline α,α-diphenyl β-picryl hydrazyl (dpph) have been investigated at weak fields at room temperature. It is found that the line shape is Lorentzian near the maximum. An estimate of the half-width is found to be in good agreement with theory.[1] Asymptotic Curie points are computed for a number of new radicals.

1. In the absence of hyperfine-structure splitting, the paramagnetic resonance absorption line shape in weak fields is determined essentially by molecular interactions in the paramagnetic system.

The effect of the dipole-dipole interaction on the absorption line shape has been investigated by Waller,[2] Broer,[3] and Van Vleck.[4] The latter characterized the line shape by its moments. The second moment is affected mainly by the central portion of the absorption curve. Higher moments are affected chiefly by the nature of the absorption curve far from the maximum, where the experimental errors are particularly large. Hence a comparison of the experimental and theoretical values of the higher moments can be made only on a qualitative basis.

The nature of the interaction can be ascertained from the central part of the absorption curve. An equation for the absorption curve in the region of the maximum, which takes into account the magnetic dipole-dipole interaction and the Coulomb exchange interaction, has been obtained by Anderson and Weiss[5] who showed that in the case of a strong exchange interaction the curve has a Lorentzian shape with a half-width given by a phenomenological constant.

A more complete quantum-mechanical analysis of the line shape has been developed by Kubo and Tomita;[1] in this treatment it is shown that the absorbed energy, as a function of frequency in the region of the absorption maximum, is proportional to the Fourier component of the function $G(t)$ if the radio-frequency magnetic field is linearly polarized. Hence the characteristics of the line are

given by the function:

$$I(\omega) = \frac{1}{2\pi} \int_{-\infty}^{+\infty} G(t) \exp(-i\omega t)\, dt. \qquad (1)$$

In cases of practical importance ($\hbar\omega \ll kT$), G(t) is determined by the symmetric correlation relation

$$G(t) = \langle \hat{M}_x(t)\, \hat{M}_x + \hat{M}_x\, \hat{M}_x(t) \rangle / 2\, \langle M_x^2 \rangle, \qquad (2)$$

where $\hat{M}_X(t)$ is the magnetization operator in the Heisenberg representation:

$$\hat{M}_x(t) = \exp(it\hat{\mathcal{H}}/\hbar)\, \hat{M}_x \exp(-it\hat{\mathcal{H}}/\hbar),$$

and $\hat{\mathcal{H}}$ is the Hamiltonian of the system in the absence of the variable field. When averages are taken in Eq. (2), the density matrix becomes a constant.

The function G(t) is calculated by a perturbation method. If the total Hamiltonian for the system, $\hat{\mathcal{H}}$, can be divided into an unperturbed part $\hat{\mathcal{H}}_0$ for which $\hat{M}_X^0(t)$ can be found easily, and the perturbation $\hat{\mathcal{H}}'$

$$\hat{\mathcal{H}} = \hat{\mathcal{H}}_0 + \hat{\mathcal{H}}', \qquad (3)$$

G(t) can be written as an expansion in terms of the small parameter which characterizes the perturbation:

$$G(t) = G_0(t) + G_1(t) + G_2(t) + \ldots \qquad (4)$$

2. The sample chosen to investigate resonance absorption was the relatively well-studied stable radical dpph [$(C_6H_5)_2N - NC_6H_2(NO_2)_3$]. The magnetic susceptibility of a radical is determined by the spin of the unpaired electron in the molecule ($g = 2.0036 + 0.0002$, cf. reference 6), and follows the Curie-Weiss law with a negative asymptotic Curie point $\Theta = -10°K$.[7] From the antiferromagnetic properties of the radical it may be assumed that there is a strong exchange interaction. In this case the unperturbed Hamiltonian $\hat{\mathcal{H}}_0$ can be given as a sum of two terms $\hat{\mathcal{H}}_1 + \hat{\mathcal{H}}_2$ where

$$\hat{\mathcal{H}}_1 = \hbar\omega_0 \sum_j \hat{s}_{jz} \quad (\hbar\omega_0 = g\mu_0 H_0) \qquad (5)$$

corresponds to the Zeeman energy in the external magnetic field H_0 while

$$\hat{\mathcal{H}}_2 = -2 \sum_{i<j} A\ (r_{ij})\, (\hat{s}_j \hat{s}_i) \qquad (6)$$

is the Coulomb exchange interaction.

If it is assumed that the perturbation is the magnetic dipole-dipole interaction and that the exchange of energy between the spin system and the lattice can be neglected, in the weak-field case a Lorentzian curve is obtained close to the maximum (cf. Appendix):

$$I(\omega) = \frac{1}{2\pi} \frac{\Delta\omega}{(\omega - \omega_0)^2 + \Delta\omega^2} \qquad (7)$$

with half-width

$$\Delta\omega = 4.18\omega_{10}^2/\omega_{20}. \qquad (8)$$

For a polycrystalline sample with a simple cubic lattice structure (constant d) and $s = 1/2$

$$\omega_{10}^2 = 3.79 g^4 \mu_0^4 \hbar^{-2} d^{-6}; \qquad (9)$$

$$\omega_{20} = 3.65\,|A|/\hbar, \qquad (10)$$

where the exchange integral A is expressed in terms of Θ and the number of nearest neighbors z:

$$A = k\Theta/2z = k\Theta/12. \qquad (11)$$

Using Eqs. (8) to (11), we can estimate the half-width of the absorption curve which, in the present case, depends on both the dipole-dipole interaction (ω_{10}) and the exchange interaction (ω_{20}).

Thus the role of exchange interactions can be explained by an analysis of the shape of the experimental absorption curve close to the maximum.

3. The shape of the resonance absorption line in dpph was determined by the oscillator reaction method.[8] A block diagram of the system is shown in Fig. 1.

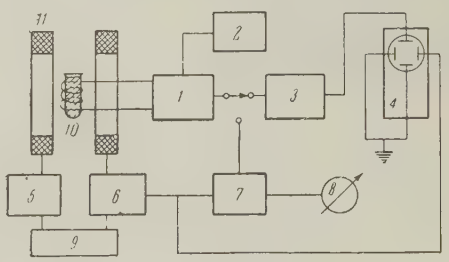

FIG. 1. Block diagram of the system. 1 – oscillator, 2 – heterodyne frequency meter, 3 – broadband amplifier, 4 – oscilloscope, 5 – balanced current-measuring circuit, 6 – modulation source, 7 – narrow-band amplifier, 8 – recorder, 9 – power supply, 10 – sample, 11 – Helmholtz coil.

The sample, containing 250 mg of dpph powder, was placed in the tank circuit of a capacitance-feedback oscillator. The peak grid voltage, at 28 Mcs, was approximately 400 millivolts. The change in oscillator grid voltage at resonance was less than 10 millivolts. Hence a linear relation between the power absorbed in the sample and the oscillator grid voltage may be assumed. The linearity of the system was checked with an auxiliary calibrated tuned circuit which was weakly coupled to the measuring circuit containing the sample being investigated. The power coupled out of the measur-

	g-factor	ΔH**, oersteds	Density, g/cm³	Free-radical concentration, percent	d, cm	|Θ|calc, °K	|Θ|exptl, °K
H	2.0042±0.0004	0.85±0.01	1.3	92	8.2	9.4	10
Cl	2.001±0.001	1.0±0.1	1.0	90	9.3	3.8	—
Br	2.002±0.002	1.9±0.1	0.8	92	10.2	1.1	—
OCH_3	2.000±0.002	2.3±0.2	1.1	88	9.0	2.0	—
F	2.000±0.004	3.5±0.4	1.0	89	9.2	1.2	—

*Coefficient in the formula $(x\,C_6H_4)(C_6H_5)\,N - NC_6H_2(NO_2)_3$.

**The value of the width $\Delta H'$, measured at points of maximum slope converted for the half-width of a Lorentzian curve using the formula $\Delta H = \sqrt{3}\,\Delta H'/2$.

ing circuit was determined from the voltage in the calibrated circuit. A linear dependence was found for the entire power range which was investigated.

The absorption lines were observed on an oscilloscope (Fig. 2) after the signal was amplified in a broadband system (30 cps to 1 Mcs) using

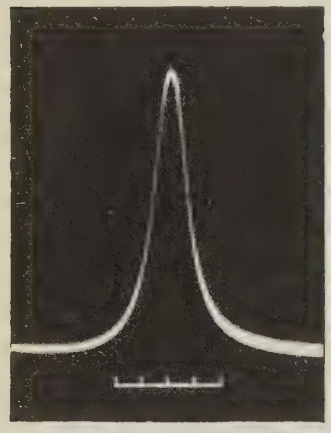

FIG. 2. Oscillogram showing paramagnetic resonance absorption in dpph (H_0 = 10 oersteds). The length of the scale corresponds to 4 oersteds.

20-oersted modulation of the fixed field at a frequency of 224 cps. A narrow-band system was used to measure the spacing between points of maximum slope. This system had a bandwidth of 0.3 cps and consisted of an amplifier, synchronous detector, and a recording device. In this work the amplitude of the modulating field was less than 0.1 oersted.

4. To compare the experimental absorption curve (Fig. 2) with a Lorentzian shape, it is convenient to write Eq. (7) in the form:

$$1/I(H) = C\Delta H + (C/\Delta H)(H - H_0)^2, \qquad (12)$$

where the constant C is determined by the choice of units. As is apparent from Fig. 3 there is a good fit between the experimental values and a line plotted according to (12).

The experimental value of the half-width of the absorption line for a polycrystalline dpph sample at room temperature and H = 10 oersteds ($\omega_0 = 1.76 \times 10^8$ cps) is found to be 0.85 ± 0.01 oersted. This result agrees with values which have been obtained earlier: (ΔH = 0.87 oersted),[7] (ΔH = 0.87 oersted),[9] and (ΔH = 0.88 oersted).[10]

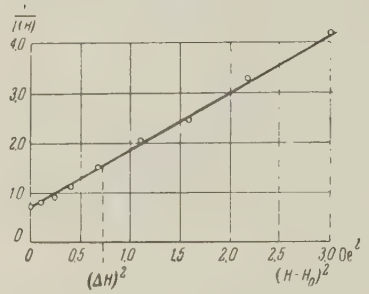

FIG. 3. The points correspond to experimental values measured on the absorption curve. The ordinate scale is arbitrary.

In weak fields, which correspond to resonance frequencies $\omega_0 \ll \omega_{2\gamma} \sim 10^{12}$ cps, it follows from Eqs. (A13) and (A15) of the Appendix that the shape and width of the line are independent of ω_0. Measurements made by us in fields ranging from 2 to 220 oersteds (values of ω_0 ranging from 3.5×10^7 cps to 3.9×10^9 cps) verify this result. In dpph at room temperature, hyperfine-structure splitting has been observed in fields on the order of 8000 oersteds.[11]

For the present sample, a theoretical estimate of the line half-width in a weak field Eq. (8) yields ΔH = 0.80 oersted.

Considering the rough nature of the estimate of the exchange integral and the fact that the actual crystal lattice of the radical differs from a simple cubic structure, the agreement between experiment and theory is quite surprising.

An estimate of the resonance absorption in weak fields for dpph has been made in reference 12 using the method proposed by Anderson and Weiss.[5] However, because of various errors the calculated width is 35 times greater than the experimental value found by these authors.*

5. The good agreement between theory and experiment in dpph allows us to make an estimate

*In particular, these authors did not take account of the so-called 10/3 effect, while the estimate of the exchange integral was carried out on the basis of the Curie-Weiss law for ferromagnets.

of the values of the asymptotic Curie points Θ for a number of derivative compounds of dpph; the line shapes for these have been studied by Chirkov and Matevosian.[13]

Using Eqs. (8) to (11) it is easily shown that

$$|\Theta| = 52.3\, g^4\mu_0^4/k\hbar d^6\Delta\omega. \tag{13}$$

The calculated and experimental results are shown in the table.

The authors wish to take this opportunity to express their gratitude to G. V. Strotskii for a discussion of this work and for a number of valuable comments and to R. O. Matevosian for making up the samples of the radicals.

APPENDIX

If it is assumed that in the case being considered the perturbation is the magnetic dipole-dipole interaction

$$\hat{\mathcal{H}}' = \sum_{\gamma} \hat{\mathcal{H}}'_{\gamma} = \sum_{\gamma} \sum_{jk} \Phi^{\gamma}_{jk} \{jk\}_{\gamma}, \tag{A.1}$$

where

$$\{jk\}_{\pm 2} = \hat{s}_j^{\pm}\hat{s}_k^{\pm}, \quad \{jk\}_{\pm 1} = \hat{s}_j^{\pm}\hat{s}_{kz} + \hat{s}_{jz}\hat{s}_k^{\pm},$$
$$\{jk\}_0 = \hat{s}_{jz}\hat{s}_{kz} - \tfrac{1}{4}(\hat{s}_j^{+}\hat{s}_k^{-} + \hat{s}_j^{-}\hat{s}_k^{+}), \qquad \hat{s}_j^{\pm} = \hat{s}_{jx} \pm i\hat{s}_{jy}; \tag{A.2}$$

$$\Phi^{\pm 2}_{jk} = -\sqrt{6\pi/5}\, g^2\mu_0^2 r_{jk}^{-3} Y_{2,\pm 2}(\vartheta_{jk}\varphi_{jk}),$$
$$\Phi^{\pm 1}_{jk} = -\sqrt{6\pi/5}\, g^2\mu_0^2 r_{jk}^{-3} Y_{2,\pm 1}(\vartheta_{jk}, \varphi_{jk}), \tag{A.3}$$
$$\Phi^{0}_{jk} = -\sqrt{16\pi/5}\, g^2\mu_0^2 r_{jk}^{-3} Y_{2,0}(\vartheta_{jk}\varphi_{jk}),$$

and the $Y_{lm}(\vartheta, \varphi)$ are the normalized spherical functions, we obtain, by carrying out the calculations indicated in (2) to (4),

$$G_0(t) = {}^1/_2 \exp(i\omega_0 t) + \text{compl. conjug.}, \quad G_1(t) = 0,$$
$$G_2(t) = -{}^1/_2 \exp(i\omega_0 t) \sum_{\gamma} \omega_{1\gamma}^2 \int_0^t (t-\tau) \tag{A.4}$$
$$\times \exp(-i\gamma\omega_0 t)\, f_{\gamma}(\tau)\, d\tau + \text{compl. conjug.}$$
$$= -{}^1/_2 \exp(i\omega_0 t)\, \psi(t).$$

Here, in accordance with reference 1, the correlation function $f_\gamma(\tau)$ can be given approximately by the expression:

$$f_{\gamma}(\tau) = \exp(-\tau^2\omega_{2\gamma}^2/2), \tag{A.5}$$

where

$$\hbar^2\omega_{2\gamma}^2 = \langle |[\hat{\mathcal{H}}_2[\hat{M}_x\hat{\mathcal{H}}'_{\gamma}]]|^2\rangle / \langle |[\hat{M}_x\hat{\mathcal{H}}'_{\gamma}]|^2\rangle. \tag{A.6}$$

For an isotropic environment

$$\omega_{12}^2 = \omega_{1-1}^2 = \frac{2}{3}\omega_{11}^2 = \frac{2}{3}\omega_{10}^2 = \frac{2}{5}\frac{s(s+1)}{\hbar^2} g^4\mu_0^4 \sum_k r_{jk}^{-6}, \tag{A.7}$$

neglecting higher terms in the expansion in (4), to second order, we may write $G(t)$ in the form

$$G(t) = {}^1/_2 \exp(i\omega_0 t - \psi(t)) + \text{compl. conjug.} \tag{A.8}$$

The line shape close to the resonance frequency is determined by the asymptotic behavior of $\psi(t)$ as $t \to \infty$

$$\psi(t) = \sum_{\gamma} \omega_{1\gamma}^2 (|t|\tau'_{\gamma} - it\tau''_{\gamma}), \tag{A.9}$$

where

$$\tau'_{\gamma} - i\tau''_{\gamma} = \sqrt{\frac{\pi}{2}}\frac{1}{\omega_{2\gamma}} \exp\left(-\frac{\gamma^2\omega_0^2}{2\omega_{2\gamma}^2}\right)$$
$$\times \left(1 - i\sqrt{\frac{2}{\pi}} \int_0^{\gamma\omega_0/\omega_{2\gamma}} \exp\left(\frac{U^2}{2}\right) dU; \right. \tag{A.10}$$

thus

$$G(t) = {}^1/_2 \exp(i\omega_0 t - \sum_{\gamma} \omega_{1\gamma}^2 (|t|\tau'_{\gamma} - it\tau''_{\gamma}))$$
$$+ \text{compl. conjug.} \tag{A.11}$$

Now it is easy to show, using the results obtained in reference 1, that the line shape close to the maximum is determined by a function of the Lorentzian form:

$$I(\omega) = \frac{1}{2\pi}\frac{\Delta\omega}{(\omega_0 - \omega + \delta)^2 + \Delta\omega^2}. \tag{A.12}$$

The half-width at half-height is

$$\Delta\omega = \sum_{\gamma} \omega_{1\gamma}^2 \tau'_{\gamma} = \sum_{\gamma} \frac{\omega_{1\gamma}^2}{\omega_{2\gamma}} \sqrt{\frac{\pi}{2}} \exp\left(-\frac{\gamma^2\omega_0^2}{2\omega_{2\gamma}^2}\right). \tag{A.13}$$

In the two limiting cases this expression becomes

$$\omega_0 \to \infty \qquad \Delta\omega_{\infty} = \frac{\omega_{10}^2}{\omega_{20}}\sqrt{\frac{\pi}{2}}, \tag{A.14}$$

$$\omega_0 \to 0 \qquad \Delta\omega_0 = \Delta\omega_{\infty} \sum_{\gamma} \frac{\omega_{1\gamma}^2}{\omega_{10}^2}\frac{\omega_{20}}{\omega_{2\gamma}}; \tag{A.15}$$

when $\omega_0 \to 0$ the shift in the resonance peak $\delta = \Sigma\, \omega_{1\gamma}^2 \tau''_{\gamma}$ vanishes.

If $\omega_{20} = \omega_{21} = \omega_{2-1} = \omega_{22}$, we obtain a simple expression for the line width in the weak-field case

$$\Delta\omega_0 = 10\Delta\omega_{\infty}/3. \tag{A.16}$$

This is called the $^{10}/_3$ effect, due to terms in the perturbation with $\gamma \neq 0$; these are important only at weak fields.

If the crystal has a simple cubic structure with lattice constant d, we get

$$\sum_k r_{jk}^{-6} = 8.4\ d^{-6}, \qquad \text{(A.17)}$$

which leads to (9). Assuming that the exchange interaction is isotropic and of the form

$$A(r_{jk}) \begin{cases} = A & r_{jk} < d \\ = 0 & r_{jk} > d \end{cases}$$

for a simple cubic lattice and $s = \frac{1}{2}$, as in reference 4, Eq. (A.6) is easily transformed to the expression

$$\omega_{20} = 3.65\,|A|/\hbar. \qquad \text{(A.18)}$$

[1] R. Kubo and K. Tomita, J. Phys. Soc. Japan **9**, 888 (1954).
[2] I. Waller, Z. Physik **79**, 370 (1932).
[3] L. J. F. Broer, Physica **10**, 801 (1943).
[4] J. H. Van·Vleck, Phys. Rev. **74**, 1168 (1948).
[5] P. W. Anderson and P. R. Weiss, Revs. Modern Phys. **25**, 269 (1953).
[6] Holden, Yager, and Merritt, J. Chem. Phys. **19**, 1319 (1951).
[7] L. S. Singer and E. G. Spencer, J. Chem. Phys. **21**, 939 (1953).
[8] E. K. Zavoiskii, J. Phys. (U.S.S.R.) **9**, 245 (1945).
[9] Garstens, Singer, and Ryan, Phys. Rev. **96**, 53 (1954).
[10] Van Gerven, Van Itterbeck, and De Wolf, J. de Phys. et Rad. **18**, 417 (1957).
[11] C. Kikuchi and V. W. Cohen, Phys. Rev. **93**, 394 (1954).
[12] F. Bruin and M. Bruin, Physica **22**, 129 (1956).
[13] A. K. Chirkov and R. O. Matevosian, J. Exptl. Theoret. Phys. (U.S.S.R.) **33**, 1053 (1957); Soviet Phys. JETP **6**, 811 (1958).

Translated by H. Lashinsky
6

SOVIET PHYSICS JETP VOLUME 35 (8), NUMBER 1 JANUARY, 1959

*SECONDARY NUCLEAR REACTIONS INDUCED IN BISMUTH AND LEAD BY HIGH-ENERGY PROTON BOMBARDMENT**

B. V. KURCHATOV, V. N. MEKHEDOV, L. V. CHISTIAKOV, M. Ia. KUZNETSOVA, N. I. BORISOVA, and V. G. SOLOV' EV

Submitted to JETP editor February 20, 1958

J. Exptl. Theoret. Phys. (U.S.S.R.) **35**, 56-63 (July, 1958)

The production of astatine isotopes ($Z = 85$) by bombardment of bismuth ($Z = 83$) and lead ($Z = 82$) with protons of energies up to 480 Mev was studied radiochemically. The cross sections for At^{211} and At^{210} production from bismuth were found to be 6×10^{-29} and $\sim 2 \times 10^{-29}$ cm^2 respectively. The formation of the light isotopes At^{205} and At^{203} was established. At^{211} was detected in lead ($\sigma \sim 10^{-31}$ cm^2).

The experimental results are attributed to secondary capture of the disintegration products (α particles or lithium nuclei). The production of light astatine isotopes is explained by high-energy proton capture with subsequent emission of π^- mesons and several neutrons. The cross section for production of α particles with $E > 20$ Mev from bismuth irradiated by 480-Mev protons was determined from the astatine yield to be 5 to 6×10^{-25} cm^2.

ONE of the characteristics of interactions between complex nuclei and fast protons is the occurrence of reactions in which the charge of the target nucleus is increased by 2 or 3. Such reactions have frequently been described in the literature[1-3] and are attributed to secondary capture of disintegration products (α particles or lithium nuclei). At high proton energies, in addition to such so-called secondary reactions, there is the additional possibility of proton capture accompanied by the emission of a π^- meson and neutrons, thus also increasing the charge by 2.

*The experimental work on which this paper is based was performed in 1951 and 1952 (cf. Report of the Institute of Nuclear Problems, Academy of Sciences, U.S.S.R. for 1951).

In the present paper we present the results of an investigation of the indicated reactions in bismuth and lead under bombardment by fast protons with energies up to 480 Mev. The production of nuclides with Z increased by 2 or more is clearly revealed through the appearance of α-radioactive astatine isotopes. Investigation of the yields of different astatine isotopes revealed both mechanisms of charge increase and enabled us to explore certain quantitative aspects of the effect which had not been studied previously.

THE PRODUCTION OF ASTATINE FROM BISMUTH

The initial material for the experiments was bismuth of high purity, shown by chemical analysis to contain < 0.001% of thorium and < 0.01% of uranium. The metal plates used in the experiments measured 10×15×2 mm and weighed up to 2 g. The plates were wrapped in aluminum foil 25 μ thick and were bombarded by a 0.2 to 0.4 μa proton current. Different proton energies from 180 to 480 Mev were obtained by varying the radius of the target position in the accelerator. The geometry of the bombardment was such that the beam passed through each plate in the direction of the 10-mm side. The initial energy of the incident proton beam was varied from 5 to 17% while the period of the bombardment ranged from 7 to 20 min.

The aluminum foil was used to monitor the current. After bombardment, the foil was unwrapped and the amount of Na^{24} activity with the half-life T = 14.8 hrs was measured. The cross section for Na^{24} production from Al^{27} was assumed to be 10^{-26} cm^2.[3]

Chemistry of Separation. The astatine was separated through coprecipitation of astatine and tellurium and the distillation of atomic astatine from an aqueous solution.[4,5] The astatine was extracted by different methods, depending on the purity and time requirements.

Quantitative Separation of Astatine. A bombarded specimen was dissolved in a minimum amount of concentrated nitric acid. The solution was diluted by 10% hydrochloric acid and an aliquot part of about 1/10 was combined with dilute hydrochloric acid to a volume of 30 to 40 milliliters. After the addition of 50 mg of tellurium (0.25 ml of a 2% solution of tellurium in nitric acid) tellurium was precipitated by 1 N stannous chloride. The precipitate was separated by centrifuging. Since a single precipitation of astatine in tellurium is insufficient, the operation was performed three times. The tellurium precipitates were combined and washed four times in 25 to 30 ml of dilute hydrochloric acid. (Such careful washing is essential for complete removal of the bismuth. If the washing is inadequate, the $Bi(OH)_3$ deposited by alkalization during the operations retains a large fraction of the astatine.) The washed tellurium was dissolved in a few drops of concentrated nitric acid; the solution was then diluted with water to a volume of 10 to 15 ml and alkalized by a 20% solution of sodium hydroxide. The tellurium was then precipitated by adding a stannite for the purpose of removing the polonium from the solution. Under these conditions, according to the literature,[4] the astatine remains in the solution. The purification from polonium was repeated. The purified solution was acidified with concentrated hydrochloric acid, 2 to 3 mg of tellurium was added, and the tellurium was precipitated by stannous chloride. The precipitation was repeated twice. The deposits were washed in water, deposited with alcohol on stainless steel plates (d = 2.5 cm), and dried on a water bath, after which the α activity was determined. The coprecipitation of astatine and tellurium is illustrated by the values given below, which are the averages of seven experiments. The amount of the carrier before the first and second precipitations was 2 mg, while the amount was 3 mg before the third precipitation. In the first precipitation 80% of the astatine was extracted, in the second precipitation 17.6%, and in the third precipitation 2.4%.

Preparation of Pure Astatine. The astatine was precipitated with tellurium by a similar method out of the solution which remained after removal of the aliquot part. The precipitates were combined and washed, and the tellurium was dissolved in 2 ml of concentrated sulfuric acid to which two drops of concentrated nitric acid had been added. The solution was diluted with water to 80 to 100 ml, 2 g of $FeSO_4$ were added, and the astatine was distilled, with 10 ml of the solution remaining in the distilling flask. The distillate was received in a vessel containing a solution of sodium hydroxide; 5 mg of tellurium was added and the latter was precipitated by adding a stannite for purification from the residue of polonium and β and γ emitters. In order to determine the amount of distilled astatine, an aliquot part of the alkaline solution was taken and the astatine was separated by the method described above. After 3 or 4 days, the daughter Po^{210} was precipitated with tellurium from the remaining solution, using the stannite in an alkaline medium, to determine the yield of At^{210}.

Rapid Separation of Pure Astatine. The sample was dissolved in concentrated nitric acid and the excess of acid was neutralized by a sodium hydroxide solution to a degree sufficient to keep the bismuth dissolved during the experiment. The solution was diluted with hot water to a volume of 10 ml and was boiled for 5 min, with the astatine being collected by the alkaline solution. About 1/20 of the astatine was boiled off with the admixture of β and γ emitters. Tellurium was precipitated from the distillate after the addition of tellurium and a stannite solution. Acidification and the addition of tellurium in the solution thus purified caused the astative to precipitate and be deposited on the target, as stated above. The entire operation of separation and preparation of the target required 20 to 25 min. This portion of the astatine was intended for the detection and measurement of short-lived α-radioactive isotopes and the determination of their relative yields.

PROCEDURE AND EXPERIMENTAL RESULTS

The α activity of the astatine targets was measured by means of an ionization chamber in conjunction with a linear accelerator. Some of the targets were also measured with a Geiger counter to study the astatine isotopes which decay through the capture of an orbital electron.

In all of the experiments we observed α activity with a half-life from 7.0 to 7.8 hrs, corresponding to At^{211} (α, K 60%), T = 7.5 hrs. The counter measurements revealed an eight-hour half-life belonging to At^{210} (K), T = 8.3 hrs. The production of the latter isotope was also confirmed by the accumulation of the long-lived α activity of the daughter Po^{210} (T = 140 days).

The utilization of the very rapid method of separating pure astatine enabled us to detect shorter periods of α activity 25 to 30 min and about 5 min, ascribed to At^{205} (α, K), (T = 25 min) and At^{203} (α, K), (T = 7 min) respectively.[6] The activities of At^{209} (α, K 95%) (T = 5.5 hrs) and At^{207} (α, K 90%) (T = 2 hrs) could not be separated on the decay curve because of the closeness of the half-lives and the small relative amount of α emission. The isotopes At^{204} (K), (T = 25 min), At^{206} (K), (T = 2.5 hrs), and At^{208} (K), (T = 6.3 hrs), which decay only by capture of an orbital electron, were not investigated.

The activity of At^{211} per gram of bismuth, under continuous bombardment and taking into account the percentage of K capture, fluctuated from 2.1×10^7 to 4.5×10^7 decays per min. The yields could not be determined with high accuracy because of a number of methodological errors. In addition to sorption losses during chemical separation, there were possible errors resulting from variations of the size of samples and the geometry of irradiation. We could also not exclude the possible loss of a small amount of astatine by evaporation from the bismuth during the dissimilar heating of the samples under bombardment.

The results obtained through bombardment by 480-Mev and 180-Mev protons are given in Tables I and II. Comparison of the average values shows

TABLE I*

Weight of Bi, g	Weight of Al, mg	A_∞ (At^{211}) per gram-atom of Bi, decays/min	A_∞ (Na^{24}) per gram-atom of Al, decays/min	σ (At^{211}), cm^2	$\frac{\sigma(At^{210})}{\sigma(At^{211})}$
1.95	32.4	$4.3 \cdot 10^9$	$5.3 \cdot 10^{11}$	$7.4 \cdot 10^{-29}$	0.43
1.69	25.5	$2.9 \cdot 10^9$	$9.1 \cdot 10^{11}$	$5.4 \cdot 10^{-29}$	0.28
1.25	18.5	$9.3 \cdot 10^9$	$1.6 \cdot 10^{12}$	$5.8 \cdot 10^{-29}$	0.31
1.18	22.5	$8.7 \cdot 10^9$	$1.5 \cdot 10^{12}$	$5.8 \cdot 10^{-29}$	0.27
0.7	2.2	$1.4 \cdot 10^{10}$	$1.9 \cdot 10^{12}$	$7.4 \cdot 10^{-29}$	
	Average			$6.3 \cdot 10^{-29}$	0.32

*E_p = 480 Mev.

TABLE II*

Weight of Bi, g	Weight of Al, mg	A_∞ (At^{211}) per gram-atom of Bi, decays/min	A_∞ (Na^{24}) per gram-atom of Al, decays/min	σ (At^{211}), cm^2	$\frac{\sigma(At^{210})}{\sigma(At^{211})}$
1.9	21.8	$3.6 \cdot 10^9$	$1.7 \cdot 10^{12}$	$2.1 \cdot 10^{-29}$	0.33
1.64	26.8	$8.7 \cdot 10^8$	$2.3 \cdot 10^{11}$	$3.8 \cdot 10^{-29}$	0.34
1.16	21.5	$3.5 \cdot 10^9$	$9.7 \cdot 10^{11}$	$3.6 \cdot 10^{-29}$	0.28
			Average	$3.2 \cdot 10^{-29}$	0.32

*E_p = 180 Mev.

TABLE III

E_p, Mev	$\sigma(At^{205})/\sigma(At^{211})$	$\sigma(At^{203})/\sigma(At^{211})$
480	0.035	~0.25
375	0.07	~0.5
275	0.12	—
180	<0.02	<0.2

that the yield of At^{211} is nearly twice as great for 480-Mev protons as for 180-Mev protons, whereas the ratio of the At^{210} and At^{211} production cross sections is unchanged. Table III shows how the cross section ratios vary for At^{205} and At^{211} and for At^{203} and At^{211} as the proton energy decreases.

The yields of At^{205} and At^{203} are lower limits because we do not know for these isotopes the relative amount of K capture which competes with α decay. The decay curve does not show a five-minute period for 275-Mev protons, and the 25-minute period disappears for $E_p = 180$ Mev. The values given in Table III are only estimates; greater accuracy will require improved apparatus, especially a multi-channel analyzer of α-particle energies.

DISCUSSION OF RESULTS

The production of the heavy isotope At^{211} cannot be attributed to the disintegration of uranium and thorium impurities. Control experiments for the purpose of determining the At^{211} yield from these elements gave cross sections $\sigma = 2.3 \times 10^{-26}$ cm^2 for thorium and 3.0×10^{-28} cm^2 for uranium. Hence the observed effect would require ~0.3% of thorium or ~10% of uranium, which considerably exceeds the limit of impurities represented by these elements.

The only reaction which accounts both for the increased charge and the mass of the products is the capture of α particles with emission of two or three neutrons. Since an admixture of α particles in the proton beam is unlikely, we assume a secondary origin of the α particles resulting from the disintegration of target atoms. We are able to relate the yields of At^{210} and At^{211} quantitatively to the observed α-particle spectrum of bismuth and to obtain the correct order of magnitude of the cross section for the production of fast α particles. The results of these calculations, and a detailed discussion of all questions arising therefrom, are given separately in the following section.

The cross sections obtained for secondary α-particle capture by bismuth are in agreement with the cross sections of similar secondary reactions in copper.[2] Without taking into account the different energies of the bombarding particles, it can be assumed that secondary capture of α particles occurs with a cross section of the same order of magnitude ($\sim 5 \times 10^{-29}$ cm^2) for various elements of the periodic system.

The foregoing mechanism for the production of heavy astatine isotopes cannot be extended to include the light isotopes. Indeed, we know from the literature that the production of At^{205} and At^{204} from bismuth requires 150-Mev α particles, while At^{203} is obtained through bombardment at 275 Mev.[6] Aside from the difficulty of explaining a considerable yield for the emission of such fast α particles, any appreciable quantity of these α particles would result in the predominance of At^{210} over At^{211} (owing to the large total $(\alpha, 3n)$ cross section; see Fig. 1), in contradiction of experiment. Therefore the production of light isotopes with a yield of the same order or one order smaller than the yield of At^{211} cannot be accounted for by secondary reactions with α particles, and requires a mechanism of π^--meson emission. The corresponding reaction for At^{203} production can be written as $Bi^{209}(p, \pi^- 7n)At^{203}$. The integral π^--emission cross section for heavy nuclei is $\sim 10^{-26}$ cm^2.[7] The cross section of the assumed particular reaction must be smaller by 2 to 3 orders of magnitude, thus not disagreeing with the observed yield of light astatine isotopes. The reaction mentioned necessitates the capture of a fast proton and the transfer of its total energy to the nucleus.

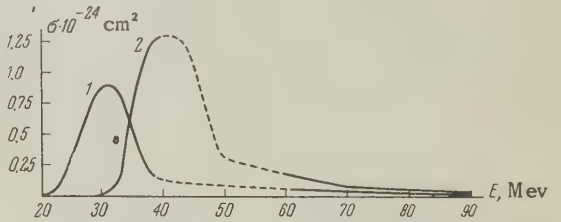

FIG. 1. Excitation functions for the $(\alpha, 2n)$ and $(\alpha, 3n)$ reactions in bismuth. 1 – $Bi(\alpha, 2n)At^{211}$; 2 – $Bi(\alpha, 3n)At^{210}$.

Taking into account the energy required for the production of a π^- meson (170 Mev) together with its kinetic energy (up to 100 or 200 Mev), we obtain the nuclear excitation energy remaining for nucleon evaporation; this is about 100 to 200 Mev. The high excitation energy will favor the emission of a large number of nucleons (in our case of production of astatine from bismuth, these can only be neutrons); thus the production of the lightest isotopes will be favored. This can also explain our observation of the predominance of

At^{203} over At^{205} and the increased yield of At^{205} as the incident proton energy decreases.

Calculation of the Yield. Figure 1 shows the excitation functions for the $(\alpha, 2n)$ and $(\alpha, 3n)$ reactions in bismuth;[6,8] the dotted lines denote our interpolations of missing portions of the curves. These experimental results furnish the only possibility to date of a quantitative analysis of a secondary reaction involving α-particle capture.

The calculation was performed as follows:

1. It was assumed that heavy astatine isotopes were produced through the capture of α particles with $20 < E < 60$ Mev emitted by bismuth when bombarded by fast protons.

2. It was necessary to determine a shape of the α-particle spectrum which would satisfy the observed ratio of At^{210} and At^{211} yields. After trials of the simplest functions that satisfy experiment (linear decay and a steep E^{-n} law) we took an intermediate spectral shape given by the theory of evaporation[9] as expressive of the physical content:

$$P(E) = \frac{E-V}{\tau^2} \exp\{-(E-V)/\tau\}.$$

3. We tried different values of the parameters V and τ, which in evaporation theory are the potential barrier and temperature of the nucleus.

4. For each pair of values of V and τ, we determined graphically the fraction K_n of α particles with $E < 20$ Mev at 5-Mev intervals, so that

$$\sum_{E=20}^{E=60} K_n = 1.$$

5. For each group of α particles, we determined the probability of α-particle capture with emission of two and three neutrons respectively. This probability W_n was obtained by summation over the entire effective range of probabilities for different portions Δl of the α-particle range. The probability w was calculated by means of the formula

$$w = \Delta l/\lambda = \Delta l n_0 \sigma_{At},$$

where n_0 is the number of Bi atoms per cm^3 and σ_{At} is the cross section for the production of the corresponding astatine isotope for a given energy interval. Δl was determined from the graph of the energy dependence of the α-particle range.[10]

6. Summation of the products $K_n W_n$ from 20 to 60 Mev gave the total probability of α-particle capture with formation of the corresponding isotope.

7. Besides the probability ratio for the production of astatine isotopes we calculated the cross section for the production of α particles with energies > 20 Mev through the disintegration of bismuth, using the equation

$$\sigma_\alpha = \frac{\sigma(At^{211})}{\Sigma W_n K_n}.$$

Table IV gives the results obtained for different values of our parameters. The experimental ratio of astatine yields (0.32 to 0.40) is satisfied

TABLE IV

τ, Mev	V, Mev	$\frac{\sigma(At^{210})}{\sigma(At^{211})}$	$\sigma_\alpha (E_\alpha > 20$ Mev), cm^2
4	13	0.26	$7.3 \cdot 10^{-25}$
4	16	0.27	$6.3 \cdot 10^{-25}$
4	19	0.33	$5.0 \cdot 10^{-25}$
4.5	13	0.34	$6.3 \cdot 10^{-25}$
5	10	0.37	$5.7 \cdot 10^{-25}$
5	13	0.41	$5.4 \cdot 10^{-25}$
5	16	0.43	$5.0 \cdot 10^{-25}$

by values of τ from 4.5 to 5 Mev and low V (10 to 13 Mev). This is higher then the value of 4 Mev obtained by Perfilov and Ostroumov[11] from the averaged spectrum of α particles emitted by Bi and W when bombarded by 460-Mev protons. Figure 2 compares our calculated curves with

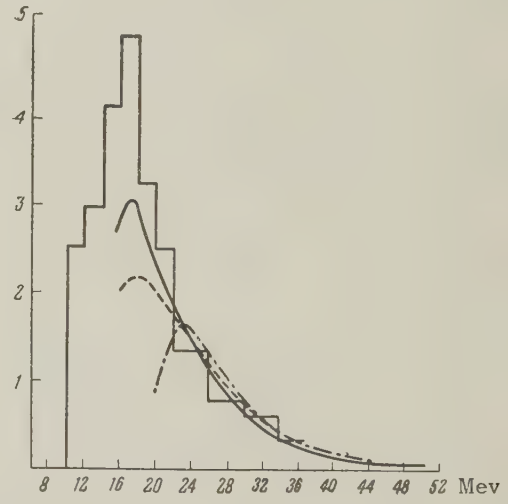

FIG. 2. Spectrum of fast α particles computed according to the yields of At^{210} and At^{211} from bismuth. Solid curve: $\tau = 5$ Mev, V = 13 Mev. Dashed curve: $\tau = 4.5$ Mev, V = 13 Mev. Dots and dashes: $\tau = 4$ Mev, V = 19 Mev.

their histogram. For the purpose of the comparison the curves are normalized to an identical area for the sum of α particles with $E_\alpha > 20$ Mev. The histogram (shifted 2 Mev to the right in accordance with a correction by the authors) fits bebetween the curves for $\tau = 4.5$ and 5.0 Mev with V = 13 Mev. Figure 2 also gives the curve for

$\tau = 4$ Mev and $V = 19$ Mev, which also satisfies the yield ratio of astatine isotopes. The difference between the peak of this curve and the corresponding experimental point does not at present justify rejection of the curve if we take into account the inadequate statistical information in connection with experiments using photographic emulsions for this range of α-particle energies, and the new results[12] which indicate the existence of a second maximum in the α spectrum under similar conditions.

Although the shape of the α spectrum according to the astatine yield agrees with other data, there is considerable disagreement with experiment in the calculation of the quantity of α particles. Perfilov and Ostroumov[11] obtained 1.5 to 1.6×10^{-25} cm^6 for the cross section of α-particle production with $E_\alpha > 20$ Mev, whereas our computations from the yield of At^{211} give a result which is 3 to 4 times larger (Table IV). Our result is not very sensitive to the assumed spectral shape and we cannot expect it to be reduced for more precise parameters. We can attempt to attribute the discrepancy to inaccurate calculation and the superimposing of experimental errors in the three independent investigations which are used for comparison. But this is evidently not the only possible explanation and the question requires further investigation.

Our results show that the yield ratio of the two heavy astatine isotopes does not depend essentially on the proton energy. This result (like the low value of the barrier V) apparently indicates that α particles with $E > 20$ Mev appear at a stage of nuclear excitation which is far from a quasi-equilibrium state. A purely evaporational mechanism for the production of the α particles would be an oversimplification. Specifically, we cannot exclude from the astatine-producing process the participation of α particles formed in a cascade process. The latter may be one of the causes of the high value of τ.

THE PRODUCTION OF ASTATINE FROM LEAD

Very pure lead was used. Spectral analysis indicated the presence of 0.01% of bismuth. By chemical analysis, the uranium content was estimated to be < 0.005% and the thorium content < 0.001%. In control experiments we used lead which we had prepared out of "Kalbaum" lead acetate. This material was converted into lead chloride and was recrystallized; the lead was then extracted by electrolysis of a hot aqueous solution, using very pure graphite electrodes. After being washed, the lead was melted in an atmosphere of electrolytic hydrogen. Spectral analysis of the purified lead revealed ~0.001% of bismuth. Chemical analysis did not reveal the presence of uranium or thorium within the limits of experimental sensitivity (U content < 10^{-3}%; Th content < 5×10^{-4}%).

The procedures for bombardment and separation of the astatine were the same as those used in the experiments with bismuth, except for the preliminary operation of precipitating lead with hydrochloric acid and longer bombardment of the sample (from 1 to 2 hrs). In each experiment we obtain α activity with a half-life of 7 to 8 hrs, which corresponds to At^{211}. Shorter periods were at the limit of detection. The astatine activity per gram of lead was considerably smaller than for bismuth; in the best case we obtained 1.9×10^4 decays/min when converted to continuous bombardment. We did not observe any dependence of the astatine yield on the purity of the original material.

The observed effect could not be caused by bismuth impurity, which would have had to be ~0.4% and thus much larger than the actual impurity. Astatine production due to uranium impurity is also excluded; this would have had to be 0.7%. An estimate of the possible influence of thorium impurity is a more complicated matter. The computed effect of thorium impurity comprises not more than one fourth of the observed activity of astatine from lead. However, we are inclined to attribute the astatine activity to reactions in lead nuclei; the actual amount of thorium impurity is unknown and may be smaller than the figure mentioned and, on the other hand, the observed At^{211} activity is a lower limit because of possible loss in chemical separation.

The formation of At^{211} from the heaviest lead isotope Pb^{208} is possible only through the capture of light nuclei resulting from the disintegration of lead. Considering lithium nuclei in the first place, the reaction can be written as Pb^{208}(Li, kn)At^{211}, although the nuclei of beryllium and other heavier elements may also participate. The cross section of At^{211} production for 480-Mev protons is estimated at 0.4 to 0.8×10^{-31} cm^2.

SEARCH FOR OTHER SECONDARY REACTIONS

For the purpose of detecting the capture of carbon nuclei we performed exploratory experiments to study the production of astatine from gold bombarded by 480-Mev protons, thus increasing the charge by 6 units. A small amount of α activity was detected (about 10 pulses/min against a back-

ground of 2 pulses/min) decaying with a half-life of 7 to 8 hrs. This small effect, which represents a cross section $\sim 10^{-33}$ cm^2, did not enable us to determine the source of the activity, as thorium impurity amounting to 5×10^{-6}% could result in the same activity. Despite special purification of the gold, thorium impurity to this extent cannot be excluded. Thus the sought reaction of carbon capture (in our case C^{14} and heavier isotopes) lies at the limit of observation and cannot be established with certainty at the bombarding energies which were used.

A similar result was obtained in our investigation of the production of iodine from silver (carbon capture) bombarded by 480-Mev protons. In this instance also the small iodine yield (16 pulses/min, representing $\sigma \approx 5 \times 10^{-33}$) did not permit us to establish its production unambiguously as the result of the sought reaction.

The authors are indebted to Professor B. M. Pontecorvo, whom they wish to thank for suggesting this research, and to Professor I. Ia. Pomeranchuk for valuable suggestions and comments during the performance of the work and the discussion of the results.

[1] L. Marquez and I. Perlman, Phys. Rev. **81**, 953 (1951).

[2] Batzel, Miller and Seaborg, Phys. Rev. **84**, 671 (1951).

[3] Vinogradov, Alimarin, Baranov, Lavrukhina, Baranova, and Pavlotskaia, Труды сессии АН СССР по мирному использованию атомной энергии (Conference of the Academy of Sciences of the U.S.S.R. on the Peaceful Uses of Atomic Energy, 1955.

[4] Corson, MacKenzie, and Segrè, Phys. Rev. **58**, 672 (1940).

[5] Johnson, Leininger, and Segrè, J. Chem. Phys. **17**, 1 (1949).

[6] Barton, Ghiorso, and Perlman, Phys. Rev. **82**, 13 (1951).

[7] Richman, Weissbluth, and Wilcox, Phys. Rev. **85**, 161 (1952).

[8] E. L. Kelly and E. Segrè, Phys. Rev. **75**, 999 (1949).

[9] K. J. Le Couteur, Proc. Phys. Soc. (London) **A63**, 259 (1950).

[10] E. Segrè, Ed., Experimental Nuclear Physics (Wiley, New York, 1953) Vol. 1, p. 222.

[11] N. A. Perfilov and V. A. Ostroumov, Dokl. Akad. Nauk SSSR **103**, 227 (1955).

[12] C. Zanger and J. Rossel, Helv. Phys. Acta **28**, 349 (1955).

Translated by I. Emin
7

SOVIET PHYSICS JETP VOLUME 35 (8), NUMBER 1 JANUARY, 1959

ENERGY SPECTRUM AND ANGULAR DISTRIBUTION OF π^+ MESONS, PRODUCED IN PROTON-PROTON COLLISIONS AT 660-670 Mev

A. G. MESHKOVSKII, Ia. Ia. SHALAMOV, and V. A. SHEBANOV

Submitted to JETP editor February 24, 1958

J. Exptl. Theoret. Phys. (U.S.S.R.) **35**, 64-70 (July, 1958)

The energy spectrum of π^+ mesons produced in p − p collisions by 670 Mev protons were measured for observation angles 19°30′, 38°, and 56°. It was found that, in the c.m.s., the shape of the π^+-meson spectrum for the $pp \rightarrow pn\pi^+$ reaction depends on the emission angle. The angular distribution of π^+ mesons produced in 660-Mev p − p collisions is given, in the c.m.s., by Eq. (1). The value found for the total cross-section is $(14.4 \pm 1.2) \times 10^{-27}$ cm^2.

1. INTRODUCTION

THE energy spectrum and the absolute yield of π^+ mesons, produced in p − p collisions at 660 Mev, were first measured by Sidorov[1] in emulsions, at five values of the observation angle from 60° to 120°. Meshcheriakov et al.[2] studied the relative spectrum of π^+ mesons at 24° by means of magnetic analysis. Meshkovskii et al.[3] measured the absolute yield of π^+ mesons at 29°, 46°, and 65°

by means of a π^+ meson magnetic spectrometer. In the present work, the spectrum was measured at 29° and 46°. Finally, Neganov and Savchenko[4] measured the energy spectrum of π^+ mesons at four angles between 108° and 160°, and determined the absolute yield at eight angles between 60° and 160°.

The results of the above experiments can essentially be summarized as follows: First, it has been found[1,3] that the shape of the energy spectrum of the π^+ mesons produced in the $pp \rightarrow pn\pi^+$ reaction depends, in the c.m.s. of the two colliding nucleons, on the angle of emission of the π^+ mesons. Second, the angular distribution of π^+ mesons in the $pp \rightarrow pn\pi^+$ reaction can be described by the expression $a + b\cos^2\vartheta^*$, where ϑ^* is the emission angle in the c.m.s.[1,4]

Since the shape of the π^+-meson spectrum varies with the angle in the c.m.s., it is interesting to study this variation for the $pp \rightarrow pp\pi^+$ reaction. The above mentioned experiments are not, however, sufficient for that purpose. The degree of accuracy of some of the measurements of reference 1 makes it impossible to find the shape of the spectrum at certain angles. In reference 4 the spectrum was investigated only for the upper half of the total energy range in the c.m.s. The results of these experiments concerning the angular distribution of π^+ mesons are not consistent. While the angular distribution of π^+ mesons in the $pp \rightarrow pn\pi^+$ reactions is almost isotropic according to reference 1, this is not the case for the distribution obtained in reference 4.

In the present work we measured the energy spectrum and differential cross-section $d\sigma/d\Omega$ of π^+ mesons, produced at 19°30′, 38°, and 56°, in p—p collisions at 670 Mev proton energy. This was done in continuation of earlier experiments,[3] in the course of which the spectrum was measured at 29° and 46°. The π^+ meson magnetic spectrometer, described in reference 3, was used in both experiments. The angle interval from 19°30′ to 56° in the laboratory system (l.s) corresponds to the interval from 35° to 90° in the c.m.s. The results of these experiments thus make is possible to study the angular dependence of the spectrum shape in the 35° to 90° interval in the c.m.s. (Sec. 5) from spectra obtained for five values of the angle. Measurements of the absolute yield of π^+ mesons at six values of the angle permitted us to calculate the corresponding angular distribution and to compare it with the results of other experiments (Secs. 3 and 4).

All measurements of the present work were carried out in the external proton beam of the synchrocyclotron of the Laboratory of Nuclear Problems, Joint Institute for Nuclear Studies.

2. EXPERIMENTAL RESULTS

Results of the measurements of differential cross-sections $d^2\sigma/d\Omega\, dE$ for the production of π^+ mesons in p—p collisions at 670 Mev proton energy at three angles of observation are given in Table I. Only the statistical errors of the measurements are given in the table.

The energy spectra of π^+ mesons based on the data of Table I are given in Fig. 1. The curves are drawn for best fit with the experimental points. Figure 2 represents the spectra in the c.m.s. The

TABLE I

19°30′		38°		56°	
Meson energy Mev	$\frac{d^2\sigma}{d\Omega\, dE}\cdot 10^{29}$ cm² sterad⁻¹ Mev⁻¹	Meson energy Mev	$\frac{d^2\sigma}{d\Omega\, dE}\cdot 10^{29}$ cm² sterad⁻¹ Mev⁻¹	Meson energy Mev	$\frac{d^2\sigma}{d\Omega\, dE}\cdot 10^{29}$ cm² sterad⁻¹ Mev⁻¹
104	0.55±0.33	80	0.65±0.17	75	0.74±0.16
130	0.59±0.32	103	0.78±0.14	88	0.82±0.16
162	0.95±0.27	128	0.95±0.17	100	1.21±0.17
190	1.38±0.18	152	1.28±0.16	116	1.14±0.15
227	1.74±0.24	172	1.68±0.16	130	1.30±0.14
263	2.37±0.26	192	1.28±0.17	143	1.13±0.14
284	2.05±0.20	212	1.40±0.15	155	1.15±0.15
301	2.32±0.23	231	1.57±0.13	163	1.00±0.12
316	2.88±0.20	240	1.33±0.15	172	0.94±0.12
322	4.04±0.32	250	1.37±0.16	186	0.90±0.09
329	5.01±0.30	256	1.41±0.14	193	1.03±0.10
338	3.81±0.27	260	1.83±0.15	200	1.04±0.09
343	2.29±0.16	263	2.16±0.14	204	0.99±0.07
350	1.52±0.17	266	2.34±0.17	207	1.06±0.08
357	0.17±0.16	269	2.18±0.11	210	0.79±0.08
—	—	275	1.75±0.13	217	0.27±0.08
—	—	279	0.65±0.11	236	0.04±0.07
—	—	284	0.51±0.13	251	−0.04±0.08
—	—	295	0.26±0.11	—	—

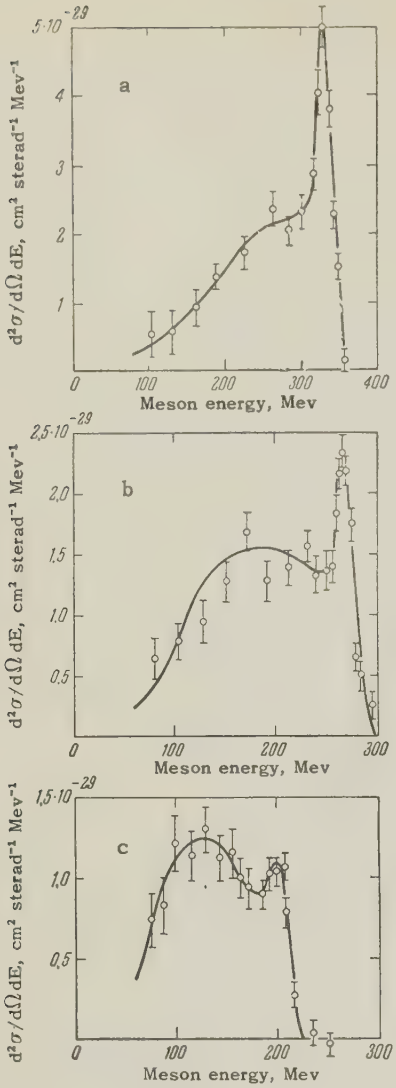

FIG. 1. Spectrum of π^+ mesons in laboratory system at emission angles: a – 19°30′, b – 38°, and c – 56°.

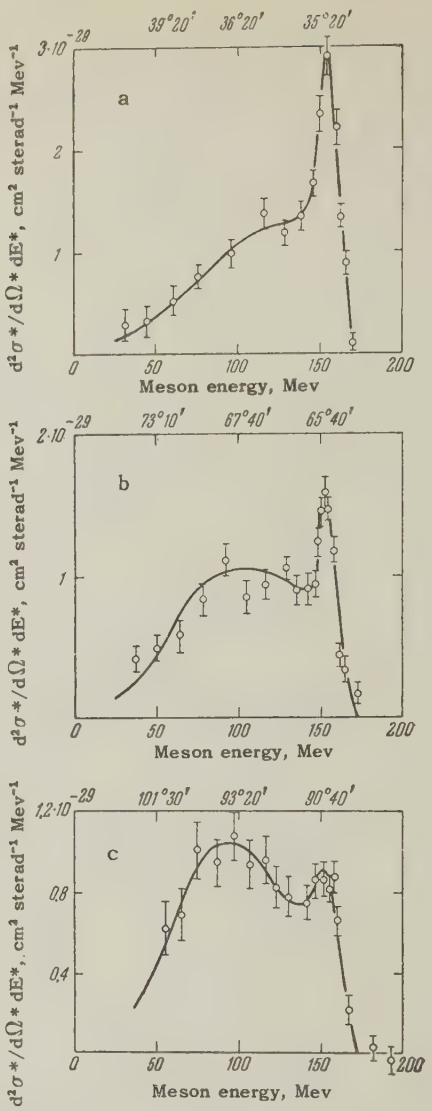

FIG. 2. Spectrum of π^+ mesons in c.m.s. at laboratory angles: a – 19°30′, b – 38°, and c – 56°.

values of the emission angle in the c.m.s. as a function of π^+ meson energy are indicated in the figure.

Results of the integration of the curves in Figs. 1 and 2, i.e., the cross sections $d\sigma/d\Omega$ in the l.s., and $d\sigma^*/d\Omega^*$ in the c.m.s., are given in Table II.

Systematic errors of the measurements, amounting to 10% for the angle 19°30′ and to 5% for the remaining angles, were taken into account, besides the statistical errors, in carrying out the integration. The tabulated values of the angle ϑ^* in the c.m.s. represent the angles of emission of π^+ mesons in the $pp \rightarrow d\pi^+$ reaction. The angles do not differ by more than 2° or 3° from the mean angles of emission of π^+ mesons in the c.m.s. for each spectrum.

TABLE II. Differential Cross-Sections at 670 Mev Proton Energy

Laboratory System		Center of Mass System	
ϑ	$d\sigma/d\Omega \cdot 10^{27}$ cm² sterad⁻¹	ϑ^*	$d\sigma/d\Omega \cdot 10^{27}$ cm² sterad⁻¹
19°30′	4.47±0.56	35°	1.42±0.18
38°	2.78±0.19	65°	1.17±0.08
56°	1.57±0.12	90°	1.01±0.08

3. ANGULAR DISTRIBUTION OF π^+ MESONS IN THE C.M.S. AND TOTAL CROSS-SECTION

It has been shown above that the results of the present experiment were obtained for three angles of observation at 670 Mev proton energy, while our earlier data for the three remaining angles[3] were obtained at 660 Mev. For the calculation of the angular distribution of π^+ mesons it is necessary to reduce all results to one energy. It is con-

TABLE III. Differential Cross-Sections in C.M.S. at 660 Mev Proton Energy

ϑ^*	35°	51°	65°	77°	90°	101°
$d\sigma^*/d\Omega^* \cdot 10^{27}$ cm^2 sterad^{-1}	1.32±0.17	1.07±0.08	1.08±0.08	1.06±0.07	0.93±0.07	0.99±0.10

venient to do this for 660 Mev, since other experiments on angular distribution have been carried out for that energy.[1,4]

A reduction to another energy value can be made using the experimental dependence of the yield of the $pp \to pn\pi^+$ reaction on the maximum meson momentum p^*_{max} in the c.m.s.[4] This dependence can be approximated by a power function of p^*_{max} (references 4 and 7). The cross-section of the reaction $pp \to d\pi^+$ in the considered narrow energy range from 660 to 670 Mev may be assumed, with an accuracy sufficient for our purposes, to remain constant, as follows from the experimental data.[5]

Results of the reduction of the values of $d\sigma^*/d\Omega^*$, obtained in the present experiment, to 660 Mev are given in Table III. The table includes also the values of $d\sigma^*/d\Omega^*$ for the three angles which were obtained by us earlier.[3]

Assuming that the angular distribution of π^+ mesons produced in $p-p$ collisions can be expressed, in the c.m.s., as $a + b\cos^2\vartheta^*$, we can find the values of a and b from Table III by the method of least squares. As a result, we obtain the following angular distribution

$$d\sigma^*/d\Omega^* = [(0.97 \pm 0.06) + (0.50 \pm 0.21)\cos^2\vartheta^*] \cdot 10^{-27} \text{ cm}^2\text{-sterad}^{-1}. \quad (1)$$

The angular distribution of π^+ mesons in the $pp \to d\pi^+$ reaction, according to the data of Meshcherakov and Neganov,[5] is

$$d\sigma^*(pp \to d\pi^+)/d\Omega^* = [(0.100 \pm 0.014) + (0.435 \pm 0.025)\cos^2\vartheta^*] \cdot 10^{-27} \text{ cm}^2\text{-sterad}^{-1}. \quad (2)$$

Subtracting Eq. (2) from Eq. (1), we obtain the angular distribution of π^+ mesons in the $pp \to pm\pi^+$ reaction:

$$d\sigma^*(pp \to pn\pi^+)/d\Omega^* = [(0.87 \pm 0.06) + (0.07 \pm 0.21)\cos^2\vartheta^*] \cdot 10^{-27} \text{ cm}^2\text{-sterad}^{-1}. \quad (3)$$

The angular distribution (1) permits us to calculate the total production cross section of π^+ mesons in $p-p$ collisions at 660 Mev. The result is $\sigma^{\pi^+}_{pp} = (14.4 \pm 1.2) \times 10^{-27}$ cm^2, in good agreement with the value $\sigma^{\pi^+}_{pp} = (14.8 \pm 2.1) \times 10^{-27}$ cm^2 obtained as the difference between the cross section for all inelastic processes, $\sigma_{pp} = (18.4 \pm 2.1) \times 10^{-27}$ cm^2 (reference 6) and the production cross section of neutral π mesons $\sigma^{\pi^0}_{pp} = (3.6 \pm 0.2) \times 10^{-27}$ cm^2.[7]

The cross-section for the $pp \to pn\pi^+$ reaction can be calculated subtracting from $\sigma^{\pi^+}_{pp}$ the value of $\sigma(pp \to d\pi^+) = (3.1 \pm 0.2) \times 10^{-27}$ cm^2.[5] This gives $\sigma(pp \to pn\pi^+) = (11.3 \pm 1.2) \times 10^{-27}$ cm^2.

4. COMPARISON OF THE MEASURED ANGULAR DISTRIBUTION WITH THE RESULTS OF OTHER EXPERIMENTS

The angular distribution of π^+ mesons in $p-p$ collisions at 660 Mev was first studied by Sidorov,[1] who found that:

$$d\sigma^*/d\Omega^* = (1.03 \pm 0.18) \times [1 + (0.1 \pm 0.2)\cos^2\vartheta^*] \cdot 10^{-27} \text{ cm}^2\text{-sterad}^{-1}. \quad (4)$$

In order to compare the above distribution with our results, we write it in the form:

$$d\sigma^*/d\Omega^* \sim 1/3 + (0.03 \pm 0.06)\cos^2\vartheta^*. \quad (5)$$

We write the angular distribution (1) found in the present work in the same form:

$$d\sigma^*/d\Omega^* \sim 1/3 + (0.17 \pm 0.07)\cos^2\vartheta^*. \quad (6)$$

If the cross-section $d\sigma^*/d\Omega^*$ is proportional to $1/3 + \alpha\cos^2\vartheta^*$ then the factor α represents the ratio of the number of anisotropically-distributed π mesons to the number of isotropically-distributed ones. It follows from Eq. (6) that the distribution obtained by us is nearly isotropic, since $\alpha = 0.17$. This result is consistent with the assumption made above, according to which the process $pp \to \pi^+$ process is nearly isotropic in the c.m.s.[3]

The distributions (5) and (6) differ somewhat from each other. It is necessary to take into account, while considering this discrepancy, that (as shown earlier[4]) Sidorov's reduction of the data contains an error which can be amended. After recalculating, we obtained the following distribution based on the corrected data of Sidorov:

$$d\sigma^*/d\Omega^* \sim 1/3 + (0.15 \pm 0.08)\cos^2\vartheta^*, \quad (7)$$

which coincides with the distribution (6).

We shall compare now the angular distribution (6) with the results of Neganov and Savchenko.[4] These authors found that

$$d\sigma^*(pp \to pn\pi^+)/d\Omega^* = [(0.58 \pm 0.13) + (0.88 \pm 0.04)\cos^2\vartheta^*] \times 10^{-27} \text{ cm}^2\text{-sterad}^{-1}. \quad (8)$$

This above expression is considerably different from Eq. (3). Combining Eq. (8) with Eq. (2) we obtain the angular distribution of π^+ mesons in p — p collisions

$$d\sigma^*/d\Omega \sim 1/3 + (0.64 \pm 0.12)\cos^2\vartheta^*, \quad (9)$$

Distribution (9) is more anisotropic than those given by Eqs. (6) and (7).

It is necessary to note, in considering the discrepancy, that the four c.m.s. π^+-meson spectra given in reference 4 have been measured only for energies larger than 70 or 80 Mev, the maximum energy in the spectra being 160 Mev. The shape of the spectrum and the value of the cross section remain therefore unknown over approximately a half of the spectrum. The authors overcame the difficulty by calculating a theoretical curve which corresponds to their results in a narrow region from 80 to 130 Mev. It is well known, however, that no theory can at present be expected to predict the results of experiments on π-meson production, and the above-mentioned agreement cannot serve as a criterion for the correctness of the curve

We think, therefore, that the spectra measured by Neganov and Savchenko cannot be used to calculate the cross-section $d\sigma^*/d\Omega^*$ in the 140° to 170° interval in which the spectrum was measured.

5. SHAPE OF THE π^+ MESON SPECTRUM IN THE C.M.S.

The gradual change of the shape of the π^+ meson spectrum in the c.m.s. with the angle of observation can be observed in Fig. 3, where the spectra measured in the present and in our earlier experiment[3] are shown together. The measurements of the present work have been reduced to 660 Mev by the method outlined in Sec. 3. The experimental points have been omitted for clarity. The dotted line represents a part of the π^+ meson spectrum measured in relative units by Meshcherakov et al.[2] at 24° in the l.s. The area of that spectrum has been normalized in the figure to the value of $d\sigma^*/d\Omega^*$ that follows from the angular distribution (1) measured in the course of the present experiment. It can be seen that the result of reference (2) is in a good agreement with our curves.

It can be seen from Fig. 3 that a marked shift

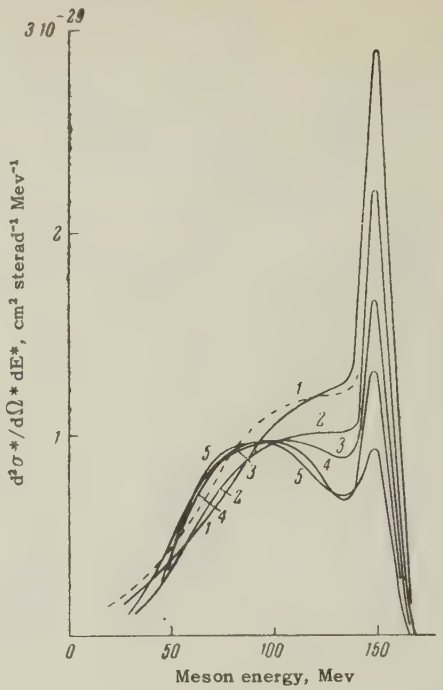

FIG. 3. Spectrum of π^+ mesons in c.m.s. at 660 Mev proton energy at the laboratory angles: 1 — 19°30, 2 — 29°, 3 — 38°, 4 — 46°, and 5 — 56°. The dotted line represents the measurements of Meshcheriakov et al.[2] at 24°.

of the maximum towards higher energies occurs in the $pp \to pn\pi^+$ reaction with decreasing angle. The maximum of spectrum 5 is obtained at about 90 Mev, while those of the spectra 1 and 2 occur at 120 to 130 Mev.

All curves in Fig. 3 are close to each other in the region below 100 Mev, so that the π^+-meson spectrum does not depend strongly on the angle below 100 Mev. It follows from Fig. 3 that the angular distribution of π^+ mesons in that region is nearly isotropic. The fact that curves 1 and 2 lie below curves 3, 4, and 5 in the 50 to 100 Mev region means that, for a π^+-meson distribution of the type $a + b\cos\vartheta^*$, the factor b should be negative in that region. Such a conclusion, however, cannot be reached on the basis of our measurements since, up to 100 Mev, the curves in Fig. 3 coincide within the limits of experimental errors.

A marked change of the spectrum shape and anisotropy of the angular distribution takes place for π^+-meson energies above 100 Mev, as can be clearly seen in Fig. 3. The fraction of anisotropically distributed π^+ mesons systematically increases with increasing meson energy, from 7% in the 100 to 110 Mev range to 25% in the 120 to 130 Mev region. We cannot trace the change of the shape of the spectrum in the $pp \to pn\pi^+$ reaction for a further increase of the π^+-meson energy, since admixture of π^+ mesons from the

$pp \rightarrow d\pi^+$ reaction becomes probable in view of instrumental limitations.

In conclusion, the authors would like to thank V. P. Dzhelepov for his interest in their work and for making the synchrocyclotron available, and to K. A. Ter-Martirosian and I. M. Kobzarev for a discussion of the results.

[1] V. M. Sidorov, J. Exptl. Theoret. Phys. (U.S.S.R.) **31**, 178 (1956), Soviet Phys. JETP **4**, 22 (1957).

[2] Meshcheriakov, Zrelov, Neganov, Vzorov, and Shabudin, J. Exptl. Theoret. Phys. (U.S.S.R.) **31**, 45 (1956), Soviet Phys. JETP **4**, 60 (1957).

[3] Meshkovskii, Pligin, Shalamov, and Shebanov, J. Exptl. Theoret. Phys. (U.S.S.R.) **31**, 560 (1956), Soviet Phys. JETP **4**, 404 (1957).

[4] B. S. Neganov and O. V. Savchenko, J. Exptl. Theoret. Phys. (U.S.S.R.) **32**, 1265 (1957), Soviet Phys. JETP **5**, 1033 (1957).

[5] M. G. Meshcheriakov and B. S. Neganov, Dokl. Akad. Nauk SSSR **100**, 677 (1955).

[6] Dzhelepov, Moskalev, and Medved', Dokl. Akad. Nauk SSSR **104**, 380 (1955).

[7] Iu. D. Prokoshkin and A. A. Tiapkin, J. Exptl. Theoret. Phys. (U.S.S.R.) **32**, 750 (1957), Soviet Phys. JETP **5**, 618 (1957).

Translated by H. Kasha
8

SOVIET PHYSICS JETP VOLUME 35 (8), NUMBER 1 JANUARY, 1959

THE DECAY SCHEME OF Mo^{99}

I. V. ESTULIN, G. M. CHERNOV, and Z. V. PASTUKHOVA

Nuclear Physics Institute, Moscow State University

Submitted to JETP editor February 27, 1958

J. Exptl. Theoret. Phys. (U.S.S.R.) **35**, 71-77 (July, 1958)

We have measured the angular correlation of the 742 — 180 kev cascade γ-rays emitted in the decay of Mo^{99}. By chemical separation of Tc^{99m} it was shown that the 1.23-Mev β-transition in Mo^{99} goes to the isomeric state in Tc^{99}, while $(7 \pm 1)\%$ of the 140 kev γ-quanta are not associated with the isomeric transition. In the discussion of the data, arguments are presented for assigning the quantum numbers $3/2^+$ to the ground state of Mo^{99}, $3/2^+$ or $5/2^+$ to the excited state of Tc^{99} at 922 kev and $7/2^+$ to the 180 kev state in Tc^{99}.

1. INTRODUCTION

THE radiation accompanying the decay of Mo^{99} has been investigated in many papers, in which the decay scheme of the isotope is also discussed. Study of the isomeric state of Tc^{99} which is produced in the decay of Mo^{99} has made it possible to assign with certainty the quantum numbers of the first two excited states of Tc^{99}, which have excitation energies of 140 and 142 kev.[1-3] A direct measurement gave $I = 9/2$ for the total angular momentum of the ground state.[4] The location of the levels in Tc^{99} at 180 and 922 kev has also been definitely established.[5-7] Different authors are in agreement on the branching ratio[1,5] for the two most intense β-transitions in Mo^{99} (with end points 0.445 and 1.23 Mev). The data of reference 8, in which a direct β-transition from Mo^{99} to the ground state of Tc^{99} was detected, are of interest. All the data enumerated above still do not enable us to make reliable assignments for various excited levels in Tc^{99} and for the ground state of Mo^{99}.

The excited state in Tc^{99} at 922 kev, which is produced in the β-decay with end point $E_\beta = 0.445$ Mev (Fig. 1), is the starting point of two γ-cascades: 742 — 180 kev and 742 — 40 — 140 kev.[7] We have measured the angular correlation for one of these cascades in order to make quantum assignments for the 180 and 922 kev levels in Tc^{99}. The results of these measurements will be presented later in the paper. We also shall consider the

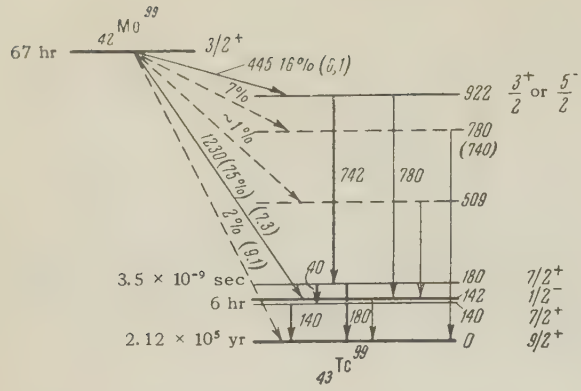

FIG. 1. Decay Scheme of Mo^{99}.

problem of determining which level in Tc^{99} is fed by the 1.23 Mev β-transition in Mo^{99}.

2. MEASUREMENT OF ANGULAR CORRELATION OF THE 742 – 180 kev CASCADE

The measurements of the angular correlation of the cascade γ-rays from Mo^{99} were done in an apparatus consisting of two scintillation counters (Fig. 2), using 20 mm thick stilbene crystals

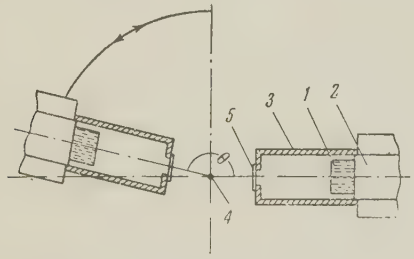

FIG. 2. Arrangement of apparatus for measurement of (γ, γ) angular correlation. 1 – stilbene crystal, 2 – FEU photomultiplier, 3 – lead case, 4 – source, 5 – lead filters in front of entrance window in the shielding.

(1 in the figure), an FEU-19 photomultiplier (2), and a coincidence circuit with a resolving time of $\tau = 3 \times 10^{-8}$ sec. The angle between the emerging γ-rays could be varied by shifting one of the counters. The crystals of the scintillation counters were covered by lead cases (3) which were 4 mm thick and had entrance windows which did not limit the solid angle subtended by the counters at the source (4). The lead shield protected the counters from the effect of scattered γ-radiation. In a control experiment with a Cs^{137} source, it was shown that there are no coincidences due to scattering from one crystal into the other for angles in the range $90° \leq \theta \leq 165°$. Such coincidences were observed for angles of 170 to 180°. We therefore limited ourselves to $\theta < 165°$ in the measurements on Mo^{99}.

The electronic equipment used in the experiment did not have amplitude discrimination, since the stilbene crystals did not permit us to separate the 140 and 180 kev γ-rays which belong to the different cascades 742-180 and 742-40-140 kev in Mo^{99}.[7] To separate the cascades we used lead filters (5 in Fig. 2) covering the entrance windows in the shielding 3. A one mm filter gave a satisfactory ratio of intensities of the 140 and 180 kev γ-lines transmitted through the filter. By measuring the number $N_{\gamma\gamma}$ of twofold coincidences as a function of filter thickness x, we determined the ratio of the contributions of the different cascades. Without filters over the entrance windows, the contribution to $N_{\gamma\gamma}$ from the 742 — 140 cascade was ~70% of that from the 742 — 180 kev cascade. With the 1 mm Pb filter used in the experiment, the contribution of the 742 — 140 kev cascade was (10 ± 5)% of that of the 742 — 180 kev cascade (the 40 kev quanta were cut out because of biasing in the amplifiers of the electronic circuit). The effect of the 742 — 140 kev cascade on the correlation function will be considered later on. The method used enabled us to take account of contributions from the different cascades without bringing in additional data on intensities I_γ and efficiencies of γ-counting ϵ_γ ($N_{\gamma\gamma}$ is proportional to $I_\gamma \epsilon_\gamma$).

The difficulty in measuring the angular correlation of the cascade γ-rays from Mo^{99} was that it constituted a small fraction of the total γ-radiation. Under such conditions it is impossible to achieve a favorable ratio of true coincidences N_t to accidentals N_a. The measurements were done with counting rates of $\sim 10^4$ pulses/sec in the channels. N_t was ~0.3 pulses/sec while $N_a \sim 1.2$ pulses/sec, i.e. $N_t/N_a \approx 1/4$.

The Mo^{99} source in the form of the metal or oxide was obtained by slow neutron irradiation of molybdenum. No differences were observed in experiments with different sources.

The coincidence measurements with the Mo^{99} source were done at angles θ equal to 90, 140 and 165°. We collected $\sim 9 \times 10^4$ true coincidences at each angle, which assured an accuracy of 1.4% in the measurements. Setting $W(\pi/2) = 1.00$, we find for $\theta = 140$ and 165 values of the correlation function $[W(\theta)/W(\pi/2)]_{exp} = 0.93 \pm 0.02$ and 0.92 ± 0.02, respectively. This result contradicts the data of Ref. 9, in which measurements of the angular correlation of the Mo^{99} cascade γ-rays gave $W(\pi)/W(\pi/2) = 1.18 \pm 0.04$. However the separate cascades were not resolved in that work. Also their coincidence circuit had a resolving time of $\tau = 2 \times 10^{-7}$ sec, which led to additional trouble in measurement of the low intensity cascade. Apparently the data of reference 9 are incorrect.

3. DISCUSSION OF RESULTS OF ANGULAR CORRELATION MEASUREMENTS

In discussing the results of the angular correlation measurements on the 742 — 180 kev cascade, we first mention some of the facts about the 180 and 922 kev levels of Tc^{99} (Fig. 1). From the 180-kev level, which has a lifetime of 3.5×10^{-9} sec,[10] radiative transitions with energies of 40 and 180 kev can occur and have approximately equal probability.[7] Data on the lifetimes of the radiative transitions, K-shell internal conversion coefficients α_K, and K-to-L ratios α_K/α_L[5-7] allow one to assert that the 40 and 180 kev γ-transitions are either M1 or E2 or a mixture M1 + E2. Consequently the 180-kev level can have the assignments $5/2^+$, $7/2^+$, $9/2^+$ or $11/2^+$. All of these values of the spin I of the 180-kev level were tried in calculating $W(\theta)$.

The 922-kev level in Tc^{99} decays mainly to the 180-kev level. Since $\beta\gamma$-coincidences are observed with the electrons from the 0.445 Mev β-transition,[7,11] the lifetime of the 922-kev level is less than 10^{-7} sec, i.e., the 742-kev transition has a multipolarity no higher than quadrupole. If the transition were octupole, the lifetime would be considerably longer, and in addition transitions with lower multipolarity should occur to the lower levels. In calculating $W(\theta)$ we therefore chose the value of I′ for the 922-kev level to satisfy the condition $|I - I'| \leq 2$, for each choice of I for the 180-kev level.

We tried 23 different sets of values of I and I′. The correlation function $W(\theta)$ was expanded in Legendre polynomials in accordance with the formulas of reference 12, which were used in the calculations. Three of the sets, sets 1, 2, 3, (cf. the table) fit the results within experimental error. The other sets give values of $W(165°)$ $W(\pi/2)$ which differ from the experimental data by more than two standard errors. The table gives the computed values of the coefficient a_2 of the polynomial P_2, and the ratio $W(\theta)/W(\pi/2)$ corrected for the contribution of the 742 — 140 kev cascade. This correction changes the ratio by no more than 1%. Uncorrected values in the table are indicated by an asterisk.

The comparatively long lifetime of the 180-kev level in Tc^{99} compels us to consider the question of possible distortions of $W(\theta)$ due to effects of atomic magnetic fields or electric quadrupole interactions, which would result in a reduction of the correlation. Only case 4 in the table gives a correlation of the same sign, but larger in magnitude, than that observed experimentally. An internal magnetic field $H \approx 5 \times 10^4$ gausses could bring case 4 into agreement with the experiment. We shall therefore include case 4 among the possible explanations of the experimental data.

So far we have listed cases of pure radiative transitions. But mixed transitions like M1 + E2 are known to occur in nuclei. It is therefore natural to consider the possibility of explaining our experimental result by such a mixed transition. We should note as a probable mixture, giving different values for the spins, case 5: $5/2\,(D)\,7/2\,(M1 + E2)\,9/2$. For the mixture of radiation with this set of spins, a_2 is determined by the equation

$$(1 + \delta^2)\, a_2 = 0.050 + 0.097\delta^2 + 0.486\delta, \qquad (1)$$

where δ^2 is the ratio of intensity of E2 to M1 radiation. Figure 3 shows the variation of a_2 with

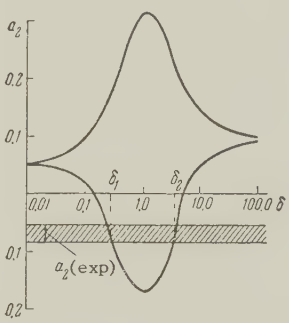

FIG. 3. Dependence of angular correlation coefficient a_2 on mixing parameter δ for the $5/2$ (D) 7/2 (M1 + E2) $9/2$ transition.

δ, taking into account a possible phase difference. The quantity a_2 varies from -0.17 to $+0.32$. The values δ_1 and δ_2 which are in agreement with the experiment determine two possible mixtures: 93% M1 and 7% E2 or 9% M1 and 91% E2, which

Correlation function $W(\theta)$

Case #	Type of transition for 922-180-0 kev	Coefficient a_2	$W(\theta)/W(\frac{\pi}{2})$ 90°	140°	165°
1	$3/2\,(D)\,5/2\,(Q)\,9/2$	−0.0714	1.00	0.95	0.91
2	$3/2\,(Q)\,7/2\,(D)\,9/2$	−0.0716	1.00	0.94	0.90
3	$7/2\,(D)\,7/2\,(D)\,9/2$	−0.0667	1.00	0.94	0.91
4	$5/2\,(Q)\,9/2\,(D)\,9/2$	−0.119	1.00	0.90*	0.84*
5	$5/2\,(D)\,7/2\,(M1 + E2)\,9/2$	$-0.17 < a_2 < +0.32$			
	Experiment	-0.07 ± 0.015	1.00	0.93 ±0.02	0.92 ±0.02

cannot be distinguished by a correlation experiment.

Of the five cases given in the table, we must select the most probable set of spins by invoking other data in addition to those from angular correlation. For this purpose, we consider the problem of assignment of quantum numbers for the Mo^{99} ground state, and the strong 1.23-Mev β-transition in Mo^{99}.

4. THE 1.23-Mev BETA-TRANSITION IN Mo^{99}

In the decay schemes of Mo^{99} which are given in two widely used handbooks,[13,14] the most intense β-transition (constituting 75% of all the β-transitions), which has an end point of 1.23 Mev, leads to the 180 kev level in Tc^{99}. Such a decay scheme for Mo^{99} is in contradiction to the data of various experimental papers.[2,7] In view of the importance of this question for the establishment of the quantum numbers of the Mo^{99} ground state, the question of the end level for the most intense β-transition was subjected to a new experimental check, the results of which are described below.

In the transition of Tc^{99} from the excited state at 180 kev (Fig. 1), 40 and 180 kev γ-quanta are radiated which bypass the isomeric state. Therefore, if 75% of the β-transitions lead to the 180 kev level, we should observe intense γ-radiation at either 40 or 180 kev. Figure 4 shows the spectrum of soft γ-radiation from Mo^{99}, measured

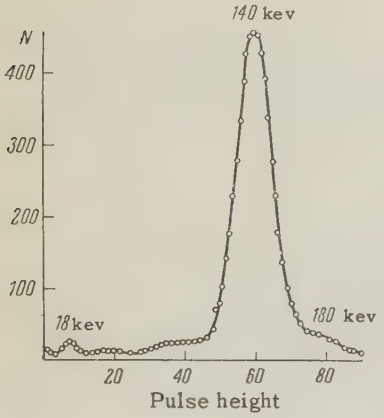

FIG. 4. Soft γ-spectrum from Mo^{99}.

with a scintillation counter having a 10 mm thick NaI (T1) crystal. As we see from the figure, the intensity of the 40 and 180 kev γ-rays is small compared to that of the 140 kev γ-radiation. The intensity of the characteristic x-rays of Tc ($\sim$ 18 kev), which are associated with internal conversion of the γ-rays in the K shell of the atom, is also small, so that taking account of possible conversion of the γ-quanta does not lead to equality of the intensities. Consequently the 1.23 Mev β-transition can lead to either the isomeric level at 142-kev or to the 140-kev level.

In a control experiment we measured the β-spectrum of Mo^{99} in coincidence with the 742-kev γ-rays and, separately, with the 140-kev γ-rays. The experiment was carried out on a coincidence apparatus consisting of two scintillation counters (a γ-counter using a NaI (T1) crystal and a β-counter with a tolane crystal) and having pulse height selection in the channels. The two β-spectra did not differ, and corresponded to the soft β-spectrum of Mo^{99}. No coincidences with the hard β-spectrum of Mo^{99} (E_β = 1.23 Mev) were observed. This experiment confirmed the data of references 2 and 7. In a direct experiment using chemical separation of Tc^{99m} it was shown that the main part of the intensity of 140-kev γ-rays is associated with the isomeric transition in Tc^{99m}.

Tc^{99m} was first separated chemically from neutron-irradiated molybdenum in reference 15. In our work the separation of Tc^{99m} was done using the extraction method proposed in reference 16, with some modifications. After neutron irradiation, MoO_3 was dissolved in a twice-molar solution of K_2CO_3, from which Tc^{99m} was separated by extraction with methylethylketone. In an auxiliary experiment, using Tc^{99m} tracer, it was determined that 99 $\pm$ 1% of the Tc^{99m} was extracted. Three samples were prepared for the physical measurements: (1) a sample of the initial Mo^{99}, (2) Mo^{99} after separation of Tc^{99m}, (3) Tc^{99m} extracted from the molybdenum. Using a scintillation counter with a NaI (T1) crystal, and a multichannel pulse-height analyzer,[17] we measured the time dependence of the intensity of the 140-kev γ-radiation. The results of one of the experiments are shown in Fig. 5. The in-

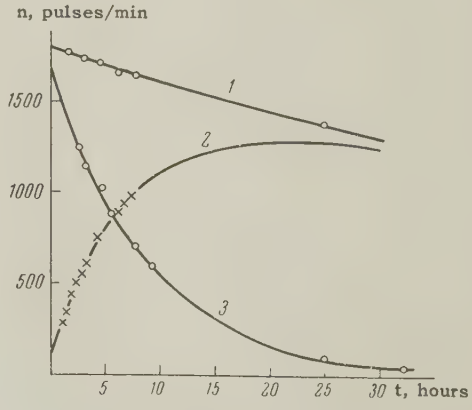

FIG. 5. Variation of intensity of 140-kev γ-rays with time t. 1 – initial Mo^{99}, 2 – Mo^{99} after separation of Tc^{99m} extracted from molybdenum.

tensity of sample 3 varied with the period of the Tc^{99m} isomer (T = 6 hours). In the Mo^{99} sample which had been freed of Tc^{99m} (Curve 2), the intensity increased with time according to the law of radioactive equilibrium (to within 1%), provided we took account of the fact that a portion of the intensity is not associated with the isomeric Tc^{99m} but is formed from Mo^{99} as a result of the 742 — 40 — 140 kev transition (Fig. 1). The magnitude of p was also computed independently from the intensity of sample 3, since the sum of the intensities from samples 2 and 3 should equal the intensity from the initial sample of Mo^{99} (Curve 1).

This experiment using chemical separation showed first that the intense β-transition leads to the isomeric state Tc^{99m}, and second that (7.5 ± 1)% of the intensity of 140-kev γ-rays is not associated with the isomeric transition but results from cascade transitions from levels with higher excitation energy. This experiment is a graphic demonstration of how quantitative chemical separation combined with absolute physical measurements can give precise spectroscopic data.

Thus the 1.23-Mev β-transition in Mo^{99} leads to the isomeric level of Tc^{99} at 142 kev (Fig. 1). This β-transition has an $f\tau$ value of 7.3 and is probably first forbidden. The ground state of Mo^{99} can therefore have the quantum numbers $5/2^+$, $3/2^+$ or $1/2^+$. With the $5/2^+$ assignment, we cannot explain the absence of an allowed transition to the 140-kev level. In addition a similar difficulty arises in explaining the absence of the β-transition to the 180-kev level. With spin $5/2$ for the ground state of Mo^{99}, we must use the set of spins of excited states of Tc^{99} which was given by case 4 of our table ($5/2$ (Q) $9/2$ (M1) $9/2$). However, this case is improbable, since it is not clear why the γ-transitions from the 922-kev level to the 140-kev level and to the ground state of Tc^{99} are absent. All of these considerations argue against the assignment of $5/2$ for the ground state of Mo^{99}.

The assignment of $1/2^+$ to the ground state of Mo^{99} does not contradict the results of the correlation measurements, but it is refuted by the data of reference 8 in which a direct β-transtion of Mo^{99} to the ground state of Tc^{99} was observed. The data of the present paper can be brought into accord with the results of reference 8 if the ground state of Mo^{99} has quantum numbers $3/2^+$. The value $3/2^+$ is among the possible values predicted by shell theory, even though it does not agree with the spins of neighboring nuclei having an odd number of neutrons in this same shell.

CONCLUSION

In the table, we gave the possible sets of total angular momenta of the 922 and 180-kev levels of Tc^{99} which are in agreement with the measured angular correlation of the 742 — 180 kev γ-cascade. As was pointed out in the preceding section, case 4 is improbable. Thus we have confirmed that the values of $[W(\theta)]_{exp}$ are not disturbed by internal fields. Case 3 is also improbable, since the assignment of $I = 7/2$ to the 922-kev level leads to difficulties in explaining the observed radiative transitions from this level (Fig. 1).

Case 1 would be probable if the ground state of Mo^{99} were $1/2^+$. With an assignment of $3/2^+$ for the Mo^{99} ground state, it is difficult in Case 1 to explain the absence of an allowed β-transition to the 180 kev level when a large number of forbidden transitions are present. Consequently the most probable schemes are those of Case 2: $3/2^+$ (E2) $7/2^+$ (M1) $9/2^+$, and Case 5, with a mixed transition ($5/2^-$ (E1) $7/2^+$ (M1 + E2) $9/2^+$), which are difficult to distinguish. In both variants the 180-kev level is definitely $7/2^+$ and the 922-kev level is tentatively assigned (as $3/2^+$ or $5/2^-$). The parity of the 922-kev level was chosen to give optimum agreement with the intensities of radiative transitions from the 922-kev level. To fix more definitely the quantum assignments of these levels of Tc^{99}, it would be desirable to determine the multipolarity of the 180 kev γ-rays by measuring their internal conversion coefficient.

In conclusion the authors thank I. S. Shapiro for discussion of the results of the paper.

[1] Medicus, Maeder and Schneider, Helv. Phys. Acta **22**, 603 (1949).

[2] Medicus, Maeder and Schneider, Helv. Phys. Acta **24**, 72 (1951).

[3] Mihelich, Goldhaber and Wilson, Phys. Rev. **82**, 972 (1951).

[4] K. G. Kessler and W. F. Meggers, Phys. Rev. **80**, 905 (1951).

[5] M. E. Bunker and R. Canada, Phys. Rev. **80**, 961 (1951).

[6] C. Levi and L. Papineau, Compt. rend. **239**, 1782 (1954).

[7] J. Varma and C. E. Mandeville, Phys. Rev. **94**, 91 (1954).

[8] Vlasov, Artem'ev, Sorokin, and Iurgenson, Тр. РИАН (Transactions, Radium Institute, Academy of Sciences, U.S.S.R.) **7**, 158 (1956).

[9] U. Cappeller and R. Klingelhöfer, Z. Physik **139**, 402 (1954).

[10] P. Lehmann and K. Miller, Compt. rend. **240**, 1525 (1955).
[11] C. E. Mandeville and M. V. Scherb, Phys. Rev. **73**, 848 (1948).
[12] Biedenharn, Blatt and Rose, Revs. Mod. Phys. **25**, 249 (1952).
[13] Hollander, Perlman and Seaborg, Revs. Mod. Phys. **25**, 469 (1953).
[14] B. S. Dzhelepov and L. K. Peker Схемы распада радиоактивных изотопов (Decay Schemes of Radioactive Isotopes), Academy of Sciences Press, 1957.
[15] C. Perrier and E. Segre, J. Chim. Phys. **5**, 712 (1937).
[16] Iu. B. Gerlit, International conference on peaceful uses of atomic energy, Geneva, 1955; Vol. 7, p. 671.
[17] Sanin, Melioranskii and Lotova, Вестник МГУ (Bulletin, Moscow State University) **12**, 87 (1955).

Translated by M. Hamermesh
9

SOVIET PHYSICS JETP VOLUME 35 (8), NUMBER 1 JANUARY, 1959

MEASUREMENT OF THE TOTAL CHARGED π MESON PRODUCTION CROSS SECTION IN NEUTRON-PROTON COLLISIONS AT 586 Mev NEUTRON ENERGY

Iu. M. KAZARINOV and Iu. N. SIMONOV

Joint Institute for Nuclear Research and Laboratory of Nuclear Problems

Submitted to JETP editor February 27, 1958

J. Exptl. Theoret. Phys. (U.S.S.R.) **35**, 78-84 (July, 1958)

The total yield of charged π mesons, produced in collisions between neutrons of 586 Mev effective energy and protons, was measured at angles in the range from 15 to 120° (in the laboratory system). Assuming charge independence of nuclear forces, the total cross-section for the production of π^+ and π^- mesons, derived from the experimental data, was found to be $\sigma(np \to \pi^+) = \sigma(np \to \pi^-) = (2.0 \pm 0.5) \times 10^{-27}$ cm^2.

THE process of production of charged π mesons in neutron-proton collisions has not, so far, been studied extensively. Comprehensive investigations were carried out only for 409 Mev neutrons. One experiment only was carried out at an energy close to 600 Mev.[2] The spectra and yields of π^+ and π^- mesons, emitted at the angle $\Phi = 90°$ in the laboratory system* (l.s.) from a target containing liquid hydrogen bombarded by neutrons originating in the charge exchange of 670-Mev protons, were measured in that work in relative units, using nuclear emulsions. The relatively small cross section for meson production, the fact that three particles are present in the final stage of the reactions studied, and also the fact that the neutron beam used is not monoenergetic, all contribute to the difficulties of experiments on π^+- and π^--meson production in n—p collisions. On the other hand, a detailed study of n—p collisions at energies considerably larger than the meson production threshold necessitates an investigation of these processes. The study of the process of meson production in n—p collisions is also of interest for understanding the character of the interaction between two nucleons with different isotropic spin ($T = 0$ and $T = 1$).

THE EXPERIMENT

The measurements were carried out with the synchrocyclotron of the Joint Institute for Nuclear Research. The neutron beam used in the experiments was obtained by charge-exchange scattering of 680-Mev protons on a Be target. The energy distribution of the neutrons in the beam had a maximum at 600 Mev and a half-width of 130 Mev.[3]

To determine the differential cross-section for charged π-meson production in n—p collisions,

*The angle Φ was measured with respect to the direction of the incident neutron beam.

we measured the ratio of the total number of π^+ and π^- mesons N_π to the number of recoil protons N_p, emitted from the scattering medium at a given angle Φ to the direction of the neutron beam. The differential π-meson production cross-section was then obtained from the determined ratio N_π/N_p and from the differential cross section for elastic $n-p$ scattering, measured earlier by the authors.[4]

To measure the π-meson yield, polyethylene and graphite were used as scattering media and were placed alternately in the neutron beam. The charged particles emitted from the scatterer were recorded by a detector. The difference between the number of particles scattered by polyethyelene and graphite, as recorded by the detector, gives the total flux of charged particles emitted from the scatterer as the result of $n-p$ collisions. Estimates have shown that, for a given neutron energy, this flux is determined essentially by the number of recoil protons and π mesons incident upon the detector. It was found that, in the conditions of the experiment, the number of μ mesons and β particles produced in π-meson decay amounted to less than 10 or 15% of the number of π mesons. This made it possible to neglect the admixture of μ mesons and β particles and to assume, in first approximation, that all particles, other than recoil protons, were π mesons. The necessary corrections were introduced later into the results of the measurements.

The π mesons and recoil protons were identified either by their range or velocity. The range method was used in the region of angles of π-meson emission $\Phi \geq 60°$. For angles $60° < \Phi < 15°$, π mesons were separated, using the velocity method, by means of a Cerenkov detector.

Two types of detectors were used in connection with the two methods of π-meson separation (Table I). A telescope consisting of three scintillation counters, connected in coincidence, was used at large angles, $\Phi \geq 60°$. Estimates based on the results of reference 2 have shown that if the threshold of such a detector is raised, by means of a suitable absorber, to the level of the maximum energy of recoil protons at a given angle Φ, then, in the range $\Phi \geq 60°$, the majority of π mesons is detected.

Velocity selection was used in measurements of the yield of charged mesons at angles $\Phi < 60°$. For this purpose, the middle counter of the telescope was replaced by a Cerenkov detector (Fig. 1), while the other two scintillation counters remained in place. For the determination of the total yield of charged particles, it was necessary to replace

TABLE I

Emission angle of π mesons (l.s.)	Energy threshold of the detector for π mesons (Mev)	Detector
15°	78.0	Cerenkov counter (water) and two scintillation counters (coincidence)
30°	78.0	
45°	78.5	Cerenkov counter (plexiglass) and two scintallation counters (coincidence)
60°	65	
90°	37	Three scintillation counters (coincidence)
120°	37	

again the exchanged scintillation detector. To preserve counter geometry in the exchange, and to effect the exchange quickly, both types of detectors used the same photomultiplier FEU-19M and the scintillator was placed in front of the photocathode directly behind the radiator of the Cerenkov detector. At the angle $\Phi = 15°$, recoil

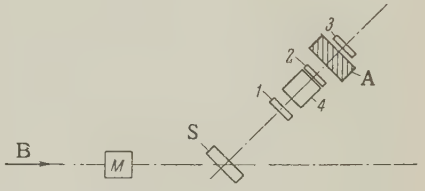

FIG. 1. Schematic diagram of the experiment. n – neutron beam, M – monitor (ionization chamber), 1, 2, 3 – scintillation counters, 4 – radiator of the Cerenkov counter, A – absorber, S – scattering medium.

protons could be detected by the Cerenkov detector. A correction was applied for that case to the results, to account for the fraction of protons recorded. The angular definition of the detector, determined by its geometry, was 3°. Energy thresholds of the detector at different angles are given in Table I.

Polyethyelene and graphite disks of equal stopping power were used as scatterers. The polyethelene disc was 0.9 g/cm^2 thick for angles $\Phi \geq 45°$ and 3.2 g/cm^2 for $\Phi < 45°$. Copper and tungsten plates were used as absorbers.

The measurements were carried out as follows: First, the total flux charged particles incident upon the detector as the result of $n-p$ collisions was determined, for a given beam intensity, under the conditions of the measurement of the differential cross sections for elastic $n-p$ scattering.[4] The usual $CH_2 - C$ difference experiment was carried out for that purpose. The detector was then set to record recoil protons and the total yield of π mesons was measured. This was

TABLE II

Angle Φ°	15°	30°	45°	60°	90°	120°
Correction for admixture of μ mesons and electrons	0.9	0.9	0.9	0.92	0.90	0.88
Correction for admixture of protons	0.15					
Correction for π mesons with energy below detector threshold					1.25	1.95
Correction for detection efficiency	1.21	1.21	1.20			
Correction for $\pi-\mu$ decay	1.03	1.03	1.03	1.04	1.06	1.10
N_π/N_p %	8.6±3.5	19±2.3	13.7±2.7	9.7±0.5	4. *±1.3	4.3 ±0.9

*The π meson yield is expressed in terms of the yield of recoil protons at $\Phi = 60°$.

done, as mentioned above, either by increasing the telescope threshold up to the maximum energy of recoil protons (for angles $\Phi > 60°$), or by exchanging one of the scintillation counters for the Cerenkov detector. Special attention was given to the measurements of the background in determination of the π-meson yield at the angles Φ = 15, 30, and 45°. In this case it was found necessary to measure, apart from the usual chance and true coincidence rate, also the background due to the fact that the detector recorded a considerable fraction of recoil proton incident directly upon the photocathode of the photomultiplier tube in the Cerenkov detector. The total background amounted to less than 5% at 60°, and increased to 20% of the number of mesons incident upon the detector from the polyethyelene scatterer at 15°.

The stability of the neutron beam intensity during the measurements was measured by means of an ionization chamber placed in the beam and connected to an integrating circuit.

RESULTS AND REDUCTION OF DATA

Determination of the Total Cross Section. The following corrections had to be applied to the results before the latter could be used for the determination of the total cross section for π-meson production.

1. Correction for the admixture of μ mesons and electrons. As mentioned above, a small amount of μ mesons and electrons was present, besides protons and π mesons, among the particles incident upon the detector. The number of electrons detected was calculated according to the data of reference 5, assuming that the angular distribution of π^0 mesons in the c.m.s. is given by the expression $0.2 + \cos^2 \vartheta$. It was also taken into account that ~1.5% of the π^0 mesons decay according to another scheme. The fraction of the μ mesons was calculated from the known yield of π mesons and the calculated angular distribution of μ mesons.

2. Correction for the admixture of protons. This correction was applied only for the 15° angle, where a considerable fraction of recoil protons could be detected by the Cerenkov detector. The correction was determined from the known neutron spectrum, and the measured dependence of the Cerenkov detector efficiency on the particle velocity (Fig. 2).

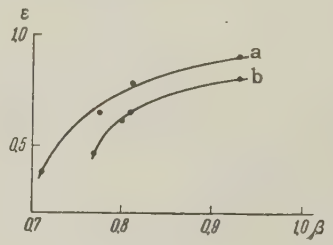

FIG. 2. Dependence of the Cerenkov-counter efficiency ε on the velocity of detected particles β. a – plexiglass, b – water.

3. Corrections for the presence of particles with energy below the detector threshold in the π-meson spectrum. These corrections were found from the π-meson spectrum calculated according to the data of reference 2 under the assumption the π-meson spectrum in c.m.s. is independent of the angle of emission. The calculated correction factors are given in the third column of Table II. These coefficients were also recalculated under the assumption that the π-meson spectra of the reactions $p + p \rightarrow \pi^+ + n + p$, $n + p \rightarrow \pi^+ + 2n$, $n + p \rightarrow \pi^- + 2p$ are identical.*

The values obtained were practically identical with those given in Table II.

4. Corrections for detector efficiency. These were necessary because of the different absorption of π mesons and protons in the detector absorbers and the properties of the Cerenkov detector. The corrections were determined experimentally on

*Evidently, this is the case at energies much higher than the threshold of meson productions. (cf., e.g., reference 6).

π-meson and proton beams of corresponding average energy.

5. Corrections for the $\pi - \mu$ decay. Correction factors were calculated from the known half-life of π mesons, accounting for the π meson spectrum cutoff (cf. point 3).

Strictly speaking, in reducing the data it would be necessary to account for the error due to the fact that the absorption of π^+ and π^- mesons in media is slightly different. An estimate based on the results of reference 7 indicates, however, that the error involved is small in the conditions of the experiment and can be neglected.

The corrected results yield, after integrating over the angles, the following value for the total production cross section of π^+ and π^- mesons in n – p collisions, under the assumption of charge independence of nuclear forces:

$$\sigma(np \to \pi^+) = \sigma(np \to \pi^-) = (2.0 \pm 0.5) \cdot 10^{-27} \text{ cm}^2.$$

The total cross sections for the studied reactions can be also determined from the π-meson yield found for the so-called "isotropic angle," i.e. the angle, for which the following relation holds between the differential cross-section $\sigma_\pi(\vartheta)$ and the total cross-section:

$$\sigma_\pi(\vartheta_i) = (1/4\pi)\,\sigma(np \to \pi).$$

The "isotropic" angle ϑ_i can be easily found in our case, considering that the obtained angular distribution of π mesons in the c.m.s. does not contain terms higher than $\cos^2\vartheta$, and can be written in the form

$$\sigma_{\pi^+}(\vartheta) + \sigma_{\pi^-}(\vartheta) = a + b\cos^2\vartheta,$$

where ϑ is the meson emission angle, and a and b are constants. As it is well known, $\vartheta_i = \cos^{-1} \times (1/\sqrt{3})$ and corresponds, in our case, to the angle $\Phi = 30°$ (l.s.). Using the value of N_π/N_p given for that angle in Table II, we find that the cross section is equal to

$$\sigma(np \to \pi^+) = \sigma(np \to \pi^-) = (1.7 \pm 0.4) \cdot 10^{-27} \text{ cm}^2.$$

The obtained values of the cross-section are very close to each other. This fact indicates, probably, that the assumptions made in reducing the data have not distorted seriously the angular distribution.

Determination of the Effective Energy. In the method used, the detector recorded π mesons produced in the collisions of particles, the energy of which varied in a very wide range, from 300 to 670 Mev. It was therefore especially important to determine the mean effective energy E_{eff}. This was done by finding the dependence of E_{eff} on the excitation function of the studied reaction for a given shape of the neutron-energy spectrum. The excitation function was taken as

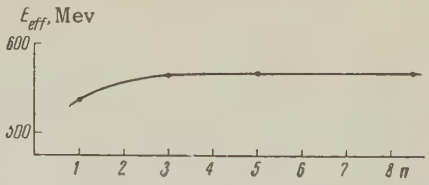

FIG. 3. Dependence of the effective neutron energy on the power exponent of the maximum π-meson momentum in Eq. (1).

$$\sigma(np \to \pi^+) \sim \eta^n_{\max}, \quad (1)$$

where η_{max} is the maximum π-meson momentum in the c.m.s. It was found that, under the given conditions, the mean effective energy is practically constant for power exponent $n \geq 3$ in Eq. (1) and does not depend on n (Fig. 3). Taking this into account, we find from the known value of $\sigma(np \to \pi^+)$ at 409 Mev that, for our case, $E_{eff} = (586 \pm 15)$ Mev.

DISCUSSION OF RESULTS

A comparison of the obtained value $\sigma(np \to \pi^+) = (2.0 \pm 0.5) \times 10^{-27}$ cm^2 with the cross-section at 409 Mev, $\sigma(mp \to \pi^+) = (0.16 \pm 0.04) \times 10^{-27}$ cm^2 (reference 1) shows that the total cross section for π^+- and π^--meson production in n – p collisions increases by more than a factor of ten for the energy increase from 409 to 586 Mev. The dependence of the cross section on the maximum π-meson momentum η_{max} can be written in the form

$$\sigma(np \to \pi^+) \sim \eta^{4.7 \pm 0.8}_{\max}.$$

This relation is in a satisfactory agreement with the relation $\sigma(pn \to \pi^+) \sim \eta^{4\pm1}_{max}$ given in reference 10, which was obtained from values of the cross section calculated for a wide energy region on the basis of the known cross-sections $\sigma(pp \to \pi^0)$, $\sigma(pp \to \pi^+)$, and $\sigma(pn \to \pi^0)$, assuming charge independence of the nuclear forces. It should be noted, however, that the authors of reference 10 give a slightly lower value for the cross-section $\sigma(pn \to \pi^+)$ at 580 Mev, equal to $(10.8 \pm 1.1) \times 10^{-27}$ cm^2. This nevertheless, is within the limit of the errors and does not contradict the value obtained in the present work.

The value found is also in a good agreement with the predictions of the isotopic invariance hypothesis, according to which we should have

$$\sigma(np \to \pi^+) = \sigma(np \to \pi^0) + \sigma(pp \to \pi^0) - {}^1/_2\sigma(pp \to \pi^+). \quad (2)$$

If we put $\sigma(np \to \pi^0) = (5.7 \pm 1.5) \times 10^{-27}$ cm^2,[5]

$\sigma(pp \to \pi^0) = (1.6 \pm 0.2) \times 10^{-27}$ cm^2,[10] and $\sigma(pp \to \pi^+) = (8.5 \pm 0.7) \times 10^{-27}$ cm^2,[11] we find that $(np \to \pi^+) = (3.1 \pm 1.6) \times 10^{-27}$ cm^2, which coincides with the measured value within the limits of accuracy.

It is well known that, according to the charge independence hypothesis, the cross sections for all π-meson production processes in nucleon-nucleon collisions can be expressed by means of three partial cross-sections σ_{10}, σ_{11}, σ_{01}.* The cross-sections σ_{11} and σ_{10} were investigated in Ref. 10 for a wide energy region. The value $\sigma(np \to \pi^+)$ found made it possible to determine σ_{01} at 586 Mev; we have $\sigma_{01} = 2\sigma(np \to \pi^+) - \sigma_{11} = (2.4 \pm 0.9) \times 10^{-27}$ cm^2. It is known, furthermore,[10] that $\sigma_{01} = (0.23 \pm 0.09) \times 10^{-27}$ cm^2 at 409 Mev. The value of σ_{01} increases therefore sharply with the energy and the dependence of σ_{01} on the maximum meson momentum can be written in the form:

$$\sigma_{01} \sim \eta_{\max}^{4.4 \pm 1.0}.$$

The total cross-section for π-meson production in $n-p$ collisions at 586 — 590 Mev is $\sigma(np \to \pi^{+0}) = (np \to \pi^0) + 2\sigma(np \to \pi^+) = (9.7 \pm 1.8) \times 10^{-27}$ cm^2. The total cross-section for the $n-p$ interaction is $(36 \pm 2) \times 10^{-27}$ cm^2. About 30% of the $n-p$ collision events is, therefore, accompanied by the production of a π meson.

In conclusion, we shall compare the probabilities of π-meson production in the collisions of two nucleons with different isotopic spin, using our result and those of references 5, 10, and 11. It can be shown[12] that the total cross-section for π-meson production in $n-p$ collisions $\sigma(np \to \pi^{\pm,0})$ can be written in the form

$$2\sigma(np \to \pi^{\pm,0}) = \sigma_\pi^1 + \sigma_\pi^0, \qquad (3)$$

where σ_π^1 and σ_π^0 are the cross-sections for π-meson production in collisions of two nucleons in the states with isotopic spin $T = 1$ and $T = 0$ respectively. On the basis of the values given above we have

$$\sigma_\pi^1 = \sigma(pp \to \pi^0) + \sigma(pp \to \pi^+) = (10.1 \pm 0.73) \cdot 10^{-27} \text{ cm}^2;$$

$$\sigma(np \to \pi^{\pm,0}) = 2\sigma(np \to \pi^+) + \sigma(np \to \pi^0)$$

$$= (9.7 \pm 1.8) \cdot 10^{-27} \text{ cm}^2,$$

and Eq. (3) yields

$$\sigma_\pi^0 = (9.3 \pm 3.7) \cdot 10^{-27} \text{ cm}^2.$$

The probabilities of π-meson production in interactions of nucleons in the states $T = 0$ and $T = 1$ are thus comparable, and the nucleons in these states interact with equal intensity.

The approximate equality of σ_π^0 and σ_π^1 indicates also that in the processes studied, at approximately 600 Mev, the transitions which result in the π-meson-nucleon system having total isotopic spins $T = 3/2$ and $T = 1/2$ have approximately the same probability. This is, evidently, the chief reason for the fact that the ratio $\sigma(pp \to \pi^+)/\sigma(mp \to \pi^+)$, equal in our case to 3.9 ± 1, is considerably less than ten. The latter value was predicted in reference 12 from the principle of isotopic invariance under the assumption that the π meson-nucleon system is always in the $T = 3/2$ state. It should be noted, however, that the value of the ratio given in reference 12 was obtained under simplifying assumptions and may, in reality, be somewhat different.

The authors would like to thank L. I. Lapidus for a discussion of the results and N. S. Amaglobeli for his help in carrying out the experiments.

*The indices refer to the total isotopic spin of the system of two nucleons in the initial and final states (before and after meson production).

[1] G. B. Yodh, Phys. Rev. **98**, 1330 (1955).

[2] V. M. Sidorov, J. Exptl. Theoret. Phys. (U.S.S.R.) **28**, 727 (1955), Soviet Phys. JETP **1**, 600 (1955).

[3] V. S. Kiselev and B. V. Fliagin, J. Exptl. Theoret. Phys. (U.S.S.R.) **32**, 962 (1957), Soviet Phys. JETP **5**, 786 (1957).

[4] Iu. M. Kazarinov and Iu. N. Simonov, J. Exptl. Theoret. Phys. (U.S.S.R.) **31**, 169 (1956), Soviet Phys. JETP **4**, 161 (1957).

[5] Dzhelepov, Oganesian, and Fliagin, J. Exptl. Theoret. Phys. (U.S.S.R.) **29**, 886 (1955), Soviet Phys. JETP **2**, 757 (1956).

[6] L. C. L. Yuan and S. J. Lindenbaum, Phys. Rev. **103**, 404 (1956).

[7] R. M. Sternheimer, Phys. Rev. **101**, 384 (1956).

[8] A. A. Tiapkin, J. Exptl. Theoret. Phys. (U.S.S.R.) **30**, 1150 (1956), Soviet Phys. JETP **3**, 797 (1956); Iu. D. Prokoshkin, J. Exptl. Theoret. Phys. (U.S.S.R.) **31**, 732 (1956), Soviet Phys. JETP **4**, 618 (1957).

[9] A. Rosenfeld, Phys. Rev. **96**, 146 (1954).

[10] Iu. D. Prokoshkin, and A. A. Tiapkin, J. Exptl. Theoret. Phys. (U.S.S.R.) **32**, 750 (1957), Soviet Phys. JETP **5**, 618 (1957).

[11] A. G. Meshcheriakov and B. S. Neganov, Dokl. Akad. Nauk SSSR **100**, 677 (1955); B. S. Neganov and O. V. Savchenko, J. Exptl. Theoret. Phys. (U.S.S.R.) **32**, 1265 (1957), Soviet Phys. JETP **5**, 1033 (1957).

[12] L. I. Lapidus, J. Exptl. Theoret. Phys. (U.S.S.R.) **31**, 865 (1956), Soviet Phys. JETP **4**, 740 (1957); D. C. Peaslee, Phys. Rev. **92**, 1085 (1954).

Translated by H. Kasha
10

HALL EFFECT IN PURE NICKEL AT HELIUM TEMPERATURES

N. V. VOLKENSHTEIN, G. V. FEDOROV, and S. V. VONSOVSKII

Institute of Metal Physics, Ural' Branch, Academy of Sciences, U.S.S.R.

Submitted to JETP editor February 11, 1958

J. Exptl. Theoret. Phys. (U.S.S.R.) **35**, 85-88 (July, 1958)

Experimental data are presented on the Hall effect in pure nickel (99.99%) in a wide temperature range down to the temperature of liquid helium. It is shown that the ferromagnetic constant R_1 drops sharply with the temperature T and has a minimum at 20 to 30°K. A physical interpretation, based on the (s-d)-exchange model, is proposed for the observed phenomenon.

A study of the Hall effect in ferromagnets discloses a sharp temperature dependence of the so-called extraordinary Hall constant R_1, determined from the experimental relation proposed in reference 1:

$$e = R_0 H + R_1 J, \qquad (1)$$

where e is the Hall field per unit current density, J the magnetization, H the magnetic field, and R_0 the ordinary Hall constant. The first data on the dependence of R_1 on the temperature T were obtained by Kikoin[2] for nickel for T ranging from room temperature to the Curie point Θ. It was observed there that R_1 increases as T rises to Θ and diminishes sharply as it passes through Θ, evidencing the ferromagnetic nature of R_1. Jan and Gijsman[3] measured R_0 and R_1 in nickel and in iron for T ranging from room temperature to that of hydrogen and observed that R_1 has a smeared minimum for nickel at 30 to 50°K and for iron at 50 to 70°K. Above these regions, R_1 drops sharply with diminishing T (thus, R_1 in nickel diminishes to $\frac{1}{20}$ its value from T = 300°K to T = 14°K). These data[3] are criticized in reference 4, whose authors state that the minimum of R_1 with temperature is in contradiction with general theoretical considerations. Most workers have believed that the ordinary constant R_0 is connected only with the concentration of the current carriers and should not change noticeably with T. Experimental data,[3,5] however, are not in agreement with these considerations. For the extraordinary constant R_1, the following theoretical relation was obtained in reference 6

$$R_1 = A\rho^2, \qquad (2)$$

where ρ is the specific resistivity and A is a constant. However, an experimental verification of (2), made by Jan,[2] gave for nickel, in the temperature range from that of nitrogen to Θ, not 2, but 1.94 as the exponent of ρ, and for iron the exponent was even 1.42. In connection with this, a hypothesis was proposed[4] that there exist two ferromagnetic effects, one obeying Eq. (2) and another that varies linearly with ρ, i.e., $R_1 = A_1\rho + A_2\rho^2$.

In view of the above, there is undoubted interest in measuring simultaneously the Hall effect and ρ in as large a temperature interval as possible, down to the lowest temperatures (helium), using the purest ferromagnetic materials possible. For this purpose we undertook to measure these quantities in pure nickel in the range from room temperature to that of liquid helium (4.2°K). The measured specimens were made of pure nickel (99.99%) with residual electric resistivity $\rho_{20.4°}/\rho_{293°} = 12.36 \times 10^{-3}$, and $\rho_{4.2°}/\rho_{293°} = 10.28 \times 10^{-3}$. The Hall voltage was measured in 9×4×0.3 mm plates using a procedure previously described,[8] which made it possible to obtain an induction B up to 22,000 gausses in the specimen with an electromagnet of magnetic field intensity of 5,000 oersteds. The potentiometric-setup sensitivity was 2×10^{-8} volts. The measurements were performed at room temperature, at 0°C, and in baths of liquid nitrogen, hydrogen, and helium. The specimen temperature was assumed equal to the normal boiling point of the liquid bath. The constants R_0 and R_1 were determined from the slope of the curve e = f(B) in the initial portion and after saturation, using the method proposed in reference 9. The measurement results are given in Figs. 1 and 2, from which it is seen that R_1 diminishes sharply with diminishing T and has a minimum at 20 to 30° [R_1(T = 300°K) ~ 100×10^{-12} v-cm/amp-gauss, R_1(T = 14°K) ~ 5×10^{-12} v-cm/amp-gauss]. The constant R_0 diminishes from 300° to 4.2°K to approximately $\frac{1}{3}$ (from 0.6 to 0.2×10^{-12} v-cm/amp-gauss),

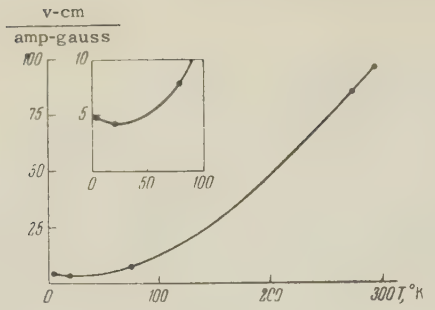

FIG. 1

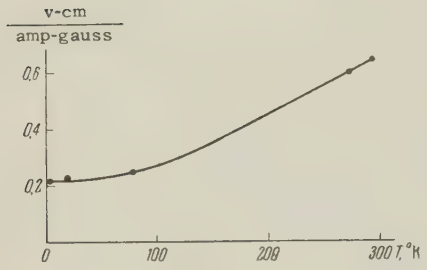

FIG. 2

and has no minimum. The observed increase in R_1 near the helium temperature raises doubts concerning the universal nature of relations of type (2), at least for a wide range of T. This is seen particularly clearly from Fig. 3, where (on

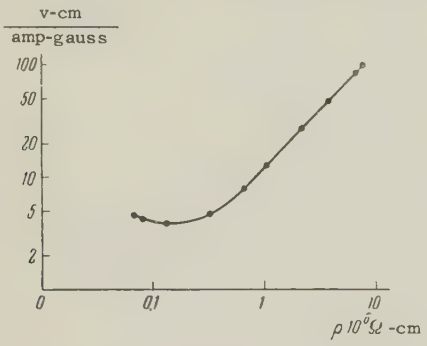

FIG. 3

a logarithmic scale) is shown the connection between R_1 and ρ as obtained in our measurements. The linear relation is retained up to the liquid-nitrogen temperature, where the exponent in the right half of (2) is 1.02. It must be noted that in references 3 and 7 this index is close to 2 only in the temperature region from Θ to room temperature. Farther down, to $T \sim 100°K$ it is closer to unity, and at still lower temperatures $\log R_1$ and $\log \rho$ are no longer linearly related. It is peculiar $\log R_1$ is linear relative to $\log \rho$ only as long as the quantity proportional to the carrier mobility (calculated from the $R_0\sigma$ formula) changes little with temperature (see Fig. 4), and ceases to be linear where the latter increases rapidly.

Attempting to understand the physical nature of the observed laws, we note that Vonsovskii et al.,[10] on the basis of sufficiently general semi-phenomenological considerations, obtained an ex-

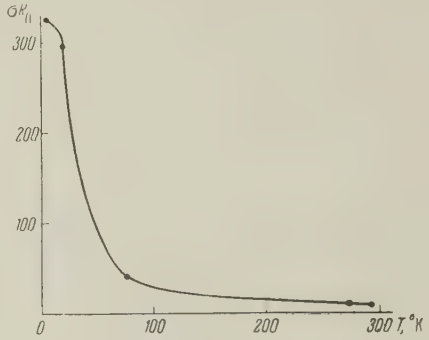

FIG. 4

pression for the electric-conductivity tensor, and the anti-symmetrical portion of its inverse value gives the Hall-constant tensor. For temperatures close to the Curie point we have*

$$R^0_{\alpha\beta\gamma} = T\,[S^{(1)}_{\alpha\gamma} + \bar{m}^2 S^{(2)}_{\alpha\gamma}]; \quad R^1_{\alpha\beta\gamma} = T\,[S^{(3)}_{\alpha\gamma} + \bar{m}^2 S^{(4)}_{\alpha\gamma}]\,4\pi\bar{a}_{\beta\gamma}{}^{1}. \tag{3}$$

Here $S^{(i)}_{\alpha\gamma}$ ($i = 1, 2, 3, 4$) are tensors that depend on T and on the limiting quasi-momentum of the conduction electron, $\bar{a}_{\beta\gamma}$ is the parameter of the internal magnetic (spin-orbit etc.) interaction, and $\bar{m}$ is the relative value of the spontaneous magnetization. From comparison with the variation of ρ of a ferromagnet below Θ,[11] it can be assumed that the signs of $S^{(1)}_{\alpha\gamma}$ and $S^{(3)}_{\alpha\gamma}$, on the one hand, and of $S^{(2)}_{\alpha\gamma}$ and $S^{(4)}_{\alpha\gamma}$, on the other, are opposite. Therefore, as T diminishes, the values of $R^0_{\alpha\beta\gamma}$ and $R^1_{\alpha\beta\gamma}$ should diminish.† This can be shown also from thermodynamic considerations.[12,13] The thermodynamic potential of the metal of the ferromagnet at values of T close to Θ can be approximately represented in the form of a sum of two terms [14]: $\Phi_1(\bar{s})$, which is the potential of the conduction electrons, and depends on their average $\bar{s}$, and $\Phi_2(\bar{s}, \bar{m})$, which is the ferromagnetism potential, which depends on $\bar{s}$ and $\bar{m}$ in addition to the usual quantities (T, pressure). Above Θ, the equilibrium conditions are

*From the most general considerations (within the framework of the s-d exchange model) it is possible to assume that (R_1/R_0) is of the same order of magnitude as (θ/θ_d), where θ_d is the temperature of degeneracy of the Fermi carrier quasi-particles. We then get $R_1/R_0 \sim 10$,[2] as experimentally observed.

†It is significant that, according to reference 3 and our measurements, the quantity $R^0_{\alpha\beta\gamma}$ in ferromagnets also depends on $\bar{m}$ and, consequently should have a different dependence on T than in nonferromagnetic materials.

$$\Phi_1'(\bar{s}_0) = 0, \quad \Phi_1''(\bar{s}_0) > 0,$$

and below Θ

$$\Phi_1'(\bar{s}) + \Phi_2'(\bar{s}, \bar{m}) = 0.$$

If one takes into account that near Θ the number $\bar{s}$ differs little from its equilibrium value $\bar{s}_0$, we have

$$\Delta\bar{s} = \bar{s} - \bar{s}_0 = -\Phi_2'(\bar{s}, \bar{m}) / \Phi_1''(\bar{s}_0).$$

Since in the first approximation[14] we have $\Phi_2(\bar{s}, \bar{m}) \sim \alpha(n - \bar{s})\bar{m}^2$, where n is the total concentration of the conduction electrons and of the ferromagnetism electrons, and $\alpha > 0$, then $\Phi_2'(\bar{s}, \bar{m}) = -\alpha\bar{m}^2$, and we have thus $\Delta\bar{s} > 0$. From theory it is known that $R \sim 1/\bar{s}e$, where $\bar{s} \approx \bar{s}_0 + \Delta\bar{s}$. Consequently,

$$R \sim \frac{1}{(\bar{s}_0 + \Delta\bar{s})e} \sim \frac{1}{\bar{s}_0 e}\left(1 - \frac{\Delta\bar{s}}{\bar{s}_0}\right) \quad (\gamma > 0).$$

If follows therefore that R diminishes with diminishing T. The same conclusion was reached also by Patrakhin[15] in his calculation of R_1 within the framework of the s-d exchange model of ferromagnetism.[16] Thus, it is possible to assume that the mechanism of the appearance of the constant R_1 and its temperature dependence near the point Θ is qualitatively understood. However, the form of the function $R_1(T)$ in the region near very low temperature, and, in particular, the occurrence of a minimum of $R_1(T)$, still remain unexplained. One can merely state that the conclusions of references 6 and 4 concerning a simple connection between R_1 and ρ do not correspond to reality, at least in the region of low temperatures. The function $R_1(T)$ and its connection with ρ can be understood only on the basis of a more rigorous s-d exchange theory, in which account is taken of the presence of two branches of the energy spectrum of the electronic system (ferromagnetic and that of the conduction electrons), and in which account is also taken of the collision processes between the carriers and the elementary excitation of the lattice vibrations (phonons) and the spin field of the ferromagnet (ferromagnons) in the presence of a magnetic interaction. The different temperature dependence of the relaxation time for these collision processes (see, for example, reference 17) can lead to a complicated temperature behavior of $R_1(T)$ at low temperatures.

For a further refinement of the data on the Hall effect in ferromagnets, we have undertaken more detailed theoretical analysis and experimental investigations of the temperature behavior of this phenomenon.

[1] E. M. Pugh, Phys. Rev. **36**, 1503 (1930).

[2] A. K. Kikoin, Sow. Phys. **9**, 1 (1936).

[3] J. P. Jan and H. M. Gijsman, Physica **18**, 339 (1952).

[4] N. S. Akulov and A. V. Cheremushkina, J. Exptl. Theoret. Phys. (U.S.S.R.) **31**, 152 (1956), Soviet Phys. JETP **4**, 150 (1957).

[5] F. E. Allison and E. M. Pugh, Phys. Rev. **107**, 103 (1957).

[6] R. Karplus and J. M. Luttinger, Phys. Rev. **95**, 1154 (1954).

[7] J. P. Jan, Helv. Phys. Acta **25**, 677 (1952).

[8] N. V. Volkenshtein and G. V. Fedorov, Физика металлов и металловедение (Phys. of Metals and Metal Research) **2**, 377 (1956).

[9] S. Foner, Phys. Rev. **88**, 955 (1956).

[10] Vonsovskii, Kobelev, and Rodionov, Izv. Akad. Nauk SSSR, Ser. Fiz. **16**, 569 (1952).

[11] W. Gerlach and K. Schneiderhan, Ann. Physki, **6**, 772 (1930). H.Potter, Proc. Roy. Soc. **132**, 560 (1931); **149**, 671 (1937).

[12] S. V. Vonsovskii, Izv. Akad. Nauk SSSR, Ser. Fiz. **11**, 617 (1947).

[13] S. V. Vonsovskii, Современное учение о магнетизме (Modern Theories of Magnetism), M—L, 1953, §17.

[14] S. V. Vonsovskii, Izv. Akad. Nauk SSSR, Ser. Fiz. **11**, 485 (1947).

[15] N. P. Patrakhin, Izv. Akad. Nauk SSSR, Ser. Fiz. **16**, 604 (1952).

[16] S. V. Vonsovskii, J. Exptl. Theoret. Phys. (U.S.S.R.) **16**, 981 (1946).

[17] E. A. Turov, Izv. Akad. Nauk SSSR, Ser. Fiz. **19**, 462 (1955), [Columbia Techn. Translations **19**, 414 (1955)].

Translated by J. G. Adashko
11

INVESTIGATION OF THE $p + p \rightarrow d + \pi^+$ REACTION WITH A POLARIZED PROTON BEAM

Iu. K. AKIMOV, O. V. SAVCHENKO, and L. M. SOROKO

Joint Institute for Nuclear Research

Submitted to JETP editor March 29, 1958

J. Exptl. Theoret. Phys. (U.S.S.R.) **35**, 89-96 (July, 1958)

The angular dependence of the asymmetry in π^+ mesons emitted in the $p + p \rightarrow \pi^+ + d$ reaction was measured for a polarized proton beam of energies 536, 616 and 654 Mev. A direct demonstration of the presence of d-state mesons in the reaction $p + p \rightarrow \pi^+ + d$ is obtained. The experimental results are consistent with the assumption that the amplitudes of s- and d-transitions are substantially less than the transition amplitude $^1D_1 \rightarrow {}^3S_2 p_2$. Estimates of limiting values for some of the partial cross sections are given.

1. INTRODUCTION

MEASUREMENTS of total cross sections for the reaction

$$p + p \rightarrow \pi^+ + d \qquad (1)$$

for proton energies from 460 to 660 Mev,[1] and also data for higher energies obtained from experiments on the inverse reaction $\pi^+ + d \rightarrow p + p$ for π^+-energies of 174 — 307 Mev,[2] made it possible to draw conclusions about the resonance character of these two mutually inverse processes coming from the strong interaction of the π meson and proton in p-states with total angular momentum $J = {}^3/_2$.

The angular distributions of the π^+ mesons in reaction (1) for proton energies from 460 to 660 Mev have been explained up to now by starting from the assumption that emission of the π^+ meson proceeds mainly in the p-state.[1] However, on the basis of only these experiments one cannot draw completely definite conclusions about the ratios of different amplitudes and, in particular, it is impossible to answer the question of the intensity of transitions in reaction (1) with emission of the π^+ meson in a d-state. More complete information on the ratios of amplitudes of different transitions can be obtained from experiments involving observation of various polarization effects. The reaction (1) was studied using a polarized 314-Mev proton beam in the work of reference 3, where the asymmetry observed came from interference between s- and p-states. Analogous experiments were also carried out at 415 Mev.[4] Values of the asymmetry obtained at two different angles in the latter case were interpreted by the authors of reference 4 only as a possible indication of the presence of d-wave effects.

It is well known that the probability of scattering of a d-state meson by a proton is very small at π^+ energies ~ 150 Mev and becomes noticeable only for energies ~ 300 Mev,[5] where $\delta_{33} \approx 10°$ and $\delta_{35} \approx -10°$. In several articles, for example in reference 6, preliminary data on the role of d-waves in the scattering of π^+ mesons by protons were considered to give a basis for neglecting d-state π mesons and analyzing both the differential cross section and the polarization effects in reaction (1), taking only s- and p-states into account. However, the well known analogy between the resonance character of process (1) and the resonance in meson-nucleon scattering, correct in general features, may not hold in detail. A difference might be caused by the second nucleon in process (1). In the phenomenological theory of processes of π-production in p-p collisions,[7] it was shown that, in reactions $p + p \rightarrow \pi^+ + n + p$ and $p + p \rightarrow \pi^0 + p + p$ for proton energies from 400 to 900 Mev, there is rather a high probability of the mechanism of the subsystem of a meson and nucleon in a $^2P_{3/2}$ state going off in a P state relative to the second nucleon. The probability of the mechanism of P emission in reaction (1) turned out to be very small. As a consequence of P emission in reaction (1), the π^+ meson is emitted in s- and also d-states. Thus, the additional angular momentum carried away by the second nucleon, not bound with the π meson, can lead to the occurrence of d-states for the π^+ meson in reaction (1), while they are absent in the meson-nucleon subsystem.

In the present work we obtained a direct demonstration of the presence of d-state mesons in

reaction (1) for proton energies of 536, 616 and 654 Mev. From the results obtained, and also on the basis of reference 4, one can conclude that the effect of d-states becomes observable, starting with energies $E_p \sim 400$ Mev. Data from polarized beams are not sufficient to determine all elements of the S-matrix for process (1), since other polarization effects must also be measured to solve this problem. However, if one makes several assumptions about relative sizes of the transition amplitudes in reaction (1), then, on the basis of the results obtained, one can indicate minimum probabilities of emission of π-mesons in s- and d-states.

2. EXPERIMENTAL ARRANGEMENT

The experiments were carried out with a polarized proton beam, obtained in scattering the internal beam of unpolarized protons of energy 673 Mev from nuclei of carbon introduced into the synchrotron chamber. Polarized protons scattered "to the right" through 6°20′ with respect to the direction of the initial beam (Fig. 1) were selected by two collimators so that the beam was directed towards the center of the deflecting magnet, the diameter of the poles of which was 100 cm. Special forms of shims[8] were set along the trajectory of the beam in the gap, equal to 13 cm, between the pole tips of this magnet. These created a region of inhomogeneous magnetic field, equivalent in its action to a system of two quadrupole lenses. The calculated value of the focal length of the lens was 2.5 m. Use of such a method of focusing made it possible to increase the intensity of the beam of polarized protons by a factor of three at the position of the hydrogen target.

The measuring apparatus was shielded from the background created by the primary beam and the scattered particles by a concrete wall of thickness 4 m, and also by lead blocks, placed in the path of the initial beam behind the carbon target and in the space between the yoke and poles of the magnet. In order to give a higher intensity of beam of unpolarized protons at the position of the carbon target, focusing quadrupole lenses with aperture 40 mm were used. At optimal values of the current in the windings of these lenses, the intensity of the polarized beam increased by a factor of 1.7.

The experimental arrangement consisted of a liquid hydrogen target,[9] scintillation counters for registering, a counter for determining the beam profile in the process of measurement, and also an ionization chamber placed past the hydrogen target.

The target and counters were accurately positioned relative to the axis of the 4-meter collimator. The establishment of this axis was carried out using a polyamide filament of diameter 0.2 mm. The target container of liquid hydrogen was positioned relative to the axis line of the target to an accuracy of 0.3 mm and was secured by screws. Control of the alignment of the axis line of the counter and axis of the collimator was carried out immediately before each experiment, and could be obtained to an accuracy of several parts of a millimeter. The adjustment of the target was not destroyed if they did not exceed 0.4 or 0.5 mm.

The absence of hidden asymmetry in the apparatus was demonstrated in experiments with the unpolarized proton beam by counting the $p + p \rightarrow \pi^+ + d$ processes without changing anything else in the experiment. The value of the asymmetry at angle $\theta_{lab} = 20°$, which would be most unfavorable with respect to hidden asymmetry, turned out to be equal to $\epsilon_0 = -2.4 \pm 1.9\%$. Besides these control measurements, measurement of the asymmetry in elastic p-p scattering with a polarized proton beam were carried out for angle $\theta_{lab} = 41°$, which corresponds to $\epsilon_{pp}(41°) = 0$. The measured value of the asymmetry turned out to be $\epsilon_{pp}(41°) = -0.5 \pm 0.9\%$.

Both the control experiments and the main ones were carried out for strengths of the magnetic field of the deflecting magnet corresponding to the maximum intensity of the polarized beam. In order to exclude drift effects in the angle of deflection of the protons, the possibility of a control on the position and profile of the beam during the course of measurements was considered. Such a control was carried out, using a movable scintillation counter placed before the hydrogen target (Fig. 1). The counter consisted of a narrow crystal of tolane (diphenyl acetylene) of dimensions $1 \times 40 \times 40$ mm, with its narrow edge turned to the beam. The current from the photomultiplier of this apparatus was registered by a potentiometer of type EPPV-51. The position of the center of the target was determined to an accuracy of ~ 1 mm by the pulse height on the tape. This corresponded to a relative drift of the current in the magnet windings of $\sim 0.5\%$, or a lack of alignment of the beam in the collimator of $\sim 0.05\%$.

The degree of polarization of the proton beam was determined by the usual method of double scattering on carbon nuclei at an angle of 6°20′ and turned out to be equal to $P_1 = 44 \pm 2.4\%$. As a control on the quantity P_1, the asymmetry ϵ in elastic p-p scattering was measured at 30° in the

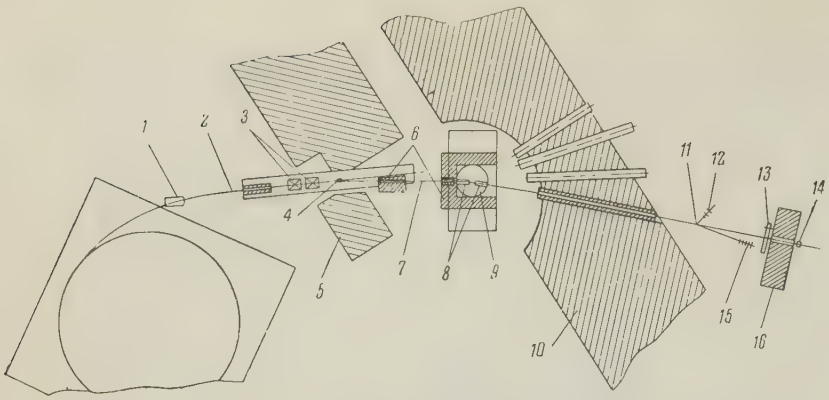

FIG. 1. Scheme of the Experiment. 1 – deflecting mouthpiece, 2 – unpolarized proton beam, 3 – magnetic quadrupole lenses of 40 mm, 4 – carbon scatterer, 5 – concrete shielding, 6 – lead shielding, 7 – polarized proton beam, 8 – focusing shim, 9 – deflecting magnet, 10 – shielding wall, 11 – target with liquid hydrogen, 12 – meson telescope, 13 – movable counter, 14 – ionization chamber, 15 – deuteron telescope, 16 – concrete shielding.

laboratory system. Its value was found in the work of reference 10 with a polarized beam of degree $P_1 = 58 \pm 3\%$. For the beam used, the value $\epsilon_{pp}(30°) = 11.9 \pm 0.6\%$ was found, whereas the value of the asymmetry[10] calculated from $P_1 = 44\%$ should be equal to $\epsilon = 12.0\%$.

The energy of the polarized beam and its spread in energy were determined by range measurements using a telescope of several scintillation counters, the last of which was connected in anti-coincidence with the first. In Fig. 2 we give two range curves:

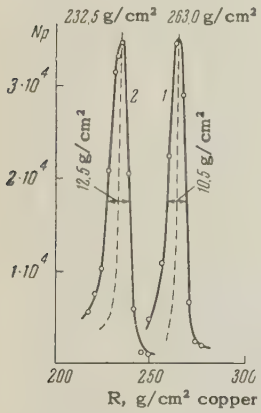

FIG. 2. Range curves in copper. 1 – unpolarized beam of protons, $E_p = 670$ Mev; 2 – polarized beam of protons, $E_p = 616$ Mev.

curve 1 with the unpolarized beam of protons of energy $E_p = 670$ Mev and spread $\Delta E = \pm 5$ Mev; curve 2 with the polarized beam, the mean energy of which turned out to be equal to $E_p = 616$ Mev, and spread $\Delta E = \pm 7$ Mev. In calculating the proton energy from the filters used in slowing down, the effect of multiple scattering in copper was taken into account.*

The remaining characteristics of the polarized beam are given in Table I for three values of the energy. Secondary particles from the reaction $p + p \rightarrow \pi^+ + d$ were counted by two conjugate telescopes of scintillation counters, connected in coincidence. The electronic scheme had the necessary stability, owing to the use of negative coefficients of selection in the telescopes of the coincidence scheme.[11] A telescope consisting of three counters counted the π^+ mesons.

TABLE I

Energy of the polarized beam Mev	536	616	654
Intensity, protons/cm² sec	$0.9 \cdot 10^5$	$5.5 \cdot 10^5$	$2.8 \cdot 10^5$
Thickness of the carbon scatterer, g/cm²	22.9	22.9	7.3
Thickness of the carbon absorber in the path of the initial beam, g/cm²	34.2	Not used	

The deuteron telescope consisted of five counters. The first three counters were connected in coincidence, and the last two in anti-coincidence with the first three. Between the second and third counters, there was a copper filter, the thickness of which corresponded to the minimum range of deuterons from reaction (1) at the conjugate angle. The interval of ranges was given by the filter placed between counters 3 and 4. With filters in this position, the telescope counted deuterons of a definite energy, and the counting efficiency for $p + p \rightarrow \pi^+ + n + p$ and $p + p \rightarrow \pi^0 + p + p$ reactions was substantially lowered by this. The measuring of the contributions from these reactions, and also of the random coincidences between telescopes was carried out with a filter of somewhat increased thickness between counters 2 and 3, so that the process (1) was not registered. The magnitude of the background was less than 10% of the considered process $p + p \rightarrow \pi^+ + d$. The angular resolution of the telescope for angle $\theta_\pi^{lab} = 20°$ ($\theta_\pi^{c.m.s.} = 35°$) was $\pm 1.9°$ ($\pm 3°$ in c.m.s.), and at angle $\theta_\pi^{lab} = 96°$ ($\vartheta_\pi^{c.m.s.} = 130°$) was $\pm 2.5°$ ($\pm 2°$ in c.m.s.).

3. RESULTS AND DISCUSSION

It is known[6] that the differential cross section for the reaction $p + p \rightarrow \pi^+ + d$ with a polarized beam of protons has the form

*The values of the coefficients were calculated by V. P. Zrelov.

$$k^2 d\sigma(\theta, \varphi)/d\Omega = (\gamma_0 + \gamma_2 \cos^2\theta + \gamma_4 \cos^4\theta) \quad (2)$$
$$+ P \sin\theta \cos\varphi (\lambda_0 + \lambda_1 \cos\theta + \lambda_2 \cos^2\theta + \lambda_3 \cos^3\theta),$$

where P is the degree of polarization of the beam, and the coefficients γ and λ[12] define elements of the S-matrix of process (1). In our case, emission of a π^+ meson to the right corresponded to azimuthal angle $\varphi = \pi$, and the polarization vector **P** pointed downwards.[13,14]

In the experiments carried out, the right-left asymmetry $\epsilon = (R-L)/(R+L)$ was measured at π^+-emission angles from 35° to 130°.

Results of the measurements of ϵ for three values of the energy are shown in Fig. 3. In the analysis of the experimental data obtained, we introduced the quantity

$$\Lambda = \frac{4\pi\,\varepsilon}{P \sin\theta\, \sigma_t} \left(\frac{d\sigma}{d\Omega}\right)_{\text{unpol}}. \quad (3)$$

The normalization factor $(\sigma/4\pi)$ is convenient for the analysis of the asymmetry in reaction (1) over a wide range of energies.

The differential cross sections $(d\sigma/d\Omega)$unpol. with an unpolarized proton beam, and also the total cross section σ_t for the reaction $p + p \to \pi^+ + d$, used in calculating Λ, were obtained by averaging the results of references 1, 2, and 15 and were taken to be the following:

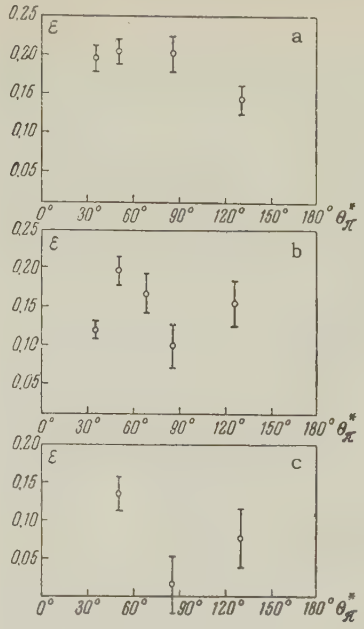

FIG. 3. Measurements of the asymmetry ε in the reaction $p + p \to d + \pi^+$ with polarized proton beams. a) E_p = 654 Mev; b) E_p = 616 Mev; c) E_p = 536 Mev.

1) $E_p = 654$ **Mev**, $d\sigma/d\Omega \sim 0.27 + \cos^2\theta$; $\sigma_t = 3.1 \cdot 10^{-27}$ cm^2;
2) $E_p = 616$ **Mev**, $d\sigma/d\Omega \sim 0.22 + \cos^2\theta$; $\sigma_t = 3.14 \cdot 10^{-27}$ cm^2;
3) $E_p = 536$ **Mev**, $d\sigma/d\Omega \sim 0.24 + \cos^2\theta$; $\sigma_t = 2.42 \cdot 10^{-27}$ cm^2.

Values of Λ as a function of θ_π in the c.m.s. are given in Fig. 4 for proton energies of 654, 616, 536 Mev. In the absence of d-transitions, the values of Λ for a given energy should be constant. The fact that a strong angular dependence of $\Lambda(\theta_\pi)$ was observed in the experiment, as can be seen by

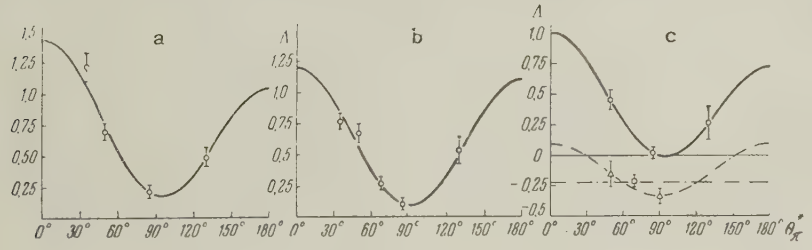

FIG. 4. Curves of $\Lambda(\theta_\pi)$: a) E_p = 654 Mev; b) E_p = 616 Mev; c) circles – date of this work, E_p = 536 Mev; triangles data from reference 4, E_p = 415 Mev; squares – data from reference 3, E_p = 314 Mev.

the graphs, is a direct demonstration of d-state π^+ mesons in reaction (1) for all three energies. The experimental values of $\Lambda(\theta_\pi)$ were approximated by the expressions

$$\Lambda = (\lambda_0 + \lambda_1 \cos\theta + \lambda_2 \cos^2\theta)/(\gamma_0 + {}^1/_3\,\gamma_2)$$

using the method of orthogonal polynomials.[16] Values of the coefficients λ_i and errors are given in Table II.

TABLE II

E_p, Mev	$\frac{\lambda_0}{\gamma_0 + \frac{1}{3}\gamma_2}$	$\frac{\lambda_1}{\gamma_0 + \frac{1}{3}\gamma_2}$	$\frac{\lambda_2}{\gamma_0 + \frac{1}{3}\gamma_2}$	$\frac{\delta\lambda_0\delta\lambda_1}{\left(\gamma_0 + \frac{1}{3}\gamma_2\right)^2}$	$\frac{\delta\lambda_0\delta\lambda_2}{\left(\gamma_0 + \frac{1}{3}\gamma_2\right)^2}$	$\frac{\delta\lambda_1\delta\lambda_2}{\left(\gamma_0 + \frac{1}{3}\gamma_2\right)^2}$
654	0.18 ± 0.03	0.20 ± 0.06	1.05 ± 0.10	$-2.2 \cdot 10^{-4}$	$-14 \cdot 10^{-4}$	$-15.0 \cdot 10^{-4}$
616	0.09 ± 0.03	0.05 ± 0.08	1.06 ± 0.11	$-7 \cdot 10^{-4}$	$-5.5 \cdot 10^{-4}$	$-6 \cdot 10^{-4}$
536	-0.003 ± 0.04	0.15 ± 0.12	0.87 ± 0.20	$-1.1 \cdot 10^{-3}$	$-3.4 \cdot 10^{-3}$	$-7.7 \cdot 10^{-3}$

Reliable values of the coefficient λ_3 could not be determined from the experimental data. In order to determine this coefficient it would be necessary to carry out very difficult measurements of the asymmetry at angles θ_π close to 0° to 180°, where the effect of the asymmetry vanishes, owing to the approximate proportionality to $\sin\theta_\pi$. The smallest errors in the coefficients were obtained for three terms in the expansion, making it possible to break off the expansion with the $\cos^2\theta_\pi$ term. The question of actual values of the coefficient λ_3 should be considered together with that of the determination of the coefficient γ_4 in the angular distribution with an unpolarized beam, since both are determined by expressions quadratic in the amplitude for d-state transtions which, as will be shown below, are rather small.

The variation of the dependence of $\Lambda(\theta_\pi)$ observed in the present work with transition from one energy to another, can be followed to the region of still smaller values if one uses results of experiment carried out at 415 Mev (reference 4) and 314 Mev.[3] The results of these experiments are given in Table III in the notation employed here.

TABLE III

E_p, Mev	$\frac{\lambda_0}{\left(\gamma_0+\frac{1}{3}\gamma_2\right)}$	$\frac{\lambda_2}{\left(\gamma_0+\frac{1}{3}\gamma_2\right)}$	$\frac{\delta\lambda_0\delta\lambda_2}{\left(\gamma_0+\frac{1}{3}\gamma_2\right)^2}$
415	-0.34 ± 0.05	0.43 ± 0.28	$-6.2\cdot10^{-3}$
314	-0.22 ± 0.03	—	—

As can be seen from Fig. 4, the sign of the asymmetry changes for proton energies $E_p \sim 500$ Mev. Values of the coefficients

$$\lambda_0/(\gamma_0+{}^1/_3\gamma_2),\ \lambda_1/(\gamma_0+{}^1/_3\gamma_2),\ \lambda_2/(\gamma_0+{}^1/_3\gamma_2)$$

are given in Fig. 5 as a function of π-meson momentum in the c.m.s., expressed in units of $m_\pi c$. At zero energy there can be only s-state mesons, and all coefficients should go to zero. For small values of the momentum of the π^+ meson, the coefficient $\lambda_0(\gamma_0+{}^1/_3\gamma_2)$, which is negative, increases with the momentum of the π^+ meson, reaches an extreme value, then decreases and, going through zero at $E_p \sim 530$ Mev, again grows, but not with a positive sign. When η is small, the change in $\lambda_0(\gamma_0+{}^1/_3\gamma_2)$ is connected with the growth of the effect of the P-wave with respect to the S-amplitude. For large values of η, the p-d interference is added to the s-p interference. It seems that the effects of these two interferences are comparable, beginning with the proton energy for which the coefficient $\lambda_0/(\gamma_0+{}^1/_3\gamma_2)$ goes through the extreme value. Verification of this follows from the fact that the coefficient $\lambda_2(\gamma_0+{}^1/_3\gamma_2)$, coming from interference between p- and d-states, becomes observable at energies $E_p \sim 400$ Mev.

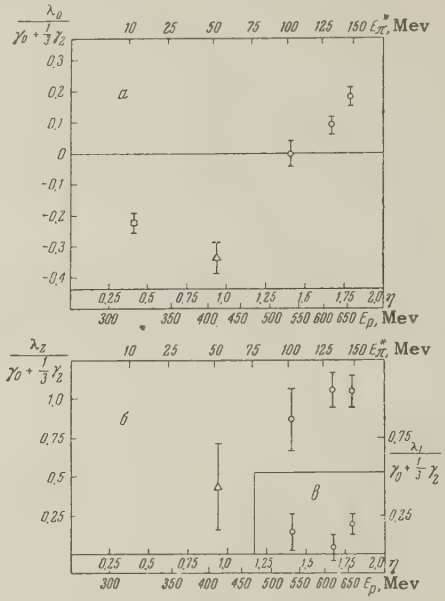

FIG. 5. Measured values of the coefficients: a) $\lambda_0/(\gamma_0+{}^1/_3\gamma_2)$, b) $\lambda_2/(\gamma_0+{}^1/_3\gamma_2)$, c) $\lambda_1(\gamma_0+{}^1/_3\gamma_2)$, circles – data of this work, squares – data from reference 3, triangles – data from reference 4.

The coefficient $\lambda_1(\gamma_0+{}^1/_3\gamma_2)$, connected with the effects of (s-d)- and (d-d)-interferences, turned out to be very small, and it was only observed with difficulty in our experiments.

All of these results can be simultaneously explained if the transition amplitude ${}^1D_2 \to ({}^3S_1 p)_2$ is taken to exceed the values of s- and d-amplitudes for $E_p \sim 600$ Mev. In this case, only s-p and p-d interferences would be observed, whereas s-d and d-d interferences would correspond to effects of second order.

The experiments carried out with a polarized proton beam add essential information about the reaction (1), but it is still not possible to evaluate all S-matrix elements connected with these reactions. However, using the smallness of s- and d-amplitudes, certain partial cross sections can be estimated. For this it is necessary to take account of the fact that d-transitions in reaction (1) are connected with a change in the orbital moment in the system of the two nucleons before and after the reaction, and also in the parity. This circumstance leads to a very small probability of d-transitions. The transitions ${}^3F_2 \to ({}^3S_1 d)_2$ and ${}^3F_3 \to ({}^3S_1 d)_3$, connected with a change in orbital momentum equal to $\Delta l = 3$ in the system of the two nucleons, should be especially impeded. This makes it possible to set the amplitudes of these

transitions equal to zero, and, for limiting values of the partial cross sections, one obtains the values:

$$\sigma(^1S_0 \rightarrow {}^3S_1 p_0) \geqslant 10^{-3} \cdot \sigma_t(pp \rightarrow d\pi^+);$$

$$\sigma(s + d) \geqslant 5.4 \cdot 10^{-2} \cdot \sigma_t(pp \rightarrow d\pi^+);$$

$$\sigma(^1D_2 \rightarrow {}^3S_1 p_2) \leqslant 0.945 \cdot \sigma_t(pp \rightarrow d\pi^+).$$

4. CONCLUSIONS

1. Experiments measuring the asymmetry in the differential cross section of the $p + p \rightarrow d + \pi^+$ reaction with polarized proton beams at energies 536, 616, and 654 Mev demonstrate the presence of π^+-meson emission in d-states.

2. From analysis of the results of this experiment, and also of those of references 3 and 4, it follows that the effect of d-state π^+ mesons in experiments with polarized beams become observable, beginning with proton energy $E_p \sim 400$ Mev.

3. The results obtained are compatible with the assumption that the transition amplitudes for emission of π^+ mesons in s- and d-states are small in comparison with the amplitude for the transition $^1D_2 \rightarrow (^3S_1 p)_2$ over all of the region of energy studied.

4. Under the assumption that transitions from initial $^3F_2$- and $^3F_3$-states can be neglected, the following limiting values were obtained:

$$\sigma(^1S_0 \rightarrow {}^3S_1 p_0) \geqslant 10^{-3} \cdot \sigma_t(pp \rightarrow d\pi^+);$$
$$\sigma(s + d) \geqslant 5.4 \cdot 10^{-2} \cdot \sigma_t(pp \rightarrow d\pi^+);$$
$$\sigma(^1D_2 \rightarrow {}^3S_1 p_2) \leqslant 0.945 \cdot \sigma_t(pp \rightarrow d\pi^+).$$

5. The phenomenological theory of production of π mesons in p-p collisions of Mandelstam[7] agrees with the values obtained.

In conclusion the authors express their gratitude to M. G. Meshcheriakov, B. S. Neganov, and L. I. Lapidus for discussion of the work and also N. P. Klepikov and S. N. Sokolov for help in processing the experimental data.

[1] M. G. Meshcheriakov and B. S. Neganov, Dokl. Akad. Nauk SSSR **100**, 677 (1955).

[2] B. S. Neganov and L. B. Parfenov, J. Exptl. Theoret. Phys. (U.S.S.R.) **34**, 767 (1958), Soviet Phys. JETP **7**, 528 (1958).

[3] F. S. Crawford and M. L. Stevenson, Phys. Rev. **95**, 1112 (1954).

[4] Fields, Fox, Kane, Stallwood, and Sutton, Phys. Rev. **96**, 812 (1954).

[5] Mukhin, Ozerov, Pontecorvo, Grigo'ev, and Mitin, CERN Symposium, Geneva, 1956.

[6] F. Mandl and T. Regge, Phys. Rev. **99**, 1478 (1955).

[7] S. Mandelstam, Proc. Roy. Soc. **A244**, 491 (1958).

[8] V. I. Danilov and O. V. Savchenko, Приборы и техника эксперимента (Instruments & Instr. Engg.) (1958).

[9] Bogomolov, Vovchenko, Soroko and Shtyrin, Preprint, Joint Institute for Nuclear Research (1958).

[10] Meshcheriakov, Nurushev and Stoletov, J. Exptl. Theoret. Phys. (U.S.S.R.) **33**, 37 (1957), Soviet Phys. **6**, 78 (1958).

[11] Iu. K. Akimov, Приборы и техника эксперимента (Instruments & Instr. Engg.) **1**, 95 (1957).

[12] L. M. Soroko, J. Exptl. Theoret. Phys. **35**, 276 (1958), Soviet Phys. JETP, **8**, 190 (this issue).

[13] L. Marshall and J. Marshall, Phys. Rev. **98**, 1398 (1955).

[14] H. Bradner and W. Isbell, Phys. Rev. **108**, 463 (1957).

[15] Dzhelepov, Kiselev, Oganesian and Fliagin, J. Exptl. Theoret. Phys. (U.S.S.R.) **35**, 854 (1958), Soviet Phys. JETP **8**.

[16] N. P. Klepikov and S. N. Sokolov, Preprint, Joint Institute for Nuclear Research (1958).

Translated by G. E. Brown
12

ON THE THEORY OF THE FERMI LIQUID

L. D. LANDAU

Institute of Physical Problems, Academy of Sciences, U.S.S.R.

Submitted to JETP editor February 5, 1958

J. Exptl. Theoret. Phys. (U.S.S.R.) **35**, 97-103 (July, 1958)

A study is made of the zero-angle scattering in collisions of quasiparticles in a Fermi liquid. It is shown that the scattering amplitude for zero angle depends on the limit approached by the ratio of the momentum and energy transfers in the collision as both these quantities go to zero. It is ascertained which of these limits is connected with the interaction energy of the quasiparticles that occurs in the general theory of the Fermi liquid developed earlier by the writer.

A general theory of the Fermi liquid* has been developed in previous papers by the writer.[1,2] One of the quantities that plays an important part in this theory in characterizing the properties of the liquid is the function $f(p, p')$ which determines the interaction energy of the quasiparticles, i.e., the variation of the energy $\epsilon(p)$ of the quasiparticles arising from a variation of their distribution function:

$$\delta\varepsilon(p) = \mathrm{Sp}_{\sigma'} \int f(\mathbf{p}, \mathbf{p}')\, \delta n(\mathbf{p}')\, d\tau' \qquad (1)$$

(where $d = d^3\mathbf{p}/(2\pi)^3$; here and below we take $\hbar = 1$).

In reference 1 it was shown that the function $f(\mathbf{p}, \mathbf{p}')$ is related in a definite way to the scattering amplitude of the quasi-particles in the liquid for their mutual collisions. The formulation given in reference 1 for this connection is not, however, quite accurate, as will be shown in the present paper.

We used below methods borrowed from quantum field theory; as is well known, these methods have recently been used with success by various authors in the study of the properties of quantum many-particle systems.

The main part in these methods is played by the Green's function G and the "vertex part" Γ. Let us recall the definitions and basic properties of these functions.

The function G is defined as the average value in the ground state of the system of the chronological product of two ψ operators:

$$G_{12} = -i\langle T(\psi_1\psi_2^+)\rangle. \qquad (2)$$

The indices 1, 2 denote sets of values of the three coordinates and the time, and also of the spin index. As usual, we shall use below instead of the space-time representation (2) the Fourier expansion of this function. The only components different from zero are those with identical values of the two momenta and the two energies (that is, of the wave vectors and frequencies): $P_1 = P_2 \equiv P$; we denote by P the "four-momentum", i.e., the combination of the momentum $\mathbf{p}$ and the energy ϵ. In respect to the spin indices (which we denote by Greek letters) the Fourier components $G_{\alpha\beta}(P) = \int G_{\alpha\beta}(X_1 - X_2)\, e^{-iP(X_1-X_2)} d^4(X_1 - X_2)$ are proportional to $\delta_{\alpha\beta}$; we shall write

$$G_{\alpha\beta}(P) = G(P)\,\delta_{\alpha\beta}. \qquad (3)$$

As is well known, the poles of the function $G(P)$ give the energies of the quasiparticles (the elementary excitations). In accordance with this, for p close to the boundary momentum p_0 and ϵ close to the boundary energy μ, $G(P)$ has the form

$$G(P) \to \frac{a}{\varepsilon - \mu - v(p - p_0) + i\delta} \qquad (4)$$

(μ is the chemical potential of the gas, and v is the speed of the quasiparticles at the Fermi boundary). This expression has a pole at

$$\varepsilon - \mu = v(p - p_0), \qquad (5)$$

and the small constant δ is introduced in the usual way to specify the rule for going around the singularity in integrating; the sign of δ agrees with the sign of $\epsilon - \mu$ (or, what is the same thing near the pole, with the sign of $p - p_0$). The "renormalization" factor a is positive and, as has been shown by Migdal,[3] is smaller than unity:

$$a < 1. \qquad (6)$$

*To avoid misunderstanding we emphasize that we are concerned not with simply a liquid composed of Fermi particles; it is also postulated that this liquid has an energy spectrum of the Fermi type, i.e., that it is not a superfluid.

The vertex part Γ is defined by means of the four-particle average value

$$\Phi_{1234} = \langle T(\psi_1\psi_2\psi_3^+\psi_4^+)\rangle. \quad (7)$$

The Fourier components of this function contain a part that is expressed in terms of functions $G(P)$ only, and a remainder that gives the definition of the Fourier component of the vertex part by the following formula:

$$\begin{aligned}&\Phi_{\alpha\beta,\gamma\delta}(P_1, P_2; P_3, P_4)\\ &= (2\pi)^8 G(P_1) G(P_2)[\delta(P_1 - P_3)\delta(P_2 - P_4)\delta_{\alpha\gamma}\delta_{\beta\delta}\\ &\quad - \delta(P_1 - P_4)\delta(P_2 - P_3)\delta_{\alpha\delta}\delta_{\beta\gamma}] \quad (8)\\ &\quad + iG(P_1) G(P_2) G(P_3) G(P_4)\\ &\times\Gamma_{\alpha\beta,\gamma\delta}(P_1, P_2; P_3, P_4)(2\pi)^4\delta(P_1 + P_2 - P_3 - P_4).\end{aligned}$$

Here the values of the arguments are connected by the relation

$$P_1 + P_2 = P_3 + P_4. \quad (9)$$

On interchange of the indices 1 and 2 (or 3 and 4) the function (7) changes sign; thus it follows from the definition (8) that Γ has the symmetry property:

$$\Gamma_{\alpha\beta,\gamma\delta}(P_1, P_2; P_3, P_4) = -\Gamma_{\beta\alpha,\gamma\delta}(P_2, P_1; P_3, P_4). \quad (10)$$

In the formation of the vertex part intermediate states occur that correspond to different values of the total number of particles in the system: the unchanged number N and the numbers $N \pm 2$. The latter arise from such arrangements of the ψ operators in the T-product as, for example, $\psi_1\psi_2\psi_3^+\psi_4^+$; the former correspond to arrangements such as, for example, $\psi_1\psi_3^+\psi_2\psi_4^+$. In accordance with this the contributions to the function Γ connected with these intermediate states have different characters in regard to their singularities. Namely, terms due to states that appear with the addition or removal of two particles have singularities with respect to the variables $P_1 + P_2$; terms corresponding to intermediate states with unchanged number of particles have singularities with respect to the variables $P_1 - P_3$ or $P_2 - P_4$.

The probability of scattering of quasi-particles with the transition

$$P_1\alpha, P_2\beta \to P_3\gamma, P_4\delta \quad (11)$$

is given in terms of the function Γ by the formula

$$\begin{aligned}&dW_{\alpha\beta,\gamma\delta}(P_1, P_2; P_3, P_4)\\ &= 2\pi|a^2\Gamma_{\alpha\beta,\gamma\delta}(P_1, P_2; P_3, P_4)|^2\delta(\varepsilon_1 + \varepsilon_2 - \varepsilon_3 - \varepsilon_4) \quad (12)\\ &\times n_1n_2(1 - n_3)(1 - n_4)\,d\tau_1d\tau_2d\tau_3\end{aligned}$$

[where $n_1, n_2, \ldots$ are the values of the distribution function for $P_1\alpha$, $P_2\beta$, and so on, and a is the renormalization constant from Eq. (4)]. The sign of Γ is defined in such a way that it corresponds to a positive scattering amplitude for repulsion and a negative amplitude for attraction.

Below we shall consider the function Γ for nearly equal values of the pairs of variables P_1, P_3 and P_2, P_4, i.e., we set $P_3 = P_1 + K$, $P_4 = P_2 - K$ with small K, and agree to write

$$\Gamma(P_1, P_2; P_1 + K, P_2 - K) \equiv \Gamma(P_1 P_2; K). \quad (13)$$

In terms of the scattering process (11) this means that we are considering collisions of quasiparticles giving nearly "forward scattering."

In the lowest order of perturbation theory contributions to the function $\Gamma(P_1, P_2; K)$ are made by the diagrams shown in the figure (a, b, c).

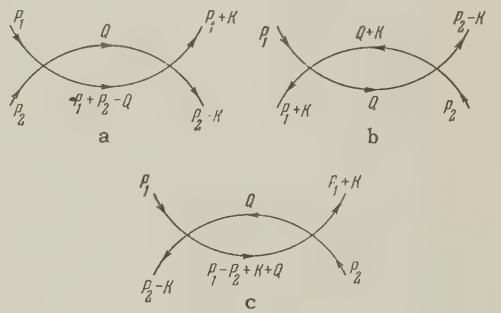

The internal parts of these diagrams correspond to the following propagation functions:

$$\text{(a) } G(Q)G(P_1 + P_2 - Q),\ \text{(b) } G(Q)G(K + Q),$$

$$\text{(c) } G(Q)G(P_1 - P_2 + K + Q),$$

where Q is the intermediate four-momentum over which one integrates. With arbitrary P_1 and P_2 there is nothing to distinguish the value $K = 0$ for the functions (a) and (c), and for small K we can put $K = 0$. In the case (b), on the other hand, for $K \to 0$ the poles of the two factors come together, so that diagrams of this type require special consideration.

To calculate Γ one must sum the entire series of perturbation theory. Since in doing this our purpose is to separate out the parts having a singularity at $K = 0$, we must first single out the contribution from all the diagrams that do not have any parallel pairs of lines with nearly equal (differing by K) values of the four-momentum. We denote by $\Gamma^{(1)}$ this part of the function Γ, which has no singularity at $K = 0$; in it we can simply put $K = 0$, so that $\Gamma^{(1)}$ will be a function of the variables P_1 and P_2 only: $\Gamma^{(1)} = \Gamma^{(1)}(P_1, P_2)$. The entire series that has to be summed can be written symbolically in the form

$$(:\Gamma:) = (:\Gamma_1:) + (:\Gamma_1:\Gamma_1:) + (:\Gamma_1:\Gamma_1:\Gamma_1:) + \cdots, \quad (14)$$

where the colons replace pairs of lines in the diagram with nearly equal values of the four-momentum, and Γ_1 denotes the set of all possible diagram elements that do not have such pairs.

The problem of summing this series (so-called "ladder" summation) reduces to the solution of an integral equation, to obtain which we "multiply" the series (14) by Γ_1, i.e., replace it by the series

$$(:\Gamma_1:\Gamma:) = (:\Gamma_1:\Gamma_1:) + (:\Gamma_1:\Gamma_1:\Gamma_1:) + \ldots .$$

Comparison of this with Eq. (14) leads to the equation

$$(:\Gamma:) - (:\Gamma_1:) = (:\Gamma_1:\Gamma:),$$

which, when written out in explicit form, is the desired integral equation

$$\Gamma_{\alpha\beta,\gamma\delta}(P_1, P_2; K) = \Gamma^{(1)}_{\alpha\beta,\gamma\delta}(P_1, P_2) \qquad (15)$$
$$- \frac{i}{(2\pi)^4}\int \Gamma^{(1)}_{\alpha\varepsilon,\gamma\zeta}(P_1, Q)\, G(Q)\, G(Q+K)\, \Gamma_{\zeta\beta,\varepsilon\delta}(Q, P_2; K)\, d^4Q$$

(in the first factor of the integrand we should, strictly speaking, have $Q + K$ instead of the argument Q; but in view of the absence of singularities in $\Gamma^{(1)}$ we can here set $K = 0$). To investigate this equation we examine the product $G(Q)G(Q + K)$ that occurs in the integrand. On substituting here $G(P)$ in the form (4) we get

$$a^2/[\varepsilon - \mu - v(q - p_0) + i\delta_1] \qquad (16)$$
$$\times [\varepsilon + \omega - \mu - v(|\mathbf{q}+\mathbf{k}| - p_0) + i\delta_2].$$

Here ϵ and $\mathbf{q}$ are the energy and momentum corresponding to the four-momentum Q, and $\epsilon + \omega$ and $\mathbf{q} + \mathbf{k}$ are those corresponding to $Q + K$.

For small $\mathbf{k}$ and ω the expression (16), as a function of ϵ and q, behaves like δ functions of the arguments $\epsilon - \mu$ and $q - p_0$; that is, it has the form

$$A\delta(\varepsilon - \mu)\,\delta(q - p_0), \qquad (17)$$

where the coefficient A depends on the angle θ between the vectors $\mathbf{k}$ and $\mathbf{q}$. Comparing Eqs. (16) and (17), we see that this coefficient is given by the integral

$$A = \iint \frac{a^2 d\varepsilon dq}{[\varepsilon - \mu - v(q - p_0) + i\delta_1][\varepsilon + \omega - \mu - v(|\mathbf{q}+\mathbf{k}| - p_0) + i\delta_2]}. \qquad (18)$$

Let us first carry out the integration with respect to $d\epsilon$. The result of the integration depends essentially on the value of q. If the two differences $q - p_0$ and $|\mathbf{q} + \mathbf{k}| - p_0$ have the same sign, then we must also assign like signs to the quantities δ_1 and δ_2. The poles of the integrand then lie in one half-plane of the complex variable ϵ, and by closing the path of integration through the other half-plane we can see that the integral vanishes. Thus the integral is nonvanishing only for opposite signs of the differences $q - p_0$ and $|\mathbf{q} + \mathbf{k}| - p_0$. Let us first suppose that $\mathbf{qk} > 0$, i.e., $\cos\theta > 0$. Then the integral is nonvanishing for $q < p_0$, $|\mathbf{q} + \mathbf{k}| > p_0$, which, because of the smallness of $\mathbf{k}$, is equivalent to the condition

$$p_0 - k\cos\theta < q < p_0. \qquad (19)$$

In addition we must have for the quantities δ that $\delta_1 < 0$, $\delta_2 > 0$, so that the poles of the integrand lie in different half-planes. Closing the path of integration through one half-plane and calculating the integral from the residue at the corresponding pole, we find

$$A = \int \frac{2\pi i a^2 dq}{\omega - v(|\mathbf{q}+\mathbf{k}| - q)}.$$

Since by Eq. (19) q is nearly equal to p_0 and varies over a range $k\cos\theta$, we can put $|\mathbf{q} + \mathbf{k}| - q = k\cos\theta$, so that

$$A = \frac{2\pi i a^2 k\cos\theta}{\omega - vk\cos\theta}.$$

Let us note the peculiar character of this expression: its limit for $k \to 0$, $\omega \to 0$ depends on the limit approached by the ratio ω/k.

It is easy to show in the same way that for $\cos\theta < 0$ (in which case the integration must be taken over the region $q > p_0$, $|\mathbf{q} + \mathbf{k}| < p_0$) one gets the same expression for $A(\theta)$. Thus we have

$$G(Q)\,G(Q+K) = \frac{2\pi i a^2 \mathbf{l}\cdot\mathbf{k}}{\omega - v\,\mathbf{l}\cdot\mathbf{k}}\delta(\varepsilon - \mu)\,\delta(q - p_0) + g(Q), \qquad (20)$$

where $\boldsymbol{l}\mathbf{k}$ has been written instead of $k\cos\theta$ ($\boldsymbol{l}$ is the unit vector in the direction of $\mathbf{q}$), and $g(Q)$ does not contain any δ-function part (for small K), so that in it we can put $K = 0$.

Substituting Eq. (20) into Eq. (15), we get the fundamental integral equation in the form

$$\Gamma_{\alpha\beta,\gamma\delta}(P_1, P_2; K) = \Gamma^{(1)}_{\alpha\beta,\gamma\delta}(P_1, P_2)$$
$$- \frac{i}{(2\pi)^4}\int_{\epsilon} \Gamma^{(1)}_{\alpha\varepsilon,\gamma\zeta}(P_1, Q)\, g(Q)\, \Gamma_{\zeta\beta,\varepsilon\delta}(Q, P_2; K)\, d^4Q \qquad (21)$$
$$+ \frac{a^2 p_0^2}{(2\pi)^3}\int \Gamma^{(1)}_{\alpha\varepsilon,\gamma\zeta}(P_1, Q)\, \Gamma_{\zeta\beta,\varepsilon\delta}(Q, P_2, K)\, \frac{\mathbf{l}\cdot\mathbf{k}}{\omega - v\,\mathbf{l}\cdot\mathbf{k}}\, do.$$

In the last term we have put $d^4Q = q^2\, dq\, do\, d\epsilon$, where do is an element of solid angle in the direction of $\boldsymbol{l}$, and have carried out the integration of the δ functions in the integrand with respect to $dq\, d\epsilon$. In the arguments of the functions $\Gamma^{(1)}$ and Γ in this term Q is taken on the Fermi surface, i.e., it consists of the momentum $\mathbf{q} = p_0\boldsymbol{l}$

and the constant energy μ.

Because of the special character of the kernel of the integral equation as noted above, its solution also has just the same character: the limit of the function $\Gamma(P_1, P_2; K)$ for $K \to 0$ depends on the way in which $\mathbf{k}$ and ω go to zero, i.e., on the limit of the ratio ω/k.

Let us denote by $\Gamma^{\omega}(P_1, P_2)$ the limit

$$\Gamma^{\omega}_{\alpha\beta,\gamma\delta}(P_1, P_2) = \lim_{K\to 0} \Gamma_{\alpha\beta,\gamma\delta}(P_1, P_2; K) \quad \text{for} \quad k/\omega \to 0 \tag{22}$$

[we shall see below that it is just this quantity with which the function $f(\mathbf{p}, \mathbf{p}')$ of Eq. (1) is related]. With this way of approaching the limit the kernel of the last term in Eq. (21) goes to zero, so that Γ^{ω} satisfies the equation

$$\Gamma^{\omega}_{\alpha\beta,\gamma\delta}(P_1, P_2) = \Gamma^{(1)}_{\alpha\beta,\gamma\delta}(P_1, P_2) - \frac{i}{(2\pi)^4}\int \Gamma^{(1)}_{\alpha\varepsilon,\gamma\zeta}(P_1, Q)\, g(Q)\, \Gamma^{\omega}_{\zeta\beta,\varepsilon\delta}(Q, P_2)\, d^4Q. \tag{23}$$

We can eliminate $\Gamma^{(1)}$ from (21) and (23). The result of the elimination is

$$\Gamma_{\alpha\beta,\gamma\delta}(P_1, P_2; K) = \Gamma^{\omega}_{\alpha\beta,\gamma\delta}(P_1, P_2) + \frac{a^2 p_0^2}{(2\pi)^3}\int \Gamma^{\omega}_{\alpha\varepsilon,\gamma\zeta}(P_1, Q)\, \Gamma_{\zeta\beta,\varepsilon\delta}(Q, P_2; K)\, \frac{1\mathbf{k}}{\omega - v1\mathbf{k}}\, do. \tag{24}$$

In fact, if we formally write Eq. (23) in the form

$$\Gamma^{(1)}_{\alpha\beta,\gamma\delta}(P_1, P_2) = \hat{L}\Gamma^{\omega}_{\alpha\beta,\gamma\delta}(P_1, P_2), \tag{25}$$

then Eq. (21) is written

$$\hat{L}\Gamma_{\alpha\beta,\gamma\delta}(P_1, P_2; K) = \Gamma^{(1)}_{\alpha\beta,\gamma\delta}(P_1, P_2) + \frac{a^2 p_0^2}{(2\pi)^3}\int \Gamma^{(1)}_{\alpha\varepsilon,\gamma\zeta}(P_1, Q)\, \Gamma_{\zeta\beta,\varepsilon\delta}(Q, P_2; K)\, \frac{1\mathbf{k}}{\omega - v1\mathbf{k}}\, do;$$

and substituting Eq. (25) and then applying the operator $\hat{L}^{-1}$ to both sides, we get Eq. (24).

Let us now introduce the function Γ^{k} defined by

$$\Gamma^{k}_{\alpha\beta,\gamma\delta}(P_1, P_2) = \lim_{K\to 0} \Gamma^{k}_{\alpha\beta,\gamma\delta}(P_1, P_2; K) \quad \text{for} \quad \omega/k \to 0. \tag{26}$$

This function (multiplied by the renormalization constant a^2) is the "forward" scattering amplitude (i.e., that for the transition $P_1, P_2 \to P_1, P_2$), corresponding to actual physical processes occurring with quasi-particles on the Fermi surface: collisions leaving the quasiparticles on this surface involve changes of momentum without change of energy, so that the passage to the limit of zero momentum transfer $\mathbf{k}$ must be made for energy transfer ω strictly equal to zero. On the other hand the function Γ^{ω} introduced above corresponds to the nonphysical limiting case of "scattering" with small energy transfer and momentum transfer strictly equal to zero.

Setting $\omega = 0$ in Eq. (24) going to the limit $K \to 0$, and multiplying both sides of the equation by a^2, we get

$$a^2\Gamma^{k}_{\alpha\beta,\gamma\delta}(P_1, P_2) = a^2\Gamma^{\omega}_{\alpha\beta,\gamma\delta}(P_1, P_2) - \frac{p_0^2}{v(2\pi)^3}\int a^2\Gamma^{\omega}_{\alpha\varepsilon,\gamma\zeta}(P_1, Q)\cdot a^2\Gamma^{k}_{\zeta\beta,\varepsilon\delta}(Q, P_2)\, do. \tag{27}$$

Thus there exists a general relation connecting the two limiting forms of the forward scattering amplitude.

Let us now turn to the study of the poles of $\Gamma(P_1, P_2; K)$ as function of K. As was already pointed out at the beginning of this paper, the poles with respect to the variable $K = P_3 - P_1$ are due to contributions to Γ associated with intermediate states in which the number of particles in the system is not changed. Therefore these poles correspond to elementary excitations of the liquid without change of the number of quasiparticles in it. It is obvious that these are the excitations which can be described as sonic excitations in the gas of quasiparticles (phonons of the "zeroth sound").

Near a pole of the function $\Gamma(P_1, P_2; K)$ the left side and the integral on the right side of the equation (24) are arbitrarily large; the term $\Gamma^{\omega}(P_1, P_2)$, on the other hand, remains finite and therefore can be dropped. We note further that the variables P_2 and also the indices β and δ are not affected by the operations applied to the function Γ in Eq. (24), i.e., they here play the role of parameters. Finally, we shall consider Γ close to the Fermi surface, i.e., we shall consider the energy of the quasiparticle, which is one of the variables P_1, to be equal to μ, and the momentum to be equal to p_0, so that we write it in the form $p_0\mathbf{n}$, where $\mathbf{n}$ is a variable unit vector. Keeping all this in mind, we conclude that the determination of the sonic excitations in the liquid reduces to the problem of the eigenvalues of the integral equation

$$\chi_{\alpha\gamma}(\mathbf{n}) = \frac{a^2 p_0^2}{(2\pi)^3}\int \Gamma^{\omega}_{\alpha\varepsilon,\gamma\zeta}(\mathbf{n},\mathbf{l})\, \chi_{\zeta\varepsilon}(\mathbf{l})\, \frac{1\mathbf{k}}{\omega - v1\mathbf{k}}\, do, \tag{28}$$

where $\chi_{\alpha\gamma}(\mathbf{n})$ is an auxiliary function.

We transform this equation, introducing instead of χ a new function, by the substitution

$$\nu_{\alpha\gamma}(\mathbf{n}) = \frac{n\mathbf{k}}{\omega - vn\mathbf{k}}\, \chi_{\alpha\gamma}(\mathbf{n}). \tag{29}$$

Then Eq. (28) takes the form

$$(\omega - vn\mathbf{k})\, \nu_{\alpha\gamma}(\mathbf{n}) = (\mathbf{k}\cdot\mathbf{n})\frac{p_0^2 a^2}{(2\pi)^3}\int \Gamma^{\omega}_{\alpha\varepsilon,\gamma\zeta}(\mathbf{n},\mathbf{l})\, \nu_{\zeta\varepsilon}(\mathbf{l})\, do. \tag{30}$$

This equation agrees precisely in form with

equation (11) found in reference 2 for the distribution function ν in the zeroth sound, and moreover a comparison of the two equations (using the definition of F by Eq. (6) of reference 2) leads to the following correspondence between the function $f(\mathbf{p}, \mathbf{p}')$* and the function Γ^{ω}:

$$f_{\alpha\beta,\gamma\delta}(\mathbf{n},\mathbf{l}) = a^2\Gamma^{\omega}_{\alpha\beta,\gamma\delta}(\mathbf{n},\mathbf{l}) \tag{31}$$

This is the desired relation between f and the properties of the scattering of the quasiparticles. For clarity we point out that the four spin indices on this function correspond to the fact that $f(\mathbf{p},\mathbf{p}')$, or more explicitly $f(\mathbf{p},\sigma;\ \mathbf{p}',\sigma')$, depends on the spin operators (two-row matrices) σ and σ' of the two particles; thus to the two particles (momenta $p_0\mathbf{n}$ and $p_0\boldsymbol{l}$) there correspond the pairs of indices α,γ and β,δ (in the function $\Gamma_{\alpha\beta,\gamma\delta}(P_1,P_2;\ P_3,P_4)$ these pairs correspond to the pairs of nearly equal four-momenta P_1, P_3 and P_2, P_4).

Having thus found the connection of the function f with the properties of the scattering of the quasiparticles, let us return to the formula (27) and obtain with its aid explicit relations between the function f and the "physical" amplitude for zero-angle scattering on the Fermi surface, which we write in the form

$$A(\mathbf{n}_1,\sigma_1;\ \mathbf{n}_2,\sigma_2) = a^2\Gamma^k(\mathbf{n}_1,\sigma_1;\ \mathbf{n}_2,\sigma_2). \tag{32}$$

On the Fermi surface the relation (27) takes the form

$$A(\mathbf{n}_1,\sigma_1;\ \mathbf{n}_2,\sigma_2) = f(\mathbf{n}_1,\sigma_1;\ \mathbf{n}_2,\sigma_2) \tag{33}$$
$$-\frac{1}{4\pi}\frac{d\tau}{d\varepsilon}\mathrm{Sp}_{\sigma'}\int f(\mathbf{n}_1,\sigma_1;\ \mathbf{n}',\sigma')\,A(\mathbf{n}',\sigma';\mathbf{n}_2,\sigma_2)\,do'$$

(where $d\tau/d\epsilon = 4\pi p_0^2/v(2\pi)^3$). The scalar functions A and f depend on all scalar combinations of the four vectors $\mathbf{n}_1$, $\mathbf{n}_2$, σ_1, σ_2. If, however, the interaction between the particles is an exchange interaction, then the only admissible scalar products are $\mathbf{n}_1\mathbf{n}_2$ and $\sigma_1\sigma_2$. Then we can expand A and f as functions of $\cos\theta$ in terms of Legendre polynomials:

$$A(\cos\theta) = \sum_l A_l P_l(\cos\theta),\quad f(\cos\theta) = \sum_l f_l P_l(\cos\theta). \tag{34}$$

*In references 1 and 2 we did not write the spin indices explicitly.

Substituting this into Eq. (33) and performing the integration with respect to do', we get

$$A_l(\sigma_1,\sigma_2) = f_l(\sigma_1\sigma_2) - \frac{1}{2l+1}\frac{d\tau}{d\varepsilon}\mathrm{Sp}_{\sigma'} f_l(\sigma_1\sigma')\,A_l(\sigma'\sigma_2). \tag{35}$$

In the case of an exchange interaction the spin dependence of the function reduces to a term proportional to $\sigma_1\sigma_2$ (cf. reference 1*), so that

$$f_l = \varphi_l + \psi_l\sigma_1\sigma_2, \tag{36}$$

where φl, ψl do not depend on the spins. Corresponding to this we also set

$$A_l = B_l + C_l\sigma_1\sigma_2. \tag{37}$$

Substituting Eqs. (36) and (37) into Eq. (35), we get without difficulty

$$B_l = \varphi_l - \frac{2}{2l+1}\frac{d\tau}{d\varepsilon}B_l\varphi_l, \tag{38}$$

$$C_l = \psi_l - \frac{1}{2(2l+1)}\frac{d\tau}{d\varepsilon}C_l\psi_l.$$

These formulas give a simple algebraic connection between the coefficients of the expansions of f and A in spherical harmonics. We note that only terms of the same l are related to each other, and that B is related only to the φ's and C only to the ψ's.

In conclusion, I would like to thank A. B. Migdal, who called my attention to the dependence of the forward scattering amplitude on the ratio ω/k, and also E. M. Lifshitz and L. P. Gor'kov for a discussion of this work.

[1] L. D. Landau, J. Exptl. Theoret. Phys. (U.S.S.R.) **30**, 1058 (1956), Soviet Phys. JETP **3**, 920 (1956).
[2] L. D. Landau, J. Exptl. Theoret. Phys. (U.S.S.R.) **32**, 59 (1957), Soviet Phys. JETP **5**, 101 (1957).
[3] A. B. Migdal, J. Exptl. Theoret. Phys. (U.S.S.R.) **32**, 399 (1957), Soviet Phys. JETP **5**, 333 (1957).

Translated by W. H. Furry
13

*We take occasion to correct a mistake which got into reference 1: Equation (27) should be

$$1/\chi = \beta^{-2}\{4\pi^2k^2/3\alpha + \bar{\psi}_0\}.$$

THE NATURE OF PARTICLES THAT CARRY AWAY MOST OF THE ENERGY IN NUCLEAR COLLISIONS AT MODERATE ENERGIES

E. FRIEDLÄNDER and E. RUCKENSTEIN

Institute of Atomic Physics, Romanian Academy of Sciences; Polytechnic Institute, Bucharest

Submitted to JETP editor January 16, 1958

J. Exptl. Theoret. Phys. (U.S.S.R.) **35**, 104-110 (July, 1958)

The electron-nuclear shower transition curve in a dense absorber is computed by assuming the existence of an energetically-preferred particle in each step of the nuclear-cascade process. The fraction of disintegrating particles in the generating component is estimated by comparing this curve with absorption in air.

1. INTRODUCTION

RECENTLY obtained experimental data indicate that in high-energy nuclear collisions that lead to multiple meson production a considerable portion of the energy of the incident particle is apparently concentrated in one of the emerging particles. This follows both from the individual observations (mostly the Schein stars[1] and the HBD star[2]) and from the behavior of the nuclear-active component of cosmic rays in the atmosphere[3,4] and the structure of extensive atmospheric showers.[5,6]

It is clear that the existence of such a preferred particle is responsible for the most important features of the nuclear-cascade process and affects substantially the comparison of experimental data with various theories concerning the elementary act.

An important problem, which can still be considered unsolved, is connected with the very nature of this particle. Thus, for example, it follows from the Heisenberg theory[7] that, at least at large impact parameters, the nucleon transfers only an insignificant portion of its energy to the meson field. Consequently, within the framework of this theory, the energetically preferred particle (abbreviated e.p.p.) must of necessity be a nucleon.

On the contrary, the Landau theory[8] leads only to a concentration of a large fraction of the system energy in a certain region that contains a small number of particles (on the order of unity). But in principle nothing contradicts the possibility of the being a meson in some cases and a nucleon in others. Calculations made by Belen'kii[9] lead only to the conclusion that the energy is concentrated somewhat more on the nucleons than on the pions.

On the other hand, in a previous work by one of us[10] it was shown that if the existence of a certain nuclear structure is admitted in the sense of the Bhabha theory,[11] a sharp difference in the distribution of the mass density in the nucleon and in the pion can cause the appearance of an e.p.p.

If such a collision model is analyzed on the basis of the Fermi theory,[12] one obtains a finite probability that the e.p.p. is a pion. If, the Heisenberg theory is applied to this model, this probability turns out to be even greater.

From the experimental point of view the situation is still unclear, for at large energies there is no direct and reliable method for distinguishing mesons from nucleons and hyperons. The presently-available information on the nature of the e.p.p. has been obtained indirectly and is in part contradictory.

Thus, starting with a comparison of the energy flux of the primary protons with the energy flux of the hard component in the atmosphere[13] and underground,[14] the authors of the works cited have concluded that the probability of concentration of a large fraction of the energy on the pion (or on some other particle, which disintegrates directly or indirectly into a pion or muon) is quite small (at any rate, less than follows, for example, from the Fermi-Landau theory). We shall deal with this problem later.

On the other hand, a study of the nuclear-active particles of moderate energies (i.e., particles that generate local electron-nuclear showers, usually recorded in experiments with counters) has disclosed[15-19] a clearly pronounced compensation effect. If the transition effect of the density[20-21] is excluded, this indicates directly the spontaneous disintegration of a certain fraction of the generated particles into nuclearly-passive ones. Consequently, these particles cannot be hyperons, for all known hyperons decay into nuclearly-active particles (p, π, Λ^0). By comparing the ranges

for absorption of the generated particles in air and in dense substances, the authors of references 15 to 17 estimated the fraction of such decaying particles at approximately $\frac{1}{3}$.

In the interpretation of experiments of this type, however, it is necessary to bear in mind that there is a principal difference between absorption measurements in air and in dense substances. In air we measure the absorption proper of individual nuclear-active particles, whereas in a dense substance all the penetrating secondary particles, including the nuclearly-passive ones, make a certain contribution to the operation of the detector. Thus, the "absorption" of the observed effect will depend also on the multiplicity of the secondary particles, on their effective cross sections, etc.

It is indeed the purpose of this article to explain the influence of these factors on the course of the transition curve of electron-nuclear showers in dense substances. The results obtained are compared with the absorption in air and can contribute to the solution of the problem concerning the existence of unstable particle along the e.p.p.

2. TRANSITION CURVE

Let us consider a detector sensitive to a penetrating component of electron-nuclear showers, placed under a dense absorber of thickness l.*

We assume for the sake of simplicity that the detector responds with equal efficiency to any shower capable of producing at least Q_0 penetrating particles at the counter level.†

We shall schematize the elementary interaction act and the cascade process in the absorber in the following manner:

(a) When a nuclear-active particle of energy E interacts with the nucleus of the absorber, a relatively small portion of the energy is transferred to the meson field. This portion goes into production of pions, whose number depends on the energy in accordance with the following power law‡

$$n = AE^{g}. \tag{1}$$

(b) The major fraction β of the energy E is carried away by a single particle, capable of experiencing further interaction in the same absorber. We shall consider β constant in the first approximation, without losing sight of the fact that actually β can have a certain spread, which we intend to take into account in a further refinement of the model. Owing to the small dimensions of the dense absorber, the nature of the e.p.p. is of no importance. It is merely important that its effective cross section be constant and equal to the geometric cross section.

(c) The energy $(1-\beta)E$ transferred to the mesons is sufficiently small and the multiplicity of the mesons is sufficiently large, so that none of them is capable of generating new penetrating particles. In this sense they are nuclearly passive, although their absorption and geometric cross sections are the same. It must borne in mind, however, that it is these particles that cause detector operation. Let Q be the number of such particles, reaching the counter level. Assume that an "event" is registered if and only if $Q \geq Q_0$.

(d) Further generation of particles under the influence of the e.p.p. ceases as soon as the energy of the latter drops below a certain threshold value E_c.

(e) Ionization losses of the charged particles can be neglected.

(f) The problem is solved in the unidimensional approximation.

Consider now an incident particle of energy E, which experiences i collisions in the absorber. The number of events of this kind is given,

$$d\nu(l, E, i) = F(E)\,dE \cdot e^{-l} l^{i}/i!, \tag{2}$$

where $F(E)dE$ is the energy spectrum of the incident nuclear-active particle; for $E > E_c$ we assume that this spectrum obeys the power law form

$$F(E)dE \sim E^{-s}dE/E. \tag{3}$$

The total number of coincidences $\nu(l)$ registered per unit time at a depth l is obtained from (2) by summation and integration over all values of i and E, compatible with conditions (c) and (d). The corresponding limits of summation and integration can be derived in the following manner.

Let E_i be the energy of the e.p.p. after the i-th collision. Condition (d) makes it possible to determine a certain critical number of collisions i_c, beyond which generation of nuclear showers ceases (i.e., the e.p.p. is absorbed). This critical number is obtained from

$$\beta^{i_c} E = E_c. \tag{4}$$

On the other hand, it follows from (a), (b), and (c) that $Q = Q(E, l, i)$. This equation admits in principle of a solution $i = i(Q, l, E)$. For a given energy E it is possible to determine the

*The unit of thickness is taken to be the interaction length.

†The generalization to the case of another form of detector-operation probability presents no difficulties in principle.

‡A system of units is used in which $\hbar = c = M = 1$, M being the mass of the nucleon.

minimum number of collisions i_0 necessary to produce, at a depth l, those Q_0 particles needed to trigger the equipment:

$$i_0 = i(Q_0,\ l,\ E). \tag{5}$$

It follows hence that the incident nuclear-active particle is registered by the instrument only if

$$i_0(Q_0, l, E) \leqslant i_c(\beta, E). \tag{6}$$

Owing to the discrete character of the quantities i_0 and i_c, the value of i' satisfying the equation

$$i_0(Q_0, l, E) = i_c(\beta, E), \tag{7}$$

corresponds to a certain finite interval of values of E.

Let E' be the minimum value of E in that interval [i.e., the minimum value of E commensurate with the solution of Eq. (7)]. It follows then from (2), (5), and (6) that

$$\nu(l) = \int_{E'}^{\infty} F(E)\,dE \sum_{i_0}^{\infty} e^{-l} l^i / i!. \tag{8}$$

This indeed is the sought equation for the transition curve.

For a specific calculation of this curve we need merely write down the explicit dependence of Q_0 on E and i. We shall use for this purpose the Rozental' cascade equations,[22] simplified for the conditions of our special model.

Let $P_i(l)$ be the number of nuclear active particles of the i-th generation at a depth l and let $M_i(l)$ be the number of "passive" mesons [in the sense of condition (c)] of the same generation. The cascade equations assume under these conditions the following simple form

$$\begin{aligned} dP_i(l)/dl &= -P_i(l) + P_{i-1}(l),\ P_0(l) = e^{-l}, \\ dM_i(l)/dl &= -M_i(l) + AE_{i-1}^{g} P_{i-1}(l). \end{aligned} \tag{9}$$

This system can be readily integrated and yields

$$\begin{aligned} P_i(l) &= e^{-l} l^i / i!, \\ M_i(l) &= A(E/\beta)^g e^{-l} (l\beta^g)^i / i!, \qquad i \geqslant 1. \end{aligned} \tag{10}$$

From this it is easy to obtain the summation over i

$$Q(i, E, l) = A\left(\frac{E}{\beta}\right)^g e^{-l} \sum_{r=1}^{l} (l\beta^g)^r / r!. \tag{11}$$

For further calculation, it is convenient to introduce a new variable z,

$$z = (E_c/E)^g. \tag{12}$$

From (11) and (5) we also obtain

$$z = \frac{A}{Q_0}\left(\frac{E_c}{\beta}\right)^g e^{-l} \sum_{r=1}^{i_0} (l\beta^g)^r / r!. \tag{13}$$

Using the spectrum (3), it is easy to transform (8) into

$$\nu(l) = \int_0^{z'(l)} \theta z^{\theta}\,\frac{dz}{z} - \int_0^{z'(l)} \theta z^{\theta}\,\frac{dz}{z} \sum_{i=0}^{i_0-1} \frac{l^i e^{-l}}{i!}, \tag{14}$$

where $\theta = s/g$, and z' is obtained from (4) by replacing E with E'.

Taking into account the discrete (jump-like) change of i_0, the second integral in (14) can be expanded into a sum of integrals; after elementary calculations we obtain

$$\nu(l) = z'^{\theta} - e^{-l} \sum_{k=1}^{k=i'} (z_k^{\theta} - z_{k-1}^{\theta}) \sum_{i=1}^{k-1} \frac{l^i}{i!}, \tag{15}$$

where

$$z_0 = 0,\ z_{i'} = z'.$$

Using (15), we have calculated the curves $\nu(l)$ for certain pairs of sensible values of β and g. It turned out that $\nu(l)$ has a sharply pronounced maximum near $l = 1$ or 2. The position of this maximum and the course of the $\nu(l)$ curve before the maximum depend little on β, but depend strongly on g. Beyond the maximum, the transition curve can be approximated by an exponential curve, the exponent is practically independent of g, and depends only on β. This can be seen also from the asymptotic behavior of (15), which for $l \gg 1$ reduces practically to

$$\nu(l) \approx [z'(l)]^{\theta}. \tag{16}$$

On the other hand, for $l \gg 1$ we have $z' \approx \beta^{i'g}$ and since under these conditions $i' \approx l$, then

$$\nu(l) \approx \exp\{-ls \ln(1/\beta)\} \tag{17}$$

and is independent of g.

3. COMPARISON WITH ABSORPTION IN THE ATMOSPHERE

Bearing in mind the positive results of the compensation experiments,[15-19] we shall assume that there exists a finite probability q that the e.p.p. is a charged pion (or any other meson that yields only nuclearly-passive particles upon disintegration). The cascade equations can be written in this case separately for the nucleons and for the nuclear-active mesons

$$\begin{aligned} dN_i^*(l)/dl &= -N_i^*(l) + (1-q)[N_{i-1}^*(l) + M_{i-1}^*(l)], \\ N_0(l) &= e^{-l}, \\ dM_i^*(l)/dl &= -M_i^*(l)(1 + k/l\beta^i) + q[N_{i-1}^*(l) + M_{i-1}^*(l)], \\ M_0(l) &= 0, \end{aligned} \tag{18}$$

where $k = 460/E$ for pions.

This system is readily integrated and, for energies that are not too high (i.e., in the approximation $k \gg 1$), yields the total number of particles of the i-th generation*

$$P_i(l) = [l(1-q)]^i e^{-l}/i!. \quad (19)$$

The total number of generating particles $P(l)$ is given by an expression similar to (8):

$$P(l) = \int_{E_c}^{\infty} F(E)\,dE \sum_{i=0}^{i=i_c(E)} [l(1-q)]^i e^{-l}/i!, \quad (20)$$

where $i_c(E)$ is determined from (4).

Equation (20), like Eq. (8), can be integrated by intervals. We get

$$P(l) \sim e^{-l(1-\Delta)}, \quad \Delta = (1-q)\beta^s. \quad (21)$$

As was to be expected, this result agrees with the known relation of Zatsepin,[23] with accuracy to a factor $(1-q)$. The same result can be derived also from simpler considerations, assuming only that all pions have a chance to disintegrate prior to interaction with the nucleus. From the considerations given above (see remark*) it follows that not more than 10% of the mesons still have a chance to interact with the nuclei in the considered range.

We can now proceed to compare the two obtained results with the experimental data. From the large number of experiments it is known (see, for example, reference 24) that $\Delta \approx 0.5$ in air. On the other hand, reference 18 reports the same value $\lambda_A \approx 3.5$ for the absorption ranges in lead, iron, and carbon. Reference 16 reports $\lambda_a \approx 2.6$ for water. Using the value $s = 1.5$ (reference 25), we obtain, with the aid of (17), $\beta \sim 0.7$ to 0.8. Inserting this value into (21), we get $q \approx 0.25$ to 0.30.

4. CONCLUSIONS

If the schematized model of interaction at moderate energies employed in this work is not too different from actuality, then the bulk of experimental data indicates apparently that, although most e.p.p. are nucleons, there is nevertheless a noticeable probability of the e.p.p. being an unstable particle other than a hyperon. Such particles can be $\pi^{\pm}$, K_μ, and K_e mesons, but not θ or τ mesons. In connection with this, it is interesting to note recent observation[26] of an electron-nuclear shower in which both the incident and emerging e.p.p. were pions.

In the present state of the problem, it is quite desirable both to refine the theoretical model and to obtain experimental data that refine the details of the phenomenon. It is important, for example, to establish whether the cited compensation experiments contain effects that are similar to the transition effect of density, and to establish the role of these effects, which can increase the apparent value of β, and consequently also of q. On the other hand it must be emphasized, that, within the framework of our model, comparison of the flux of high-energy μ mesons with the flux of primary protons does not give a negligible value of q. Using the relation, introduced by Zatsepin et al.,[14] for the flux of μ mesons with $E > 10^{13}$ arising from the first collision of the primary protons, but using merely the spectrum of the primary protons multiplied by q for the creation spectrum of the pions, we obtain $q \sim 0.14$.

Although the independence of q of the energy does not follow of necessity from the different theories of the elementary act, let us note merely that the discrepancy between the two values (0.14 and 0.25) obtained for q can be ascribed, at least partially, to the copious production, at high energies, of mesons that do not disintegrate directly or indirectly into muons or pions.

We express our gratitude to Academician D. V. Skobel'tsyn and the staff of the Cosmic-Rays Laboratory of the Physics Institute, Academy of Sciences, U.S.S.R. for critical evaluation of this work and for valuable comments.

*The solution of the system of equations (18) actually has the form

$$P_i(l) = e^{-l}\, l^i\, \Phi(i) \prod_{j=1}^{i-1} \Phi(j)/(j+1),$$

where

$$\Phi(j) = 1 - q + qj\beta^j/(j\beta^j + k).$$

$\Phi(j)$ has a maximum at $j \ln \beta = -1$; for $\beta \approx 0.8$ this corresponds to values of $j \approx 4$ and $j\,\beta^j \approx 1.6$. Introducing for E its value averaged over the spectrum (assuming $E_c \approx 10$, i.e., $\bar{E} \approx 30$), we find that the value of q, approximately calculated from (19), is ~ 10% below the actual value.

[1] Glasser, Haskin, Schein, and Lord, Phys. Rev. **99**, 1555 (1955).

[2] Hopper, Bismas, and Darby, Phys. Rev. **80**, 970 (1950).

[3] N. L. Grigorov and N. V. Murzin, Izv. Akad. Nauk SSSR, Ser. Fiz. **17**, 21 (1953).

[4] N. L. Grigorov, Dokl. Akad. Nauk SSSR **94**, 835 (1954).

[5] Dobrotin, Zatsepin, Nikol'skii, Sarycheva, and Khristiansen, Izv. Akad. Nauk SSSR, Ser. Fiz. **19**, 666 (1955) [Columbia Techn. Transl. **19**, 605 (1955)].

[6] N. A. Dobrotin, Paper delivered at International Cosmic-Rays Conference, Budapest, 1956.

[7] W. Heisenberg, Z. Physik, **126**, 569 (1949).
[8] L. D. Landau, Izv. Akad. Nauk SSSR, Ser. Fiz. **17**, 51 (1953).
[9] S. Z. Belen'skii, Dokl. Akad. Nauk SSSR **99**, 523 (1954).
[10] E. Friedländer, Hung. Phys. Acta **5**, 237 (1956).
[11] H. Bhabha, Proc. Roy. Soc. **A219**, 293 (1953).
[12] E. Fermi, Progr. Theoret. Phys. **5**, 570 (1950).
[13] Vernov, Grigorov, Zatsepin, and Chudakov, Izv. Akad. Nauk SSSR, Ser. Fiz. **19**, 493 (1955) [Columbia Techn. Transl. **19**, 445 (1955)].
[14] Guzhavina, Guzhavin, and Zatsepin, J. Exptl. Theoret. Phys. (U.S.S.R.) **31**, 819 (1956), Soviet Phys. JETP **4**, 690 (1957).
[15] Veksler, Kurnosova, and Liubimov, J. Exptl. Theoret. Phys. (U.S.S.R.) **17**, 1026 (1947).
[16] Azimov, Vishnevskii, and Khilko, Dokl. Akad. Nauk SSSR, **76**, 231 (1951).
[17] S. Azimov and V. F. Vishnevskii, Izv. Akad. Nauk SSSR, Ser. Fiz. **17**, 88 (1953).
[18] Azimov, Dobrotin, Liubimov, and Ryzhkova, Izv. Akad. Nauk SSSR, Ser. Fiz. **17**, 80 (1953).
[19] Friedländer, Jussim, and Mayer, Studii si Cer. de Fizica, **6**, 229 (1955).
[20] M. I. Podgoretskii, J. Exptl. Theoret. Phys. (U.S.S.R.) **21**, 1090 (1951).
[21] Podgoretskii, Barchikov, and Rakitin, Dokl. Akad. Nauk SSSR **73**, 685 (1950).
[22] I. L. Rozental', J. Exptl. Theoret. Phys. (U.S.S.R.) **23**, 440 (1952).
[23] G. T. Zatsepin, J. Exptl. Theoret. Phys. (U.S.S.R.) **19**, 1104 (1949).
[24] G. B. Zhdanov, Usp. Fiz. Nauk **54**, 435 (1954).
[25] Camerini, Fowler, Lock, and Muirhead, Phil. Mag. **41**, 413 (1950).
[26] Birger, Guseva, Kotel'nikova, Maksimenko, Riabikov, Slavatinskii, and Stashkov, J. Exptl. Theoret. Phys. (U.S.S.R.) **31**, 982 (1956), Soviet Phys. JETP **4**, 836 (1957).

Translated by J. G. Adashko
14

SOVIET PHYSICS JETP VOLUME 35 (8), NUMBER 1 JANUARY, 1959

POSSIBILITY OF DETERMINING THE INTERACTION CONSTANTS FROM EXPERIMENTS ON $K_{\mu 3}$ DECAYS

I. G. IVANTER

Institute of Scientific Information, Academy of Sciences, U.S.S.R.

Submitted to JETP editor January 16, 1958

J. Exptl. Theoret. Phys. (U.S.S.R.) **35**, 111-115 (July, 1958)

Expressions are derived for the spectra and polarization of μ mesons created in $K_{\mu 3}$ decays for fixed pion energies and arbitrary complex interaction functions. It is shown that, accurate to within an unimportant phase shift, it is possible to determine all interaction functions from measurements of the spectra and three polarizations, with the exception of the second vector function. The latter cannot be separated in the above experiments from the first-vector and scalar interaction functions. The presence of tensor interaction can be ascertained from measurements of the spectrum and polarizations of μ mesons at an energy close to maximum.

EXPRESSIONS for the spectrum of μ mesons, as well as for their polarization, were obtained by various authors.[1-11] However, no calculations were made for the case of arbitrary complex constants,* nor were they analyzed from the point of view of the possibility of determining all the constants experimentally. If the interaction is assumed to be local, the most general expression for the transition matrix element is of the form

$$\langle\bar{\psi}_\mu\{(g_S+i\gamma_5 g_S')+(g_V+i\gamma_5 g_V')\gamma_4+{}^1/_2 M^{-1}(g_T+i\gamma_5 g_T')\times(\gamma_4\hat{p}_\pi-\hat{p}_\pi\gamma_4)\}\psi_\nu\rangle(2M^{3/2}E_\pi^{1/2})^{-1}. \quad (1)$$

Here M is the mass of the K meson, and p_π

*In fact, the interaction constants may depend on the pion energy, and shall henceforth be referred to as "functions."

and E_π are the 4-momentum and energy of the pion respectively.

Only one vector variant is taken into account in the matrix element, because the second vector variant can be reduced to the first vector and scalar variants, as was noted by Pais and Treiman.[11] It must be indicated that this reduction is possible only if the electromagnetic interaction is neglected. The expression for the spectrum is written in the following manner:

$$\delta W_1(E_\pi, E_\mu) = (32\pi^3 M^3)^{-1} dE_\pi dE_\mu \{A_0 + A_1 E_\mu + A_2 E_\mu^2\}. \quad (2)$$

Here A_i, like B_i, C_i, and D_i below, are functions of the pion energy and of the interaction function. The expressions for A_i, B_i, C_i and D_i are given in the Appendix.

For the degree of longitudinal polarization, multiplied by the probability of decay with given meson energies (or, in other words, for the differences of the spectra of μ-mesons polarized with and against the momentum at fixed pion energy), we obtain the following expression

$$\delta W_2(E_\pi, E_\mu) = (32\pi^3 M^3)^{-1} dE_\pi dE_\mu \{B_0 + B_1 E_\mu + B_2 E_\mu^2 + B_3 E_\mu^3\}. \quad (3)$$

In the case of transverse polarization in the plane of the decay (along the direction of $\mathbf{J}_2$, which makes a sharp angle with the pion momentum and a right angle with the muon momentum) the analogous expression is

$$\delta W_3(E_\pi, E_\mu) = -|p_\pi||\sin\theta|(32\pi^3 M^3)^{-1} dE_\pi dE_\mu \{C_0 + C_1 E_\mu + C_2 E_\mu^2\}.$$

Here θ is the angle between the pion and muon momenta.

For the difference in the spectra of muons polarized in the direction $\mathbf{J}_3 = (\mathbf{p}_\pi \times \mathbf{p}_\mu)/|(\mathbf{p}_\pi \times \mathbf{p}_\mu)|$, perpendicular to the plane of decay (which is forbidden by the law of conservation of combined parity), we obtain, for a fixed pion energy, the following expression

$$\delta W_4(E_\pi, E_\mu) = p_\mu p_\pi |\sin\theta| \{D_0 + D_1 E_\mu\} dE_\pi dE_\mu (32\pi^3 M^3)^{-1} \quad (4)$$

The expressions for δW_2 and δW_3 contain six combinations of interaction functions. These expressions are polynomials of third and second degree respectively. It is possible therefore to set up seven equations from the experimental data. An investigation of the determinant of the system has shown that at least six of the seven equations are linearly independent.

From the spectral data it is possible to obtain three more equations and the polarization perpendicular to the plane of the decay yield two more. A total of eleven equations can thus be obtained. Hence, with accuracy to a non-essential phase shift, it is possible to obtain all the interaction functions. Naturally, the second vector variant cannot differ in this case from S or V_1. However, with this reservation, a complete experiment is possible.

It is of interest, however, to obtain certain information on the interaction functions from data on only part of the experiments. Such information can be obtained from data on the spectra of the longitudinally-polarized muons at fixed energy E_π. If we regroup the terms in expression (3), the result is

$$\delta W_2(E_\pi, E_\mu) = dE_\pi dE_\mu (32\pi^3 M^3)^{-1} \{b_T \Phi_T + b_V \Phi_V + b_{VT} \Phi_{VT} + b_{ST} \Phi_{ST} + b_S \Phi_S + b_{SV} \Phi_{SV}\}. \quad (5)$$

Here

$$b_T = -2\mathrm{Re}(g'_T g_T^*); \quad b_V = -2\mathrm{Re}(g'_V g_V^*);$$
$$b_S = -2\mathrm{Re}(g'_S g_S^*); \quad b_{VT} = -2\mathrm{Re}(g_V g_T'^* - g'_V g_T^*);$$
$$b_{ST} = -2\mathrm{Re}(g_S g_T'^* + g'_S g_T^*); \quad b_{SV} = -2\mathrm{Re}(g_S g_V'^* - g'_S g_V^*).$$

The values of the functions Φ_i are given in the Appendix.

The diagram shows the region of variation of the pion and muon energies, allowed by the laws of momentum and energy conservation. This region is plotted for K^0 decays, i.e., the following mass values are assumed: $M_{K^0} = 495$ Mev, $m_{\pi^\pm} = 139.6$ Mev, $m_\mu = 105.7$ Mev, $c^2 = 1$.

The diagram shows, inside the allowed zone, the curves on which the functions Φ_i vanish. The closer a point is to the curve, the less the probability contribution due the term corresponding to the curve. These curves intersect at several points. If a probability other than zero is observed at such points, it means that there is at least one non-vanishing variant, whose line does not pass through the given point. Of particular in-

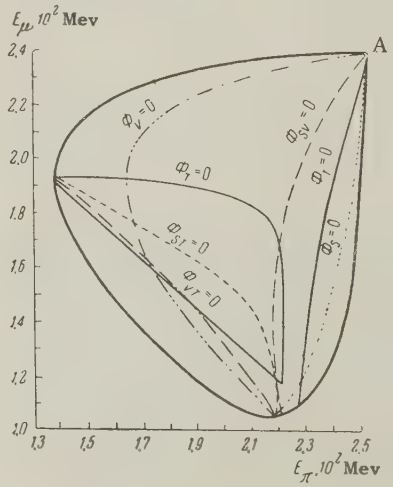

Zero lines of pure and interference terms.

terest is point A, corresponding to maximum muon energy. It is not necessary to know the pion energy to carry out measurements at this point, and the experiment can thus be facilitated somewhat. If it is found that the probability density for the emission of longitudinally polarized mesons differs from zero near the point, this means that at least one of the S or T variants is present, provided the measurement is carried out in a region on the order of 3 to 5 Mev from the limiting energy. The line of the zeros of the first vector variant will approach quite gently the boundary of the region in the boundary energy. If the above energy density is seen to be unequal to zero in a region on the order of 0.5 Mev, this means the existence of the tensor variant, for in this case the interference term ST would differ from zero. Naturally, if the π-meson energy is fixed, no such accuracy is necessary.

It must be emphasized here again that in our notation the second vector variant $\langle\bar{\psi}_\mu p_\pi(g_\mu - i\gamma_5 g'_{V_2})\psi_\nu\rangle$ is reduced to the first vector and scalar variants. Therefore the presence of a scalar variant can be interpreted also as the presence of the second vector variant. In connection with this, it is particularly important to establish the presence of a tensor variant.

The remaining points require simultaneous measurement of the pion energy.

We call attention to the fact that $\delta W_3/|\sin\theta|$ is a second-order polynomial in E_m if, and only if, the interference term VT differs from zero, i.e., if the tensor and vector variants exist simultaneously. If there is no such term, then $\delta W_3/|\sin\theta|$ depends linearly on the muon energy or becomes constant.

The expressions for the spectrum and for the longitudinal polarization of the pions were integrated by various authors (the spectra by Furuchin et al.[2] and Matinina,[7,8] and the spectra and polarizations by Okun'[1]) under the assumption that the interaction functions are independent of the pion energy. From the expressions obtained by Okun' it is easily seen that if the interaction constants are considered independent of the pion energy, it is possible to determine experimentally, from measurements of the spectrum and of the longitudinal polarization, all twelve combinations of the interaction constant.

I thank L. B. Okun' for suggesting the problem and for evaluation, and K. A. Ter Martirosian for discussions.

APPENDIX

We give below the values of the functions A_i, B_i, C_i, and D_i:

$$A_0 = a_T\left[\left(ME_\pi - \frac{\Delta}{2}\right)(2ME_\pi - \Delta - E_\pi^2 + m_\pi^2) - m_\pi^2 m_\mu^2 + m_\mu^2 E_\pi^2\right]M^{-2} + a_{VT}\left(\frac{\Delta}{2} - ME_\pi - m_\pi^2 + E_\pi^2\right)m_\mu M^{-1}$$
$$+ a_V\left(m_\mu^2 + ME_\pi - \frac{\Delta}{2}\right) + a_{SV}m_\mu(M - E_\pi) + a_{ST}\left(ME_\pi - \frac{\Delta}{2}\right)(E_\pi - M)M^{-1} + a_S\left(\frac{\Delta}{2} - ME_\pi - m_\mu^2\right);$$
$$A_1 = a_T 2(2ME_\pi - \Delta)(M - E_\pi)M^{-2} + a_{VT}(E_\pi - M) + a_V 2(M - E_\pi) + a_{ST}(2E_\pi M - m_\pi^2 - M^2)M^{-1} + a_{SV}(-m_\mu);$$
$$A_2 = a_T 2M^{-2}(m_\pi^2 - 2ME_\pi + 2M^2) - 2a_V.$$

Here

$$\Delta = M^2 + m_\pi^2 + m_\mu^2;\ a_T = |g_T|^2 + |g'_T|^2;\ a_V = |g_V|^2 + |g'_V|^2;\ a_S = |g_S|^2 + |g'_S|^2;\ a_{VT} = 2\mathrm{Re}(g_V g_T^* - g'_V g'^*_T);$$
$$a_{ST} = 2\mathrm{Re}(g_T g_S^* + g'_T g'^*_S);\ a_{SV} = 2\mathrm{Re}(g_S g_V^* - g'_S g'^*_V).$$

$$B_0 = b_S m_\mu^2(M - E_\pi) + b_{SV}\left(\frac{\Delta}{2} - ME_\pi - m_\mu^2\right)m_\mu + b_{ST}\left[m_\mu^2\left(\frac{\Delta}{2} - m_\pi^2\right) + (E_\pi - M)E_\pi m_\mu^2\right]M^{-1} + b_V m_\mu^2(M - E_\pi)$$
$$+ b_{VT}M^{-1}m_\mu\left(ME_\pi - \frac{\Delta}{2}\right)(M - E_\pi) + b_T(M - E_\pi)(E_\pi^2 - m_\pi^2)m_\mu^2 M^{-2};$$
$$B_1 = b_S\left(ME_\pi - \frac{\Delta}{2}\right) + b_{SV}m_\mu(E_\pi - M) + b_{ST}M^{-1}\left(m_\mu^2 + \frac{\Delta}{2} - ME_\pi\right)(E_\pi - M) + b_V\left(\frac{\Delta}{2} - ME_\pi - 2m_\mu^2\right)$$
$$+ b_{VT}M^{-1}\left[\frac{\Delta}{2}m_\mu + E_\pi^2 m_\mu + Mm_\mu(M - 3E_\pi)\right] + b_T M^{-2}\left[2m_\mu^2 m_\pi^2 - 2E_\pi^2 m_\mu^2 + \left(\frac{\Delta}{2} - ME_\pi\right)(2ME_\pi - \Delta - E_\pi^2 + m_\pi^2)\right];$$
$$B_2 = b_{SV}m_\mu + b_{ST}(m_\pi^2 - 2ME_\pi + M^2)M^{-1} + b_V 2(E_\pi - M) + b_{VT}m_\mu(E_\pi - M)M^{-1} + b_T 4M^{-1}\left(\frac{\Delta}{2} - E_\pi\Delta/2M - ME_\pi + E_\pi^2\right);$$
$$B_3 = 2b_V + b_T(4E_\pi M - 2m_\pi^2 - 2M^2)M^{-2};\quad C_0 = -b_S m_\mu + b_{ST}m_\mu(E_\pi - M)M^{-1} + b_V m_\mu - b_{VT}m_\mu^2 M^{-1}$$
$$+ b_T m_\mu\left[2\left(ME_\pi - \frac{\Delta}{2}\right) - E_\pi^2 + m_\pi^2\right]M^{-2};\quad C_1 = b_{SV} + b_{ST}\frac{m_\mu}{M} + b_{VT}(E_\pi - M)M^{-1} + b_T 2m_\mu(M - E_\pi);$$
$$C_2 = b_{VT}2M^{-3}.\ D_0 = M^{-1}\left(d_{SV} + \frac{m_\mu}{M}d_{ST} + \frac{M - E_\pi}{M}d_{VT}\right);\ D_1 = -2d_{VT}M^{-2}.$$

Here

$$d_{SV} = -2\mathrm{Im}\,(g_S g_V^* - g_S' g_V'^*);\quad d_{ST} = 2\mathrm{Im}\,(g_T g_S^* + g_T' g_S'^*);\ d_{VT} = -2\mathrm{Im}\,(g_V g_T^* - g_V' g_T'^*).$$

$$\Phi_S = E_\mu\left(ME_\pi - \frac{\Delta}{2}\right) + m_\mu^2 (M - E_\pi);\ \Phi_{SV} = E_\mu^2 m_\mu + E_\mu (E_\pi - M)\, m_\mu + m_\mu\left(\frac{\Delta}{2} - ME_\pi - m_\mu^2\right);$$

$$\Phi_{ST} = E_\mu^2\left(\frac{m_\pi^2}{M} - 2E_\pi + M\right) + E_\mu\left\{-m_\mu^2 + \frac{E_\pi m_\mu^2}{M} + (E_\pi - M)\left(\frac{\Delta}{2M} - E_\pi\right)\right\} + M^{-1}\left\{m_\mu^2\left(\frac{\Delta}{2} - m_\pi^2\right) + (E_\pi - M)\, E_\pi m_\mu^2\right\};$$

$$\Phi_V = 2E_\mu^3 + E_\mu^2(-2M + 2E_\pi) + E_\mu\left\{\left(\frac{\Delta}{2} - ME_\pi\right) - 2m_\mu^2\right\} + m_\mu^2 (M - E_\pi);$$

$$\Phi_{VT} = E_\mu^2 M^{-1} m_\mu (E_\pi - M) + E_\mu M^{-1}\left\{\frac{\Delta}{2} m_\mu + E_\pi^2 m_\mu + M m_\mu (M - 3E_\pi)\right\} + M^{-1}\left\{m_\mu\left(ME_\pi - \frac{\Delta}{2}\right)(M - E_\pi)\right\};$$

$$\Phi_T = M^{-2}E_\mu^3\{4E_\pi M - 2m_\pi^2 - 2M^2\} + E_\mu^2 M^{-1} 4\left(\frac{\Delta}{2} - \frac{E_\pi \Delta}{2M} - ME_\pi + E_\pi^2\right) + E_\mu M^{-2}\left\{2m_\pi^2 m_\mu^2 - 2E_\pi^2 m_\mu^2\right.$$

$$\left. + \left(\frac{\Delta}{2} - ME_\pi\right)(2ME_\pi - \Delta - E_\pi^2 + m_\pi^2)\right\} + (M - E_\pi)(E_\pi^2 - m_\pi^2) m_\mu^2 M^{-2}.$$

[1] S. Furuichi et al., Progr. Theoret. Phys. **17**, 89 (1957).

[2] S. Furuichi et al., Progr. Theoret. Phys. **17**, 89 (1957).

[3] S. Furuichi et al., Nuovo cimento **5**, 285 (1957).

[4] J. Werle, Preprint, 1957.

[5] J. Werle, Nucl. Phys. **1**, 171 (1957).

[6] J. M. Charap, Preprint, 1957.

[7] S. G. Matininan, J. Exptl. Theoret. Phys. (U.S.S.R.) **33**, 797 (1957), Soviet Phys. JETP **6**, 614 (1958).

[8] S. G. Matinian, J. Exptl. Theoret. Phys. (U.S.S.R.) **32**, 929 (1957), Soviet Phys. JETP **5**, 757 (1957).

[9] S. G. Matinian, J. Exptl. Theoret. Phys. (U.S.S.R.) **31**, 529 (1956), Soviet Phys. JETP **4**, 434 (1957).

[10] L. B. Okun', Nucl. Phys. **5**, 455 (1958).

[11] A. Pais and S. B. Treiman, Phys. Rev. **105**, 1616 (1957).

Translated by J. G. Adashko
15

SOVIET PHYSICS JETP VOLUME 35 (8), NUMBER 1 JANUARY, 1959

THEORY OF EXCITATION OF HYDROMAGNETIC WAVES

A. I. AKHIEZER and A. G. SITENKO

Physico-Technical Institute, Academy of Sciences, Ukrainian S.S.R.

Submitted to JETP editor January 29, 1958

J. Exptl. Theoret. Phys. (U.S.S.R.) **35**, 116-120 (July, 1958)

Excitation of hydromagnetic and magnetoacoustic waves by external currents is investigated. Damping of the waves as a result of conductivity and viscosity is taken into account. The intensity of excitation by currents is compared with the intensity of excitation by mechanical means.

1. As is well known, propagation of hydromagnetic and magnetoacoustic waves is possible in a conducting liquid located in an external magnetic field.[1] In the experiments of Lundquist,[2] hydromagnetic waves were excited in liquid mercury by mechanical means, with the use of a rotating disk equipped with blades. Excitation of hydromagnetic waves is also possible by means of external variable currents. It is therefore of interest to determine the intensity of the excitation of hydromagnetic waves by this method and to compare this intensity with that of the excitation of hydromagnetic waves by mechanical means. The present paper is devoted to a consideration of this problem.

2. Let us consider an ideal compressible conducting liquid located in an external magnetic field $\mathbf{H}_0$. The motion of the liquid in the present of external currents $\mathbf{j}_0$ will be determined by the equations of hydrodynamics:

$$\rho \frac{\partial \mathbf{v}}{\partial t} + \rho (\mathbf{v}\nabla)\mathbf{v} = -\nabla p + \frac{\mu}{c}[\mathbf{j} \times \mathbf{H}], \qquad (1)$$

$$\frac{\partial \rho}{\partial t} + \operatorname{div}(\rho \mathbf{v}) = 0$$

and Maxwell's equations

$$\operatorname{curl} \mathbf{E} = -\frac{\mu}{c}\frac{\partial \mathbf{H}}{\partial t}, \quad \operatorname{div} \mathbf{H} = 0, \operatorname{curl} \mathbf{H} = \frac{4\pi}{c}(\mathbf{j} + \mathbf{j}_0), \qquad (2)$$

where $\mathbf{v}$ and ρ are the velocity and density of the liquid, p is the pressure, $\mathbf{E}$ and $\mathbf{H}$ are the electric and magnetic fields arising in the liquid, $\mathbf{j}$ is the current density defined by the relation

$$\mathbf{j} = \sigma\left(\mathbf{E} + \frac{\mu}{c}[\mathbf{v} \times \mathbf{H}]\right),$$

and σ and μ are the conductivity and magnetic susceptibility of the liquid.

In the case of a liquid of infinite conductivity, which we shall consider first, it follows from the last equation that

$$\mathbf{E} = -\frac{\mu}{c}[\mathbf{v} \times \mathbf{H}]. \qquad (3)$$

If the current $\mathbf{j}_0$ is sufficiently small, then we can linearize the set of equations (1). In such a case, we obtain the following equation for the determination of the velocity of the liquid $\mathbf{v}$:

$$\frac{\partial^2 \mathbf{v}}{\partial t^2} - S^2 \operatorname{grad} \operatorname{div} \mathbf{v} \qquad (4)$$

$$-[\operatorname{curl} \operatorname{curl}[\mathbf{v} \times \mathbf{V}_0] \times \mathbf{V}_0] = \frac{\mu}{c\rho_0}\left[\mathbf{H}_0 \times \frac{\partial \mathbf{j}_0}{\partial t}\right],$$

where ρ_0 is the equilibrium liquid density, S the velocity of sound, and $\mathbf{V}_0 = \sqrt{\mu/4\pi\rho_0}\,\mathbf{H}_0$ the Alfven velocity.

The variable magnetic field $\mathbf{h} = \mathbf{H} - \mathbf{H}_0$ and the change in the density associated with the wave are determined by the equations:

$$\frac{\partial \mathbf{h}}{\partial t} = \operatorname{curl}[\mathbf{v} \times \mathbf{H}_0], \quad \frac{\partial \rho}{\partial t} + \rho_0 \operatorname{div} \mathbf{v} = 0. \qquad (5)$$

By means of Eqs. (1) and (2), we can show that the increase in the total energy of the medium per unit time, including the kinetic energy, the energy of the sound waves, and the energy of the magnetic field is determined by the following formula:

$$I = \frac{\partial}{\partial t}\int\left\{\frac{\rho_0 v^2}{2} + \frac{S^2\rho^2}{2\rho_0} + \frac{\mu H^2}{8\pi}\right\} dv = \frac{\mu}{c}\int \mathbf{v}\cdot[\mathbf{H}_0 \times \mathbf{j}_0]\, dv. \qquad (6)$$

The intensity of radiation of the hydromagnetic and magnetoacoustic waves is also determined by this equation.

3. We shall look for $\mathbf{v}$ in the form of a Fourier integral

$$\mathbf{v}(\mathbf{r}, t) = \int \mathbf{v}(\mathbf{k}, \omega)\, e^{i\mathbf{k}\cdot\mathbf{r} - i\omega t}\, d\mathbf{k}\, d\omega.$$

Substituting this expression in (4), we get

$$\{\omega^2 - (\mathbf{k}\cdot\mathbf{V}_0)^2\}\,\mathbf{v} - \{(S^2 + \mathbf{V}_0^2)\,\mathbf{k} - (\mathbf{k}\cdot\mathbf{V}_0)\,\mathbf{V}_0\}\,(\mathbf{k}\cdot\mathbf{v}) \qquad (7)$$

$$+ \mathbf{k}\,(\mathbf{k}\cdot\mathbf{V}_0)\,(\mathbf{V}_0\cdot\mathbf{v}) = i\omega\frac{\mu}{c\rho_0}[\mathbf{H}_0 \times \mathbf{j}_0],$$

where $\mathbf{j}_0(\mathbf{k}, \omega)$ is the Fourier component of the external current density

$$\mathbf{j}_0(\mathbf{k}, \omega) = (2\pi)^{-4}\int \mathbf{j}_0(\mathbf{r}, t)\, e^{-i\mathbf{k}\cdot\mathbf{r} + i\omega t}\, d\mathbf{r}dt.$$

Setting the determinant of (7), equal to zero, we obtain the dispersion equation for free waves in an ideally conducting medium in the presence of an external magnetic field:

$$[\omega^2 - (\mathbf{k}\cdot\mathbf{V}_0)^2]\,\{\omega^2[\omega^2 - (S^2 + V_0^2)\,k^2] + S^2k^2\,(\mathbf{k}\cdot\mathbf{V}_0)^2 = 0. \qquad (8)$$

This equation has three different solutions, corresponding to the three different types of waves that can be propagated in an ideally conducting, compressible liquid located in an external magnetic field. The squares of the phase velocities of the hydromagnetic and the two magnetoacoustic waves are respectively equal to

$$u_1^2 = V_0^2 \cos^2\vartheta,$$

$$u_{2,3}^2 = {}^1/_2\{(S^2 + V_0^2) \pm \sqrt{(S^2 + V_0^2)^2 - 4S^2V_0^2\cos^2\vartheta}\},$$

where ϑ is the angle between the direction of wave propagation and the magnetic field $\mathbf{H}_0$. All three types of waves are excited in the medium in the general case in the presence of an external magnetic field.

Starting out with $\mathbf{v}$ from (7) and using Eq. (6), we get the following general expression for the intensity of radiation of the three types of waves per element of solid angle do:

$$dI = 8\pi^5\mu\frac{V_0^2}{c^2}\omega_0^2\left\{\left|j_\perp\left(\frac{\omega_0}{u_1}, \vartheta, \varphi\right)\right|^2 \frac{\cos^2\varphi}{u_1^3}\right.,$$

$$+ \frac{u_2^2 - S^2\cos^2\vartheta}{u_2^2 - u_3^2}\left|j_\perp\left(\frac{\omega_0}{u_2}, \vartheta, \varphi\right)\right|^2 \frac{\sin^2\vartheta}{u_2^3} \qquad (9)$$

$$\left. + \frac{S^2\cos^2\vartheta - u_3^2}{u_2^2 - u_3^2}\left|j_\perp\left(\frac{\omega_0}{u_3}, \vartheta, \varphi\right)\right|^2 \frac{\sin^2\varphi}{u_3^3}\right\} do,$$

where $\mathbf{j}_\perp(\mathbf{k}, \vartheta, \varphi)$ is the Fourier component of the component of the current density in the plane perpendicular to the direction of the magnetic field $\mathbf{H}_0$; φ is the angle between two planes, one defined by $\mathbf{j}_0$ and $\mathbf{H}_0$, and the other by the direction of wave propagation and $\mathbf{H}_0$; ω_0 is the frequency of the external current (we consider the

external current $\mathbf{j}_0$ to be a harmonic function of the time).

The first component in (9) determines the intensity of excitation of hydromagnetic waves with phase velocity u_1, the second and third components the intensities of excitation of the magnetoacoustic waves with phase velocities u_2 and u_3.

We note that only the excitation of hydromagnetic waves is possible in an incompressible fluid, wherein the intensity of radiation is equal to

$$dI = 8\pi^5 \mu \frac{\omega_0^2 V_0^2}{c^2 u_1^3} \left| j_\perp\left(\frac{\omega_0}{u_1}, \vartheta, \varphi\right)\right|^2 d\sigma. \qquad (10)$$

4. Let us now consider several special cases.

(a) Surface current. If the surface current

$$\mathbf{j}_0 = \mathbf{j}_S \delta(z)\, e^{-i\omega_0 t}, \qquad (11)$$

exists in a plane perpendicular to the magnetic field $\mathbf{H}_0$, then only hydromagnetic waves will be propagated. These travel along the field. The total radiation intensity of these waves for a unit surface current is equal to

$$I_S = \pi\mu V_0 c^{-2} j_S^2. \qquad (12)$$

We note that the radiation intensity does not depend on the frequency of excitation of the current.

(b) Line current. In this case,

$$\mathbf{j}_0 = \mathbf{j}_L \delta(x)\, \delta(z)\, e^{-i\omega_0 t},$$

and the total intensity of radiation of the hydromagnetic waves per unit length is determined by the expression

$$I_L = (\pi\mu\omega_0 / 2c^2)\, j_L^2. \qquad (13)$$

The radiation intensity is proportional to the frequency of the current.

(c) Current loop. In this case,

$$j_0 = j_C \frac{\delta(\rho - a)}{2\pi\rho}\, \delta(z)\, e^{-i\omega_0 t},$$

and only the magnetoacoustic waves are excited. In such a case the radiation intensity is equal to

$$dI_C = \frac{\mu\omega_0^2}{8\pi c^2} V_0^2 j_C^2 \left\{ J_1^2\left(\frac{a\omega_0}{u_2}\sin\vartheta\right) \frac{u_2^2 - S^2\cos^2\vartheta}{u_2^3(u_2^2 - u_3^2)} \right. \qquad (14)$$

$$\left. + J_1^2\left(\frac{a\omega_0}{u_2}\sin\vartheta\right) \frac{S^2\cos^2\vartheta - u_3^2}{u_3^3(u_2^2 - u_3^2)} \right\} d\sigma.$$

We can find the total intensity in two limiting special cases: if $V_0^2 \gg S^2$, then

$$u_2^2 = V_0^2 + S^2\sin^2\vartheta, \quad u_3^2 = S^2\cos^2\vartheta.$$

Here only the magnetoacoustic wave with phase velocity u_2 is excited. The angular distribution of the radiation is determined from the formula

$$dI_C = \frac{\mu\omega_0^2}{8\pi V_0 c^2} j_C^2 J_1^2\left(\frac{a\omega_0}{V_0}\sin\vartheta\right) d\sigma.$$

If the inequality $a\omega_0/V_0 \ll 1$ is satisfied, the total radiation intensity becomes

$$I_C = (\mu a^2\omega_0^4 / 12c^2 V_0^3)\, j_C^2. \qquad (15)$$

If $V_0^2 \ll S^2$, then

$$u_2^2 = S^2 + V_0^2\sin^2\vartheta, \quad u_3^2 = V_0^2\cos^2\vartheta.$$

Here only waves with the phase velocity u_3 are excited. The angular distribution of the radiation of these waves is determined from the relation

$$dI_C = \frac{\mu\omega_0^2}{8\pi c^2 V_0} j_C^2 J_1^2\left(\frac{a\omega_0}{V_0}\tan\vartheta\right)\tan\vartheta\, d\sigma.$$

The total radiation intensity is equal to

$$I_C = \frac{\mu\omega_0^2}{2c^2 V_0} j_C^2 I_1\left(\frac{a\omega_0}{V_0}\right) K_1\left(\frac{a\omega_0}{V_0}\right).$$

If $a\omega_0/V_0 \ll 1$, then

$$I_C = (\mu\omega_0^2 / 4c^2 V_0)\, j_C^2. \qquad (16)$$

5. We now consider the effect of finite conductivity and the viscosity of the fluid on the excitation of hydromagnetic waves. Limiting ourselves for simplicity to the case of an incompressible fluid, we have the following system of equations for the velocity $\mathbf{v}$ and magnetic field $\mathbf{h}$:

$$\frac{\partial \mathbf{v}}{\partial t} = \nu\nabla\nabla\cdot\mathbf{v} + \frac{\mu}{4\pi\rho_0}[\operatorname{curl}\mathbf{h}\times\mathbf{H}_0] - \frac{\mu}{c\rho_0}[\mathbf{j}_0\times\mathbf{H}_0],$$

$$\frac{\partial \mathbf{h}}{\partial t} = \operatorname{curl}[\mathbf{v}\times\mathbf{H}_0] - \frac{c^2}{4\pi\mu\sigma}\operatorname{curl}\operatorname{curl}\mathbf{h} + \frac{c}{\mu\sigma}\operatorname{curl}\mathbf{j}, \qquad (17)$$

where ν is the viscosity of the liquid.

The radiation intensity can be found from the formula

$$I = -\int \mathbf{E}\cdot\mathbf{j}_0 dv,$$

where the intensity of the electric field $\mathbf{E}$ is equal to

$$\mathbf{E} = -\frac{\mu}{c}[\mathbf{v}\times\mathbf{H}_0] + \frac{c}{4\pi\sigma}\operatorname{curl}\mathbf{h} - \frac{\mathbf{j}_0}{\sigma}.$$

We can show that the intensity of the radiation of the hydromagnetic waves will be determined by the expression

$$dI = 16\pi^4 \int_0^\infty \left\{ \frac{\mu c^{-2}\omega_0^2 k^2 (\nu + c^2/4\pi\mu\sigma)}{[\omega^2 - (\mathbf{k}\cdot\mathbf{V}_0)^2 - c^2k^4\nu/4\pi\mu\sigma]^2 + \omega_0^2 k^4 (\nu + c^2/4\pi\mu\sigma)^2} |[\mathbf{V}_0\times\mathbf{j}_0(\mathbf{k})]|^2 \right. \qquad (18)$$

$$\left. + \frac{\omega_0^2 (\mathbf{k}\mathbf{V}_0)(1/4\pi\sigma)[\omega_0^2 - (\mathbf{k}\mathbf{V}_0)^2 - c^2k^4\nu/2\pi\mu\sigma - (c^2k^2/4\pi\mu\sigma)^2]}{[\omega_0^2 + (c^2k^2/4\pi\mu\sigma)^2]\{[\omega^2 - (\mathbf{k}\mathbf{V}_0)^2 - c^2k^4\nu/4\pi\mu\sigma]^2 + \omega_0^2 k^4 (\nu + c^2/4\pi\mu\sigma)^2\}} |\mathbf{j}_0(\mathbf{k})|^2 + \frac{\omega_0^2/4\pi\sigma}{\omega_0^2 + (c^2k^2/4\pi\mu\sigma)^2} |\mathbf{j}_0(\mathbf{k})|^2 \right\} k^2\, dk\, d\sigma.$$

In a viscous liquid with finite conductivity, the harmonic current with frequency ω_0 [in contrast to (1)] excites hydromagnetic waves with different frequencies $\omega = ku_1$. The spectral distribution of the hydromagnetic waves radiated is determined from (18).

Making use of the formula

$$\delta(x) = \lim \frac{1}{\pi} \frac{\alpha}{\alpha^2 + x^2},$$

it is easy to show that for $\nu \to 0$ and $\sigma \to \infty$, Eq. (18) goes over into (10).

6. We now compare the intensity of the excitation of hydromagnetic waves by currents with the intensity of excitation of hydromagnetic waves by mechanical means, in which case, for a certain plane perpendicular to the magnetic field $\mathbf{H}_0$ (the plane $z = 0$), the velocity of the liquid perpendicular to the magnetic field is given by

$$\mathbf{v} = \mathbf{v}_0 e^{-i\omega_0 t}, \quad \mathbf{v}_0 \perp \mathbf{H}_0, \quad z = 0.$$

Assuming $\mathbf{v}, \mathbf{h} \sim \exp\{-i\omega_0(t - z/V_0)\}$, and taking the liquid to be incompressible, we get, by (3) and (5),

$$\mathbf{E} = -\frac{\mu}{c}[\mathbf{v} \times \mathbf{H}_0], \quad \mathbf{h} = -\sqrt{\frac{4\pi\rho_0}{\mu}}\mathbf{v}. \tag{19}$$

The energy flow is determined primarily by the flow of electromagnetic energy

$$I = \frac{c}{8\pi} \operatorname{Re}[\mathbf{E} \times \mathbf{h}^*].$$

Substituting this expression in (19), we get

$$I = {}^1/_2 \rho_0 V_0 v_0^2. \tag{20}$$

A comparison of (20) with Eq. (12) shows that the surface current j_S is equivalent to a velocity

$$v_0 = \sqrt{2\pi\mu/\rho_0}\, j_S/c$$

from the viewpoint of the excitation of hydromagnetic waves.

[1] H. Alfvén, Cosmical Electrodynamics (Oxford, 1950).

[2] S. Lundquist, Phys. Rev. **76**, 1805 (1949).

Translated by R. T. Beyer
16

SOVIET PHYSICS JETP VOLUME 35(8), NUMBER 1 JANUARY, 1959

QUANTUM-MECHANICAL PROBABILITIES AS SUMS OVER PATHS

G. V. RIAZANOV

Moscow State University

Submitted to JETP editor January 28, 1958

J. Exptl. Theoret. Phys. (U.S.S.R.) **35**, 121-131 (July, 1958)

A new formulation of nonrelativistic quantum mechanics is proposed, namely a general definition of the probability of any event. The physical content of quantum mechanics is reduced to a single principle similar to the principle of Gibbs; this makes it possible to solve problems without resorting to the use of wave functions and operators.

THE idea that there may exist in quantum mechanics a general expression for the probability amplitude of any event is due to Feynman.[1] These amplitudes are multiplied and combined like classical probabilities; this leads to the idea of constructing quantum mechanics according to the model of classical statistical physics. In statistical physics the probability of finding a system to have some given property is equal to the sum over all configurations having this property; each configuration is used with the weight assigned by Gibbs. In quantum mechanics the role of the configurations is played by the paths of the particle; according to Feynman's idea the probabilities are replaced by amplitudes. A simple and complete "atomistic" description is obtained (see Sec. 8).

This program has not, however, been completely carried out. According to Feynman, the amplitude of any state must be the sum over all paths consistent with the conditions of the experiment, but,

as is stated in reference 1 (Sec. 11), "which properties [of the paths] correspond to which physical measurements has not been formulated in a general way."

This problem is solved in the present paper, but in a different way. We have to give up certain of Feynman's ideas. The question of a general expression for the amplitude does not have to be dealt with, since, as will be shown below, something more is available — a general expression for the probability of any event.

1. A FORMULATION OF QUANTUM MECHANICS

Any experiment can be completely analyzed by means of the following rule:

The probability for finding a particle possessing any given property is equal to the sum over all paths that have this property; each path occurs with the weight $\cos(S/h)$; S is the change of the classical action along the path, and h is Planck's constant.

The probability for finding a given value a for the physical quantity $a\{x(t)\}$, which depends on the path $x(t)$ (a can be a coordinate, a velocity, the energy at a particular time, two coordinates at different times, etc.), is given symbolically by

$$W(a) = \int_a \cos\frac{S}{h}\, d\Gamma; \tag{1}$$

$\int_a d\Gamma$ denotes the integral over all paths for which $a\{x(t)\} = a$.

If we specify the path by a succession of coordinates x_k and momenta p_k at times t_k, and if $t_k - t_{k-1} = \epsilon_k$ is much smaller than the characteristic time of the system, then

$$W(a) = \sum_{\pm} \int\int \cdots \int_a \cos\frac{S}{h} \prod_k \frac{d^3x_k d^3p_k}{(2\pi)^3}; \tag{2}$$

$\sum_{\pm}$ denotes the sum over all signs of the ϵ_k; S is the change of the action along the broken-line path with the vertices x_k, p_k:

$$S(\ldots x_k p_k \ldots) = \int p^\nu dx^\nu = \sum_k \mathbf{p}_k(\mathbf{x}_k - \mathbf{x}_{k-1}) - H(\mathbf{p}_k, \mathbf{x}_k)\varepsilon_k.$$

The integration is taken over the region $a(\ldots x_k p_k \ldots) = a$. All the paths begin and end at the times $-T$ and T, and the index k runs through the finite number of values $-N < k < N$. For $N \to \infty$ and $T \to \infty$ one gets all possible paths. It is assumed that the entire history of the particle is known, i.e., all macrofields.

If the physical quantities are expressed in terms of coordinates and velocities (not momenta), the condition $a(\ldots x_k p_k \ldots) = a$ is replaced by $a(\ldots x_k \ldots) = a$. We can integrate over all the p_k, and there remains a sum over purely spatial paths.

Thus a simple construct (though one poorly described by usual notations) — the sum over all paths, i.e., over all ways of realizing the event a — contains in itself all the principles and rules of quantum mechanics, and provides in general form a way of writing down the solution of any quantum mechanical problem.

2. THE UNIVERSAL DISTRIBUTION OF PATHS

Like the Gibbs distribution, the distribution (1) can in some measure be proved.

We start from the classical ideas about the microscopic world. Particles move along paths $x(t)$, and each path occurs with a probability $W\{x(t)\}$. Knowing $W\{x(t)\}$, one can find the probability of any event a:

$$W(a) = \int_a W\{x(t)\}\, d\Gamma. \tag{3}$$

We assume that $W\{x(t)\}$ depends only on the change of the action along the path. In classical mechanics the sign of the action can be arbitrary; therefore $W\{x(t)\} = W(S) + W(-S)$. For two noninteracting particles the probability must fall apart into a product of probabilities, i.e., we must have the relation:

$$W(S_1 + S_2) + W(-S_1 + S_2) + W(S_1 - S_2) + W(-S_1 - S_2) = [W(S_1) + W(-S_1)]\,[W(S_2) + W(-S_2)].$$

From this we have $W(S) = \cos \alpha S$, where α is a constant; comparing Eq. (3) with quantum mechanics (or with experiment) we get $\alpha = 1/h$. The quantity $\cos(S/h)$ can be negative (our assumptions are in part untrue), but the probabilities measured in experiments turn out to be positive. These are probabilities associated with the measurement of commuting quantities, in which it is not necessary to take into account the reaction of the instruments.

It is interesting that many formulas are simplified and "given meaning" (see Sec. 3) if we assume that the two signs of the action correspond to two ways of traversing the path (not at all related to the actual direction of motion of the particle along a path in the classical limit).

Repeating the above considerations, we get

$$W(a) = \int_a e^{iS/h} d\Gamma. \tag{4}$$

Here the integration is taken over directed paths, i.e., paths with different directions of traversal are distinguished. According to Eq. (4) the quantity $\exp[iS\{x(t)\}/h]$ is the formal probability (for short we shall call it the probability) for the particle to pass along the path $x(t)$, and $\cos[S\{x(t)\}/h]$ in Eq. (1) is the probability for finding the path $x(t)$.

For the further discussion we introduce the notations: $(xt \to x't')$ is the sum over all directed paths (each with the factor $\exp iS$) passing from x,t to x',t'; $(xt \sim x't')$ is the sum over all closed paths (each with the factor $\exp iS$) passing through x,t and x',t'; $(xt \underset{a}{\sim} x't')$ is the sum over all closed paths passing through x,t and x',t' and possessing the property a.

3. THE PRINCIPLES OF QUANTUM MECHANICS

To make clear the connection of Eq. (1) with the usual formalism, let us calculate $W(x,t)$, the probability for finding the particle at the point x at the time t. This is the sum over all paths passing through the point x at the time t; it can be obtained if we multiply the sum over all paths (each with the factor $\exp iS$) arriving at the point x,t [we denote this sum by $\psi(x,t)$] by the sum over all paths that come out from the point x,t. The second sum will be equal to the complex conjugate expression $\psi^+(x,t)$, since for each departing path there exists one just like it but oppositely directed. Thus $W = \psi\psi^+$. As can be verified, the quantity ψ satisfies the Schrödinger equation, and consequently is identical with the wave function, although the definition given above contains some arbitrariness and will be made more precise in Sec. 4.

According to Eq. (4) $\psi(x,t)$ is the probability of arriving at the point x,t; $\psi^+(x,t)$ is the probability of emerging from the point x,t; $W(x,t)$ is the probability of passage through x,t, obtained by multiplication of the probabilities of these two events, which always appear together.

Let us now calculate the average value of the momentum of the particle at the time t. According to Eq. (2)

$$\bar{p}(t_l) = \sum_{\pm} \iint \ldots \int p_l \cos S \prod_k \frac{dx_k dp_k}{2\pi},$$

and we now replace $\cos S$ by $(e^{iS} + e^{-iS})/2$ and set $\epsilon_l = 0$. Then

$$\bar{p}(t_l) = \frac{1}{2}\int \psi(x_l, t_l)\, p_l e^{ip_l(x_l - x_{l-1})}\psi^+(x_{l-1}, t_l)\, dx_l dp_l dx_{l-1} \tag{5}$$

$$+ \text{Compl. conj.} = \frac{1}{2}\int \psi(x, t_l)\frac{1}{i}\frac{\partial \psi^+}{\partial x}(x, t_l)\, dx + \text{Compl. conj.}$$

In a similar way one can show that Eq. (2) gives the correct values for the first powers of such quantities as momentum, energy, and angular momentum. In calculating the average values of higher powers of most physical quantities, however, it is necessary to take precautions against possible inaccuracies associated with the replacement of continuous paths by broken ones. In order that the value of the physical quantity $f(x,p)$ at the time t shall not depend on the way the time axis is broken up into intervals ϵ_k, one must replace

$f(t)$ by $\lim\limits_{\epsilon \to 0} \int\limits_{t-\epsilon}^{t+\epsilon} f\, dt$; $\epsilon \to 0$, $\epsilon_k \to 0$, but $\epsilon \gg \epsilon_k$.

Or, more simply, inside the interval $(t-\epsilon,\ t+\epsilon)$ we take N intermediate time intervals t_k and set

$f = \frac{1}{N}\sum\limits_{k=1}^{N} f_k$ (f_k is the value of f at the time t_k).

Then

$$\bar{f}^n = \lim_{N\to\infty} \int \left(\frac{\Sigma f_k}{N}\right)^n \cos S d\Gamma.$$

Here $|t_k - t_{k-1}|$ remains of the order of magnitude of ϵ, and the sign of the difference $|t_k - t_{k-1}|$ can be arbitrary.

For $N \to \infty$ there remain only those terms in $\left(\sum f_k\right)^n$ in which the f_k are taken at different times, but, as can easily be shown, for $t_k \to t_{k-1}$ the quantity $\int f_{k_1} \ldots f_{k_n} \cos S\, d\Gamma$ becomes equal to $\int \psi^+(x,t)\, f^n(x, -i\partial/\partial x)\, \psi(x,t)\, dx$. If Eq. (1) gives the correct value for all a^n, then the correct value is also obtained for $W(a)$. This can be verified by direct calculation of the probabilities (see Sec. 5).

We note that since every measurement reduces in the final analysis to measurements of coordinates, it is sufficient that Eq. (2) give the correct value for $W(x,t)$.

We shall now show that $(xt \to x't')$ is the same as the propagation function of Schrödinger's equation. Unlike the corresponding Feynman expression, $(xt \to x't')$ contains paths with change of the sign of the time [because of the operation $\sum\limits_{\pm}$ in Eq. (2)]. In the case in question, however, these paths make no contribution to the sum.

In fact, let us compare $(xt \to x't')$ — the sum over all paths (each with the factor $\exp iS$) connecting the points x,t and x',t' without change of the sign of the time — and $(xt \underset{1}{\to} x't')$ — the sum over the paths connecting x,t and x',t' with a single change of the sign of the time at the time

t'' (t'' lies outside the interval (t, t')):

$$(xt \xrightarrow[1]{} x't') = \int (xt \xrightarrow[0]{} x''t'')(x''i'' \xrightarrow[0]{} x't')\,dx''.$$

As is well known,[1] the sum over the paths connecting the points x, t and x', t' without change of the sign of the time is the propagation function of Schrödinger's equation, so that $(xt \xrightarrow[1]{} x't') = (xt \xrightarrow[0]{} x't')$.

Let us now consider the probability of this event: at the time t_0 a measurement was made of the complete set of quantities $L_i(x,p)$ and they were found to be equal to the numbers L_i, and the time t the quantity $M_1(x,p)$ is equal to M_1. The quantities L_i form a complete set if $W(L_1 \ldots L_n t)$ comes apart into the product of two functions: ψ, the sum over the paths arriving, and ψ^+, the sum over the paths departing. Let $M_2 \ldots M_n$ be quantities that make a complete set together with M_1.

According to quantum mechanics

$$W(M_1 t \mid L_1 \ldots L_n t_0) = \int W(M_1 \ldots M_n t \mid L_1 \ldots L_n t_0)\,dM_2 \ldots dM_n \qquad (6)$$
$$= \int G(M_1 \ldots M_n t \mid L_1 \ldots L_n t_0)|^2\,dM_2 \ldots dM_n;$$

G is the propagation function in the mixed L, M representation. Since G is the sum over all paths going from t_0 to t, and G^+ is the sum over all paths going from t to t_0, $W(M_1 t \mid L_1 \ldots L_n t_0)$ is the sum over all closed paths (in the x,t space), for which at the time t_0 $L_i(x,p) = L_i$ and at the time t $M_1(x,p) = M_1$, that is,

$$W(M_1 t \mid L_1 \ldots L_n t_0) = \int \cos S\,d\Gamma = (M_1 t \sim L_1 \ldots L_n t_0). \qquad (7)$$

$$M_1 t \rightleftarrows L_1 \ldots L_n t_0.$$

This formula makes it possible to solve both scattering problems and problems relating to stationary states. In the latter case W does not depend on t and t_0.

The closed paths in Eq. (7) have no special physical meaning; their appearance can be understood if one traces through the proof of Eqs. (7) and (1) presented in Sec. 4. The expression (7) does not mean that the particles move along closed paths.

There is one further relation, similar to Eq. (7) and interesting from the point of view of a causal description. A comparison of $W(x,p,t)$ and $W(x,p,t')$ as calculated from Eq. (1) gives

$$W(x,p,t) = \int (xpt \sim x'p't')\,W(x',p',t')\,dx'dp'. \qquad (8)$$

4. EQUIVALENCE TO THE USUAL FORMALISM

The expression (1) is an obvious analogue of the Gibbs distribution; the number N (cf. Sec. 1) plays the role of the number of particles, but the dependence of the expression (1) on N for $N \to \infty$ is completely different from that existing in statistical physics. Because of this fact, problems arise in quantum mechanics that do not have to be solved in statistical physics.

Let us go back to Eq. (1). Suppose that measurements of some kind are carried out; we must find the relation between them. The probability for each measurement to give a prescribed result is defined by Eq. (1), and at first sight is not related in any way to the results of the other measurements. In actual fact, however, the integral on the right side of Eq. (1) is not completely defined. The time ranges from $t = -\infty$ to $t = +\infty$, and the integral is infinitely manifold even for discrete time, so that it can be defined only as a limit of an N-fold integral for $N \to \infty$. It is easy to show by examples, however, that such a limit does not exist; the result depends on the assumptions that are made about the positions of the final and initial points of the path. For example, one can assume that at the initial instant the particle is at the point 0, or that the particle can be at any point.

In the general case the behavior depends on two functions which give the distributions of the initial and final points for the two possible directions of motion:

$$W(a) = \iint u(x)(x, -T_{\tilde{a}}\ x', T)\,u(x')\,dxdx' + \iint v(x)(x, -T_{\tilde{a}}\ x', T)\,v(x')\,dxdx'. \qquad (9)$$

Part of the measurements serves to determine the behavior as T goes to infinity, i.e., to determine u and v, and the probability of the other results is calculated just from this limiting behavior. The connection between the mean values with this approach agrees with the quantum-mechanical results (see below), but the hypothesis that the behavior of the paths for $t \to \pm\infty$ affects the results of measurement is, generally speaking, an abstraction. This is the quantum-mechanical form of Laplace determinism.

In actual fact the past and future histories of the particle are unknown to us; from this point of view, the behavior at infinity is unimportant and one can fix on some single rule, for example the hypothesis that all particles appear from the point 0 at the time $-\Theta$ and disappear into this point at the time Θ. In this case the probability of an event

is found to depend on unknown past and future forces. For definiteness we may suppose that a prescribed external field acts on the particles during the time interval $(-T, T)$, an unknown field X during the interval $(-\Theta, -T)$, and the field Y during the interval (T, Θ):

$$W(a) = (0, -\Theta_{\tilde{a}}\ 0, \Theta);$$

$$S = \int_{-\Theta}^{\Theta} L dt = \int_{-\Theta}^{-T} L(X)\, dt + \int_{-T}^{T} L dt + \int_{T}^{\Theta} L(Y)\, dt. \quad (10)$$

To find the connection between observed quantities, one must use Eq. (10) to express them in terms of the unknown fields X and Y, and then eliminate X and Y from the resulting system of equations. The result again agrees with that of quantum mechanics, though the dependence on future forces seems rather strange. This dependence exists also in the classical principle of least action; if the coordinates of a particle are given at the times t_1 and t_2, then the value of a coordinate at a time t $(t_1 < t < t_2)$ depends both on the past and also on the future history.

This formalism can be somewhat simplified if we equate to zero the density of "sources" at $t = \Theta$. There remains only the sum over paths beginning at $t = -\Theta$ and ending at $t = -\Theta$. In this case the probability depends only on the past history:

$$W(a) = (0, -\Theta\ \tilde{a}\ 0, -\Theta)$$

$$S = \int_{-\Theta}^{-T} L(X)\, dt + \int_{-T}^{-T} L dt + \int_{-T}^{-\Theta} L(X)\, dt. \quad (11)$$

Thus the sum in Eq. (1) must be taken either over paths with prescribed behavior for $T \to \pm\infty$, or else over paths in a field of unknown past and future (or only past) forces.

The agreement of the consequences of Eqs. (9), (10), and (11) with quantum mechanics can be shown easily by relating u, v and X, Y with the wave function. In Eq. (9)

$$\psi(x, -T) = u(x) + iv(x)$$

$$+ \int (x, -T - x', T)\,[u(x') + iv(x')]\, dx'.$$

In Eq. (10)

$$\psi(x, -T) = (0, -\Theta \to x, -T)$$

$$+ \int (x, -T \to x', T)\,(x', T \to 0, \Theta)\, dx'.$$

In Eq. (11)

$$\psi(x, -T) = (0, -\Theta \to x, -T).$$

Unknown forces and "densities of sources" exist also in statistical physics. For example, the statistical sum for a gas will be different for the cases of free and fixed piston. In statistical physics, however, the forces acting on the piston, or the probability of a given position of the piston are usually known, whereas in quantum mechanics they have to be calculated from the results of measurements.

The operation of eliminating u, v or X, Y is in general complicated, but it is no more complicated than the elimination of ψ in quantum mechanics. For example, the problem of finding the coordinate distribution at time t' for given coordinate distribution and momentum distribution at the time t is difficult also in the usual formalism (it is hard to find ψ at the time t). Just as in the usual formulation, the problem is considerably simplified if part of the measurements gives a complete description of the state (this case includes all known problems of quantum mechanics). Let us consider this case (for simplicity we take a one-dimensional problem).

It is required to determine $W(M, t) = \int_{M,t} \cos S\, d\Gamma$ if it is known that

$$W(L', t_0) = \int_{L', t_0} \cos S d\Gamma = \delta(L' - L).$$

To find $W(M, t)$ we go back to Eq. (1); this formula, however, depends on the unknown past and future history [or only the past, if we use Eq. (11)] of the particle, i.e., on X and Y. We need some sort of information about this history. We get this information from the condition $W(L', t_0) = \delta(L' - L)$.

In other words, we have two equations

$$W(M, t) = \int_{M, t} \cos S d\Gamma, \qquad \delta(L' - L) = \int_{L', t_0} \cos S d\Gamma$$

[with S taken from Eq. (10) or Eq. (11)] from which we must eliminate the unknown forces X and Y. We obtain the conditional probability $W(M, t \mid L, t_0)$.

We shall show that $W(M, t \mid L, t_0)$ agrees with the expression (7). Let $\psi(x, t_0)$ be the sum over all paths that arrive at x, t_0. According to Sec. 3,

$$W(L, t) = \int \psi^+(x, t)\, \delta(L - \hat{L})\, \psi(x, t)\, dt.$$

From the condition

$$W(L', t_0) = \int \psi^+ \delta(L' - \hat{L})\, \psi dx = \delta(L' - L)$$

(this is a condition on the unknown forces or behavior for $T \to \pm\infty$), we get: $\psi(x, t_0) = \psi_L(x, t_0)$, an eigenfunction of the operator L. Similarly,

$$W(M, t) = \int \psi^+ \delta(M - \hat{M}) \psi dx$$

$$= \int \psi^+ \delta(M - M') \psi dM' = |\psi(M, t)|^2.$$

Since

$$\psi(x, t) = \int (xt \leftarrow x't_0) \psi(x', t_0) dx,$$

$$\text{then } \psi(x, t) = G(x, t \mid L, t_0).$$

In the M-representation $\psi(M, t) = G(M, t \mid L, t_0)$, so that

$$W(M, t) = |G(M, t \mid L, t_0)|^2.$$

In just the same way one obtains Eq. (8). According to Eq. (1) $W(x, p, t)$ and $W(x, p, t')$ depend on the unknown past and future history. Comparing these dependences, we get the relation (8). One has to write out detailed expressions for $W(x, p, t)$ and $W(x, p, t')$, draw the corresponding paths, and note that for $t > t'$ the contribution to $W(x, p, t')$ from the paths $-\infty \to t' \to t \to \infty$ is the same as that from the paths $-\infty \to t \to t' \to t \to \infty$. These last differ from the paths $-\infty \to t \to \infty$, which occur in $W(x, p, t)$, by the loop $t \to t' \to t$. This loop gives $(xpt \sim x'p't')$ in Eq. (8).

In practice, however, there is no need to use the general scheme; Eq. (7), which contains no unknown forces and densities, is sufficient.

5. EXAMPLES

The equivalence of the expression (7) to the usual formalism can be verified by examples.

(a) A scattering problem.

Let us calculate $W(p, t \mid x, t_0)$ — the probability for the particle to have the momentum p at the time t, if at the time t_0 it had the coordinate x. According to Eq. (7),

$$W = (pt \sim xt_0) = \lim_{\varepsilon \to 0} \int (yt \underset{p}{\to} y't + \varepsilon)$$

$$\times (y't + \varepsilon \to xt_0)(xt_0 \to yt)\, dydy'$$

$$= \int \frac{e^{ip(y-y')}}{2\pi} G(y't \mid xt_0) G^+(yt \mid xt_0)\, dydy'$$

$$= |(2\pi)^{-1/2} \int e^{ipy} G(yt \mid xt_0)\, dy|^2.$$

(b) The distribution of the coordinate in the stationary state with energy E, $W(x \mid E)$.

It is more convenient to consider a more general quantity, $W(xt \mid Et')$. This is the sum over all paths that pass through the point x at the time t and have the energy E at the time t'.

Prescription of the energy means prescription of the average energy in an infinitely small neighborhood (t_1, t_N) of the point t'. We denote the coordinates at the times t_1 and t_N by x_1 and x_N.

The more precisely written expression for W, with meaning clear from the notations, is

$$W(xt\ Et') = \int\int (x_1 t_1 \underset{\bar{E}=E}{\longrightarrow} x_N t_N)$$

$$\times (x_N t_N \to xt)(xt \to x_1 t_1)\, dx_1 dx_N.$$

Inside the interval (t_1, t_N) we choose $N - 2$ instants of time

$$t_2, t_3, \ldots, t_{N-1} (t_k = t_{k-1} + \varepsilon_k);$$

and replace the continuous paths by broken lines with vertices at x_k, p_k:

$$W = \int\limits_{\bar{E}=E} \exp\left\{i \sum_k (p_k \Delta x_k - H_k \varepsilon_k)\right\}$$

$$\times \prod_k \frac{dx_k dp_k}{2\pi} (x_N t_N \to xt)(xt \to x_1 t_1).$$

The condition

$$\bar{E} = \frac{1}{N} \sum_1^N H_k = \frac{1}{N} \sum_1^N H(p_k x_k) = E$$

is now replaced by a factor $(2\pi)^{-1} \int \exp\{i\tau(E - \bar{E})\}\, d\tau$:

$$W = \int \exp\left\{i\tau E + i \sum_k [p_k \Delta x_k - H_k(\varepsilon_k + \tau/N)]\right\}$$

$$\times \prod_k \frac{dx_k dp_k}{2\pi} (x_N t_N \to xt)(xt \to x_1 t_1) \frac{d\tau}{2\pi}$$

$$= \int e^{i\tau E} (x_1 t_1 \to x_N t_N + \tau)(x_N t_N \to xt)$$

$$\times (xt \to x_1 t_1)\, dx_1 dx_N d\tau / 2\pi.$$

Substituting in this the relation

$$(xt \to x't') = G = \sum_E \varphi_E^+(x) \varphi_E(x') e^{iE(t-t')},$$

we get: $W = |\varphi_E(x)|^2$.

(c) Diffraction from two apertures.

We have to calculate $W(x \mid x_0)$ — the probability of finding the particle at the point x if the source is at the point x_0 behind the screen. This is the sum over all closed paths passing through x and x_0 (Sec. 7), each with the weight $\cos S$. The paths for which the time direction does not change at the points of integration can be omitted, and there remain only paths for which the sign of the time changes at the points x and x_0.

The sum over paths falls into three parts:

$$(x_0 \sim x) = (x_0 \underset{1}{\overset{1}{\rightleftarrows}} x) + (x_0 \underset{2}{\overset{2}{\rightleftarrows}} x) + \{(x_0 \underset{2}{\overset{1}{\rightleftarrows}} x) + (x_0 \underset{1}{\overset{2}{\rightleftarrows}} x)\}.$$

The arrows represent the path, and the numbers

1 and 2 refer to the apertures. These three terms correspond to the three terms of the quantum-mechanical expression for the probability:

$$W = |\psi_1 + \psi_2|^2 = \psi_1^+\psi_1 + \psi_2^+\psi_2 + (\psi_1^+\psi_2 + \psi_2^+\psi_1).$$

6. THE PAULI PRINCIPLE

We shall show that imposition of the Pauli principle is equivalent to the exclusion from the sum over paths of paths that have a common part traversed in different directions.

Let us consider $W(x, y, t | x', y', t')$ — the probability of finding two particles at the points x and y at the time t, if at the time t' there were two particles at the points x' and y'. There are two possibilities: the transition $x' \rightleftarrows x$, $y' \rightleftarrows y$ and the transition $x' \rightleftarrows y$, $y' \rightleftarrows x$. The sum over paths breaks up into two parts, each of which separates into the product of two sums over paths, i.e.,

$$W(x, y | x', y') = W(x | x')\, W(y | y') + W(x | y')\, W(y | x').$$

From this we must subtract the sum over all paths that have a common part. Suppose the two paths coincide on the transition $\xi'\tau' \rightarrow \xi\tau$.

The path $x' \rightarrow x \rightarrow \xi \rightarrow \xi' \rightarrow x'$, $y' \rightarrow y \rightarrow \xi' \rightarrow \xi \rightarrow y'$ must be subtracted from the sum over paths. But this path comes in with the same contribution as the path

$$x' \rightarrow x \rightarrow y' \rightarrow y \rightarrow x'.$$

(This becomes clear if one draws the corresponding paths.)

Symbolically we can write:

$$x'y' \sim xy = x' \rightleftarrows x \cdot y' \rightleftarrows y + x' \rightleftarrows y \cdot y' \rightleftarrows x - \quad (12)$$
$$- x' \rightarrow x \rightarrow y' \rightarrow y \rightarrow x' - x' \rightarrow y \rightarrow y' \rightarrow x \rightarrow x'.$$

Since the sum over each of the transitions represented by an arrow is the same as a quantum-mechanical propagation function,

$$W(x, y | x', y') = |G(x | x')\, G(y | y') - G(x | y')\, G(y | x')|^2.$$

This is the same as the quantum-mechanical expression (for Fermi particles).

When we consider Bose particles the last two terms in Eq. (12) must be taken with the plus sign. If a boson is a bound state of two fermions, this rule can be explained. The forbidden paths will be subtracted for each of the fermions, and the twice-forbidden term comes in with a plus sign, but since the paths of the two particles must coincide, only this term remains in Eq. (1) (in addition to the main term). The minus sign in Eq. (12) is replaced by a plus sign.

7. COMPARISON WITH THE FEYNMAN FORMULATION

The approach that has been presented differs from that of Feynman primarily as to results. The Feynman formula for the transition amplitude replaces only the Schrödinger equation, whereas Eq. (1) contains within it, in addition to the Schrödinger equation, relations of the types $W = \psi^+\psi$, $p = -ih\partial/\partial x$, and the whole theory of representations. Equation (1) makes it possible to solve any problem, whereas the Feynman principle is insufficient, for example, for the problems (a) and (b) of Sec. 5.

We note that Eq. (1) cannot be obtained by simple multiplication of the Feynman expressions for the amplitudes, since, firstly, a general expression for the amplitudes is not known, and secondly, even in the special case in which the amplitude is equal to $\psi(x, t)$, multiplication of $\psi(x, t)$, written according to reference 1 as a sum over paths, by $\psi^+(x, t)$ does not give the sum over all possible paths as is required by the meaning of Eq. (1) (see below).

The limited nature of Feynman's results is due to a lack of consistency in the description of the "quantum microscopic world", i.e., of such events as the passage of a particle along a prescribed path. Dirac[2] has shown how, without contradiction, one can associate with each path a formal probability, and how this probability differs from the square of the absolute value of the Feynman amplitude [this contradiction has been noted in a paper by Stratonovich,[5] where there are some indications of the existence of the formula (1)]. It can be shown (as will be done in another place) that the difference is due to a different definition of the concept "path of the particle," and that in sums over paths a path must be taken just in the Dirac sence, not in the Feynman sense.

Thus it is necessary to abandon the belief in the deep physical meaning of the concept of amplitude, as it exists in quantum mechanics and in reference 1. According to Eq. (1), not all probabilities separate into products of amplitudes.

Another lack of consistency in Feynman's treatment is the absence of paths with change of sign of the time, whereas the basic idea is to include all conceivable possibilities. No limitations at all are to be imposed on the path; they appear only after the averaging. It can be said in advance that in the majority of cases the paths with changing sign of the time will make no contribution in the nonrelativistic region, but inclu-

sion of both signs turns out to be necessary, for example, to get the right value for the average of any function that depends on the velocity (if purely spatial paths are taken). Because paths with both signs of the time are absent in reference 1 the product of the Feynman ψ and ψ^+ does not give the W of Eq. (1), but the ψ defined in Sec. 3 differs from that of Feynman, since in addition to the paths coming from $t = -\infty$ it contains paths coming from $t = +\infty$.

Whereas in reference 1 $\psi(x,t) = (-\infty \rightarrow xt)$, in Sec. 3

$$\psi(x, t) = (-\infty \rightarrow xt) + (xt \leftarrow \infty).$$

A further necessary addition to reference 1 is the refinement made in Sec. 4 of the concept of the sum over paths for paths going out to $t = \pm\infty$. In quantum mechanics wave functions are prescribed by the value of a complete set of quantities, and from this point of view it is not clear what wave function appears in the Feynman relation $\psi(x,t) = (-\infty \rightarrow xt)$. This is a purely symbolic expression. In Sec. 4 it is assumed that such expressions depend on the way in which T goes to infinity (or on an unknown history); this is equivalent to the quantum-mechanical dependence on a complete set of quantities.

Furthermore, we get a logical source of the Feynman rule that in calculating $\overline{v^n}$ (v is the velocity) all the factors must be taken at times arbitrarily close together, but still distinct. By the meaning of Eq. (1), the sum must be taken over paths with arbitrary values of the higher derivatives at the point x,t, and such a sum is not obtained by the use of broken paths. In order for this not to affect the results, the instantaneous value of a physical quantity along a broken path must be defined as the average in an infinitely small neighborhood of the point t (just such quantities are measured in experiments). With such an approach a particle has at the time t both a coordinate x and a momentum $\tilde{p}$ [$\tilde{p} = \frac{1}{2\epsilon}\int_{t-\epsilon}^{t+\epsilon} p\,dt$, ϵ much smaller than the characteristic time of the system, but much larger than ϵ_k in Eq. (2)]. As can be shown, the sum over the paths with prescribed x and p gives the Wigner[3] distribution W(x,p). This distribution cannot, however, be used for the calculation of the average value of an arbitrary quantity f(x,p), since generally speaking $\tilde{f}(x,p) \neq f(\tilde{x}, \tilde{p})$. This is one of the objections against the statistical interpretation of quantum mechanics (cf. reference 4); it is removed if we suppose that what is measured is always $\tilde{f}(x,p)$, and not $f(\tilde{x}, \tilde{p})$.

Thus, unlike the situation in reference 1: (1) the probability of any event is written as the sum of formal probabilities (and not the amplitude as a sum of amplitudes, see beginning of paper); (2) paths with changing time direction are taken into account; (3) the peculiarities of paths receding to infinity are taken into account; (4) the special features of broken paths are more consistently treated.

We note that certain amplitudes agree with the formal probabilities. For example, the probability amplitude for a particle to pass through x,t agrees with the formal probability for the particle to arrive at the point x,t. Just for this reason the amplitudes have the properties of probabilities and the Feynman approach (see beginning of paper) is correct in a certain region.

The present treatment is also directly related to references 2 to 5, which are devoted to the statistical interpretation of quantum mechanics, but its purpose and ideas are quite different from those of these papers.

In references 2 to 5 it is shown how one can, within the framework of quantum mechanics, "restore" the classical picture, if it exists. The distribution of paths has been defined, firstly by the principles and rules of quantum mechanics, secondly by the prescription of the wave function or, what is the same thing, by the prescription of a complete set of physical quantities. The idea of a universal distribution is absent (if the history of the particle is known).

Above, unlike in references 2 to 5: (1) the statistical interpretation is used for the derivation of the principles of quantum mechanics (the approach is in a certain sense an inverse one to that of references 2 to 5; (2) the difference of the quantum distributions from the classical (see beginning of Sec. 4) is interpreted in the framework of the statistical picture.

Two considerations — the possibility of "inverting" the exposition of quantum mechanics (with the Gibbs distribution as a model), and the calculation of conditional probabilities by elimination of the unknown history of the particle — are basic to the present communication.

8. CONCLUSION

Equation (1) is of interest from various points of view.

First of all, the logical structure of quantum mechanics is simplified and clarified. Beyond this, the reduction of all the principles of quantum

mechanics to Eq. (1) and the possibility of deriving Eq. (1) from simple and general assumptions about the physical world (this question is not discussed in the present paper) may be of importance for possible generalizations of quantum mechanics to new domains.

It can be expected that in the relativistic domain the language of possible classes of paths will turn out to be the only mode of description (like the Gibbs distribution in statistical physics). For example, it may happen that there is a retarded interaction between particles that is not reducible to a field (cf. reference 1). In this case the probability does not separate into the product of wave functions, the Schrödinger equation cannot be written, and problems can be solved only by means of Eq. (1).

On the mathematical side, Eq. (1) broadens the domain of application of the functional integration (as compared with reference 1), and there is a hope that in time simplicity and generality will appear not only in the way of writing the general principle, but also in the methods of solving all concrete problems. At present there are a few problems that are solved very simply by means of Eq. (1).

Also of interest is the possibility of using Eq. (1) to carry over accustomed classical ideas into the microscopic world. True, a simple imposition of the probabilities on the the classical picture is somewhat hindered by the "negative probabilities," but everything that has been presented can be translated in the most varied ways into the language of ordinary probabilities. It can be shown that the "negative probabilities" are in no way connected with the formalism of wave functions and operators and are not the cause of the sharp difference between classical physics and the canonical quantum description. The difference exists only in the means of describing mathematically analogous objects (for example, ensembles of configurations in classical statistical physics and ensembles of paths of particles), and in the problems that have to be solved.

It can also be shown that Eq. (1) bears the same relation to the canonical formalism that the Gibbs distribution does to thermodynamics (there is a precise and far-reaching analogy). Therefore the success of the atomistic (not phenomenological) approach may possibly repeat itself for Eq. (1). It is interesting that Eq. (4) can be united with the Gibbs principle, if one introduces a formal integration over paths with a complex time and takes the change of the time equal to ih/kT (k is Boltzmann's constant and T the temperature). Equation (4) will contain both the Gibbs principle and Hamilton's principle.

In conclusion I thank V. Ia. Fainberg for directing this work and for helpful advice.

[1] R. P. Feynman, Revs. Modern Phys. **20**, 367 (1948).

[2] P. A. M. Dirac, Revs. Modern Phys. **17**, 195 (1945).

[3] E. Wigner, Phys. Rev. **40**, 749 (1932).

[4] J. E. Moyal, Proc. Camb. Phil. Soc. **45**, 99 (1949).

[5] R. L. Stratonovich, J. Exptl. Theoret. Phys. (U.S.S.R.) **32**, 1483 (1957), Soviet Phys. JETP **5**, 1206 (1957).

Translated by W. H. Furry
17

ON THE CASCADE THEORY OF SHOWERS

I. P. IVANENKO

Moscow State University

Submitted to JETP editor February 4, 1958

J. Exptl. Theoret. Phys. (U.S.S.R.) 35, 132-136 (July, 1958)

The equation for the average number of particles with energy greater than a given value, produced in a layer of finite thickness, has been solved with account of collision losses. The solutions obtained are compared with those of the usual cascade theory. An expression has been obtained for the mean energy of particles of a cascade shower at any stage of its development.

EQUATIONS for the distribution function of the number of particles produced in a layer of matter between t and t + dt with energy between E and E + dE, and their solution for the mean number of particles $\epsilon\{P(E_0, E, t)\}$ neglecting ionization losses, have been given in reference 1.

It is interesting to solve the equations for the mean number of particles produced in a layer of thickness dt, taking the ionization losses into account, and to compare the results with those of the usual cascade theory[2] dealing with the number of particles $P(E_0, E, t)$ with energy between E and E + dE at the distance t to t + dt from the considered layer.

The equations in question are (we consider a shower initiated by a primary electron with energy E_0):

$$\varepsilon\{P(E_0, E, t)\} = 2\int_E^{E_0} \Gamma(E_0, E', t)\, W_p(E, E')\, dE', \quad \varepsilon\{\Gamma(E_0, E_0, t)\} = \int_E^{E_0} P(E_0, E', t)\, W_e(E' - E, E')\, dE', \tag{1}$$

where Γ denotes the corresponding photon distributions. Equation (1) can be solved easily by means of the Mellin transformation. For further calculations it is convenient to use the Laplace transforms of the solutions of Eq. (1). We obtain the following expression for the number of electrons produced in the layer between 0 and t with energy greater than E (at the place of production):

$$\varepsilon\{N_p(E_0, E, t)\} = -\frac{1}{4\pi}\int_{\delta-i\infty}^{\delta+i\infty} ds \int_{d-i\infty}^{d+i\infty} d\lambda\, \varepsilon\{P(E_0, s, \lambda)\}\, E^{-s}(e^{\lambda t} - 1)/s\lambda, \tag{2}$$

where

$$\varepsilon\{P(E_0, s, \lambda)\} = \Gamma(E_0, s, \lambda)\, B(s), \quad \varepsilon\{\Gamma(E_0, s, \lambda)\} = P(E_0, s, \lambda)\, C(s);$$

the values of B(s), C(s), and $P(E_0, s, \lambda)$ have been determined in reference 2. The explicit expression for $\epsilon\{N(E_0, E, t)\}$, accounting for ionization losses, can be written in the form*

$$\varepsilon\{N_p(E_0, E, t)\} = -\frac{1}{2\pi i}\int_{\sigma-i\infty}^{\sigma+i\infty} ds 2\sigma_0 D(s)\, H_1'(s) \exp\{\lambda_1(s)\, t + ys - \ln(-\lambda_1(s))\} \tag{3}$$

$$\times G_k(s, \varepsilon)/s + \frac{1}{2\pi i}\int_{\sigma-i\infty}^{\sigma+i\infty} ds 2\sigma_0 D(s)\, H_1'(s) \exp\{ys - \ln(-\lambda_1(s))\}\, G_k(s, \varepsilon)/s.$$

Here

$$H_1'(s) = 1/(\lambda_1(s) - \lambda_2(s)); \quad \varepsilon = Ef(\lambda_1(s))/\beta; \quad G_k(s, \varepsilon) = \int_0^1 x^{s-1}(x + \varepsilon)^{-s}\left\{\sum_{\substack{n=0 \\ n\neq 1}}^{\infty} (-1)^n x^n/n!\,(1 - n) - (1 - C)\, x\right\} dx;$$

C is the Euler constant, and other values are given in reference 2.

For $\epsilon > 1$, the function $G_k(s, \epsilon)$ can be written in the form

*We use the simplified expressions for B(s) and C(c) given reference 3. These do not differ by more than 3% from the more accurate values, and greatly simplify the calculations.

$$G_k(s, \varepsilon) = \sum_{\substack{n=0 \\ n \neq 1}}^{\infty} (-1)^n \varepsilon^{-s} F(s, s+n, s+n+1, -1/\varepsilon)/n!\,(1-n)(s+n) + (C-1)\,\varepsilon^{-s} F(s, s+1, s+2, -1/\varepsilon)/(s+1), \tag{4}$$

where $F(a, b, c, x)$ is the hypergeometric function; the integral can be evaluated numerically for $\epsilon \leq 1$ and noninteger s. It should be noted that the expression written is true for $y = \ln(E_0/\beta) > 1$ and $t > 1$.

The corresponding formulae, obtained neglecting ionization losses, are

$$\varepsilon\{N_p(E_0, E, t)\} = -\frac{1}{2\pi i}\int_{\sigma-i\infty}^{\sigma+i\infty} ds 2\sigma_0 H_1'(s) \exp\{\lambda_1(s)\,t + ys \tag{5}$$

$$-\ln(-\lambda_1(s))\}/s^2(1+s) + \frac{1}{2\pi i}\int_{\sigma-i\infty}^{\sigma+i\infty} ds 2\sigma_0 H_1'(s) \exp\{ys - \ln(-\lambda_1(s))\}/s^2(1+s).$$

The function $\epsilon\{N_p(E_p, E, t)\}$ should not be compared with $N_p(E_0, E, t)$ of the usual cascade theory, as it has been done in reference 2, but with the function

$$N_{ps}(E_0, E, t) = \int_0^t N_p(E_0, E, \tau)\, d\tau, \tag{6}$$

which represents the area under the curve $N_p(E_0, E, t)$ from 0 to t. Carrying out the necessary computations, we obtain (neglecting the ionization losses):

$$N_{ps}(E_0, E, t) = -\frac{1}{2\pi i}\int_{\sigma-i\infty}^{\sigma+i\infty} ds H_1(s) \exp\{\lambda_1(s)\,t + ys - \ln(-\lambda_1(s))\}/s + \frac{1}{2\pi i}\int_{\sigma-i\infty}^{\sigma+i\infty} ds H_1(s) \exp\{ys - \ln(-\lambda_1(s))\}/s \tag{7}$$

and, taking the ionization losses into account:

$$N_{ps}(E_0, E, t) = -\frac{1}{2\pi i}\int_{\sigma-i\infty}^{\sigma+i\infty} ds H_1(s)\, D(s) \exp\{\lambda_1(s)\,t + ys - \ln(-\lambda_1(s))\} \tag{8}$$

$$\times G(s, \varepsilon)/s + \frac{1}{2\pi i}\int_{\sigma-i\infty}^{\sigma+i\infty} ds H_1(s)\, D(s) \exp\{ys - \ln(-\lambda_1(s))\}\, G(s, \varepsilon)/s.$$

where

$$G(s, \varepsilon) = e^{\varepsilon}\int_{\varepsilon}^{\varepsilon+1} \left(1 - \frac{\varepsilon}{x}\right)^s e^{-x} dx,$$

and other values have been given in reference 2. The values of the function $G_k(s, \epsilon)$, calculated according to Eq. (4) for several values of s and ϵ, are given in Table I.

It should be noted that the second term in Eqs. (3) and (5) gives the number of particles produced in the layer $(0 - \infty)$ and the first term gives the number of particles produced in the layer $(t - \infty)$. In Eqs. (7) and (8), the second term represents the area under the cascade curve from $t = 0$ to $t = \infty$, and the first term — from t to ∞. The results of computation of the functions $\overline{N}_{ps}(E_0, E, t)$ and $\epsilon\{\overline{N}_p(E_0, E, t)\}$, neglecting and accounting for ionization losses, given in Table II, represent, therefore, the area under the cascade curve and the number of electrons produced in the layer t to ∞, respectively. For the functions calculated neglecting ionization losses, $y = \ln(E_0/E)$; for those accounting for ionization losses, $y = \ln(E_0/\beta)$. In the latter case, particle energy is measured in units of $\beta/f(\lambda_1(s))$.

If the range of electrons is determined solely

TABLE I. The function $G_k(s, \epsilon)$

s	ε				
	1.5	3.18	6.36	12.7	25.4
1.00	0.329	0.180	0.0950	0.0489	0.0248
1.04	0.303	0.162	0.0835	0.0418	0.0207
1.10	0.268	0.139	0.0690	0.0332	0.0158
1.15	0.244	0.123	0.0590	0.0275	0.0126
1.25	0.200	0.0958	0.0434	0.0190	0.00815
1.35	0.167	0.0754	0.0321	0.0132	0.00530
1.45	0.139	0.0597	0.0240	0.00918	0.00347

by radiation processes, then the values of $\overline{N}_{ps}(y,t)$ and $\epsilon\{\overline{N}_p(y,t)\}$ should be equal. It can be seen from Table II that, within the accuracy of calculations (< 5%), such is the case. It can therefore be maintained that if ionization losses are taken into account, the functions N_{Γ_S} and $\epsilon\{N_{\Gamma_S}(E_0, E, t)\}$ for photons should coincide as well.

In the energy region where the range of electrons is determined by radiation and ionization processes, it is necessary to assume that $\epsilon\{\overline{N}_p(E_0, E, t)\} > \overline{N}_{ps}(E_0, E, t)$. For instance, in the limiting case $E \to 0$, we have $\epsilon\{\overline{N}_p(E_0, E, t)\} \to \infty$, while $\overline{N}_{ps}$ remains finite. For $\epsilon = 1.5$, we have $\epsilon\{\overline{N}_p\} \approx 2\overline{N}_{ps}$, and for $\epsilon = 25.4$, $\epsilon\{\overline{N}_p\} \approx 1.3\,\overline{N}_{ps}$. It is, therefore, necessary to bear in mind the difference between the functions

TABLE II.* The functions $\overline{N}_{ps}(E_0, E, t)$ and $\epsilon\{\overline{N}_p(E_0, E, t)\}$, with and without account of ionization losses, giving the area under the cascade curve, and the number of electrons produced in the layer from t to ∞, respectively.

$y = 15.9$

	ε	t = 0	4.8	7.9	12.7	18.4	23.2	27.8
$N_{ps}(y,t)$		3.61(6)	3.36(6)	3.07(6)	2.29(6)	9.88(5)	3.09(5)	7.06(4)
$\epsilon\{N_p(y,t)\}$		3.57(6)	3.31(6)	3.02(6)	2.23(6)	9.58(5)	2.99(5)	6.85(4)
N_{ps}	0	8.45(6)	7.93(6)	7.30(6)	5.53(6)	2.48(6)	8.02(5)	1.90(5)
N_{ps}	1.5	2.26(6)	2.12(6)	2.10(6)	1.53(6)	6.26(5)	1.85(5)	4.02(4)
ϵN_p	1.5	5.31(6)	4.89(6)	4.44(6)	3.25(6)	1.36(6)	4.10(5)	9.12(4)
N_{ps}	3.18	1.64(6)	1.51(6)	1.36(6)	9.68(5)	3.85(5)	1.10(5)	2.28(4)
ϵN_p	3.18	2.81(6)	2.56(6)	2.30(6)	1.70(6)	6.49(5)	1.86(5)	3.91(4)
N_{ps}	6.36	9.84(5)	8.94(5)	7.99(5)	5.62(5)	2.20(5)	6.27(4)	1.33(4)
ϵN_p	6.36	1.42(6)	1.30(6)	1.14(6)	7.87(5)	2.94(5)	7.91(4)	1.57(4)
N_{ps}	12.7	5.18(5)	4.53(5)	3.98(5)	2.70(5)	9.71(4)	2.53(4)	4.84(3)
ϵN_p	12.7	7.04(5)	6.26(5)	5.51(5)	3.67(5)	1.28(5)	3.25(4)	6.01(3)
N_{ps}	25.4	2.60(5)	2.30(5)	2.00(5)	1.31(5)	4.45(4)	1.09(4)	1.97(3)
ϵN_p	25.4	3.43(5)	3.03(5)	2.61(5)	1.69(5)	5.52(4)	1.30(4)	2.27(3)

$y = 11.7$

	ε	t = 0	2.94	7.36	12.3	16.1	19.7
$N_{ps}(y,t)$		5.35(4)	4.99(4)	3.98(4)	2.06(4)	8.25(3)	2.61(3)
$\epsilon\{N_p(y,t)\}$		5.27(4)	4.90(4)	3.89(4)	2.00(4)	7.98(3)	2.54(3)
N_{ps}	0	1.26(5)	1.19(5)	9.63(4)	5.17(4)	2.14(4)	7.03(3)
N_{ps}	1.5	3.69(4)	3.42(4)	2.66(4)	1.30(4)	4.95(3)	1.49(3)
ϵN_p	1.5	7.80(4)	7.22(4)	5.66(4)	2.83(4)	1.09(4)	3.38(3)
N_{ps}	3.18	2.37(4)	2.21(4)	1.68(4)	8.02(3)	2.93(3)	8.44(2)
ϵN_p	3.18	4.08(4)	3.74(4)	2.85(4)	1.35(4)	4.96(3)	1.45(3)
N_{ps}	6.36	1.42(4)	1.30(4)	9.79(3)	4.58(3)	1.67(3)	4.93(2)
ϵN_p	6.36	2.07(4)	1.86(4)	1.37(4)	6.12(3)	2.11(3)	5.82(2)
N_{ps}	12.7	7.20(3)	6.48(3)	4.70(3)	2.02(3)	6.75(2)	1.79(2)
ϵN_p	12.7	9.98(3)	8.95(3)	6.39(3)	2.68(3)	8.67(2)	2.23(2)
N_{ps}	25.4	3.66(3)	3.25(3)	2.29(3)	9.28(2)	2.91(2)	7.31(1)
ϵN_p	25.4	4.84(3)	4.24(3)	2.94(3)	1.15(3)	3.48(2)	8.41(1)

$y = 9.25$

	ε	t = 0	4.20	8.68	11.9	14.8
$N_{ps}(y,t)$		4.27(3)	3.55(3)	2.06(3)	9.64(2)	3.71(2)
$\epsilon\{N_p(y,t)\}$		4.19(3)	3.47(3)	2.00(3)	9.33(3)	3.60(2)
N_{ps}	0	1.01(4)	8.60(3)	5.18(3)	2.50(3)	9.98(2)
N_{ps}	1.5	2.92(3)	2.37(3)	1.31(3)	5.78(2)	2.12(2)
ϵN_p	1.5	6.17(3)	5.06(3)	2.83(3)	1.28(3)	4.79(2)
N_{ps}	3.18	1.88(3)	1.50(3)	8.03(2)	3.43(2)	1.20(2)
ϵN_p	3.18	3.20(3)	2.54(3)	1.35(3)	5.80(2)	2.06(2)
N_{ps}	6.36	1.11(3)	8.75(2)	4.59(2)	1.96(2)	7.00(1)
ϵN_p	6.36	1.59(3)	1.47(3)	6.13(2)	2.47(2)	8.26(1)
N_{ps}	12.7	5.53(2)	4.19(2)	2.03(2)	7.89(1)	2.55(1)
ϵN_p	12.7	7.65(2)	7.34(2)	2.68(2)	1.01(2)	3.16(1)
N_{ps}	25.4	2.08(2)	2.04(2)	9.29(1)	3.40(1)	1.04(1)
ϵN_p	25.4	3.63(2)	2.62(2)	1.15(2)	4.07(1)	1.19(1)

TABLE II. (Continued)*

$y = 5.94$

	ε	t = 0	t = 3.84	t = 6.32	t = 8.43
$N_{ps}(y, t)$		1.45(2)	9.94(1)	5.79(1)	2.75(1)
$\varepsilon\{N_p(y, t)\}$		1.43(2)	9.63(1)	5.61(1)	2.67(1)
N_{ps}	0	3.51(2)	2.50(2)	1.50(2)	7.41(1)
N_{ps}	1.5	9.68(1)	6.29(1)	3.47(1)	1.57(1)
εN_p	1.5	2.06(2)	1.36(2)	7.69(1)	3.56(1)
N_{ps}	3.18	6.14(1)	3.87(1)	2.06(1)	8.88
εN_p	3.18	1.04(2)	6.52(1)	3.48(1)	1.53(1)
N_{ps}	6.36	3.57(1)	2.21(1)	1.17(1)	5.19
εN_p	6.36	4.99(1)	29.53	14.84	6.13
N_{ps}	12.7	1.71(1)	9.76	4.74	1.89
εN_p	12.7	2.33(1)	1.29(1)	6.09	2.34
N_{ps}	25.4	8.33	4.48	2.04	0.769
εN_p	25.4	10.70	5.55	2.45	0.89

$y = 3.32$

	ε	t = 0	t = 1.89	t = 3.35
$N_{ps}(y, t)$		9.15	6.50	4.15
$\varepsilon\{N_p(y, t)\}$		8.87	6.30	4.03
N_{ps}	0	23.0	16.9	11.2
N_{ps}	1.5	5.80	3.90	2.37
εN_p	1.5	12.6	8.64	5.37
N_{ps}	3.18	3.56	2.31	1.34
εN_p	3.18	6.01	3.91	2.30
N_{ps}	6.36	2.04	1.32	0.78
εN_p	6.36	2.72	1.67	0.92
N_{ps}	12.7	0.900	0.53	0.28
εN_p	12.7	1.19	0.68	0.35

*The number in parenthesis indicates the power of 10, a factor by which the corresponding value should be multiplied.

$N_{ps}(E_0, E, t)$ and $\epsilon\{N_p(E_0, E, t)\}$ in the interpretation of emulsion and diffusion-chamber measurements.

It should be noted that while $N_{ps}(E_0, 0, t) \to E_0/\beta$ for $t \to \infty$[2], direct computations according to Eq. (2) yield a value differing from E_0/β by less than 5% for $y > 5$, which makes it possible to appreciate the influence of the approximations made in the calculation. For $y = 3.32$, the value of $N_{ps}(0, \infty)$ differs from E_0/β by 20%, which indicates that the integrals should be computed more accurately, i.e., the integrand should be expressed in the form $\exp\{\Phi(s, y, t)\}$ and the integral evaluated by the saddle-point method.

It should be noted, furthermore, that the expressions for the function $\overline{N}_{ps}(E_0, E, t)$ make it possible to find easily the mean energy of shower particles at a given depth:

$$\overline{E(t)} = \overline{N}_{ps}(E_0, 0, t)/N_p(E_0, 0, t). \qquad (9)$$

Analogous expressions for the distribution function of electrons in showers initiated by a single primary photon, as well as for the photon distribution function, can be obtained easily.

The author wishes to thank T. V. Klopkova for help in the computations.

[1] A. Ramakrishnan and S. K. Srinivasan, Proc. Ind. Acad. Sci. **44**, 263 (1956); **45**, 133 (1957); S. K. Srinivasan and N. R. Ranganathan, Proc. Ind. Acad. Sci. **45**, 69, 268 (1957).

[2] S. Z. Belen'kii, Лавинные процессы в космических лучах (Cascade Processes in Cosmic Rays), Gostekhizdat, 1948.

[3] B. Rossi and K. Greisen, Revs. Modern Phys. **13**, 240 (1941).

Translated by H. Kasha
18

SCATTERING OF SLOW NEUTRONS BY DEUTERONS

V. N. EFIMOV

P. N. Lebedev Physics Institute, Academy of Sciences, U.S.S.R.

Submitted to JETP editor February 5, 1958

J. Exptl. Theoret. Phys. (U.S.S.R.) **35**, 137-142 (July, 1958)

The neutron-deuteron scattering lengths were computed by a variational method, taking into account deformation of the deuteron. The radial dependence of the nuclear force potential was chosen to be a Gaussian, with parameters adjusted to agree with low energy data on the n-p interaction. The computation was done only for Serber-type exchange forces. The values of the scattering lengths agree with the experimental values within the experimental errors.

AT low energies, the scattering of neutrons by deuterons is characterized by two scattering lengths: a_4 for total spin $S = 3/2$ and a_2 for $S = 1/2$. Analysis of the experimental data gives two possible sets of values of a_4 and a_2:[1]

$$a_4 = 6.2 \cdot 10^{-13}\ \text{cm}; a_2 = 0.8 \cdot 10^{-13}\ \text{cm} \qquad (1)$$

or

$$a_4 = 2.4 \cdot 10^{-13}\ \text{cm}; a_2 = 8.3 \cdot 10^{-13}\ \text{cm}. \qquad (2)$$

The scattering lengths have been calculated by different methods in various theoretical papers.[2-7] In calculating the s-phases of low energy n-d scattering, Christian and Gammel[5] used the Hulthen[8] variational method and assumed that the deuteron is not distorted by the incoming neutron. The appropriate Euler equations were then solved and values of $a_4 = 5.9 \times 10^{-13}$ cm, $a_2 = 1.5 \times 10^{-13}$ cm were found for the scattering lengths.

Burke and Robertson[7] made use of the approximation of an undistorted deuteron directly in the Schrödinger equation and computed the scattering lengths for several values of the radius of nuclear forces. Their results are in poorer agreement with experiment than those of reference 5. The solutions found in references 5 and 7 require complicated calculations which have to be done on electronic computers, but the values found for the scattering lengths are not in sufficiently good agreement with experiment.

Verde[3] and Clementel[4] used the direct variational method, which leads to less complicated calculations. However, their results are not satisfactory, apparently owing to too crude an approximation to the deuteron wave function and to the assumption that the deuteron is not deformable. Even though Verde's results are in agreement with the experimental values (2) for the scattering lengths, from later work[5-7] and from considerations of symmetry of the wave function which are presented in reference 9, it appears that the set in (1) are the correct values. It is therefore of interest to obtain the correct values of the scattering lengths by a direct variational method taking into account the deformation of the deuteron. Instead of using Hulthèn's method,[8] it seemed to us more effective to start from the variational principle for nucleon-nucleon scattering phases which was given by Rubinow.[10] According to Rubinow, the variation of a certain functional is zero for the solution of the wave equation, and its extremal value determines the scattering phase. The functional depends only on "interior" wave functions which are different from zero only within the range of action of the scattering potential. Such functions are easily approximated by damped exponentials. The generalization of Rubinow's variational method to n-d scattering is presented below.

Let the index 1 refer to the incident neutron, and 2, 3 to the neutron and proton forming the deuteron. $\mathbf{r}_i$ is the radius vector to the i-th nucleon; M is the nucleon mass; E is the kinetic energy of the neutron in the center-of-mass system, E_d the binding energy of the deuteron; S is the total spin of the system, equal to $3/2$ or $1/2$; σ_i are the spin variables, which take on values $\pm 1/2$. The nucleon-nucleon interaction is assumed to be central and charge-invariant:

$$V(ik) = U(ik)(w + bB_{ik} + mM_{ik} + hH_{ik}), \qquad (3)$$

where U(ik) is a function of the distance $|\mathbf{r}_i - \mathbf{r}_k|$ between the i-th and k-th nucleons; w, b, m, and h are respectively the fractions of Wigner, Bartlett,

Majorana, and Heisenberg forces, $w + b + m + h = 1$, B_{ik}, M_{ik}, and H_{ik} are the corresponding exchange operators. Introducing the coordinates

$$\mathbf{r} = (\sqrt{3}/2)(\mathbf{r}_3 - \mathbf{r}_2),\ \mathbf{q} = -\mathbf{r}_1 + {}^1/_2(\mathbf{r}_2 + \mathbf{r}_3)$$

the Schrödinger equation takes the form

$$(\Delta_r + \Delta_q + k^2 - k_d^2 + W)\,\Psi^{(S)}(\mathbf{r}, \mathbf{q}, \sigma_1, \sigma_2, \sigma_3) = 0, \quad (4)$$

where

$$k^2 = 4ME/3\hbar^2,\ k_d^2 = 4ME_d/3\hbar^2,$$
$$W = V(12) + V(13) + V(23),$$

$\Delta_{\mathbf{r}}$ and $\Delta_{\mathbf{q}}$ are the Laplacians with respect to the variables $\mathbf{r}$ and $\mathbf{q}$, respectively.

The functions $\Psi^{(S)}$ are assumed to be everywhere finite, continuous, and antisymmetric under interchange of the neutrons, and to have the following asymptotic form as $q \to \infty$:

$$\Psi^{(3/2)} \approx \chi^{(3/2)}(\sigma_1, \sigma_2, \sigma_3)(f\cot\delta_4 + g), \quad (5a)$$

$$\Psi^{(1/2)} \approx \chi^{(1/2)}(\sigma_1, \sigma_2, \sigma_3)(f\cot\delta_2 + g), \quad (5b)$$

where δ_4 and δ_2 are the s-scattering phases in the states with $S = 3/2$ and $S = 1/2$, respectively;

$$f = \frac{1}{2\pi^{1/2}}\varphi_d(r)\frac{1}{q}\sin kq,\ g = \frac{1}{2\pi^{1/2}}\varphi_d(r)\frac{1}{q}\cos kq, \quad (6)$$

$\varphi_d(\mathbf{r})$ is the wave function of the deuteron,

$$\chi^{(3/2)} = \alpha_1(\sigma_1)\alpha_2(\sigma_2)\alpha_3(\sigma_3),$$

$$\chi^{(1/2)} = \{\alpha_1(\sigma_1)[\alpha_2(\sigma_2)\beta_3(\sigma_3) + \beta_2(\sigma_2)\alpha_3(\sigma_3)]$$
$$- 2\beta_1(\sigma_1)\alpha_2(\sigma_2)\alpha_3(\sigma_3)\}/\sqrt{6}.$$

α and β are defined as usual:

$$\alpha({}^1/_2) = 1,\ \alpha(-{}^1/_2) = 0,\ \beta({}^1/_2) = 0,\ \beta(-{}^1/_2) = 1.$$

We expand the functions $\Psi^{(S)}$ in eigenfunctions of the total spin S and its z projection S_z. These functions have the form:

$$\text{for } S = 3/2,\ S_z = 3/2,\ \chi^{(3/2)} = \alpha_1(\sigma_1)\alpha_2(\sigma_2)\alpha_3(\sigma_3); \quad (7)$$

$$\text{for } S = 1/2,\ S_z = 1/2,$$

$$\chi_1^{(1/2)} = [\beta_1(\sigma_1)\alpha_2(\sigma_2) - \alpha_1(\sigma_1)\beta_2(\sigma_2)]\alpha_3(\sigma_3)/\sqrt{2}; \quad (8a)$$

$$\chi_2^{(1/2)} = \{[\alpha_1(\sigma_1)\beta_2(\sigma_2) + \beta_1(\sigma_1)\alpha_2(\sigma_2)]\alpha_3(\sigma_3) \quad (8b)$$
$$- 2\alpha_1(\sigma_1)\alpha_2(\sigma_2)\beta_3(\sigma_3)\}/\sqrt{6},$$

where the function (8a) is antisymmetric and (7) and (8b) are symmetric in the spins of the two neutrons. Then

$$\Psi^{(3/2)} = \chi^{(3/2)}\psi(\mathbf{r}, \mathbf{q}), \quad (9)$$

$$\Psi^{(1/2)} = \chi_1^{(1/2)}\varphi_1(\mathbf{r}, \mathbf{q}) + \chi_2^{(1/2)}\varphi_2(\mathbf{r}, \mathbf{q}). \quad (10)$$

Substituting (9) and (10) in (4) and separating spin variables, we get for $\psi(\mathbf{r}, \mathbf{q})$ the equation

$$(\tau + W_4)\psi = 0, \quad (11)$$

where

$$\tau = \Delta_r + \Delta_q + k^2 - k_d^2,\ W_4 = (\chi^{(3/2)}, W\chi^{(3/2)}),$$

while for $\varphi_1(\mathbf{r}, \mathbf{q})$ and $\varphi_2(\mathbf{r}, \mathbf{q})$ we have the pair of equations

$$(T + W_2)\varphi = 0, \quad (12)$$

where

$$T = \begin{pmatrix} \tau & 0 \\ 0 & \tau \end{pmatrix}, \qquad W_2 = \begin{pmatrix} W_{11} & W_{12} \\ W_{21} & W_{22} \end{pmatrix},$$
$$\varphi = \begin{pmatrix} \varphi_1 \\ \varphi_2 \end{pmatrix},\ W_{ik} = (\chi_i^{(1/2)}, W\chi_k^{(1/2)}).$$

To construct total wave functions $\Psi^{(S)}$ which are antisymmetric under interchange of the two neutrons, we need the following combinations of the functions f and g defined in (6):

$$F_4 = (1 - P_{12})f,\ G_4 = (1 - P_{12})g,$$
$$F_2^{(1)} = -(\sqrt{3}/2)(1 + P_{12})f,\ G_2^{(1)} = -(\sqrt{3}/2)(1 + P_{12})g,$$
$$F_2^{(2)} = -{}^1/_2(1 - P_{12})f,\ G_2^{(2)} = -{}^1/_2(1 - P_{12})g, \quad (13)$$

where P_{12} is the exchange operator for the coordinates of the two neutrons.

If in place of ψ, φ_1, φ_2 we introduce new functions Y_4, $Y_2^{(1)}$ and $Y_2^{(2)}$:

$$\psi = F_4\cot\delta_4 + G_4 - Y_4, \quad (14)$$

$$\varphi_1 = F_2^{(1)}\cot\delta_2 + G_2^{(1)} - Y_2^{(1)},\ \varphi_2 = F_2^{(2)}\cot\delta_2 + G_2^{(2)} - Y_2^{(2)}$$

and impose the conditions:

$$P_{12}Y_4 = -Y_4,\ P_{12}Y_2^{(1)} = Y_2^{(1)},\ P_{12}Y_2^{(2)} = -Y_2^{(2)}, \quad (15)$$

we find that all the functions Y and G are finite and continuous, and all the Y's go to zero for $q \to \infty$, so that it follows from (7) to (10), (13), and (14) that $\Psi^{(3/2)}$ and $\Psi^{(1/2)}$ are finite, continuous, have the required symmetry and take on the form (5) as $q \to \infty$.

Substituting (14) in (11) and (12), we get the equations for Y_4, $Y_2^{(1)}$ and $Y_2^{(2)}$:

$$(\tau + W_4)(Y_4 - G_4)$$
$$-\cot\delta_4[W_4F_4 - (1 - P_{12})U(23)f] = 0, \quad (16)$$
$$(T + W_2)(Y_2 - G_2) - \operatorname{ctg}\delta_2(W_2 - U_2)F_2 = 0.$$

Here

$$F_2 = \begin{pmatrix} F_2^{(1)} \\ F_2^{(2)} \end{pmatrix},\ G_2 = \begin{pmatrix} G_2^{(1)} \\ G_2^{(2)} \end{pmatrix},\ Y_2 = \begin{pmatrix} Y_2^{(1)} \\ Y_2^{(2)} \end{pmatrix},$$

$$U_2 = \begin{pmatrix} {}^1/_2(1 + P_{12})U(23) & (\sqrt{3}/2)(1 - P_{12})U(23) \\ (1/2\sqrt{3})(1 - P_{12})U(23) & {}^1/_2(1 + P_{12})U(23) \end{pmatrix},$$

and $U(ik)$ is defined in (3). In deriving (16) we used the fact that F_4 and F_2 satisfy the equations

$$\tau F_4 + (1 - P_{12}) U(23) f = 0, \quad (T + U_2) F_2 = 0, \quad (17)$$

which follow from (6) and (13).

The set of equations (16) and (17) enable us to find the phases δ_4 and δ_2 by using the variational principle[10] which states that the solutions of equation (16) annul the variation of the functional $L(Y-G)$, while $<L>_{extr.} = k \cot \delta$. The functional L has the form:

$$L = k \cot \eta (1 + B)^2 - C, \quad (18)$$

where η is the s-phase shift in Born approximation; the quantities B, C for $S = 3/2$ are given by the formulas:

$$B = \frac{1}{2k} \int d\tau (Y_4 - G_4) \{W_4 F_4 - (1 - P_{12}) U(23) f\},$$

$$C = \frac{1}{2} \int d\tau (Y_4 - G_4)(\tau + W_4)(Y_4 - G_4), \quad (d\tau = d\mathbf{r}\, d\mathbf{q}),$$

and for $S = 1/2$ by

$$B = \frac{1}{2k} \int d\tau [(Y_2 - G_2), (W_2 - U_2) F_2],$$

$$C = \frac{1}{2} \int d\tau [(Y_2 - G_2), (T + W_2)(Y_2 - G_2)],$$

where

$$[A, B] = A_1^* B_1 + A_2^* B_2, \quad \text{if} \quad A = \begin{pmatrix} A_1 \\ A_2 \end{pmatrix}, \; B = \begin{pmatrix} B_1 \\ B_2 \end{pmatrix}$$

The computation of the scattering lengths was done with the potential used in reference 5:

$$U(r) = U_0 \exp(-\lambda^2 r^2), \; U_0 = 86.4 \text{ Mev}, \quad (19)$$

$$\lambda^{-1} = 1.332 \cdot 10^{-13} \text{ cm}$$

and the Serber exchange force. The potential (19) was chosen to agree with the data on the n-p interaction at low energies. For the potential (19), the approximate deuteron function has the form:[5]

$$\varphi_d(x) = 0.02133 e^{-0.03x^2} + 0.08582 e^{-0.16x^2} + 0.18115 e^{-0.76x^2}, \quad (20)$$

where $x = \lambda r$.

The minimum of the functional (18) was found by the direct Ritz method, using trial functions satisfying the conditions (15). For $S = 3/2$, we chose:

(1) in first approximation, neglecting deformation of the deuteron:

$$Y_4 = (1 - P_{12}) \varphi_d(r) \left[\exp(-\lambda^2 q^2)/2\pi^{1/2} q + \sum_{n=1}^{N} C_n \exp(-n\lambda^2 q^2) \right], \quad (21)$$

(2) in second approximation, including deformation of the deuteron:

$$Y_4 = (1 - P_{12}) \Phi,$$

where P_{12} is the operator which interchanges the coordinates of the neutrons,

$$\Phi = \varphi_d(r) \exp(-\lambda^2 q^2)/2\pi^{1/2} q + \sum_{p,n} C_{pn} \exp(-\gamma_p \lambda^2 r^2 - n\lambda^2 q^2), \quad (22)$$

$$p = 1, 2, 3; \; n = 1, 2 \ldots, N;$$

$$\gamma_1 = 0.03, \; \gamma_2 = 0.16, \; \gamma_3 = 0.76.$$

For each n, the sum over p in (22) contains the same exponentials $\exp(-\gamma_p x^2)$ as in (20), but the coefficients are varied.

For $S = 1/2$ the trial functions took into account deformation of the deuteron:

(1) In first approximation, the deformation was included as in (22)

$$Y_2^{(1)} = -(\sqrt{3}/2)(1 + P_{12}) \Phi, \quad Y_2^{(2)} = -1/2 (1 - P_{12}) \Phi.$$

(2) In the second approximation, in the spin state (8a) we added an unknown multiple of a function which is symmetric in the coordinates of all the nucleons. The introduction of such a function takes account of the fact that in the state (8a) the neuteron penetrates deep into the deuteron and all three nucleons interact strongly with one another. We chose this function in the form

$$v = \sum_{m=1}^{M} A_m \exp[-m\lambda^2 (r^2 + q^2)/2]. \quad (23)$$

Thus in this case the trial function had the form

$$Y_2^{(1)} = -(\sqrt{3}/2)(1 + P_{12}) \Phi - v,$$

$$Y_2^{(2)} = -1/2 (1 - P_{12}) \Phi.$$

The computational results for the scattering lengths a_4 and a_2 are given in the table, in which the values of M and N indicate the number of terms included in the sums which appear in the trial functions (21), (22), and (23). It is clear that

Dependence of a_4 and a_2 on number of terms in the trial functions (21), (22) and (23). For each n in (22), p runs through the values 1, 2, 3.

	First approximation	Second approximation	Experiment[1]
$a_4 \cdot 10^{13}$ cm^{-1}	$N=1$ 11.8 $N=2$ 7.5 $N=3$ 7.5	$N=1$ 7.7 $N=2$ 6.3 $N=3$ 6.3	6.2 ± 0.2
$a_2 \cdot 10^{13}$ cm^{-1}	$N=1$ 1.7 $N=2$ 1.7	$N=1$, $M=2$ } 1.1 $N=2$, $M=3$ } 1.1	0.8 ± 0.3

the contributions of the terms in the trial functions drop off rapidly with increasing n and m, and that $a_4 = 6.3 \times 10^{-13}$ cm and $a_2 = 1.1 \times 10^{-13}$ cm coincide within the limits of error with the experimental values (1) for the scattering lengths.

We are now in the course of calculation of the energy dependence of the s-phase, the depth of the potential and the type of exchange force, as well as the analysis of low energy proton-deuteron scattering, by the present method.

In conclusion, the author thanks M. V. Kazarnovskii and A. S. Davydov for valuable discussions and continued interest in the work.

[1] Wollan, Shull, and Koehler, Phys. Rev. **83**, 700 (1951).

[2] L. Motz and J. Schwinger, Phys. Rev. **58**, 26 (1940).

[3] M. Verde, Helv. Phys. Acta **22**, 339 (1949); A. Troesch and M. Verde, Helv. Phys. Acta **24**, 39 (1951).

[4] E. Clementel, Nuovo cimento **8**, 185 (1951).

[5] R. S. Christian and J. L. Gammel, Phys. Rev. **91**, 100 (1953).

[6] T. V. Skorniakov and K. A. Ter-Martirosian, Dokl. Akad. Nauk SSSR **106**, 425 (1956), Soviet Phys. "Doklady" **1**, 53 (1956).

[7] P. G. Burke and H. H. Robertson, Proc. Phys. Soc. **A70**, 777 (1957).

[8] L. Hulthen, Kgl. Fysiograf. Sällskap. Lund. Förh. **14**, No. 21, 257 (1944).

[9] A. S. Davydov and G. F. Filippov, J. Exptl. Theoret. Phys. (U.S.S.R.) **31**, 340 (1956); Soviet Phys. JETP **4**, 267 (1957).

[10] S. I. Rubinow, Phys. Rev. **98**, 183 (1955).

Translated by M. Hamermesh
19

SOVIET PHYSICS JETP VOLUME 35 (8), NUMBER 1 JANUARY, 1959

NONEQUILIBRIUM PROCESSES IN IMPURITY SEMICONDUCTORS

V. P. SHABANSKII

P. N. Lebedev Physics Institute, Academy of Sciences, U.S.S.R.

Submitted to JETP editor February 5, 1958

J. Exptl. Theoret. Phys. (U.S.S.R.) **35**, 143-153 (July, 1958)

A treatment is given of the kinetic equations for impurity semiconductors, which describe transitions from the impurity levels to the conduction band. On the assumption that the distribution function of the free electrons (or holes) has the form of an equilibrium distribution function with a certain effective temperature that can be determined from the equations, explicit expressions are given for the energy and kinetic coefficients for cases in which the lifetime of the electrons in the conduction band is determined by photorecombination and triple-collision recombination processes. Nonradiative transitions other than those occurring in triple recombination are included by a phenomenological method. In this case the kinetic and energy coefficients can be expressed in terms of the lifetime of the electrons against such transitions in the equilibrium state. The equations obtained make it possible to determine the electron temperature and the number of electrons in the conduction band in various nonequilibrium processes.

1. THE KINETIC EQUATIONS FOR THE FREE ELECTRONS, INCLUDING EFFECTS OF RECOMBINATION AND IONIZATION

THE kinetic equations for the distribution function $\bar{n}$ of electrons or holes, including effects of their possible heating up, have the form [cf. e.g., Eqs. (3.1) ff. in reference 1]

$$\frac{\partial \bar{n}_0}{\partial t} + \frac{v}{3}\nabla\hat{\bar{n}}_1 + \frac{1}{N_e}\frac{\partial}{\partial\varepsilon}(N_e S_1) + \Sigma_{ee}(\bar{n}_0, \bar{n}_0) + \varphi(\varepsilon) = 0, \quad (1.1)$$

$$\frac{\partial \bar{n}_1}{\partial t} + v\nabla\bar{n}_0 + e\mathbf{E}v\frac{\partial \bar{n}_0}{\partial\varepsilon} + \frac{e}{mc}[\mathbf{H}\times\bar{n}_1] + \frac{v}{L}\bar{n}_1 = 0. \quad (1.2)$$

Here

$$S_1 = {}^1/_3\, e\mathbf{E}\cdot\bar{\mathbf{n}}_1 v - S \qquad (1.3)$$

$$= {}^1/_3\, e\mathbf{E}\cdot\bar{\mathbf{n}}_1 v - (2mv_s^2\varepsilon v/l)\,[\bar{n}_0(1-\bar{n}_0)/kT + \partial\bar{n}_0/\partial\varepsilon]$$

is the energy flux density in the energy space. The notations are as follows: $\bar{n}_0$ is the part of the distribution function that is symmetric in the momenta (the average number of electrons in a given energy level); $\mathbf{v}\cdot\bar{\mathbf{n}}_1/v$ is the part added to the symmetric part of the distribution function — together these two parts give the total function $\bar{n}$; ϵ is the energy, $v = \partial\epsilon/\partial p$ is the speed, m the effective mass, e the charge of an electron (or hole), v_s the velocity of sound, and T the lattice temperature. The reciprocal of the mean free path L in which the electron loses its momentum is given by

$$1/L = 1/l_{el} + 1/l_{ei} + 1/l_{ee}, \qquad (1.4)$$

where $l = l_{el}$ is the mean free path against loss of momentum by scattering by phonons, l_{ei} by scattering by impurities, and l_{ee} by electrons and holes. E and H are the external electric and magnetic fields, c the speed of light, and N_e the doubled (because of spin degeneracy) density of electron (or hole) levels. The expression Σ_{ee} describes the interaction between the electrons in the conduction band. The term $\varphi(\epsilon)$ in Eq. (1.1), which was not included in reference 1, describes the change of the average number of electrons (or holes) with the energy ϵ on account of transitions between the conduction band, the valence band, and the impurity levels. We neglect the analogous term in Eq. (1.2). Together with the normalization condition

$$n = \int \bar{n}_0 N_e d\varepsilon \qquad (1.5)$$

the system of equations completely determines the distribution function

$$n = n_0 + \mathbf{v}\cdot\mathbf{n}_1/v. \qquad (1.6)$$

We shall choose the concrete form of $\varphi(\epsilon)$ for impurity semiconductors for conditions such that transitions from one band to another, and also between a band and local levels far removed from it can be neglected. Thus for semiconductors with electron conductivity we include only transitions between donor levels and the conduction band, and for semiconductors with hole conductivity only transitions between acceptor levels and the valence band. The construction of the scheme for semiconductors with hole conductivity does not differ at all in principle from the treatment of electronic semiconductors. Therefore for definiteness we shall speak hereafter about an electronic semiconductor in which in addition to the donors there are N_a acceptors. In the ground state the acceptors will be filled up with electrons which have gone to them from the donor levels. We shall denote by N_d the number of donor levels that are filled in the ground state. Thus we arrive at a Neiburov scheme of a semiconductor with N_d donors and N_a acceptors, located at the distance ϵ_0 below the bottom of the conduction band.

Ejection of electrons from the donor levels into the conduction band cannot be accomplished by the phonons, because their maximum energy is considerably smaller than ϵ_0. Thermal fluctuations, under the action of which impurity electrons get ionized, can occur in the form of photons of black-body radiation. The dispersion formula for this excitation branch is given by the equation $\omega^2 = \omega_0^2 + v_\nu K^2$, where v_ν is the speed of light of frequency ν in the medium, K is the wave vector of the photon, and $\omega_0 = (4\pi ne^2/m)^{1/2}$ is the Debye frequency determined by the total number n of free electrons. For semiconductors in which n is small compared with the value in metals, the quantity ω_0 can be neglected for frequencies that can produce transitions ($\omega \gtrsim \epsilon_0/h$). In addition to the processes of ionization by black-body radiation, ionization can be produced by fast electrons with energies larger than ϵ_0. The inverse processes are those of photorecombination, accompanied by the emission of a photon, and of triple-collision recombination, i.e., recombination with an empty impurity by one of two electrons colliding with it simultaneously. For a number of semiconductors in which the numbers of free electrons are small, and for which it is known that in equilibrium one can neglect processes of ionization by collision and of radiationless triple-collision recombination, radiative recombination alone cannot explain the short lifetimes of electrons in the free state that are observed experimentally. The source and character of the perturbations that cause the nonradiative transitions in these semiconductors have not been ascertained as yet. We shall for the time being leave this class of semiconductors to one side, so that we confine ourselves to the consideration of semiconductors in which the lifetime of the free electrons in the equilibrium state is fixed either by radiative recombination or by nonradiative triple recombination.

Let $\tilde{Z}(\epsilon) - \tilde{Z}'(\epsilon)$ denote the increase of the number of free electrons with the energy ϵ per unit volume and unit time owing to processes of photoionization and photorecombination, and $Z(\epsilon) - Z'(\epsilon)$ that owing to processes of ionization by

collision and triple recombination. Then

$$\varphi(\varepsilon) = -\tilde{Z} + \tilde{Z}' - Z + Z'. \qquad (1.7)$$

We confine ourselves to the consideration of semiconductors of relatively small conductivity, in which the number of electrons is so small ($n < 6 \times 10^{14} T^{3/2}$) that they obey classical statistics. Then for the photoprocesses we have

$$\tilde{Z}(\varepsilon) = (N_d - n)\,\varkappa_\nu v_\nu \bar{N}_\nu\, d\Gamma_\nu / d\Gamma_e, \qquad (1.8)$$

$$\tilde{Z}'(\varepsilon) = (N_a + n)\,\varkappa_e v\,(1 + \bar{N}_\nu)\,\bar{n}, \qquad (1.9)$$

where $\bar{n}$ is the average number of free electrons in the level in question, n is the total number of free electrons, $d\Gamma_e = N_e(\epsilon)\,d\epsilon$ is the number of electronic levels with the energy ϵ, $d\Gamma_\nu$ is the number of photon levels, κ_ν is the cross-section for photoionization by a photon of frequency given by $h\nu = \epsilon_0 + \epsilon$, and κ_e is the cross-section for photorecombination. The cross-sections κ_ν and κ_e are connected by the relation

$$\varkappa_\nu = \varkappa_e \frac{d\Gamma_e}{d\Gamma_\nu}\frac{v}{v_\nu}. \qquad (1.10)$$

In Eq. (1.9) the factor $(1 + \bar{N}_\nu)$, where $\bar{N}_\nu$ is the average number of photons with the frequency ν, includes the effects of both spontaneous and stimulated emission.

Taking account of the effects of dispersion, we have for the number of photon levels

$$d\Gamma_\nu = 8\pi K^2\, dK = \frac{8\pi\nu^2}{c^3}\zeta^3\frac{d\ln\zeta\nu}{d\ln\nu}\,d\nu,$$

where the photon wave vector $K = \zeta\nu/c$, and ζ is the index of refraction. The speed of a photon in material with the index of refraction ζ is

$$v_\nu = d\nu/dK = (c/\zeta)\,d\ln\nu/d\ln\zeta\nu.$$

The quantity $v_\nu d\Gamma_\nu$ itself has the simple form

$$v_\nu\, d\Gamma_\nu = (8\pi\nu^2/c^2)\,\zeta^2\, d\nu = v_\nu 8\pi\nu^2\, d\nu / v_\nu^3, \qquad (1.11)$$

just as if there were no dependence of ζ on ν. For frequencies $h\nu \sim \epsilon_0$ in the majority of semiconductors the relation $\epsilon_d \approx \zeta^2$ between the index of refraction and the dielectric constant holds with good accuracy.

To describe the processes of ionization by collision and triple recombination we introduce the cross-section $S^{1,2}(\epsilon_1, \epsilon_2)$ for the process in which an electron with energy ϵ_1 produces ionization by collision with the ejected electron going into an energy interval at ϵ_2 and the original electron left still in the conduction band (the indices 1, 2 on S mean that at the start of the process there was one electron in the conduction band, and at the end there are two). The cross-section $S^{2,1}(\epsilon_1, \epsilon_2)$ describes the inverse process, in which one of the two electrons recombines (namely the first one) while they are both interacting with the impurity. The change of the number of electrons with energy ϵ owing to ionization processes $S^{1,2}$ consists of three parts: (1) the electron ionized from the impurity goes into the interval $d\epsilon$, (2) the electron producing the ionization goes into the interval $d\epsilon$, and (3) an electron that itself has the energy ϵ produces ionization and leaves the interval $d\epsilon$. Corresponding to these three processes we have:

$$Z(\varepsilon) = (N_d - n)\,n\left\{\int_{\varepsilon+\varepsilon_0}^{\infty} v(\varepsilon_1)\frac{\bar{n}(\varepsilon_1)}{n}\frac{S^{1,2}(\varepsilon_1,\varepsilon)}{N_e(\varepsilon)}N_e(\varepsilon_1)\,d\varepsilon_1 + \int_{\varepsilon+\varepsilon_0}^{\infty} v(\varepsilon_1)\frac{\bar{n}(\varepsilon_1)}{n}\frac{S^{1,2}(\varepsilon_1,\varepsilon_1-\varepsilon-\varepsilon_0)}{N_e(\varepsilon)}N_e(\varepsilon_1)\,d\varepsilon_1 - \int_0^{\varepsilon-\varepsilon_0} v(\varepsilon)\frac{\bar{n}(\varepsilon)}{n}\frac{S^{1,2}(\varepsilon,\varepsilon_1)}{N_e(\varepsilon)}N_e(\varepsilon_1)\,d\varepsilon_1\right\}. \qquad (1.12)$$

In a similar way we find for the decrease of the number of electrons with the energy ϵ owing to the inverse processes $S^{2,1}$:

$$Z'(\varepsilon) = (N_a+n)\,n^2\left\{\int_0^{\infty} v(\varepsilon)\frac{\bar{n}(\varepsilon)}{n}v(\varepsilon_1)\frac{\bar{n}(\varepsilon_1)}{n}S^{2,1}(\varepsilon,\varepsilon_1)N_e(\varepsilon_1)\,d\varepsilon_1 + \int_0^{\infty} v(\varepsilon)\frac{\bar{n}(\varepsilon)}{n}v(\varepsilon_1)\frac{\bar{n}(\varepsilon_1)}{n}S^{2,1}(\varepsilon_1,\varepsilon)N_e(\varepsilon_1)\,d\varepsilon_1 - \int_0^{\infty} v(\varepsilon-\varepsilon_1-\varepsilon_0)\frac{\bar{n}(\varepsilon-\varepsilon_1-\varepsilon_0)}{n}v(\varepsilon_1)\frac{\bar{n}(\varepsilon_1)}{n}S^{2,1}(\varepsilon_1,\varepsilon-\varepsilon_1-\varepsilon_0)\,d\varepsilon_1\right\}. \qquad (1.13)$$

Furthermore, as follows from the principle of detailed balance, or from the equation $Z = Z'$, for equilibrium [cf. Eq. (2.1)] we have the following relation between the cross-sections of the direct and inverse processes

$$S^{2,1}(\varepsilon_1,\varepsilon_2) = \frac{v(\varepsilon_1+\varepsilon_2+\varepsilon_0)}{v(\varepsilon_1)v(\varepsilon_2)}\frac{N_e(\varepsilon_1+\varepsilon_2+\varepsilon_0)}{N_e(\varepsilon_1)N_e(\varepsilon_2)}S^{1,2}(\varepsilon_1+\varepsilon_2+\varepsilon_0,\varepsilon_2). \qquad (1.14)$$

The cross-section $q(\epsilon)$ for ionization by collision is defined in terms of $S^{1,2}$ in the following way:

$$q(\varepsilon) = \int_0^{\varepsilon-\varepsilon_0} S^{1,2}(\varepsilon,\varepsilon_1)\,d\varepsilon_1, \qquad (1.15)$$

and the concrete expression for $S^{1,2}$, for example as given by the classical Thomson formula, is

$$S^{1,2}(\varepsilon, \varepsilon_1) = \pi e^4 / \varepsilon (\varepsilon_1 + \varepsilon_0).$$

As will be seen from what follows, it is necessary to take into account all three possibilities for ionization and recombination. Usually only the first term is used in calculating the ionization. This would, however, lead to an incorrect result in calculating the change of the total energy of the free electrons.

Equations (1.1) to (1.3), with the $\varphi(\epsilon)$ determined by Eq. (1.7) and the equations following it, describe the change of the distribution function n of the electrons in various sorts of processes, on condition that the distribution $\overline{N}_\nu$ of the photons at each point of coordinate space is a known function. $\overline{N}_\nu$ is determined by the equation of diffusion of radiation and the appropriate boundary conditions. This equation clearly has the form

$$\frac{\partial N_\nu(\vartheta, \varphi)}{\partial t} + \mathbf{v}_\nu \nabla N_\nu(\vartheta, \varphi) + (N_d - n)\varkappa_\nu v_\nu N_\nu(\vartheta, \varphi) \quad (1.16)$$

$$- (N_a + n)\varkappa_e v \left(\frac{1}{4\pi} + N_\nu(\vartheta, \varphi)\right) \bar{n} \frac{d\Gamma_e}{d\Gamma_\nu} = 0,$$

where $N_\nu(\vartheta, \varphi)$ is the number of photons of frequency ν in the direction ϑ, φ, so that $\int N_\nu(\vartheta, \varphi) \sin\vartheta \, d\vartheta \, d\varphi = \overline{N}_\nu$.

Using Eqs. (1.12) to (1.14), and also (in the intermediate steps) the concrete expression for $S^{1,2}$, we calculate the integral of Eq. (1) times $N_e d\epsilon$. As the result we get the equation of conservation of charge in the form

$$\frac{\partial n}{\partial t} - (N_d - n)\tilde{\beta} + (N_a + n) n\tilde{\beta}' - (N_d - n) n\beta \quad (1.17)$$

$$+ (N_a + n) n^2 \beta' + \operatorname{div} \mathbf{j}/e = 0,$$

where the ionization and recombination coefficients are

$$\tilde{\beta} = \int_{\nu_0}^{\infty} \varkappa_\nu \overline{N}_\nu v_\nu \, d\Gamma_\nu; \quad (1.18)$$

$$\tilde{\beta}' = \frac{1}{n}\int_0^\infty \varkappa_e v (1 + \overline{N}_\nu) \bar{n} \, d\Gamma_e = \frac{1}{n}\int_{\nu_0}^\infty \varkappa_\nu (1 + \overline{N}_\nu) \bar{n} v_\nu \, d\Gamma_\nu; \quad (1.19)$$

$$\beta = \frac{1}{n}\int_{\varepsilon_0}^\infty v(\varepsilon) \bar{n}(\varepsilon) N_e(\varepsilon) \, d\varepsilon \int_0^{\varepsilon - \varepsilon_0} S^{1,2}(\varepsilon, \varepsilon_1) \, d\varepsilon_1, \quad (1.20)$$

$$\beta' = \frac{1}{n^2}\int_{\varepsilon_0}^\infty v(\varepsilon) N_e(\varepsilon) \, d\varepsilon \int_0^{\varepsilon - \varepsilon_0} \bar{n}(\varepsilon_1) \bar{n}(\varepsilon - \varepsilon_1 - \varepsilon_0) S^{1,2}(\varepsilon, \varepsilon_1) \, d\varepsilon_1, \quad (1.21)$$

and the electric current density is

$$\mathbf{j} = -\frac{e}{3}\int_0^\infty v \bar{\mathbf{n}}_1 N_e \, d\varepsilon. \quad (1.22)$$

By integrating the product of Eq. (1) times $\epsilon N_e(\epsilon) d\epsilon$ we can obtain the equation of conservation of energy. Here the integration of the expressions (1.12) and (1.13) for Z and Z′ gives a negative quantity, unlike the case of integration of $\tilde{Z}$ and $\tilde{Z}'$. This corresponds to the physics of the situation: when recombination occurs the electronic system receives the liberated binding energy of the electron and impurity. On performing the integration we get the equation of conservation of energy

$$\partial \varepsilon_e / \partial t + \operatorname{div} \mathbf{W}_e - \mathbf{E}\cdot\mathbf{j} + Q_{el} + Q_{ep} + Q_{ei} = 0. \quad (1.23)$$

Here the average energy of the n electrons is

$$\varepsilon_e = n\bar{\varepsilon} = \int \varepsilon \bar{n} N_e d\varepsilon; \quad (1.24)$$

the electronic thermal flux is

$$\mathbf{W}_e = \frac{1}{3}\int \varepsilon v \bar{\mathbf{n}}_1 N_e d\varepsilon; \quad (1.25)$$

the energy transferred from the electrons to the lattice on account of emission of phonons is

$$Q_{el} = \int S N_e d\varepsilon, \quad (1.26)$$

where S is to be taken from Eq. (1.3); the energy lost by the electrons in interaction with the photons is

$$Q_{ep} = (N_a + n) n (\tilde{\tilde{\gamma}}' - \varepsilon_0 \tilde{\beta}') - (N_d - n)(\tilde{\gamma} - \varepsilon_0 \tilde{\beta}) \quad (1.27)$$

and that lost in processes of ionization by collision and of recombination is

$$Q_{ei} = -\varepsilon_0 (N_a + n) n^2 \beta' + \varepsilon_0 (N_d - n) n\beta, \quad (1.28)$$

where the quantities

$$\tilde{\gamma} = \int_{\nu_0}^\infty \varkappa_\nu \overline{N}_\nu h\nu v_\nu d\Gamma_\nu, \quad (1.29)$$

$$\tilde{\tilde{\gamma}}' = \frac{1}{n}\int_{\nu_0}^\infty \varkappa_\nu (1 + \overline{N}_\nu) \bar{n} h\nu v_\nu d\Gamma_\nu \quad (1.30)$$

differ from $\tilde{\beta}$ and $\tilde{\beta}'$ by the factor $h\nu$ in the integrands.

The first term in Q_{ep} is the energy lost by the electrons in the conduction band in photorecombination; the second term in Q_{ep} is the energy received by the electrons in the absorption of radiation. Here $(N_a + n) n\tilde{\tilde{\gamma}}'$ is the radiated energy, and $(N_d - n)\tilde{\gamma}$ is the absorbed energy. The terms $\epsilon_0\tilde{\beta}'$ and $\epsilon_0\tilde{\beta}$ allow for the change of the binding energy.

The conservation equations (1.17) and (1.23) are not a complete system unless supplemented by the

equation of conservation of energy for the photons, which is obtained by integrating the product of Eq. (1.16) by $h\nu \sin\vartheta\, d\vartheta\, d\varphi$:

$$\partial\varepsilon_p/\partial t + \nabla\cdot\mathbf{W}_p + (N_d - n)\,\tilde{\gamma} - (N_a + n)\,n\tilde{\gamma}' = 0, \quad (1.31)$$

where the energy of the photons producing ionization is

$$\varepsilon_p = \int_{\varepsilon_0}^{\infty} h\nu \overline{N}_\nu d\Gamma_\nu, \quad (1.32)$$

the radiative energy flux is

$$\mathbf{W}_p = \int v_\nu \nabla N_\nu(\vartheta, \varphi) \sin\vartheta\, d\vartheta\, d\varphi\, d\Gamma_\nu \quad (1.33)$$

and the last two terms in Eq. (1.31) represent the energy going into ionization.

The energy transferred by the electrons to the lattice either goes to increase the lattice energy, or else is carried away owing to the thermal conductivity of the lattice, which is described by the equation

$$\partial\varepsilon_l/\partial t + \operatorname{div}\mathbf{W}_l - Q_{el} = 0, \quad (1.34)$$

where ϵ_l is the average lattice energy and $\mathbf{W}_l$ is the thermal flux transferred by the phonons.

We shall not write out the differential equation corresponding to (1.34) for the distribution function of the phonons since, owing to the strong interaction between phonons at temperatures above the Debye temperature, the equilibrium distribution for the temperature T, determined from Eq. (1.34) and the boundary conditions, is not upset by the action of the external field and illumination. Thus the problem is the following one. For concrete physical conditions we have to determine the distribution functions of the electrons and photons, Eqs. (1.1), (1.2), and (1.16), and, knowing these distribution functions, we must use the conservation equations (1.17) and (1.23) and the transport equations (1.22) and (1.25) to describe the various nonequilibrium processes.

It is convenient, particularly for thin specimens, to separate the radiation into an internal part, which will be denoted by $\overline{N}_\nu$ as before, and an external part $\overline{N}^{ext}$

Then, introducing the notations

$$\beta_{ext} = \int_{\nu_0}^{\infty} \varkappa_\nu \overline{N}_\nu^{ext} v_\nu d\Gamma_\nu, \quad (1.35)$$

$$\gamma_{ext} = \int_{\nu_0}^{\infty} \varkappa_\nu \overline{N}_\nu^{ext} h\nu v_\nu d\Gamma_\nu, \quad (1.36)$$

we have instead of Eqs. (2.16) and (2.22)

$$\frac{\partial n}{\partial t} - (N_d - n)(\tilde{\beta} + \beta_{ext}) + (N_a + n)\,n\tilde{\beta}' - (N_d - n)\,n\beta + (N_a + n)\,n^2\beta' + \operatorname{div}\frac{\mathbf{j}}{e} = 0, \quad (1.37)$$

$$\frac{\partial\varepsilon_e}{\partial t} + \operatorname{div}\mathbf{W}_e - \mathbf{E}\cdot\mathbf{j} + Q_{el} + Q_{ep} + Q_{ei} = Q_{ep}^{ext}, \quad (1.38)$$

where the energy received by the electrons as a result of the irradiation is

$$Q_{ep}^{ext} = (N_d - n)(\gamma_{ext} - \varepsilon_0\beta_{ext}). \quad (1.39)$$

Here we do not necessarily mean by β_{ext} irradiation by light; it may also be any other agency that produces ionization of the electrons, for example an electron beam, etc.

2. THE CONSERVATION EQUATIONS FOR AN EQUILIBRIUM DISTRIBUTION FUNCTION OF THE ELECTRONS WITH AN EFFECTIVE TEMPERATURE

In the presence of external fields and irradiation of the semiconductor the distribution functions of the electrons and photons will be of a nonequilibrium nature. Owing to the slowness of transfer of energy from the electrons to the lattice, as compared with the transfer of momentum, in strong electric fields the electron gas gets heated up.* The energy distribution of the electrons of this heated gas will be mainly determined by the interaction with the phonons, since the characteristic times for exchange of energy between electrons and photons are considerably longer than the time for exchange of energy with the phonons.

The first manifestation of the nonequilibrium nature of the electron distribution is a shift of the maximum of the distribution function toward higher energies. The nonequilibrium distribution function can be approximated by an equilibrium function with a certain effective electron temperature, which is determined from the equations. The kinetic coefficients found by means of this function differ very little from the coefficients found from the exact distribution function. Moreover, such an approximation facilitates the calculations and makes the meanings of the effects clearer. Therefore we shall assume that the distribution function of the electrons is an equilibrium function with the temperature T_e.

*Generally speaking, the electron gas will get heated up in a field also in the case in which the energy is transferred to the lattice in the same time as the momentum (as, for example, in ionic semiconductors, in which the mean free path l_ε against energy transfer and the free path l_p against momentum transfer are of the same order). And this heating up will also manifest itself in effects for which it is of importance. For this case, however, the very method of solving the kinetic equation is, strictly speaking, not valid for arbitrary fields, because in sufficiently strong fields (for which the heating up is appreciable) the asymmetrical part of the distribution function becomes comparable with the symmetrical part.

The energy distribution of the photons is determined on one hand by the electron distribution, and on the other hand by the penetration of the external irradiation into the interior of the specimen. It is clear that far inside a massive specimen the distribution function $\overline{N}_\nu$ of the photons will correspond to the electron distribution; i.e., if the electrons have the temperature T_e, then $\overline{N}_\nu$ is the equilibrium function with this same temperature.

In a thin specimen, where the additional radiation that appears because of the recombination of the heated-up electrons gets out of the specimen without being absorbed, the photon distribution is the equilibrium distribution with the temperature T. Just this case, which is the least favorable one for the increase of the total number of free electrons under the action of a field, is the one we shall now consider. Corresponding to the above statements, our assumptions are

$$\overline{n} = \frac{n}{N_{\text{eff}}(T_e)} e^{-\varepsilon/kT_e}, \quad N_{\text{eff}}(T_e) = 2(2\pi mkT_e/h^2)^{3/2}, \tag{2.1}$$

$$\overline{N}_\nu = [e^{h\nu/kT} - 1]^{-1}. \tag{2.2}$$

In the calculation of the quantities β, Eqs. (1.18) to (1.21), we assume that the density of the electron levels is the same as for free electrons with the effective mass m, and that the cross-section $q(\epsilon)$ for ionization by collision is given by the Thomson formula

$$q(\varepsilon) = (\pi e_1^4/\varepsilon^2)(\varepsilon/\varepsilon_0 - 1),$$

where e_1 is the effective charge of the impurity.

Then, substituting Eqs. (2.1) and (2.2) into Eqs. (1.18) to (1.21), we get for the case $kT/\epsilon_0 \ll 1$, $kT_e/\epsilon_0 \ll 1$:

$$\tilde{\beta} = \tilde{B}e^{-\varepsilon_0/kT}, \tag{2.3}$$

$$\tilde{\beta}' = (\tilde{B}/N_{\text{eff}}(T))(T/T_e)^{1/2}, \tag{2.4}$$

$$\beta = B(T_e/T)^{1/2}e^{-\varepsilon/kT_e}, \tag{2.5}$$

$$\beta' = (B/N_{\text{eff}}(T))\,T/T_e, \tag{2.6}$$

where

$$\tilde{B} = 8\pi\varkappa_\nu^0\varepsilon_0^2\varepsilon_{\text{d}}kT/c^2h^3, \tag{2.7}$$

$$B = (4\pi e_1^4/\varepsilon_0^2)\sqrt{kT/2\pi m}. \tag{2.8}$$

Here κ_ν^0 is the absorption coefficient of light of frequency ν_0 by a single atom, and ϵ_d is the dielectric constant ($\epsilon_d \approx \xi^2$). To first approximation with respect to kT/ϵ_0, kT_e/ϵ_0 the expressions (1.29), (1.30) for $\tilde{\gamma}$ give

$$\tilde{\gamma} = \varepsilon_0\tilde{\beta} \qquad \tilde{\gamma}' = \varepsilon_0\tilde{\beta}', \tag{2.9}$$

so that according to Eq. (1.27) the energy Q_{ep} transferred to the photons is zero. In the next approximation we get

$$\tilde{\gamma} - \varepsilon_0\tilde{\beta} = kT\tilde{\beta}, \qquad \tilde{\gamma}' - \varepsilon_0\tilde{\beta}' = kT_e\tilde{\beta}', \tag{2.10}$$

$$Q_{ep} = (N_a + n)\,nkT_e\tilde{\beta}' - (N_d - n)\,kT\tilde{\beta}. \tag{2.11}$$

The concrete form of the expression (1.39) for the energy received by the electrons in ionization by an external source depends on the spectral composition of the irradiation. For monochromatic light of frequency $\nu_{ext} = \epsilon_{ext}/h$, or for a monochromatic electron beam with energy $\epsilon_{ext} = eV_{ext}$

$$Q_{\text{ext}} = (N_d - n)(\varepsilon_{\text{ext}} - \varepsilon_0)\beta_{\text{ext}}, \tag{2.12}$$

where for light

$$\beta_{\text{ext}} = (I\Delta\nu\varkappa_\nu/h\nu)_{\nu=\nu_{\text{ext}}} = n_{\text{qu}}\varkappa_{\nu\,\text{ext}}, \tag{2.13}$$

and for an electron beam

$$\beta_{\text{ext}} = n_{\text{el}}q(\varepsilon_{\text{ext}}) = (j_{\text{ext}}/e)\,q(\varepsilon_{\text{ext}}). \tag{2.14}$$

Here n_{qu} and n_{el} are the numbers of quanta and electrons of energy ϵ_{ext} incident per unit time on one square centimeter of surface; I is the intensity of the incident light.

The total energies incident and radiated by the specimen in the form of photons are obviously given by the expressions:

$$Q'_{\text{ext}} = (N_d - n)\,\varepsilon_{\text{ext}}\beta_{\text{ext}}, \tag{2.15}$$

$$Q'_{ep} = (N_a + n)\,n\varepsilon_0\tilde{\beta}'. \tag{2.16}$$

To evaluate the quantity B by Eq. (2.7) we must know the experimental values of the absorption coefficient and the index of refraction of the light (or the value of the dielectric constant) for the frequency ν_0. On the other hand, these quantities can be evaluated by means of the hydrogen-like model of the impurity, if one knows the depth ϵ_0 of the local level, the effective mass of the electron, and the resonance absorption cross-section of hydrogen.

If we regard the impurity as a Coulomb center placed in a medium of dielectric constant ϵ_d, then the depth ϵ_0 of the impurity level and the "radius" r_0 of the impurity are determined from the relations

$$\varepsilon_R/\varepsilon_0 = \varepsilon_{\text{d}}^2 m_e/m, \quad r_0 = r_{\text{H}}\varepsilon_{\text{d}}m_e/m, \tag{2.17}$$

where ϵ_R is the Rydberg energy, r_H is the Bohr radius, and m_e and m are the true and effective masses of the electron. The actual depth of the impurity level does not, however, correspond to the dielectric constant ϵ_d in the way shown in Eq. (2.17) for all semiconductors. Therefore in estimating the impurity radius r_0 it is better to use the expression

$$r_0 = r_{\text{H}}(\varepsilon_R m_e/\varepsilon_0 m)^{1/2}, \tag{2.18}$$

which is obtained by eliminating ϵ_d from Eq. (2.17).

The photoionization cross-section κ_ν is proportional both to r_0^2 and to the electromagnetic interaction constant in the medium, i.e., $\kappa_{\nu_0} \sim e_1^2/h\nu_\nu = e^2/hc\epsilon_d^{1/2}$, where $e_1 = e\epsilon_d^{1/2}$ is the effective charge. Eliminating ϵ_d, we get*

$$\kappa_{\nu_0} = \kappa_H (\varepsilon_R/\varepsilon_0)^{3/4} (m_e/m)^{5/4}. \quad (2.19)$$

In just the same way, eliminating the effective charge e_1 from the expression (2.8) for B, we get:

$$B = (4\pi e^4/\varepsilon_0\varepsilon_R) \sqrt{kT/2\pi m_e}\, (m_e/m)^{3/2}. \quad (2.20)$$

If we introduce the maximum value of the collision ionization for hydrogen, which according to the Thomson formula is reached at energy $2\epsilon_R$ and is given by $q_{max}^H = e^4/4\epsilon_R^2 \sim 10^{-16}\,cm^{-2}$, (which agrees with the experimental value), then we get the following expressions for B and $\tilde{B}$:

$$\tilde{B} = (8\pi\kappa_H kT\varepsilon_d \varepsilon_0^2/c^2h^3) (\varepsilon_R/\varepsilon_0)^{3/4} (m_e/m)^{5/4}, \quad (2.21)$$

$$B = 16 q_{max}^H (\varepsilon_R/\varepsilon_0) \sqrt{kT/2\pi m_e}\, (m_e/m)^{3/2}. \quad (2.22)$$

If for example, we set $\epsilon_0 = 0.15$ ev, $m = m_e$ and use the data for hydrogen, $\epsilon_R = 13.6$, $q_{max}^H = 10^{-16}\,cm^{-2}$, $\kappa_H = 6.3 \times 10^{-18}\,cm^2$, we find that for $T = 300°$ we have $B \approx 4 \times 10^{-9}$, $\tilde{B} \approx 5 \times 10^5$. The value $\epsilon_0 = 0.15$ ev corresponds to a dielectric constant $\epsilon_d = (\epsilon_R/\epsilon_0)^{1/2} \sim 9.5$.

The characteristic times for photoelectric and triple-collision recombination — lifetime of the electron in the free state — are connected with the quantities $\tilde{B}$ and B in the following way:

$$\tilde{\tau}' = 1/(N_a + n_0)\tilde{\beta}' = N_{eff}(T)/(N_a + n_0)\tilde{B}, \quad (2.23)$$

$$\tau' = 1/(N_a + n_0) n_0 \beta' = N_{eff}(T)/(N_a + n_0) n_0 B, \quad (2.24)$$

where n_0 is the equilibrium number of free electrons.

For the distribution function (2.1) the expression (1.25) for the energy transferred to the lattice by the electrons takes the form

$$Q_{el} = An \frac{T_e - T}{T} \left(\frac{T_e}{T}\right)^{1/2}, \quad (2.25)$$

where we have used the notation

$$A = -\left(\frac{T}{T_e}\right)^{1/2} \frac{2mv_s^2}{n} \int_0^\infty \frac{\varepsilon v N_e}{l} \frac{\partial \bar{n}}{\partial \varepsilon}\, d\varepsilon. \quad (2.26)$$

If we assume that l does not depend on the energy, which is correct for atomic semiconductors, then

$$A = (16mv_s^2/l)(kT/2\pi m)^{1/2}. \quad (2.27)$$

For example, with $m = m_e$, $v_s \sim 10^5$ cm/sec, $T = 300°$, and $l \sim 10^{-6}$ cm, we have the numerical value $A \sim 5 \times 10^{-4}$.

Let us now assume that there exists a type of nonradiative recombination in which the energy is in some way transferred directly to the lattice. This means that there are in the lattice excitations other than the photons of blackbody radiation that are capable of ionizing the impurity. Of whatever type these excitations may be — boson or fermion — for $kT/\epsilon_0 \ll 1$ the probabilities of ionization through the action of these excitations and of recombination with appearance of excitation will be of the forms (2.3) and (2.4), but with an unknown coefficient B, which we denote by B_b. The value of B_b can be estimated if we know the experimental value of the lifetime for radiationless recombination, by the relation (2.23):

$$\tau_b' = N_{eff}(T)/(N_a + n_0) B_b. \quad (2.28)$$

The next question is that of the rate at which equilibrium is established for the excitations that produce the nonradiative transitions, i.e., the question of the rate at which the transfer of the excitation energy by the phonons occurs. If the time for transport of the excitation energy by the phonons is smaller than the time for recombination with production of these excitations, then the temperature of the excitations will be the same as the lattice temperature. This natural assumption corresponds to the most favorable case for the increase of the number of free electrons under the action of the external factors. Then, just as for the interaction with the photons that get away without being absorbed, we have

$$\beta_b = B_b e^{-\varepsilon_0/kT}, \quad \beta_b' = (B_b/N_{eff}(T))(T/T_e)^{1/2}. \quad (2.29)$$

In Eq. (1.37) one adds the term $-(N_d - n)\beta_b + (N_a + n) n \beta_b'$. The energy Q_{el} transferred in unit time from the electrons to the lattice, which we have to put into Eq. (1.38) instead of the expression (2.25), is given, in analogy with Eq. (2.11), by

$$Q_{el} = An \frac{T_e - T}{T} \left(\frac{T_e}{T}\right)^{1/2} + (N_a + n) nkT_e \beta_b' - (N_d - n) kT\beta_b. \quad (2.30)$$

In the equation (1.34) for the transfer of energy by phonons, however, we must use instead of this value the total energy received by the lattice

$$Q_{el}' = An \frac{T_e - T}{T} \left(\frac{T_e}{T}\right)^{1/2} + (N_a + n) n\varepsilon_0 \beta_b' - (N_d - n)\varepsilon_0 \beta_b \quad (2.31)$$

[cf. Eqs. (1.31) and (2.16)].

Thus the conservation equations for the electrons have the form:

*The same result is also obtained on the basis of the Kramers formula for the photoionization cross-section of hydrogen.

$$\frac{\partial n}{\partial t} + \operatorname{div}\frac{\mathbf{j}}{e} - (N_d - n)(\tilde{\beta} + \beta_b + n\beta + \beta_{ext}) + (N_a + n)\, n\,(\tilde{\beta}' + \beta_b' + n\beta') = 0, \quad (2.32)$$

$$\frac{\partial \varepsilon_e}{\partial t} + \operatorname{div}\mathbf{W}_e - \mathbf{E}\cdot\mathbf{j} + An\frac{T_e - T}{T}\left(\frac{T_e}{T}\right)^{1/2} - (N_d - n)\,[kT\tilde{\beta} + kT\beta_b - n\varepsilon_0\beta + (\varepsilon_{ext} - \varepsilon_0)\beta_{ext}] + (N_a + n)\, n\,[kT_e\tilde{\beta}' + kT_e\beta_b' - n_0\beta'] = 0. \quad (2.33)$$

By solving this system of two equations together with the transport equations one can uniquely determine T_e and the non-equilibrium values of n for various processes.

[1] V. P. Shabanskii, J. Exptl. Theoret. Phys. (U.S.S.R.) **31**, 657 (1956), Soviet Phys. JETP **4**, 497 (1957).

Translated by W. H. Furry
20

SOVIET PHYSICS JETP VOLUME 35 (8), NUMBER 1 JANUARY, 1959

PHOTOPRODUCTION OF ELECTRON AND μ - MESON PAIRS ON NUCLEONS

I. T. DIATLOV

Submitted to JETP editor February 8, 1958

J. Exptl. Theoret. Phys. (U.S.S.R.) **35**, 154-158 (July, 1958)

Production of electron or μ-meson pairs on nucleons by high-energy gamma-quanta is examined. It is shown under what conditions the cross sections for these processes can be expressed in terms of the electromagnetic form factors of the free nucleon.

1. An investigation of the cross sections of the radiation processes involving production of electrons and μ mesons from nucleons at large angles, makes it possible to judge the electromagnetic properties of the nucleon (form factors)[1] or, if these are known from other experiments, to determine the limits of validity of modern quantum electrodynamics.

It was indicated in reference 2 that the electromagnetic form factor of the free nucleon can be written in the form ($\hbar = c = 1$):

$$\Gamma_\mu(q^2) = a(q^2)\gamma_\mu + i\frac{b(q^2)}{2M}\frac{1}{2}(\gamma_\mu\hat{q} - \hat{q}\gamma_\mu),$$

where q is the momentum transferred by the electromagnetic field to the nucleon ($q^2 = \mathbf{q}^2 - q_0^2$; $\hat{q} = q_\nu\gamma_\nu$), M is the nucleon mass, and $a(q^2)$ and $b(q^2)$ are real functions. When q^2 goes to zero, $a(q^2)$ goes to 1 or 0 for protons and neutrons respectively, and $b(q^2)$ goes to the anomalous magnetic moment μ_0 (in nuclear magnetons). Substantial deviations from these limiting values of $a(q^2)$ and $b(q^2)$ are expected when $q \gtrsim \mu$, where μ is the mass of the pion. We shall therefore be interested in recoils $q \gtrsim \mu$, i.e., as will be seen later on, in sufficiently large angles. Furthermore, to determine the form factor $b(q^2)$ it is necessary to consider large recoils, since $b(q^2)$ enters into the formula together with the factor $q(M)(1)$.

2. We consider the production of electron or muon pairs on nucleons by gamma quanta. Graphs corresponding to this process are divided into two groups. In the first group (1a) only one photon line goes to the nucleon line. Along this photon line the nucleon acquires a recoil momentum $q = k - p_+ - p_-$ (p_+ and p_- are the momenta of the pair components and k is the momentum of the incident quantum). These are graphs having the electromagnetic vertex part of the free nucleon, and can be expressed in terms of functions a and b of formula (1) by inserting Γ_μ from formula (1) when writing the matrix elements corresponding to graphs (1a). In the second group, two photon lines go to the nucleon portion of the graph (Figs. 1b and 1c indicate the general form of such a graph and two simplest graphs for a nucleon interacting only with the electromagnetic field). It is impossible to account for the meson interactions for these by introducing simple form factors of type (1).

As to the matrix elements of such graphs, it can be assumed that they are of the same order of magnitude (or less) as the matrix elements of the simplest graphs (1c), corresponding to the

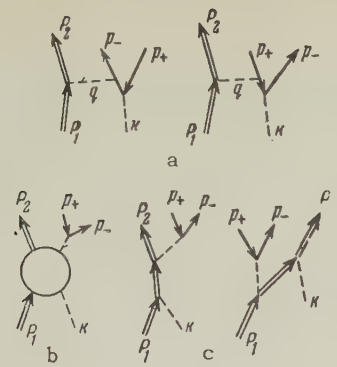

FIG. 1

process that takes place on a point nucleon interacting only with the electromagnetic field. The interaction with meson fields leads to a smearing of the electromagnetic charge of the nucleon which, apparently, reduces the matrix elements compared with the corresponding ones for the point nucleon. These considerations can be confirmed by direct examination of several very simple meson graphs. Consequently, under these conditions, when it is possible to neglect graphs 1c compared with 1a, the cross section of the process can be expressed in terms of the quantities $a(q^2)$ and $b(q^2)$ and this takes care of the influence of the meson fields.

The matrix elements corresponding to graphs 1a and 1c are:

$$M_a = -e^3(2\pi)^4\overline{U}(P_2)\Gamma_\mu U(P_1)\bar{u}(p_-)\left\{\frac{\gamma_\mu}{q^2}\frac{i(-\hat{p}_+ + \hat{k}) - m}{-2p_+\cdot k}\frac{\hat{e}}{\sqrt{2\omega}} + \frac{\hat{e}}{\sqrt{2\omega}}\frac{i(\hat{p}_- - \hat{k}) - m}{-2p_-\cdot k}\frac{\gamma_\mu}{q^2}\right\}v(p_+); \tag{2}$$

$$M_c = -e^3(2\pi)^4\overline{U}(P_2)\left\{\gamma_\mu\frac{i(\hat{P}_1 + \hat{k}) - M}{2P_1\cdot k}\frac{\hat{e}}{\sqrt{2\omega}} + \frac{\hat{e}}{\sqrt{2\omega}}\frac{i(\hat{P}_2 - \hat{k}) - M}{-2P_2\cdot k}\gamma_\mu\right\}U(P_1)\bar{u}(p_-)\frac{\gamma_\mu}{q_1^2}v(p_+), \tag{3}$$

$$pk = \mathbf{p}\cdot\boldsymbol{\omega} - \varepsilon\omega; \quad P_2 = P_1 + q; \quad q_1 = p_+ + p_-;$$

P_1 and P_2 are the momenta of the initial and final nucleons, m is the mass of the light particles, and $\hat{e} = e_\mu\gamma_\mu$ where e_μ is the polarization vector of the gamma quantum.

In order of magnitude

$$M_a \sim \frac{e^3(2\pi)^4}{V\omega}\frac{\mathbf{e}\cdot\mathbf{p}}{p\cdot k}\left(1 - \frac{\mathbf{q}\cdot\mathbf{p}}{Ep}\right)\frac{1}{q^2};$$
$$M_c \sim \frac{e^3(2\pi)^4}{V\omega}\frac{\mathbf{e}\cdot\mathbf{p}}{P\cdot k}\left(1 - \frac{\mathbf{q}\cdot\mathbf{p}}{Ep}\right)\frac{1}{q_1^2}; \tag{4}$$

p is the momentum of any one of the light particles (we assume that their momenta are of the same order), P is the momentum of the nucleon, and E is its energy.

From the Weizsäker[3] analysis of radiation processes it is clear that the principal contribution to the total cross section will be made at large energies by M_a, since the principal contribution to the double cross section is introduced by the angles $\vartheta \lesssim m/p$, and at such angles $M_a \gg M_b$. We are interested, however, in large Q ($q \gtrsim \mu > m$), which corresponds to large angles ($\vartheta \geq \mu/p$). It is therefore necessary to examine the ratio of M_a to M_c at such angles.

From (4) we see that M_a consists of two terms whose ratio is proportional to $\sim|\mathbf{q}|/E$. Neglecting the terms $\sim|\mathbf{q}|/E$ means considering only small recoils $|\mathbf{q}| \ll M$, neglecting the energies transferred to the nucleon, and neglecting the term containing $b(q^2)$ in the expression (1). In order to be able to discard graphs 1c without making such approximations, it is necessary to satisfy the condition

$$\frac{\mathbf{q}\cdot\mathbf{p}}{Ep}\frac{P\cdot k}{p\cdot k}\frac{q_1^2}{q^2} \gg 1. \tag{5}$$

Recoils $|\mathbf{q}| \geq \mu$ mean that the momenta of the light particles should be greater than μ (ω, $|\mathbf{p}_+|$, $|\mathbf{p}_-| > \mu > m$). Then, when $\vartheta \ll 1$ (it will be shown below that only this case is of importance), we have

$$p\cdot k \sim \frac{\omega}{p}[m^2 + (p\vartheta)^2], \quad \mathbf{q}\cdot\mathbf{p} \sim p(E - M) + O(p^2\vartheta^2),$$
$$q^2 \sim O(p^2\vartheta^2), \quad q_1^2 \sim 2m^2 + O(p^2\vartheta^2), \tag{6}$$
$$P\cdot k \sim M\omega + O(p^2\vartheta^2).$$

From the energy-conservation law (the nucleon was at rest before collision) we have

$$E - M \approx 0(p^2\vartheta^2/M). \tag{7}$$

Insertion of (6) and (7) into (5) gives the conditions under which it is possible to consider only graphs 1a

$$\vartheta^2 \ll M/p, \qquad p \gg M. \tag{8}$$

The first of conditions (8) imposes limitations on the energies acquired by the recoil nucleon during the process. It follows from (7) and (8) that the recoil energies are considerably smaller than the energies of the light particles ($\epsilon \cong p$): $E \ll p$. If the second condition of (8) is not satisfied ($p \lesssim M$), then $M_a \gg M_c$ as before, but the terms with $|\mathbf{q}|/E$ in M_a are of the same order as in M_c, and consequently all these, including those containing $b(q^2)$, should be discarded. We then obtain for the quanta with energy $\omega \lesssim M$ and

angles $\vartheta^2 \ll M/\omega \sim 1$ the ordinary Bethe-Heitler formula multiplied by $a^2(q^2)$ ($q^2 = q^2$ for $|q| \ll M$, and the recoil energy of the nucleon is neglected).

3. If conditions (8) are satisfied we obtain, by inserting expression (1) in lieu of Γ_μ into Eq. (3), the probability of pair production on a nucleon at rest.

$$dW = (2\pi)^{-4} |M_a|^2 (2\pi)^{-9} d^3p_+ d^3p_- \delta(M+\omega-\varepsilon_+-\varepsilon_- \quad (9)$$
$$-[M^2+(\omega-p_+-p_-)^2]^{1/2}).$$

Integrating (9) over the absolute value of the momentum p_- and then averaging over the polarization of the gamma-quantum and summing over the spins of the pair components, we obtain ($\alpha = 1/137$):

$$d\sigma = \frac{\alpha^3}{(2\pi)^2} \frac{p_+p_-dp_+}{\omega^3} do_+ do_- \frac{1}{q^4} \left\{a^2(q^2)\left[f_{B-H} + \frac{q^2}{4M^2} f_1\right]\right. \quad (10)$$
$$\left. + 2a(q^2) b(q^2) \frac{q^2}{4M^2} f + b^2(q^2) \frac{q^2}{4M^2}\left[f_{B-H} + \frac{q^2}{4M^2} f_1 - f\right]\right\},$$

where

$$f_{B-H} = \frac{16 p_+^2 p_-^2 (p_+\vartheta_+)^2}{[m^2+(p_+\vartheta_+)^2]^2} + \frac{16 p_+^2 p_-^2 (p_-\vartheta_-)^2}{[m^2+(p_-\vartheta_-)^2]^2}$$
$$- \frac{16 p_+^2 p_-^2 (p_+^2+p_-^2)(\vartheta_+\vartheta_-)}{[m^2+(p_+\vartheta_+)^2][m^2+(p_-\vartheta_-)^2]}$$
$$- 8\omega^2 \frac{[(p_+\vartheta_+)^2+(p_-\vartheta_-)^2] p_+p_-}{[m^2+(p_+\vartheta_+)^2][m^2+(p_-\vartheta_-)^2]}; \quad (11)$$

$$f = -8\omega^2 [(p_+\vartheta_+)^2 + (p_-\vartheta_-)^2] / [m^2+(p_+\vartheta_+)^2][m^2+(p_-\vartheta_-)^2];$$
$$f_1 = 8m^2 (p_+ - p_-)^2 \omega^2 / [m^2+(p_+\vartheta_+)^2][m^2+(p_-\vartheta_-)^2];$$
$$q^2 = (p_+\vartheta_+ + p_-\vartheta_-)^2 = 2M(\omega - p_+ - p_-); \quad (12)$$

ϑ_+ and ϑ_- are the angles between ω and p_+ and p_- respectively ($\omega \cdot \vartheta_\pm = 0$). The modulus of p_- should be expressed in terms of the remaining variables from the conservation laws. f_{B-H} is the usual angular distribution of pairs at relativistic energies (Bethe-Heitler). The remaining terms of (10) represent either corrections to account for the recoil or pair production due to the magnetic moment. All these tend to zero as $M \to \infty$. Formulas (10) and (11) are correct for all angles $\vartheta^2 \ll M/p$, i.e., $q^2 \ll Mp$. Consequently, there exists a sufficiently broad region in which these formulas are of definite interest from the point of view of investigating the limits of validity of quantum electrodynamics and a study of the nucleon form factors

$$\mu^2 \leqslant q^2 \ll Mp, \quad \mu^2/p^2 \leqslant \vartheta^2 \ll M/p. \quad (13)$$

If small $q \sim \mu$ are considered it is possible to neglect recoil in (10). We then obtain the usual Bethe-Heitler formula for the angular distribution at higher energies, multiplied by $a^2(q^2)$:

$$d\sigma = a^2(q^2)\, d\sigma_{B-H}. \quad (14)$$

For lower energies, $p \lesssim M$, formula (14), as already indicated, remains valid in the angle interval $\vartheta \ll 1$.

However, if we do not neglect recoil, then formula (10) holds for angles $\vartheta \sim \mu/p$, and the terms with f_1 can be neglected for angles $\vartheta \gg \mu/p$ in production of a pair of muons, and for all angles (13) in production of a pair of electrons, since then

$$|f_1|/|f_{B-H}| \sim 2m^2/(p\vartheta)^2 \ll 1$$

($|f_1|/|f_{B-H}| \ll 1$ also for $|p_+ - p_-| \ll p_\pm$). In all the above cases formula (10) becomes

$$d\sigma = \frac{\alpha^3}{(2\pi)^2} \frac{p_+p_-dp_+}{\omega^3} do_+do_- \cdot q^{-4} \left\{a^2(q^2) f_{B-H}\right. \quad (15)$$
$$\left. + 2a(q^2) b(q^2) \frac{q^2}{4M^2} f + b^2(q^2) \frac{q^2}{4M^2}[f_{B-H} - f]\right\}.$$

By determining the angular distribution at various energies it is possible, in principle, using formulas (10) to (15), to obtain the values of the form factors[2] or, if these are known, to check how substantially the electromagnetic interaction varies at high energies.

4. If we integrate the δ-function in (9) over the angle between the projections of the vectors p_+ and p_- on a plane perpendicular to the direction ω ($p_+\vartheta_+$ and $p_-\vartheta_-$), and then integrate over the angles ϑ_+ and ϑ_- to a certain ϑ_{max} ($\vartheta_{max} \ll M/p$) at constant p_+ and p_-, i.e., at constant q^2 (12), we obtain the energy distribution of the pair particles that travel in the cone $\vartheta_\pm \lesssim \vartheta_{max}$.

The integration should be over the region bounded by inequalities

$$|q^2 - x^2 - y^2| \leqslant 2xy; \quad x \leqslant \Lambda_+, \quad y \leqslant \Lambda_-, \quad (16)$$
$$x = p_+\vartheta_+; \quad y = p_-\vartheta_-; \quad \Lambda_+ = p_+\vartheta_{max}; \quad \Lambda_- = p_-\vartheta_{max}.$$

Integration over region (16) can be performed rigorously only if $|p_+ - p_-| \geq \sqrt{q^2/\vartheta_{max}}$ or approximately if $\Lambda_+^2 \gg q^2$ ($p_+ \leq p_-$ in the formulas that follow).

For the case $\Lambda_+^2 \gg q^2$ we get

$$d\sigma = \alpha^3 \frac{dp_+dp_-}{\omega^3} \frac{2M}{q^4} \left\{a^2(q^2)\left[\Phi_{B-H} + \frac{q^2}{4M^2}\Phi_1\right]\right.$$
$$\left. + 2a(q^2) b(q^2) \frac{q^2}{4M^2}\Phi + b^2(q^2) \frac{q^2}{4M^2}\left[\Phi_{B-H} + \frac{q^2}{4M^2}\Phi_1 - \Phi\right]\right\}; \quad (17)$$

$$\Phi_{B-H} = (p_+^2+p_-^2)\frac{q^2}{\sqrt{q^4+4q^2m^2}} L - 2p_+p_-\left[1 + \frac{2m^2}{\sqrt{q^4+4q^2m^2}} L\right];$$
$$\Phi = -2\omega^2\left\{2\ln\frac{p_+\vartheta_{max}}{m} + \frac{m^2}{\sqrt{q^4+4q^2m^2}} L\right\}; \quad (18)$$
$$\Phi_1 = -\frac{(p_+-p_-)^2}{p_+p_-}\omega^2 \frac{m^2}{\sqrt{q^4+4q^2m^2}} L;$$
$$L = \ln\frac{[\sqrt{q^4+4q^2m^2} - q^2]\, m^2}{\sqrt{q^4+4q^2m^2}(q^2+m^2) + q^2(q^2+3m^2)}.$$

For $q^2 \ll M^2$ ($q^2 \lesssim \mu^2$) we neglect all the terms in (17) except for the first one, containing Φ_{B-H}. For $q^2 \gg m^2$ it is possible to neglect Φ_1 entirely, the remaining functions assume the simple form

$$\Phi_{B-H} = (p_+^2 + p_-^2)\, q^2 L / \sqrt{q^4 + 4q^2m^2} - 2p_+p_-;$$
$$\Phi = -4\omega^2 \ln (p_+\vartheta_{max}/m). \qquad (19)$$

We leave L in its previous form, in view of the large coefficients in the terms with m^2.

Formula (17) can still be integrated over dp_+ for $p_+ + p_- = \text{const} \approx \omega$ ($q^2 = \text{const}$) and $2Mdp_- = -dq^2$. Then, for $q^2 \gg m^2$:

$$d\sigma = -\alpha^3 \frac{dq^2}{3q^4}\left\{a^2(q^2)\left[\frac{q^2}{\sqrt{q^4+4q^2m^2}}L - \frac{1}{2}\right] - 3ab\frac{q^2}{M^2}\left[\ln\frac{\omega\vartheta_{max}}{2m} - 1\right] + b^2\frac{q^2}{4M^2}\left[\frac{q^2L}{\sqrt{q^4+4q^2m^2}} + 6\ln\frac{\omega\vartheta_{max}}{2m} - \frac{13}{2}\right]\right\}. \qquad (20)$$

Analogous results can also be obtained for bremsstrahlung. For this purpose it is necessary to replace in the matrix elements (2)

$$p_+, \varepsilon_+ \to -p_1, \ -\varepsilon_1, \quad p_-, \varepsilon_- \to p_2, \varepsilon_2; \quad \omega, \omega \to -\omega, \ -\omega$$

and in formulas (9) to take $d^3p_2 d^3\omega/(2\pi)^6$ instead of the statistical factor $d^3p_+d^3p_-/(2\pi)^6$. The results can be obtained from formulas (10) to (15) by substituting

$$\frac{p_+p_-dp_+}{\omega^3}do_+do_- \to \frac{p_2}{p_1}\frac{d\omega}{\omega}do_{p_2}do_\omega;$$
$$\vartheta_+ \to \vartheta; \ \vartheta_- \to \vartheta - \vartheta_2, \ p_+ \to -p_1$$

(ϑ_2 is the angle between p_2 and p_1).

In conclusion, the author expresses sincere gratitude to I. M. Shmushkevich for suggesting the topic and for valuable advice.

[1] G. E. Masek and W. K. H. Panofsky, Phys. Rev. **101**, 1094 (1956); Masek, Lazarus, and Panofsky, Phys. Rev. **103**, 374 (1956).

[2] Akhiezer, Rozentsveig, and Shmushkevich, J. Exptl. Theoret. Phys. **33**, 765 (1957), Soviet Phys. JETP **6**, 588 (1958).

[3] C. F. Weizsaker, Z. Physik **88**, 612 (1934).

Translated by J. G. Adashko
21

SOVIET PHYSICS JETP VOLUME 35 (8), NUMBER 1 JANUARY, 1959

THE POLARIZATION OF THE INTERNAL-CONVERSION ELECTRONS EMITTED AFTER β-DECAY

V. B. BERESTETSKII and A. P. RUDIK

Submitted to JETP editor February 8, 1958

J. Exptl. Theoret. Phys. (U.S.S.R.) **35**, 159-164 (July, 1958)

A discussion is given of the correlation of the polarization of internal-conversion electrons with the direction of emission of the electrons in the preceding β-decay. If one neglects the Coulomb field of the nucleus, then in the case of a magnetic multipole the polarization is longitudinal and does not depend on the energy. In the case of an electric multipole both longitudinal and transverse polarizations occur, with dependence on the energy.

1. Owing to the nonconservation of parity in β-decay the daughter nucleus is polarized in the direction of the emitted β-decay electron (the parent nucleus is supposed unpolarized, and the direction of emission of the neutrino is not observed). Therefore if an internal-conversion process occurs after the β-decay, the conversion electrons must possess a preferred polarization.* This effect can be used both in studying β-decay and also in studying the properties of nuclear levels, since (as will be shown below) the character of the polarization

*Our attention was called to the existence of such an effect by A. I. Alikhanov and V. A. Liubimov.

of the conversion electrons depends in an essential way on the order and type (electric or magnetic) of the multipole involved in the nuclear transition.

The general expression for the polarization vector $\langle\sigma\rangle$ of the internal-conversion electron, for the case of an allowed β-decay transition, has the following form:

$$a(\mathbf{v}\cdot\mathbf{n})\mathbf{n} + b(\mathbf{v} - (\mathbf{v}\cdot\mathbf{n})\mathbf{n}), \qquad (1)$$

where a and b are constants depending on the angular momenta of the nuclear states and the energy of the transition, $c\mathbf{v}$ is the velocity of the β particle, and $\mathbf{n}$ is the unit vector of the direction of the conversion transition.

In fact, Eq. (1) is a general expression with the following properties: (1) it is a polar vector, corresponding to the fact that the polarization appears only as a result of the nonconservation of parity in β-decay ($\langle\sigma\rangle$ is an axial vector); (2) it is invariant under replacement of $\mathbf{n}$ by $-\mathbf{n}$, which corresponds to the conservation of parity in the internal-conversion process; (3) it is proportional to the velocity vector of the β particle, which determines the polarization of the daughter nucleus.

2. Let us find the density matrix characterizing the polarization state of the nucleus formed as a result of the β-decay. If this nucleus is in a state with angular momentum j_2, and if the initial nucleus was unpolarized and the direction of the neutrino was not observed, then the general expression for the density matrix that determines the distribution of the angular-momentum component m_2 must have the following form:

$$\rho_{m_2 m_2'} = \frac{1}{2j_2+1}\left\{\delta_{m_2 m_2'} + \left(\frac{j_2+1}{j_2}\right)^{1/2} \zeta C^{j_2 m_2}_{j_2 m_2', 1\mu} v^\mu\right\}, \qquad (2)$$

where $v^\mu = (-1)^\mu v_{-\mu}$ are the components of the vector ($v^0 = v_z$; $v^{\pm 1} = \mp (v_x \mp i v_y)/2^{1/2}$), and $C^{\ldots}_{\ldots}$ are the coefficients of vector composition (Clebsch-Gordan coefficients), which differ from the matrix elements of the angular-momentum operator $\mathbf{J}$ only by a normalizing factor:

$$(jm|J_\mu|jm') = (jm'|J^\mu|jm) = \sqrt{j(j+1)}\, C^{jm}_{jm',\,1\mu}.$$

The constant ζ can be expressed in terms of the constant that appears in the expression W for the angular distribution of the β particles from the decay of polarized nuclei.

For this purpose let us consider the β-decay of a polarized nucleus with angular momentum j_2 into a nucleus with angular momentum j_3. The probability for the decay can be written in the form

$$W = \mathrm{Sp}\,\rho^0 U^+ U,$$

where U is the operator describing the transition $j_2 \to j_3$ and ρ^0 is the density matrix of the state j_2. If the state of polarization is defined by the average angular momentum vector $\langle \mathbf{J} \rangle$, then

$$\rho^0_{m_2 m_2'} = \frac{1}{2j_2+1}\left\{\delta_{m_2 m_2'} + \frac{3\langle J_\mu\rangle}{\sqrt{j_2(j_2+1)}} C^{j_2 m_2}_{j_2 m_2',\,1\mu}\right\}.$$

The matrix U^+U is proportional to the expression (2). Indeed, the density matrix (2) is determined by the transition $j_3 \to j_2$, and since the state j_3 is not polarized,

$$\rho_{m_2 m_2'} = (U^+U)_{m_2 m_2'} / \mathrm{Sp}\, U^+U.$$

Consequently, apart from a common factor

$$W \sim \left(\delta_{m_2 m_2'} + \frac{3\langle J_\nu\rangle}{\sqrt{j_2(j_2+1)}} C^{j_2 m_2}_{j_2 m_2',\,1\nu}\right)$$

$$\times \left(\delta_{m_2 m_2'} + \left(\frac{j_2+1}{j_2}\right)^{1/2} \zeta C^{j_2 m_2}_{j_2 m_2',\,1\mu} v^\mu\right).$$

Performing the summation over m_2 and m_2', we get

$$W = 1 + \zeta \langle \mathbf{J}\rangle \mathbf{v} / j_2. \qquad (3)$$

Thus we can omit consideration of the β-decay stage of the process, and determine the constant ζ in Eq. (2) from a comparison of Eq. (3) with the known expression for W.[1,2] In particular, for an allowed β transition in the case of S, T, A, and V interaction variants (with neglect of Coulomb forces) ζ is given by

$$\zeta = 2\,\mathrm{Re}\left\{(c_S c_T'^* + c_S' c_T^* - c_V c_A'^* - c_V' c_A^*)\right.$$

$$\times \left(\frac{j_2}{j_2+1}\right)^{1/2} \delta_{j_2 j_3} M_F M_{GT}^* + (c_T c_T'^* - c_A c_A'^*)\,\Lambda_{j_2 j_3} |M_{GT}|^2\Big\}$$

$$\times \{(|c_S|^2 + |c_S'|^2 + |c_V|^2 + |c_V'|^2)|M_F|^2$$

$$+ (|c_T|^2 + |c_T'|^2 + |c_A|^2 + |c_A'|^2)|M_{GT}|^2\}^{-1},$$

where

$$\Lambda_{j_2 j_3} = \{j_2(j_2+1) - j_3(j_3+1) + 2\}/\{2j_2(j_2+1)\},$$

$$M_F = \left(\int 1\right), \quad M_{GT} = \left(\int \sigma\right).$$

3. Suppose the nucleus makes a further transition from the state $j_2 m_2$ to the state $j_1 m_1$. The matrix element of the internal-conversion process can be written in the following form[3] (omitting common factors that are of no importance for our purpose):

$$M_{m_2 m_1} = (j_2 m_2 | Q^{(\lambda)}_{LM} | j_1 m_1)^* \int \psi_2^*(\mathbf{r})\, B^{(\lambda)}_{LM}(\mathbf{r})\, \psi_1(\mathbf{r})\, d\mathbf{r}. \qquad (4)$$

Here $Q^{(\lambda)}_{LM}$ is the operator of the 2^L-pole electric ($\lambda = 1$) or magnetic ($\lambda = 0$) moment of the nucleus, corresponding to the transition in question; ψ_1 and ψ_2 are the wave functions of the electron for the initial and final states; and $B^{(\lambda)}_{LM}$

is the operator of the interaction of the electron with the multipole field. This operator has the following form

$$B^{(0)}_{LM} = \boldsymbol{\alpha}\mathbf{Y}_{LLM}(\mathbf{r}/r)\,G_L(\omega r),$$

$$B^{(1)}_{LM} = Y_{LM}\left(\frac{\mathbf{r}}{r}\right)G_L(\omega r)$$

$$+\sqrt{\frac{2L+1}{L}}\,\boldsymbol{\alpha}\mathbf{Y}_{L,\,L-1,\,M}\left(\frac{\mathbf{r}}{r}\right)G_{L-1}(\omega r).$$

$$G^l(x) = i^l H^{(1)}_{l+1/2}(x)/\sqrt{x},$$

where α is the Dirac matrices, ω is the energy of the transition, $H^{(1)}$ is a Hankel function, Y_{LM} is a spherical harmonic, and $\mathbf{Y}_{LlM}$ is a spherical vector, the components of which are defined in the following way:

$$(Y_{Ll\mathcal{M}})^{\mu} = C^{LM}_{lm,1\,\mu}Y_{lm}.$$

We confine ourselves here to the free-electron approximation

$$\psi_2 = \begin{pmatrix} u \\ \dfrac{\mathbf{q}\sigma}{\varepsilon+m}\,u \end{pmatrix} e^{i\mathbf{q}\mathbf{r}};\quad \psi_1 = \begin{pmatrix} u_0 \\ 0 \end{pmatrix};\quad \varepsilon = m+\omega,$$

where ϵ and $\mathbf{q}$ are the energy and momentum of the conversion electron, u and u_0 are two-component spinors, and σ is the Pauli matrices. Then the integral in Eq. (4) reduces to the following:

$$\int e^{i\mathbf{q}\mathbf{r}}Y_{lm}\left(\frac{\mathbf{r}}{r}\right)G_l(\omega r)\,d\mathbf{r} \sim Y_{lm}(\mathbf{n})\left(\frac{q}{\omega}\right)^l;\quad \mathbf{n} = \frac{\mathbf{q}}{q}.$$

Omitting unimportant factors, we get the expression for the matrix element

$$M_{m_2m_1} = (j_2m_2\,|\,Q^{(\lambda)}_{LM}\,|\,j_1m_1)\,u^*V^{(\lambda)}_{LM}u_0, \tag{5}$$

where in the case of a magnetic multipole ($\lambda = 0$)

$$V^{(0)}_{LM} = (\sigma\cdot\mathbf{n})\,\sigma\mathbf{Y}_{LLM}(\mathbf{n}), \tag{5a}$$

and in the case of an electric multipole ($\lambda = 1$)

$$V^{(1)}_{LM} = Y_{LM}(\mathbf{n}) + \sqrt{\frac{2L+1}{L}}\,\varkappa(\sigma\cdot\mathbf{n})\,\sigma\mathbf{Y}_{L,\,L-1,\,M}(\mathbf{n}); \tag{5b}$$

$$\varkappa = \frac{\varepsilon-m}{\varepsilon+m}.$$

The probability of internal conversion is given by the quantity

$$W = \rho_{m_2m_2'}M_{m_1m_2}M^*_{m_2'm_1}. \tag{6}$$

If we represent W in the form

$$W = P_{\alpha\beta}u_\alpha u^*_\beta,$$

then the density matrix of the conversion electron is obviously equal to P/Sp P. Furthermore, if P has the form

$$P = A(1+\xi\sigma), \tag{6a}$$

then the polarization vector of the conversion electron is given by

$$\langle\sigma\rangle = \xi. \tag{6b}$$

4. Substituting Eq. (5) into Eq. (6), we use the fact that since the electron in the initial state is not polarized $u^0_\alpha u^{0*}_\beta = \delta_{\alpha\beta}$. Then we get the following expression for P:

$$P = \rho_{m_2m_2'}\,(j_2m_2\,|\,Q^{(\lambda)}_{LM}\,|\,j_1m_1)^*\,(j_2m_2'\,|\,Q^{(\lambda)}_{LM'}\,|\,j_1m_1)\,V^{(\lambda)}_{LM}V^{(\lambda)*}_{LM'}. \tag{7}$$

The product of the last two factors, which is a matrix with respect to the spin variables, can be represented in the form

$$V^{(\lambda)}_{LM}V^{(\lambda)*}_{LM'} = R^{(\lambda)}_{MM'} + \sigma\mathbf{S}^{(\lambda)}_{MM'}. \tag{8}$$

Using the expressions (5a) and (5b), we get

$$R^{(0)}_{MM'} = \mathbf{Y}_{LLM}\cdot\mathbf{Y}^*_{LLM'},\quad \mathbf{S}^{(0)}_{MM'} = i\,[\mathbf{Y}_{LLM}\times\mathbf{Y}^*_{LLM}];$$

$$R^{(1)}_{MM'} = (1+2\varkappa)\,Y_{LM}Y^*_{LM'} + \frac{2L+1}{L}\,\varkappa^2\mathbf{Y}_{L,\,L-1,\,M}\mathbf{Y}^*_{L,\,L-1,\,M}; \tag{8a}$$

$$\mathbf{S}^{(1)}_{MM'} = i\,\frac{L+1}{L}\,\varkappa^2\,[\mathbf{Y}_{LLM}\times\mathbf{Y}^*_{LLM}]$$

$$-(\varkappa+\varkappa^2)\sqrt{\frac{L+1}{L}}\,(\mathbf{Y}_{LLM}Y^*_{LM'} + Y_{LM}\mathbf{Y}^*_{LLM'}).$$

The matrix element of the multipole moment can be represented in the following form:

$$(j_2m_2\,|\,Q^{(\lambda)}_{LM}\,|\,j_1m_1) = Q^{(\lambda)}C^{j_2m_2}_{j_1m_1,\,LM}, \tag{9}$$

where $Q^{(\lambda)}$ does not depend on the quantum numbers m_1 and m_2. Substituting Eqs. (2), (8) and (9) into Eq. (7), we get, omitting unimportant common factors:

$$P = \left[\delta_{m_2m_2'} + \left(\frac{j_2+1}{j_2}\right)^{1/2}\zeta C^{j_2m_2}_{j_2m_2',\,1\mu}v^\mu\right]C^{j_2m_2}_{j_1m_1,\,LM}C^{j_2m_2'}_{j_1m_1,\,LM'}\,[R^{(\lambda)}_{MM'} + \sigma\mathbf{S}^{(\lambda)}_{MM'}]$$

(summation over all repeated indices is understood), and using the relations

$$C^{j_2m_2}_{j_1m_1,\,LM}C^{j_2m_2}_{j_1m_1,\,LM'} = \frac{2j_2+1}{2L+1}\delta_{MM'};\quad C^{j_2m_2}_{j_2m_2',\,1\mu}C^{j_2m_2}_{j_1m_1,\,LM}C^{j_2m_2'}_{j_1m_1,\,LM'} = \frac{2j_2+1}{2L+1}\,\frac{L(L+1)+j_2(j_2+1)-j_1(j_1+1)}{2\sqrt{L(L+1)}\,j_2(j_2+1)}\,C^{LM}_{LM',\,1\mu},$$

we have

$$P = R^{(\lambda)}_{MM} + \sigma\mathbf{S}^{(\lambda)}_{MM} + \zeta v^\mu\,\frac{L(L+1)+j_2(j_2+1)-j_1(j_1+1)}{2j_2\sqrt{L(L+1)}}\,C^{LM}_{LM',\,1\mu}(R^{(\lambda)}_{MM'} + \sigma\mathbf{S}^{(\lambda)}_{MM'}). \tag{10}$$

In Eq. (10) the first two terms, after they are summed over M, cannot depend on $\mathbf{n}$. Therefore

$$S^{(\lambda)}_{MM} = 0, \quad R^{(\lambda)}_{MM} = \text{const} = \frac{1}{4\pi}\int R^{(\lambda)}_{MM} d\sigma.$$

From the expression (8a) it follows that

$$R^{(0)}_{MM} = \frac{2L+1}{4\pi}, \quad R^{(1)}_{MM} = \left(1 + 2\varkappa + \frac{2L+1}{L}\varkappa^2\right)\frac{2L+1}{4\pi}.$$

For the calculation of the last two terms in Eq. (10) we take the z axis in the direction of the vector $\mathbf{v}$. Then instead of the sum over μ there remains just the one term with $\mu = 0$, and $M' = M$. Using the explicit expression of the coefficient

$$C^{LM}_{LM,\,10} = M/\sqrt{L(L+1)}$$

and the fact that $R^{(\lambda)}_{MM}$ does not depend on the sign of M, we get

$$\sum_M M R^{(\lambda)}_{MM} = 0.$$

We have still to find the last term in Eq. (10), i.e., the quantity

$$v C^{LM}_{LM',\,10} S^{(\lambda)}_{MM}. \tag{11}$$

According to Eq. (8a), in the case of a magnetic multipole the vector $\mathbf{S}^{(0)}$ is directed along $\mathbf{n}$, since $\mathbf{Y}_{LLM}$ is a transverse vector. This means that for magnetic transitions the coefficient b in Eq. (1) is zero.

Comparing Eq. (11) with the first term in Eq. (1), we see that

$$v\sum_M M S^{(0)}_{MM} = f(\mathbf{v}\cdot\mathbf{n})\,\mathbf{n} = f v n_z \mathbf{n}' \tag{12}$$

where f is a constant. To determine this constant we integrate Eq. (12) with respect to the solid angle; this gives

$$\frac{4\pi}{3} f = \sum_M M \int S^{(0)}_{z\,MM}\, d\sigma.$$

Substituting the explicit expression for $S^{(0)}_{MM}$, we find

$$f = \frac{3}{4\pi}\frac{1}{L(L+1)}\sum_M M^2 = \frac{2L+1}{4\pi}.$$

According to Eq. (8a), in the case of an electric multipole $\mathbf{S}^{(1)}$ contains two terms. The first term, $\mathbf{S}^{(1)}_{\parallel}$, is directed along $\mathbf{n}$ and is calculated in the same way as $\mathbf{S}^{(0)}$. The second term $\mathbf{S}^{(1)}_{\perp}$, proportional to $\mathbf{Y}_{LLM}$, is perpendicular to $\mathbf{n}$, and consequently must have the form of the second term in Eq. (1), i.e.,

$$v\sum_M M S^{(1)}_{\perp\,MM} = g(\mathbf{v} - (\mathbf{v}\cdot\mathbf{n})\,\mathbf{n}).$$

Using the explicit form of $\mathbf{S}^{(1)}_{\perp}$ and integrating this equation over the angles, we find

$$g = \frac{2L+1}{4\pi}\sqrt{L(L+1)}.$$

Substituting these results into Eq. (10), we get on the basis of Eqs. (6a) and (6b) the following expressions for the polarization vector of the conversion electron:

(a) in the case of a magnetic multipole

$$\langle\sigma\rangle = (r\zeta/j_2)\,\mathbf{n}(\mathbf{n}\cdot\mathbf{v}); \tag{13}$$

(b) in the case of an electric multipole

$$\langle\sigma\rangle = r\frac{L+1}{1+2\varkappa+\varkappa^2(2L+1)/L}\frac{\zeta}{j_2}$$
$$\times\left\{(\varkappa+\varkappa^2)(\mathbf{n}(\mathbf{n}\cdot\mathbf{v}) - \mathbf{v}) + \frac{\varkappa^2}{L}(\mathbf{n}\cdot\mathbf{v})\mathbf{n}\right\}, \tag{14}$$

$$r = [L(L+1) + j_2(j_2+1) - j_1(j_1+1)]/2L(L+1).$$

We see from Eq. (13) that in the case of a magnetic multipole the polarization is longitudinal and does not depend on the energy of the polarization electron. This feature is, however, closely connected with the free-electron approximation which has been used here. Therefore a treatment of this problem with exact wave functions for the conversion electron would be of interest.

According to Eq. (14), in the case of an electric dipole the polarization is decidedly energy-dependent. When the speed v_k of the conversion electron is small, the transverse polarization is proportional to v_k^2/c^2, and the longitudinal polarization to $(v_k/c)^4$. These results also need to be made more precise, since for small velocities the effect of the Coulomb field of the nucleus can be important.

We express our sincere gratitude to Academician A. I. Alikhanov and V. A. Liubimov for their interest in the work and a number of helpful discussions.

[1] T. D. Lee and C. N. Yang, Phys. Rev. **104**, 254 (1956).

[2] Berestetskii, Ioffe, Rudik, and Ter-Martirosian, Nuclear Phys. **5**, 464 (1958). I. M. Schmushkevich, J. Exptl. Theoret. Phys. (U.S.S.R.) **33**, 1477 (1957), Soviet Phys. JETP **6**, 1139 (1959); B. T. Feld, Phys. Rev. **107**, 797 (1957). Alder, Stech, and Winther, Phys. Rev. **107**, 728 (1957).

[3] A. I. Akhiezer and V. B. Berestetskii, Квантовая электродинамика (Quantum Electrodynamics), GITTL 1953. [Engl. Transl. publ. by U. S. Dept. of Commerce].

Translated by W. H. Furry
22

DETERMINATION OF THE ENERGY OF FAST PARTICLES FROM THE ANGULAR DISTRIBUTION OF THEIR REACTION PRODUCTS

A. I. NIKISHOV and I. L. ROZENTAL'

P. N. Lebedev Physics Institute, Academy of Sciences, U.S.S.R.

Submitted to JETP editor February 8, 1958

J. Exptl. Theoret. Phys. (U.S.S.R.) **35**, 165-169 (July, 1958)

An analysis is given of the error in determining the energy E of fast colliding particles from the angular distribution of the produced particles. It turns out that to determine the energy by this method one should take account of the connection between the total number of observed star tracks and the energy E. The dependence predicted by the Landau theory is used in the present paper. An approximate distribution of E as a function of the angles and the number of tracks observed is obtained.

1. A method widely used at present for determining the energy of colliding particles is based on the analysis of the angular distribution of the particles produced in the collision process and on the simplest relations of relativistic kinematics. In the course of this analysis two assumptions are usually made: (1) the velocity of the secondaries is close to light velocity, and (2) in the center-of-mass system, the outgoing particles emerge on the average symmetrically with respect to the plane perpendicular to the line of motion.

The first assumption is well satisfied for sufficiently high energies of the primaries ($\gtrsim 10^{12}$ ev), with which we shall deal from now on (cf., for example, the direct measurements of energy of primaries in reference 1).

The second assumption, which is strictly true for nucleon-nucleon collisions, requires additional justification in the most commonly occurring case of collision of nucleons with heavy nuclei. By using the hydrodynamical theory of multiple production proposed by Landau,[2] one can evaluate the degree of asymmetry, if one invokes the additional assumption that the "tube" model[3,4] is valid. According to the results of Amai et al.[5] using this model, the asymmetry in the c.m. system is small, and we shall neglect it in what follows.

Under these assumptions, the energy E of the primary particles, expressed in units of Mc^2 (where M is the nucleon mass), is determined by the formulas

$$-\ln\gamma = \frac{1}{n}\sum_{i=1}^{n} \ln\tan\vartheta_i, \qquad (1)$$

$$E = 2\mu\gamma^2, \qquad (2)$$

where θ_i is the angle in the laboratory system between the direction of motion of the i-th secondary and the direction of the primary; n is the number of tracks of charged secondaries from which the value of E is computed, and μ is the mass of a "tube."

The following important question concerns the size of the possible error in this method. This question was posed in the paper of Castagnoli et al.[6] who estimated the errors taking into account only fluctuations in the value of the energy as a function of the angular distribution. However such an approach is inadequate since it does not take into account several factors, each of which can even change the errors by an order of magnitude. Among these factors are the effect of the energy spectrum of the primaries,* the distribution of "tube" lengths and the relation between the number of observed particles and the energy E. Neglect of the last factor means essentially that the calculations of Castagnoli et al. refer to an artificial case where the dispersion of the distribution of the total number of particles as a function of the energy E is infinite. Furthermore, computations carried out by us show that using the actual dependence can shift the most probable value of E by an order of magnitude from the value obtained when this relation is not taken into account.

In the present paper an attempt is made to treat the problem of the possible errors of the method of determining the energy E from the angular distribution of the secondaries.

The analysis will be based on the hydrodynam-

*The possible importance of the spectrum was first pointed out by N. L. Grigorov.

ical theory of multiple production, extended to the case of the collision of a nucleon with heavy nuclei by using the "tube" model.

2. Let us first start with the case where we know that nucleon-nucleon collisions occur.*

We consider the two stochastic variables,

$$-\eta = \frac{1}{N}\sum_{i=1}^{N} \ln \tan \vartheta_i$$

and the total number of charged particles, N.

According to Landau's theory, the expectation value of N is

$$MN = {}^4/_3 (E/2)^{1/4} = N_0.$$

The (conditional) probability density of the quantity η under the condition that the energy is E and the number of observed particles is n† is given by the relation (cf. reference 6)

$$p\left(\eta/E,n\right) = \left(\frac{2\pi\sigma^2(E)}{n}\right)^{-1/2} \exp\left\{-\left(\eta - \frac{1}{2}\ln\frac{E}{2}\right)\frac{n}{2\sigma^2(E)}\right\}, \quad (3)$$

where

$$\sigma^2(E) = {}^1/_2 \ln(E/2).$$

Omitting unimportant normalization factors from now on, we can write the probability p(N|E) for fixed E in the form

$$p\left(\frac{N}{E}\right) \sim N_0^{-1/2} \exp\left\{-\frac{(N-N_0)^2}{\alpha N_0}\right\}, \quad (4)$$

where α is a constant which we set equal to unity‡ (cf. Appendix). In order to find the desired probability density p(E|η, N) for the energy of the primary to be in the interval E to E + dE under the condition that definite values of η and N were observed, we must use Bayes' formula

$$p(E|\eta, N) \sim p(E)\, p(\eta, N|E) = p(E)\, p(\eta|N, E)\, p(N|E), \quad (5)$$

where p(E) is the spectrum of incident particles, which was set equal to $E^{-2.7}$ in the numerical calculations.**

Figures 1 and 2 show examples of the variation of p(E|η, N) for nucleon-nucleon collisions, for different values of N and of E_{eff}, which is defined from the relation $\eta = {}^1/_2 \ln(E_{eff}/2)$.

*Such a case was realized experimentally by using an emulsion stack sandwiched with light material (brass).[7]

†As a special case, we may have n = N.

‡The final result depends very strongly on the numerical value of α. Within the framework of the Landau theory, we know only that its order of magnitude is unity.

**The shape of the spectrum in the high-energy region is not known; however, as auxiliary computations showed, a small change of the exponent (say to 2.5) practically does not change the final result.

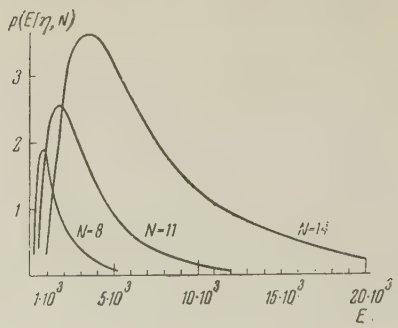

FIG. 1. η = 4.3; $E_{eff} = 10^4$.

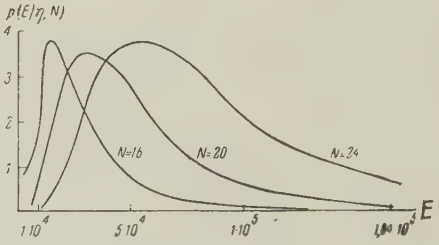

FIG. 2. η = 5.4; $E_{eff} = 10^5$.

3. Let us consider next the collision of a nucleon with a heavy nucleus. In using the tube model we must also take account of the distribution of paths in the nuclear matter and the change (compared to the case of nucleon-nucleon collision) which this distribution produces in the dependence of the mean number of particles N and the angular distribution on the value of E.

Expressing the tube length l in terms of number of nucleons, we have approximately[3,4]:

$$\bar{N} = N_0 l^{3/4}; \quad \sigma^2(E) = \frac{1}{2}\ln\left[E/2\left(\frac{l+1}{2}\right)^3\right].$$

Remembering that the probability p(l) of collision with a tube of length l has the form p(l) ~ l, $1 \le l \le l_{max}$, and again using Bayes' formula, we get:

$$p\left(E|\eta,\ N,\ l\right) = \frac{p(\eta,\ N,\ l|E)\,p(E)}{\int_0^\infty p(\eta,\ N,\ l|E)\,p(E)\,dE} \quad (6)$$

$$= \frac{p(\eta|N,\ l,\ E),\ p(N|l,E)\,p(E)}{\int_0^\infty p(\eta|N,\ l,\ E)\,p(N|l,\ E)\,p(E)\,dE}$$

where

$$p(\eta|N,\ l,\ E) = \left(2\pi\frac{\sigma^2(E)}{N}\right)^{-1/2} \exp\left\{-\left(\eta - \ln\sqrt{\frac{E}{2l}}\right)^2 \frac{N}{2\sigma^2(E)}\right\},$$

$$p(N|l,\ E) = (2\pi\bar{N})^{-1/2} \exp\{-(N-\bar{N})^2/2\bar{N}\}.$$

Since

$$p(E,\ l|\eta,\ N) = \frac{p(\eta|N,\ l,\ E)\,p(N|l,\ E)\,p(E)\,p(l)}{\int_0^\infty p(\eta|N,\ l,\ E)\,p(N|l,\ E)\,p(E)\,dE}, \quad (7)$$

we have finally:

$$p(E|\eta, N) = \int_0^{l_{max}} p(E, l|\eta, N)\, dl \qquad (8)$$

$$\sim \int_0^{l_{max}} \frac{p(\eta|N, l, E)\, p(N|l, E)\, p(E)\, l}{\int_0^{\infty} p(\eta|N, l, E)\, p(N|l, E)\, p(E)\, dE}\, dl.$$

Figure 3 shows the function $p(E|\eta, N)$ for $N = 14$; $\eta = 4.3$; $l_{max} = 5$ (the energy E_{eff} determined from the angular distribution is equal to 10^4).

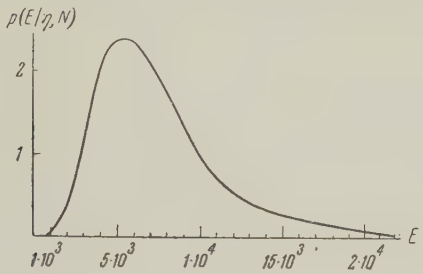

FIG. 3

4. On the basis of the computations and the graphs presented here we can draw the following conclusions.

1. In determining E it is necessary, in addition to its relation to the angular distribution (through the quantity η), to take account of its dependence on the total number N of observed tracks.

2. For given values of η and N, the distribution of possible values of E is characterized by considerable dispersion. The size of the dispersion as well as the location of the maximum of the distribution depend essentially on the relation between η and N.

3. The probability distribution is also affected by the parameters of the collision model (for example, by the value of the dispersion α).

In conclusion the authors express their indebtedness to G. B. Zhdanov for a fruitful discussion of the questions treated in this paper, and to Z. S. Maksimova and R. M. Povarova for carrying out the numberical computations.

APPENDIX

If the probability distribution $p(N_t)$ of the total number of particles is known, the probability that N of the particles are charged is given by

$$p(N) = \sum_{N_t=N}^{\infty} p(N|N_t)\, p(N_t),$$

where

$$p(N/N_t) = \frac{N_t!}{N!(N_t - N)!}\, q^N (1-q)^{N_t - N},$$

and q is the probability of production of a charged particle, which we may set equal to $2/3$. As usual, for sufficiently large N and N_t, these distributions can be represented by a Gaussian.

If the total number of particles is distributed according to the law

$$p(N_t|E) = (2\pi\sigma^2(E))^{-1/2} \exp\left\{-\frac{(N_t - \overline{N}_t)^2}{2\sigma^2(E)}\right\},$$

where $\sigma^2(E) = DN_t$ is the dispersion of N_t, and $DN_t = \alpha' N_t = \alpha' \overline{N}_t$ ($\alpha' = \text{const}$), the dispersion $D(N)$ of the quantity N is given by the relation

$$D(N) = \overline{N}\,[1 + (\alpha' - 1)\, q] = \alpha N.$$

According to reference 8, $\alpha' \sim 1$; then $\alpha \sim 1$. Unfortunately at present, within the framework of the hypotheses which are the basis of Landau's theory, one can only determine the order of magnitude of the lower limit on the value of α. Quantum fluctuations and peripheral collisions, which were not included in Ref. 8, should apparently increase the value of α.

[1] Debenedetti, Garelli, Tallone, and Vignone, Nuovo cimento **4**, 1151 (1956).

[2] L. D. Landau, Izv. Akad. Nauk SSSR, Ser. Fiz. **17**, 51 (1953).

[3] I. L. Rozental' and D. S. Chernavskii, Usp. Fiz. Nauk **52**, 185 (1954).

[4] S. Z. Belen'kii and G. A. Milekhin, J. Exptl. Theoret. Phys. (U.S.S.R.) **29**, 20 (1955), Soviet Phys. JETP **2**, 14 (1956).

[5] Amai, Fukuda, Iso, and Sato, Progr. Theor. Phys. **17**, 241 (1957).

[6] Castagnoli, Cortini, Franzinetti, Manfredini, and Moreno, Nuovo cimento **10**, 1539 (1953).

[7] Kaplon, Ritson, and Walker, Phys. Rev. **90**, 716 (1953).

[8] Podgoretskii, Rozental' and Chernavskii, J. Exptl. Theoret. Phys. (U.S.S.R.) **29**, 296 (1955), Soviet Phys. JETP **2**, 211 (1956).

Translated by M. Hamermesh
23

ON THE THEORY OF THE WEAK INTERACTIONS. I

Iu. A. GOL' FAND

N. P. Lebedev Physics Institute, Academy of Sciences, U.S.S.R.

Submitted to JETP editor February 8, 1958

J. Exptl. Theoret. Phys. (U.S.S.R.) 35, 170-177 (July, 1958)

A scheme for a universal four-fermion interaction is constructed which differs from the usual schemes in the way the quantized fields are introduced into the theory. The electron and positron β-decays are described by different variants of the Fermi interaction. The CPT theorem does not hold, but the theory is invariant with respect to the transformations CP, CT, and PT. Various experimental and theoretical consequences are discussed.

1. INTRODUCTION

THE hypothesis of the universal character of the four-fermion interaction seems extremely plausible in the light of the latest studies in the field of weak-interaction physics.[1] The existing experimental data on β-decay are not, however, in agreement with any of the variants of the Fermi interaction, and the possibility cannot be excluded that this situation will not change as the experimental results become even more precise. It is therefore of interest to try to construct a universal theory of the weak interactions that differs from the usual theoretical schemes.

In the construction of the theory of elementary particles quantum electrodynamics is taken as a model. Moreover, the methods and concepts of quantum electrodynamics are to a considerable extent carried over into the other theories. In particular, the quantization of the fermion fields is carried out like the quantization of the electron-positron field, and this imposes certain limitations on the structure of the theory. In the present paper the quantized fields are introduced into the theory in a different way, and owing to this the nature of the theory is qualitatively changed. For example, in the theory of β-decay the electron and positron decays are described by different variants of the four-fermion interaction.

The construction of a theory of the weak interactions with the degree of completeness inherent in contemporary field theories is not the purpose of the present paper. On the contrary, in this paper we consider only the most primitive aspects of the theory. The theoretical scheme is based on certain assumptions that give a unique way of constructing the Hamiltonian of the weak interactions, which enables us (at any rate in the framework of the perturbation theory) to obtain from the theory consequences that can be subjected to comparison with experiment. Relatively little attention is given in this paper to general theoretical questions. Thus the theory has the character of a working hypothesis that makes it possible to check by experiment the correctness or incorrectness of certain theoretical ideas and to obtain a general orientation in the group of phenomena that are due to the weak interactions.

2. THE HAMILTONIAN OF THE WEAK INTERACTIONS

The proposed scheme is a certain form of universal theory of contact four-fermion interaction. We assume that all fermions have the spin $\frac{1}{2}$. The requirement of relativistic invariance determines essentially uniquely (i.e., apart from the charge and isotopic variables) the possible states of a free particle. When, however, we come to associate with the particles quantized fields, in terms of which the interaction Hamiltonian is expressed, there is a lack of uniqueness, to remove which it is necessary to formulate a number of additional rules.

Since at the present time no general principle is known from which the nonconservation of parity in weak interactions would follow, we are forced to introduce the requirement of nonconservation of parity into the theory as an additional postulate. The simplest way to do this is to assume that in the theory of the weak interactions all particles are described by two-component fields. To give an exact meaning to this concept, let us first consider a four-component spinor ψ independent of x. With respect to Lorentz transformations (without reflections) ψ separates into two two-

component quantities. If we choose a representation of the Dirac matrices in which the matrix γ_5 is diagonal, this separation has the form

$$\psi = \begin{pmatrix} \varphi \\ \dot{\varphi} \end{pmatrix}. \tag{2.1}$$

The quantities φ and $\dot{\varphi}$ transform according to nonequivalent representations of the Lorentz group. More precisely, the quantity $\dot{\varphi}$ transforms in the same way as the quantity $\epsilon\varphi^*$, where the asterisk means that the complex-conjugate quantity is taken and use in made of the matrix

$$\varepsilon = \begin{pmatrix} 0 & 1 \\ -1 & 0 \end{pmatrix}.$$

In the case of a field depending on x one can further decompose quantities $\psi(x)$ into parts corresponding to the creation and annihilation of particles.

The two-component fields of creation and of annihilation of particles already admit of no further decomposition. These fields will be used for the construction of the interaction Hamiltonian. We write down the explicit forms of the fields for the creation of particles:

$$\begin{aligned} \varphi_c(x) &= \sum \sqrt{(1-\sigma v)/2}\, \varepsilon a^+(p)\, e^{ipx}, \\ \dot{\varphi}_c(x) &= \sum \sqrt{(1+\sigma v)/2}\, \varepsilon a^+(p)\, e^{ipx}, \end{aligned} \tag{2.2}$$

and of those for the annihilation of particles:

$$\begin{aligned} \varphi_a(x) &= \sum \sqrt{(1-\sigma v)/2}\, a(p)\, e^{-ipx}, \\ \dot{\varphi}_a(x) &= \sum \sqrt{(1+\sigma v)/2}\, a(p)\, e^{-ipx}, \end{aligned} \tag{2.3}$$

where σ denotes the Pauli matrices, $\mathbf{v} = \mathbf{p}/E$ is the velocity vector of the particle (we use everywhere a system of units in which $\hbar = c = 1$), and $a^+(\mathbf{p})$ and $a(\mathbf{p})$ are creation and annihilation operators. The connection between the fields (2.2) and (2.3) and the ordinary spinor fields is established in the Appendix.

From the quantities $\varphi(x)$ and $\dot{\varphi}(x)$ we can construct two types of scalars:

$$\varphi_1 \varepsilon \varphi_2, \quad \dot{\varphi}_1 \varepsilon \dot{\varphi}_2. \tag{2.4}$$

We adopt the hypothesis of a scalar interaction, which states that each possible weak-interaction process corresponds to the presence in the Hamiltonian of a single term which is the product of two scalars of the type (2.4). We note that although our assumption imposes serious limitations on the form of the interaction it contains in principle nothing new in comparison with the usual form of the theory, since in any variant of the four-fermion theory the Hamiltonian can be transformed into a sum of terms of the type indicated. The limitation lies in the fact that one here chooses a single term from each such sum.

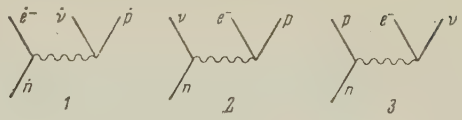

FIG. 1

It is convenient to use a graphical description of the processes. Figure 1 shows three possible diagrams for the process $n \rightarrow p + e^- + \nu$. We agree to associate with the solid lines scalars of the type (2.4). The wavy line does not correspond to any intermediate field; it is introduced just to separate the solid lines. The three diagrams of Fig. 1 correspond to three different variants of the theory of β-decay.

To get a unique variant of the theory, we introduce the rule of change of charge, according to which the electric charge must change by unity along each solid line, and the nuclear charge must suffer the maximum possible change.

From the three possible diagrams of Fig. 1 the rule of change of charge selects diagram 1. It is easy to see that an analogous situation exists for the other processes.

For complete uniqueness of the choice of the interaction variant it is still necessary to specify the types of fields corresponding to a given process. This is done by the rule of polarization of the lines, according to which fields of definite types always correspond to the charged particles, namely

to e^-, μ^+, p correspond fields $\dot{\varphi}_c(x)$ and $\dot{\varphi}_a(x)$,

to e^+, μ^-, $\tilde{p}$ correspond fields $\varphi_c(x)$ and $\varphi_a(x)$.

There is no need to specify the types of fields for the neutral particles, since according to the rule of change of charge only one charged particle corresponds to each line. Thus by the forms (2.4) the types of field for the neutral particles in a given process are uniquely determined. We note that the type of field for a neutral particle can change, depending on the process in which it occurs. In Fig. 1, diagram 1, dots are placed over the symbols for the particles, since according to the rule of polarization of lines in this case fields of the type $\varphi(x)$ correspond to all of the particles.

The rules formulated above uniquely determine the form of the interaction Hamiltonian, since the character of a process determines the required choice of the creation and annihilation fields, the rule of change of charge determines the distribution of these fields in scalar expressions of the types (2.4), and the rule of polarization of the

lines determines which of the scalars (2.4) is to be used in each case.

The last assumption is that the interaction constant g is the same in absolute value for all processes.

3. SOME GENERAL PROPERTIES OF THE THEORY

The essential difference between the proposed scheme and all theories based on the usual way of quantizing fields is due to the rule of polarization of lines (Sec. 2). For example, in the theory of Feynman and Gell-Mann,[1] which is also based on two-component fields, to the creation of an electron there corresponds the field $\dot{\varphi}_c(x)$, and to the annihilation of an electron the field $\varphi_a(x)$. In our theory fields of the type $\dot{\varphi}(x)$ correspond to both the creation and the annihilation of an electron. As a result of this kind of construction the part of the Hamiltonian that corresponds to the weak interactions is non-Hermitian. As an illustration of this fact let us consider two mutually inverse processes, for example

$$p \to n + e^+ + \nu, \tag{3.1}$$

$$n + e^+ + \nu \to p. \tag{3.2}$$

Corresponding to the process (3.1) the Hamiltonian contans the term

$$g(\varphi_{cn}\varepsilon\varphi_{ce^+})(\dot{\varphi}_{c\nu}\varepsilon\dot{\varphi}_{ap}), \tag{3.3}$$

and for the process (3.2) the term

$$g(\varphi_{ae^+}\varepsilon\varphi_{an})(\dot{\varphi}_{cp}\varepsilon\dot{\varphi}_{a\nu}). \tag{3.4}$$

Using the obvious relations

$$\varepsilon\varphi_a^+(x) = \dot{\varphi}_c(x), \qquad \varepsilon\dot{\varphi}_a^+(x) = \varphi_c(x)$$

we find that the expression Hermitian adjoint to (3.3) is

$$-g(\dot{\varphi}_{ae^+}\varepsilon\dot{\varphi}_{an})(\varphi_{cp}\varepsilon\varphi_{a\nu}), \tag{3.5}$$

which is not the same as (3.4).

Generally speaking the non-Hermitian character of the Hamiltonian could lead to the appearance of imaginary additions to the masses of particles. We shall show that in the present case such imaginary terms cannot arise. For this purpose we examine the symmetry properties of our scheme with respect to reflections. Obviously the theory is not invariant with respect to the space inversion P and the charge conjugation C, since these transformations are not allowed by the rule of polarization of lines. We shall show that the theory is invariant with respect to the combined inversion CP.

Let $\varphi(x)$ be any one of the two-component fields for a certain particle; we denote the corresponding field for the antiparticle by $\varphi'(x)$. Under the action of CP the fields transform in the following way:

$$\begin{aligned} &\varphi_a(x) \to \dot{\varphi}'_a(x), \ \varphi_c(x) \to -\dot{\varphi}'_c(x), \\ &\dot{\varphi}_a(x) \to \varphi'_a(x), \ \dot{\varphi}_c(x) \to -\varphi'_c(x). \end{aligned} \tag{3.6}$$

The rule of polarization of lines is invariant with respect to the transformations (3.6), and consequently the theory is invariant with respect to the CP transformation. Besides the combined inversion, the theory is also invariant with respect to the transformation PT — the simultaneous reversal of all four space-time axes. The proof is analogous to that above, since the transformation of the fields under the action of PT has the form:

$$\varphi_a(x) \leftrightarrow \varphi_c(-x), \ \dot{\varphi}_a(x) \leftrightarrow \dot{\varphi}_c(-x).$$

Thus the theory is invariant with respect to inversions of the following types: CP, PT, and CT (since $CT = CP \cdot PT$). The theory is not invariant with respect to the transformation CPT. There is nothing surprising in the fact that this theory violates the CPT theorem of Pauli,[2] since the proof of this theorem is based on the ordinary type of quantization of fields, in which the CPT transformation has the form

$$\psi(x) \to i\gamma_5\psi(-x).$$

Using the invariance of the theory with respect to the transformation PT, we shall show that the masses of the particles must be real. We shall consider the weak-interaction Hamiltonian H_W as a perturbation. Suppose the state of an unperturbed stationary particle is characterized by the rest mass m_0. The state in question is degenerate as to the spin directions, but since the Hamiltonian H_W is invariant with respect to space rotations, the degeneracy as to the spin direction is not removed by the action of the perturbation. Thus the perturbed state is characterized by a single mass value $m = m_0 + \delta m$. We now apply the operation PT to the state in question. Since the total Hamiltonian is invariant with respect to this transformation, the original state goes over into some other state of the same particle, characterized by a mass m^* (the operation PT includes in itself complex conjugation). Since there exists only one value of the mass of the particle, $m^* = m$, i.e., the total mass is real.

If instead of the transformation PT we use the combined inversion CP, we can prove by similar considerations the precise equality of the masses of particle and antiparticle.

Because of the non-Hermitian character of the weak-interaction Hamiltonian H_W, in this theory there is no detailed balancing for reactions with the weakly interacting particles. On the basis of the PT invariance we can assert only the equality of the probabilities of direct and reversed processes (in the sense of PT) — the analogue of the reciprocity theorem. After averaging over the spins of the interacting particles, however, the probabilities of the direct and inverse processes do turn out to be equal.

Without question the introduction of the non-Hermitian Hamiltonian H_W into the theory is a serious infraction of the formal foundations of quantum mechanics. Therefore the term "Hamiltonian" must in this case be understood in a provisional sense. In this paper we regard H_W as a phenomenological quantity, by means of which one can extract results in the framework of the perturbation theory. Later on the author proposes to develop a certain quantum-mechanical scheme which permits the non-Hermitian Hamiltonian H_W to be introduced into the theory in a way free from contradictions.

4. COMPARISON OF THE THEORY WITH EXPERIMENT

We begin the consideration of the concrete results of this theory with β-decay. Figure 2 shows the diagrams: 1 — for electron β-decay, 2 — for positron β-decay, and 3 — for K-capture. The

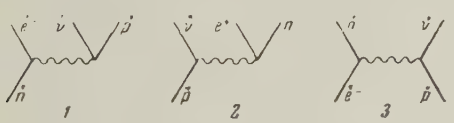

FIG. 2

forms of the corresponding terms in the Hamiltonian H_W are, for β^--decay

$$g\,(\dot{\varphi}_{cp}\varepsilon\dot{\varphi}_{cv})\,(\dot{\varphi}_{ce^-}\varepsilon\dot{\varphi}_{an}), \tag{4.1}$$

and for β^+-decay

$$g\,(\varphi_{cn}\varepsilon\varphi_{ce^+})\,(\dot{\varphi}_{cv}\varepsilon\dot{\varphi}_{ap}). \tag{4.2}$$

The expressions (4.1) and (4.2) differ from each other in the types of fields occurring in them. If we transform these expressions to the ordinary form of the β-decay theory, we find that the β^--decay involves the S, T, and P variants of the theory, whereas the β^+-decay involves the A and V variants.

Using the explicit forms of the fields (2.2) and (2.3) we can easily calculate the probabilities of the various processes. We confine ourselves to allowed β-transitions. The angular correlation between the electron and neutrino is given by the well known expression $1 + \lambda v \cos\theta$, but, unlike the case of the usual theory, the coefficient λ has opposite signs for the β^+ and β^- decays:

$$\lambda = \pm(\gamma^2 - 1/3)/(1+\gamma^2) \quad (\text{for } \beta^{\pm}\text{-decay}) \tag{4.3}$$

where $\gamma^2 = |M_F|^2/|M_{GT}|^2$ is the ratio of the squares of the nuclear matrix elements for Fermi and Gamov-Teller transitions. This result is in agreement with the experiments on the β^--decay of He^6 (reference 3) and the β^+-decay of A^{35} (reference 4). The values of λ for the decays of other nuclei are known with considerably less accuracy, but they also agree qualitatively with the theoretical values. The average longitudinal polarization of the electrons is $\pm v$ (for $\beta^{\pm}$-decay). This result is the direct consequence of the rule of polarization of lines, and is confirmed by a large number of measurements. The values of the asymmetry coefficient in the angular distribution of the electrons from the β-decay of oriented nuclei are also in qualitative agreement with the experimental data.[5-8]

An interesting experiment on the capture of a K electron by the Eu^{152} nucleus[9] shows that the neutrino emitted in the K-capture is polarized opposite to the direction of motion. This result is in agreement with the theory, since according to diagram 3 (Fig. 2), in the K-capture process the field $\dot{\varphi}_{c\nu}$ corresponds to the neutrino.

The decay of $\mu^{\pm}$ mesons goes according to the diagrams of Fig. 3. In both cases the two neutrinos emitted in the decay are differently polarized, which leads to the value $\rho = 3/4$ for the Michel parameter, which is in agreement with experiment.[10]

The decay of $\pi^{\pm}$ and $K^{\pm}$ mesons occurs by way of virtual pairs of heavy particles. The relative fraction of $\pi^{\pm} \to e^{\pm} + \nu$ decays cannot be calculated without an accurate treatment of the part played by the strong interactions. It is curious,

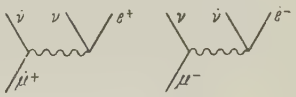

FIG. 3

however, that different variants of the weak-interaction theory are involved in the $\pi \to \mu$ and $\pi \to e$ decays. Figure 4 shows the corresponding lowest-order diagrams, from which it can be seen that the decay $\pi^{\pm} \to \mu^{\pm} + \nu$ goes through the pseudoscalar variant of the theory of the Fermi interactions, and the decay $\pi^{\pm} \to e^{\pm} + \nu$ through the pseudovector variant. When higher-order virtual processes are

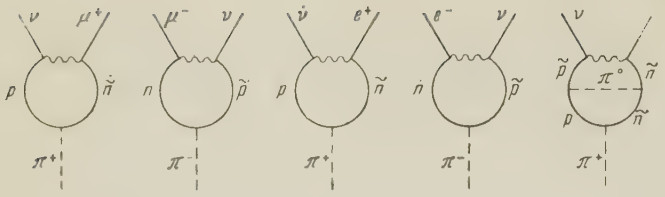

FIG. 4

taken into account, the decay $\pi^{\pm} \to e^{\pm} + \nu$ can go through the pseudoscalar variant (cf. diagram 3 of Fig. 4).

5. CONCLUDING REMARKS

The main feature that distinguishes the proposed theoretical scheme from the usual schemes is the rule of polarization of lines (Sec. 2). Therefore a direct experimental check of this rule is desirable. An exact measurement of the polarization of the electrons from β-decay would be very useful for this purpose, and also measurement of the polarization of the μ^+ mesons from the $K^+_{\mu 3}$-decay.

In formulating the rules for the construction of the Hamiltonian of the weak interactions (Sec. 2) the writer has tried to give the briefest possible expression of all the experimental data. Such a problem of course does not have a unique solution, and the choice of one procedure or another is to a considerable extent arbitrary. On the other hand, the rules must necessarily provide an extrapolation of the experimental data into a very broad uninvestigated domain. It is quite possible that the concrete rules presented in Sec. 2 will be contradicted by experiment and will have to be changed. It is to be specially emphasized that the literal content of these rules is not to be regarded as a final result.

The main idea of this entire construction, in the writer's opinion, is that the system of rules considered here leads to a theoretical scheme of a new type.

The writer expresses his sincere gratitude to B. L. Ioffe for exceptionally valuable discussions.

APPENDIX

We shall establish the connection between the two-component fields (2.2) and (2.3) and the four-component spinor field $\psi(x)$, which satisfies the Dirac equation. Let us consider the expansion of $\psi(x)$ in plane waves

$$\psi(x) = \sum (u(\mathbf{p})\, a(\mathbf{p})\, e^{-ipx} + v(\mathbf{p})\, b^+(\mathbf{p})\, e^{ipx}), \qquad (1)$$

where $u(\mathbf{p})$ and $v(\mathbf{p})$ are matrices of four rows and two columns which satisfy the relations

$$\hat{p}u(\mathbf{p}) = mu(\mathbf{p}), \quad \hat{p}v(\mathbf{p}) = -mv(\mathbf{p}). \qquad (2)$$

$$a(\mathbf{p}) \equiv \begin{pmatrix} a_1(\mathbf{p}) \\ a_2(\mathbf{p}) \end{pmatrix} \quad \text{and} \quad b^+(\mathbf{p}) \equiv \begin{pmatrix} b_1^+(\mathbf{p}) \\ b_2^+(\mathbf{p}) \end{pmatrix}$$

are the operators for annihilation of a particle and for creation of an antiparticle.

Let us determine the explicit form of $u(\mathbf{p})$ and and $v(\mathbf{p})$ in a representation of the matrices γ_μ in which γ_5 is diagonal. In this representation the matrices are written down in the following "separated" form:

$$\gamma_\mu = \begin{pmatrix} 0 & \sigma_\mu \\ \sigma^\mu & 0 \end{pmatrix}, \quad \gamma_5 = \begin{pmatrix} 1 & 0 \\ 0 & -1 \end{pmatrix},$$

where $\sigma_\mu = (1, \boldsymbol{\sigma})$, $\sigma^\mu = (1, -\boldsymbol{\sigma})$ are two-row matrices. From this it is easy to find the form of the operator $\hat{p}$:

$$\hat{p} = \begin{pmatrix} 0 & E - \sigma\mathbf{p} \\ E + \sigma\mathbf{p} & 0 \end{pmatrix} = m \begin{pmatrix} 0 & \left(\frac{1 - \sigma\mathbf{v}}{1 + \sigma\mathbf{v}}\right)^{1/2} \\ \left(\frac{1 + \sigma\mathbf{v}}{1 - \sigma\mathbf{v}}\right)^{1/2} & 0 \end{pmatrix}. \qquad (3)$$

Using Eq. (3), we find the solution of the first of the equations (2) in the "separated" form:

$$u(\mathbf{p}) = \begin{pmatrix} \sqrt{(1 - \sigma\mathbf{v})/2} \\ \sqrt{(1 + \sigma\mathbf{v})/2} \end{pmatrix}. \qquad (4)$$

The factor $2^{-1/2}$ is introduced for normalization: $u^+(\mathbf{p})\, u(\mathbf{p}) = 1$. For $v(\mathbf{p})$ we take the quantity which is charge-conjugate to (4):

$$v(\mathbf{p}) = cu^*(\mathbf{p}) = \begin{pmatrix} 0 & \varepsilon \\ -\varepsilon & 0 \end{pmatrix} \begin{pmatrix} \sqrt{(1 - \sigma\mathbf{v})/2} \\ \sqrt{(1 + \sigma\mathbf{v})/2} \end{pmatrix}^* \qquad (5)$$

$$= \begin{pmatrix} \sqrt{(1 - \sigma\mathbf{v})/2}\, \varepsilon \\ -\sqrt{(1 + \sigma\mathbf{v})/2}\, \varepsilon \end{pmatrix}.$$

Substituting Eqs. (4) and (5) into Eq. (1) and comparing with Eqs. (2.2) and (2.3), we find the expression for $\psi(x)$ in terms of the two-component fields:

$$\psi(x) = \begin{pmatrix} \varphi_a(x) + \varphi'_c(x) \\ \dot{\varphi}_a(x) - \dot{\varphi}'_c(x) \end{pmatrix}, \qquad (6)$$

where the prime means that the field φ refers to the antiparticle.

Using the relation (6) and knowing the law of transformation of $\psi(x)$, one can easily find the transformation properties of the two-component fields considered in Sec. 3.

[1] R. P. Feynman and M. Gell-Mann, Phys. Rev. 109, 193 (1958).

[2] W. Pauli, in Niels Bohr and the Development of Physics, London 1955.

[3] B. M. Rustad and S. L. Ruby, Phys. Rev. 97, 991 (1955).

[4] Hermannsfeldt, Maxson, Stähelin, and Allen Phys. Rev. **107**, 641 (1957).
[5] Wu, Ambler, Hayward, Hoppes, and Hudson, Phys. Rev. **105**, 1413 (1957).
[6] Ambler, Hayward, Hoppes, Hudson, and Wu, Phys. Rev. **106**, 1361 (1957).
[7] Ambler, Hayward, Hoppes, and Hudson, Phys. Rev. **108**, 503 (1957).
[8] Burgy, Epstein, Krohn, Novey, Raboy, Ringo, and Telegdi, Phys. Rev. **107**, 1731 (1957).
[9] Goldhaber, Grodzins, and Sunyar, Phys. Rev. **109**, 1015 (1958).
[10] L. Rosenson, Phys. Rev. **109**, 958 (1958).

Translated by W. H. Furry
24

SOVIET PHYSICS JETP VOLUME 35 (8), NUMBER 1 JANUARY, 1959

POLARIZATION CORRELATION OF BETA PARTICLES AND GAMMA QUANTA IN ALLOWED DECAY OF ORIENTED NUCLEI

A. Z. DOLGINOV

Leningrad Physico-Technical Institute, Academy of Sciences, U.S.S.R.

Submitted to JETP editor February 10, 1958

J. Exptl. Theoret. Phys. (U.S.S.R.) **35**, 178-183 (July, 1958)

Formulas are obtained for the correlation between the polarization of particles and the circular polarization of the subsequent gamma quanta in allowed beta decay of oriented nuclei.

THE extensive study of angular and polarization correlation in beta transformations, undertaken recently, have made it possible to gather much important information on beta interactions. It was established that the assumed A-V interaction in parity nonconservation is apparently not in contradiction with existing experiments. However, there are clearly not enough data for an unambiguous statement. This is why the determination of the type of beta interaction remains the most important problem in the theory of beta decay. It is also desirable to know the values and the relative signs of the β-interaction constants. To explain these problems, it is desirable to study all aspects of the beta transformations and, in particular, to investigate the polarization correlation between the β-particles and subsequent gamma quanta in beta decay of oriented nuclei. The advantages of such experiments is that they can yield complete information on the β-interaction constants. The pseudoscalar interaction does not make a noticeable contribution in allowed beta transitions. This leaves therefore eight (generally speaking complex) constants c_S, c_T, c_V, c_A and c'_S, c'_T, c'_V, and c'_A for the scalar, tensor, vector and axial-vector beta interactions, which must be determined experimentally. The quantities c'_i, unlike c_i, enter into those interaction terms that vanish when parity is conserved (these terms contain an additional matrix $\gamma_5 = \gamma_1\gamma_2\gamma_3\gamma_4$, where $\gamma_4 = -\beta$). A study of the correlation considered here, in accordance with (1), makes it possible to determine the real and imaginary parts of eight independent combinations of c_i and c'_i. The information obtained in this manner will actually be complete. Let us remark however that the quantity $\mathrm{Im}\,(c_S c'^{*}_V + c'_S c^{*}_V)$ enters only with a small multiplier $\alpha Z/E$, where $\alpha = 1/137$, Z is the charge of the nucleus, and E the total energy of the beta electron (we use units in which $\hbar = m = c = 1$). Therefore, if the experimental accuracy is insufficient to discern quantities of order $\alpha Z/E$ from quantities of order $p/E \equiv v/c$, we obtain not 16 but only 15 independent relations for the 16 real quantities. In practice however, this causes no complications, for it is enough to take into account the results of any of the already-performed independent experiments to obtain more relations than necessary.

Since the procedural aspect of the calculation of the sought correlation has been treated in an earlier work by this author,[1] we merely cite the end results.

We introduce the following notation: j_0, j_1, and j_2 are the angular moments of the nucleus for the β-γ transition $j_0(\beta)j_1(\gamma)j_2$; μ_0, μ_1, and μ_2 are their projection on the z axis. $\mathbf{k}(k, \theta, \Phi)$ is the momentum of the gamma quantum, I is its multiplicity, $\sigma = 1$ or -1 determines the right-handed or left-handed circular polarization of the quantum; $\mathbf{p}(p, \vartheta, \varphi)$ is the electron momentum and $\boldsymbol{\zeta}(1, \chi, \omega)$ is the pseudovector of its polarization in the rest system. The angles θ, Φ and ϑ, φ are given in a coordinate system in which the z axis is along the direction of the predominant orientation of the nuclear spins, while the angles χ and ω are in a coordinate system with the z axis along the direction of $\mathbf{p}$ (see diagram).

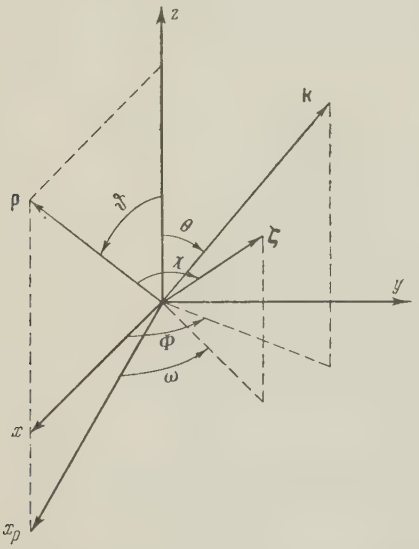

The expression for the correlation beween j_0, $\mathbf{p}$, $\mathbf{k}$, and $\boldsymbol{\zeta}$ for $\sigma = \pm 1$ can be represented in the following form*

$$W(j_0, \mathbf{p}, \boldsymbol{\zeta}, \mathbf{k}, \sigma) = \sum (-1)^g \sqrt{2S+1}\, h_g(j_0) B_{S\sigma} \times Z^{ba}_{Jg S} F^{ba}_{Jg S}(\mathbf{p}, \boldsymbol{\zeta}, \mathbf{k}); \quad (1)$$

$$h_g(j_0) = \sum_{\mu_0} (-1)^{j_0-\mu_0} C^{g0}_{j_0\mu_0 j_0-\mu_0} w(\mu_0); \quad (2)$$

$$B_{S\sigma} = U(j_2 I j_1 S;\ j_1 I)\, C^{I\sigma}_{I\sigma S0}; \quad (3)$$

$$F^{ba}_{Jg S}(\mathbf{p}, \boldsymbol{\zeta}, \mathbf{k}) = 4\pi i^{\lambda} (-1)^{J-a} \sqrt{2a+1} \sum_{\sigma,\beta} C^{J\sigma}_{g0S\sigma} \times Y_{S\sigma}(\vartheta\Phi)\, D^{J*}_{\sigma\beta}(\varphi\vartheta 0)\, C^{J\beta}_{a0b\beta} Y^{*}_{b\beta}(\chi\omega). \quad (4)$$

The summation in (1) is over all possible values of the indices a, d, J, g, and S within the following limits: $b + J \geq a \geq |b - J|$; $0 \leq S \leq 2I$; $J + S \geq g \geq |J - S|$; $b = 0, 1$; $J = 0, 1$; $2\lambda = 1 - (-1)^{a+b+S+g}$.

The quantities $C^{c\gamma}_{a\alpha b\beta}$ are the known Clebsch-Gordan coefficients. $w(\mu_0)$ is the probability of a given value of the projection μ_0 of an oriented nucleus. $h_g(j_0)$ determines the degree of orientation of the initial nuclei; the values for $f_g(j_0) = h_g(j_0)/j_0^g$ for various particular cases are given in reference 2. For aligned nuclei, g can be only even. The quantity

$$U(j_2 I j_1 S;\ j_1 I) = \sqrt{(2j_1+1)(2I+1)}\, W(j_2 I j_1 S;\ j_1 I), \quad (5)$$

where $W(j_2 I j_i S;\ j_1 I)$ is the Racah function. In the particular case when S = 0 or 1, we have

$$B_{00} = 1, \quad B_{1\sigma} = \sigma \frac{j_1(j_1+1) - j_2(j_2+1) + I(I+1)}{2I(I+1)\sqrt{j_1(j_1+1)}} \quad (6)$$

If the γ-quanta polarization is not investigated, it is necessary to take $B_S = B_{S_1} + B_{S_{-1}}$ instead of B_S. $B_S \neq 0$ only for even S

$$B_S = \left[1 - \frac{S(S+1)}{2I(I+1)}\right] U(j_2 I j_1 S;\ j_1 I)\, C^{I0}_{I0S0}. \quad (7)$$

If the observed β-γ cascade is of the form $j_0(\beta)j_1(\gamma_1)j_2(\gamma_2)\ldots j_{N-1}(\gamma)j_N$ and if the experiment is aimed at investigation of the gamma quanta of the $j_{N-1}(\gamma)j_N$ transition, then, denoting the multiplicities of the quanta by $I_1, I_2, \ldots I_{n-1}, I$ respectively, we obtain a formula for the correlation, provided we multiply the expression $B_{S\sigma}$ in (1) by the product

$$\prod_{k=2}^{N-1} U(j_k I_k S j_{k-1};\ j_{k-1} j_k). \quad (8)$$

The quantity $F^{ba}_{JgS}(\mathbf{p}, \boldsymbol{\xi}, \mathbf{k})$ depends only on the angles. Its explicit form is given in the Appendix for several specific cases.

We give here the values of the quantities Z^{ba}_{JgS} that enter into (1):

$$Z^{00}_{0gS} = [M_0 - \gamma E^{-1} N_0 + U(g j_1 j_0 1;\ j_1 j_0)(M_1 - \gamma E^{-1} N_1)]\, \delta_{Sg};$$

$$Z^{01}_{1gS} = (2/3)\, U(j_0 S j_0 1;\ j_0 g)\, E^{-1} [-(p \operatorname{Re} Q_m + \alpha Z \operatorname{Im} Q_n)\, \delta_{gS\pm 1} + (p \operatorname{Im} Q_m - \alpha Z \operatorname{Re} Q_n)\, \delta_{gS}] - \sqrt{2(2g+1)(2j_0+1)(2j_1+1)/3}\, X(j_1 j_0 1,\ j_1 j_0 1,\ Sg1) \times E^{-1}(p \operatorname{Re} Q_1 + \alpha Z \operatorname{Im} Q_1);$$

$$Z^{10}_{1gS} = (2/9)\, U(j_0 S j_0 1;\ j_0 g)\, [\operatorname{Re} D \delta_{Sg\pm 1} - \operatorname{Im} D \delta_{Sg}] + (1/3)\sqrt{2(2g+1)(2j_0+1)(2j_1+1)/3}\, X(j_1 j_0 1, j_1 j_0 1, Sg1)\, G;$$

$$Z^{11}_{0gS} = \sqrt{1/3}\, E^{-1} [p \operatorname{Re} Q_0 + \alpha Z \operatorname{Im} Q_0 + U(g j_1 j_0 1;\ j_1 j_0)(p \operatorname{Re} Q_1 + \alpha Z \operatorname{Im} Q_1)]\, \delta_{gS};$$

$$Z^{11}_{1gS} = (2/3)\sqrt{2/3}\, U(j_0 S j_0 1,\ j_0 g)\, E^{-1} [(p \operatorname{Re} Q_n + \alpha Z \operatorname{Im} Q_m)\, \delta_{gS} - (p \operatorname{Im} Q_n - \alpha Z \operatorname{Re} Q_m)\, \delta_{Sg\pm 1}] - 2\sqrt{(2g+1)(2j_0+1)(2j_1+1)}\, X(j_1 j_0 1,\ j_1 j_0 1,\ Sg1) E^{-1} \times (p \operatorname{Im} Q_1 - \alpha Z \operatorname{Re} Q_1)\, \delta_{Sg\pm 1};$$

$$Z^{12}_{1gS} = (2/3)(1 - \gamma E^{-1}) \{(\sqrt{2}/3)\, U(j_0 S j_0 1,\ j_0 g)\, [\operatorname{Im}(D_0 + D_1)\, \delta_{Sg} - \operatorname{Re}(D_0 + D_1)\, \delta_{Sg\pm 1}] - \sqrt{(2g+1)(2j_0+1)(2j_1+1)/3} \times X(j_1 j_0 1,\ j_1 j_0 1,\ Sg1)(M_1' + N_1)\};$$

$$\gamma = \sqrt{1 - (\alpha Z)^2}.$$

*The common factors that do not affect the correlation are omitted everywhere.

The quantities X(abc, def, ghi) are the Fano functions. Their explicit form, many of their properties, and particular values, are given in references 3 and 4. The number triplets abc, def, and ghi can be transposed cyclically without changing the function X. Non-cyclic transposition of the numbers changes the function by a factor $(-1)^{\nu}$, where $\nu = a+b+c+d+e+f+g+h+i$. X(abc, def, ghi) = X(adg, beh, cfi) and X(abc, def, gh0) = U(gdbc; ae) $\delta_{cf}\delta_{gh}/\sqrt{(2g+1)(2c+1)(2a+1)(2e+1)}$.

The quantities M_0, N_0, Q_m, etc., which enter into $Z^{ba}_{JgS'}$ have the following explicit form:

$$M_0 = (|c_S|^2 + |c'_S|^2)|K_S|^2 + (|c_V|^2 + |c'_V|^2)|K_V|^2;$$
$$M_1 = (|c_T|^2 + |c'_T|^2)|K_T|^2 + (|c_A|^2 + |c'_A|^2)|K_A|^2;$$
$$N_0 = 2\mathrm{Re}\,(c_S c^*_V + c'_S c'^*_V) K_S K^*_V;$$
$$N_1 = 2\mathrm{Re}\,(c_T c'^*_A + c'_T c'^*_A) K_T K^*_A;$$
$$\mathrm{Re}\,Q_0 = \mathrm{Re}\,(c_S c'^*_S |K_S|^2 - c_V c'^*_V |K_V|^2);$$
$$\mathrm{Im}\,Q_0 = \mathrm{Im}\,(c_V c'^*_S + c'_V c^*_S) K_V K^*_S;$$
$$\mathrm{Re}\,Q_1 = \mathrm{Re}\,(c_T c'^*_T |K_T|^2 - c_A c'^*_A |K_A|^2);$$
$$\mathrm{Im}\,Q_1 = \mathrm{Im}\,(c_A c'^*_T + c'_A c^*_T) K_A K^*_T;$$
$$Q_m = (c'_S c^*_T + c_S c'^*_T) K_S K^*_T - (c_V c'^*_A + c'_V c^*_A) K_V K^*_A;$$
$$Q_n = (c_V c'^*_T + c'_V c^*_T) K_V K^*_T - (c_S c'^*_A + c'_S c^*_A) K_S K^*_A;$$
$$D_0 = (c_S c^*_T + c'_S c'^*_T) K_S K^*_T + (c_V c^*_A + c'_A c'^*_A) K_V K^*_A;$$
$$D_1 = (c_V c^*_T + c'_V c'^*_T) K_V K^*_T + (c_S c^*_A + c'_S c'^*_A) K_S K^*_A;$$
$$D = (D_0 - \gamma E^{-1} D_1) - 2(D_1 - \gamma E^{-1} D_0);$$
$$G = (M_1 - \gamma E^{-1} N_1) - 2(N_1 - \gamma E^{-1} M_1).$$

The quantities K_S, K_V, K_T, and K_E are the nuclear matrix elements for the S, V, T, and A interactions

$$K_S = \int \psi_{j_1\mu_1} \beta \psi_{j_0\mu_0} d\mathbf{r} \equiv \int \beta; \qquad (9)$$

$$K_T = -[C^{j_0\mu_0}_{10 j_1\mu_1}]^{-1} \int \psi^*_{j_1\mu_1} \beta\sigma_z \psi_{j_0\mu_0} d\mathbf{r} \equiv -\int \beta\sigma; \qquad (10)$$

K_V and K_A differ from K_S and K_T in the absence of the matrix β under the integral sign. In the non-relativistic approximation for the nucleons we have

$$K_V \equiv \int 1 = -K_S, \qquad K_A \equiv \int \sigma = -K_T. \qquad (11)$$

Since the strong interactions are apparently invariant under time inversion, the phase shift between K_S, K_T, etc. is zero or π.

If the beta interaction is invariant under time inversion, the constants c and c′ should be real. In references 5 to 7 it was proposed to study the β-γ correlation in oriented nuclei to determine Im Q_m. The first experimental results[8] do not lead to definite conclusions. Assuming the AV or TS interaction to take place, proof of the absence of Im Q_m would be sufficient to establish the invariance of the beta interaction under time inversion. However, if some other combination of the β-interaction variants takes place, say TV or AVS etc, it becomes necessary to study the phenomena that are determined by Im Q_n, Im Q_1, etc. To clarify the problem of the invariance under time inversion, it is not essential to investigate the correlation (1) completely. It is enough to study the polarization of the electrons emitted by the polarized nuclei. The corresponding formulas are given in our earlier work.[1]

Let us note that it is not essential to have oriented nuclei in order to investigate this correlation. The same results are obtained by studying the correlation between the electron polarization and the circular polarization of the subsequent gamma quanta. For a given circular polarization σ, the probability of definite $\mathbf{p}$, $\boldsymbol{\zeta}$, and $\mathbf{k}$ is of the form

$$W(\mathbf{p}, \boldsymbol{\zeta}, \mathbf{k}, \sigma) = \sum_{L=0}^{1} [M_L - \gamma E^{-1} N_L] + E^{-1}[p\,\mathrm{Re}\,(Q_0 + Q_1) + \alpha Z\,\mathrm{Im}\,(Q_0 + Q_1)]\cos\chi - B_{1\sigma}\{[-2p\,\mathrm{Re}\,Q_m - 2\alpha Z\,\mathrm{Im}\,Q_n + \lambda_{j_1 j_0}(p\,\mathrm{Re}\,Q_1 + \alpha Z\,\mathrm{Im}\,Q_1)]E^{-1}\cos\theta + (1/3)[2\mathrm{Re}\,D + \lambda_{j_1 j_0} G][\cos\theta\cos\chi + \sin\theta\sin\chi\cos\omega] + [2p\,\mathrm{Im}\,Q_n - 2\alpha Z\,\mathrm{Re}\,Q_m - \lambda_{j_1 j_0}(p\,\mathrm{Im}\,Q_1 - \alpha Z\,\mathrm{Re}\,Q_1)]E^{-1} \times \sin\theta\sin\chi\sin\omega + (1/3)(1 - \gamma E^{-1})[2\mathrm{Re}\,(D_0 + D_1) - \lambda_{j_1 j_0}(M_1 + N_1)][2\cos\theta\cos\chi - \sin\theta\sin\chi\cos\omega]\}; \qquad (12)$$

$$\lambda_{j_1 j_0} = [j_1(j_1+1) - j_0(j_0+1) + 2][2\sqrt{j_1(j_1+1)}]^{-1}. \qquad (13)$$

Since the nuclei are not oriented in the given case, the angles θ and χ are measured from the direction of $\mathbf{p}$, which was taken to be the z axis. The plane (pk) is chosen the same as the (zx) plane and the angle ω is measured from the x axis in a right-handed system of coordinates.

If there exists a $t \to -t$ invariance then, according to (12), the probability of observing an electron polarized with or against the y axis ($\chi = \pi/2$, $\omega = t\pi/2$) is very small. In this case Im Q_n = Im Q_1 = 0, and the projection of the polarization vector (14) on the y axis is proportional to a small quantity, namely $2\alpha Z E^{-1} \times$ Re $(Q_m - \lambda_{j_1 j_0} Q_1)$. Observation of a noticeable electron polarization ($\sim p/A$ and not $\sim \alpha Z/E$) along this axis would be evidence of the existence of a contribution from the VT or AT interaction and of violation of the $t \to -t$ invariance.

Since the observation of the circular polarization of gamma quanta yields information on the orientation of the nuclear spin after the beta decay,

a study of the correlation (12) is equivalent to a study of the polarization of the electrons emitted by oriented nuclei. To proceed to this case and to obtain $W(j_0, \mathbf{p}, \boldsymbol{\xi})$, it is sufficient to replace $B_{1\sigma}$ in formula (12) by $-h_1(j_0) = -\sum_{\mu_0} \mu_0 w(\mu_0)/\sqrt{j_0(j_0+1)}$, to replace $\lambda_{j_1 j_0}$ by $\lambda_{j_0 j_1}$, and to replace θ by ϑ.

If we know the probability (1), then the polarization of the electrons emitted in the beta decay is determined by the vector $\bar{\xi}$, where $|\bar{\xi}| \leq 1$ gives the degree of polarization. Let $w(\chi, \omega)$ denote, in abbreviated form, the probability $W(j_0, \mathbf{p}, \boldsymbol{\xi}, \mathbf{k}, \sigma)$ as a function of the angles χ and ω. Then the expression for the projection of $\bar{\xi}$ on the coordinate axes (in a system with z parallel to $\mathbf{p}$) can be represented in the form

$$\bar{\zeta}_k = [w_k - w_{-k}]/[w_k + w_{-k}], \quad k \to x, y, z,$$
$$w_z = w(0, 0) \quad w_{-z} = w(\pi, 0) \quad w_x = w\left(\frac{\pi}{2}, 0\right), \qquad (14)$$
$$w_{-x} = w\left(\frac{\pi}{2}, \pi\right) \quad w_y = w\left(\frac{\pi}{2}, \frac{\pi}{2}\right) \quad w_{-y} = w\left(\frac{\pi}{2}, -\frac{\pi}{2}\right).$$

All the above formulas pertain to a β^- decay. For β^+ decay it is necessary to make the substitutions

$$c_S \to -c_S^*, \quad c_V \to c_V^*, \quad c_T \to c_T^*, \quad c_A \to -c_A^*.$$
$$c'_S \to c'^*_S, \quad c'_V \to -c'^*_V, \quad c'_T \to -c'^*_T, \quad c'_A \to c'^*_A. \qquad (15)$$

If the polarization of the beta particles is not being investigaged, it is necessary to put $b = 0$ in formula (1). Therefore only Z^{00}_{0gS} and Z^{01}_{1gS} will enter into $W(j_0, \mathbf{p}, \mathbf{k}, \sigma)$. When $S = g$, the quantity Z^{01}_{1gS} contains the term $(p/E)\,\mathrm{Im}\,Q_m$. This makes it possible, by investigating $W(j_0, \mathbf{p}, \mathbf{k})$ or $W(j_0, \mathbf{p}, \sigma)$ to obtain information on the $t \to -t$ invariance for the TS or AV interaction.

APPENDIX

The expression (4) contains the quantity $D^j_{\alpha\beta}(\varphi\vartheta 0)$. This equals

$$D^0_{\sigma\beta} = \delta_{\sigma 0}\delta_{\beta 0}, \quad D^1_{00} = \cos\vartheta,$$
$$2D^1_{11} = 2D^{1*}_{-1-1} = (1 + \cos\vartheta)\, e^{i\varphi},$$
$$2D^1_{1-1} = 2D^{1*}_{-11} = (1 - \cos\vartheta)\, e^{i\varphi};$$
$$\sqrt{2}D^1_{0-1} = -\sqrt{2}D^1_{01} = \sin\vartheta,$$
$$\sqrt{2}D^1_{10} = -\sqrt{2}D^1_{-10} = \sin\vartheta e^{i\varphi}.$$

References 1 and 5 give particular values of the quantity $F_{SgJ}(\vartheta\varphi\theta\Phi)$, which in our notation is $i^{-\lambda} F^{0J}_{JgS}(\mathbf{p}, \boldsymbol{\xi}, \mathbf{k})$. The following are a few particular values of $F^{ba}_{JgS}(\mathbf{p}, \boldsymbol{\xi}, \mathbf{k})$ for $b \neq 0$):

$$F^{11}_{000} = \sqrt{3}\cos\chi; \; F^{11}_{110} = \frac{3}{\sqrt{2}}\sin\vartheta\sin\chi\sin\omega;$$
$$F^{11}_{101} = 3\sqrt{3/2}\{\cos\theta\sin\vartheta\sin\chi\sin\omega$$
$$+ \sin\theta\sin\chi\cos\omega\sin(\Phi - \varphi)$$
$$- \cos\vartheta\sin\chi\sin\omega\sin\theta\cos(\Phi - \varphi)\};$$
$$F^{10}_{110} = -\sqrt{3}[\cos\vartheta\cos\chi - \sin\vartheta\sin\chi\cos\omega];$$
$$F^{12}_{101} = (3/\sqrt{2})\{\cos\theta[2\cos\vartheta\cos\chi + \sin\chi\sin\vartheta\cos\omega]$$
$$+[2\sin\vartheta\cos\chi - \sin\chi\cos\vartheta\cos\omega]\sin\theta\cos(\Phi - \varphi)$$
$$-\sin\chi\sin\omega\sin\theta\sin(\Phi - \varphi)\};$$
$$F^{12}_{110} = \sqrt{3/2}[2\cos\vartheta\cos\chi + \sin\vartheta\sin\chi\cos\omega].$$

[1] A. Z. Dolginov, Nucl. Phys. **5**, 512 (1958).
[2] I. A. M. Cox and H. A. Tolhoek, Physica **19**, 101 (1953).
[3] H. Matsunobo and H. Takebe, Progr. Theoret. Phys. **14**, 589 (1955).
[4] Kennedy, Sears, and Sharp, Chalk River Report CRT, 569, 1954.
[5] A. Z. Dolginov, J. Exptl. Theoret. Phys. (U.S.S.R.) **33**, 1363 (1957), Soviet Phys. JETP **6**, 1047 (1958).
[6] M. Morita and R. S. Morita, Phys. Rev. **107**, 1316 (1957).
[7] R. B. Curtis and R. R. Lewis, Phys. Rev. **107**, 1381 (1957).
[8] Ambler, Hayward, Hoppes, and Hudson, Phys. Rev. **108**, 503 (1957).

Translated by J. G. Adashko
25

ALPHA DECAY OF NONSPHERICAL NUCLEI

L. L. GOL' DIN, G. M. ADEL' SON-VELSKII, A. P. BIRZGAL, A. D. PILIIA,
and K. A. TER-MARTIROSIAN

Submitted to JETP editor February 17, 1958

J. Exptl. Theoret. Phys. (U.S.S.R.) **35**, 184-202 (July, 1958)

We consider the system of equations for the radial functions describing the motion of alpha particles emitted in the α decay of nonspherical nuclei of arbitrary spin. We obtain equations which determine the boundary conditions for the radial functions on the nuclear surface, and formulas expressing the α-decay probability in terms of the values of the radial functions at the nuclear surface and the shape of the nucleus. A simple approximate formula is found for the dependence of the α-decay probability on the angular momentum l carried off by the α particle and the energy of the level in the daughter nucleus.

Various methods for approximate solution of the system of equations for the radial functions are analyzed for even nuclei (spin 0). It is shown that the terms that give rise to a coupling of the equations (due to the nonspherical part of the Coulomb interaction between the α particle and the nucleus) cannot be treated as a perturbation for $l > 2$.

An exact numerical solution of the system of equations is given for an elliptical nucleus, taking into account all multipole interactions, under the condition of constancy of the wave function on the nuclear surface. An estimate is made of the influence of higher harmonics in the expansion of the equation of the nuclear surface in Legendre polynomials. The computational results are compared with experiment.

1. INTRODUCTION

THE study of the intensity of α transitions to rotational levels enables us to obtain important information concerning the properties of nonspherical nuclei. The theory of the excitation of rotational levels in α decay has been treated by Rasmussen and Segal,[1] Strutinskii,[2,3] Nosov,[4,5] and Fröman.[6] However, comparison of the results of the theoretical computations with experiment shows systematic disagreements: the results differ by a factor of 1 to 10 for the 4^+ levels of even-even nuclei, and by a factor of several hundred for the 6^+ levels of these nuclei. (So far it has not been possible to reduce the theoretical formulas for odd nuclei to a form suitable for practical computation, which would allow one to compare them with experiment.) The published theoretical papers contain a variety of simplifications: neglect of certain terms in the expression for the kinetic energy of the nuclear top,[1] neglect of 2^4-pole (in all the published papers) and sometimes even of the quadrupole[2] interaction between the nucleus and the α particle, etc. The effect of such omissions has not been properly appreciated, even though the results for large angular momenta l turn out to be extremely sensitive to such simplifications.

Rasmussen and Segal[1] give the results of numerical computations of intensity of α decay. These computations, however, not only contain various simplifications which are not completely justified but they are also done for certain special values of the eccentricity which were selected on the basis of extrapolation of experimental data for the rare earths. It is therefore not clear whether one could choose the eccentricity in such a way as to explain the intensity of the decay to all known levels.

The computations which are presented below had three purposes. The first of these was to bring the formulas describing the α decay of nonspherical nuclei of arbitrary spin to a form suitable for practical calculations. In addition, we wanted to explain the applicability of the usual methods of computation, in which the quadrupole moment of the electrical interaction of the α particle and the nucleus (as well as the higher multipole moments) are treated as a perturbation. Anticipating our results, we may say that for $l \geq 4$ (where l is the angular momentum carried off by the α particle) this treatment proved to be impossible. Finally, we wanted to find out whether the disagreement between experiment and computations which we mentioned above

is the result of the approximations and omissions of the particular papers themselves, or whether it is related to the approximate nature of the fundamental starting points of the whole theory: the assumption of the constancy of the α particle wave function on the boundary of the nucleus and the assumption of a simple shape for the nucleus (i.e., the assumption that in the expansion of the radius vector $R(\theta)$ to the nuclear surface in Legendre polynomials one can drop all terms except the first two or three.

2. GENERAL THEORY OF ALPHA DECAY

The fundamental equations describing the α decay of nonspherical nuclei of arbitrary spin have already been obtained in references 1 and 6. The formulas which we shall find for the boundary conditions at the nucleus make these equations suitable for practical computations. In our calculations we shall limit ourselves to the simplest case of "favored" α transitions, i.e., transitions in which the parity of the state and the projection of the angular momentum on the nuclear axis do not change during the α-decay process.

If the angular momentum I_0 of the decaying nucleus is different from zero, the probability of excitation in α decay of the rotational level of the daughter nucleus having angular momentum I ($I = I_0,\ I_0 + 1,\ I_0 + 2 \ldots$ etc.) is given by

$$W_I = \frac{\hbar k_I}{\mu} \sum_{l=|I-I_0|}^{I+I_0}{}' |a_{Il}|^2. \qquad (2.1)$$

The sum in (2.1) extends only over even values of l (we shall indicate such sums by a prime on the summation sign).

The quantities a_{Il} are the amplitudes at infinity of the radial functions $f_{Il}(r)$, describing α particles carrying off angular momentum l (and the residual daughter nucleus in a state with angular momentum I):

$$f_{Il}(r) \to a_{Il} \exp\{i(k_I r - \eta_I \ln 2k_I r)\}, \quad r \to \infty, \qquad (2.2)$$
$$k_I^2 = 2\mu E_I / \hbar^2, \quad \eta_I = 2Ze^2\mu / \hbar^2 k_I,$$

where E_I is the α-decay energy in the transition to the level I. We shall denote the corresponding quantities for the transition to the ground level with $I = I_0$ simply as k, η, E.

The system of equations[1,2] satisfied by the radial functions $f_{Il}(r)$ (cf. also Appendix) is

$$\frac{d^2 f_{Il}}{dr^2} + \left(k_I^2 - \frac{l(l+1)}{r^2} - \frac{2k_I\eta_I}{r}\right) f_{Il}(r) \qquad (2.3)$$
$$= \sum_{l'=0}^{\infty}{}' \sum_{l'=|l'-I_0|}^{l'+I_0} V_{Il;l'l'}(r)\, f_{l'l'}(r).$$

The quantities $V_{Il;I'l'}(r)$ are the matrix elements of the noncentral part of the coulomb interaction of the α particle and the nonspherical nucleus, which can be represented as

$$V_{Il;\,l'l'}(r) = \sum_{L=2}^{\infty}{}' Q_L(Il;\ I'l')\, V_L(r);$$
$$Q_L(Il;\ I'l') = (-1)^{I-I'} \sqrt{(2l'+1)(2I'+1)}$$
$$\times W(I'I_0Ll;\ l'I)\, C^{I0}_{L0;\,l'0}\, C^{II_0}_{l'I_0;\,L0}; \qquad (2.4)$$
$$V_L(r) = \frac{2\mu}{\hbar^2}\frac{2L+1}{2} \int_{-1}^{1} V(r, \theta) P_L(\cos\theta)\, d(\cos\theta),$$

where W is a Racah coefficient,[7] the quantities $C^{IM}_{I_1M_1;I_2M_2}$ are Clebsch-Gordan coefficients, and the $V_L(r)$ are the coefficients in the Legendre polynomial expansion of the coulomb energy $V(r, \theta)$ of the α particle in the field of the nonspherical nucleus (θ is the polar angle in the coordinate system fixed in the nucleus.

The system (2.3) should be solved under some boundary condition on the nuclear surface $r = R(\theta)$. At the nuclear surface the wave function $\Psi(r, \theta, \varphi)$, which describes the motion of the α particle formed in the decay, depends only on the angle θ:

$$\Psi(R(\theta), \theta, \varphi) \equiv \chi(\theta)$$

(where one usually assumes that $\chi(\theta) = \text{const.}$). It can be shown (cf. Appendix) that this condition gives the system of equations

$$\sum_{I,\,l} C^{II_0}_{I_0,\,I_0+\Omega;\,l,\,-\Omega} f_{Il}[R(\theta)]\, Y_{l\Omega}(\theta, \varphi) = R_0(\theta)\chi(\theta)\delta_{\Omega,0}, \qquad (2.5)$$

where Ω (the projection of the α particle angular momentum on the nuclear axis) takes on all possible values.

The boundary conditions (2.5) (for given $R(\theta)$ and $\chi(\theta)$) together with Eqs. (2.3) uniquely determine the functions $f_{Il}(r)$, and consequently via (2.2) give the amplitudes a_{Il}.

Making use of (2.5) we can obtain the approximate formula for the α-decay intensity which we have used previously.[8] Let us replace the functions f_{Il} by functions $\varphi_{Il}(r)$ which, for $r \to \infty$, go over into $\exp\{i(k_I r - \eta_I \ln 2k_I r)\}$, so that

$$\varphi_{Il}(r) = f_{Il}(r) / a_{Il}. \qquad (2.6)$$

We multiply both sides of (2.5) by

$$C^{II_0}_{I_0,\,I_0+\Omega;\,l,\,-\Omega} Y^*_{l\Omega}(\theta, \varphi) / \varphi_{Il}[R(\theta)],$$

sum over Ω and integrate over θ and φ. Using the orthogonality property of the Clebsch-Gordan coefficients and the orthogonality of the spherical harmonics, we get

$$a_{Il} + \sum_{I'l'}{}'' B(I, l;\ I'l')\, a_{I'l'} = A_{Il} C^{II_0}_{I_0 I_0;\ l_0} \qquad (2.7)$$

(the summation is extended over all values of I' and l' except the one pair for which $I = I'$ and $l = l'$). In (2.7) we have introduced the notation

$$A_{Il} = 2\pi \int_{-1}^{1} \frac{R(\theta)\chi(\theta)}{\varphi_{Il}[R(\theta)]} Y_{l_0}(\theta)\, d(\cos\theta), \qquad (2.8)$$

$$B(I, l;\ I', l') = \sum_{\Omega} C^{II_0}_{I_0, I_0+\Omega;\ l, -\Omega} C^{I'I_0}_{I_0, I_0+\Omega;\ l', -\Omega}$$

$$\times \int Y^{*}_{l\Omega} \frac{\varphi_{I'l'}[R(\theta)]}{\varphi_{Il}[R(\theta)]} Y_{l'\Omega}\, d\varphi\, d(\cos\theta).$$

As numerical estimates show, all the quantities $B(Il;\ I'l')$ are small, so that to a good approximation the whole summation in (2.7) can be dropped. This comes about because the functions $Y_{l\Omega}$ with different l are orthogonal, while the ratio $\varphi_{I'l'}[R(\theta)]/\varphi_{Il}[R(\theta)]$ varies only little with angle θ.* Neglecting the dependence of this ratio on angle, we find that for $l \neq l'$ the integral appearing in $B(Il;I'l')$ vanishes while for $l = l'$, $B(Il;I'l')$ vanishes because of the orthogonality of the Clebsch-Gordan coefficients with $I \neq I'$. We therefore get

$$a_{Il} \approx A_{Il} C^{II_0}_{I_0 I_0;\ l_0}. \qquad (2.9)$$

Now let us consider the quantities A_{Il} defined in (2.8). The functions $\varphi_{Il}(r)$ in the denominator depend on r essentially in the same way as the Coulomb functions $\varphi^{(0)}_{Il}(r)$ which are the exact solution of (2.3) when we neglect the right hand side (and satisfy the same boundary condition at $r \to \infty$,

$$\varphi^{(0)}_{Il}(r) \to \exp i(k_I r - \eta_I \ln 2k_I r),$$

as the functions $\varphi_{Il}(r)$). At the nucleus, this function falls off exponentially with increasing r, so that the principal contribution to the integral (2.8) comes from the neighborhood of $\theta = 0$, where $R(\theta)$ reaches a maximum. Also making use of the fact that all the functions $\varphi_{Il}[R(\theta)]$ depend on angle in approximately the same way, we find

$$A_{Il} \approx C\sqrt{2l+1}\,/\,\varphi_{Il}[R(0)], \qquad (2.10)$$

where $\sqrt{2l+1} = \sqrt{4\pi}\,[Y_{l_0}(\theta)]_{\theta=0}$. In α decay, the constant η_I in (2.3) is always large compared to unity: $\eta_I \gg 1$, which is the reason why the quasi-classical approximation is well justified. In this approximation it is well known (also cf. the next section) that $\varphi_{Il}(r)$ is representable in the form

$$\varphi_{Il}(r) = \exp\{-S_l(r, k_l)\},$$

where S_l can be expanded in a rapidly converging series

$$S_l = A(r, k_I) + B(r, k_I)\, l(l+1) + C(r, k_I)\, l^2(l+1)^2 \qquad (2.11)$$

and

$$k_I = k\sqrt{1 - \Delta E_I/E} \approx k - k\Delta E_I/2E,$$

$$\Delta E_I = \frac{\hbar^2}{2\mathcal{J}}\{I(I+1) - I_0(I_0+1) \qquad (2.12)$$

$$+ a[(-1)^{I+1/2}(I + 1/2) + 1]\,\delta_{I_0 1/2}\}$$

(E is the energy of the α-decay to the lowest level of the rotational band, which has spin I_0).

Expanding the coefficients of the series (2.11) in powers of $\Delta E_I/E$, we find that the function $\varphi_{Il}[R = 0] = \varphi_{Il}(a)$ can be represented as the rapidly converging series

$$\varphi_{Il}(a) = c_1 \exp\left\{-\frac{\alpha}{2} l(l+1) - \frac{\beta}{2}\frac{\Delta E_I}{E} + \ldots\right\}. \qquad (2.13)$$

For estimating orders of magnitude, it is useful to expand the Coulomb function $\varphi^{(0)}_{Il}(a)$, which is of the same order of magnitude as $\varphi_{Il}(a)$, in a series of the type of (2.13). As is easily verified [cf. formulas (3.11) and (3.12)],

$$\varphi^{(0)}_{Il}(a) = c_2 \exp\left\{-\frac{\alpha_c}{2} l(l+1) - \frac{\beta_c}{2}\frac{\Delta E_I}{E}\right\}, \qquad (2.14)$$

$$\alpha_c = \tan\varepsilon/\eta \approx 0.1, \quad \beta_c = 2\eta(\varepsilon + 1/2 \sin 2\varepsilon) \approx 75,$$

$$\varepsilon = \arccos\sqrt{ka/2\eta}.$$

Substituting (2.9), (2.10), and (2.13) in (2.1), we get finally

$$W_I = W_0 \sum_{l=I-I_0}^{I+I_0}{}' |C^{II_0}_{I_0 I_0;\ l_0}|^2 (2l+1) \exp\left\{-\alpha l(l+1) - \beta\frac{\Delta E_I}{E}\right\}. \qquad (2.15)$$

The coefficients α and β in (2.15) should be regarded as parameters whose values are determined from experiment, since the connection with the shape of the nucleus was lost in getting equation (2.10) from (2.8).

We note, finally, that for the case of even-even nuclei, when $I_0 = 0$, $I = l$ and $\Delta E_I/E \sim l(l+1)$, formula (2.15) assumes a simple form, given by Landau:[9]

$$W_l = (2l+1)\, W_0 e^{-\alpha' l(l+1)}. \qquad (2.16)$$

Let us make one more remark concerning the derivation of formula (2.15). The one assumption in the derivation which was not completely justi-

*Each of the quantities $\varphi_{Il}[R(\theta)]$ has a strong angular dependence, but their ratio depends only slightly on angle. For the functions $\varphi^{(0)}_{Il}[R(\theta)]$, which are the solutions of (2.3) with the right side set equal to zero, this can be seen from the formulas of the next section. As the numerical computations show, this assertion is also valid for the functions $\varphi_{Il}[R(\theta)]$.

TABLE I. Alpha Decay of Some Even Nuclei*

Decaying Nucleus	α'	Level spin and parity	Particle energy kev	Level energy kev	Intensity of α decay (%)	
					Experiment	Computation
Pu^{240}	0.457	0+	5158.9	0	75.5	75.5
		2+	5114.4	45.3	24.4	24.4
		4+	5014	147	$9.1\cdot10^{-2}$	$7.3\cdot10^{-2}$
Pu^{238}	0.435	0+	5491	0	71.1	71.1
		2+	5448	43.7	28.7	28.7
		4+	5352	141.5	0.13	0.11
U^{232}	0.394	0+	5318	68	68	68
		2+	5261	32	32	32
		4+	5134	0.3	0.3	0.23
Cm^{242}	0.441	0+	6110	0	73.7	73.7
		2+	6066	44	26.3	26.3
		4+	5965	148	$3.5\cdot10^{-2}$	$9.9\cdot10^{-2}$

*Formula (2.16) was used for the computations. The probability of α decay to the 2^+ level was used for the determination of the parameter α'.

TABLE II. Alpha Decay of Some Odd Nuclei*

Decaying Nucleus	α	β	Level spin and parity	Particle energy kev	Level energy kev	Intensity of α decay (%)	
						Experiment	Computation
Pu^{239}	0.309	115	$1/2\pm$	5147	0	72	72
			$3/2\pm$	5134	13.2	16.8	16.8
			$5/2\pm$	5096	51.7	10.7	10.8
			$7/2\pm$	5064	84	$3.7\cdot10^{-2}$	$9\cdot10^{-2}$
			$9/2\pm$	4991	151	$1.3\cdot10^{-2}$	$2.6\cdot10^{-2}$
Am^{241}	0.283	99	$5/2\pm$	5482	0	85	85
			$7/2\pm$	5439.1	43.4	12.8	12.8
			$9/2\pm$	5386.0	97.4	1.66	1.7
			$11/2\pm$	5321	164	$1.5\cdot10^{-2}$	$3.4\cdot10^{-2}$
			$13/2\pm$	5241	245	$2\cdot10^{-3}$	$2.4\cdot10^{-3}$

*Formula (2.15) was used for the computations. The probabilities of α decay to the levels with spin $I_0 + 1$ and $I_0 + 2$ were used for determining the constants α and β.

fied was that the integral (2.8) can be replaced by a quantity proportional to the value of the integrand at the point $\theta = 0$. However, the form of (2.15) does not depend in any essential way on this assumption, since (2.15) also follows from (2.8) and (2.9) if we expand the whole integral (2.8) in series:

$$\int_{-1}^{1} \frac{R(\theta)\chi(\theta)}{\varphi_{Il}[R(\theta)]} Y_{l0}(\theta)\, d(\cos\theta)$$

$$= (2l+1)\exp\left[-\frac{1}{2}\left\{c + \alpha l(l+1) + \beta\frac{\Delta E_I}{E}\right.\right. \quad (2.17)$$

$$\left.\left. + \alpha_1 l^2(l+1)^2 + \beta_1\left(\frac{\Delta E_I}{E}\right)^2 + \gamma l(l+1)\frac{\Delta E_I}{E} + \ldots\right\}\right].$$

It is clear from this that formula (2.15) is quite exact. But this precision is obtained at the expense of giving up the possibility of theoretical evaluation of the constants α and β starting from the nuclear shape. Thus formula (2.15) cannot be used for determining the shape of α-active nuclei. It is not difficult to obtain an approximate formula of the same type as (2.15) but without this defect. To do this we need only replace $\varphi_{Il}[R(\theta)]$ in (2.8) by the Coulomb function $\varphi^{(0)}_{Il}[R(\theta)]$. From (2.1), (2.8) and (2.9) we then find

$$W_I = 4\pi^2\frac{\hbar k_I}{\mu}\sum_{l=I-I_0}^{I+I_0}{}' |C^{II_0}_{I_0 I_0;\, l0}|^2 \left|\int_{-1}^{1}\frac{R(\theta)\chi(\theta)}{\varphi^{(0)}_{Il}[R(\theta)]} Y_{l0}(\theta)\, d(\cos\theta)\right|^2. \quad (2.18)$$

The integral in this formula can be computed numerically for any nuclear shape $R(\theta)$, as soon as we choose the form of the function $\chi(\theta)$ (usually we assume that $\chi(\theta) = \text{const}$). Formula (2.18) cannot of course pretend to be particularly exact, in particular for large values of l, since at $l = 4$ (cf. the following section) the effect of the right-hand side of (2.3) already produces a sizeable difference getween the true radial functions $\varphi_{Il}(r)$ and the Coulomb functions $\varphi^{(0)}_{Il}(r)$, which are the solution of (2.3) without the right-hand side.

In conclusion we give some numerical data illustrating the applicability of formulas (2.15) and (2.16) to the description of the experimental data. As we see from Table I, Landau's formula (2.16) with the single parameter α' gives a good description of the experimental data for $l \leq 4$. For $l = 6$, this formula already leads to a marked disagreement with experiment (by a factor of hundreds!), which shows the need for considering the next term, $\alpha'' l^2 (l+1)^2$, in the expansion of the exponential. It is therefore natural to expect that formula (2.15) will give a good description of the intensities of α decay to the first five levels of the rotational band (for which $l \leq 4$), as is shown in Table II.

As we see from formula (2.8), the intensity of the α decay to particular levels can take on anomalously large or small values if some particular term in the Legendre polynomial expansion of $R(\theta)\chi(\theta)/\varphi_{ll}[R(\theta)]$ is "resonantly" large or small. The smooth representation (2.17) is not possible in such a case. This may be the explanation of the large (factor of three) discrepancy between the calculated and experimental amplitudes for the α decay of Cm^{242} to the 4^+ level of the daughter nucleus (cf. Table I).

3. ANALYSIS OF SOME APPROXIMATE METHODS OF SOLUTION OF EQUATIONS (2.3)

The system of equations (2.3) cannot be solved exactly by analytic methods even in the simplest case of $I_0 = 0$. Various authors have either completely omitted the right hand side of (2.3) or have regarded it as a perturbation and taken it into account by a method of successive approximations. In doing this, only the quadrupole part of the Coulomb interaction was included. We shall show that such a procedure for solution of the problem is incorrect, since the correction provided by the first approximation is of the same order of magnitude de as the zeroth approximation.

For the case of $I_0 = 0$, the equations for the radial functions and the appropriate boundary conditions have a very simple form, which can be obtained by setting $I_0 = 0$, $I = l$, $I' = l'$ in (2.3), (2.4), and (2.5). In this case

$$Q_L(l, l, l', l') = \sqrt{\frac{2l'+1}{2l+1}} |C^{l_0}_{L0;\, l'0}|^2 = \int Y^*_{l'0} P_L Y_{l0}\, d\Omega.$$

Introducing the dimensionless variable

$$x = r/r_0, \quad r_0 = 2Ze^2/E = 2\eta/k$$

(where r_0 is the barrier radius) into (2.3), and setting

$$f_{ll}(r) = a_l \varphi_l(r), \quad \varphi_l(r) \to \exp i(k_l r - \eta_l \ln 2k_l r) \text{ for } r \to \infty,$$

we get

$$\varphi_l''(x) + (\varkappa_l^2 - \nu_l)\varphi_l(x) = \frac{4\eta^2}{x} \sum_{l'}{}' \frac{a_{l'}}{a_l} \varphi_{l'}(x) U_{l'l}(x). \quad (3.2)$$

Here we have introduced the notation

$$\varkappa_l^2 = 4\eta^2\left[1 - \frac{\Delta E}{6E} l(l+1)\right]; \quad \nu_l = 4\eta^2\left[\frac{1}{x} + \frac{l(l+1)}{4\eta^2 x^2}\right]. \quad (3.3)$$

ΔE is the excitation energy of the first rotational level,

$$U_{l'l} = \int Y_{l'0}(\mu) U(x, \mu) Y_{l0}(\mu)\, d\Omega; \quad \mu = \cos\theta, \quad (3.4)$$

and U is the noncentral part of the Coulomb interaction, which is given by

$$V(r, \theta) = \frac{E}{x}[1 + U(x, \mu)]. \quad (3.5)$$

The dimensionless constant η (cf. text following Eq. 2.12) is approximately equal to 25.

The solution of Eq. (3.2) without the right hand side is the coulomb function $\varphi_l^{(0)}(x)$, which can be represented quite accurately* as

$$\varphi_l^{(0)}(x) = \sqrt{\frac{\pi}{2}}\, e^{2\pi i/3} \left(\frac{\varkappa_l^2}{\varkappa_l^2 - \nu_l}\right)^{1/4} \quad (3.6)$$

$$\times \left(\int_{x_l}^{x} \sqrt{\varkappa_l^2 - \nu_l}\right)^{1/2} H^{(1)}_{1/3}\left(\int_{x_l}^{x} \sqrt{\varkappa_l^2 - \nu_l}\, dx\right),$$

where $H^{(1)}_{1/3}$ is the Hankel function of the first kind of order $1/3$, and x_l is the turning point (the value at which $\varkappa_l^2 = \nu_l$). The function (3.6) coincides with the exact solution (3.2) in the region of the turning point, and has the correct asymptotic behavior far away from that point. The constant in (3.6) is chosen so that all the functions $\varphi_l^{(0)}$ are real at and near the nucleus.

The goal of the computation is to calculate the amplitudes $a_{ll} = a_l$, which determine the α-decay probability W_l through (2.1). According to (2.8) and (2.9),

$$a_l = 2\pi \int_{-1}^{1} \frac{R(\theta)\chi(\theta)}{\varphi_l[R(\theta)]} Y_{l0}(\theta)\, d(\cos\theta). \quad (3.7)$$

We obtain the zeroth approximation $a_l^{(0)}$ to the value of a_l by replacing $\varphi_l[R(\theta)]$ in (3.7) by the Coulomb function $\varphi_l^{(0)}[R(\theta)]$, in accordance with (2.18). To find $a_l^{(1)}$ we must substitute the first approximation $\varphi_l^{(1)}$ in (3.7). In calculating $\varphi_l^{(1)}$, the functions $\varphi_l^{(0)}(x)$ and the values $a_l^{(0)}$ and $a_{l'}^{(0)}$ were substituted on the right side

*Formula (3.6) describes the variation of the function $\varphi_l^{(0)}$ in the neighborhood of the nucleus and its dependence on l with an accuracy which is no worse than 1%.

of (3.2). It is then convenient to look for a solution of (3.2) in the form $\varphi_l^{(1)}(x) = \lambda_l(x)\varphi_l^{(0)}(x)$. We then find for λ_l the equation

$$2\lambda_l'\varphi_l'^{(0)}(x) = \frac{4\eta^2}{x}\sum_{l'}\frac{a_{l'}^{(0)}}{a_l^{(0)}}U_{l'l}\varphi_{l'}^{(0)}(x)$$

with the boundary condition $\lambda_l(\infty) = 1$. (On the left hand side we have neglected the term $\lambda_l''(x)\varphi_l^{(0)}(x)$, which is vanishingly small compared to $\lambda_l'(x)\varphi_l'^{(0)}(x)$. This is obvious simply from the fact that in the region below the barrier the function $\varphi_l^{(0)}(x)$ changes by 20 orders of magnitude whereas $\lambda_l(x)$ only changes by a factor of 1 to 10.)

Performing the integration, we get

$$\lambda_l(x) = 1 + \eta\sum_{l'}\frac{a_{l'}^{(0)}}{a_l^{(0)}}\int_x^\infty \frac{\varphi_{l'}^{(0)}(x)}{\varphi_l^{(0)}(x)}\frac{U_{l'l}(x)}{\sqrt{x(1-x)}}dx. \quad (3.8)$$

According to (3.7),

$$a_l^{(1)} = a_l^{(0)}/\lambda_l(a), \quad a = [R(\theta)]_{\theta=0}/r_0 \quad (3.9)$$

(a is the nuclear radius in units of r_0).

For practical computations it is convenient to use the asymptotic representation (3.6) which gives a quite accurate description of the behavior of $\varphi_l^{(0)}$ near the nuclear surface:

$$\varphi_l^{(0)}(x) \approx \left(\frac{\varkappa_l^2}{\nu_l - \varkappa_l^2}\right)^{1/4}\exp\left\{\int_x^{x_l}\sqrt{\nu_l - \varkappa_l^2}\,dx\right\}, \quad \frac{x}{x_l} \ll 1. \quad (3.10)$$

The exponent is well approximated by the series

$$\int_x^{x_l}\sqrt{\nu_l - \varkappa_l^2}\,dx = A + Bl(l+1) + Cl^2(l+1)^2, \quad (3.11)$$

where

$$A(x) = 2\eta(\alpha - {}^1/_2\sin 2\alpha),$$
$$B(x) = 2\eta\left[\frac{\Delta E}{12E}\left(\alpha + \frac{1}{2}\sin 2\alpha\right) + \frac{\tan\alpha}{4\eta^2}\right],$$
$$C(x) = \frac{1}{2\eta}\frac{\Delta E}{6E}\cot\alpha + \eta\left(\frac{\Delta E}{6E}\right)^2\left(\cot\alpha + \frac{3}{2}\alpha + \frac{1}{4}\sin 2\alpha\right) + \frac{1}{3\eta^3}\left(\cot 2\alpha - \frac{1}{8\sin\alpha\cos^3\alpha}\right), \quad (3.12)$$
$$\alpha = \arccos\sqrt{x}.$$

(Formulas (3.10), (3.11), and (3.12) are also valid for nuclei with $I_0 \neq 0$. In this case $(\Delta E/6E)\,l(l+1)$ must be replaced by ΔE_I and κ_I by κ_l.)

We point out for orientation that at the nuclear surface $A \approx 40$, $B \approx 0.1$ and $C \approx 10^{-4}$, so that for small l the term $Cl^2(l+1)^2$ is unimportant. Substitution of (3.10) and (3.11) in (3.8) gives

$$\lambda_l(x) = 1 + \eta\sum_{l'=0}^{\infty}\frac{a_{l'}^{(0)}}{a_l^{(0)}}\int_x^1\frac{U_{l'l}(x)}{\sqrt{x(1-x)}} \times \exp\{B(x)[l'(l'+1) - l(l+1)]\}\,dx. \quad (3.13)$$

In (3.13) the upper limit of integration has been replaced by 1. This step is necessary since the expansion (3.11) is not valid in the region $\nu_l - \kappa_l^2 < 0$. Because of the rapid falloff of $U_{l'l}$ with increasing x and the oscillatory character of the functions $\varphi_l^{(0)}$ in the region $x > 1$, the integral from 1 to ∞ contributes practically nothing.

For numerical computations it is necessary to choose a specific shape for the nucleus,

$$R(\theta) = x_1[1 + \alpha_2 P_2(\cos\theta) + \alpha_4 P_4(\cos\theta) + \ldots]. \quad (3.14)$$

For an ellipsoid with eccentricity $u = \sqrt{1 - b^2/a^2}$ and semiaxes a and b (in units of r_0),

$$\alpha_2 = \frac{15}{4u^2}\left[1 - \frac{2}{3}u^2 - \frac{u\sqrt{1-u^2}}{\arcsin u}\right] = \frac{u^2}{3} + 0.16\,u^4 + 0.098\,u^6 + \ldots,$$
$$\alpha_4 = \frac{27}{64\,u^2}[35 - 40u^2 + 8u^4] + \frac{45}{64}\frac{\sqrt{1-u^2}}{u^3\arcsin u}(10\,u^2 - 21) = 0.086\,u^4 + 0.083\,u^6 + \ldots, \quad (3.15)$$

The quantities $U_{l'l}$ appearing in (3.13) are given by the coefficients in the Legendre polynomial expansion of $U(x, \mu)$. In the region outside the nucleus (but not in the interior!) the potential of a uniformly charged ellipsoid is correctly given by the formula

$$U(x, \mu) = 3\sum_{n=1}^{\infty}\frac{1}{(2n+1)(2n+3)}\left(\frac{ua}{x}\right)^{2n}P_{2n}(x). \quad (3.16)$$

Formula (3.16) is not the same expansion as that usually used for the potential of an ellipsoid, and is considerably more convenient. (The possibility of having different expansions of the potential in Legendre polynomials in the region $b \leq x \leq a$ is related to the fact that when this inequality is satisfied the Legendre polynomials are not orthogonal in the region external to the nucleus.)

For an arbitrary nuclear shape (3.14), the expansion (3.16) is not exact. As we shall show later, the details of the shape of the nucleus have a significant effect on the probability of emission of particles with high l. This effect is, however, associated mainly with the change in the boundary conditions, whereas the effect of nuclear shape which is associated with changes in the potential is not so important and was not taken into account. In our computations we therefore assumed the nucleus to be elliptical and used formula (3.16). Then

$$U_{l'l} = 3\sum_{n=1}^{\infty}\frac{1}{(2n+1)(2n+3)}\left(\frac{ua}{x}\right)^{2n}\frac{\sqrt{(2l+1)(2l'+1)}}{4n+1}(C_{l'0;l0}^{2n,0})^2. \quad (3.17)$$

In Tables III and IV we give the results of computation of the amplitudes $a_l^{(0)}$ and the factors

TABLE III. Probability of α decay to successive rotational levels, computed in zeroth approximation for U^{236}

	Computational results							Experimental data
α_2	0.07	0.095	0.117	0.141	0.168	0.195	0.227	
u^2	0.20	0.25	0.30	0.35	0.40	0.45	0.50	
$a_2^{(0)}/a_0^{(0)}$	0.38	0.46	0.55	0.62	0.69	0.74	0.77	0.57
$a_4^{(0)}/a_0^{(0)}$	0.025	0.038	0.054	0.072	0.086	0.106	0.122	0.035
$a_6^{(0)}/a_0^{(0)}$	$4.7\cdot10^{-4}$	$9.1\cdot10^{-4}$	$1.6\cdot10^{-3}$	$2.4\cdot10^{-3}$	$3.3\cdot10^{-3}$	$4.4\cdot10^{-3}$	$5.8\cdot10^{-3}$	$6.7\cdot10^{-3}$

$\lambda_l^{(1)}(a)$, which determine the first order correction through Eq. (3.9). The computations were done for U^{236} (α decay of Pu^{240}). $\chi(\theta)$ was set equal to a constant in (3.7). The size of the nucleus was fixed by the condition $\chi^2(\theta)V_n = 1$, where V_n is the nuclear volume.

TABLE IV. First approximation factors $\lambda_l^{(1)}$ for U^{236}

u^2	0.25	0.30	0.35	0.40	0.45	0.50
$\lambda_0^{(1)}$	1.13	1.18	1.24	1.31	1.38	1.45
$\lambda_2^{(1)}$	1.22	1.23	1.25	1.26	1.27	1.29
$\lambda_4^{(1)}$	1.77	1.82	1.85	1.87	1.89	1.91
$\lambda_6^{(1)}$	2.13	2.21	2.31	2.42	2.51	2.56

As we see from Table IV, for actually occurring deformations ($u^2 = 0.3$), the correction factor λ is close to unity only for $l = 0$ and 2. Starting with $l = 4$ the correction reaches an order of magnitude of 100% and the method of successive approximations is not consistent.*

We tried to improve the successive approximation method by substituting $\varphi_l(x) = \lambda_l(x)\varphi_l^{(0)}(x)$ on the right as well as the left side of (3.2). When this is done one gets a system of coupled equations for the relatively slowly varying functions $\lambda_l(x)$. If one assumes that the $\lambda_l(x)$ vary significantly only near the nucleus, expands $\lambda_l(x)$ in powers of $(x-a)$ around the point $x = a$, and keeps only the zeroth and first powers, a relatively simple system of algebraic equations is obtained for $\lambda(a)$. The coefficients in these equations are integrals which can be computed numerically. However, the computation showed that the solutions obtained by this method diverge for actually occurring values of the deformation.

It should be mentioned that, aside from the inaccuracy associated with the use of the successive-approximation method, the computations involved the use of the approximate value (3.11) of the coulomb function and the approximate formula (3.7) which is a consequence of the boundary conditions on the nuclear surface. Estimates showed that both these approximations are very good, and do not contribute errors exceeding a few percent. Thus the divergence of the method of successive approximations is caused only by the use of the method itself. We were therefore faced with the necessity of an exact numerical solution of equations (3.2).

4. NUMERICAL SOLUTION OF THE EQUATIONS

The numerical solution of Eq. (3.2) expressed in terms of the functions $f_l(x) = a_l\varphi_l(x)$ was carried out on the M-2 electronic computer of the Laboratory for Control Machines and Systems of the Academy of Sciences, U.S.S.R. Seven functions ($l = 0, 2, \ldots 12$) were included in the computations, while the remainder were set equal to zero. The solution of the equations was carried "inward" from $x = \infty$ (actually from $x = 3$) to the surface of the nucleus (to $x \approx 0.1$). To determine the a_l, we constructed the 7 fundamental systems of solutions φ_{ln} ($n = 0, 2, \ldots 12$). The solution with number n was normalized at $x = 3$ by the requirement that $\varphi_{ln}(3) = \delta_{ln}\varphi_l^{(0)}(3)$. Every solution of (3.2) can be represented as a linear combination of these seven solutions. Thus each of the functions we are trying to find can be written as

$$f_l(x) = \sum_{n=0}^{12}{}' a_n \varphi_{ln}(x), \quad l = 0, 2 \ldots 12 \qquad (4.1)$$

(where the prime on the summation sign means that the sum runs over even n). It is easy to see that the functions $f_l(x)$ have the correct asym-

*The values found for a_0 and a_2 can be used to determine the dimensions and eccentricity of the nucleus. However, when this is done there are no quantities left which can be compared with experiment in order to check the theory. We also mention that the divergence of the successive approximation method for $l \geq 4$ means that the excitation of higher rotational levels occurs to a considerable extent through the coulomb interaction of the α particle with the nucleus.

ptotic behavior for $x \to \infty$, so that the a_n are the required decay amplitudes. After substituting (4.1), the boundary condition (2.5) gives (in our case where $I_0 = 0$, $I = l$),

$$\sum_{n=0}^{12}{}' a_n \chi_n(\theta) = \chi(\theta), \tag{4.2}$$

where

$$\chi_n(\theta) = \sum_{l=0}^{12}{}' \frac{\varphi_{ln}[R(\theta)]}{R(\theta)} Y_{l0}(\theta) \tag{4.3}$$

are well-defined functions which are uniquely determined from the shape of the nucleus. The requirement

$$\chi(\theta) = \text{const} \tag{4.4}$$

enables us to find the ratio a_n/a_0.

As a check, the fundamental systems of solutions $\varphi_{ln}(x)$ were computed for $n = 0, 2, 4, 6, 8$, when only five functions f_0, f_2, f_4, f_6, f_8 were included. A comparison showed that then the first four functions are changed negligibly. The various stages of the solution can be followed on the graphs of Figs. 1 to 5.

To illustrate the orders of magnitude, Fig. 1 shows the real part of $\varphi_l^{(0)}(x)$ for U^{236} (α decay of Pu^{240}) as a function of x.

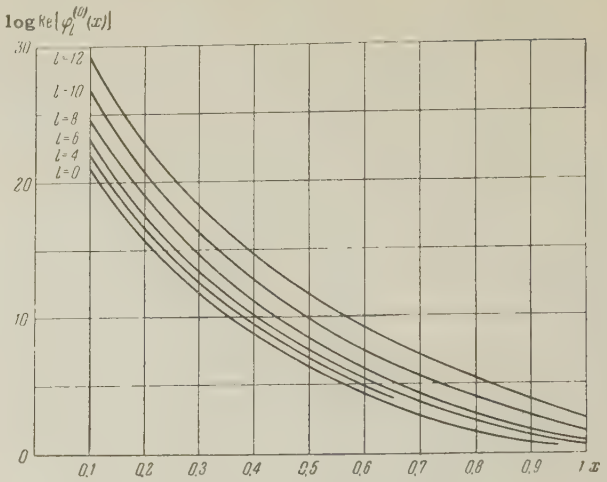

FIG. 1. Real part of the zeroth approximation functions $\varphi_l^{(0)}(x)$ for U^{236}; $\eta = 26.0$.

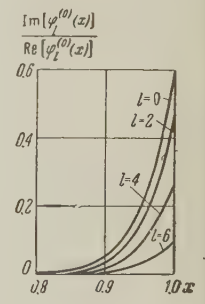

FIG. 2. Ratio of imaginary to real part of $\varphi_l^{(0)}(x)$.

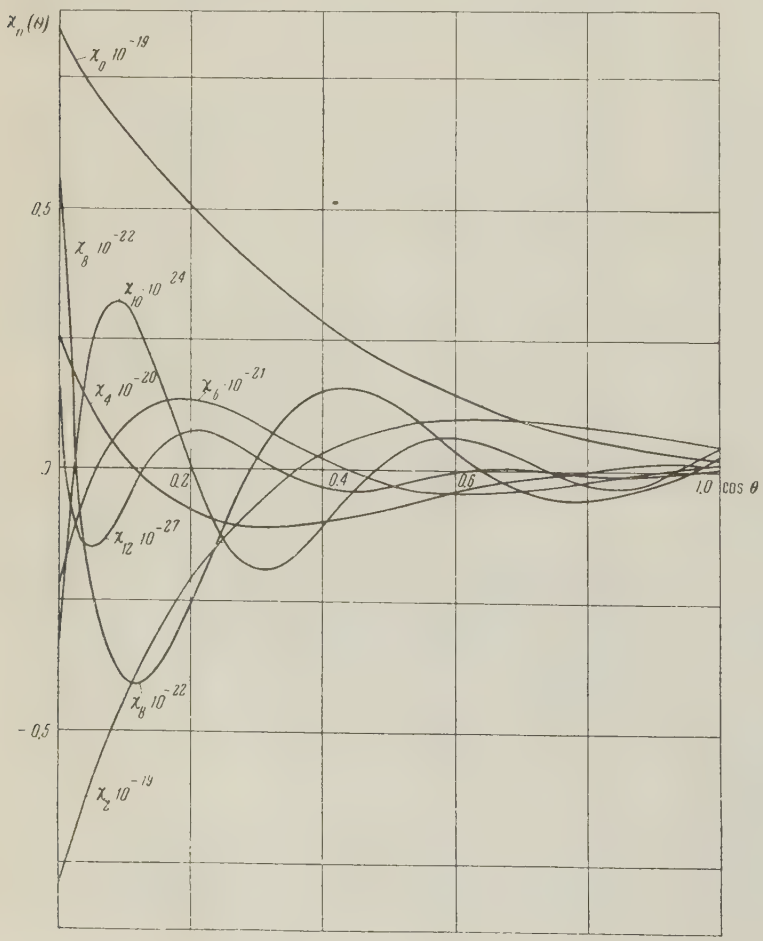

FIG. 3. Graph of the functions $\chi_n(\theta)$.

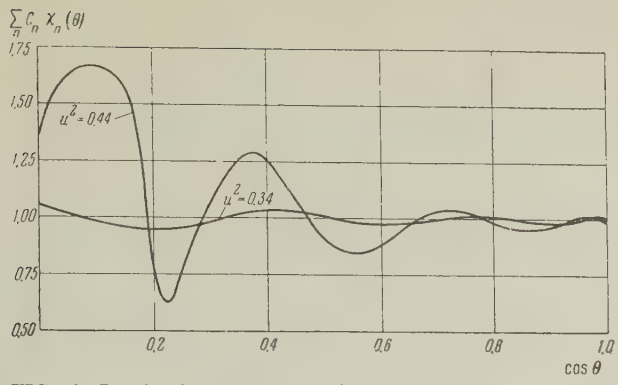

FIG. 4. Graph of the function $\sum_n c_n \chi_n(\theta)$. The coefficients c_n were selected by the least squares method so that the deviation of $\sum_n c_n \chi_n(\theta)$ from unity was a minimum. (The constants correspond to U^{236}).

Figure 2 shows the ratio of the imaginary part of $\varphi_l^{(0)}(x)$ to the real part. As we see from the figure, at $x = 0.8$ all the functions $\varphi_l^{(0)}(x)$ can already be assumed to be real, as should be the case according to (3.10). The functions $\varphi_{ln}(x)$ also turn out to be real at the nucleus. Choosing a real constant in (4.4), we also get real values for the amplitudes a_n.

Figure 3 shows graphs of the functions $\chi_n(\theta)$, calculated for $\eta = 25.4$, $a = 0.19$, $u^2 = 0.35$. The calculations were done keeping all the terms in the multipole expansion (3.16), (3.17) of the interaction potential. Linear combinations must be built up from the functions $\chi_n(\theta)$ so as to obtain a constant value on the nuclear surface, in accordance with (4.2) and (4.4). Each of the functions χ_n has $n/2$ roots on the nuclear surface. All of the functions increase rapidly as we move from the "nose" of the nucleus toward the equator, in accordance with the decrease of $R(\theta)$ in this direction. A practical choice of coefficients a_n satisfying the condition (4.4) was made by applying the least squares method to 17 points on the nucleus, at which the functions χ_n were calculated. In applying least squares, we used a weight factor of $1/\chi_0(\theta)$. The introduction of the weight factor enabled us to avoid excess sensitivity to the unimportant equatorial region of the nucleus. The large number of functions which were to combine to give the constant enabled us to fit it quite accurately. This is illustrated in Fig. 4 for the example of U^{236}. We see from this figure that the curve of the "deviations" intersects the value 1, to which the fit was made, a number of times which is one greater than the number of zeros in the highest function $\chi_n(\theta)$ included in the computation. We also note that the fit is quite good for $u^2 \leq 0.35$, while it is rather bad for $u^2 > 0.45$. Thus the

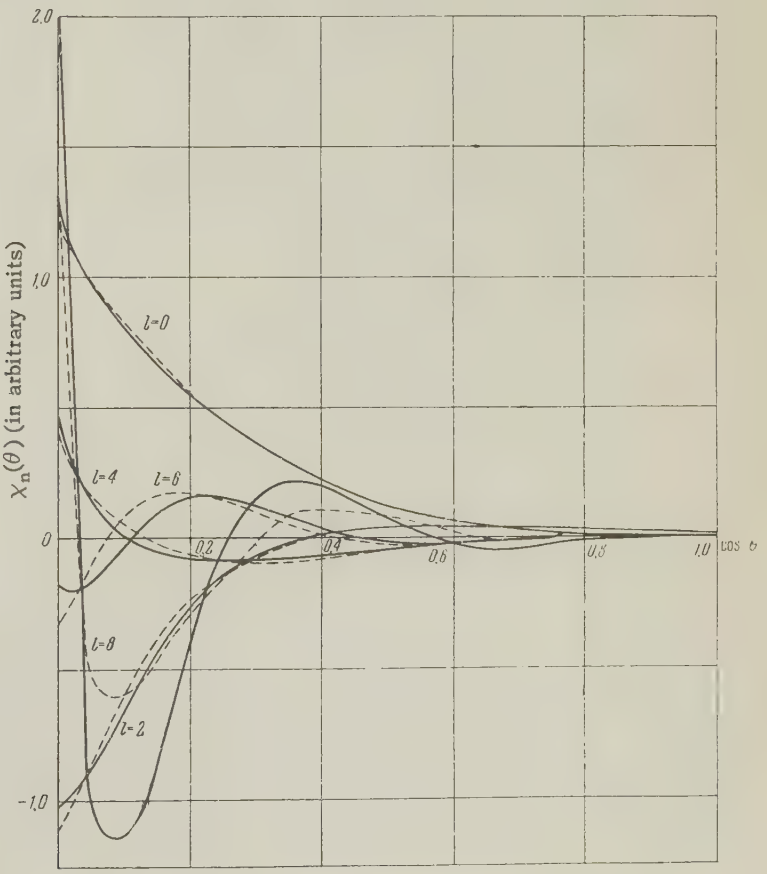

FIG. 5. Graph of the functions $\chi_n(\theta)$, calculated including five (f_0, f_2, ... f_8) or seven (f_0, f_2, ... f_{12}) functions f_n. The solid curves are for $l_{max} = 8$, the dotted curves for $l_{max} = 12$.

number of functions $\chi_n(\theta)$ included was insufficient for the latter case. This example illustrates especially clearly the need to include a large number of functions, and the inapplicability of the usual analytic methods. Figure 5 shows the functions $\chi_n(\theta)$ calculated including five (f_0, f_2, ... f_8) and seven (f_0, f_2, ... f_{12}) functions f_n.

In our computational procedure we had first to assign the nuclear size (the computation was done for one volume and various eccentricities), so that it is important to examine the extent to which the results are sensitive to the size of the nucleus.

The results of such a computation are contained in Table V.

TABLE V. Effect of nuclear size on α-decay probability (for U^{236})

Major semi-axis a	Ratio of decay probabilities		
	a_2/a_0	a_4/a_0	a_6/a_0
0.156	0.56	0.062	0.0022
0.173	0.59	0.071	0.0027
0.190	0.62	0.080	0.0034

Comparing Table V with Table VI, which shows the effect of the nuclear shape, we easily discover that the nuclear size has a subordinate role in determining the relative intensities of α decays. In evaluating the results it should be remembered that a change in size of 10% (the extreme values of a in Table V differ by 10% from the middle value) gives a change of a factor of 5 in the absolute value of the function f_0, and consequently a change of a factor of 25 in the α-decay intensity.

TABLE VI. Intensity of α decay to rotational levels as a function of nuclear shape (for U^{236})

	Computational results				Experimental data
α_2	0.095	0.141	0.186	0.238	
u^2	0.25	0.35	0.44	0.52	
a_2/a_0	0.41	0.59	0.85	0.93	0.57
a_4/a_0	0.033	0.070	0.113	0.163	0.035
a_6/a_0	0.0011	0.0030	0.0072	0.011	0.0067

Table VI gives the results of numerical computation of α-decay intensities for U^{236} (α-decay of Pu^{240}) which were carried out on an electronic computer.

The data of Table VI are plotted in Fig. 6. The crosses on the curves are the experimental values.

Comparison of Table VI with Table III shows good agreement of the results of the exact calculations with those of the approximate calculations [using formula (2.18)]. As mentioned earlier, for

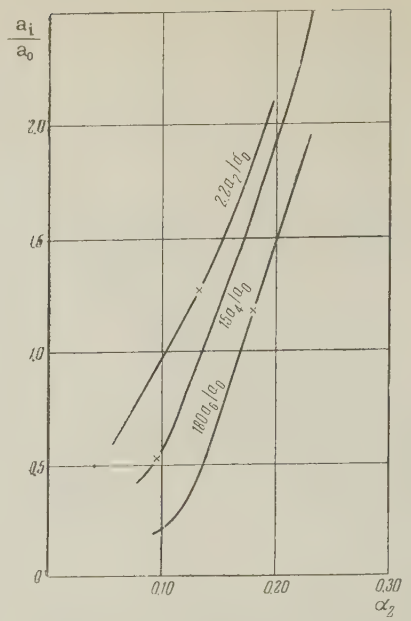

FIG. 6. Dependence of intensity of α decay to successive rotational levels on elongation of the nucleus (computation for U^{236}).

reasonable values of the eccentricity the first order corrections in the analytic computation are not small, so that the close agreement between the results of the numerical and approximate computations was unexpected. This leads one to think that applying (2.18) to odd nuclei with $I_0 \neq 0$ also should give good results and enable one to determine the eccentricity of the nucleus simply.

Such computations were done for Am^{241} and Pu^{239}. Only one parameter, the eccentricity u^2, was varied; the nuclear size was chosen to give the correct expression for the α-decay intensity to the ground state. The results of the computation are given in Table VII.

One striking feature of the results in Table VI is the clear, though not very large, discrepancy between the experimental and calculated values. Thus, by setting $\alpha_2 = 0.133$ we would obtain exact agreement of the theoretical and experimental values of a_2/a_0, but we then get a difference of a factor of 1.8 in the values of a_4/a_0 (and a discrepancy of a factor of 2.7 in the value of a_6/a_0). This discrepancy can be eliminated by a suitable choice of the coefficient α_4 in formula (3.14) which determines the nuclear shape. For arbitrary α_4 the nucleus is of course no longer ellipsoidal, and the matrix elements of the potential are determined by a formula which is different from (3.17), a point which was not taken into account in the computations. However, this selection of the coefficient α_4 does not improve the agreement with experiment for the ratio a_6/a_0 but rather makes it worse. This ratio, in turn,

TABLE VII. Intensity of α decay to rotational levels for some odd nuclei*

Daughter nucleus	Spin of rotational level	Relative intensity of α decay		
		Exptl.	Calculated for elliptical nucleus	Calculated for oval nucleus
Np^{237} $I_0 = 5/2$	7/2	0.150	0.150	0.146
	9/2	$2 \cdot 10^{-2}$	$2.8 \cdot 10^{-2}$	$2.5 \cdot 10^{-2}$
	11/2	$1.8 \cdot 10^{-4}$	$1.2 \cdot 10^{-3}$	$1.8 \cdot 10^{-4}$
	13/2	$2.4 \cdot 10^{-5}$	$1.2 \cdot 10^{-4}$	$1.8 \cdot 10^{-5}$
U^{235} $I_0 = 1/2$	3/2	0.232	0.232	0.232
	5/2	0.148	0.190	0.195
	7/2	$5 \cdot 10^{-4}$	$6 \cdot 10^{-3}$	$5.7 \cdot 10^{-4}$
	9/2	$1.4 \cdot 10^{-4}$	$2.7 \cdot 10^{-3}$	$2.6 \cdot 10^{-4}$

*The intensity was computed using formula (2.18). For N_p^{237}, we set $a = 0.193$ and $u^2 = 0.283$ in the case of the ellipse and $u^2 = 0.30$ and $\alpha_4 = -0.04$ in the case of the oval. For U^{235}, we used $a = 0.173$ and $u^2 = 0.285$ for the ellipse and $u^2 = 0.32$ and $\alpha_4 = -0.043$ for the oval. It is interesting to note that the two nuclei should be assigned almost exactly the same shape.

can be "fitted into place" by a suitable choice of α_6 in formula (3.14), but such a procedure can hardly be meaningful. For illustration, we give in Table VIII the results of the computation with this optimum choice of α_4.

We note that the quadrupole moment Q_0 calculated for an elliptical nucleus with $\alpha_2 = 0.121$, is equal to 10×10^{-24}, in beautiful agreement with the data found for this region of the periodic table from experiments on coulomb excitation.[10]

In conclusion, Table IX gives numerically computed intensities for some α transitions in even-even nuclei. In the computations the nucleus was assumed to be elliptical, and the eccentricity was chosen to give closest possible agreement with experiment for the value of a_2/a_0. A striking feature is the increase in α_2 as we move away from the closed shell corresponding to lead, the passage through a maximum and the subsequent decrease of α_2 as we go toward heavier nuclei.

TABLE VIII. Intensities of α decay to successive rotational levels, for elliptical ($\alpha_2 = 0.121$, $\alpha_4 = 0.011$) and oval ($\alpha_2 = 0.142$, $\alpha_4 = -0.029$) shape of the nucleus (U^{236})

	Experimental data	Elliptical nucleus	Oval nucleus
a_2/a_0	0.57	0.57	0.57
a_4/a_0	0.035	0.063	0.035
a_6/a_0	0.0067	0.0024	0.00015

APPENDIX

We give a short derivation of the system of equations (2.3) and the boundary condition (2.5).

The wave function ψ of the decaying nucleus corresponds to a definite value of the total angular momentum I_0 (the spin of the decaying nucleus) and its projection M on the z axis of a fixed coordinate system, and depends on the radius vector $\mathbf{r}(r, \theta_\alpha, \varphi_\alpha)$ to the position of the α-particle in the laboratory system and the Euler angles $\Theta_i = \Theta, \Phi, \Psi$ which determine the orientation of the elongated nucleus:

$$\psi = \psi_{I_0 M}(r, \theta_\alpha, \varphi_\alpha, \Theta_i). \qquad (A.1)$$

We introduce a system of orthonormal functions $\Phi^{(Il)}_{I_0 MK}(\theta_\alpha, \varphi_\alpha, \Theta_i)$, which are eigenfunctions of:

TABLE IX. Intensities of α transitions in some even-even nuclei

Daughter nucleus	Decaying nucleus	u^2	α_2	a_2/a_0		$10\,(a_4/a_0)$		$10^3\,(a_6/a_0)$		$10^5\,(a_8/a_0)$	
				comp.	exp.	comp.	exp.	comp.	exp.	comp.	exp.
Cf^{250}	Fm^{254}	0.235	0.088	0.45	0.45	0.53	0.70	2.5		5	
Cm^{248}	Cf^{252}	0.226	0.094	0.41	0.41	0.40	0.50	1.4			
Cm^{242}	Cf^{246}	0.272	0.104	0.52	0.53	0.67	0.47	3	14	7	
Pu^{240}	Cm^{244}	0.291	0.113	0.52	0.55	0.60	0.13	3	8	5	
Pu^{238}	Cm^{242}	0.328	0.130	0.60	0.60	0.83	0.22	4.5	8	10	50
U^{238}	Pu^{242}	0.275	0.106	0.60	0.60	0.70		2.5		2	
U^{236}	Pu^{240}	0.330	0.121	0.57	0.57	0.63	0.35	2.5	6		
U^{234}	Pu^{238}	0.335	0.143	0.63	0.63	0.87	0.47	4	8	7	
Th^{226}	U^{230}	0.406	0.168	0.69	0.69	0.87	0.77	3		5	
Ra^{224}	Th^{228}	0.374	0.153	0.54	0.63	0.50	0.53	1		0.7	
Em^{218}	Ra^{222}	0.165	0.060	0.021	0.021	0.08		0.05			

(1) the angular momentum $\hat{\boldsymbol{l}}$ of the α particle with eigenvalue $l(l+1)$ (in the fixed system); (2) the angular momentum of the nucleus, $\hat{\mathbf{I}} = \hat{\mathbf{R}} + \eta_\zeta \hat{I}_0$, where $\mathbf{R}$ is the angular momentum of the rotation of the nucleus and η_ζ is a unit vector along the symmetry axis of the nucleus (eigenvalue $I(I+1)$); (3) the total angular momentum of the system $\hat{\mathbf{I}}_0 = \hat{\mathbf{I}} + \hat{\boldsymbol{l}}$ (eigenvalue $I_0(I_0+1)$): (4) the projection $\hat{I}_{0z}$ of the vector $\hat{\mathbf{I}}_0$ on the fixed z axis (value M); and (5) the projection $\hat{I}_\zeta$ of the vector $\hat{\mathbf{I}}$ on the symmetry axis η_ζ of the nucleus, $\hat{I}_\zeta = \eta_\zeta \cdot \hat{\mathbf{I}}$ (value K). It is not hard to show that these functions have the form

$$\Phi^{(Il)}_{I_0MK}(\theta_\alpha, \varphi_\alpha, \Theta_i) \qquad (A.2)$$
$$= \sum_{m=-l}^{l} C^{I_0M}_{lm;\, I,\, M-m}\, Y_{lm}(\theta_\alpha, \varphi_\alpha)\, \tilde{D}^{(I)}_{M-m,K}(\Theta_i).$$

Here the Y_{lm} are normalized spherical harmonics, while the $\tilde{D}^{(I)}_{MK}$ are the coefficients in the representation of the rotation group, normalized so that

$$\int \tilde{D}^{(I_2)*}_{M_2K_2} \tilde{D}^{(I_1)}_{M_1K_1}\, d(\cos\Theta)\, d\Phi d\Psi = \delta_{I_1I_2}\delta_{M_1M_2}\delta_{K_1K_2},$$

where

$$\tilde{D}^{(l)}_{0m}(\Theta, \Phi, \Psi) = \frac{1}{\sqrt{2\pi}} Y^*_{lm}\left(\Theta, \frac{\pi}{2} - \Phi\right);$$
$$\tilde{D}^{(l)}_{m0}(\Theta, \Phi, \Psi) = \frac{1}{\sqrt{2\pi}} Y_{lm}\left(\Theta, \Psi - \frac{\pi}{2}\right); \qquad (A.3)$$
$$Y_{lm}(\theta_\alpha, \varphi_\alpha) = \sum_{\Omega=-l}^{l} \sqrt{\frac{8\pi^2}{2l+1}}\, \tilde{D}^{(l)}_{m\Omega}(\Theta, \Phi, \Psi)\, Y_{l\Omega}(\theta, \varphi),$$

and θ, φ are the polar angles of the vector $\mathbf{r}_\alpha$ in the coordinate system fixed in the nucleus.

Substituting (A.3) in (A.2) and using the identity

$$\sqrt{\frac{8\pi^2}{2l+1}} \sum_{m=-l}^{l} C^{I_0M}_{lm;\, I,\, M-m}\, \tilde{D}^{(l)}_{m\Omega}(\Theta_i)\quad D^{(I)}_{M-m,\,K}(\Theta_i)$$
$$= \sqrt{\frac{2I+1}{2I_0+1}}\, C^{I_0,\,K+\Omega}_{l\Omega;\,IK} D^{(I_0)}_{M,\,K+\Omega}(\Theta_i),$$

we easily obtain $\Phi^{(Il)}_{I_0MK}$ an expression not in terms of $\theta_\alpha, \varphi_\alpha$, as in (A.2), but in terms of the angles θ and φ in the coordinate system fixed in the nucleus:

$$\Phi^{(I,\,l)}_{I_0MK} = \sqrt{\frac{2I+1}{2I_0+1}} \sum_{\Omega=-l}^{l} C^{I_0,\,K+\Omega}_{l\Omega;\,IK}\, \tilde{D}^{(I_0)}_{M;\,K+\Omega}\, Y_{l\Omega}(\theta, \varphi). \qquad (A.4)$$

We represent the wave function (A.1) by a series in the functions $\Phi^{(Il)}_{I_0MK}$ defined by either (A.2) or (A.4). The expansion coefficients F_{IlK} will be functions of r:

$$\psi_{I_0M} = \sum_{IlK} F_{IlK}(r)\, \Phi^{(Il)}_{I_0MK}(\theta_\alpha, \varphi_\alpha, \Theta_i). \qquad (A.5)$$

The function ψ_{I_0M} is a solution of the Schrodinger equation:

$$\left\{-\frac{\hbar^2}{2\mu}\nabla^2_\alpha + \frac{\hbar^2}{2\mathcal{J}}(\hat{R}^2_\zeta + \hat{R}^2_\eta) \right. \qquad (A.6)$$
$$\left. + \frac{\hbar^2}{2\mathcal{J}'}\hat{R}^2_\zeta + V(r, \theta)\right\}\psi_{I_0M} = E\psi_{I_0M}.$$

$\mathcal{J}'$ is the moment of inertia with respect to the nuclear symmetry axis, and $\mathcal{J}$ with respect to the perpendicular axis. We note that

$$\hat{R}_\zeta \Phi^{(Il)}_{I_0MK} = (\hat{\mathbf{I}} - \hat{\boldsymbol{\eta}}_\zeta \hat{I}_0)_\zeta\, \Phi^{(Il)}_{I_0MK}$$
$$= (\hat{I}_\zeta - I_0)\, \Phi^{(Il)}_{I_0MK} = (K - I_0)\, \Phi^{(Il)}_{I_0MK}.$$

If $\mathcal{J}' \to 0$, which is the only case we shall treat, the terms involving $\hat{R}^2_\zeta$ must be absent (since they give an infinite energy), from which it follows very easily that all terms with $K \neq I_0$ must be absent from (A.5). We should therefore set $F_{Il K} = r^{-1} f_{Il}(r)\, \delta_{KI_0}$, which gives

$$\psi_{I_0M} = \sum_{Il} \frac{f_{Il}(r)}{r}\, \Phi^{(Il)}_{I_0MI_0}(\theta_\alpha, \varphi_\alpha, \Theta_i). \qquad (A.7)$$

Formula (2.1) follows quickly from equation (A.7).

Writing $\hat{\mathbf{R}} = \hat{\mathbf{I}} - \eta_\zeta I_0$ and noting that $\hat{R}_\zeta \Phi^{(Il)}_{I_0MI_0} = 0$, we get

$$(\hat{R}^2_\xi + \hat{R}^2_\eta)\, \Phi^{(Il)}_{I_0MI_0} = \hat{\mathbf{R}}^2 \Phi^{(Il)}_{I_0MI_0}$$
$$= (\hat{I}^2 - I_0^2)\, \Phi^{(Il)}_{I_0MI_0} [I(I+1) - I_0^2]\, \Phi^{(Il)}_{I_0MI_0}.$$

Using this equality, substituting (A.7) in (A.6), we get, after multiplying by $\Phi^{(I'l')}_{I_0MI_0}$ and integrating over angles, the system of equations (2.3) for the functions f_{Il}, where

$$V_{Il I'l'}(r) = \frac{2\mu}{\hbar^2}\int \Phi^{(Il)*}_{I_0MI_0}\left[V(r, \theta) - \frac{2Ze^2}{r}\right]\Phi^{(I'l')}_{I_0MI_0}\, d\Omega\, d\Theta_i.$$

Let us expand the potential energy of interaction of the α particle with the nucleus in Legendre polynomials:

$$\frac{2\mu}{\hbar^2}\left[V(r, \theta) - \frac{2Ze^2}{r}\right] = \sum_{L=0}^{\infty} V_L(r)\, P_L(\mu), \quad \mu = \cos\theta,$$

and substitute this expression and (A.4) in the formula defining $V_{Il I'l'}(r)$. We then get expression (2.4) for the $V_{Il I'l'}$, where

$$Q_L(Il;\, I'l') = \int \Phi^{(Il)*}_{I_0MI_0} P_L \Phi^{(I'l')}_{I_0MI_0}\, d\Omega\, d\Theta_i = \frac{\sqrt{(2I+1)(2I'+1)}}{2I_0+1}$$
$$\times \sqrt{\frac{2l'+1}{2l+1}}\, C^{l0}_{L0;\,l'0} \sum_{\Omega} C^{I_0,\,I_0+\Omega}_{l'\Omega;\,I'I_0} C^{I_0,\,I_0+\Omega}_{l\Omega;\,II_0} C^{l\Omega}_{l'\Omega;L0}.$$

Summation over Ω using the well known formula of Racah[7] gives the value (2.4) for Q_L. Substitution of (A.4) in (A.7) gives

$$\psi_{I_0 M} = \sum_{I\Omega} \sqrt{\frac{2I+1}{2I_0+1}}\, C^{I_0, I_0+\Omega}_{I\Omega;\, II_0} \frac{f_{Il}(r)}{r}\, Y_{l\Omega}(\theta, \varphi)\, \tilde{D}^{(I_0)}_{M, I_0+\Omega}(\Theta_i). \quad (A.8)$$

On the nuclear surface, where $r = R(\theta)$, the wave function should not depend on φ. This will be the case only if, when we substitute $r = R(\theta)$ in (A.8), all terms in the sum over Ω except the term for $\Omega = 0$ vanish.

It then follows from (A.8) that at the nuclear surface

$$\psi_{I_0 M}[R(\theta), 0, \varphi; \Theta_i] = \chi(\theta)\, \tilde{D}^{(I_0)}_{MI_0}(\Theta_i), \quad (A.9)$$

where

$$\chi(\theta) = \sum_{Il} \sqrt{\frac{2I+1}{2I_0+1}}\, C^{II_0}_{l0;\, II_0} \frac{f_{Il}[R(\theta)]}{R(\theta)}\, Y_{l0}(\theta)$$

is some function of θ whose specific form will depend on the structure of the α-particle function in the interior of the nucleus. Substituting $r = R(\theta)$ in (A.8), equating the right sides of (A.8) and (A.9), multiplying both sides of the resulting equations by $\{\tilde{D}^{(I_0)}_{M, I_0+\Omega}(\Theta_i)\}^*$ and integrating over Θ_i, we get the boundary condition (2.5).

[1] J. O. Rasmussen and B. Segall, Phys. Rev. **103**, 1298 (1956).

[2] V. M. Strutinskii, J. Exptl. Theoret. Phys. (U.S.S.R.) **30**, 411 (1956), Soviet Phys. JETP **3**, 450 (1956).

[3] V. M. Strutinskii, J. Exptl. Theoret. Phys. (U.S.S.R.) **32**, 1412 (1957), Soviet Phys. JETP **5**, 1150 (1957).

[4] V. G. Nosov, Dokl. Akad. Nauk SSSR **112**, 414 (1957), Soviet Phys. "Doklady" **2**, 48 (1957).

[5] V. G. Nosov, J. Exptl. Theoret. Phys. (U.S.S.R.) **33**, 226 (1957), Soviet Phys. JETP **6**, 176 (1958).

[6] P. O. Fröman, Mat.-fys. Skrifter Kgl. Danske Videnskab. Selskab **1**, #3 (1957).

[7] G. Racah, Phys. Rev. **62**, 438 (1942).

[8] Gol'din, Novikova, and Tret'iakov, Izv. Akad. Nauk SSSR, Ser. Fiz. **20**, 868 (1956).

[9] L. D. Landau, Report to the 6th All-Union Conference on Nuclear Spectroscopy, Moscow, 1956.

[10] Alder, Bohr, Huus, Mottelson, and Winther, Revs. Modern Phys. **28**, 430 (1956).

Translated by M. Hamermesh
26

SOVIET PHYSICS JETP VOLUME 35 (8), NUMBER 1 JANUARY, 1959

PROPAGATION OF DETONATION WAVES IN THE PRESENCE OF A MAGNETIC FIELD

E. LARISH and I. SHEKHTMAN

Applied Mechanics Institute, Academy of Sciences, Romanian People's Republic; Atomic Physics Institute, Academy of Sciences, Romanian People's Republic

Submitted to JETP editor February 13, 1958

J. Exptl. Theoret. Phys. (U.S.S.R.) **35**, 203-207 (July, 1958)

It is shown that relativistic detonation waves in a magnetic field possess properties similar to those of the ordinary waves. Solutions of the equations at the discontinuity are presented for the relativistic and nonrelativistic cases.

SHOCK waves in a plasma situated in a magnetic field have been discussed frequently in recent times. In some of this work, for example that of Hoffman and Teller,[1] use was made of the relativistic hydrodynamic equations.

In the present article we consider "perpendicular" detonation waves, i.e., waves propagated at right angles to the direction of the magnetic field. One may expect that the influence of the magnetic field will become noticeable when its energy per unit mass of the medium becomes comparable with the energy liberated in the medium. The calculations are made in a relativistic manner, although for those thermonuclear fuels which are now known

and for fields which can be achieved at the present time there is no necessity to take relativistic effects into account. Nevertheless, a relativistic treatment is interesting because it indicates the behavior of the different quantities in the case of more powerful fuels and fields, and gives their limiting values.

1. EQUATIONS AT THE DISCONTINUITY

We now undertake the derivation of the relation between the physical parameters of the cold and of the burnt gas in a detonation wave, leaving aside for the time being the question of the structure of the wave.

We assume that the shock wave, which forms the front of the detonation wave, converts the medium into a plasma with infinite conductivity and with magnetic permeability $\mu = 1$. Moreover, we assume that the width of the wave is sufficiently large that we do not need to take losses into account.

The equations at the discontinuity express the continuity of the components of the energy-momentum tensor. In writing them down we should take into account the fact that the detonation energy is obtained at the expense of converting a certain fraction (α) of the rest mass of the initial gas. In the reference system in which the wave is at rest, they have the following form:

$$\rho_1 v_1/\gamma_1 = \rho_2 v_2/\gamma_2 (1-\alpha) = j, \tag{1}$$

$$\gamma_1^{-2}\left[\left(e_1 + \frac{H_1^2}{2}\right)\frac{v_1^2}{c^2} + p_1 + \frac{H_1^2}{2}\right] = \gamma_2^{-2}\left[\left(e_2 + \frac{H_2^2}{2}\right)\frac{v_2^2}{c^2} + p_2 + \frac{H_2^2}{2}\right], \tag{2a}$$

$$\frac{v_1}{c\gamma_1^2}\left[e_1 + \frac{H_1^2}{2} + p_1 + \frac{H_1^2}{2}\right] = \frac{v_2}{c\gamma_2^2}\left[e_2 + \frac{H_2^2}{2} + p_2 + \frac{H_2^2}{2}\right], \tag{3a}$$

$$H_1/\rho_1 = H_2/\rho_2 (1-\alpha), \quad \gamma = \sqrt{1-v^2/c^2}. \tag{4}$$

Here p is the pressure, $\sqrt{4\pi}$ H is the intensity of the magnetic field, e the internal energy per unit volume in the proper reference system, v the velocity of the medium, c the velocity of light, ρ the rest-mass density in the proper reference system (the one associated with the gas), and j the flux density of the rest mass. Equation (1) expresses conservation of rest mass, (2a) the continuity of the momentum flux, (3a) conservation of energy, and (4) expresses continuity of the field. Equation (4) is valid in virtue of the assumed infinite conductivity of the plasma, and expresses the "freezing" of the lines of force into the medium.

Let us reduce these equations to a more usual form by introducing the quantities

$$p^* = p + H^2/2, \qquad w^* = e + p + H^2. \tag{5}$$

On calculating v and γ from (1), and on substituting these expressions into (2a), we obtain

$$p_2^* - p_1^* = -(j/c)^2 [w_2^*(1-\alpha)/\rho_2^2 - w_1^*/\rho_1^2]. \tag{2}$$

Repeating the same calculations with respect to (3a), we obtain the equation for the detonation adiabatic

$$p_2^* - p_1^* = \frac{(1-\alpha)^2 w_2^{*3}/\rho_2^2 - w_1^{*3}/\rho_1^2}{(1-\alpha)^2 w_2^{*2}/\rho_2^2 + w_1^{*2}/\rho_1^2}. \tag{3}$$

To Eqs. (1) to (4) one should also add the equation of state, which can be written in the form

$$w^* = w^*(p^*, \rho, H_1). \tag{6}$$

2. THE JOUGUET POINT

Equations (1) to (6) form a complete system of equations at the discontinuity. In order to solve it we must also give one further additional relation, which must be found from the boundary conditions. As is well known, the latter lead often (e.g. in the case of spontaneous detonation) to the fact that the detonation wave is propagated with the least possible velocity. The system then corresponds to the so called Jouguet point on the detonation adiabatic.

We can derive certain general relationships which hold at the Jouguet point. To do this, we shall utilize the method given by Zel'dovich. It is well known that the usual detonation wave consists of two regions: of a shock wave of not very great width in which the material is heated to the required temperature, and of a considerably more extensive zone of combustion. In such a case Eq. (2) is valid for all the intermediate states if α is assumed variable.

In the case of stronger detonation waves, a strict separation into a shock wave and into a combustion zone loses its meaning. Combustion begins inside the shock wave, which is considerably broadened by ordinary and radiant thermal conductivity and by slow establishment of equilibrium between electrons and ions. By utilizing the schematic representations of the structure of the shock wave developed by Zel'dovich[2] and Shafranov,[3] we can represent the detonation wave in the form shown in Fig. 1.

Within the region $1-1'$ a gradual heating of the gas takes place owing to the thermal conductivity and to the slowing down in the gas of un-

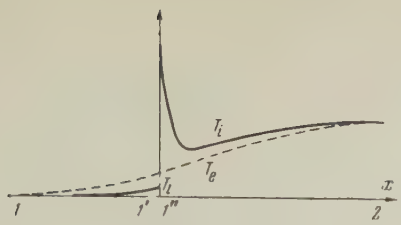

FIG. 1

charged particles formed during combustion. Between 1′ and 1″ the ionic (and, possibly, also the electronic) temperature undergoes a sharp discontinuity. Combustion, the establishment of electron-ion equilibrium, and the slowing down of uncharged particles occur simultaneously in the region $1''-2$.

In order that the following arguments be valid, it is necessary that combustion should be the slowest of all these processes, for otherwise it would be continued in the region in which energy is absorbed. The final state for the shock adiabatic is the state 1″, in which the combustion starts. This adiabatic is situated below the detonation adiabatic. In order to find it, we must generally solve the whole problem of the structure of the wave.

We shall represent the state of the gas on the plane $(p^*, (1-\alpha)^2\omega^*/\rho^2)$. In this plane the detonation adiabatic is determined by Eq. (3). As may be seen from Eq. (2), the detonation process is represented in this plane by a straight line passing through the point 1 (cf. Fig. 2) situated

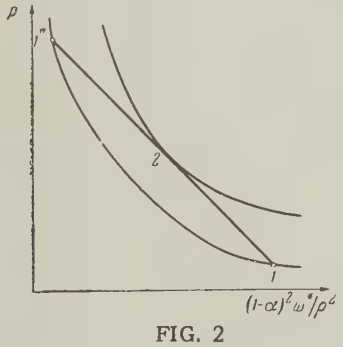

FIG. 2

on the shock adiabatic and intersecting the detonation adiabatic. A displacement along the segment $1-1''$ corresponds to the shock wave. Combustion is represented by the segment $1''-2$. The speed of the wave is determined by the slope of this straight line. The wave with the minimum speed corresponds to the tangent to the detonation adiabatic constructed at the point 1; the point of tangency is the Jouguet point. As is well known, the part of the adiabatic below this point has no physical meaning.

On differentiating (2) and (3), and on taking into account the identity

$$d(w^*/\rho) = dp^*/\rho + Tds \tag{7}$$

(s is the entropy per unit rest mass), we obtain the following relation:

$$\left[\frac{(1-\alpha)^2 w_2^*}{\rho_2^2} - \frac{w_1^*}{\rho_1^2}\right]^2 \frac{dj^2}{c^2} = 2(1-\alpha)^2 \frac{w_2^*}{\rho_2} T_2 ds_2. \tag{8}$$

From this we see that at the Jouguet point, where dj = 0, we must have

$$ds_2 = 0. \tag{9}$$

From Eq. (3) we now obtain the flux

$$\frac{j^2}{c^2} = -\frac{1}{(1-\alpha)^2}\left[\frac{\partial p_2^*}{\partial (w_2^*/\rho_2^2)}\right]_s. \tag{10}$$

This relation gives us immediately

$$v_2^2/c^2 = (\partial p_2^*/\partial e_2^*)_s. \tag{11}$$

The derivative should be taken after replacing H_2 by its value from Eq. (4).

As is well known, $c(\partial\rho/\partial e)_s^{1/2}$ is the relativistic expression for the speed of sound. The right-hand side of (11) is the speed of sound in the magnetic field. We obtain the usual result: the wave moves over the detonation products with the speed of sound.

3. SOLUTION OF THE EQUATIONS

For a definite detonation process we know the parameter α, the thermodynamic state of the gas 1, and the magnetic field H_1. To be able to find the remaining quantities, we must express explicitly thermodynamic functions for the detonation products. We give below the solution of Eqs. (1) to (4) and (6) for the detonation wave which corresponds to the Jouguet point in the case when the detonation products may be regarded as an ideal gas.

For a relativistic ideal gas the following equation of state remains valid

$$p = \rho RT = \rho c^2 \sigma, \tag{12}$$

where $\sigma = RT/c^2$. The heat function has the form

$$w = \rho c^2 g(\sigma)$$

and the speed of sound is given by

$$a = c\left[\frac{H^2/\rho c^2 + f(\sigma)}{H^2/\rho c^2 + g(\sigma)}\right]^{1/2}$$

We introduce the dimensionless variables

$$R = \rho_2/(1-\alpha)\alpha_1, \quad h = H_1^2/\rho_1 c^2 \tag{13}$$

The functions $f(\sigma)$ and $g(\sigma)$ which depend on the kind of gas have, generally speaking, a fairly complicated form for a gas heated to tem-

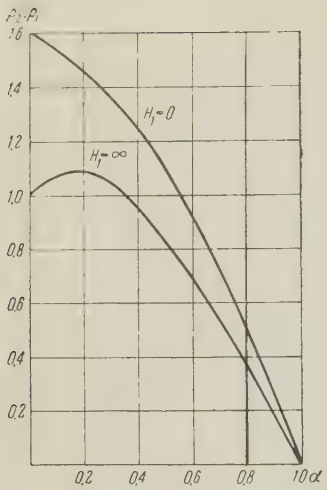

FIG. 3

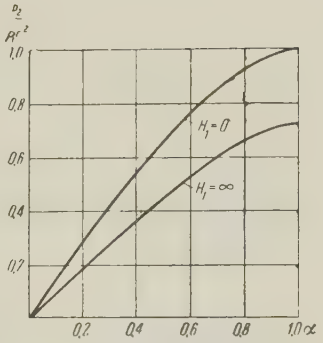

FIG. 4

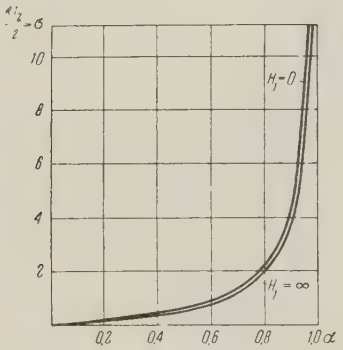

FIG. 5

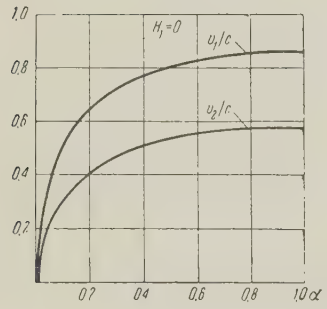

FIG. 6

peratures at which relativistic effects come into play (for the electronic component of the gas this occurs at $T \sim 10^{9}$°K). It is therefore convenient to express the solution of the system of equations in parametric form (the parameters are R and σ). It may be written down in the form of a quadratic equation for h:

$$h^2[-3R^2+2(3g-f)R+2(g-f)(\sigma-g)-g^2]+h[-2R^2+(3g-4f)R+4gf+4\sigma(g-f)-g^3/R]+2[-fR+gf+\sigma(g-f)]=0 \quad (14)$$

and of the equation

$$\frac{1}{1-\alpha^2}=(g+hR)^2-\frac{hR+f}{g-f}\,\frac{R-g}{(1+h)^2}\,[g+(2h+1)R]. \quad (15)$$

The results of sample numerical calculations are shown in Figs. 3 to 6.

4. THE NONRELATIVISTIC CASE

We shall examine in greater detail the case when the energy liberated and the energy of the magnetic field are both low in comparison with the energy of the gas. We may set in Eqs. (1) to (4) and (6)

$$v_1/c \ll 1; \quad v_2/c \ll 1; \quad \alpha \ll 1; \quad (16)$$

$$H_1^2/\rho_1 c^2 \ll 1; \quad \alpha\rho_1 c^2 = q; \quad w \to \rho c^2 + w.$$

Here q denotes the quantity of heat liberated per unit mass, while the nonrelativistic heat function

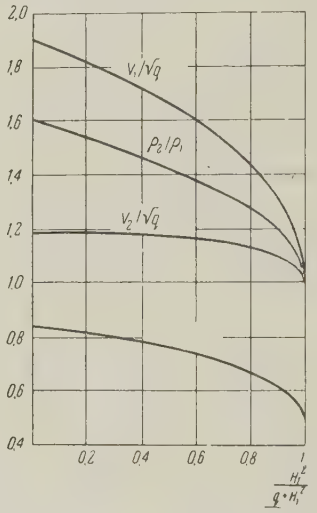

FIG. 7. The lower curve corresponds to RT_2/q.

is denoted by the same letter w. The system (1) to (4) and (6) now assumes the usual form:

$$\rho_1 v_1 = \rho_2 v_2, \quad p_1+\rho_1 v_1^2+H_1^2/2 = p_2+\rho_2 v_2^2+H_2^2/2,$$
$$q+w_1+v_1^2/2+H_1^2/\rho_1 = w_2+v_2^2/2+H_2^2/\rho_2, \quad H_1/\rho_1 = H_2/\rho_2. \quad (17)$$

The speed of sound is given by

$$v_2 = (\varkappa p_2/\rho_2 + H_2^2/\rho_2)^{1/2}. \quad (18)$$

For those cases which are of interest in connection with the foregoing, the detonation can always be regarded as strong, i.e., we can set $p_1 = w_1 = 0$. Moreover, we shall assume that the product of detonation is an ideal gas.

We introduce the dimensionless variables

$$\rho_2 = \rho_1 R_2, \quad v_1 = \sqrt{q}V_1, \quad v_2 = \sqrt{q}V_2,$$
$$H_1^2 = \rho_1 q h_1, \quad H_2^2 = \rho_2 q h_2, \quad p_2 = \rho_2 q z_2.$$

The solution may be given in parametric form (parameter R_2):

$$\frac{1}{h_1} = \frac{[1-(2-\varkappa)R_2^2(1-R_2)]\,[(\varkappa/2)(1-R_2^2)+\varkappa/(\varkappa-1)]}{2R_2[\varkappa(1-R_2)+1]} + \frac{2-\varkappa}{4}R_2(1-R_2^2) - \frac{2-\varkappa}{2(\varkappa-1)}R_2 - 1; \quad (19)$$

$$z_2 = h_1[1-(2-\varkappa)R_2^2(1-R_2)]/2R_2[\varkappa(1-R_2)+1];$$

$$V_2^2 = \varkappa z_2 + \frac{2-\varkappa}{2}h_1R_2, \quad V_1 = R_2V_2,$$

where $\varkappa$ is the adiabatic coefficient. This solution is given in Fig. 7 for $\varkappa = 5/3$.

[1] G. Hoffman and E. Teller, Phys. Rev. **80**, 692 (1950).

[2] Ia. B. Zel'dovich, J. Exptl. Theoret. Phys. (U.S.S.R.) **32**, 1126 (1957), Soviet Phys. JETP **5**, 919 (1957).

[3] V. D. Shafranov, J. Exptl. Theoret. Phys. (U.S.S.R.) **32**, 1453 (1957), Soviet Phys. JETP **5**, 1183 (1957).

Translated by G. Volkoff
27

SOVIET PHYSICS JETP VOLUME 35 (8), NUMBER 1 JANUARY, 1959

A NONLINEAR THEORY OF VECTOR FIELDS

V. Iu. URBAKH

Institute of Biological Physics, Academy of Sciences, U.S.S.R.

Submitted to JETP editor February 17, 1958

J. Exptl. Theoret. Phys. (U.S.S.R.) **35**, 208-215 (July, 1958)

In analogy with Einstein's theory of gravitation, the existence of a physical vector field is treated as the curvature in a "non-Pythagorean" space whose metric is $ds = \gamma_i dx^i$. This leads to nonlinear field equations which in the linear approximation (for weak fields) become the usual equations. In spite of its potential being singular, the total energy in the field of a point charge is finite.

1. STATEMENT OF THE PROBLEM

As a rule, the nonlinear generalizations of field theories are constructed in an attempt to eliminate divergences in ordinary field theory. It is known, however, that this can be done also in other ways (nonlocal interactions, the use of higher drivatives, space quantization, etc.). Furthermore, one likes to hope that it is possible to go on without essentially leaving the framework of the existing theory. This would seem to be why the nonlinear theories do not receive wide recognition at present.

We wish to emphasize that a nonlinear generalization of field theory is necessary, independently of the divergences in the linear theory and independently of the possible necessity for other generalizations. Our argument is based on the following considerations.

(a) In principle, nonlinearity in field theory follows unavoidably from the fact of pair creation and annihilation, which leads to nonlinear effects such as scattering of light by light. It is not, therefore, merely accidental that when dealing with interactions in modern field theory we arrive at nonlinear equations. Nonlinearity whould therefore not be considered simply one of many possible methods for eliminating the difficulties of the theory, but as a reflection of the objective properties of the field.

(b) It is well known that in all nonlinear theories there appears a characteristic length which, although it has different meanings in different versions, is always of the order of magnitude of the "classical radius" $r_0 = e^2/m_0c^2$ of the field's source. This parameter serves as a criterion that can be used to define weak fields (with $r \gg r_0$) for which nonlinear effects can be neglected. It turns out that in electrodynamics all real processes take place in a region for which $r \gg r_0$ (weak fields and low energies), and the linear theory is insufficient only when one needs to consider virtual processes with arbitrary energies. The situation is different, however, where in mesodynamcs, weak fields (in the above sense

of the word) practically never exist. In this case the critical parameter will be $R_0 = g^2/M_0c^2$, where M_0 is the nucleon mass. If we take $g^2/hc \approx 14$ (as is presently believed), we obtain $R_0 \approx 3 \times 10^{-13}$ cm. But because the range of nuclear forces is so short that they practically vanish at a distance $\Lambda_\mu = h/\mu c \approx 1.4 \times 10^{-13}$ cm (where μ is the meson mass), there is essentially no field at $r > R_0$. Therefore the values of r equal to and less than Λ_μ, at which the field is measurably different from zero, lie entirely within a region whose radius is less than R_0, a region in which the linear theory is no longer applicable. This means that the Yukawa potential cannot serve as a first approximation, and this may be the cause of many of the difficulties in the meson theory of nuclear forces. It is important to see that it is not so much a matter of g^2/hc being greater than 1, but of R_0 being greater than Λ_μ (which is determined by the value of μ). It is not accidental, therefore, that an expansion in inverse powers of g^2/hc also fails. The difficulties in linear mesodynamics lie not in the fact that the nuclear interaction is strong, but that it is of such short range.

(c) It is thought that an important deficiency of nonlinear theories is that on the one hand, they are difficult to quantize, while on the other hand an unquantized (classical) nonlinear theory can hardly be of interest. This is because much before the nonlinear deviations become of importance (at distances of the order of the classical radius of the particle which is the source of the field), quantum effects begin to predominate (at distances of the order of the Compton wavelength of this particle). But this also is true only for electrodynamics, where $r_0/\lambda_0 = (e^2/m_0c^2)/(h/m_0c) = e^2/hc = 1/137$. In mesodynamics, on the other hand, $R_0/\Lambda_0 = (g^2/M_0c^2)(h/M_0c) = g^2/hc \approx 14$, so that progress in classical mesodynamics should indeed begin with the nonlinearities.

(d) In the special theory of relativity it becomes clear that Newtonian mechanics is good only if $v \ll c$ and must be generalized at high velocities. The general theory of relativity shows that mechanics must be generalized also for high accelerations, i.e., for large forces or intense fields (and this generalization leads to a nonlinear theory). But it has been shown by Fock[1] that Einstein's theory does not describe arbitrary accelerated motion, but only motion in the gravitational field. The theory therefore refers only to the gravitational field, and is not a general theory of noninertial motion. The problem then arises of performing analogous generalizations for other fields as well, in particular for the practically most important cases of the electromagnetic and meson fields.

At first glance such a statement of the problem (to the extent, at any rate, that it refers to the electromagnetic field) may seem confusing, since there already exists a very well known general relativistic covariant formulation of electrodynamics. This generalization, however, deals only with the gravitational field associated with the electromagnetic one, and leads, in particular, to a criterion of nonlinearity which is not e^2/m_0c^2, but $(e^2/m_0c^2)(\xi/e)$, where $\xi = m_0\sqrt{\kappa}$ is the gravitational charge. For this reason this generalization has little practical meaning. What we are discussing, on the other hand, is a generalization that makes electrodynamics itself nonlinear, without considering any other kinds of fields (even the gravitational). From this point of view, Einstein's theory (and, in particular, the geometrical methods he uses) should be thought of as a model for the construction of the nonlinear field theory, a model which, although it has been applied to a tensor (specifically, the gravitational) field, is one that can be used in attempts to construct a nonlinear theory also for vector, spinor, and other fields. In the present work, this will be done for a vector field,* and the first field treated will be the simple electromagnetic one (with zero rest mass, in quantum terms).

It may seem that a geometric treatment of the electromagnetic field is impossible even if only because this field produces in general different accelerations in different bodies, so that one cannot formulate an equivalence principle. Also, one may point out that the four components of the electromagnetic potential are insufficient for a generalization of the Pythagorean theorem, since they cannot be identified with the components of a metric tensor.

These difficulties can, however, be overcome.

(a) If we admit to "Einstein's elevator" only those bodies whose charge-to-mass ratio (specific charge) e/m_0 has a given fixed value, the situation arising for these bodies is the same as in the theory of gravitation, since by a suitable coordinate change the external field can be eliminated and the desired relations obtained. For any other group of bodies with another specific charge, we obtain (formally) the same relations. The specific charge will enter only in the form of a parameter (replacing the gravitational constant in the gravitational equations). Such a device has

*A preliminary version has already been published.[2]

already been used by other authors, for instance by Rumer.[3]

(b) The four-component electromagnetic field can be treated geometrically by associating with it a "non-Pythagorean" four-space, whose metric is given by four functions making up a four-vector, so that the line element in this space is given in terms of increments in the coordinates by the equation

$$ds = \gamma_i dx^i, \quad i = 1, 2, 3, 4, \tag{1}$$

where $dx^4 = ic\,dt$. This "space" is simply a model; so far it is in no way related to any physical space, and is merely an accessory similar to the n-dimensional space of statistical mechanics or "isotopic spin space."

A non-Pythagorean metric such as (1) has been used before. It was first introduced by Fock and Ivanenko[4] and was later analyzed in detail by Mirura et al.[5] More recently it has been studied by Flint and Williamson.[6] In all these works, however, the γ_i were treated as modifications of the Dirac matrices and were used to generalize the Dirac equation, mostly in order to account for the gravitational field, so that it was assumed that $\gamma_i\gamma_k + \gamma_k\gamma_i = 2g_{ik}$.

Here we propose an entirely different problem, namely that of studying the field γ_i itself. With this field we associate a definite physical field whose equations we wish to find.

2. CURVED "NON-PYTHAGOREAN" SPACE

A construction of a curved non-Pythagorean space whose metric is given by $ds = \gamma_i dx^i$ has already been given.[2] In particular, the following expressions were obtained.

(a) The equation of a geodesic is

$$d^2x^i/ds^2 + \Gamma^i_k dx^k/ds = 0; \tag{2}$$

(b) The action function is

$$\mathscr{L} = \text{const}\,\Gamma_{im}\Gamma^{im}, \tag{3}$$

(c) The energy-momentum tensor is

$$\mathscr{T}^{ik} = \mathscr{T}^i_s b^{sk} = \text{const}'\,(\Gamma_{sn}\Gamma^{in} - \tfrac{1}{4} b^i_s \Gamma_{mn}\Gamma^{mn})\, b^{sk}, \tag{4}$$

with

$$\Gamma^i_k = \Gamma_{km} b^{mi}, \quad \Gamma^{im} = \Gamma_{kn} b^{ik} b^{mn},$$

$$\Gamma_{ik} = \partial\gamma_k/\partial x^i - \partial\gamma_i/\partial x^k = -\Gamma_{ki},$$

$$b_{ik} = \tfrac{1}{2}(\gamma_i\gamma_k + \gamma_k\gamma_i) = b_{ki}, \quad b^{ik} = \tfrac{1}{2}(\gamma^i\gamma^k + \gamma^k\gamma^i) = b^{ki},$$

$$\gamma^i = b^{ik}\gamma_k, \quad \gamma_i = \alpha_i + h_i,$$

where the α_i are Dirac matrices, and the h_i are c-number increments which give the deviation of the space from Euclidean.

In addition, we have the relations

$$b^{il}b_{kl} = b^i_k = \delta^i_k; \tag{5}$$

$$\partial\Gamma_{kl}/\partial x^n + \partial\Gamma_{ln}/\partial x^k + \partial\Gamma_{nk}/\partial x^l = 0. \tag{6}$$

The generalization given by Eq. (3) of the Maxwell Lagrangian

$$L_0 = -F_{im}F_{im}/16\pi \tag{7}$$

follows obviously from the concepts described at the start: the Lagrangian should be invariant in the non-Euclidean space defined by the metric (1).

Thus the geometric interpretation can be used to unite the formalism of electrodynamics in the "general theory of relativity" with the well known idea of Mie. In the expression $F^{ik} = F_{mn}g^{im}g^{kn}$ we make the substitution $g_{ik} \to b_{ik} = \tfrac{1}{2}(\gamma_i\gamma_k + \gamma_k\gamma_i)$, where $\gamma_i = \alpha_i + \xi A_i$, so that we obtain, in agreement with Mie, a tensor of the form $H^{ik} = u^{ik}(F_{mn}, A_l)$, and, as must occur in his scheme,

$$\Gamma^{im} = \text{const}\,(\partial\mathscr{L}/\partial\Gamma_{im}).$$

Roughly speaking, what happens is that the action of the gravitational field on the electromagnetic one is replaced by the electromagnetic field acting on itself.

The fact that the Lagrangian of Eq. (3) contains the field potentials explicitly (in terms of the b^{ik}) might seem to be a contradiction in our theory, which then is no longer gauge invariant. But it is known that Einstein's theory of gravitation also has this property, and this is never considered a defect. The fact is that a direct relation between gauge invariance of the field equations and the zero rest mass of the quanta associated with this field is necessary only in a linear theory. Thus all we can demand from a nonlinear theory is that the equations be gauge invariant in linear approximation. Our theory satisfies this condition, since in the linear approximation the Lagrangian of Eq. (3) becomes the Maxwell Lagrangian of Eq. (7).

3. THE ELECTROMAGNETIC FIELD

Let us base the theory of the electromagnetic field on Eqs. (2), (6), (3), and (4). It is clear that the expressions entering into these equations are matrix expressions. They can therefore be treated as operators in some function space, and the "ordinary" expressions (for instance the Lagrangian and the components of the energy momentum tensor) can be treated as sort of "mean values" given by relations of the form

$$L = {}^{t}\text{Sp}\,\mathscr{L}. \tag{8}$$

These then establish the relation between subsidiary ("matrix") space of Eq. (1) and "ordinary" Riemannian space.*

In addition, we must yet establish the relation between the Γ_{im} from the nonlinear theory and the F_{im} from the linear one, as well as find the constants in Eqs. (3) and (4).

For a weak field, the geodesic equation (2) gives

$$\dot{u}_i \approx c\Gamma_{ik}u_k,$$

since $b^{mi} \approx b_0^{mi} = \delta^{mi}$, and $ds = c\,d\tau$. Comparing this with the Lorentz formula

$$m_0\dot{u}_i = \frac{e}{c}F_{ik}u_k$$

and noting that $\gamma_i = \gamma_i^0 + h_i = \alpha_i + h_i$, we have

$$h_i = (e/m_0c^2)A_i. \tag{9}$$

Similarly

$$L \approx \text{const}\,\Gamma_{im}\Gamma_{im} = \text{const}\,(e/m_0c^2)^2F_{im}F_{im},$$

so that comparing with (7), we have

$$\mathscr{L} = -(1/16\pi)(m_0c^2/e)^2\Gamma_{im}\Gamma_{kn}b^{ik}b^{mn}. \tag{10}$$

Similarly, we obtain

$$\mathscr{T}^{ik} = -\frac{1}{4\pi}\left(\frac{m_0c^2}{e}\right)^2\left(\Gamma_{sn}\Gamma^{in} - \frac{1}{4}\Gamma_{mn}\Gamma^{mn}\right)b^{sk}. \tag{11}$$

Here e and m_0 are the charge and rest mass of a test body. It should be noted that the properties of the test body enter into our theory in a very important way, since they give the criterion of smallness (and therefore nonlinearity) of the field. According to this criterion the field may be considered weak (and described with sufficient accuracy by the linear theory) if the energy of the charge in this field is much less than the self-energy of the charged body, that is if $e\varphi \ll m_0c^2$ or $h \ll 1$.

It is a well known fact that no such test body enters into the theory of gravitation, and that the limit of applicability of the linear approximation to the gravitational field is the same for all test bodies and is uniquely determined by the field "strength" at the given point (for a static spherically symmetric field this is the ratio of the gravitational radius $\kappa M/c^2$ of a source of mass M to the length of the radius vector at the given point). In other words, no test-body parameters enter into the solution of the field equations. This is related to the fact that the gravitational charge of any body is proportional to its mass (with the same coefficient of proportionality for all bodies), so that $(\xi/m_0c^2)^2 = (m_0\sqrt{\kappa}/m_0c^2)^2 = \kappa/c^4$, which does not involve the test body. The fact that the test-body parameters enter into the solution of the field equations in the nonlinear theory of the electromagnetic field was pointed out at the very start when we spoke of using an equivalence principle in this theory.

To obtain and solve the field equations for the general case involves great mathematical difficulties. It is therefore useful to consider the simple but important special case of a static spherically-symmetric field. In this case we may attempt to find a solution of the form $h_\mu = 0$ (for $\mu = 1$, 2, or 3), and $h_4 = ih \neq 0$. Then all the $\Gamma_{\mu\nu} = 0$, and $\Gamma_{\mu 4} = -\Gamma_{4\mu} = \partial h_4/\partial x^\mu$, so that

$$\mathscr{L} = \Gamma_{im}\Gamma^{im} = \Gamma_{im}\Gamma_{kn}b^{ik}b^{mn} = 2\frac{\partial h_4}{\partial x^\mu}\frac{\partial h_4}{\partial x^\nu}(b^{\mu\nu}b^{44} - b^{\mu 4}b^{\nu 4}). \tag{12}$$

Since

$$b_{ik} = \delta_{ik} + \alpha_ih_k + \alpha_kh_i + h_ih_k,$$

we have

$$b_{\mu\nu} = \delta_{\mu\nu},\ b_{\mu 4} = \alpha_\mu h_4,\ b_{44} = 1 + 2\alpha_4h_4 + h_4^2.$$

Using the relation $b^{ik}b_{kl} = \delta_l^i$, which gives ten equations for the ten desired b^{ik}, we arrive at

$$b^{\mu\mu} = 1 + h_4^2\frac{g}{H} + \frac{2h_4^3}{H}\alpha_4,\ b^{44} = \frac{g}{H} - \frac{2h_4}{H}\alpha_4,$$

$$b^{\mu\nu} = h_4^2\frac{g}{H}\alpha_\mu\alpha_\nu + (-1)^\lambda\frac{2h_4^3}{H}\alpha_5\alpha_\lambda,\ \nu \neq \mu,\ \lambda \neq \mu,\ \nu, \tag{13}$$

$$b^{\mu 4} = -h_4\frac{g}{H}\alpha_\mu + \frac{2h_4^2}{H}\alpha_\mu\alpha_4,$$

where $g = 1 - 2h_4^2$, and $H = 1 - 8h_4^2 + 4h_4^4$.

From this it follows immediately that

$$\text{Sp}\,(b^{\mu\nu}b^{44} - b^{\mu 4}b^{\nu 4}) = 0\ (\mu \neq \nu), \tag{14}$$

and

$$\text{Sp}\,(b^{\mu\mu}b^{44} - b^{\mu 4}b^{\mu 4}) = 4g/H, \tag{15}$$

since the trace of all the α_i and products of different α_i vanishes.

Thus

$$L = \text{const}\,(\nabla h_4)^2g/H, \tag{16}$$

so that in agreement with the usual expressions

$$\frac{\delta L}{\delta h_i} = \frac{\partial L}{\partial h_i} - \frac{\partial}{\partial x^k}\frac{\partial L}{\partial(\partial h_i/\partial x^k)} = 0$$

we obtain the field equation in the form

$$\nabla^2h_4 + \frac{1}{2}(\nabla h_4)^2\frac{(\partial/\partial h_4)(g/H)}{g/H} = 0$$

or

$$h'' + \frac{2}{r}h' + \frac{1}{2}(h')^2\frac{\partial \ln(g/H)}{\partial h} = 0, \tag{17}$$

*This idea is due to E. S. Fradkin.

where $g = 1 + 2h^2$, and $H = 1 + 8h^2 + 4h^4$, since $h_4 = ih$.

Integration gives

$$\int \left[\frac{1+2h^2}{1+8h^2+4h^4}\right]^{1/2} dh = \frac{C}{r} + C_1. \qquad (18)$$

Further calculations are difficult, since it is necessary not only to write the elliptical integral on the left as an explicit function of h, but to find the inverse function $h = h(r)$.

It is therefore convenient to obtain an approximate but simple solution, writing

$$\left[\frac{1+2h^2}{1+8h^2+4h^4}\right]^{1/2} \approx \left[\frac{1+2h^2}{1+4h^2+4h^4}\right]^{1/2} = (1+2h^2)^{-1/2}. \qquad (19)$$

It should be noted that the difference between the approximate answer and the exact one increases neither as $h \to 0$, nor as $h \to \infty$. On the contrary, in these limits this difference vanishes, and is as large as about 20 percent only in a small interval about $h \approx 1$.

With (19), the solution of (18) becomes

$$\int dh / \sqrt{1+2h^2} = \frac{C}{r} + C_1$$

or

$$\frac{1}{\sqrt{2}} \sinh^{-1}(\sqrt{2}\, h) = \frac{C}{r} + C_1.$$

Since in the linear approximation we must have $h = r_0/r$, where $r_0 = e^2/m_0c^2$, we have $C = r_0$ and $C_1 = 0$, so that finally

$$\sinh^{-1}(\sqrt{2}\, h) = \sqrt{2}\, r_0/r,$$

whence

$$h = \sinh(\sqrt{2}\, r_0/r)/\sqrt{2}, \qquad (20)$$

$$\varphi = (e/r_0\sqrt{2}) \sinh(r_0\sqrt{2}/r). \qquad (21)$$

As r approaches 0, the potential starts increasing very rapidly at a distance of the order of r_0, so that one may say that two colliding electrons behave like solid spheres of radius r_0. For $r \gg r_0$, we obtain the usual Coulomb potential. In the second approximation, we have

$$\varphi \approx (e/r)(1 + r_0^2/3r^2);$$

so that the correction for the first Bohr orbit ($r = a_0 = h^2/me^2$) is of the order of α^4, where $\alpha = e^2/hc$.

Although the potential of (21) has a high singularity at $r = 0$, for $r > r_0$ stable orbits are possible. This can be seen using the virial theorem, according to which if periodic motion is to take place, then $\overline{E} < 0$, where $\overline{E} = \overline{T} + \overline{V} = \frac{1}{2} r\overline{V}' + \overline{V}$.

In our case we have

$$V = -\frac{e}{r_0\sqrt{2}} \sinh\frac{r_0\sqrt{2}}{r}, \quad V' = \frac{e}{r^2}\cosh\frac{r_0\sqrt{2}}{r},$$

so that

$$E = \frac{e}{r_0\sqrt{2}}\cosh\frac{r_0\sqrt{2}}{r}\left(\frac{1}{2}\frac{r_0\sqrt{2}}{r} - \tanh\frac{r_0\sqrt{2}}{r}\right)$$

$$= \frac{e}{r_0\sqrt{2}}\cosh x\left(\frac{x}{2} - \tanh x\right),$$

where $x = r_0\sqrt{2}/r$. Since $\tanh x > x/2$ for $x \lesssim 2$, and since $(e/r_0)\cosh x > 0$, it follows that $\overline{E} < 0$ for all $r > \sqrt{2}\, r_0/2$, or almost always.

The potential of (21) can now be used to calculate the total energy of the electromagnetic field of the electron. In our case of a static spherically symmetric potential ($h_\alpha = 0$, $\partial h_i/\partial x^4 = 0$), we obtain

$$T^{44} = -\frac{1}{4\pi}\left(\frac{m_0c^2}{e}\right)^2 \frac{1}{2}\Gamma_{\mu 4}\Gamma_{\nu 4}\frac{1}{4}\,\mathrm{Sp}\,\{(b^{\mu\nu}b^{44} - b^{\mu 4}b^{\nu 4})\, b^{44}\}$$

$$= -(e^2/8\pi r_0^2)(h')^2(1+4h^4)/(1+8h^2+4h^4)^2;$$

so that

$$m = -\frac{1}{ic}P^4 = \frac{1}{c^2}\int_0^\infty T^{44}d\tau = \frac{e^2}{2\sqrt{2}\, r_0c^2}J,$$

where

$$J = \int_0^\infty \frac{\cosh^2 x\,(\cosh^4 x - 2\sinh^2 bx)}{(\cosh^4 x + 2\sinh^2 x)^2}dx \approx 1,$$

or

$$m \approx m_0/2\sqrt{2}. \qquad (22)$$

In spite of the highly singular potential given by (21), the total energy of the field is finite.

It follows from (22) that in the given theory the classical electromagnetic electron mass is only part of the total electron mass (the question of the "bare" mass remains open) so that the condition of Laue's theorem ($\int T^{ik}d\tau = 0$ for all components except T^{44}) is naturally not fulfilled in this case. This is not a defect in the theory, but speaks in its favor, since certain phenomena (such as electron production in μ-meson decay) indicate that the electron has some elements in common with other "elementary" particles. In addition, we must yet "leave room" for the quantum ("transverse") mass (this quantity will be calculated later; it is also found to be finite and of the correct order of magnitude αm_0).

[1] V. A. Fock, Теория пространства, времени и тяготения (Theory of Space, Time and Gravity). GITTL, M., 1955.

[2] V. Iu. Urbakh, Dokl. Akad. Nauk SSSR **101**, 1043 (1955).
[3] Iu. B. Rumer, Исследования по 5-оптике (Investigations in 5-Optics) GITTL, M., 1956.
[4] W. A. Fock and D. D. Iwanenko, Z. Physik **54**, 798 (1929).
[5] Mimura, Morinaga, Takeno, et al., J. Sci. Hiroshima Univ., Series **A5**, 99, 151, 205 (1935); **6**, 103 (1936); **7**, 39, 81 (1937).
[6] H. T. Flint and E. M. Williamson, Z. Physik **135**, 260 (1953).

Translated by E. J. Saletan
28

SOVIET PHYSICS JETP VOLUME 35 (8), NUMBER 1 JANUARY, 1959

THEORY OF THE ANISOTROPY OF THE WIDTH OF FERROMAGNETIC RESONANCE ABSORPTION LINE

G. V. SKROTSKII and L. V. KURBATOV

Ural Polytechnic Institute

Submitted to JETP editor February 19, 1958

J. Exptl. Theoret. Phys. (U.S.S.R.) **35**, 216-220 (July, 1958)

The dependence of the width of a resonance absorption line on the internal field is found from the Landau-Lifshitz equations. Specific examples of ferrites with single-axis and cubic symmetry are considered.

1. The width of a radio-frequency resonance absorption line, considering only spin-spin relaxation, can be described with the equation[1,2]

$$\dot{\mathbf{M}} = \gamma[\mathbf{M}\times\mathbf{H}] - \frac{1}{\tau}(\mathbf{M} - \chi_0\mathbf{H}), \qquad (1)$$

where χ_0 is the equilibrium susceptibility, and $M = \chi_0 H_M$. In the case of weak radio-frequency fields, when $|h| \ll H_M$, this equation leads to a Lorentzian line shape. When applied to ferromagnets, however, χ_0 is no longer constant. The magnitude of χ_0 can be deduced from Eq. (1), assuming a constant magnitude for the vector $\mathbf{M}$. Then

$$\chi_0 = M^2/(\mathbf{M}\cdot\mathbf{H})$$

and

$$\dot{\mathbf{M}} = \gamma[\mathbf{M}\times\mathbf{H}] - \lambda M^{-2}[\mathbf{M}\times[\mathbf{M}\times\mathbf{H}]], \qquad (2)$$

where $\lambda = \chi_0/\tau$.

The Landau-Lifshitz equation (2), in which the magnitude of the magnetization vector $\mathbf{M}$ is constant, is conveniently expressed in polar coordinates, where the orientation of the vector $\mathbf{M}$ is given by its polar angle ϑ and its azimuthal angle φ. Introducing the radial, polar, and azimuthal components of the field, H_M, H_ϑ, and H_φ, Eq. (2) becomes

$$\dot{\vartheta} = -\gamma(H_\varphi - \alpha H_\vartheta), \quad \dot{\varphi}\sin\vartheta = \gamma(H_\vartheta + \alpha H_\varphi), \qquad (3)$$

where a dimensionless attenuation parameter $\alpha = \lambda/\gamma M$ has been introduced.

Analogously, Eq. (1) becomes in spherical coordinates

$$\dot{M} = \frac{1}{\tau}(\chi_0 H_M - M), \qquad (4)$$

$$\dot{\vartheta} = \frac{\chi_0}{M\tau}H_\vartheta - \gamma H_\varphi, \quad \dot{\varphi}\sin\vartheta = \frac{\chi_0}{M\tau}H_\varphi + \gamma H_\vartheta. \qquad (5)$$

When $M = \text{const.}$, with $\chi_0 = \alpha\gamma M\tau$, these equations reduce to Eqs. (3).

2. In a state of thermodynamic equilibrium the direction of the magnetization vector $\mathbf{M}$ in a ferromagnet coincides with the direction of the effective internal field $\mathbf{H}_M$, whose magnitude in turn can be found using the free energy F:

$$H_M = -F_M \equiv -\partial F/\partial M. \qquad (6)$$

The equilibrium orientation of the vector $\mathbf{M}$, given by the angles ϑ_0 and φ_0, is found from the conditions

$$F_\vartheta \equiv \partial F/\partial\vartheta = 0, \quad F_\varphi \equiv \partial F/\partial\varphi = 0. \qquad (7)$$

If the free energy at this point is a minimum, the equilibrium is stable.

Now let us consider the non-equilibrium state, which arises when the effective field changes with time. In this event the orientation of the vector **M** will change, owing to the appearance of the components H_ϑ and H_φ in the non-equilibrium state. It is not difficult to show that

$$H_\vartheta = -F_\vartheta / M;\ H_\varphi = -F_\varphi / M \sin\vartheta_0. \tag{8}$$

If the deviation from equilibrium is small, i.e., for small values of

$$\Delta\vartheta(t) = \vartheta(t) - \vartheta_0;\ \Delta\varphi(t) = \varphi(t) - \varphi_0, \tag{9}$$

we can restrict ourselves to linear terms in the expansions of F_ϑ and F_φ,

$$F_\vartheta = F_{\vartheta\vartheta}\Delta\vartheta + F_{\vartheta\varphi}\Delta\varphi;\ F_\varphi = F_{\vartheta\varphi}\Delta\vartheta + F_{\varphi\varphi}\Delta\varphi, \tag{10}$$

where the second derivatives $F_{\vartheta\vartheta}$, $F_{\vartheta\varphi}$, and $F_{\varphi\varphi}$ are evaluated at equilibrium.

Now from Eq. (3), using Eqs. (8) to (10), we arrive at a system of linear equations, describing small damped oscillations of the magnetization vector about its equilibrium position:

$$\begin{aligned}\gamma^{-1}M\sin\vartheta_0\dot{\Delta\vartheta} &= \{F_{\varphi\vartheta} - \alpha F_{\vartheta\vartheta}\sin\vartheta_0\}\Delta\vartheta \\ &+ \{F_{\varphi\varphi} - \alpha F_{\vartheta\varphi}\sin\vartheta_0\}\Delta\varphi; \\ -\gamma^{-1}M\sin\vartheta_0\dot{\Delta\varphi} &= \{F_{\vartheta\vartheta} + \alpha F_{\vartheta\varphi}(\sin\vartheta_0)^{-1}\}\Delta\vartheta \\ &+ \{F_{\vartheta\varphi} + \alpha F_{\varphi\varphi}(\sin\vartheta_0)^{-1}\}\Delta\varphi.\end{aligned} \tag{11}$$

In the absence of attenuation terms ($\alpha = 0$), these reduce to the equations used successfully in previous work[3,4] to determine the spectrum of the natural frequencies of oscillation of the magnetization.

The system of homogeneous equations (11) possesses a periodic solution with frequency ω, if this frequency satisfies the secular equation

$$\omega^2 - i\omega\Delta\omega - \omega_0^2 = 0,$$

where ω_0 is the resonant frequency of oscillation,

$$\begin{aligned}\omega_0/\gamma &= (1+\alpha^2)^{1/2}H^* \\ &\equiv (1+\alpha^2)^{1/2}(M\sin\vartheta_0)^{-1}\{F_{\vartheta\vartheta}F_{\varphi\varphi} - F_{\vartheta\varphi}^2\}^{1/2},\end{aligned} \tag{12}$$

and $\Delta\omega$ is the breadth of the resonance absorption line.

$$\Delta\omega/\gamma \equiv \Delta H = (\alpha/M)\{F_{\vartheta\vartheta} + F_{\varphi\varphi}(\sin^2\vartheta_0)^{-1}\}. \tag{13}$$

To find the resonant frequency ω_0 and the line breadth ΔH, it is therefore necessary to have an exact expression for the free energy per unit volume of the crystal.

When the allowance for attenuation $\alpha \neq 0$, leads, owing to the smallness of the parameter α, to a negligible shift of the resonant frequency ω_0. This explains the good agreement between experiment and Artman's theoretical calculations[5] of the angular variation of the resonant field in ferrites with cubical symmetry of the crystal lattice.

In the case where the effective field H_M, given by Eq. (6), does not coincide at equilibrium with the direction of the external applied field, the width of an absorption line may become anisotropic relative to different crystallographic directions. In non-metallic ferromagnets this can depend on anisotropy of the shape of the sample as well as on the crystalline anisotropy.

3. As an example, let us consider the case of a uniaxial single-crystal ferrite. Let the polar axis of the coordinate system lie along the hexagonal axis of the crystal, which is the axis of least magnetization, and let the aximuth angle be measured from the direction $[10\bar{1}0]$. Then the angle-dependent part of the free energy per unit volume of an ellipsoidal specimen has the form

$$\begin{aligned}F &= K\sin^2\vartheta - MH(\sin\theta\cos\phi\sin\vartheta\cos\varphi \\ &+ \sin\theta\sin\phi\sin\vartheta\sin\varphi + \cos\theta\cos\vartheta) \\ &+ \tfrac{1}{2}M^2(N_x\sin^2\vartheta\cos^2\varphi + N_y\sin^2\vartheta\sin^2\varphi + N_z\cos^2\vartheta),\end{aligned} \tag{14}$$

where ϑ and φ are respectively the polar and azimuth angles, which determine the orientation of the external field. We limit ourselves here to anisotropy of the first order, and neglect magnetostriction effects.

The problem of determining the equilibrium orientation of the vector **M** for an arbitrary orientation of the external applied field (equivalent, in the absence of this field, to the problem of domain structure) is very complicated. The calculation can be performed comparatively simply only for the case where the external field lies in the base plane, i.e., where $\theta = \pi/2$.

In this event, if $\phi = \pi/2$, and

$$(N_y - N_x)M < H < \frac{2K}{M} + (N_y - N_z)M,$$

then

$$\begin{aligned}H^{*2} &= \left\{\left[\frac{2K}{M} + (N_y - N_z)M\right]^2 - H^2\right\}\frac{2K + (2N_y - N_x - N_z)M^2}{2K + (N_y - N_z)M^2}; \\ \frac{\Delta H}{\alpha} &= \frac{2K}{M} + (2N_y - N_x - N_z)M \\ &+ \frac{[2K + (N_y - N_z)M^2]^2 - H^2M^2}{M[2K + (N_y - N_z)M^2]}.\end{aligned} \tag{15}$$

If, on the other hand, $\phi = \pi/2$ and $H \geq 2K/M + (N_y - N_z)M$ then

$$\begin{aligned}H^{*2} &= H^2 - 2KH/M - (N_y - N_x)(HM - 2K) \\ &- M(N_y - N_z)[H - (N_y - N_x)M]; \\ \Delta H/\alpha &= 2H - 2K/M - (2N_y - N_x - N_z)M.\end{aligned} \tag{16}$$

Material	Direction of External field	H_{res}	ΔH	$\lvert\alpha\rvert$	$1/\tau$, sec^{-1}
Manganese ferrite with zinc impurities	[111]	3176	82	$12.5\cdot10^{-3}$	$7.0\cdot10^{8}$
	[110]	3225	70	$10.7\cdot10^{-3}$	$6.1\cdot10^{8}$
	[100]	3407	56	$8.4\cdot10^{-3}$	$5.1\cdot10^{8}$
Manganese ferrite	[111]	3214	66	$9.9\cdot10^{-3}$	$5.8\cdot10^{8}$
	[110]	3280	50	$7.5\cdot10^{-3}$	$4.3\cdot10^{8}$
	[100]	3442	46	$6.8\cdot10^{-3}$	$4.1\cdot10^{8}$

In the case where $\varphi = 0$ (field directed along the $[10\bar{1}0]$ axis) it is necessary only to interchange N_x and N_y everywhere. For an arbitrary ellipsoid, $N_x \neq N_y$, and in general the line width will be anisotropic with different orientations of the external field with respect to the base plane.

For a spheroidal sample ($N_x = N_y = N$, $N_z = 4\pi - 2N$), there is no anisotropy of the line width within the base plane, since for a given orientation of the field within this plane we have

$$\frac{\Delta H}{\alpha} = \frac{2\,[2K/M - (4\pi - 3N)\,M]^2 - H^2}{2K/M - (4\pi - 3N)\,M},$$

$$\text{for } H < 2K/M - (4\pi - 3N)\,M,$$

$$\frac{\Delta H}{\alpha} = 2H - \frac{2K}{M} + (4\pi - 3N)\,M, \tag{17}$$

$$\text{for } H \geqslant 2K/M - (4\pi - 3N)\,M.$$

If attenuation is neglected ($\alpha = 0$), we arrive at the expression for the resonant frequency given in reference 4.

4. As a second example, consider the case of a single crystal with cubic symmetry. This case is of especial interest, since the majority of single-crystal ferrites have this symmetry. For the coordinate axes x, y, and z, we select the axes [010], [001], and [100], respectively. The chosen polar axis is [100], which for the monocrystals with negative anisotropy of interest here is the axis of difficult magnetization. The azimuth angle is measured from the [010] axis. We limit ourselves henceforth to a spherical specimen ($N_x = N_y = N_z = 4\pi/3$), for which we assume that the applied external field H lies in the plane [110].

If, as before, we confine our attention only to anisotropy of the first order (which is possible except at excessively low temperatures) and neglect effects of magnetostriction, then the angle-dependent part of the free energy per unit volume has the form

$$F = \frac{1}{4} K [\sin^2 2\vartheta + \sin^4\vartheta \sin^2 2\varphi] \tag{18}$$

$$- MH [\cos\theta\cos\vartheta + \sin\theta\sin\vartheta\sin(\varphi + \pi/4)],$$

where θ is the polar angle that determines the orientation of **H** in the (110) plane.

It is not difficult to show that if the external applied field **H** is sufficiently large, and lies along one of the principal crystallographic directions belonging to the plane (110), then **M** is parallel to **H** at equilibrium.

Calculating the second derivatives of the free energy at equilibrium from Eq. (18), and substituting these in Eqs. (12) and (13), we find the resonant frequencies and line breadths for different directions of the external field.

If $\theta = 54°44'$, i.e., if the field **H** lies along the [111] axis, which, for a crystal with negative anisotropy, is the axis of easy magnetization, then

$$\Delta H = 2\alpha H\,(1 + 4|K|/3MH). \tag{19}$$

If $\theta = \pi/2$, i.e., the field **H** lies along the [110] axis, then

$$\Delta H = 2\alpha H\,(1 + |K|/2MH) \tag{20}$$

Finally, if $\theta = 0$, where the field lies along the axis [100] of difficult magnetization, then

$$\Delta H = 2\alpha H\,(1 - |K|/MH) \tag{21}$$

The corresponding formulas for the resonant frequencies, neglecting relaxation, have been computed by Artman.[5] We notice that for a single-crystal ferrite with positive anisotropy the signs in front of $|K|/MH$ in the expressions (19) to (21) are reversed.

It follows from the above definitions that the spin-spin relaxation time is related to α by the expression

$$\frac{1}{\tau} = \gamma M^{-2}\,(\mathbf{M}\cdot\mathbf{H})\,\alpha, \tag{22}$$

in which we can set $\mathbf{M}\cdot\mathbf{H} = MH$.

The angle dependence of the width of a resonance absorption line in a ferrite of cubic symmetry has been studied previously.[6,7] In the first of these references, a manganese ferrite with a small zinc impurity was investigated at 9100 Mcs. The effective anisotropic field K/M at room temperature amounted to -71 ± 1 oersteds. In the second reference a manganese ferrite of composition $Mn_{0.98}Fe_{1.86}O_4$ was studied at 9300 Mcs. The effective anisotropic field at room temperature was -79 ± 3 oersteds.

The experimental results for both ferrites and the calculated values of α and $1/\tau$ are given in the table.

It is evident from the table that α and $1/\tau$ are decreasing functions of the applied external field, with $1/\tau$ decreasing more slowly.

It is also not difficult to verify that, as a consequence of the smallness of the term $|K|/MH$, the variation of τ with different directions of the applied external field cannot be explained solely by the presence of the crystalline anisotropy of the sample. Calculation of second-order anisotropy cannot substantially alter this situation. Thus the relaxation time τ in Eq. (1), turns out to be a slowly rising function of the field strength when $M = \text{const}$. Therefore the Landau-Lifshitz equation (1) agrees best with experiment if the parameter λ is determined from the relation

$$\lambda = M^2/\tau(\mathbf{M}\cdot\mathbf{H}) \qquad (23)$$

Further experimental investigation of the angular variation of the breadth of resonance absorption lines in ferrites of different compositions at various microwave frequencies and temperatures is of interest for a more detailed explanation of the dependence of the relaxation time τ on the intensity of the applied magnetic field.

[1] G. V. Skrotskii and L. V. Kurbatov, Izv. Akad. Nauk SSSR, Ser. Fiz. **21**, 833 (1957) [Columb. Tech. Transl. **21**, 833 (1957)].

[2] G. V. Skrotskii and V. T. Shmatov, J. Exptl. Theoret. Phys. (U.S.S.R.) **34**, 740 (1958), Soviet Phys. JETP **7**, 508 (1958).

[3] H. Suhl, Phys. Rev. **97**, 555 (1955).

[4] J. Smit and H. J. Beljers, Philips Res. Rep. **10**, 113 (1955).

[5] J. O. Artman, Phys. Rev. **105**, 62 (1957).

[6] P. E. Tannenwald, Phys. Rev. **100**, 1713 (1955).

[7] Dillon, Geschwind, and Jaccarino, Phys. Rev. **100**, 750 (1955).

Translated by P. Thaddeus
29

SOVIET PHYSICS JETP VOLUME 35 (8), NUMBER 1 JANUARY, 1959

ON THE $\pi \to e + \nu + \gamma$ DECAY

V. G. VAKS and B. L. IOFFE

Submitted to JETP editor February 20, 1958

J. Exptl. Theoret. Phys. (U.S.S.R.) **35**, 221-227 (July, 1958)

The $\pi \to e + \nu + \gamma$ decay is investigated for vector and axial-vector interactions. An exact relation between the probability of the vector-type part of the decay $\pi \to e + \nu + \gamma$ and the probability of the decay $\pi^0 \to 2\gamma$ can be established by assuming that the direct interaction between π mesons and the electron-neutrino field, suggested by Gell-Mann and Feynman, exists in the vector-type theory. It is found that the axial-vector-type decay accounts for the main part of the total probability for the $\pi \to e + \nu + \gamma$ decay. The ratio of the total probability for the $\pi \to e + \nu + \gamma$ decay to the probability for the $\pi \to \mu + \nu$ decay is of order 5×10^{-6}. Expressions for the angular and energy distributions of the electrons and quanta are obtained.

GELL-MANN and Feynman[1] suggested a scheme for a universal weak interaction of the nucleons with the electron-neutrino field is of the vector- and axial-vector-type. The interaction Hamiltonian has the form

$$H_1 = (\bar{\psi}\gamma_\mu(G_V + \gamma_5 G_A)\tau^+\psi)J_\mu + \text{Herm. conj.}, \qquad (1)$$
$$J_\mu = (\bar{\psi}_e\gamma_\mu{}^1/_2(1+\gamma_5)\psi_\nu),$$

where

$$\psi = \begin{pmatrix}\psi_P\\ \psi_N\end{pmatrix},\quad \tau^+ = \sqrt{2}\begin{pmatrix}01\\00\end{pmatrix} = \frac{1}{\sqrt{2}}(\tau_x + i\tau_y),$$
$$\gamma_5 = -\begin{pmatrix}01\\10\end{pmatrix},\quad \gamma_\mu = \{\beta,\ \beta\alpha\},$$

and G_V and G_A are coupling constants. Gell-Mann and Feynman (see also reference 2) assume that there exists a direct interaction of the π mesons with the electron-neutrino field, which is described by the Hamiltonian

$$H_2 = 2iG_V [\Phi^+ T^+ \nabla_\mu \Phi - (\nabla_\mu \Phi^+) T^+ \Phi] J_\mu \quad (2)$$
$$+ \text{Herm. conj.},$$

where $\Phi = \{\varphi, \varphi^0, \varphi^+\}$ are the wave functions of the π mesons, and

$$T^+ = \frac{1}{\sqrt{2}}(T_x + iT_y) = \begin{pmatrix} 0 & -1 & 0 \\ 0 & 0 & 1 \\ 0 & 0 & 0 \end{pmatrix}$$

is the isotopic spin operator for the π mesons. The vector part of the interaction (1) together with the interaction (2) is completely analogous to the interaction of π mesons with the electromagnetic field

$$H_{el} = e\left\{\bar{\psi}\gamma_\mu\left(\frac{1}{2}\tau_z + \frac{1}{2}\right)\psi \right. \quad (3)$$
$$\left. + i[\Phi^+ T_z \nabla_\mu \Phi - (\nabla_\mu \Phi^+) T_z \Phi]\right\} A_\mu.$$

This allows us to establish an exact relation between the probability of the vector-type part of the $\pi^\pm \to e^\pm + \nu + \gamma$ decay and the probability of the decay of a neutral π meson into two γ quanta. Since the axial-vector-type part of the $\pi^\pm \to e^\pm + \nu + \gamma$ decay is mainly determined by terms which are simply related to the $\pi^\pm \to e^\pm + \nu$ decay, it is possible to estimate the probabilities for the $\pi \to e + \nu + \gamma$ decays in the A- and V-type theory more correctly than was done earlier by Treiman and Wyld.[3]

We write the matrix elements for the $\pi^0 \to 2\gamma$ decay (M_γ) and for the vector-type part of the $\pi \to e + \nu + \gamma$ decay (M_V) decay in the form

$$M_\gamma(k_1, k_2) = e^2 \varphi^0(q) A_\mu(k_1) A_\nu(k_2) U^\gamma_{\mu\nu}(k_1, k_2),$$
$$M_V(k_1, k_2) = eG_V \varphi^+(q) A_\mu(k_1) J_\nu(k_2) U^V_{\mu\nu}(k_1, k_2). \quad (4)$$

Here, for the $\pi^0 \to 2\gamma$ decay, k_1 and k_2 are the 4-momenta of the quanta, $\varphi^0(q)$ is the wave function of the neutral meson, and $q = k_1 + k_2$ is its momentum; for the $\pi \to e + \nu + \gamma$ decay, k_1 is the momentum of the quantum, $k_2 = p_e + p_\nu$ is the total momentum of electron-neutrino system, and $\varphi(q)$ is the wave function of the charged meson.

We shall show that, with the strong interactions treated exactly (but neglecting the radiative corrections connected with the electromagnetic and weak interactions),

$$U^\gamma_{\mu\nu}(k_1, k_2) = U^V_{\mu\nu}(k_1, k_2). \quad (5)$$

We shall assume that the momenta of the emitted γ quanta and the leptons ($k \sim \mu/2$) are small compared with the average momenta Λ of the virtual particles participating in the decay.*

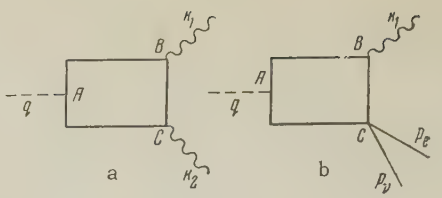

FIG. 1. (a) $\pi^0 \to 2\gamma$ decay; ---- meson line, ~~~ photon line; (b) $\pi \to e + \nu + \gamma$ decay; —— electron and neutrino lines; p_e and p_ν are the 4-momenta of the electron and the neutrino, $p_e + p_\nu = k_2$.

We restrict ourselves first to the case when only π mesons and nucleons participate in the strong interactions. We consider an arbitrary Feynman diagram (Fig. 1) for the processes which we are concerned with. The quantities $U^\gamma_{\mu\nu}(k_1, k_2)$ and $U^V_{\mu\nu}(k_1, k_2)$ for this diagram are products of two factors: (1) the integral over the momenta of the virtual particles and the sum over the spin variables, and (2) the sum over the isotopic spin variables. We see from the comparison of the interaction Hamiltonians (1) and (2) with (3) that the spin-momentum part of the diagram is the same for $U^\gamma_{\mu\nu}$ and $U^V_{\mu\nu}$. Thus $U^\gamma_{\mu\nu}$ and $U^V_{\mu\nu}$ have the form

$$U^{\gamma,V}_{\mu\nu}(k_1, k_2) = J_{\mu\nu}(k_1, k_2) F^{\gamma,V}_{ABC};$$
$$F^{\gamma,V}_{ABC} = \mathrm{Sp}\{\tau_A \ldots \tau_B \ldots \tau_C \ldots\}, \quad (6)$$

where τ_A, τ_B, τ_C are isotopic spin operators; index A denotes the initial π meson, B and C denote the two γ quanta for the π^0 decay, and the γ quantum and the leptonic current in the decay $\pi \to e + \nu + \gamma$. In the case of the π^0 decay, τ_A is to be substituted by τ_z, and τ_B and τ_C are to be substituted by $(\tau_z + 1)/2$ for γ quanta emitted by nucleons, and by T_z for γ quanta emitted by mesons. In the case of the decay $\pi^- \to e^- + \nu + \gamma$, τ_A is replaced by $\tau = (\tau_x - i\tau_y)/\sqrt{2}$, τ_B by $(\tau_z + 1)/2$ (or T_z), and τ_C by τ^+ (or T^+).

The quantity $J_{\mu\nu}(k_1, k_2)$ should be a pseudotensor of second rank, i.e.,

$$J_{\mu\nu}(k_1, k_2) = A\varepsilon_{\mu\nu\lambda\sigma} k_{1\lambda} k_{2\sigma}, \quad (7)$$

where A is independent of k_1 and k_2 with an accuracy up to terms of order $(k/\Lambda)^2$, which we discard. Together with the diagram of Fig. 1 we

*It follows from the experimental lifetime of the π^0 meson that Λ cannot be essentially smaller than M, the mass of the nucleon, for the condition $\Lambda \ll M$ would introduce an additional factor $(\Lambda/M)^4$ into the estimate for the lifetime of the π^0 meson, in disagreement with experiment. (This conclusion is not derived from perturbation theory, since the succeeding terms in the expansion with respect to g^2 would be of order $g^2(\Lambda/M)^2 \lesssim 1$.)

now consider a diagram in which the vertices B and C are interchanged. It is easily seen that due to the symmetry of (7) under the interchange $\mu \to \nu$, $k_1 \to k_2$, the sum of these diagrams is equal to

$$U^{\gamma,V}_{\mu\nu}(k_1, k_2) + U^{\gamma,V}_{\nu\mu}(k_2, k_1) = J_{\mu\nu}(k_1, k_2)\,[F^{\gamma,V}_{ABC} + F^{\gamma,V}_{ACB}]. \tag{8}$$

We investigate the vector structure of the expression $F_{ABC} + F_{ACB}$ in the isotopic spin space. We note here that the interaction with the electromagnetic field can formally be described (neglecting the radiative corrections with respect to e^2) by a sum of the interactions of the nucleons and the π mesons with an isotopic spin vector α^{γ}_i (components $\alpha^{\gamma}_z = 1/2$, $\alpha^{\gamma}_x = \alpha^{\gamma}_y = 0$), and an isotopic spin scalar $\beta = 1/2$. Then the Hamiltonian for the interaction with the electromagnetic field is written in this way:

$$H_{el} = e\{\bar{\psi}\gamma_\mu\tau_i\psi + i[\Phi^+ T_i \nabla_\mu \Phi - (\nabla_\mu\Phi^+)\,T_i\Phi]\}\,A_\mu\alpha^{\gamma}_i + e\bar{\psi}\gamma_\mu\psi A_\mu\beta \tag{3'}$$

which is formally invariant in isotopic spin space. The expression F_{ABC} also takes a form invariant in isotopic spin space:

$$F^{\gamma}_{ABC} = F_{ikl}\varphi^0_i\alpha^{\gamma}_k\alpha^{\gamma}_l + F'_{ik}\varphi^0_i\alpha^{\gamma}_k\beta + F''_{il}\varphi^0_i\alpha^{\gamma}_l\beta + F'''_i\varphi^0_i\beta^2, \tag{9}$$

where φ^0_i is the isotopic spin vector of the π^0 meson ($\varphi^0_1 = \varphi^0_2 = 0$, $\varphi^0_3 = 1$). The term F'_{ik} corresponds to the case when the quanta emitted at vertex B refer to α, and those emitted at C refer to β. the term F''_{il} corresponds to the opposite case. In analogy, the interaction with the leptonic field can be written in the form of an interaction with the isotopic spin vector α^{V}_i (components $\alpha^{V}_z = 0$, $\alpha^{V}_x = 1/\sqrt{2}$, $\alpha^{V}_y = i/\sqrt{2}$). Here the expressions for F^{V}_{ABC} and F^{V}_{ACB} take the form (φ^+_i is the isotopic spin vector of the π^- meson; $\varphi^+_1 = 1/\sqrt{2}$, $\varphi^+_2 = -i/\sqrt{2}$, $\varphi^+_3 = 0$):

$$F^{V}_{ABC} = F_{ikl}\varphi_i\alpha^{\gamma}_k\alpha^{V}_l + F''_{il}\varphi_i\beta\alpha^{V}_l, \qquad F^{V}_{ACB} = F_{ikl}\varphi_i\alpha^{V}_k\alpha^{\gamma}_l + F'_{ik}\varphi_i\alpha^{V}_k\beta, \tag{9'}$$

since the isotopic scalar β participates only in the emission of quanta (i.e. at the vertex B in the diagram of Fig. 1). It is easily seen that those terms in the expression $F^{\gamma,V}_{ABC} + F^{\gamma,V}_{ACB}$ in which both interactions in the vertices B and C involve the isotopic spin vector, reduce to zero. Indeed, in this case the quantity F_{ikl} in (9) and (9′) should be a pseudotensor of third rank in isotopic spin space. However, after the summation of the isotopic spin variables of the mesons and after taking the spur of the isotopic spin variables of the nucleons, the only expression left to represent $F_{ikl} + F_{ilk}$ is the unit tensor ϵ_{ikl}. But ϵ_{ikl} is antisymmetric in the indices k, l, while $F_{ikl} + F_{ilk}$ is symmetric in the same indices. Hence $F_{ikl} + F_{ilk} = 0$ (so that, for example, the γ quanta in the π^0 decay cannot be both emitted by virtual π mesons).

In the same way, all terms F_{ABC} reduce to zero in which both γ quantum emissions in the vertices B and C involve the isotopic spin scalar. Indeed, it is impossible to construct an isotopic spin vector F^{γ}_i, since there is no distinguished direction in isotopic spin space in expression (6). The only non-zero terms in (9) and (9′) are the terms F'_{ik} and F''_{il}. The quantities F'_{ik} and F''_{ik} are tensors of second rank in isotopic spin space, and they can therefore be expressed in terms of the unit tensor δ_{ik}, i.e. $F'_{ik} = C\delta_{ik}$, $F''_{ik} = D\delta_{ik}$, where C and D are certain numerical constants. Substituting these expressions for F'_{ik} and F''_{ik} in (9) and (9′), we find without difficulty that $F_{ABC} + F_{ACB} = F^{V}_{ABC} + F^{V}_{ACB} = 1/2\,(C + D)$, as can also be seen from (5).

The above proof is easily generalized for the case when hyperons and K mesons also participate in the strong interactions. In the interaction Hamiltonian describing the interaction of the hyperons and K mesons with the electromagnetic field we then have to replace the matrices $(\tau_z + 1)/2$ and T_z by $T_z + 1/2 + S/2$ and $T_z + S/2$, respectively (S is the strangeness), We also assume that the Hamiltonian for the interaction of the hyperons and K mesons with the leptonic field has the form (1), (2), where τ^+ and T^+ are replaced by the corresponding projection of the isotopic spin of the strange particle.

With the help of (4), (5), and (7) we can write the matrix elements M_γ and M_V in the form

$$M_\gamma(k_1, k_2) = ae^2\varphi^0(q)\,A_\mu(k_1)\,A_\nu(k_2)\,\varepsilon_{\mu\nu\lambda\sigma}k_{1\lambda}k_{2\sigma}; \qquad M_V(k_1, k_2) = aeG_V\varphi^+(q)\,A_\mu(k_1)\,J_\nu(k_2)\,\varepsilon_{\mu\nu\lambda\sigma}k_{1\lambda}k_{2\sigma} \tag{10}$$

The constant a is to be determined from the experimental lifetime of the π^0 meson.

It is convenient to split up the matrix element $M_A(k_1, k_2)$ (corresponding to the axial-vector-type part of the $\pi \to e + \nu + \gamma$ decay) into two parts. The first part contains the diagram of Fig. 2, in which a γ quantum is emitted by an electron, as well as terms of zeroth order in k_1,

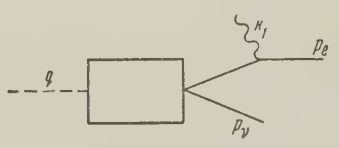

FIG. 2

k_2 from the expancion of diagram Fig. 1 in powers of k. The second part contains the terms of seccond order in k_1, k_2 in the expansion of diagram Fig. 1.

As is known,[3-5] it is not necessary to calculate the closed loops for the determination of the first part of $M_A(k_1, k_2)$. It can be obtained by introducing the phenomenological interaction

$$H_{\pi e\nu} = g_{\pi e\nu}\frac{\partial\varphi^+}{\partial x_\mu}\left(\bar{\psi}_e\gamma_\mu\frac{1}{2}(1+\gamma_5)\psi_\nu\right) + \text{Herm. conj.}, \tag{11}$$

for the description of the decay $\pi \to e + \nu$, and by observing that on the strength of the gauge invariance $\partial\varphi^+/\partial x_\mu$ should be changed to $\partial\varphi^+/\partial x_\mu + ieA_\mu\varphi^+$. (The expression $ieg_{\pi e\nu}A_\mu\varphi^+J_\mu$ corresponds to the terms of zero order in k_1, k_2 in the expansion of diagram Fig. 1). Then[3-5] the Hamiltonian (11) is equivalent to the Hamiltonian:

$$H_{\pi e\nu} = m_e g_{\pi e\nu}\varphi^+(\bar{\psi}_e\,{}^1/_2(1+\gamma_5)\psi_\nu) + \text{Herm. conj.}, \tag{12}$$

where the emission of the γ quantum is effected only through the bremsstrahlung of the electron. The radiative decay of the π meson with the Hamiltonian (12) was considered earlier.[4] Therefore we have to concern ourselves only with the part of $M_A(k_1, k_2)$ containing the terms quadratic in k_1, k_2. It is easily seen that the general expression for this matrix element must have the form:

$$M_A(k_1, k_2) = iteG_A\varphi^+(q)\,[A_\mu(k_1)k_{1\nu} - A_\nu(k_1)k_{1\mu}]\,J_\mu(k_2)k_{2\nu}. \tag{13}$$

Strictly speaking, we cannot determine the constant b by theoretical considerations.* However, since it is determined in perturbation theory by integrals of the same type as those determining the constant a in (10), we may assume that b is of the same order as a. Direct calculation shows that the matrix element of Hamiltonian (12) does not interfere with the matrix elements (10) and (13), if we neglect higher powers of the ratio m_e/μ. It is therefore convenient to first compute $dW^{(1)}$, the probability of the transition $\pi \to e + \nu + \gamma$ on account of the terms $M_V + M_A$.

After the summation over the polarizations of the emitted quantum and over the spins of the electron, we obtain for the differential probability of the decay $dW^{(1)}$ the following expression:

$$dW^{(1)} = \frac{1}{\pi^2}\frac{G_V^2}{e^2}W_{\pi^0}\frac{k}{\mu^2}\left\{(1+\lambda^2)\left(1-\frac{(\mathbf{k}\cdot\mathbf{n})(\mathbf{k}\cdot\nu)}{k^2}\right)\right. \tag{14}$$
$$\left. + 2\lambda\,\frac{\mathbf{k}\cdot\nu - \mathbf{k}\cdot\mathbf{n}}{k}\right\}\delta(E_e + E_\nu + k - \mu)\frac{dk\,d\mathbf{p}_e}{(2\pi)^3}.$$

Here $\mathbf{p}_e = n\mathbf{p}_e$ and $\mathbf{k}$ are the momenta of the electron and the γ quantum, respectively, ν is a unit vector in the direction of the neutrino momentum, W_{π^0} is the probability for the decay of the π^0 meson into two γ quanta, μ is the mass of the π meson, $\lambda = bG_A/aG_V$. W_{π^0} is connected with the constant a in (10) through the relation:

$$W_{\pi^0} = \pi^2\mu^3a^2.$$

By integration we may obtain various partial distributions from (14). Thus the energy distribution of the electrons has the form [$p_e = (\mu/2)y$]

$$dW_e^{(1)} = \frac{1}{2^6\pi^3}\frac{G_V^2}{e^2}W_{\pi^0}\mu^4y^2\left\{(1+\lambda^2)\left[(1-y)^2 + \frac{1}{6}y^2\right]\right. \tag{15}$$
$$\left. + \lambda(1-y)\left(1 - 2y + \frac{1}{2}y^2\right)\right\}dy,$$

and the energy distribution of the γ quanta ($k = (\mu/2)y$) is:

$$dW_\gamma^{(1)} = \frac{1}{2^6\pi^3}\frac{G_V^2}{e^2}W_{\pi^0}\mu^4\frac{4}{3}(1+\lambda^2)x^3(1-x)\,dx. \tag{16}$$

The integral probability $W^{(1)}$ is equal to

$$W^{(1)} = \frac{1}{960\pi^3}\frac{G_V^2\mu^4}{e^2}W_{\pi^0}(1+\lambda^2). \tag{17}$$

We estimate the numerical value of $W^{(1)}$. The constant G_V^2 was determined in experiments[6] on the β decay of O^{14}: $G_V^2\mu^4 = 0.51\times10^{-13}$. We estimate the lifetime of the π^0 meson with Orear[7] to be $W_{\pi^0} \gtrsim 0.5\times10^{16}$ sec^{-1}, and we find $W^{(1)} = 2.4$ sec^{-1} ($\lambda = 1$). Thus the ratio of $W^{(1)}$ to the total probability for the $\pi \to \mu + \nu$ decay is

$$W^{(1)}/W_{\mu+\nu} \approx 6\cdot10^{-8}. \tag{18}$$

This estimate of the number of the $\pi \to e + \nu + \gamma$ decays is very close to the estimate of Treiman and Wyld (reference 3).*

Let us now consider $W^{(2)}$, which is the $\pi \to e + \nu + \gamma$ decay probability due to the terms in which a γ quantum is emitted by the electron. A corresponding calculation was made in reference 4† for the $\pi \to \mu + \nu + \gamma$ case. The results can be easily translated for the $\pi \to e + \nu + \gamma$ decay. We obtain for the differential probability the expression:

*The quantity b has the same phase as a, so that we may take them to be real. This follows from the invariance of the strong and electromagnetic interactions under time reversal (or charge conjugation). The proof may be carried through with the help of the phenomenological Hamiltonian corresponding to the matrix elements (10) and (13).

*An analogous calculation for the $\pi \to \mu + \nu + \gamma$ decay gave the negligibly small value $W^V_{\mu+\nu+\gamma} \sim 5\times10^{-10}\,W_{\mu+\nu}$ for the probability of a $\pi \to \mu + \nu + \gamma$ decay through the V variant.

†We note that formula (6) in reference 4, which gives the total probability for the $\pi \to \mu + \nu$ decay, contains the incorrect factor ½. Accordingly, the values in the tables of this reference should be multiplied by ½.

$$dW^{(2)} = \frac{1}{8\pi^3}\frac{e^2}{\mu^2} W_{e+\nu} \frac{1}{E_e E_\nu k}\left\{2(E_e k - \mathbf{k}\cdot\mathbf{p}_e)(k\mu - kE_e + \mathbf{k}\cdot\mathbf{p}_e) + \mu^2\left[p_e^2 - \frac{(\mathbf{p}_e\cdot\mathbf{k})^2}{k^2}\right]\right\}\frac{dp_e dk}{(E_e k - \mathbf{k}\cdot\mathbf{p}_e)^2}\delta(E_e + E_\nu + k - \mu), \quad (19)$$

where $W_{e+\nu}$ is the probability for the $\pi \to e + \nu$ decay, equal to $1.3 \times 10^{-4} W_{\mu+\nu}$ in the Gell-Mann-Feynman scheme. The energy distribution of the electrons has the form

$$dW_e^{(2)} = \frac{1}{2\pi} e^2 W_{e+\nu}(1-y)\left\{\ln\left[\left(\frac{\mu}{m}\right)^2 \frac{y^2}{1-y}\right] + \frac{2y}{(1-y)^2}\left[-2 + \ln\left(\frac{\mu}{m}y\right)^2\right]\right\} dy. \quad (20)$$

The electron spectrum diverges near the upper limit ($y \to 1$), which corresponds to the emission of long-wave quanta. Therefore the total probability for a $\pi \to e + \nu + \gamma$ decay in which the electron is emitted with an energy below a certain maximum value y_{max} increases logarithmically with y_{max}. Because of this, and also because of the presence of the large term $\ln(\mu/m)^2$ in (20), the probability for the radiative decay with the quantum emitted by a virtual electron in comparatively large, and substantially surpasses the probability $W^{(1)}$.

It follows that we need consider only the term $W^{(2)}$ in the computation of the total probability for the $\pi \to e + \nu + \gamma$ decay. The results of the computation of this probability as a function of the maximal electron energy are tabulated in the table. (We use $W_{e+\nu} = 1.3 \times 10^{-4} W_{\mu+\nu}$).

y_{max}	0.3	0.5	0.7	0.9
$\frac{10^6 W_{e+\nu+\gamma}}{W_{\mu+\nu}}$	0.36	0.85	1.8	3.3

The table shows that the probability for the $\pi \to e + \nu + \gamma$ decay is greater by almost two orders of magnitude than the probability $W^{(1)}$ for the decay through the V variant.

Besides the energy distribution of the electrons, we are also interested in the angular distribution of the quanta over the angle θ between the directions of emission of the electron and of the quantum. This distribution is obtained from (19) by integrating over the energies of the electron and the quantum. For $\theta \gg m_e/\mu$ it is equal to

$$dW^{(2)}(\theta) = \frac{e^2}{4\pi} W_{e+\nu} \frac{\sin\theta d\theta}{\alpha^3} \times \left\{\alpha + (1-\alpha)\ln(1-\alpha) + 2\alpha^2(1-\alpha)\left(\ln\frac{1}{1-y_{max}} - 1\right)\right\}, \quad (21)$$

where $\alpha = \sin^2\theta/2$ and y_{max} is the maximal energy (measured in $\mu/2$) up to which the electron spectrum is integrated. Expression (21) behaves like $d\theta/\theta$ for small θ. However, the divergence at $\theta \to 0$ in (21) is only seeming. It derives from the neglect of quantities $\sim m/\mu$ in the calculation of (21). For $\theta \sim m/\mu$ we really have an expression of order $1/(\theta^2 + 4(m^2/\mu^2))$ instead of $1/\theta^2$. The presence of this factor is perfectly reasonable: it is related to the fact that in the relativistic case the bremsstrahlung of the electron is concentrated in the narrow solid angle $\sim m/E$ around the direction of the momentum of the electron. This also accounts for the appearance of the large logarithmic term $\ln(\mu/m)^2$ in (20). Thus we have the most favorable conditions for the detection of the $\pi \to e + \nu + \gamma$ decay through the vector and axial-vector variant if the registering electron and quantum move in the same direction.

Of special interest is the experimental investigation of the vector-type part of the $\pi \to e + \nu + \gamma$ decay, since this would give the possibility to verify the hypothesis of Gell-Mann and Feynman about the existence of a direct interaction of the π mesons with the electron-neutrino field, as well as the theorem about the connection between the $\pi^0 \to 2\gamma$ decay and the vector-type part of the $\pi \to e + \nu + \gamma$ decay. It is possible in principle to single out the vector-type part of the $\pi \to e + \nu + \gamma$ decay from the background of the more probable axial-vector variant if one selects the electrons and quanta flying in opposite directions, since in the vector variant of the decay the greater part of the quanta is emitted into angles close to 180° relative to the direction of flight of the electron. In this case, as seen from (21), the probability for the axial-vector variant of such a decay, where the γ quantum is emitted by the electron, will be of order $10^{-7} W_{\mu+\nu} \sin\theta\, d\theta$. The probability for the vector variant of the decay will be of the same order. For a unique isolation of those terms in the probability of the transition which correspond to the vector variant (i.e., the determination of λ in (14)) one needs identical measurements for two different energies of the electron, which further complicates an already difficult task.

In conclusion the authors express their deep gratitude to I. Iu. Kobzarev and L. B. Okun' for helpful discussions.

Note added in proof (June 16, 1958): After the completion of this paper new data[8] appeared on the relation between the probabilities of the decays $\pi \to e + \nu$ and $\pi \to \mu + \nu$, from which it follows that $W_{e+\nu}/W_{\mu+\nu} < 10^{-5}$. This ratio $W_{e+\nu}/W_{\mu+\nu}$ contradicts the theory of Gell-Mann and Feynman, and indicates a significant suppression of the axial-vector variant of the decay $\pi \to e + \nu$. In this situation it is of even greater interest to verify the

theory of Gell-Mann and Feynman for the vector variant, and to investigate experimentally the decay $\pi \to e + \nu + \gamma$. This decay should go mainly through the vector variant because of the suppression of the axial-vector variant, so that the probability of the $\pi \to e + \nu + \gamma$ decay will be determined by formulas (14) to (18).

[1] R. Feynman and M. Gell-Mann, Phys. Rev. **109**, 193 (1958).

[2] S. S. Gershtein and Ia. B. Zel'dovich, J. Exptl. Theoret. Phys. (U.S.S.R.) **29**, 698 (1955); Soviet Phys. JETP **2**, 576 (1956).

[3] S. B. Treiman and H. W. Wyld, Phys. Rev. **101**, 1552 (1956).

[4] B. L. Ioffe and A. P. Rudik, Dokl. Akad. Nauk SSSR **87**, 359 (1952).

[5] S. A. Bludman and M. A. Ruderman, Phys. Rev. **101**, 910 (1956).

[6] J. B. Gerhart, Phys. Rev. **95**, 288 (1954).

[7] Harris, Orear, and Taylor, Phys. Rev. **106**, 327 (1957).

[8] H. L. Anderson and C. M. Lattes, Nuovo cimento **6**, 1356 (1957).

Translated by R. Lipperheide
30

COUPLED MAGNETOELASTIC WAVES IN FERROMAGNETIC MEDIA AND FERROACOUSTIC RESONANCE

A. I. AKHIEZER, V. G. BAR'IAKHTAR, and S. V. PELETMINSKII

Physico-Technical Institute

Submitted to JETP editor February 20, 1958

J. Exptl. Theoret. Phys. (U.S.S.R.) **35**, 228-239 (July, 1958)

A phenomenological theory is given for coupled magnetoacoustic waves in ferromagnetic media and ferrites (the coupling between the elastic and magnetic waves is due to magnetostriction and spontaneous magnetization). The acoustic velocity in ferromagnetic media is determined and is found to be a function of the magnetization and longitudinal magnetic field. The acoustic absorption factor associated with the electrical conductivity and relaxation of the magnetization is determined. The possibility of resonant ultrasonic excitation of magnetic waves is indicated.

1. As is well known, any deviation of the magnetization from the equilibrium value (at a given temperature) in ferromagnetic media and ferrites is propagated in the form of waves, the dispersion properties of which are similar to those of spin waves.[1]

Because of magnetostriction and ponderomotive effects due to spontaneous magnetization, there is coupling in an elastically deformed ferromagnetic material between what we shall call "magnetic" waves and the elastic waves. In media of high conductivity, the coupled magnetoelastic waves produced in this way are similar to the magnetoelastic waves that propagate in metals in an external magnetic field and to the magnetohydrodynamic waves in liquid conductors. However, in contrast with magnetohydrodynamic waves, the magnetoelastic waves considered here can propagate in both ferromagnetic media and ferrites and, in addition, do not require an external magnetic field.

The coupling between magnetic and elastic waves offers the possibility of acoustic excitation of magnetic waves; moreover, the excitation should be especially intense in those cases in which the frequency and wave vector of the magnetic wave coincide with the frequency and wave vector of the elastic wave.

The interaction between magnetic and elastic waves leads to a dependence of the acoustic velocity in ferromagnetic media on the spontaneous magnetization and the external magnetic field. This interaction means additional acoustic absorption in ferromagnetic media; this absorption depends on the electrical conductivity of the medium and the magnetization relaxation mechanism. It is to be distinguished from another acoustic absorption mechanism, also characteristic of ferromagnetic media, in which the presence of an external acoustic field causes a deviation in the spin wave distribution function from the equilibrium value by virtue of the increased entropy.[2]

In the present paper we present a phenomenological theory of coupled magnetoelastic waves in ferromagnetic media and ferrites. Pure magnetic waves are considered first.

2. The free energy in a ferromagnetic medium can be given in the form:

$$\mathcal{H} = \int \left\{ \frac{1}{2} \alpha_{ik} \frac{\partial \mathbf{M}}{\partial x} \frac{\partial \mathbf{M}}{\partial x_k} + \beta(\mathbf{M}) + \frac{\mathbf{h}^2 + \mathbf{e}\cdot\mathbf{d}}{8\pi} - \mathbf{M}\cdot\mathbf{H}_0 \right\} dV. \tag{1}$$

Here the first term represents the exchange energy associated with inhomogeneity of the magnetization $\mathbf{M}$ (the α_{ik} are the exchange integrals*), the second term includes the exchange energy which depends on M and the anisotropy energy, while the third and fourth terms are the energy of the electromagnetic field and the energy of the magnetic moment in the external magnetic field $\mathbf{H}_0$ ($\mathbf{h}$ and $\mathbf{e}$ are the magnetic and electric fields respectively, $\mathbf{d}$ is the induction associated with the changing magnetization).

In the case of a uniaxial crystal the function $\beta(\mathbf{M})$ can be given by

$$\beta(\mathbf{M}) = \beta_1(M^2) + \beta_2(\mathbf{M}\cdot\mathbf{n}/M), \tag{2}$$

*In order-of-magnitude the quantities $\alpha_{ik} \sim \Theta_c a^2/\hbar g M_0$, where Θ_c is the Curie temperature, a is the lattice constant, and M_0 is the saturation magnetization.

where $\mathbf{n}$ is a unit vector in the direction of easiest magnetization.

The time derivative of the magnetization of the ferromagnetic medium is determined by the Landau-Lifshitz equation[3]

$$\partial \mathbf{M}/\partial t = g[\mathbf{M}\times\mathbf{H}^{(e)}] - \lambda M^{-2}[\mathbf{M}\times[\mathbf{M}\times\mathbf{H}^{(e)}]], \qquad (3)$$

where $\mathbf{H}^{(e)}$ is the effective magnetic field, an expression for which is given below, λ is the damping factor and g is the gyromagnetic ratio.

We determine the time derivative of the energy in a volume V. Using Maxwell's equations we have:

$$\frac{d\mathcal{H}}{dt} = \int_V \left\{ -\frac{\partial \mathbf{M}}{\partial t}\left[\mathbf{H}_0 + \mathbf{h} - \frac{\partial \beta}{\partial \mathbf{M}} + \alpha_{ik}\frac{\partial^2 \mathbf{M}}{\partial x_i \partial x_k}\right] - \mathbf{j}\cdot\mathbf{e} \right\} dV$$
$$+ \int_S \left\{ \frac{c}{4\pi}[\mathbf{h}\times\mathbf{e}]_k + \alpha_{ik}\frac{\partial \mathbf{M}}{\partial x_i}\frac{\partial \mathbf{M}}{\partial t} \right\} ds_k,$$

where $\mathbf{j}$ is the density of the conduction current and S is the surface which encloses the volume V.

If $\lambda = 0$ and $\sigma = 0$, from energy conservation considerations, the exchange integral must vanish. Whence, using Eq. (3) for $\partial \mathbf{M}/\partial t$ with $\lambda = 0$, it is easy to obtain the following expression for the effective magnetic field:

$$\mathbf{H}^{(e)} = \mathbf{H}_0 + \mathbf{h} - \partial \beta(\mathbf{M})/\partial \mathbf{M} + \alpha_{ik}\partial^2 \mathbf{M}/\partial x_i \partial x_k. \qquad (4)$$

For finite values of λ and σ the time derivative of the energy is

$$\frac{d\mathcal{H}}{dt} = -\int_V \frac{j^2}{\sigma} dV - \int_V \frac{\lambda}{M^2}[\mathbf{M}\times\mathbf{H}^{(e)}]^2 dV \qquad (5)$$
$$+ \int_S \left\{ \frac{c}{4\pi}[\mathbf{h}\times\mathbf{e}]_k + \alpha_{ik}\frac{\partial \mathbf{M}}{\partial x_i}\frac{\partial \mathbf{M}}{\partial t} \right\} ds_k,$$

where σ is the electrical conductivity of the media.

3. We now explain the dispersion properties of the magnetic waves. We use the symbol $\mathbf{M}_0$ to denote the equilibrium value of the magnetization per unit volume of the ferromagnetic medium at a given temperature and $\mu(\mathbf{r}, t)$ to express the deviation of the magnetization from the equilibrium value at a point $\mathbf{r}$ and time t.

The quantity $\mathbf{M}_0$ can be determined from the minimum energy condition which yields

$$(\partial \beta/\partial \mathbf{M})_{\mathbf{M}=\mathbf{M}_0} = \mathbf{H}_0. \qquad (6)$$

Assuming that $\mu \ll M_0$, from Eqs. (2), (4) and (6) we obtain the following expression for the effective magnetic field in the case of a uniaxial crystal with $\mathbf{H}_0 \parallel \mathbf{n}$:

$$\mathbf{H}^{(e)} = \mathbf{h} - H_0\boldsymbol{\mu}/M_0 - \beta\boldsymbol{\mu}_\perp - a\mathbf{n}(\mathbf{n}\cdot\boldsymbol{\mu}) + \alpha\Delta\boldsymbol{\mu},$$

where β is the anisotropy constant $\beta = -\beta_2'(1)/M_0^2$ and $a = 4M_0^2\beta_1''(M_0^2)$.

With $\lambda = 0$ the complete system of linearized equations is

$$\frac{\partial \boldsymbol{\mu}}{\partial t} = gM_0\left[\mathbf{n}\times\left(\mathbf{h} - \frac{H_0}{M_0}\boldsymbol{\mu} - \beta\boldsymbol{\mu} + \alpha\Delta\boldsymbol{\mu}\right)\right],$$
$$\operatorname{curl}\mathbf{h} = \frac{1}{c}\frac{\partial \mathbf{d}}{\partial t} + \frac{4\pi}{c}\mathbf{j}, \qquad (7)$$
$$\operatorname{curl}\mathbf{e} = -\frac{1}{c}\frac{\partial}{\partial t}(\mathbf{h} + 4\pi\boldsymbol{\mu}).$$

We seek a solution for this system in the form of plane waves $e^{-i(\omega t - \mathbf{k}\cdot\mathbf{r})}$. First we consider the case $\sigma = 0$. Neglecting the displacement current, the relation between ω and $\mathbf{k}$ is of the form:

$$\omega = (\Omega\Omega_1)^{1/2}, \qquad (8)$$

where

$$\Omega = gM_0(\alpha k^2 + \beta + H_0/M_0 + 4\pi\sin^2\vartheta),$$
$$\Omega_1 = gM_0(\alpha k^2 + \beta + H_0/M_0) \qquad (9)$$

and ϑ is the angle between $\mathbf{k}$ and $\mathbf{M}_0$.

This relation is the same as the well known relation between frequency and wave vector for Bloch spin waves.[4] It is valid when $\epsilon\omega \ll \sigma \ll c^2k^2/\omega$.

We now consider the magnetic and electromagnetic waves in ferrites, taking the displacement current into account. Writing $\mathbf{d} = \epsilon(\omega)\mathbf{e}$, where $\epsilon(\omega)$ is the dielectric constant, the following dispersion equation is obtained from Eq. (7):

$$\left\{1 + \frac{\tau\xi^2}{x^2 - \xi^2}\right\}\left\{1 + \frac{\tau\xi^2}{x^2 - \xi^2}\cos^2\vartheta\right\} - x^2 = 0, \qquad (10)$$

where

$$\tau = \frac{4\pi gM_0}{4\pi gM_0 + \Omega_1}, \qquad \xi^2 = \frac{\tau^2}{\varepsilon}\left(\frac{ck}{4\pi gM_0}\right)^2, \qquad x = \tau\frac{\omega}{4\pi gM_0}.$$

If $\xi^2 \gg 1$, Eq. (10) leads to the solution:

$$\omega^2 = \frac{c^2k^2}{\varepsilon}\left\{1 \pm \frac{4\pi gM_0}{\omega}\cos\vartheta\right\}, \qquad \omega^2 = \Omega\Omega_1. \qquad (11)$$

The first of these equations determines the frequency of the electromagnetic waves which propagate in a medium of anisotropic magnetic susceptibility with the following values for the two waves (right-handed and left-handed circular polarization):

$$\mu_1(\omega) = 1 - (4\pi gM_0/\omega)\cos\vartheta,$$
$$\mu_2(\omega) = 1 + (4\pi gM_0/\omega)\cos\vartheta. \qquad (12)$$

The second solution coincides with (8).

If $\xi^2 \ll 1$, Eq. (10) has the following roots:

$$\omega = ck\sqrt{\frac{1-\tau}{\varepsilon}}, \qquad \omega = ck\sqrt{\frac{1-\tau\cos^2\vartheta}{\varepsilon}}, \qquad (13)$$
$$\omega = 4\pi gM_0/\tau = \Omega_1 + 4\pi gM_0 = g(B_0 + \beta M_0).$$

If the conductivity of the medium is high, ($\sigma \gg \epsilon\omega$, $\sigma \gg c^2k^2/\omega$) the frequency of the magnetic waves is

$$\omega = \Omega_1 + 4\pi g M_0. \tag{14}$$

4. We now determine the damping of the magnetic waves due to the finite conductivity and relaxation processes.

If the absorption is small, the damping factor can be defined as

$$\Gamma = -(1/\overline{\mathcal{H}})\,\overline{d\mathcal{H}/dt}, \tag{15}$$

where the bar denotes time averages of expressions defined in Eqs. (1) and (5); in place of the fields **e** and **h** we substitute their values for $\sigma = 0$, $\lambda = 0$ or $\sigma = \infty$ and $\lambda = 0$.

If $\epsilon\omega \ll \sigma \ll c^2k^2/\omega \sim c^2\hbar^2/\Theta_C a^2$, it can be shown that:

$$\Gamma = 16\pi^2 \frac{\sigma g M_0}{c^2k^2}(\Omega + \Omega_1\cos^2\vartheta) + 2\frac{\lambda}{gM_0}(\Omega_1 + 2\pi g M_0 \sin^2\vartheta). \tag{16}$$

If $\sigma \gg 4\pi g M_0$ and $\sigma \gg c^2k^2/4\pi g M_0$

$$\Gamma = \frac{1}{\sigma}(ck)^2 \frac{gM_0}{\Omega_1 + 4\pi g M_0}(1 + \sin^2\vartheta) + 2\frac{\lambda}{gM_0}(\Omega_1 + 4\pi g M_0). \tag{17}$$

5. It can be easily shown that the absorption of the magnetic waves is small ($\Gamma \ll \omega$) if

$$\lambda \ll gM_0, \quad \sigma \ll c^2k^2/gM_0.$$

These inequalities are obviously the existence conditions for Bloch spin waves.

It follows from the second condition that

$$k \gg k_0,$$

where

$$k_0 = \begin{cases} \delta_0^{-1}, & l \ll \delta_0 \\ (\delta_0^2 l)^{-1/3}, & l \gg \delta_0, \end{cases} \tag{18}$$

l is the electron free path length and δ_0 is the depth of the skin layer corresponding to the frequency $\omega = gM_0$ ($\delta_0^2 = c^2/2\pi g M_0\sigma_0$, σ_0 is the static conductivity; when $l \gg \delta_0$ the expression for k_0 corresponds to the anomalous skin effect).

Thus, there are no spin waves for wavelengths large compared with $\lambda_0 = 1/k_0$.

If $k \ll k_0$, the magnetic wave spectrum is determined by Eq. (14). In this case the frequency is a weak function of wave vector.

The dependence of spin-wave frequency on wave vector, as is well known, is associated with the dependence of the magnetization and other thermodynamic quantities on temperature. A Bloch law ($T^{3/2}$) for the magnetization corresponds to the spectrum $\omega = \Theta_C(ak)^2/\hbar$ which is obtained if we neglect the terms $\beta + H_0/M_0$ and $4\pi\sin^2\vartheta$ in Eq. (9), i.e., if the magnetic interaction and anisotropy are neglected. It can be shown that frequencies $\omega = \Theta_C(ak)^2/\hbar$ are excited at temperatures much higher than $4\pi g M_0\hbar$ ($\sim 1°K$).

At temperatures $T \leq 4\pi g M_0\hbar$ the magnetic interaction plays an important role in the spectrum and the frequency is determined by Eq. (8). In this case we have a T^2 relation for the magnetization instead of the $T^{3/2}$ relation.[5] Equation (8) applies only when $k \gg k_0$. Whence it may be concluded that the spectrum $\omega \sim k\sin\vartheta$ is excited at temperatures which satisfy the condition

$$gB_0\hbar\,(a^2\sigma\Theta_c/\hbar c^2)^{1/3} < T < gB_0\hbar.$$

In the temperature region $T \ll gB_0\hbar\,(a^2\sigma\Theta_C/\hbar c^2)^{1/2}$, in place of the spectrum given in (8) we must use that given in (14) which yields an exponential dependence for deviations of the magnetization from the saturation value.

6. We now investigate coupled magnetoacoustic waves in ferromagnetic media.

The equation of motion for the magnetization and the elasticity equation are:

$$\frac{\partial \mathbf{M}}{\partial t} + \frac{\partial}{\partial x_k}(\mathbf{M}\dot{u}_k) = g[\mathbf{M}\times\mathbf{H}^{(e)}] - \frac{\lambda}{M^2}[\mathbf{M}\times[\mathbf{M}\times\mathbf{H}^{(e)}]], \tag{19}$$

$$\rho\ddot{\mathbf{u}} = \mathbf{f},$$

where $\mathbf{u}$ is the elastic displacement, $\mathbf{H}^{(e)}$ is the effective magnetic field and $\mathbf{f}$ is the force which acts on a unit volume of the medium (expressions for these are given below).

The energy in the ferromagnetic medium can be given in the form:

$$\mathcal{H} = \int\left\{\frac{1}{2}\alpha_{ik}\frac{\partial \mathbf{M}}{\partial x_i}\frac{\partial \mathbf{M}}{\partial x_k} + \frac{h^2 + \mathbf{e}\cdot\mathbf{d}}{8\pi} + \beta(\mathbf{M}) - \mathbf{M}\cdot\mathbf{H}_0 \right. \tag{20}$$

$$\left. + \frac{1}{2}\rho\dot{\mathbf{u}}^2 + \frac{1}{2}\lambda_{iklm}u_{ik}u_{lm} + F_{lm}(\mathbf{M})\,u_{lm}\right\} dV.$$

This expression differs from that given in (1) in the presence of the three last terms; the first two represent elastic energy and the third the magnetostriction energy (λ_{iklm} is the elasticity tensor).

Using Maxwell's equations and (19), and assuming that the current density is

$$\mathbf{j} = \sigma\left\{\mathbf{e} + \frac{1}{c}[\dot{\mathbf{u}}\times\mathbf{B}]\right\}, \quad \mathbf{B} = \mathbf{H} + 4\pi\mathbf{M},$$

it is easy to show that

$$\frac{d\mathcal{H}}{dt} = \int\Big\{-\Big(g\,[\mathbf{M}\times\mathbf{H}^{(e)}] - \frac{\lambda}{M^2}\,[\mathbf{M}\times[\mathbf{M}\times\mathbf{H}^{(e)}]]\Big)\Big(\mathbf{H}_0 + \mathbf{h} - \frac{\partial\beta}{\partial\mathbf{M}} + \alpha_{ik}\frac{\partial^2\mathbf{M}}{\partial x_i\partial x_k} - \mathbf{G}\Big) - \frac{1}{\sigma}\,j^2 + \dot{u}_i\Big[f_i - \frac{\partial\sigma_{ik}}{\partial x_k} - \frac{1}{c}\,[\mathbf{j}\times\mathbf{B}]_i - \mathbf{M}\frac{\partial}{\partial x_i}\Big(\mathbf{H}_0 + \mathbf{h} - \frac{\partial\beta}{\partial\mathbf{M}} + \alpha_{pr}\frac{\partial^2\mathbf{M}}{\partial x_p\partial x_r} - \mathbf{G}\Big)\Big]\Big\}\,dV + \int\Big\{\frac{c}{4\pi}\,[\mathbf{h}\times\mathbf{e}]_k + \alpha_{ik}\frac{\partial\mathbf{M}}{\partial x_i}\frac{\partial\mathbf{M}}{\partial t} + \dot{u}_i\Big[\sigma_{ik} + \delta_{ik}\mathbf{M}\Big(\mathbf{H}_0 + \mathbf{h} - \frac{\partial\beta}{\partial\mathbf{M}} + \alpha_{pr}\frac{\partial^2\mathbf{M}}{\partial x_p\partial x_r} - \mathbf{G}\Big)\Big]\Big\}\,ds_k,$$

where

$$\sigma_{ik} = \lambda_{iklm}u_{lm} + F_{ik}(\mathbf{M}), \quad \mathbf{G} = u_{lm}\partial F_{lm}(\mathbf{M})/\partial\mathbf{M}. \tag{21}$$

When $\sigma = \lambda = 0$ the volume integral vanishes. Whence it is easy to show that the effective magnetic field $\mathbf{H}^{(e)}$ and the volume force $\mathbf{f}$ are

$$\mathbf{H}^{(e)} = \mathbf{H}_0 + \mathbf{h} - \frac{\partial\beta}{\partial\mathbf{M}} + \alpha_{ik}\frac{\partial^2\mathbf{M}}{\partial x_i\partial x_k} - \mathbf{G},$$
$$f_i = \frac{\partial\sigma_{ik}}{\partial x_k} + \frac{1}{c}\,[\mathbf{j}\times\mathbf{B}]_i + \mathbf{M}\frac{\partial}{\partial x_i}\mathbf{H}^{(e)}. \tag{22}$$

Thus, for finite values of λ and σ the time derivative of the energy is given by

$$\frac{d\mathcal{H}}{dt} = -\int\frac{j^2}{\sigma}\,dV - \int_V\frac{\lambda}{M^2}\,[\mathbf{M}\times\mathbf{H}^{(e)}]^2\,dV + \int_S\Big\{\dot{u}_i(\sigma_{ik} + \delta_{ik}\mathbf{H}^{(e)}\mathbf{M}) + \frac{c}{4\pi}\,[\mathbf{h}\times\mathbf{e}]_k + \alpha_{ik}\frac{\partial\mathbf{M}}{\partial x_i}\frac{\partial\mathbf{M}}{\partial t}\Big\}\,ds_k.$$

7. We consider first coupled magnetoacoustic waves with $\lambda = 0$.

For simplicity it will be assumed that the medium is isotropic in both its elastic and magnetostrictive properties. The last condition means that $F_{ik}(\mathbf{M})$ is of the form

$$F_{ik}(\mathbf{M}) = \delta_{ik}M^2F_1(M^2) + M_iM_kF_2(M^2), \tag{23}$$

where F_1 and F_2 are certain functions of M^2.

Assuming that at equilibrium $u_{ik} = 0$, from the minimum energy condition it is easy to show that $F_{ik}(\mathbf{M}_0) = 0$.

Linearizing Eq. (22) and assuming for simplicity that F_1 and F_2 are constant, we obtain the following expressions for $\mathbf{H}^{(e)}$ and $\mathbf{f}$:

$$\mathbf{H}^{(e)} = \mathbf{h} - \beta\boldsymbol{\mu}_\perp - \boldsymbol{\mu}\frac{H_0}{M_0} - a\mathbf{n}(\boldsymbol{\mu}\mathbf{n}) + \alpha\Delta\mu - \delta_1\mathbf{M}_0\operatorname{div}\mathbf{u} - \frac{1}{2}\,\delta_2M_0((\mathbf{n}\nabla)\cdot\mathbf{u} + \nabla(\mathbf{n}\cdot\mathbf{u})),$$

$$f_i = \rho c_l^2\Delta u_i + \rho(c_l^2 - c_t^2)\frac{\partial}{\partial x_i}\operatorname{div}\mathbf{u} + \frac{1}{c}\,[\mathbf{j}\times\mathbf{B}_0]_i + \mathbf{M}_0\frac{\partial}{\partial x_i}\mathbf{H}^{(e)} + \delta_1\frac{\partial}{\partial x_i}(\mathbf{M}_0\cdot\boldsymbol{\mu}) + \frac{\delta_2}{2}\Big(M_{0i}\operatorname{div}\boldsymbol{\mu} + M_{0k}\frac{\partial\mu_i}{\partial x_k}\Big),$$

where δ_1 and δ_2 are the magnetostriction constants

$$\delta_1 = 2F_1 \text{ and } \delta_2 = 2F_2.$$

The linearized equations of motion for the magnetization and elasticity are of the form:

$$\frac{\partial\boldsymbol{\mu}}{\partial t} + \mathbf{M}_0\operatorname{div}\dot{\mathbf{u}} = gM_0\,[\mathbf{n}\times\mathbf{H}^{(e)}],$$

$$\ddot{\mathbf{u}} = c_t^2\Delta\mathbf{u} + (c_l^2 - c_t^2)\nabla\operatorname{div}\mathbf{u} + \frac{\delta_1}{\rho}\nabla(\mathbf{M}_0\boldsymbol{\mu}) + \frac{\delta_2}{2\rho}\Big(\mathbf{M}_0\operatorname{div}\boldsymbol{\mu} + (\mathbf{M}_0\nabla)\cdot\boldsymbol{\mu}\Big) + \frac{1}{c\rho}\,[\mathbf{j}\times\mathbf{B}_0] + \frac{1}{\rho}\nabla\mathbf{M}_0\cdot\mathbf{H}^{(e)}, \tag{24}$$

where $\mathbf{B}_0 = \mathbf{H}_0 + 4\pi\mathbf{M}_0$, c_l and c_t are the velocities of the longitudinal and transverse acoustic oscillations. Assuming that all quantities vary as $e^{-i(\omega t - \mathbf{k}\cdot\mathbf{r})}$ and that $\sigma = 0$, we obtain the following dispersion relation

$$(v^2 - c_t^2)^2(v^2 - \tilde{c}_l^2)(v^2 - \Omega\Omega_1/k^2) - \zeta(v^2 - c_t^2)f_1 - \zeta^2f_2 = 0, \tag{25}$$

where

$$v = \frac{\omega}{k},\ \zeta = \frac{M_0^2}{4\rho}\delta_2^2,\ \tilde{c}_l^2 = c_l^2 - \frac{M_0^2}{\rho}\Big[2(\delta_2 - 2\pi)\cos^2\vartheta + 2\delta_1 - a - \frac{H_0}{M_0} - \alpha k^2\Big],$$

$$f_1 = \frac{gM_0\Omega_1}{k^2}\Big\{v^2 - c_t^2 + (c_t^2 - c_l^2)\cos^2 2\vartheta + \frac{\Omega}{\Omega_1}(v^2 - c_l^2)\cos^2\vartheta + \frac{16\pi^2}{\delta_2^2}\Big(1 - \frac{\delta_2}{2\pi}\Big)(v^2 - c_t^2)\sin^2 2\vartheta\Big\},$$

$$f_2 = \frac{(gM_0)^2}{k^2}(c_t^2 - c_l^2)\cos^2\vartheta\cos^2 2\vartheta.$$

From this equation it is easy to obtain the velocities for the longitudinal (v_1) and transverse (v_2, v_3) acoustic waves:

$$v_1^2 = \tilde{c}_l^2\Big\{1 + \frac{gM_0^3}{4\rho c_l^2}(\delta_2 - 4\pi)^2\frac{\Omega_1}{\omega^2 - \Omega\Omega_1}\sin^2 2\vartheta\Big\},$$

$$v_2^2 = c_t^2\Big\{1 + \frac{gM_0^3}{8\rho c_t^2}\delta_2^2\frac{\Omega_1\cos^2 2\vartheta + \Omega\cos^2\vartheta + [(\Omega_1\cos^2 2\vartheta - \Omega\cos^2\vartheta)^2 + 4\omega^2\cos^2\vartheta\cos^2 2\vartheta]^{1/2}}{\omega^2 - \Omega\Omega_1}\Big\}, \tag{26}$$

$$v_3^2 = c_t^2\Big\{1 + \frac{gM_0^3}{8\rho c_t^2}\delta_2^2\frac{\Omega_1\cos^2 2\vartheta + \Omega\cos^2\vartheta - [(\Omega_1\cos^2 2\vartheta - \Omega\cos^2\vartheta)^2 + 4\omega^2\cos^2\vartheta\cos^2 2\vartheta]^{1/2}}{\omega^2 - \Omega\Omega_1}\Big\}.$$

These formulas apply if ω^2 is not close to $\Omega\Omega_1$.

If ω^2 is approximately the same as $\Omega\Omega_1$ the magnetic and acoustic branches of the oscillations "cross"; this effect is now considered for $\vartheta = \pi/2$ and $\vartheta = 0$.[6]

If $\vartheta = \pi/2$, the roots of the dispersion equation are:

$$v^2 = \begin{cases} \tilde{c}_l^2 \\ c_t^2 \\ \frac{1}{2}\left(c_t^2 + \frac{\Omega\Omega_1}{k^2}\right) + \frac{1}{2}\left[\left(c_t^2 - \frac{\Omega\Omega_1}{k^2}\right)^2 + \zeta\frac{gM_0\Omega_1}{k^2}\right]^{1/2}, \\ \frac{1}{2}\left(c_t^2 + \frac{\Omega\Omega_1}{k^2}\right) - \frac{1}{2}\left[\left(c_t^2 - \frac{\Omega\Omega_1}{k^2}\right)^2 + \zeta\frac{gM_0\Omega_1}{k^2}\right]^{1/2}. \end{cases} \tag{27}$$

The first two roots determine the phase velocities of the longitudinal and one of the transverse acoustic waves. When $kc_t < \sqrt{\Omega\Omega_1}$ the third root determines the phase velocity of the magnetic wave while the fourth determines that of the other transverse wave. When $kc_t > \sqrt{\Omega\Omega_1}$, on the other hand, the fourth root determines the phase velocity of the magnetic wave while the third determines the phase velocity of the acoustic wave.

If $\vartheta = 0$, the roots of the dispersion equation are:

$$v = \begin{cases} \tilde{c}_l \\ c_t - \frac{1}{2}\frac{\zeta}{c_t}\frac{gM_0}{kc_t + \Omega_1} \\ \frac{1}{2}\left(c_t + \frac{\Omega_1}{k} - \frac{1}{2}\frac{\zeta}{c_t}\frac{gM_0}{kc_t + \Omega_1}\right) + \frac{1}{2}\left[\left(c_t - \frac{\Omega_1}{k}\right)^2 + \zeta\frac{gM_0}{kc_t}\frac{3kc_t + \Omega_1}{kc_t + \Omega_1}\right]^{1/2} \\ \frac{1}{2}\left(c_t + \frac{\Omega_1}{k} - \frac{1}{2}\frac{\zeta}{c_t}\frac{gM_0}{kc_t + \Omega_1}\right) - \frac{1}{2}\left[\left(c_t - \frac{\Omega_1}{k}\right)^2 + \zeta\frac{gM_0}{kc_t}\frac{3kc_t + \Omega_1}{kc_t + \Omega_1}\right]^{1/2}. \end{cases} \tag{28}$$

When $kc_t < \Omega_1$, the third root determines the phase velocity of the magnetic wave while the fourth determines that of the transverse acoustic wave; if, however, $kc_t > \Omega_1$ the third root determines the phase velocity of the transverse acoustic wave while the fourth determines that of the magnetic wave.

Equations (27) and (28) apply if

$$(\lambda/gM_0)^2 \ll \delta_2^2 (M_0^2/4\rho c_t^2)\, M_0/(H_0 + \beta M_0).$$

It can be shown that the transverse waves are elliptically polarized and are of the following form:

$$\mathbf{u} = U\left\{\left(\frac{\mathbf{k}_\perp}{k_\perp^2} - \frac{\mathbf{k}_\parallel}{k_\parallel^2}\right)\cos(\omega t - \mathbf{k}\cdot\mathbf{r}) - \frac{[\mathbf{n}\times\mathbf{k}]}{k_\perp^2\eta}\sin(\omega t - \mathbf{k}\cdot\mathbf{r})\right\};$$

$$\boldsymbol{\mu} = \frac{gM_0^2}{2c_t}\delta_2 \frac{U\cos\vartheta}{\eta - \frac{\Omega_1}{\omega}\cos 2\vartheta}\left\{\frac{\mathbf{k}_\perp}{k_\perp^2}\sin(\omega t - \mathbf{k}\cdot\mathbf{r}) + \frac{[\mathbf{n}\times\mathbf{k}]}{k_\perp^2\eta}\cos 2\vartheta\cos(\omega t - \mathbf{k}\cdot\mathbf{r})\right\}, \tag{29}$$

where U is a constant,

$$\eta = \frac{\Omega_1}{\omega}\left\{1 + \frac{2\cos^2\vartheta}{\Omega_1^2}\frac{\omega^2 - \Omega\Omega_1}{\cos^2 2\vartheta + \frac{\Omega}{\Omega_1}\cos^2\vartheta \pm \left[\left(\cos^2 2\vartheta - \frac{\Omega}{\Omega_1}\cos^2\vartheta\right)^2 + 4\frac{\omega^2}{\Omega_1^2}\cos^2\vartheta\cos^2 2\vartheta\right]^{1/2}}\right\}\cos 2\vartheta \tag{30}$$

and $k_\parallel$ and $k_\perp$ are the longitudinal and transverse components of $\mathbf{k}$ (with respect to $\mathbf{M}_0$). The ratio of the semi-axes of the ellipse is

$$b/a = \cos\vartheta/\eta \tag{29'}$$

(the semi-axis a lies in the $(\mathbf{n}, \mathbf{k})$ plane and is perpendicular to $\mathbf{k}$).

When $\theta = 0$ we obtain two cylindrically polarized waves; with $\theta = \pi/2$ we have two linearly polarized waves for which the vector $\mathbf{u}$ has components along $\mathbf{M}_0$ and $\mathbf{M}_0 \times \mathbf{k}$.

8. We can analyze coupled magnetoacoustic oscillations in the high-conductivity case $\sigma \gg \omega c^2/c_t^2$ in similar fashion.

Here we present only the formulas for the phase velocities of the acoustic waves for $\vartheta = 0$ and $\vartheta = \pi/2$. If $\vartheta = 0$,

$$v_1 = c_t\left[1 - \frac{M_0^2}{2\rho c_t^2}\left(2\delta_1 + 2\delta_2 - a - 4\pi - \frac{H_0}{M_0}\right)\right],$$
$$v_2 = v_3 = c_t\left\{1 + \frac{M_0^2}{2\rho c_t^2}\left[\frac{B_0^2}{4\pi M_0^2} - \frac{1}{4}\frac{gM_0}{\Omega_1 + 4\pi g M_0}\left(\delta_2 - 2\frac{B_0}{M_0}\right)\right]\right\}. \quad (31)$$

When $\vartheta = \pi/2$

$$v_1 = c_t\left[1 - \frac{M_0^2}{2\rho c_t^2}\left(\delta_2 - \frac{H_0}{4\pi M_0}\right)^2\right], \quad (31')$$
$$v_2 = c_t\left[1 - \frac{M_0^2}{8\rho c_t^2}\frac{gM_0}{\Omega_1 + 4\pi g M_0}\right], \quad v_3 = c_t,$$

Taking $M_0 = 0$ and $\delta_1 = \delta_2 = 0$ in these expressions we obtain the velocity of acoustic waves in a high conductivity metal located in an external magnetic field H_0. If $H_0^2/8\pi\rho c_t^2 \ll 1$ these expressions assume the following form: for $\vartheta = 0$

$$v_1 = c_t,\ v_2 = v_3 = c_t(1 + H_0^2/8\pi\rho c_t^2); \quad (32)$$

for $\vartheta = \pi/2$

$$v_1 = c_t(1 + H_0^2/8\pi\rho c_t^2),\ v_2 = v_3 = c_t. \quad (32')$$

9. In the previous formulas we have neglected terms containing λ and σ. Taking these terms into account leads, firstly, to damping and, secondly, to an additional variation in phase velocity. We consider the second problem, having in mind a number of effects for which the condition $(\lambda/gM_0)^2 \gg \delta_2^2(M_0^2/4\rho c_t^2)M_0(H_0 + \beta M_0)^{-1}$ is satisfied. It can be shown that if this condition is satisfied the dispersion equation leads to the following expression for the phase velocity of the acoustic wave when $\vartheta = 0$

$$v_2^2 = v_3^2 = c_t^2\left[1 - \frac{\zeta}{c_t^2}gM_0\frac{\omega - \Omega_1}{(\omega - \Omega_1)^2 + (\lambda/gM_0)^2\Omega_1^2}\right]. \quad (33)$$

The relative change in the acoustic velocity $\Delta v/v$ for $\lambda/gM_0 \sim 10^{-1}$ and $\beta \sim 10^{-1}$ is approximately 0.1%.

10. We now consider the absorption factor for magnetoacoustic oscillations. For this purpose, in accordance with Eq. (15), we compute the quantities $\overline{\mathcal{H}}$ and $\overline{d\mathcal{H}/dt}$ with values of the field corresponding to $\lambda = 0$ and $\sigma = 0$. Here we present only the final results.

For small σ the absorption factors for longitudinal $\Gamma^{(l)}$ and transverse $\Gamma^{(t)}$ waves are

$$\Gamma^{(l)} = \lambda\omega^2\frac{M_0^2}{4\rho c_t^2}(4\pi - \delta_2)^2\frac{\omega^2 + \Omega_1^2}{[\omega^2 - \Omega\Omega_1]^2}\sin^2\vartheta$$
$$+\sigma\frac{M_0^2}{\rho c^2}\left\{\left[\frac{H_0}{M_0} + (4\pi - \delta_2)\frac{4\pi g M_0\Omega_1}{\omega^2 - \Omega\Omega_1}\cos^2\vartheta\right]^2 + (4\pi - \delta_2)^2\left[\frac{4\pi g M_0\omega}{\omega^2 - \Omega\Omega_1}\right]^2\cos^2\vartheta\right\}\sin^2\vartheta, \quad (34)$$

$$\Gamma^{(t)} = \lambda\omega^2\frac{M_0^2}{4\rho c_t^2}\delta_2^2\frac{\eta^2 + \cos^2 2\vartheta}{\eta^2 + \cos^2\vartheta}\frac{\cos^4\vartheta}{[\omega\eta - \Omega_1\cos 2\vartheta]^2} + \frac{\sigma B_0^2}{\rho c^2}\frac{\cos^2\vartheta}{\eta^2 + \cos^2\vartheta}$$
$$\times\left\{\left[1 - \frac{2\pi M_0}{B_0}\delta_2\frac{gM_0\cos^2\vartheta}{\eta\omega - \Omega_1\cos 2\vartheta}\right]^2\eta^2 + \left[1 - \frac{2\pi M_0}{B_0}\delta_2\frac{gM_0\cos 2\vartheta}{\eta\omega - \Omega_1\cos 2\vartheta}\right]^2\cos^2\vartheta\right\}.$$

It is apparent that the acoustic absorption is highly anisotropic and that the absorption is especially high at resonances at which the magnetic and acoustic frequencies coincide.

To determine the acoustic absorption coefficient in the resonance region it is necessary to use the exact dispersion equation, which takes account of the conductivity σ and the absorption factor λ. It can be shown that in this case the absorption factor is given by (30) and (34) if in the denominators of these expressions we replace $[\omega^2 - \Omega\Omega_1]^2$ by $[\omega^2 - \Omega\Omega_1]^2 + \Gamma\Omega\Omega_1$ where Γ is the damping factor for the magnetic wave as given by Eq. (16).

The longitudinal absorption factor for acoustic waves at resonance when $\vartheta = \pi/2$ is given by

$$\Gamma^{(l)} \approx \frac{M_0^2}{\rho c_t^2}\frac{(4\pi - \delta_2)^2}{4\pi}\frac{\omega_0^2}{\lambda},\quad \omega_0^2 = \Omega\Omega_1. \quad (35)$$

We compare the damping at resonance with the damping due to thermal conductivity. The latter is determined from the expression[7]

$$\gamma \approx (\Omega\Omega_1/C^2)\,\varkappa T\alpha_T^2\rho, \qquad (36)$$

where $\varkappa$ is the thermal conductivity, T is the temperature in degrees, C is the heat capacity per unit volume and α_T is the thermal expansion coefficient.

The ratio $\Gamma^{(l)}/\gamma$ is

$$\Gamma^{(l)}/\gamma \approx (4\pi - \delta_2)^2\, C^2 M_0^2/4\pi\alpha_T^2\lambda\varkappa c_l^2 T; \qquad (37)$$

with

$$\alpha_T = 10^{-5},\ C = 10^6,\ \varkappa \sim 10^6,\ T \sim 10^2\ ^\circ\mathrm{K},$$

$$\lambda/gM_0 \sim 10^{-1},\ \delta_2 \sim 1,\ c_l \sim 5\cdot 10^5,\ M_0 \sim 10^3,$$

this ratio becomes $\Gamma^{(l)}/\gamma \sim 10^2$.

Finally, we present the formulas which determine the acoustic absorption in ferromagnetic media of high conductivity $\sigma \gg c^2\omega/c_t^2$. When $\vartheta = 0$

$$\Gamma^{(l)} = \lambda\left(\delta_2 - 2\frac{B_0}{M_0}\right)^2 \frac{M_0^2}{4\rho c_t^2}\left(\frac{M_0}{B_0+\beta M_0}\right)^2\left(\frac{\omega}{gM_0}\right)^2 \qquad (38)$$

$$+\frac{\omega^2}{\sigma}\frac{M_0^2}{\rho c_t^2}\left(\frac{c}{c_t}\right)^2\left\{\frac{B_0}{4\pi M_0}+\frac{1}{2}\frac{M_0}{B_0+\beta M_0}\left(\delta_2 - 2\frac{B_0}{M_0}\right)\right\}^2,\ \Gamma^{(l)} = 0.$$

when $\vartheta = \pi/2$

$$\Gamma_2^{(t)} = 0,\ \Gamma_3^{(t)} = \lambda\omega^2\,(M_0^2/4\rho c_t^2)\,\delta_2^2/\Omega^2, \qquad (38')$$

$$\Gamma^{(l)} = (\omega^2/16\pi^2\sigma)\,(c/c_l)^2\,H_0^2/\rho c_t^2.$$

We see that the acoustic absorption is non-resonant at high values of σ.

We compare this absorption factor (38) with that associated with thermal conductivity and internal viscosity. In metals the latter is determined from the expression:[8]

$$\gamma \sim \tau\omega^2 n\varepsilon_0/\rho c_t^2,\ \omega\tau \ll c_t/v_0, \qquad (39)$$

where ϵ_0 is the Fermi energy and v_0 is the corresponding limiting electron velocity, n is the number of conduction electrons per unit volume and τ is the relaxation time. The ratio of the absorption factors (38) and (39) is

$$\frac{\Gamma}{\gamma} \sim \left(\frac{gM_0}{\sigma}\right)^2\left(\frac{c^2}{c_t v_0}\right)^2\left[\frac{B_0}{4\pi M_0}+\frac{1}{2}\frac{M_0}{B_0+\beta M_0}\left(\delta_2 - 2\frac{B_0}{M_0}\right)\right]^2. \qquad (40)$$

With $\sigma \sim 10^{17}$ and $\omega < 10^7$ both factors are of the same order of magnitude.

11. In conclusion, we consider the problem of exciting magnetic waves by means of an external acoustic field.

Suppose that the half-space $z > 0$ is filled with a ferromagnetic medium at the external surface of which ($z = 0$) is applied a displacement $\mathbf{u} = \mathbf{u}_0 e^{-i\omega t}$ or a stress $\sigma_{i3} = f_i e^{-i\omega t}$ ($\mathbf{u}_0$ and $\mathbf{f}$ are assumed constant). It is required to determine $\mathbf{u}(\mathbf{r}, t)$ and $\mathbf{u}(\mathbf{r}, t)$.

Since we wish to consider low resonance frequencies, the magnetization vector $\mathbf{M}_0$ will be taken perpendicular to the boundary $z = 0$ (to satisfy this condition we imagine a magnetization equal to $\mathbf{M}_0$ in the region $z < 0$).

It follows from Eq. (28) that when $\vartheta = 0$ the interaction of the transverse sound with magnetic waves is distinctive only in the resonance effect. Hence we will assume that $\mathbf{u}_0$ and $\mathbf{f}$ are in the (x, y) plane which contains the vector $\boldsymbol{\mu}$.

In our case, the basic equations (24) can be written in the form:

$$\ddot{\mathbf{u}} - c_t^2\frac{\partial^2\mathbf{u}}{\partial z^2} - \frac{M_0\delta_2}{2\rho}\frac{\partial\boldsymbol{\mu}}{\partial z} = 0,$$

$$\dot{\boldsymbol{\mu}} = gM_0\left[\mathbf{n}\times\left(-\frac{\omega_0}{gM_0}\boldsymbol{\mu} + \mathbf{h}^{(s)}\right)\right] + \lambda\left(\frac{\omega_0}{gM_0}\boldsymbol{\mu} - \mathbf{h}^{(s)}\right) = 0,$$

where

$$\mathbf{h}^{(s)} = -\frac{\delta_2 M_0}{2}\frac{\partial\mathbf{u}}{\partial z},\quad \omega_0 = gM_0\left(\beta + \frac{H_0}{M_0}\right)$$

It follows from the second equation that

$$\boldsymbol{\mu} = \hat{\chi}\mathbf{h}^{(s)},$$

where the tensor $\hat{\chi}$ is of the form:

$$\hat{\chi} = \frac{-gM_0\omega_0}{\omega_0^2 - \left(\omega - i\omega_0\frac{\lambda}{gM_0}\right)^2}$$

$$\times\begin{pmatrix} 1 - i\frac{\lambda}{gM_0}\frac{\omega}{\omega_0} + \left(\frac{\lambda}{gM_0}\right)^2 & i\frac{\omega}{\omega_0} \\ -i\frac{\omega}{\omega_0} & 1 - i\frac{\lambda}{gM_0}\frac{\omega}{\omega_0} + \left(\frac{\lambda}{gM_0}\right)^2 \end{pmatrix}.$$

Assuming that $\mathbf{u}$ and $\boldsymbol{\mu}$ are proportional to $e^{-i\omega t}$, we have

$$\omega^2\mathbf{u} + (c_t^2 - \zeta\hat{\chi})\,\partial^2\mathbf{u}/\partial z^2 = 0,$$

whence

$$\mathbf{u} = \mathbf{c}_1 e^{ik_1 z} + \mathbf{c}_2 e^{ik_2 z},$$

where $\mathbf{c}_1$ and $\mathbf{c}_2$ are integration constants and

$$k_1^2 = \frac{\omega^2}{c_t^2}\frac{c_t^2}{c_t^2 - \zeta\left(\chi_{xx} - \sqrt{\chi_{xy}\chi_{yx}}\right)},\quad k_2^2 = \frac{\omega^2}{c_t^2}\frac{c_t^2}{c_t^2 - \zeta\left(\chi_{xx} + \sqrt{\chi_{xy}\chi_{yx}}\right)}.$$

If $\mathbf{u}|_{z=0} = \mathbf{u}_0$ is given,

$$c_{1x} = c_{2x} = ic_{1y} = -ic_{2y} = u_0/2$$

($\mathbf{u}_0$ is taken along the x axis) and

$$\mathbf{u}(z, t) = \frac{1}{2} u_0 \{e^{i(k_1 z - \omega t)} + e^{i(k_2 z - \omega t)}\} \mathbf{i} + \frac{i}{2} u_0 \{e^{i(k_1 z - \omega t)} - e^{i(k_2 z - \omega t)}\} \mathbf{j},$$

$$\boldsymbol{\mu}(z, t) = -{}^1/_2 M_0 \hat{\delta}_2 \hat{\chi} \partial \mathbf{u} / \partial z.$$

Here $\mathbf{i}$ and $\mathbf{j}$ are unit vectors along the x and y axes. Whence:

$$\mu_x(z, t) = \frac{\delta_2 \omega \omega_0 g M_0^2 u_0}{2c_t \left[(\omega^2 - \omega_0^2)^2 + 4\omega^2 \omega_0^2 \left(\frac{\lambda}{gM_0}\right)^2\right]} \left\{(\omega^2 - \omega_0^2) \sin(\omega t - kz) - 2\omega\omega_0 \frac{\lambda}{gM_0} \cos(\omega t - kz)\right\},$$

$$\mu_y(z, t) = \frac{\delta_2 \omega^2 g M_0^2 u_0}{2c_t (\omega^2 - \omega_0^2)^2 + 4\omega^2 \omega_0^2 (\lambda / gM_0)^2]} \left\{(\omega^2 - \omega_0^2) \cos(\omega t - kz) + 2\omega\omega_0 \frac{\lambda}{gM_0} \sin(\omega t - kz)\right\}, \quad (41)$$

$$u(z, t) = u_0 \cos(\omega t - kz)$$

(here we have made use of the fact that k_1 and k_2 are approximately the same; thus $k_1 = k_2 = k = \omega/c_t$).

The equations in (41) apply if:

$$\lambda / gM_0 \gg (\zeta / c_t^2)\, gM_0 / \omega_0.$$

At resonance:

$$\mu_{res} / M_0 \approx \delta_2 (gM_0)^2 u_0 / \lambda c_t.$$

Assuming $\lambda/gM_0 \sim 10^{-1}$, $\omega_0 \sim 10^7$, and $\omega_0 u_0 / c_t \sim 10^{-6}$ we find $\mu_{res}/M_0 \sim 10^{-2}$.

If the stress is given at the boundary,

$$\mu_x(z, t) = \frac{\delta_2 \omega_0 g M_0^2 f}{2\rho c_t^2} \frac{(\omega^2 - \omega_0^2) \cos(\omega t - kz) + 2\omega\omega_0 (\lambda / gM_0) \sin(\omega t - kz)}{(\omega^2 - \omega_0^2)^2 + 4\omega^2 \omega_0^2 (\lambda / gM_0)^2},$$

$$\mu_y(z, t) = -\frac{\delta_2 \omega_0 g M_0^2 f}{2\rho c_t^2} \frac{(\omega^2 - \omega_0^2) \sin(\omega t - kz) - 2\omega\omega_0 (\lambda / gM_0) \cos(\omega t - kz)}{(\omega^2 - \omega_0^2)^2 + 4\omega^2 \omega_0^2 (\lambda / gM_0)^2},$$

$$u(z, t) = \frac{-f}{\rho \omega c_t} \sin(\omega t - kz).$$

These formulas apply when $\lambda/gM_0 \gg (\zeta/c_t^2)\, gM_0/\omega_0$.

The authors wish to express their gratitude to Academician L. D. Landau for a number of valuable comments and to M. I. Kaganov for illuminating discussions.

[1] C. Herring and C. Kittel, Phys. Rev. **81**, 869 (1951).

[2] A. I. Akhiezer and L. A. Shishkin, J. Exptl. Theoret. Phys. (U.S.S.R.) **34**, 1267 (1958), Soviet Phys. JETP **7**, 875 (1958).

[3] L. D. Landau and E. M. Lifshitz, Soviet Phys. **8**, 157 (1935).

[4] T. Holstein and H. Primakoff, Phys. Rev. **58**, 1098 (1940).

[5] M. I. Kaganov and V. M. Tsukernik, J. Exptl. Theoret. Phys. (U.S.S.R.) **34**, 1610 (1958), Soviet Phys. JETP **7**, 1107 (1958).

[6] E. A. Turov and Iu. P. Irkhin, Физика металлов и металловедение (Physics of Metals and Metal Research) **3**, 15 (1956).

[7] L. D. Landau and E. M. Lifshitz, Механика сплошных сред (Mechanics of Continuous Media) GITTL 2nd ed., p. 776.

[8] Akhiezer, Kaganov and Liubarskii, J. Exptl. Theoret. Phys. (U.S.S.R.) **32**, 837 (1957), Soviet Phys. JETP **5**, 685 (1957).

Translated by H. Lashinsky
31

MOMENT OF INERTIA OF NONSPHERICAL NUCLEI

Iu. K. KHOKHLOV

P. N. Lebedev Physics Institute, Academy of Sciences, U.S.S.R.

Submitted to JETP editor February 24, 1958

J. Exptl. Theoret. Phys. (U.S.S.R.) **35**, 240-243 (July, 1958)

The formula proposed by Inglis for the nuclear moment of inertia is calculated by perturbation theory in an approximation that is quadratic in the deformation parameter. An infinite rectangle well is assumed. The obtained moment of inertia of closed shells is several times larger than the hydrodynamic moment of inertia.

1. Assume a nonspherical potential well, rigidly coupled to a massive rotator. If we fill the lower levels of the well with non-interacting nucleons, we obtain a certain system (called the Inglis model[1]), the rotary properties of which are of procedural interest in the study of the rotation of real nuclei. The moment of inertia of the system comprises the moment of inertia of the rotator and the moment of the inertia of the nucleons entrained by the rotator. The latter moment is given by formula (4), previously investigated by Inglis[1,2] and by Bohr and Mottelson.[3] These authors used the potential of the anisotropic harmonic oscillator, and were thus able to calculate (4) in closed form.. In the case of closed shells, the result obtained does not differ substantially from the hydrodynamic result.

The present paper concerns results obtained for an infinite rectangular potential well. Because of the great mathematical difficulties, we restrict ourselves to closed shells. The wave functions were calculated by perturbation of the boundary conditions, up to and including the fourth approximation. The perturbation due to the rotation was considered [see Eq. (4)] in the first order of perturbation theory. Alltogether the moment of inertia of the closed shells was determined up to terms quadratic in the deformation parameter.

2. In a coordinate system that rotates, together with the nucleus, around the x axis with angular velocity Ω, the boundary S of the potential well is given by

$$r = R_0(1+\alpha), \text{ where } \alpha = \sum_{\lambda=0} \alpha_\lambda P_\lambda(\cos\theta). \tag{1}$$

Here α_λ are coefficients which will be considered in the following small compared to unity, θ is the polar angle, and $P_\lambda(\cos\theta)$ are Legendre polynomials with the usual normalization $P_\lambda(1) = 1$.

The wave function Ψ obeys inside S the time-independent Schrödinger equation of a free particle, augmented by a term describing the Coriolis force

$$\left(\nabla^2 + k^2 + \frac{2}{\hbar} M\Omega L_x\right)\Psi = 0, \tag{2}$$

with the boundary condition

$$\Psi|_S = 0. \tag{3}$$

Here k is the wave number, M the nucleon mass, and L_x the projection of the angular momentum on the x axis.

The contribution to the moment of inertia from the given nucleon equals

$$I = \hbar\left[\frac{\partial}{\partial\Omega}(\Psi, L_x\Psi)\right]_{\Omega=0} = \frac{2M}{k^2}\frac{(\varphi, L_x\varphi)}{(\psi,\psi)}. \tag{4}$$

Here

$$\psi = \sqrt{N}\Psi_{\Omega=0};\ \varphi = \sqrt{N}\frac{\hbar k^2}{M}\frac{\partial\Psi}{\partial\Omega}\Big|_{\Omega=0};$$
$$N = (\psi,\psi). \tag{5}$$

The functions ψ and φ obey the following equations and boundary conditions

$$(\nabla^2 + k^2)\psi = 0;\ (\nabla^2 + k^2)\varphi = -2k^2 L_x\psi; \tag{6}$$

$$\psi|_s = 0;\ \varphi_s = 0. \tag{7}$$

In an unperturbed spherically-symmetrical square well the functions ψ have the form

$$\psi^{(0)} = j_l(k_0 r)\, Y_{lm}. \tag{8}$$

Here Y_{lm} are spherical harmonics, $j_l(x)$ the spherical Bessel functions, and k_0 the eigenvalue determined by the condition $j_l(k_0R_0) = 0$. In the following we shall denote $k_0R_0 \equiv X$. We shall characterize the excited states by the same numbers, l and X. We shall speak about closed l-shells in the nonspherical well in the sense that the participating states form closed l-shells for vanishing deformation.

In general ψ and φ are given by

$$\psi = \sum_{l'} a_{l'} j_{l'}(x) Y_{l'm}, \quad a_l = 1; \tag{9}$$

$$\varphi = \frac{1}{2}(\varphi^{(+)} + \varphi^{(-)}), \tag{10}$$

$$\varphi^{(+)} = \sum_{l'} [a_{l'} f_{l'}(x) + b_{l'} j_{l'}(x)] B_{l'} Y_{l', m+1},$$

$$\varphi^{(-)} = \sum_{l'} [a_{l'} f_{l'}(x) + b_{l'} j_{l'}(x)] C_{l'} Y_{l', m-1}. \tag{11}$$

Here

$$B_l = (L_+)_{m+1, m} = \sqrt{(l+m+1)(l-m)};$$

$$C_l = (L_-)_{m-1, m} = \sqrt{(l+m)(l-m+1)};$$

$$L_\pm = L_x \pm i L_y; \quad x = kr;$$

the numbers k, $a_{l'}$, $b_{l'}$, and c_l obviously depend on l, m, and X.

It is easy to see that the terms which contain the functions $f_{l'}(x) \equiv x \frac{d}{dx} j_{l'}(x)$ are particular solutions of the inhomogeneous equation for φ, while the terms containing $j_{l'}(x)$ are solutions of the corresponding homogeneous equation. The coefficients $b_{l'}$ are determined by the boundary condition $\varphi^{(+)}|_S = 0$ and the coefficients $c_{l'}$ are obtained from the $b_{l'}$ by changing m to $-m$.

The moment of inertia is now given by

$$I = \frac{1}{2}(I_+ + I_-); \; I_+ = \frac{M}{k^2} \frac{(\psi, L_- \varphi^{(+)})}{(\psi\psi)} \tag{12}$$

$$= \frac{M}{k^2} \cdot \frac{\left(\sum_{l'} a_{l'} j_{l'}(x) Y_{l'm}, \; \sum_{l'} [a_{l'} f_{l'}(x) + b_{l'} j_{l'}(x)] B_{l'}^2 Y_{l'm}\right)}{\left(\sum_{l'} a_{l'} j_{l'}(x) Y_{l'm}, \; \sum_{l'} a_{l'} j_{l'}(x) Y_{l'm}\right)}.$$

The moment I_- follows from I_+ by the substitution of m by $-m$. We therefore do not have to investigate I_- separately, and correspondingly do not need the function $\varphi^{(-)}$.

We now expand all quantities in power series of α_λ:

$$k \approx k_0 + k_1 + k_2 + k_3 + k_4;$$

$$a_{l'} \approx a_{l'}^{(1)} + a_{l'}^{(2)} + a_{l'}^{(3)} \text{ for } l' \neq l; \quad a_l = 1; \tag{13}$$

$$b_{l'} \approx b_{l'}^{(-1)} + b_{l'}^{(0)} + b_{l'}^{(1)} + b_{l'}^{(2)}.$$

We have here written the terms needed to calculate the moment of inertia in the quadratic approximation. All these terms are successively determined by the boundary conditions (7).

The moment I_+ can be written as the series

$$I_+ \approx I_+^{(-1)} + I_+^{(0)} + I_+^{(1)} + I_+^{(2)}. \tag{14}$$

In summing over m, the terms $I_+^{(-1)}$, $I_+^{(0)}$ and $I_+^{(1)}$ vanish. Thus, as could be expected, the expansion of the moment of inertia for closed shells begins with the quadratic term:

$$I_{l,X}^{(2)} = \sum_m I_+^{(2)}. \tag{15}$$

After extensive calculations we obtain

$$I_{l,X}^{(2)} = \sum_m \frac{M}{k_0^2} \Big\{ \frac{1}{12} [(2l-1)(2l+5) + 2X^2] B_l^2 (p_{ll} - q_{ll})^2 + \sum_{l'}{}' \Big[\frac{1}{4} (B_l^2 + B_{l'}^2)(p_{ll'}^2 + q_{ll'}^2) - B_l B_{l'} p_{ll'} q_{ll'} \Big] \times [2X^2 + (1 + 2\varphi_{l'}) \psi_{l'}] \Big\}. \tag{16}$$

Here

$$\varphi_{l'} = 1 + f_{l'}(X)/j_{l'}(X), \; \psi_{l'} = l'(l'+1) - X^2 + \varphi_{l'} - \varphi_{l'}^2;$$

$$p_{ll'} = (l, m \,|\, \alpha \,|\, l', m); \; q_{ll'} = (l, m+1 \,|\, \alpha \,|\, l', m+1). \tag{17}$$

Taking for α the particular value

$$\alpha = \alpha_2 P_2(\cos\theta) \tag{18}$$

and summing over m, we have

$$I_{l,X}^{(2)} = \frac{9}{10} M R_0^2 \alpha_2^2 \times \Big\{ \frac{2}{9} \Big[1 + \frac{(2l-1)(2l+5)}{2X^2} \Big] \frac{l(l+1)(2l+1)(2l+5)}{(2l-1)(2l+3)^2} + 2X^4 \Big[\frac{l(l-1)}{(2l-1)^4} - \frac{(l+1)(l+2)}{(2l+3)^4} \Big] + X^2 \Big[\frac{l(l-1)}{(2l-1)^2} \Big(\frac{4}{2l-1} - 1 \Big) + \frac{(l+1)(l+2)}{(2l+3)^2} \Big(\frac{4}{2l+3} + 1 \Big) \Big] \Big\}. \tag{19}$$

The moment of inertia of the whole nucleus equals

$$I \approx g \sum_{l,X} I_{l,x}^2. \tag{20}$$

Here $g = 4$ is the number of nucleons which can simultaneously occupy the state with given l, X, and m.

3. Table I lists the moments of inertia of several nuclei obtained by numerically summing (19), in terms of the hydrodynamic moment of inertia I_{hydr} which is given in the quadratic approximation by

$$I_{hydr} = \frac{9}{10} M A R_0^2 \alpha_2^2; \tag{21}$$

here A is the atomic number of the nucleus.

We see that in the considered range of A the ratio I/I_{hydr} is several times larger than unity. Thus the results obtained in references 1 to 3 do not occur in our case.

Concerning the region of applicability of the quadratic approximation, we can make the following remarks. As was known earlier and confirmed in the present paper, the range of applicability of perturbation theory is rather small for states with angular momentum $l \approx 0$. In this case the effective expansion parameter turns out not to be α_2 (which is true for extremely large l) but $X^2\alpha_2$,

A	136	180	184	212	264	276	312	372	392
I/I_{hydr}	10.5	8.8	7.9	10.4	9.4	5.0	6.5	6	15.6

where $X \equiv k_0 R_0$, and $X^2 \approx 100$. Therefore the range of applicability of perturbation theory for the moment of inertia is determined, strictly speaking, by $X^2\alpha_2$ since the states with $l = 0; 1; \ldots$ give a large contribution. However, one can expect that the averaged value of the moment will be correct over a substantially larger range of α_2. This can be explained as follows. We divide all states into two groups, states with large l and states with small l, where the latter contain the cases $l = 0; 1; \ldots$. Both groups will give approximately equal but opposite contributions to the moment of inertia, with an appreciable mutual cancellation of terms containing the parameter $(\alpha_2 X^2)^2$ taking place. This cancellation, incidentally, turns out to be incomplete. This explains the obtained oscillations of the moment of inertia as a function of A.

[1] D. Inglis, Phys. Rev. **96**, 1059 (1954).
[2] D. Inglis, Phys. Rev. **103**, 1786 (1956).
[3] A. Bohr and B. Mottelson, Kgl. Dansk. Vidensk. Selsk. Mat.-Fys. Medd, **30**, No. 1 (1955).

Translated by M. Danos
32

SOVIET PHYSICS JETP VOLUME 35 (8), NUMBER 1 JANUARY, 1959

ON THE POLARIZATION OF RECOIL NUCLEONS IN THE PHOTOPRODUCTION OF PIONS

N. F. NELIPA and V. A. FEOKTISTOV

P. N. Lebedev Physics Institute, Academy of Sciences, U.S.S.R.

Submitted to JETP editor February 24, 1958

J. Exptl. Theoret. Phys. (U.S.S.R.) **35**, 244-248 (July, 1958)

A general expression for the polarization of recoil nucleons appearing during the production of pions by photons has been obtained on the basis of the momentum and parity conservation laws. As an example, an expression is derived for the polarization in pion production in s, p, and d states.

1. Measurement of the polarization of the recoil nucleons that appear in photoproduction of mesons would help clarify, in principle, many important problems connected with the difference between the Fermi and Yang solutions, with the determination of small phase shifts in meson-nucleon scattering, with the elimination of the Miñami ambiguity, etc.

A theoretical study of the problems of polarization can be made, roughly speaking, in two ways. The first,[1] based on the use of the density matrix, leads to the most general expressions for polarization, a particular case of interest to us being the expression for the polarization P of recoil nuclei in meson photoproduction. The second method, which employs the phenomenological scattering S matrix,[2] is simpler, albeit more limited. An expression for P, was obtained by the last method in reference 3.*

In the present work we should like to call attention to still another possibility of obtaining a general expression for P within the framework of the S matrix. Unlike the authors of reference 3, we obtained a more general expression for P, in which summation over the spin projections of the initial particles leads to the Racah coefficient.† The use of such a formula facilitates the calcula-

*An expression for P, in the particular case when the mesons are produced only in the s and p states, is given by Fel'd[4] without proof.

†Naturally, the expression we obtained for P is the same as obtained with the aid of the density matrix.

tions considerably, for tables are available for the coefficients that enter into the formula. By way of an example, we have calculated the expression for P in that case when the mesons are produced in the s, p, and d states. If d-state meson production is disregarded, our expression for P goes into the corresponding expression of Fel'd.[4]

2. We shall consider the reaction

$$\gamma + N \to N' + \pi. \tag{1}$$

To simplify the calculations we assume that the incident photon moves along the z axis and that the nucleon is emitted in the xz plane. Then the non-vanishing nucleon polarization will be that along the y axis, i.e., we must find an expression for the following quantity

$$P = (d\sigma_+ - d\sigma_-)/(d\sigma_+ + d\sigma_-), \tag{2}$$

where $d\sigma_+$ and $d\sigma_-$ are the differential cross sections for meson photoproduction, corresponding to the production of recoil nucleons with spins along and against the y axis. We calculate $d\sigma_+$ and $d\sigma_-$ by the same method as used to derive an expression for the differential cross section for photoproduction (see for example reference 5 and the bibliography contained therein). The only difference is that we do not sum over the finite nucleon spin projections, but calculate the cross sections for the two spin projections separately, thus obtaining $d\sigma_+$ and $d\sigma_-$.

We shall perform the calculations in the center-of-mass system. The initial photon-nucleon system can be described in terms of the total angular momentum L of the incident photon, for the electric and magnetic multiplicities p = 0 or 1 respectively, and a nucleon spin I. The final meson-nucleon system will be described by a relative orbital meson momentum l' and a total meson and nucleon spin s', so that $s' = 1/2$. The probability of the transition from a photon-nucleon with total momentum J = L + I into a nucleon-meson state having the same total momentum will be characterized by the matrix $S^J_{l's',LI}$. Then the amplitude of process (1), corresponding to the production of particles with definite values of each spin projection, is written as follows:[5]

$$f = \sum_{JLpl'} i^{L-l'+p} \sqrt{\frac{\pi}{2}} \times (2L+1)^{1/2} m^p C^{JM}_{Lm;\,Im_I} C^{JM}_{l'\mu';\,s'm_{s'}} S^J_{l's';\,LI} Y^{\mu'}_{l'}(\vartheta). \tag{3}$$

Here $m = \pm 1$ (two transverse photon polarizations), $C^{JM}_{j_1 m_1 j_2 m_2}$ are the Clebsch-Gordan coefficients, $Y^{\mu'}_{l'}(\vartheta)$ spherical functions, ϑ the angle between the directions of motion of the photon and meson, and m_I, $m_{s'}$, μ' are the projections of I, s' and l'. Here $m_{s'} = 1/2$ corresponds to a recoil-nucleon spin directed along the z axis (let this state be described by the function α), and $m_{s'} = -1/2$ is directed along the negative z axis (this state is described by the function β). We are interested in the polarization of the recoil nucleons along the y axis, i.e., the relation between the state of a nucleon with spins along the positive y axis (this state will be described by the function γ) and the state of one with spins along the negative y axis (function δ). The functions α and β are expressed in terms of the functions γ and δ as follows:

$$\alpha = (\gamma + \delta)/\sqrt{2}, \quad \beta = -i(\gamma - \delta)/\sqrt{2}. \tag{4}$$

Taking these relations into account, the expressions for the amplitudes f_+ and f_-, for meson photoproduction accompanied by production of recoil nucleons with spins along the positive and negative y axis, are written

$$f_\pm = \sum_{JLpl'} i^{L-l'+p} \frac{\sqrt{\pi}}{2} (2L+1)^{1/2} m^p C^{JM}_{LmIm_I} S^J_{l's',LI} Y^{\mu'}_{l'}(\vartheta) \times [C^{JM}_{l'\mu' 1/2\,1/2} \mp C^{JM}_{l'\mu' 1/2\,-1/2}]. \tag{5}$$

The differential cross section averaged over the projections of the initial spins (m and m_I) will be of the form

$$d\sigma_\pm = \frac{1}{4k^2} \sum_{mm_I} |f_\pm|^2 \, d\Omega, \tag{6}$$

where k is the wave number of the photon.

The expressions for $d\sigma_+$ and $d\sigma_-$ contain terms with products of the Clebsch-Gordan coefficients, both with equal signs of the projections $m_{s'}$ (denoted by a_+ and a_-) and with different signs of $m_{s'}$ (i.e., b_+ and b_-). It turns out that $a_+ = a_- = a$ and $b_+ = -b_-$, i.e.,

$$d\sigma_+ = a\,d\Omega + d\sigma_n, \quad d\sigma_- = a\,d\Omega - d\sigma_n, \tag{6'}$$

where $d\sigma_n = b_+ d\Omega$.

Using the relation

$$Y^{\mu^*}_l(\vartheta)\, Y^{\mu'}_{l'}(\vartheta) = (-1)^\mu \sum_{n=|l-l'|}^{l+l'} \sqrt{\frac{(2l+1)(2l'+1)}{4\pi(2n+1)}}\, C^{n0}_{l'0l0} C^{nM}_{l-\mu l'\mu'} Y^M_n(\vartheta), \tag{7}$$

we obtain

$$d\sigma_n = \frac{1}{16k^2} \sum_{\substack{J_1 L_1 p_1 l_1' \\ J_2 L_2 p_2 l_2' n}} i^{L_1 - L_2 - l_1' + l_2' + p_1 - p_2} \sqrt{\pi} \left[(2L_1+1)(2L_2+1)\right.$$

$$\times (2l_1'+1)(2l_2'+1)\frac{1}{(2n+1)}\Big]^{1/2} \mathrm{Im}\{S^*(1)\,S(2)\} \sum_{mm_I} (-1)^{\mu_2'} m^{p_1+p_2} C^{J_1 M_1}_{L_1 m J m_I} \tag{8}$$

$$\times C^{J_2 M_2}_{L_2 m J m_I} C^{n0}_{l_1' 0 l_2' 0} C^{n\mu_1' - \mu_2'}_{l_1' \mu_1' l_2' - \mu_2'} \left(C^{J_1 M_1}_{l_1' \mu_1' 1/2\, 1/2} C^{J_2 M_2}_{l_2' \mu_2' 1/2 - 1/2} - C^{J_1 M_1}_{l_1' \mu_1' 1/2 - 1/2} C^{J_2 M_2}_{l_2' \mu_2' 1/2\, 1/2} \right) Y^{\mu_1' - \mu_2'}_{n-1}(\vartheta)\, d\Omega.$$

Inserting (6′) into (2) and bearing in mind that $d\sigma_+ + d\sigma_- = d\sigma$, we find

$$P = 2d\sigma_n / d\sigma. \tag{9}$$

The quantity P can be sought with the aid of (8), but this leads to rather cumbersome computations. The calculations become much simpler if the summation in expression (8) is over the projections of the spins m_I and m. To perform this summation, we use the following relations:[6]

$$C^{e\alpha+\beta}_{a\alpha b\beta} C^{c\alpha+\beta+\delta}_{e\alpha+\beta d\delta} = \sum_f \sqrt{(2e+1)(2f+1)}\, C^{c\alpha+\beta+\delta}_{a\alpha f\beta+\delta} C^{f\beta+\delta}_{b\beta d\delta}\, W(abcd; ef), \tag{10}$$

$$\sum_\beta C^{e\alpha+\beta}_{a\alpha b\beta} C^{c\gamma}_{c\alpha+\beta d\gamma-\alpha-\beta} C^{f\gamma-\alpha}_{b\beta d\gamma-\alpha-\beta} = \sqrt{(2e+1)(2f+1)}\, C^{c\gamma}_{a\alpha f\gamma-\alpha}\, W(abcd; ef), \tag{11}$$

where W(abcd; ef) are the Racah coefficients (the Latin and Greek letters denote momenta and projections of momenta respectively).

Using the symmetry properties of the Clebsch-Gordan coefficients together with relation (10) and (11) we get

$$d\sigma_n = \frac{1}{4k^2} \sum i^{L_1 - l_1' + p_1 - L_2 + l_2' - p_2} \sqrt{\frac{\pi}{2}} \left[(2L_1+1)(2L_2+1)(2l_1'+1)(2l_2'+1)\right]^{1/2}$$

$$\times (2J_1+1)(2J_2+1)\left[\frac{2n(n+1)}{2n+1}\right]^{1/2} C^{n0}_{l_1' 0 l_2' 0} C^{n0}_{L_1 1 L_2 - 1}\, W\left(L_1 J_1 L_2 J_2;\ \tfrac{1}{2}\, n\right) \tag{12}$$

$$\times \left[W\left(\tfrac{1}{2}\, l_1' n - \tfrac{1}{2}\, l_2';\ J_1\, n\right) W\left(l_2' J_1\ \tfrac{1}{2}\, n;\ n - \tfrac{1}{2}\, J_2\right) - W\left(\tfrac{1}{2}\, l_1' n + \tfrac{1}{2}\, l_2';\ J_1\, n\right) W\left(l_2' J_1\, \tfrac{1}{2}\, n;\ n + \tfrac{1}{2}\, J_2\right)\right]$$

$$\times \mathrm{Im}\ \{S^*(1)\, S(2)\}\ Y_{n-1} d\Omega.$$

The summation is over $J_1 J_2 L_1 L_2 p_1 p_2 l_1' l_2'$ and n. Using (12), and bearing (9) in mind, an expression can be found for P. Here it is necessary to employ the tabulated numerical values of the Racah coefficients[7] and of the Clebsch-Gordan coefficients.[8]

3. To illustrate the use of the formula obtained, let us find an expression for P for the case when the mesons are formed in the s, p and d states. The transitions possible in this case are listed in the table.

Transition	L	J	l′
E_{11}	1	$^1/_2-$	0
E_{13}	1	$^3/_2-$	2
M_{11}	1	$^1/_2+$	1
M_{13}	1	$^3/_2+$	1
E_{23}	2	$^3/_2+$	1
M_{23}	2	$^3/_2-$	2
M_{25}	2	$^5/_2-$	2
E_{35}	3	$^5/_2-$	2

The letters in the first column denote the matrix elements of the corresponding transitions; E and M represent electric and magnetic transitions respectively (the first index is determined by the quantity L, and the second equals 2J).

Taking these transitions into account, the expression for P becomes

$$P = \frac{\sin\vartheta\, d\Omega}{4k^2 d\sigma} \mathrm{Im}\left\{E_{11}^* \left[-M_{11} - \tfrac{1}{2}\, M_{13} - \frac{\sqrt{3}}{2} E_{23}\right) + \left(\frac{3}{2} E_{13} - \frac{3\sqrt{3}}{2} M_{23}\right.\right.$$

$$\left.\left. - \sqrt{3} M_{25} - \sqrt{6} E_{35}\right) \cos\vartheta \right] + M_{11}^* \left[\left(\frac{3}{2}\, M_{13} + \frac{3\sqrt{3}}{2} E_{23}\right) \cos\vartheta\right.$$

$$+\left(-\frac{1}{2}E_{13}+\frac{\sqrt{3}}{2}M_{23}+\frac{\sqrt{3}}{2}XM_{25}+\sqrt{\frac{3}{2}}XE_{35}\right)\Big]+M_{13}^{*}\Big[2E_{13}$$

$$+\sqrt{3}(1-3\cos^2\vartheta)M_{23}+\sqrt{3}\left(-1+\frac{1}{2}\cos^2\vartheta\right)M_{25}-\frac{\sqrt{6}}{8}XE_{35}\Big]$$

$$+E_{23}^{*}\Big[-\sqrt{3}(1-3\cos^2\vartheta)E_{13}-6\cos^2\vartheta M_{23}-\frac{3}{2}\cos^2\vartheta M_{25} \tag{13}$$

$$+\frac{3}{8}\sqrt{2}(-3-\cos^2\vartheta)E_{35}\Big]+E_{13}^{*}\Big[-\frac{5\sqrt{3}}{2}M_{25}-\frac{5\sqrt{6}}{56}(19+9\cos^2\vartheta)E_{35}\Big]\cos\vartheta$$

$$+M_{23}^{*}\Big[\frac{5}{14}(15+6\cos^2\vartheta)M_{25}+\frac{5\sqrt{2}}{56}(69+15\cos^2\vartheta)E_{35}\Big]\cos\vartheta\Big\},$$

where $X = (5\cos^2\vartheta - 1)$.

If meson production in the d state is disregarded (i.e., putting $E_{13} = M_{23} = M_{25} = E_{35} = 0$), Eq. (13) goes into the corresponding expression obtained by Fel'd (reference 4).*

[1] A. Simon, Phys. Rev. **92**, 1050 (1953).

[2] J. Blatt and V. E. Weiskopf, Theoretical Nuclear Physics, N. Y., 1952.

[3] Hayakaw, Kawaguchi, and Minami, Progr. Theoret. Phsy. **12**, 355 (1953).

[4] B. T. Fel'd, Nuovo cimento **12**, 425 (1954).

[5] N. F. Nelipa, Usp. Fiz. Nauk (in press).

[6] G. Ia. Liubarskii, Теория групп и ее применения в физике (Group Theory and its Applications in Physics), GITTL, M. 1957.

[7] Simon, VanderSluis, and Biedenharn, Oak Ridge National Laboratory report ORNL-1679.

[8] A. Simon, Oak Ridge National Laboratory Report ORNL-1718 (1954).

[9] Keck, Tollestrup, and Walker, Phys. Rev. **101**, 1159 (1956).

*It must be noted that the expression given in reference 9 for P, follows from our expression if we make, in addition, the following substitutions:

$$E_{11}\to E_{11},\ M_{11}\to -M_{11},\ M_{13}\to -M_{13},\ E_{23}\to E_{23}/2\sqrt{3}.$$

Translated by J. G. Adashko
33

INFLUENCE OF DEFORMATIONS ON OSCILLATION EFFECTS IN METALS AT LOW TEMPERATURES

A. M. KOSEVICH

Physico-Technical Institute, Academy of Sciences, Ukrainian S.S.R.

Submitted to JETP editor February 26, 1958

J. Exptl. Theoret. Phys. (U.S.S.R.) **35**, 249-253 (July, 1958)

The influence of elastic strains on the properties of the electron gas in a metal is considered. It is shown that if the metal contains electron groups with significantly different numbers of electrons, the de Haas — van Alphen effect is very sensitive to deformations of the metal. An explanation is offered for the oscillations of the thermodynamic quantities, which can be produced, by changing the external pressure, in a metal placed in a constant magnetic field.

MANY recent articles deal with experimental investigations of the influence of elastic deformations (particularly uniform compression) in metals on the physical phenomena that are due to the character of the energy spectrum of the conduction electrons.[1-4] In the present work we shall study certain effects in deformed metals, starting with a semi-phenomenological account of the influence of elastic deformations on the electron spectrum.

1. Following Akhiezer et al.[5] we shall assume that the influence of elastic deformation on the law of electron dispersion can be taken into account in the form of a small addition to the electron energy in the undeformed metal:*

$$\varepsilon^{\alpha}(\mathbf{p}) = \varepsilon_0^{\alpha}(\mathbf{p}) + g_{ik}^{\alpha}(\mathbf{p})\, u_{ik}, \qquad (1)$$

where $\epsilon^{\alpha}(\mathbf{p})$ and $\epsilon_0^{\alpha}(\mathbf{p})$ are the energies of the electrons of group α in the deformed and undeformed metal respectively,† u_{ik} is the deformation tensor, and $g_{ik}^{\alpha}(\mathbf{p})$ is a tensor function of the quasi-momentum $\mathbf{p}$, characteristic for the given group. In writing (1) it is assumed that the inhomogeneity in the deformation field is small, i.e., that u_{ik} changes substantially over distances that exceed considerably the average de-Broglie wavelength for the electron. Note that if u_{ik} in (1) is taken to be the field of the sound wave, then the second term in (1) becomes the classical analogue of the electron-phonon interaction Hamiltonian. Therefore the $g_{ik}(\mathbf{p})$ are connected with the effective cross sections for the absorption and emission of a phonon by an electron.

Starting with (1), it is easy to calculate the spectral characteristics of the electron gas in a homogeneously-deformed metal: the number of states of an electron of group α with energies less than ϵ is $n^{\alpha}(\epsilon)$ and the total number of states is $n(\epsilon) = \sum_{\alpha} n^{\alpha}(\epsilon)$. It turns out that in an approximation linear in u_{ik} we have

$$n^{\alpha}(\varepsilon) = n_0^{\alpha}(\varepsilon) - u_{ik}\bar{g}_{ik}^{\alpha}\rho_0^{\alpha}(\varepsilon), \quad \rho_0^{\alpha}(\varepsilon) = dn_0^{\alpha}(\varepsilon)/d\varepsilon,$$

where $\bar{g}^{\alpha}$ is the average value of $g^{\alpha}(\mathbf{p})$ over the equal-energy surface $\epsilon_0^{\alpha}(\mathbf{p}) = \epsilon$:

$$\bar{g}^{\alpha} = \oint g^{\alpha}\frac{d\Omega}{v_0} \Big/ \oint \frac{d\Omega}{v_0},$$

(integration over the surface $\epsilon_0^{\alpha}(\mathbf{p}) = \epsilon$), and also

$$n(\varepsilon) = n_0(\varepsilon) - u_{ik}\bar{g}_{ik}\rho_0(\varepsilon), \qquad (2)$$

where

$$\bar{g} = \sum_{\alpha}\bar{g}^{\alpha}\rho_0^{\alpha}(\varepsilon)/\rho_0(\varepsilon), \quad \rho_0(\varepsilon) = \sum_{\alpha}\rho_0^{\alpha}(\varepsilon).$$

Let us consider an electron gas in a homogeneously-deformed metal of volume V at low temperatures ($kT \ll \zeta$, where ζ is the chemical potential of the electron gas at $T = 0°K$), when the number of electrons per unit volume can be

*Since the electron energy $\varepsilon(\mathbf{p})$ in the metal is a periodic function of $\mathbf{p}$ with the period of the reciprocal lattice, the deformation of a metal changes not only the form of the function $\varepsilon(\mathbf{p})$ itself, but also its period. In the case of electron trajectories in quasi-momentum space, located in one or several neighboring elementary cells of the reciprocal lattice, both these changes in $\varepsilon(\mathbf{p})$ can be described, in the case of small deformations, by formula (1). If, however, the electron trajectory covers a very large number of reciprocal-lattice cells, then a small change in the period of the deformation cannot be taken into account in the form of a small addition to the function $\varepsilon(\mathbf{p})$; however, we shall not be interested henceforth in such trajectories.

†Hereinafter, zero in the subscript will denote the corresponding quality in the undeformed metal.

considered equal to $n(\zeta)$. From (2), and from the condition that the number of electrons is constant,

$$Vn(\zeta) = V_0 n_0(\zeta_0) = \text{const}$$

we can then determine the change in the chemical potential $\delta\zeta$, due to the deformation of the metal

$$\delta\zeta = -\alpha_{ik}u_{ik},\ \alpha_{ik} = \frac{n_0(\zeta_0)}{\rho_0(\zeta_0)}\delta_{ik} - \bar{g}_{ik}, \qquad (3)$$

where δ_{ik} is the Kronecker symbol.

Naturally, the coefficients α_{ik} are determined in terms of the functions g_{ik} for all electron groups. If the metal contains electron groups with substantially differing numbers of electrons then, generally speaking, α_{ik} is determined essentially by the groups with large numbers of electrons i.e., $\alpha_{ik} \sim \zeta^{gr}$, where ζ^{gr} is the chemical potential reckoned from the "bottom" of the energy band of the fundamental group of electrons. Assuming the usual value of ζ^{gr} for metals, the order of magnitude of α_{ik} can be estimated to be 1 ev.

Since α_{ik} is a symmetrical tensor of second rank, the number of its independent components, meaning also the number of independent experimental measurements of $\delta\zeta$ from which α_{ik} can be established, is determined by the symmetry of the crystal. For example, for cubic metals α_{ik} has one independent component ($\alpha_{ik} = \alpha\delta_{ik}$), and for uniaxial metals it has two independent components.

In case of uniform hydrostatic compression at a pressure p, Eq. (3) becomes

$$\delta\zeta = ap,\ a = \alpha_{ik}s_{ikll}, \qquad (4a)$$

where s_{iklm} is the tensor of the coefficients of elasticity of the metal (repeated indices are summed).

The value of the scalar coefficient a in (4) can be readily estimated from the following considerations. Were the examined "electron gas in the metal" a free gas, then at constant temperature it would obey the relation $\delta\zeta = v_0\delta p$, where v_0 is the volume per gas particle. For an electron gas in metal, this relation can be satisfied only in order of magnitude, i.e., $a \sim v_0$. Considering that in a metal there is approximately one electron for each atom, we obtain, in order of magnitude, $a \sim 10^{-23}$ cm^3. This estimate, as expected, corresponds to the values of the coefficients α_{ik} estimated above.

In the case of uniaxial compression of a metal at a pressure p (for example, along the x_3 axis), formula (3) becomes even simpler:

$$\delta\zeta = b_{33}p,\ b_{33} = \alpha_{ik}s_{ik33}. \qquad (4b)$$

Finally, we note that the change in the electron work function of the deformed metal follows from (3) and (4). As a result, a contact potential difference arises between two specimens of the same metal, if one specimen is elastically deformed.

2. Consider a metal having one or several groups with an anomalously small number of electrons. For such a group, $\zeta^\beta \ll \zeta^{gr}$ (ζ^β is the chemical potential, reckoned from the bottom of the β energy band). As is known, the presence of such a group of electrons leads to a very strong de Haas — van Alphen effect. Here the period of the corresponding oscillations due to a change in magnetic field H is determined by the extremal area $S_m^\beta(\zeta_\beta)$ of the intersection between the Fermi surface for the anomalously small group and the plane perpendicular to H.[6] In the deformed metal, the area cut from the Fermi surface varies both because of change in the form of the equal-energy surfaces and because of the change in ζ. Taking account of both factors that influence the variation of S_m, we readily obtain from (1) the area of the central section of the Fermi surface after deformation.

$$S_m^\beta(\zeta^\beta) = S_m^{0\beta}(\zeta_0^\beta + \delta\zeta)\{1 + \beta_{ik}u_{ik}\}; \qquad (5)$$

Here β_{ik} is a coefficient that takes into account the change in the form of the β-equal-energy surface. This coefficient depends on the orientation of the plane of intersection. If the intersection considered is fully contained in one cell or covers only several cells of the reciprocal lattice, then

$$\beta_{ik} = -2\pi m_\beta^0 \bar{g}_{ik}^{*\beta}/S_m^{0\beta},\ 2\pi m_\beta^0 = dS_m^{0\beta}/d\zeta_\beta,$$

where $\bar{g}^{*\beta}$ is the average value of $g^\beta(\mathbf{p})$ along the trajectory which encloses the area $S_m^{0\beta}(\zeta_0^\beta)$ in the quasi-momentum space. Generally speaking, $\beta_{ik} \sim 1$.

Since, in order of magnitude, $\delta\zeta \sim u_{ik}\zeta^{gr}$, we can use in (5)

$$\delta\zeta/\zeta_0^\beta \sim u_{ik}(\zeta^{gr}/\zeta_0^\beta).$$

For anomalously small electron groups we usually have $\zeta^{gr}/\zeta_0 \sim 10^2$ to 10^3, and therefore for deformations $u_{ik} \sim 10^{-2}$ to 10^{-3} it turns out that $\delta\zeta \sim \zeta_0^\beta$, i.e., the change in the chemical potential is commensurate with ζ_0^β. In this case it follows from Eq. (5) that

(a) with varying H, the oscillation period changes, because of $\delta\zeta$, by an amount comparable with the period itself, in spite of the fact that the deformation, and hence the relative changes of the crystal-lattice constants, is small;

(b) anisotropic changes in the period of the oscillation determined by the second term in the

curly brackets of (5) give a relatively small contribution to the total change in the period.

This means that of the two indicated factors that influence the oscillations in a deformed metal, the change in the chemical potential of the electron gas is the more significant. The change in the form of the β Fermi surface affects very little the oscillations due to the β group of electrons.

If the electron dispersion in the undeformed metal is not quadratic, then the effective mass m^0_β of the electron depends in general on the energy, and should therefore be considerably changed by the above deformations. This leads, in particular, to a considerable change in the temperature dependence of the amplitude of the oscillation that is determined by the quantity m^0_β.

A similar type of period variation and a similar temperature dependence of the deformation were observed for single crystals of zinc by Dmitrenko, Verkin, and Lazarev,[2,3]

Let us note that simultaneous measurements of the changes in the oscillation periods, i.e., δS_m, and of the effective mass of the electron m^0 in one form of deformation makes it possible to determine $\delta\zeta$, and consequently the coefficients a or b in (4). With several loads it is possible to determine the coefficient α_{ik} in (3). In fact, we have

$$\delta S^\beta_m \approx 2\pi m_\beta \delta\zeta = 2\pi\,[m^0_\beta(\zeta_0) + \delta m_\beta]\,\delta\zeta, \qquad (6)$$

where δm_β is the average change in the electron mass due to the deformation. Relation (6), together with (3) and (4), solves the above problem.

If the coefficient a (or b) is known, it is possible to establish the energy dependence of S^0_m, over a considerable range of energies, from the dependence of the period on p. This energy dependence makes it possible to establish the law of electron dispersion in the anomalously small group for a sufficiently large region of the Fermi boundary energy.

Finally, since $S^{0\beta}_m(\epsilon)$ is a monotonic function of energy for closed equal-energy surfaces, then the following is true:

(a) In the presence of anomalously small groups of carriers of opposite polarity, the corresponding periods will change upon deformation in different directions (increase for particles of one sign and diminish for those of the opposite sign).

(b) Changing the sign of the pressure in uniaxial loading, as can be seen from (4b), leads to a change in the sign of δS^β_m for anomalously small groups (in the case of a quadratic dispersion law, the effect should be symmetrical, accurate to terms $\beta_{ik}u_{ik}$).

A change in the sign of δS^β_m was observed by Verkin and Dmitrenko upon reversal of the uniaxial loading of single crystals of zinc.[7]

3. Equation (5) leads also to an explanation of another possible oscillation effect, namely oscillations of thermodynamic quantities in a constant magnetic field due to changes in the external load applied to the metal.* Actually, at low temperatures, oscillations produced in any thermodynamic quantity by the β group of electrons are determined by a factor of the form[6]

$$\sin\left(cS^\beta_m(\zeta_\beta)/e\hbar H + \varphi\right), \qquad (7)$$

where φ is a certain practically-constant phase.

A change of 2π in the argument of (7) corresponds to one period of oscillation. As can be seen from (5) and (7), this change can result, at constant H, from a change in ζ due to the deformation of the metal. In the presence of an anomalously small group of electrons, it is easy to determine from (5) and (7) what change in chemical potential corresponds to one period of oscillations:

$$\Delta\zeta = 2\pi e\hbar H/c\,(dS^\beta_m/d\zeta) = e\hbar H/m_\beta c = \mu_\beta H. \qquad (8)$$

Naturally, (8) coincides with the distance between the electron energy levels in the magnetic field. Formula (8) becomes quite obvious in the case of a quadratic dispersion law, when the argument of (7) contains $2\pi\zeta_\beta/\mu_\beta H$.

In the case of uniform hydrostatic compression, the change in pressure p, corresponding to the oscillation period, is

$$\Delta p = \Delta\zeta/a = \mu_\beta H/a. \qquad (9a)$$

In uniaxial compression along the x_3 axis, the period of the pressure oscillations is determined by the formula

$$\Delta p = \mu_\beta H/b. \qquad (9b)$$

Formulas (8) and (9) show (a) that the period of oscillations due to changes in applied pressure p is proportional to the magnetic field H, and (b) that the anistropy of the period and its dependence on p are determined by the anistropy and pressure dependence of the effective mass m averaged over the period.

Measurement of the oscillation periods due to a change in pressure in weak magnetic fields, when the energy period of $\Delta\zeta = \mu_\beta H$ is small, makes it possible to determine directly the effective mass of the electrons of anomalously small groups and its dependence on p (meaning also on the energy).

The possibility of experimental observation of

*That such oscillations can be observed is suggested also by Alekseyevskiy, Brandt, and Kostina.[4]

the above oscillations is confirmed by the fact in references 2 and 3, at $p = 1500$ atmos, the change $\delta\zeta$ is comparable with ζ_β for an anomalous group of electrons in zinc, while in weak fields usually $\mu_\beta H \ll \zeta_\beta$.*

In conclusion, I use this opportunity to thank I. M. Lifshitz for counsel and discussions, and also B. I. Verkin and I. M. Dmitrenko for discussing the results of the work.

[1] B. I. Verkin and I. M. Dmitrenko, J. Exptl. Theoret. Phys. (U.S.S.R.) **31**, 538 (1956), Soviet Phys. JETP **4**, 432 (1957). N. E. Alekseevskii and N. B. Brandt, J. Exptl. Theoret. Phys. (U.S.S.R.) **28**, 379 (1955), Soviet Phys. JETP **1**, 384 (1955). Alekseevskii, Brandt, and Kostina, Dokl. Akad. Nauk SSSR **105**, 46 (1955), J. Exptl. Theoret. Phys. (U.S.S.R.) **31**, 943 (1956), Soviet Phys. JETP **4**, 813 (1957). W. Overton and T. Berlincourt, Phys. Rev. **99**, 1165 (1955).

[2] Dmitrenko, Verkin, and Lazarev, J. Exptl. Theoret. Phys. (U.S.S.R.) **33**, 287 (1957), Soviet Phys. JETP **6**, 223 (1958).

[3] Dmitrenko, Verkin, and Lazarev, J. Exptl. Theoret. Phys. (U.S.S.R.) **35**, 328 (1958), Soviet Phys. JETP **8** (1959) (in press).

[4] Alekseevskii, Brandt, and Kostina, Izv. Akad. Nauk SSSR, Ser. Fiz. **21**, 790 (1957) [Columbia Tech. Transl. **21**, 792 (1957)].

[5] A. I. Akhiezer, J. Exptl. Theoret. Phys. **8**, 1330 (1938); Akhiezer, Kaganov, and Liubarskii, J. Exptl. Theoret. Phys. (U.S.S.R.) **32**, 837 (1957), Soviet Phys. JETP **5**, 685 (1957).

[6] I. M. Lifshitz and A. M. Kosevich, J. Exptl. Theoret. Phys. (U.S.S.R.) **29**, 730 (1955), Soviet Phys. JETP **2**, 636 (1956).

[7] B. I. Verkin and I. M. Dmitrenko, J. Exptl. Theoret. Phys. (U.S.S.R.) **35**, 291 (1958), Soviet Phys. JETP **8**, 200 (1959) (this issue).

*All the calculations of Secs. 2 and 3 of this article were made assuming $\mu H \ll \zeta$. If this more stringent inequality is satisfied we can, in particular, disregard the quantum oscillations of ζ.

Translated by J. G. Adashko
34

SOVIET PHYSICS JETP VOLUME 35 (8), NUMBER 1 JANUARY, 1959

ON A POSSIBLE LIMIT ON THE APPLICABILITY OF QUANTUM ELECTRODYNAMICS

D. I. BLOKHINTSEV

Joint Institute for Nuclear Research

Submitted to JETP editor February 28, 1958

J. Exptl. Theoret. Phys. (U.S.S.R.) **35**, 254-257 (July, 1958)

Processes that can compete with electromagnetic processes at high energies are considered. It is shown that these can be processes associated with four-fermion interactions.

1. INTRODUCTION

It has been shown in reference 1 that the application of the present method of renormalization in quantum electrodynamics leads to a difficulty in principle — to the vanishing of the renormalized charge. Although objections have been raised[2] against the unconditional cogency of the proof, nevertheless it seems to be quite convincingly demonstrated that there are difficulties in principle in the range of energies E defined by the condition $\alpha \ln(E/mc^2) \sim 1$ ($\alpha = e^2/\hbar c$). The typical length corresponding to this energy, $l \sim (\hbar/mc)e^{-3\pi/\alpha}$, lies far beyond the limit of the gravitational radius of the electron, as was first shown in reference 3. The limiting energy itself is enormously large ($E_0 \sim mc^2 e^{3\pi/\alpha}$).

It can therefore be expected that in actual fact the limits of the applicability of the present electrodynamics will show up considerably earlier,

for example through a possible change of the space-time structure in regions of space and time that are small, but still markedly larger than l.

There is, however, another limitation on the meaningfulness of quantum electrodynamics, more accessible to theoretical analysis.

Besides the purely electrodynamic interactions of photons, electrons, and positrons there occur processes involving mesons and nucleons. These processes can be brought about in a purely electrodynamic way, for example by the interaction of a photon with an electron.

If it should turn out that the contribution of these nonelectromagnetic processes exceeds that of the electromagnetic processes, then we should lose the possibility of dealing with pure electrodynamics without including other types of interactions in an essential way. In particular, beginning at a certain energy E_{cr} it would become meaningless to think of an expansion in powers of $e^2/\hbar c$.

We shall show that the weak four-fermion Fermi interaction can be a competing interaction of this kind. The validity of this interaction in the high-energy region has not been experimentally verified, and various theoretical doubts as to the applicability of this interaction for energies $E \gg mc^2$ can be put forward. We shall, however, start from the assumption that this interaction can be used right up to very high energies, and we shall consider the consequences following from this assumption.

A physical peculiarity of the pure fermion interactions is the fact that the matrix elements of these interactions do not fall off with increase of the energies of the fermions taking part in the process, whereas the matrix elements of processes that involve bosons (photons, π mesons and K particles) decrease with increasing energy of the bosons. The reason for this is that with increasing boson energy the boson field falls off like $k^{-1/2}$:

$$\Phi_k = \sqrt{\hbar/2k}e^{ikx}b_k + \text{conjugate};$$

(here k is the momentum of the boson and b_k is the creation operator of the boson), whereas the fermion field remains constant with increasing energy of the fermion:

$$\psi_k \sim u_k e^{ikx}a_k + \text{conjugate},$$

(u_k is a spinor amplitude, and a_k is the creation operator of the fermion).

In what follows we shall show that because of this peculiarity of the fermion interactions they become important in electromagnetic processes considerably before the logarithmic limit $E \sim mc^2e^{3\pi/\alpha}$ is reached.

2. THE FERMION-ELECTROMAGNETIC INTERACTION

Let us consider the process of interaction of a photon (k) with an electron (e) leading to the formation of a μ meson (μ) and two neutrinos (ν, $\tilde{\nu}$):

$$k + e \to \mu + \nu + \tilde{\nu}. \tag{1}$$

Such a process will be described by the interaction Lagrangian W:

$$W = eW_e + eW_\mu + gW_{\mu e\nu}, \tag{2}$$

where $eW_e = (J_eA)$ is the interaction of the electron (J_e is the electron current) with the electromagnetic field (A is the vector potential); eW_μ has the same meaning for the μ meson. Finally, $gW_{e\mu\nu}$ is the four-fermion interaction of electron, μ meson, and neutrino; $g = \hbar c\Lambda_0^2 \approx 10^{-49}$ erg-cm^3 is the Fermi constant ($\Lambda_0 = 6 \times 10^{-17}$ cm), and

$$W_{e\mu\nu} = (\bar{\psi}_e O_1 \psi_\mu)(\bar{\psi}_\nu O_2 \psi_\nu) + \text{conjugate}$$

Here ψ_e, ψ_μ, ψ_ν are the spinor fields of electrons, μ mesons, and neutrinos, respectively, and O_1 and O_2 are certain spinor operators.

The total effective cross-section for the process (1) will be:

$$\sigma_\mu = \frac{2\pi}{\hbar c}\int |W_{af}|^2 \frac{p_\nu^2 dp_\nu d\Omega_\nu \tilde{p}_\nu'^2 dp_\nu' d\Omega_\nu'}{(2\pi\hbar)^6 dE_f}, \tag{3}$$

where W_{af} is the matrix element of the interaction energy (2) for the process (1), p_ν, $\tilde{p}_\nu$ are the momenta of the neutrino and antineutrino, and E_f is the energy of the final state. The structure of this matrix element is such that in the first nonvanishing approximation it is given by:

$$W_{af} = eg\sum_i \left\{ \frac{(a|W_e|c)(c|W_{e\mu\nu}|f)}{E_0 - E_c} + \frac{(a|W_{e\mu\nu}|c)(c|W_\mu|f)}{E_0 - E_c'} \right\}, \tag{4}$$

where E_0 is the energy of the initial state and E_c that of the intermediate state. In the center-of-mass system of the photon and electron $E_0 - E_c \sim \hbar ck$ (k is the wave vector of the photon); $(a|W_e|c) \sim k^{-1/2}$, $(c|W_\mu|f) \sim k^{-1/2}$. Therefore $|W_{af}|^2 \sim e^2gk^{-3}$. The weight factor in Eq. (3) is proportional to k^5. Thus the total cross-section is

$$\sigma_\mu \approx \alpha\Lambda_0^4 k^2 F, \tag{5}$$

where F is a factor of the order 1 which depends weakly on k.*

In a similar way we can consider the process of collision of two electrons with simultaneous transformation into two mesons,

$$e' + e'' \to \mu' + \mu''. \tag{1'}$$

The differential cross-section (in the center-of-mass system) for this process will be

$$d\sigma_{\mu\mu} \cong \Lambda_0^8 q^4 p^2 F \, d\Omega, \tag{6}$$

where q is the momentum transfer and p is the initial momentum of the electron, measured in reciprocal-length units.

On the other hand, the cross-sections for the purely electromagnetic processes are given by ($\alpha = e^2/\hbar c$):

$$\sigma_c = \frac{\pi\alpha^2}{2k^2}\left(\ln\frac{4k^2}{k_c^2} + \frac{1}{2}\right) \tag{7}$$

for the Compton effect,

$$d\sigma_{ee} = \alpha^2 (p^2/q^4)\, d\Omega \tag{8}$$

for the elastic collision of electrons,

$$\sigma_p = \frac{28}{9}\frac{\alpha^3}{k_c^2}\left(\ln\frac{4k^2}{k_c^2} - 3.5\right) \tag{9}$$

for pair production (here $k_C = mc/h$), and

$$\sigma_\gamma = \frac{4\alpha^3}{k_c^2}\left|\ln\frac{4k^2}{k_c^2} - 3.5\right| \tag{10}$$

for bremsstrahlung from electron collisions.

A comparison of these cross-sections with those for the mixed processes (1) and (1') shows that

$$\sigma_\mu > \sigma_c \quad \text{for} \quad k \gtrsim \alpha^{1/4}/\Lambda_0; \tag{11}$$

$$\sigma_\mu > \sigma_p \quad \text{for} \quad k \gtrsim \alpha^{1/2}(\alpha/\Lambda_0 k_c)/\Lambda_0; \tag{12}$$

$$d\sigma_{\mu\mu} > d\sigma_{ee} \quad \text{for} \quad q \gtrsim \alpha^{1/4}/\Lambda_0; \tag{13}$$

$$\sigma_{\mu\mu} > \sigma_\gamma \quad \text{for} \quad q \sim p \gtrsim (\alpha^3/k^2\Lambda_0^2)/\Lambda_0. \tag{14}$$

As can be seen from these inequalities, if the four-fermion interaction can be regarded as applicable in the energy region $k > 1/\Lambda_0$, then the processes with the production of neutrinos and μ mesons are more intense than the purely electromagnetic processes. For this the corresponding energies of the photons or electrons in the center-of-mass system must be larger than $\hbar c/\Lambda_0 \sim 2$ Bev. This is an enormous energy, but it is nevertheless much smaller than that from the logarithmic formula.

It must be noted that the production of pairs of nucleons and mesons will play a much smaller role, since their production cross-section will be smaller by a factor $(m/M)^2$ than that for the production of electron-positron pairs.

Processes with production of neutrinos and boson mesons will also become important only at higher energy because of the above-mentioned difference in the behaviors of the matrix elements of bosons and fermions.

Thus the fermion interaction may be the one which limits the range of applicability of electrodynamics to dimensions larger than Λ_0. For smaller lengths, and consequently for energies larger than $\hbar c/\Lambda_0$, there is no sense at all in studying electrodynamics without directing attention to processes with μ mesons and neutrinos and to the Fermi constant g as well as $e^2/\hbar c$.

*These qualitative conclusions are confirmed by more detailed calculations carried out by Doctor M. Meier (Romania), to whom the writer expresses his thanks.

[1] Landau, Abrikosov, and Khalatnikov, Dokl. Akad. Nauk SSSR **95**, 1177 (1954).

[2] N. N. Bogoliubov and D. V. Shirkov, **Введение в теорию квантованных полей** (Introduction to the Theory of Quantized Fields), pp. 355-356. GITTL, Moscow, 1957.

[3] M. A. Markov, J. Exptl. Theoret. Phys. (U.S.S.R.) **17**, 661 (1947).

Translated by W. H. Furry
35

ON THE THEORY OF THE INTERACTION OF FAST NEUTRONS OF VARIOUS ANGULAR MOMENTA WITH SEMI-TRANSPARENT NUCLEI

L. E. PARGAMANIK and V. V. UL' IANOV

Khar' kov State University

Submitted to JETP editor February 28, 1958

J. Exptl. Theoret. Phys. (U.S.S.R.) **35**, 258-264 (July, 1958)

The participation of fast neutrons with various angular momenta in the interaction with semi-transparent nuclei is studied within the framework of the complex square-well model for the nucleus. The exact expressions for the partial cross sections are approximated with the help of special asymptotic formulas for the cylindrical functions which are valid throughout the momentum range of interest. This approximation allows a more precise determination of the participation of waves with angular momentum $l \sim kR$ in neutron scattering and absorption processes as compared with the results obtained in the quasi-classical approximation. Corrections to the integral absorption and scattering cross sections are obtained, which are important for high and low effective absorption.

In many recent papers[1-4] on the scattering of particles from nuclei use is made of the model of a complex potential well. With this model it was possible to determine accurately the dependence of the cross section on energy in both the low- and high-energy regions. For small neutron energies only the wave with low angular momenta participate in the interactions with the nucleus. In the calculation of the cross section one can therefore sum directly over the partial cross sections.

For high neutron energies many waves (with momenta $l \lesssim kR$), interact with the nucleus, and for the calculation of the cross section it is necessary to sum over the whole contributing interval of momenta, and to determine accurately the upper limit of this interval. In addition, the diffuseness of the nuclear boundary also affects the value of the cross section.

Fernbach, Serber, and Taylor[1] regard the nucleus as a homogeneous sphere with a certain absorption coefficient and a certain refraction index. Applying a quasi-classical method based on an optical analogy (in the following we shall call this the optical approximation) to this model, it was possible to fit satisfactorily the neutron scattering experiments for energies of order 100 Mev. However, the differential scattering cross sections came out incorrectly. As shown by Pasternack and Snyder,[5] this discrepancy is for the most part due to the inaccuracy of the optical approximation, and not due to the model. The optical approximation gives the true partial cross sections only for waves with momenta $l \lesssim kR/2$. In the region of momenta $l \lesssim kR$ the values for the partial cross sections appear to be too low, and waves with momenta $l > kR - \frac{1}{2}$ are not accounted for at all.

Drozdov[3] obtained an expression for the absorption cross section for fast neutrons, solving the Schrödinger equation approximately with the help of the semi-classical method of Petrashen'.[6] This paper improves on the results of the crude optical approximation, since the Petrashen' method gives good accuracy in the region $l < kR$; however, Drozdov applies without justification the formulas thus obtained also in the region $l \sim kR$ and cuts off the integration at the momentum $l = kR - \frac{1}{2}$, arguing that only waves with momentum corresponding to an impact parameter smaller than the nuclear radius participate in scattering and absorption processes.

Thus both methods[1,3] give a good approximation only for partial waves with momenta $l < kR$. The momentum region $l \sim kR$ is treated incorrectly, and in the calculation of the cross section the integration is cut off at the momentum $l = kR - \frac{1}{2}$. It is therefore of interest to investigate in more detail the role of the momenta $l \sim kR$ in the interaction of neutrons with the nucleus, and to determine the behavior of the scattering and absorption coefficients in this momentum region. This paper treats this question on the basis of the simpler model of a complex square potential well. This well, for which the Schrödinger equation can be solved exactly, permits an estimate of the accuracy of the results obtained. In addition, the

effect of the diffuseness of the nuclear boundary is excluded.

1. REGION OF SMALL MOMENTA

With the model of a square complex potential well it is appropriate not to start from an approximate solution of the Schrödinger equation, but to obtain the exact expressions for the scattering and absorption coefficients. In summing these we use more exact approximations, taking account of all waves participating in the interaction.

If the interaction potential of the neutron-nucleus system has the form $U(r) = -V - iW$ for $r \leq R$ and $U(r) = 0$ for $r > R$, where R is the nuclear radius, the Schrödinger equation for the radial neutron wave function with momentum l and energy E can be solved exactly. The reflection coefficient has the form:

$$\beta_l = -\frac{xJ_{l+1/2}(z)H^{(2)}_{l-1/2}(x) - zJ_{l-1/2}(z)H^{(2)}_{l+1/2}(x)}{xJ_{l+1/2}(z)H^{(1)}_{l-1/2}(x) - zJ_{l-1/2}(z)H^{(1)}_{l+1/2}(x)}, \qquad (1)$$

$$x = kR = \sqrt{2m}E^{1/2}R/\hbar, \quad z = \sqrt{2m}(E + V + iW)^{1/2}R/\hbar,$$

where m is the reduced mass of the neutron-nucleus system.

In order to get from (1) expressions for the coefficients of scattering, $|1-\beta_l|^2$, and absorption, $1-|\beta_l|^2$, which are convenient for inspection and for the integration over the whole contributing momentum interval, we have to use approximate formulas for the cylindrical functions. However, the usual formulas for $l \ll x$ and $l \sim x$ are applicable only in a rather narrow region of momenta: to those of order $x^{1/2}$ for small momenta, and to those below $x^{1/3}$ for $l \sim x$. Below we shall therefore use special formulas for the cylindrical functions in the region $l < x$ (see reference 7), and the formulas of Fock[8] for the region $l \sim x$.

In the region $l < x$ the asymptotic formulas used, e.g. for the Bessel functions, have the form:

$$J_\nu(\nu\sec\beta) = \sqrt{\frac{2}{\pi\nu\tan\beta}}\,[\cos(\nu\tan\beta - \nu\beta) + O(1/\nu\tan\beta)].$$

The retention of only the first term in this expansion gives an error of order $1/3\nu\ \tan\beta$; in the momentum region $l < 3x/4$ this error does not surpass 5%. This approximation gives for the reflection coefficient the formula

$$\beta_l = \exp\left\{2i\left[\sqrt{z^2-(l+1/2)^2} - \sqrt{x^2-(l+1/2)^2} + (l+1/2)\left(\cos^{-1}\frac{l+1/2}{x} - \cos^{-1}\frac{l+1/2}{z}\right)\right]\right\}, \qquad (2)$$

which agrees with the result obtained by Drozdov.[3]

For high energies, where $\eta \equiv \mathrm{Im}\ z \ll x$ and $\xi \equiv \mathrm{Re}\ z - x \ll x$, the phase at infinity δ_l, which is related to the reflection coefficient by $\beta_l = e^{2i\delta_l}$, has the form:

$$\delta_l = (\xi + i\eta)\left[1 - \frac{1}{2}\left(\frac{l+1/2}{x}\right)^2 - \frac{1}{8}\left(\frac{l+1/2}{x}\right)^4 - \cdots\right] \approx (\xi + i\eta)\sqrt{1-(l+1/2)^2/x^2}.$$

In the optical approximation[1]

$$\delta_l = [(n-1)x + iKR/2]\sqrt{1-(l+1/2)^2/x^2}, \qquad (3)$$

where K is the absorption coefficient, and n the refraction index. At high energies we have thus the following correspondence between the parameters: η corresponds to KR/2, and ξ corresponds to $(n-1)x$. This enables us to compare the results of the optical approximation with ours. Since η depends not only on the imaginary part W of the potential, but also on the real part V, on the neutron energy, and on the mass of the nucleus, we shall in the following call this parameter the "effective absorption." Analogously, we shall call ξ the "effective refraction."

2. REGION OF INTERMEDIATE MOMENTA

Of special interest is the momentum region $l \sim x$. For an approximation of expression (1) in this momentum region we use the asymptotic formulas for the cylindrical functions of Fock.[8] For example, for the Bessel function we have:

$$J_{l+1/2}(z) = \frac{1}{\sqrt{\pi}}\left(\frac{z}{2}\right)^{-1/3} \times\left\{v(\tau) - \frac{1}{60}\left(\frac{z}{2}\right)^{-2/3}[\tau^2 v'(\tau) + 4\tau v(\tau)] + \cdots\right\}. \qquad (4)$$

With the help of these formulas the reflection coefficient takes the form

$$\beta_l = \frac{xv(\tau)w^*(t') - zv(\tau')w^*(t)}{xv(\tau)w(t') - zv(\tau')w(t)}, \qquad (5)$$

where

$$w(t) = \sqrt{\pi/3}\,e^{2\pi i/3}(-t)^{1/2}H^{(1)}_{1/3}[^2/_3(-t)^{3/2}] = u(t) + iv(t),$$

$$w^*(t) = u(t) - iv(t),$$

$$t = (l+1/2-x)/(x/2)^{1/3}, \quad t' = (l-1/2-x)/(x/2)^{1/3},$$

$$\tau = (l+1/2-z)/(z/2)^{1/3}, \quad \tau' = (l-1/2-z)/(z/2)^{1/3}.$$

In formula (5) we retain only the first terms of expansion (4). This approximation introduces an error of order $|t|^{5/2}/60\,(x/2)^{2/3}$; in the region of momenta $|l-x| \lesssim x^{1/2}$ this error does not surpass 2%. Hence formula (2) gives a good approximation for the reflection coefficient in the region $l < x$, while formula (5) applies to the region $l \sim x$. Thus the whole contributing mo-

mentum interval is covered.

We calculate the scattering and absorption coefficients with the help of formula (5) and expand the resulting expression in powers of $(x/2)^{1/2}$ We obtain:

$$|1-\beta_l|^2 = 4(\xi^2+\eta^2)\frac{[v'(t)^2 - tv(t)^2]^2}{(x/2)^{2/3}}, \quad (6)$$

$$1-|\beta_l|^2 = 4\eta\frac{v'(t)^2 - tv(t)^2}{(x/2)^{1/3}}. \quad (7)$$

In going from negative to positive values of the argument, the Airy function $v(t)$ changes from an oscillating function to an exponentially decreasing function. Therefore the scattering and absorption coefficients decrease rapidly after some characteristic value $l_0 \sim x - 1/2$. However, l_0 does not in general equal $x - 1/2$: for absorption coefficients with high effective absorption ($\eta > (x/2)^{1/3}$) $l_0 \gtrsim x - 1/2$, for those with low effective absorption ($\eta \ll 1$) $l_0 < x - 1/2$. It was found that the waves with momentum $l > x - 1/2$ contribute significantly to the absorption cross section for high effective absorption (see Fig. 1): their inclusion gives a correction of order 20% at relatively low energies ($x \sim 10$, $\eta \sim 2$). For small effective absorption ($\eta \ll 1$) the partial cross sections begin to decrease rapidly already for $l < x - 1/2$ (see Fig. 2), so that the approximations of references 2 and 3 give these incorrectly in the region $l \lesssim x$. As a result, these approximations yield too high values for the cross section (of order 20% for $x \sim 10$). It was found that the region $l > x - 1/2$ contributes

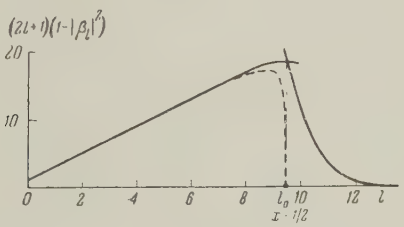

FIG. 1. Partial absorption cross sections for the parameters $x = 10$, $\xi = 1$, $\eta = 1.875$; the solid curves are obtained with formulas (2) and (7), the dotted curve is obtained with the optical approximation (3).

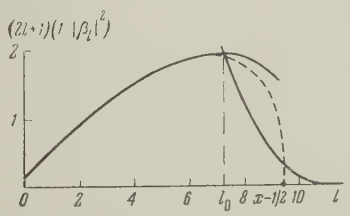

FIG. 2. Partial absorption cross sections for the parameters $x = 10$, $\xi = 1$, $\eta = 0.05$; the solid curves are obtained with formulas (2) and (7), the dotted curve is obtained with the optical approximation (3).

nothing to the partial cross sections for all conceivable values of the effective absorption and refraction. A comparison is possible only with the optical approximation, since Drozdov[3] investigated only the absorption of neutrons. We shall show below that our results differ from those of the optical approximation only for small effective absorption and refraction. The optical approximation gives somewhat larger values in this case.

3. CROSS SECTIONS FOR SCATTERING AND ABSORPTION

With the approximations obtained for the coefficients of reflection, scattering, and absorption it is possible to calculate the cross sections by integrating* over the whole momentum interval (separately for $l \le l_0$ and for $l \ge l_0$). Integrating, we obtain:

$$\frac{\sigma_s}{\pi R^2} = \int_0^\infty (2l+1)|1-\beta_l|^2\,dl = \left[1 + \frac{t_0}{(x/2)^{2/3}} + \cdots\right]$$
$$\times\left\{1 + e^{-4\eta}[1+\eta+\cdots] - 2e^{-2\eta}\left[\cos 2\xi\left(1+\frac{\eta}{2}+\cdots\right)\right.\right.$$
$$\left.\left. + \sin 2\xi\left(\frac{\xi}{2}+\cdots\right)\right]\right\} + \frac{4(\xi^2+\eta^2)}{(x^{4/3}}(0.011 - 0.044t_0 + \cdots), \quad (8)$$

$$\frac{\sigma_c}{\pi R^2} = \int_0^\infty (2l+1)(1-|\beta_l|^2)\,dl = \left[1 + \frac{t_0}{(x/2)^{2/3}} + \cdots\right] \quad (9)$$
$$\times\left\{1 - e^{-4\eta}[1+\eta+\cdots] + \frac{8\eta}{x}[0.096 - 0.21\ t_0 + \cdots]\right\},$$

where t_0 is related to the characteristic l_0 by

$$t_0 = (l_0 + 1/2 - x)/(x/2)^{1/3},$$

and is separately determined, for the scattering coefficient from the identification of the expression $|1-\beta_l|^2$ in formulas (2) and (6), and for the absorption coefficient from the identification of the expression $1-|\beta_l|^2$ in formulas (2) and (7). For example, for $\eta \ll 1$ and $\xi \ll 1$, t_0 is the same for the scattering and for the absorption, and has the form

$$t_0 = 0.685 - 1.315(x/2)^{1/3} + 0.1/(x/2)^{1/3} - \cdots, \quad (10)$$

while, for large η, t_0 for the absorption is

$$t_0 = 0.53 - 0.63(x/2)^{1/3}/\eta + \cdots. \quad (11)$$

For comparison with the results of the optical approximation and with the approximation of Drozdov, we consider formulas (8) and (9) for,

*The relative error introduced by changing the summation over the partial scattering and absorption cross sections (to be performed in the calculation of the cross section) into an integration is very small ($\sim x^{-2}$) and can be neglected.

the cross sections, expressed in terms of the effective absorption η and the effective refraction ξ, in the limiting cases. Depending on the relation between the neutron energy and the parameters of the potential well the expressions for η and ξ have the following form:

for $W < V < E$ $(x > y,\ \zeta < 1)$:

$$\eta = \sqrt{\frac{mR^2}{2\hbar^2 E}}\, W\left(1 - \frac{V}{2E} + \cdots\right) = \frac{\zeta y^2}{2x}\left(1 - \frac{y^2}{2x^2} + \cdots\right),$$
$$\xi = \sqrt{\frac{mR^2}{2\hbar^2 E}}\, V\left(1 - \frac{V}{4E} + \cdots\right) \tag{12}$$
$$= \frac{y^2}{2x}\left(1 - \frac{(1-\zeta^2)\, y^2}{4x^2} + \cdots\right);$$

for $W < E < V$ $(\zeta y^2 < x^2 < y^2)$:

$$\eta = \sqrt{\frac{mR^2 V}{2\hbar^2}}\, W\left(1 - \frac{E}{2V} + \cdots\right) = \frac{\zeta y}{2}\left(1 - \frac{x^2}{2y^2} + \cdots\right),$$
$$\xi = \sqrt{\frac{2mR^2 V}{\hbar^2}}\left(1 - \sqrt{\frac{E}{V}} + \frac{E}{2V} - \cdots\right) \tag{13}$$
$$= y\left(1 - \frac{x}{y} + \frac{x^2}{2y^2} - \cdots\right),$$

where

$$y = \sqrt{2m}\, V^{1/2} R/\hbar, \quad \zeta = W/V.$$

For small effective absorption $(\eta \ll 1)$ we obtain from (9), (10), and (12):*

$$\frac{\sigma_c}{\pi R^2} = 2.72\eta\left(1 - \frac{1.86}{x^{1/2}} + \frac{1.48}{x^{2/3}} - \cdots\right)$$
$$= 1.36\,\frac{\zeta y^2}{x}\left(1 - \frac{1.86}{x^{1/2}} + \frac{1.48}{x^{2/3}} - \cdots\right); \tag{14}$$

in the same case references 1 and 3 give, respectively:

$$\sigma_c/\pi R^2 = 2.67\eta, \quad \sigma_c/\pi R^2 = 2.72\eta.$$

We see that the optical approximation and Drozdov's results give too large values for the cross section (with a relative error of order $-0.6\,x^{-1/2}$).

For large effective absorption $(\eta > (x/2)^{1/3})$ we obtain from (9), (11), and (13):

$$\frac{\sigma_c}{\pi R^2} = 1 + 1.66\,\frac{\eta}{x} - 0.63\,\frac{1}{\eta\,(x/2)^{2/3}} + \cdots$$
$$= 1 + 0.83\,\frac{\zeta y}{x} - 0.415\,\frac{\zeta x}{y} - \frac{1.59}{\zeta y x^{2/3}} + \cdots; \tag{15}$$

in references 1 and 2 $\sigma_c/\pi R^2 = 1$. The correction to the absorption cross section is in this case $\sim \eta/x$.

As mentioned above, for the scattering cross section we are interested in the results for small effective absorption and refraction $(\eta \ll 1,\ \xi \ll 1)$; we find from (8), (10), and (12) (see footnote*):

$$\frac{\sigma_s}{\pi R^2} = 2(\xi^2 + \eta^2)\left(1 - \frac{1.86}{x^{1/2}} + \frac{0.865}{x^{2/3}} - \cdots\right)$$
$$= \frac{y^4}{2x^2}(1 + \zeta^2)\left(1 - \frac{1.86}{x^{1/2}} + \frac{0.865}{x^{2/3}} - \cdots\right), \tag{16}$$

while reference 1 gives

$$\sigma_s/\pi R^2 = 2(\xi^2 + \eta^2).$$

For a graphical illustration of the accuracy of the above calculations see Fig. 3. The points represent the exact values of the absorption coefficient for the parameters $\xi = 1$, $\eta = 0.5$, $x = 10$;

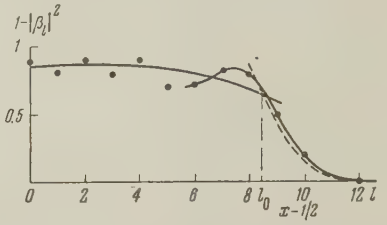

FIG. 3. Absorption coefficients for the parameters $x = 10$, $\xi = 1$, $\eta = 0.5$; the points denote the exact values, the solid curves are obtained with the formulas (2) and (5), the dotted curve is obtained with the approximate formula (7).

the solid curve represents the values of the absorption coefficient calculated with the approximate formulas (2) in the region $l < x$, and (5) in the region $l \sim x$. In addition, in the region $l \sim x$ the dotted curve represents the absorption coefficient calculated with formula (7), i.e., retaining only the first term in expansion (5). We see from Fig. 3 that the approximate values are close to the exact ones. Although in region $l < x$ the approximation gives only a smooth curve for the absorption coefficient, the error in the calculation of the cross section is found to be insignificant. The absorption coefficients are integrated over the momenta (with weights $2l + 1$). Estimates show that the accuracy of the cross section calculations is on the order of 1 or 2%; thus the corrections to the cross sections obtained with the optical approximation and by Drozdov are greater than the calculational error by an order of magnitude. We note that our asymptotic expressions tally well (in the mean) in the region $l \lesssim l_0$ (see Fig. 3; in Figs. 1 and 2 the region of overlapping of the asymptotic curves is not shown).

CONCLUSION

Let us estimate the neutron energies for which the above results are valid. We base our estimate of the upper limit on the assumption that the neu-

*We emphasize in relation to formulas (14) to (16) that the inclusion of the region of intermediate momenta changes somewhat the dependence of the cross sections on energy.

tron-nucleus interaction can be summarily described with the model of a complex potential only for energies corresponding to a wavelength of the same order or larger than the average distance between the nucleons in the nucleus. Then this limit is in the region of energies of order 100 Mev. In addition, the asymptotic formulas for the cylindrical functions used in this paper are valid only for sufficiently large arguments ($x \ll 1$). This limits the applicability of the above results at the low energy side. Our results refer thus to energies of 20 to 200 Mev.

We note further that for an accurate calculation of the cross sections in the framework of the complex potential well model one must, together with the effect of the intermediate momenta, also consider the effect of the diffuseness of the nuclear boundary. Both effects are included in the paper of Nemirovskii.[4] His numerical treatment of the formulas containing the cylindrical functions allows him to circumvent the difficulties connected with the approximation of these functions in the region of intermediate momenta. However, the great number of approximations in his paper makes it difficult to estimate the accuracy of his results.

The comparison of the results of the present paper with the results of Nemirovskii shows that the consideration of the diffuseness of the nuclear boundary always leads to an increase in the absorption cross section, while the inclusion of the intermediate momenta leads to an increase in the cross section for large effective absorption, but to a decrease for small effective absorption. Hence, for neutron energies of order 100 Mev and small ξ the two effects work in opposite directions. The increase of the cross section due to the diffuseness of the nuclear boundary (for diffuseness $\gtrsim k^{-1}$)* is of order 10% (for heavy nuclei).[4] On the other hand, we have shown above that the decrease in the cross section due to the proper inclusion of the intermediate momenta for a nucleus with sharp boundary is of the same order of magnitude. As a result, the proper inclusion of the region of intermediate momenta for neutron energies of order 100 Mev is just as essential as the consideration of the effects of the diffuseness of the nuclear boundary.

The authors express their gratitude to A. I. Akhiezer for a discussion of the results of this paper.

*The comparison of the effects of the region of intermediate momenta and of the diffuseness of the nuclear boundary is made difficult by the absence of experimental data on the diffuseness parameter for $E \gtrsim V$.

[1] Fernbach, Serber, and Taylor, Phys. Rev. **75**, 1352 (1949).

[2] Feshbach, Porter, and Weisskopf, Phys. Rev. **96**, 448 (1954).

[3] S. I. Drozdov, Dokl. Akad. Nauk SSSR **106**, 409 (1956), Soviet Phys. "Doklady" **1**, 37 (1956).

[4] P. E. Nemirovskii, J. Exptl. Theoret. Phys. (U.S.S.R.) **30**, 551 (1956); Soviet Phys. JETP **3**, 484 (1956).

[5] S. Pasternack and H. S. Snyder, Phys. Rev. **80**, 921 (1950).

[6] M. I. Petrashen', Uch. Zap. LGU, seriia fizich. **7**, 59 (1949).

[7] G. N. Watson, A Treatise on the Theory of Bessel Functions, Cambridge, 1945.

[8] V. A. Fock, Дифракция радиоволн вокруг земной поверхности (Diffraction of Radio Waves on the Surface of the Earth) M.—L., 1946.

Translated by R. Lipperheide
36

A SUPERCONDUCTOR IN A HIGH FREQUENCY FIELD

A. A. ABRIKOSOV, L. P. GOR'KOV, and I. M. KHALATNIKOV

Institute for Physical Problems, Academy of Sciences, U.S.S.R.

Submitted to JETP editor March 4, 1958

J. Exptl. Theoret. Phys. (U.S.S.R.) 35, 265-275 (July, 1958)

We derive an equation describing the behavior of superconductors in a high frequency field. With the aid of this equation the frequency and temperature dependence of the impedance of a bulk superconductor have been evaluated.

As is well known Bardeen, Cooper, and Schrieffer[1] have recently constructed a microscopic theory of superconductivity in which they succeeded in explaining a whole number of properties of superconductors. In particular, in that paper they considered the behavior of superconductors in a constant weak field and obtained a new equation expressing the connection of the current with the field, replacing the equation of the phenomenological theory of F. and H. London. This equation turned out to be non-local; with its help the problem of the penetration of a weak static field into a bulk superconductor was solved in reference 1 and the dependence of the penetration depth on the temperature was found.

In the present paper we consider the behavior of a superconductor in a high frequency field. The calculation given below shows that in an alternating field the character of the connection between the current and the vector potential changes, and depends in an essential way on the frequency. For non-zero temperatures or a sufficiently high frequency this equation, written down for the Fourier components of the current, contains imaginary components, which are connected with the absorption of radiation in the superconductor. The impedance of the bulk superconductor is determined with the aid of the equation obtained.

1. THE EQUATION FOR THE CURRENT IN THE SUPERCONDUCTOR

In the non-stationary problem under consideration, it is most convenient to start directly from the expression for the current operator in second quantization:

$$\hat{\mathbf{j}}(x) = -\frac{ie}{2m}\{\tilde{\psi}^+(x)\nabla\tilde{\psi}(x) - \nabla\tilde{\psi}^+(x)\tilde{\psi}(x)\} - \frac{e^2}{mc}\tilde{\psi}^+(x)\tilde{\psi}(x)\mathbf{A}(x) \quad (1)$$

The operators $\tilde{\psi}^+$ and $\tilde{\psi}$ are here written down in the Heisenberg representation and depend on the field $\mathbf{A}$. This dependence has the usual form

$$\tilde{\psi}(x) = \hat{S}^{-1}(t)\psi(x)\hat{S}(t), \quad (2)$$

where $\psi(x)$ is the second quantization operator in the absence of the field, and $\hat{S}(t)$ the S-matrix satisfying the equation

$$i\frac{\partial}{\partial t}\hat{S}(t) = -\frac{1}{c}\left(\int \hat{j}(x)\mathbf{A}(x)\,d^3x\right)\hat{S}(t). \quad (3)$$

The field $\mathbf{A}(x)$ is, as usual, assumed to be adiabatically switched on at $t = -\infty$. The value of the current in the superconductor at a given point and at a given instant can clearly be obtained by taking the average of the operator (1) over the Heisenberg state of the system coinciding with the state of the system in the absence of the field:

$$\mathbf{j}(x) = -\frac{ie}{2m}\langle\tilde{\psi}^+\nabla\tilde{\psi} - \nabla\tilde{\psi}^+\tilde{\psi}\rangle - \frac{e^2}{mc}\langle\tilde{\psi}^+\tilde{\psi}\rangle\mathbf{A}(x).$$

In a weak field it is sufficient to perform the calculations up to terms linear in $\mathbf{A}$. We can therefore in the second term at once put $\tilde{\psi} = \psi$; this is the usual "London" term

$$-(e^2N/mc)\mathbf{A}(x). \quad (4)$$

In the first term it is necessary to expand the operators $\tilde{\psi}$ and $\tilde{\psi}^+$ according to (2) and (3) up to terms of the first order in $\mathbf{A}$:

$$\tilde{\psi}(x) = \psi(x) - \frac{i}{c}\int_{-\infty}^{t}[\hat{j}_\alpha(y), \psi(y)]A_\alpha(y)\,d^4y \quad (5)$$

with a similar formula for $\tilde{\psi}^+$. It is sufficient in turn to retain in formula (5) for $\hat{\mathbf{j}}(y)$ only the first part of expression (1)

$$\hat{\mathbf{j}}_1(x) = -\frac{ie}{2m}(\nabla_x - \nabla_{x'})\psi^+(x')\psi(x)\Big|_{x'\to x}. \quad (6)$$

After substituting (5) into (6) we obtain the term in $\mathbf{j}_1(x) \equiv \langle \hat{\mathbf{j}}_1(x) \rangle$ which is linear in the field:

$$\mathbf{j}_1(x) = \frac{ie^2}{4m^2c}(\nabla_x - \nabla_{x'}) \int_{-\infty}^{t} (\mathbf{A}(y)(\nabla_y - \nabla_{y'})) \langle \{\psi^+(y')\psi(y)\psi^+(x')\psi(x) - \psi^+(x')\psi(x)\psi^+(y')\psi(y)\} \rangle d^4y. \tag{7}$$

Here and henceforth the primed coordinates differ only in the space variables, which must be put equal after performing the differentiation.

The evaluation of the averages of the products of the four ψ and ψ^+ operators in (7) can most conveniently be performed by using the method developed by one of the authors in reference 2. These averages are expressed in terms of pair averages:

$$G_{\alpha\beta}(x-x') = -i\langle T(\psi_\alpha(x)\psi^+_\beta(x'))\rangle; \quad F^+_{\alpha\beta}(x-x') = \langle T(\psi^+_\alpha(x)\psi^+_\beta(x'))\rangle; \quad F_{\alpha\beta}(x-x') = \langle T(\psi_\alpha(x)\psi_\beta(x'))\rangle.$$

The dependence of these quantities on the spinor indices is as follows:

$$G_{\alpha\beta}(x-x') = \delta_{\alpha\beta}G(x-x'); \qquad F^+_{\alpha\beta}(x-x') = -F_{\alpha\beta}(x-x') = F(x-x')\begin{pmatrix} 0 & 1 \\ -1 & 0 \end{pmatrix}_{\alpha\beta}.$$

Performing the averaging in (7) we get

$$\mathbf{j}_1(x) = \frac{ie^2}{2m^2c}(\hat{\mathbf{p}}_x - \hat{\mathbf{p}}_{x'}) \int_{-\infty}^{t} (\mathbf{A}(y)(\hat{\mathbf{p}}_y - \hat{\mathbf{p}}_{y'})) \{[G(y-x')G(x-y') - F(x'-y')F(x-y)] - \text{C.C.}\} d^4y. \tag{8}$$

Going over to Fourier components we find:

$$\mathbf{j}_1(\mathbf{k},\omega) = \frac{2e^2}{m^2c}\int \frac{d^3p}{(2\pi)^3} \int_{-\infty}^{\infty} \frac{d\omega_1}{2\pi} \int_{-\infty}^{\infty} \frac{d\omega_2}{2\pi} \mathbf{p}(\mathbf{A}(\mathbf{k},\omega)\mathbf{p})$$

$$\times \left[G\left(\mathbf{p} - \frac{\mathbf{k}}{2}, \omega_1\right) G\left(\mathbf{p} + \frac{\mathbf{k}}{2}, \omega_2\right) - F\left(\mathbf{p} - \frac{\mathbf{k}}{2}, \omega_1\right) F\left(\mathbf{p} + \frac{\mathbf{k}}{2}, \omega_2\right) - \text{C.C.}\right] \frac{1}{\omega_1 - \omega_2 - \omega - i\delta}.$$

The Fourier components of the functions $G(x - x')$ and $F(x - x')$ were found in reference 2. It is convenient to write them in the form

$$\begin{aligned} G(\mathbf{p},\omega) &= \frac{u_p^2(1-n_p)}{\omega - \varepsilon_p + i\delta} + \frac{v_p^2 n_p}{\omega + \varepsilon_p + i\delta} + \frac{v_p^2(1-n_p)}{\omega + \varepsilon_p - i\delta} + \frac{u_p^2 n_p}{\omega - \varepsilon_p - i\delta}; \\ F(\mathbf{p},\omega) &= iu_p v_p \left[\frac{1-n_p}{\omega - \varepsilon_p + i\delta} - \frac{n_p}{\omega + \varepsilon_p + i\delta} - \frac{1-n_p}{\omega + \varepsilon_p - i\delta} + \frac{n_p}{\omega - \varepsilon_p - i\delta}\right], \end{aligned} \tag{9}$$

where

$$u_p^2 = {}^1/_2(1 + \xi_p/\varepsilon_p); \quad v_p^2 = {}^1/_2(1 - \xi_p/\varepsilon_p); \quad \xi_p = v(p - p_0); \quad \varepsilon_p = \sqrt{\xi_p^2 + \Delta^2}; \quad n_p = (e^{\varepsilon_p/T} + 1)^{-1}.$$

The quantity Δ depends on the temperature in the way found in the paper by Bardeen et al.

Substituting equations (9) into the expression for the current and integrating we find for the Fourier components of the current:

$$\begin{aligned} \mathbf{j}(\mathbf{k},\omega) = \frac{2e^2}{(2\pi)^3 m^2 c}\int d^3p\, \mathbf{p}(\mathbf{pA}(\mathbf{k},\omega)) \Bigg[(v_1u_2 - u_1v_2)\left(\frac{v_1u_2}{\varepsilon_1 + \varepsilon_2 + \omega + i\delta} + \frac{u_1v_2}{\varepsilon_1 + \varepsilon_2 - \omega - i\delta}\right) \\ \times (1 - n_1 - n_2) + (u_1u_2 + v_1v_2)\left(\frac{u_1u_2}{\varepsilon_2 - \varepsilon_1 + \omega + i\delta} + \frac{v_1v_2}{\varepsilon_2 - \varepsilon_1 - \omega - i\delta}\right)(n_1 - n_2)\Bigg] - \frac{e^2}{mc}N\mathbf{A}(\mathbf{k},\omega), \end{aligned} \tag{10}$$

when the index 1 corresponds to the momentum $\mathbf{p} + \frac{1}{2}\mathbf{k}$, and the index 2 to the momentum $\mathbf{p} - \frac{1}{2}\mathbf{k}$. Substituting into (7), assuming the vector $\mathbf{A}$ to lie in the surface plane of the specimen and performing the integration over φ we get

$$\begin{aligned} \mathbf{j}(\mathbf{k},\omega) = \frac{3e^2N\mathbf{A}(\mathbf{k},\omega)}{32mc}\int_{-1}^{1} d\cos\theta \sin^2\theta \int_{-\xi_0}^{\xi_0} d\xi \Bigg[\left(1 - \frac{\xi_1\xi_2 + \Delta^2}{\varepsilon_1\varepsilon_2}\right)\left(\tanh\frac{\varepsilon_1}{2T} + \tanh\frac{\varepsilon_2}{2T}\right)\left(\frac{1}{\varepsilon_1 + \varepsilon_2 + \omega + i\delta} + \frac{1}{\varepsilon_1 + \varepsilon_2 - \omega - i\delta}\right) \\ + \left(1 + \frac{\xi_1\xi_2 + \Delta^2}{\varepsilon_1\varepsilon_2}\right)\left(\tanh\frac{\varepsilon_1}{2T} - \tanh\frac{\varepsilon_2}{2T}\right)\left(\frac{1}{\varepsilon_1 - \varepsilon_2 + \omega + i\delta} + \frac{1}{\varepsilon_1 - \varepsilon_2 - \omega - i\delta}\right)\Bigg] - \frac{e^2}{mc}N\mathbf{A}(\mathbf{k},\omega). \end{aligned} \tag{11}$$

In this expression we used the fact that terms containing one ξ give zero on integration. Indeed, we have

$$\xi_{1,2} = \xi \pm {}^1/_2\, vk\cos\theta, \tag{12}$$

and the integrations over $\cos\theta$ and ξ are performed over a symmetric domain. The quantity ξ_0 determines the upper limit of integration over ξ.

2. PIPPARD'S LIMITING CASE

Further evaluations are impossible to perform without more concrete assumptions about the magnitude of the parameters important for the problem considered. Of the greatest importance for us is the fact that, apparently, the penetration depth of the field for the majority of superconductors is much less than the quantity v/Δ, i.e., $vk \gg \Delta$ (See reference 1).* This inequality is violated only in the neighborhood of the transition point T_c, where the region with $vk \ll \Delta$ occurs. As was shown in reference 1, the basic domain of electrodynamics is founded upon the equation proposed earlier by Pippard.[3] We shall call this region the Pippard region. In the second region the applicability of the London electrodynamics[4] is conserved (London region).†

In the case of a variable field the London region gets narrowed. This is clear, though, from the fact that a normal metal is a Pippard one, since $\Delta = 0$ for it, whence follows that the London region cannot continue up to the transition point itself. Leaving a detailed analysis of this problem until the next section, we shall consider here how Eq. (11) simplifies in the Pippard region. We shall at the same time also assume $vk \gg \omega$. As we shall see in the following, this is always correct in the range of frequencies of most interest.

Equation (11) can be transformed in the following way. In view of the fact that ω only enters into denominators such as $\epsilon_1 + \epsilon_2 + \omega + i\delta$, we can subtract from the coefficient for $A(k, \omega)$ which we denote as $-(3e^2N\Delta/4mcvk)\,Q(\omega)$ its value in the static case. The remainder will be the integral over ξ and $\cos\theta$ where the important region of integration is the region $\xi \ll vk$, $\cos\theta \ll 1$. We introduce now as new variables ξ_1 and ξ_2. If we put $vk \gg T$ (this will be shown below) we can assume that the integrations over ξ_1 and ξ_2 proceed independently with limits from $-\infty$ to $+\infty$. Terms with the product $\xi_1\xi_2$ will thus drop out of the integral. Apart from that, the factor $\sin^2\theta$ can be replaced by unity. Finally we go over to the variables ϵ_1/Δ and ϵ_2/Δ (denoting them again by ϵ_1 and ϵ_2). As a result we get:

$$Q(\omega) - Q(0) = -\frac{1}{2}\int_1^\infty \frac{d\varepsilon_1}{\sqrt{\varepsilon_1^2-1}}\int_1^\infty \frac{d\varepsilon_2}{\sqrt{\varepsilon_2^2-1}}\left[(1-\varepsilon_1\varepsilon_2)\left(\tanh\frac{\varepsilon_1\Delta}{2T}+\tanh\frac{\varepsilon_2\Delta}{2T}\right)\left(\frac{1}{\varepsilon_1+\varepsilon_2+\omega/\Delta+i\delta}\right.\right.$$
$$\left.\left.+\frac{1}{\varepsilon_1+\varepsilon_2-\omega/\Delta-i\delta}-\frac{2}{\varepsilon_1+\varepsilon_2}\right)-(1+\varepsilon_1\varepsilon_2)\left(\tanh\frac{\varepsilon_1\Delta}{2T}-\tanh\frac{\varepsilon_2\Delta}{2T}\right)\left(\frac{1}{\varepsilon_1-\varepsilon_2+\omega/\Delta+i\delta}+\frac{1}{\varepsilon_1-\varepsilon_2-\omega/\Delta-i\delta}-\frac{2}{\varepsilon_1-\varepsilon_2}\right)\right]. \tag{13}$$

To fix ideas we shall now assume $\omega > 0$ and isolate the imaginary part from the integral (13). By means of slight transformations one can convince oneself that the real part of expression (13) is always of the same form as at $T = 0$, but with Δ depending on the temperature. The final expression is of the form

$$Q(\omega) - Q(0) = \int_1^\infty \frac{d\varepsilon_1}{\sqrt{\varepsilon_1^2-1}}\int_1^\infty \frac{d\varepsilon_2}{\sqrt{\varepsilon_2^2-1}}\left[(1-\varepsilon_1\varepsilon_2)\left(\frac{1}{\varepsilon_1+\varepsilon_2+\omega/\Delta}+\frac{1}{\varepsilon_1+\varepsilon_2-\omega/\Delta}-\frac{2}{\varepsilon_1+\varepsilon_2}\right)\right]$$
$$-\frac{i\pi}{2}\,\theta\left(\frac{\omega}{2\Delta}-1\right)\int_1^{\omega/\Delta-1} d\varepsilon\,\frac{[\varepsilon(\omega/\Delta-\varepsilon)-1]\,[\tanh(\omega/2T-\varepsilon\Delta/2T)+\tanh(\varepsilon\Delta/2T)]}{\sqrt{\varepsilon^2-1}\sqrt{(\omega/\Delta-\varepsilon)^2-1}} \tag{14}$$
$$-i\pi\int_1^\infty d\varepsilon\,\frac{[\varepsilon(\omega/\Delta+\varepsilon)+1]\,[\tanh(\omega/2T+\varepsilon\Delta/2T)-\tanh(\varepsilon\Delta/2T)}{\sqrt{\varepsilon^2-1}\sqrt{(\varepsilon+\omega/\Delta)^2-1}}, \qquad \text{where } \theta(x) = \begin{cases} 1 & x>0 \\ 0 & x<0. \end{cases}$$

*Strictly speaking, the strong inequality $vk \gg \Delta$ is not valid. But the applicability of the formulae obtained in this limiting case is provided by the insertion of significant numerical factors.

†Such a family of superconductors we shall call Pippard superconductors. The opposite case (which can be called the London case) when the superconductor for $\omega = 0$, is described by the equations of F and H. London in the whole temperature range is, apparently, less common, and we shall not consider it.

One integration in the real part of $Q(\omega)$ can be performed. After this there remains

$$\mathrm{Re}\,[Q(\omega)-Q(0)]=\mathcal{J}(\omega/\Delta)+\mathcal{J}(-\omega/\Delta)-2\mathcal{J}(0), \tag{15}$$

where

$$\mathcal{J}\left(\frac{\omega}{\Delta}\right)=\int_1^\infty \frac{d\varepsilon\,[\varepsilon(\varepsilon+\omega/\Delta)+1]}{\sqrt{\varepsilon^2-1}\,\sqrt{(\varepsilon+\omega/\Delta)^2-1}}\cosh^{-1}\left(\varepsilon+\frac{\omega}{\Delta}\right). \tag{16}$$

Although each of the integrals in (15) diverges, together they give a finite expression. In the integral $\mathcal{J}(-\omega/\Delta)$ in the region where $1>\epsilon-\omega/\Delta>0$, we must replace

$$\cosh^{-1}\left(\varepsilon-\frac{\omega}{\Delta}\right)\Big/\sqrt{\left(\varepsilon-\frac{\omega}{\Delta}\right)^2-1}\to\cos^{-1}\left(\varepsilon-\frac{\omega}{\Delta}\right)\Big/\sqrt{1-\left(\varepsilon-\frac{\omega}{\Delta}\right)^2},$$

and in the region where $\epsilon-\omega/\Delta$ is negative we must take $-\arccos(\omega/\Delta-\epsilon)$ or, respectively, $\frac{1}{2}\pi+\sin^{-1}(\omega/\Delta-\epsilon)$. The limiting value of this expression in the region of small frequencies is of the form

$$\mathrm{Re}\,[Q(\omega)-Q(0)]\approx(5\pi^2/12)(\omega/\Delta)^2. \tag{17}$$

In the region $\omega/\Delta\gg1$ we get

$$\mathrm{Re}\,[Q(\omega)-Q(0)]=2\ln(2\omega/\Delta)-\pi^2. \tag{18}$$

An expression for $Q(0)$ was found in Bardeen, Cooper, and Schrieffer's paper.[1] It is of the form

$$Q(0)=\pi^2\tanh(\Delta/2T). \tag{19}$$

The integration (16) can be carried out in the case $\omega=2\Delta$. In view of the fact that according to (14) the imaginary part of $Q(\omega)$ is equal to zero for $\omega<2\Delta$, we get

$$Q(2\Delta)-Q(0)=2\pi+2\sqrt{3}+4\ln(\sqrt{3}+1)$$
$$-2\ln2-\pi^2\approx2.5.$$

Hence it is clear that for $T=0$ the magnitude of the current, and consequently the penetration depth which is proportional to $Q(\omega)^{1/3}$ (see Sec. 4), changes little when the frequency is changed from 0 to 2Δ:

$$\delta(2\Delta)/\delta(0)|_{T=0}\approx0.93.$$

The imaginary part of formula (13) depends in an essential way on the relations between Δ, ω, and T. We consider first of all the case $T=0$. Then there remains only the first term of the imaginary part in equation (14) (we shall call it the "pair" term) which is different from zero only for $\omega>2\Delta$. Physically this is completely clear. As is well known, the imaginary part of the current determines the absorption and in the absence of an excitation such an absorption can only take place thanks to the destruction of a pair. The quantity 2Δ determines the energy necessary for this, when the statistics are taken into account.

Performing some simple transformations of the integral we find

$$\mathrm{Im}\,Q(\omega)=-2\pi\theta\left(\frac{\omega}{2\Delta}-1\right)$$
$$\times\int_0^{\omega/2\Delta-1}d\varepsilon\,\frac{[(\omega/2\Delta)^2-\varepsilon^2-1]}{\{[(\omega/2\Delta+\varepsilon)^2-1]\,[(\omega/2\Delta-\varepsilon)^2-1]\}^{1/2}}. \tag{20}$$

This integral can be reduced to an elliptical one. Near the threshold, i.e., for $\omega/2\Delta-1\ll1$ it has the form

$$\mathrm{Im}\,Q(\omega)=-\pi^2(\omega/2\Delta-1). \tag{21}$$

In the limiting case of large frequencies $\omega\gg\Delta$ it becomes equal to

$$\mathrm{Im}\,Q(\omega)=-\pi\omega/\Delta. \tag{22}$$

In the case of temperatures different from zero, of most interest are some limiting cases, as we shall see in the next section.

(a) The case $T\sim\omega\ll\Delta$. Here, of course, only the second term of the imaginary part of Eq. (14) (which we shall call the "electron" term) will take part. Transforming it, we find

$$\mathrm{Im}\,Q(\omega)=-4\pi\sinh\frac{\omega}{2T}K_0\left(\frac{\omega}{2T}\right)e^{-\Delta/T}, \tag{23}$$

where $K_0(x)$ is a Hankel function of an imaginary argument. In particular, we have for $T\ll\omega\ll\Delta$

$$\mathrm{Im}\,Q(\omega)=-2\pi\sqrt{\pi T/\omega}\,e^{-\Delta/T}, \tag{24}$$

and for $\omega\ll T\ll\Delta$

$$\mathrm{Im}\,Q(\omega)=-2\pi\frac{\omega}{T}\ln\frac{4T}{\gamma\omega}e^{-\frac{\Delta}{T}};\quad(\gamma=e^C\approx1.78). \tag{25}$$

(b) The case $\omega\ll T\sim\Delta$. Again only the electron term takes part. By means of a series of transformations we find

$$\mathrm{Im}\,Q(\omega)=-\pi\left[\frac{\omega}{T}\cosh^{-2}\frac{\Delta}{2T}\ln2\sqrt{\frac{2\Delta}{\omega}}\right.$$
$$\left.+\frac{\omega}{\Delta}\left(1-\tanh\frac{\Delta}{2T}\right)-2\frac{\omega}{T}P\left(\frac{\Delta}{T}\right)\right], \tag{26}$$

where the function $P(x)$ is the integral

$$P(x)=\int_1^\infty\frac{d\varepsilon}{\varepsilon^2-1}\,\frac{\cosh x\varepsilon-\cosh x}{(\cosh x\varepsilon+1)(\cosh x+1)}. \tag{27}$$

The limiting values of this function are as follows:

$$x \gg 1 \quad P(x) = e^{-x}\ln 2\gamma x, \qquad x \ll 1 \quad P(x) = 4x\pi^{-2}\zeta(3) \approx 0.485x. \tag{28}$$

From expression (26) we find that for $\omega \ll T \ll \Delta$ the result coincides with (25) while for $\omega \ll \Delta \ll T$

$$\operatorname{Im} Q(\omega) = -\pi\omega/\Delta. \tag{29}$$

(c) The case $\omega \sim \Delta \ll T$. Although the pair term in principle takes part in Im Q, its contribution turns out to be small. As to the electron term, we get from it again equation (29).

(d) The case $T \ll \omega \sim \Delta$. Here there are two possibilities. If $\omega < 2\Delta$, only the electron term will take part which gives

$$\operatorname{Im} Q(\omega) = -2\pi\sqrt{\pi}\sqrt{\frac{T}{2\Delta}+\frac{T}{\omega}}\,e^{-\frac{\Delta}{T}}. \tag{30}$$

In particular, Eq. (24) is obtained for $T \ll \omega \ll \Delta$. If $\omega > 2\Delta$, expression (30) is exponentially small compared to the contribution from the pair term (of course slightly away from the threshold). In view of the smallness of the temperature we can then use Eqs. (20) to (21).

(e) The case $\Delta \ll T \sim \omega$. Here both the pair term and the electron term take part to an equal degree. The calculation leads to the result

$$\operatorname{Im} Q(\omega) = -\pi\left(\frac{\omega}{\Delta} - 2\tanh\frac{\omega}{2T}\right). \tag{31}$$

Although in this formula the second term is much smaller than the first one, we have retained it for a reason which will be given below.

(f) The case $T \sim \Delta \ll \omega$. Here the most important contribution is given by the pair term, and it is sufficient to consider only the main expression which is the same as Eq. (29).

At the end of this section we must note that in all cases when $\omega \gg \Delta$ the real part of $Q(\omega)$ is small compared to the imaginary part which is, independently of the temperature, equal to $-\pi\omega/\Delta$. In this way the relation between the current and the vector potential is in the case $\omega \gg \Delta$ of the form

$$j(\mathbf{k}, \omega) = i\,(3\pi e^2 N\omega/4mcvk)\,A(\mathbf{k}, \omega). \tag{32}$$

This relation does not contain Δ and is exactly the same as the one obtained from the theory of the anomalous skin effect in a normal metal. This result is natural.

However, in the cases $\omega \gg \Delta$ we can not restrict ourselves only to the main term. In order that the difference between the superconducting state and the normal state can be revealed, it is necessary to take into account also terms of the next order. In the case $\Delta \ll T \sim \omega$ these terms come both from the real and from the imaginary part of $Q(\omega)$. Just for that reason was the main expression in Eq. (31) supplemented by a small term. In the last case $T \sim \Delta \ll \omega$ the main correction gives only the real part of $Q(\omega)$.

3. THE LONDON REGION

We shall now elucidate under what conditions the London region $vk \ll \Delta$ occurs. We shall not consider, as already stated, the possible, but apparently very uncommon, case when under static conditions the superconductor is a London one for the whole temperature range.

As was already noted in the preceding section the London region can appear only near T_c. On the other hand near T_c the gap width Δ becomes very small and since for $\omega \gg \Delta$ the metal differs little from a normal conductor, the London region cannot extend to the critical temperature itself and in any case has an upper limit through the condition $\omega \ll \Delta$.

To find the more exact location of the London region we find first of all the connection between the current and the vector potential in the case $\Delta \gg vk$. To do this we take into account the earlier noted fact that for the whole range of frequencies of interest we can assume $\omega \ll vk$ and also that the London region occurs only in the immediate neighborhood of T_c, i.e., that we can assume that $\Delta \ll T$. The necessary equation is obtained from Eq. (14). Only the integral with the difference of the tangents is then essential and the last term in that equation.

We find in that way

$$j(\mathbf{k}, \omega) = -\frac{e^2 N A(\mathbf{k}, \omega)}{mc}\left\{\alpha\,\frac{\Delta^2}{T_c^2} - \frac{3i\pi\omega}{4vk}\right\}; \tag{33}$$

where

$$\alpha = \frac{1}{4}\int_0^\infty \frac{\sinh x\,dx}{x\cosh^3 x} = \frac{7}{4\pi^2}\zeta(3) = 0.21.$$

If we restrict ourselves to the real part of this relation, we obtain the equation of the Londons, where the expression within the braces plays the role of the ratio of the number of superconducting electrons N_s to the total number of electrons. The imaginary part corresponds to absorption. We note that this expression is obtained under the assumption $\omega \ll \Delta \ll T$ and $\omega \ll vk$ but the relation between vk and Δ and between vk and T can be arbitrary. This explains indeed also the fact that this expression coincides within a

small correction term with the corresponding equation for the Pippard case.

As a criterion for the transition from the Pippard region to the London region one can take the equality of the coefficients of $\mathbf{A}$ in the expression for the current. For the Pippard case, assuming $\omega \ll \Delta \ll T$, we find from (17), (19), and (29)

$$\mathbf{j}(k, \omega) = -\frac{e^2 N}{mc} \mathbf{A}(k, \omega) \left\{ \frac{3\pi^2}{8} \frac{\Delta^2}{vkT_c} - i \frac{3}{4} \pi \frac{\omega}{vk} \right\}. \quad (34)$$

We shall compare this formula with Eq. (33). We assume that the imaginary parts in both equations are small compared to the real parts. In that case the criterion coincides with the criterion for the static case. The London region occurs for

$$vk \ll vk_1 = 3\pi^2 T_c / 8\alpha \approx 17.7 T_c. \quad (35)$$

Assuming $k \sim 1/\delta$ where δ is the penetration depth, one can show, using the well-known London equation for the penetration depth $\delta_L = (mc^2/4\pi N_S e^2)^{1/2}$ and Eq. (33), that this corresponds to the condition

$$\Delta \ll \frac{3}{16} \left(\frac{\pi}{\alpha} \right)^{2/3} \left(\frac{mc^2}{Ne^2 v^2} \right)^{1/3} T_c^2. \quad (36)$$

From this inequality it follows that for instance for aluminium the London region occurs for $(T_c - T)/T_c \sim 4 \times 10^{-4}$, for tin for $(T_c - T)/T_c \sim 3 \times 10^{-2}$.*

When the temperature is increased the real part in Eq. (33) becomes small compared to the imaginary part. But since in the latter case the superconductor differs little from a normal metal, we obtain necessarily the Pippard case (we remember that the imaginary part in (33) refers to that case). In that way we can assume that the London region is bounded by the condition

$$vk \gg vk_2 = (3\pi\omega/4\alpha)(T_c/\Delta)^2 \quad (37)$$

or, after substituting for the London penetration depth,

$$\Delta \gg \frac{3^{1/3}\pi^{1/6}}{(4\alpha)^{1/3}} \left(\frac{mc^2}{Ne^2 v^2} \right)^{1/6} T_c \omega^{1/3}. \quad (38)$$

Comparing Eqs. (34) and (35) we get the condition for the occurrence of the London region

$$\omega \ll \omega_c = \frac{9\pi^4}{(8\alpha)^3} \left(\frac{mc^2}{Ne^2 v^2} \right) T_c^3. \quad (39)$$

*Tin is in fact not a genuine Pippard metal and is on the boundary between the London and the Pippard situations, since for tin $vk \approx vk_1$ already at $T = 0$. But since far from T_c the temperature dependence and the penetration depth are very weak, essential departures from the Pippard equations occur only in the neighborhood of T_c.

Such a limitation can mean completely different frequencies for different substances. For aluminium, for instance, this frequency corresponds to $2 \times 10^{-2} T_c$ or $\sim 3 \times 10^9$ sec^{-1}. For tin it is equal to $0.5\, T_c \approx 2 \times 10^{11}$ sec^{-1}.

In view of the fact that of the greatest interest is the range of frequencies not too far from $\Delta(0)$ which for a Pippard metal is practically always beyond the limits of the region bounded by the inequality (39) we shall in general not consider the London region.

It is appropriate to note here also that apart from a limitation as to frequencies, the applicability of F. and H. London's equations in the form (33) is also limited from the high temperature side by the condition that the dimensions of pairs, which is of the order of v/Δ, must be small compared to the mean free path. In the opposite case the constant coefficient occurring in F. and H. London's equation can no longer be described by the first term within the brackets of Eq. (33). Since the mean free path can on the average be assumed to be of the order of 10^{-3} cm, and $v/\Delta(0) \sim 10^{-4}$ cm, the region of applicability of Eq. (33) is generally speaking small. As to the case $v/\Delta \gg l$, the electrodynamics for it has not been formulated and we shall not discuss it.

To conclude this section, we note that, as can be easily seen, for frequencies larger than ω_c a direct estimate gives $vk \gg T_c$ for the whole range of temperatures, including the neighborhood of T_c where the penetration depth is maximum. Such a relation between vk and T was essential for the conclusion reached in Sec. 2.

4. THE IMPEDANCE

The relation between $\mathbf{j}$ and $\mathbf{A}$ can be substituted into the Maxwell equations and one can obtain an expression for the dependence of the vector potential on the coordinates.

In the Pippard case considered by us the corresponding calculations are not different from the static case 1. Assuming the reflection of the electrons from the surface to be diffuse, we get for the penetration depth:

$$\delta = \frac{1}{H(0)} \operatorname{Re} \int_0^\infty H\, dz = \frac{\operatorname{Re} A(0)}{H(0)} = \frac{\sqrt{3}}{2\pi} \left(\frac{c^2 mv}{3\pi e^2 N \Delta} \right)^{1/3} \operatorname{Re} [Q(\omega)]^{-1/3}. \quad (40)$$

The impedance is determined as follows:

$$Z = R + iX = E(0) \Big/ \int_0^\infty j\,dz = -\frac{4\pi}{c}\frac{E(0)}{H(0)} = -\frac{4\pi i\omega}{c^2}\frac{A(0)}{H(0)} = -\frac{2\sqrt{3}\,\pi i\omega}{c^2}\left(\frac{mc^2 v}{3\pi e^2 N \Delta Q(\omega)}\right)^{1/3} \tag{41}$$

For complex $Q(\omega)$ the value of the root is determined as the analytical continuation of the real root for real $Q(\omega)$.

It is convenient to relate the magnitude of the impedance to the value of the active resistivity in the normal state which is equal to

$$R_n = \sqrt{3}\,(mvc^2\pi/3Ne^2)^{1/3}\,\omega^{2/3}/c^2. \tag{42}$$

Such an expression is obtained by substituting $Q(\omega) = -i\pi\omega/\Delta$ into (41) (see also reference 5). The ratio Z/R_n is determined by the equation

$$Z(\omega)/R_n = -2i\,(\pi\omega/\Delta Q(\omega))^{1/3}. \tag{43}$$

For the case $T = 0$ the frequency dependence of the impedance is obtained from Eqs. (43), (15), (19), and (20).

In the case of non-zero temperatures we carry out an analysis of the temperature dependence of the impedance for different frequencies.

(A) The case $\omega \ll \Delta(0)$

(1) For the lowest temperatures there occurs the region $T \ll \omega \ll \Delta$. Then T becomes of the order of ω and finally we go over to the region $\omega \ll T \ll \Delta$. A description of that transition is given by Eqs. (19), (23). Substituting into (43) and taking into account that $\mathrm{Re}\,Q(\omega) \gg \mathrm{Im}\,Q(\omega)$ we get

$$\frac{Z(\omega)}{R_n} = 2\left(\frac{\omega}{\pi\Delta}\right)^{1/3}\left[\frac{4}{3\pi}\sinh\frac{\omega}{2T}K_0\left(\frac{\omega}{2T}\right)e^{-\Delta/T} - i\right]. \tag{44}$$

(2) When the temperature is raised further, we get into the range $\omega \ll \Delta \sim T$ which then goes over into the range $\omega \ll \Delta \ll T$. This transition is described by Eqs. (19) and (26). As long as $\Delta/T \gg \omega/\Delta$, the imaginary part of $Q(\omega)$ will be small compared to the real part, as before, and we get in that way

$$\frac{Z(\omega)}{R_n} = 2\left[\frac{\omega}{\pi\Delta\tanh(\Delta/2T)}\right]^{1/3}\left[\frac{2\omega}{3\pi T}\frac{1}{\sinh(\Delta/T)}\ln 2\sqrt{\frac{2\Delta}{\omega}} + \frac{1}{3\pi}\frac{\omega}{\Delta}\left(\coth\frac{\Delta}{2T} - 1\right) - \frac{2}{3\pi}P\left(\frac{\Delta}{T}\right)\coth\frac{\Delta}{2T} - i\right], \tag{45}$$

where $P(\Delta/T)$ is given by expression (27).

(3) For still higher temperatures, Δ decreases so much that it becomes comparable with and then less than ω. This region is described by Eqs. (19), (15), and (29); for $\omega \sim \Delta$ the real and imaginary parts of $Q(\omega)$ are of the same order of magnitude, and for $\omega \gg \Delta$ the real part of $Q(\omega)$ turns out to be small compared to the imaginary part. In that limiting case the equation for the impedance is of the form

$$\frac{Z(\omega)}{R_n} = 1 + \frac{1}{\sqrt{3}\pi}\frac{\Delta}{\omega}\left(2\ln\frac{2\omega}{\Delta} + \pi^2\right) - i\sqrt{3}\left[1 - \frac{1}{3\sqrt{3}\pi}\frac{\Delta}{\omega}\left(2\ln\frac{2\omega}{\Delta} + \pi^2\right)\right]. \tag{46}$$

(B) The case $\omega \sim \Delta(0)$

(1) At low temperatures we have $T \ll \omega \sim \Delta$. In this region one applies Eqs. (15), (19), and (30) in the case when $\omega < 2\Delta(0)$, or Eq. (20) if $\omega > 2\Delta(0)$. In the first case the imaginary part of $Q(\omega)$ will be small compared to the real part, and the expression for the impedance will be of the form

$$\frac{Z(\omega)}{R_n} = 2\sqrt{\frac{\omega\pi}{\Delta\,\mathrm{Re}\,Q(\omega)}} \times \left[\frac{2\pi\sqrt{\pi}}{3\,\mathrm{Re}\,Q(\omega)}\sqrt{\frac{T}{2\Delta} + \frac{T}{\omega}}\;e^{-\Delta/T} - i\right], \tag{47}$$

where $\mathrm{Re}\,Q(\omega)$ is given by Eq. (15) with an additional π^2. In the case $\omega > 2\Delta(0)$ the equations for the case $T = 0$ can be used.

(2) When the temperature is raised we go over to the range $\omega \sim \Delta \sim T$ and finally we get into the range $\Delta \ll T \sim \omega$. Here we can use equations (18) and (31). Inasfar as the real part of $Q(\omega)$ is less than the imaginary part we can again use an expansion. As a result we find:

$$\frac{Z(\omega)}{R_n} = 1 + \frac{1}{\sqrt{3}\,\pi}\frac{\Delta}{\omega}\left(2\ln\frac{2\omega}{\Delta} + \pi^2 + \frac{2\pi}{\sqrt{3}}\tanh\frac{\omega}{2T}\right) - i\sqrt{3}\left[1 - \frac{1}{3\sqrt{3}\,\pi}\frac{\Delta}{\omega}\left(2\ln\frac{2\omega}{\Delta} + \pi^2 - 2\pi\sqrt{3}\tanh\frac{\omega}{2T}\right)\right]. \tag{48}$$

It is interesting to note that when the temperature is lowered starting from T_c, the real part of the impedance initially does not decrease, but slightly increases.

(C) The case $\omega \gg \Delta(0)$

In this case only the relation between T and Δ changes, but ω is all the time large compared with them. Here we apply Eqs. (18), (19), and (29). Taking into account again that the real part is small, we find:

$$\frac{Z(\omega)}{R_n} = 1 + \frac{1}{\sqrt{3}\,\pi}\frac{\Delta}{\omega}\left(2\ln\frac{2\omega}{\Delta} + \pi^2\left(1 - \tanh\frac{\Delta}{2T}\right)\right) - i\sqrt{3}\left[1 - \frac{1}{3\sqrt{3}\,\pi}\frac{\Delta}{\omega}\left(2\ln\frac{2\omega}{\Delta} + \pi^2\left(1 - \tanh\frac{\Delta}{2T}\right)\right)\right]. \tag{49}$$

In view of the fact that a detailed comparison of the theory with experimental data requires large numerical calculations (first of all a tabulation of the functions (15) and (20), which at this moment has not yet been concluded) such a comparison will be given in a later paper.

In conclusion the authors express their deep gratitude to academician L. D. Landau for his interest in this paper.

[1] Bardeen, Cooper, and Schrieffer, Phys. Rev. **108**, 1175 (1957).

[2] L. P. Gor'kov, J. Exptl. Theoret. Phys. (U.S.S.R.) **34**, 735 (1958), Soviet Phys. JETP **7**, 505 (1958).

[3] A. B. Pippard, Proc. Roy. Soc. (London) **A216**, 547 (1953).

[4] F. and H. London, Proc. Roy. Soc. (London) **A149**, 71 (1935); Physica **2**, 341 (1935).

[5] G. E. H. Reuter and E. H. Sondheimer, Proc. Roy. Soc. (London) **A195**, 336 (1948).

Translated by D. ter Haar
37

Letters to the Editor

PROTON-PROTON SCATTERING IN THE $^1D_2$ STATE AT 616 Mev

L. M. SOROKO

Joint Institute for Nuclear Research

Submitted to JETP editor March 28, 1958

J. Exptl. Theoret. Phys. (U.S.S.R.) **35**, 276-277 (July, 1958)

PRODUCTION of π mesons in p-p collisions, which proceeds rather intensively beginning with proton energies of ~400 Mev, complicates substantially the character of the elastic scattering. The connection between elastic and inelastic scattering is analyzed with the aid of the unitarity of the S matrix. In the region of proton energies of ~600 Mev, the initial $^1D_2$ state of the two protons plays an essential role.

If we consider only processes with the production of a single π meson, and also neglect d-states of the π meson, then the following processes can go through the $^1D_2$ state: (1) elastic p-p scattering; (2) the transition $^1D_2 \to (^3S_1 p)_2$ in the reaction $p+p \to d+\pi^+$; (3) the transition $^1D_2 \to (^3S_1 p)_2$ in the reaction $p+p \to n+p+\pi^+$; (4) the transition $^1D_2 \to (^3P_2 s)_2$ in the reaction $p+p \to \pi^0+p+p$.

The probability of emission of π^0 meson in an s state is rather low, since process (4) is negligible in the energy region considered. Then the S matrix for the initial $^1D_2$ state ($T=1$; $J=2$; $\Pi=+$) can be written

$$S=\begin{pmatrix} S_{11} & iS_{12} & iS_{13} \\ -iS_{12} & S_{22} & S_{23} \\ -iS_{13} & S_{23} & S_{33} \end{pmatrix},$$

where the suffix 1 denotes the p-p system, 2 the (π^+d) system, and 3 the (π^+np) system.

The values of $|S_{12}|^2$ and $|S_{13}|^2$ can be determined using the results of references 1 and 2 and also of reference 3. For the energy $E_p = 654$ Mev we obtain $|S_{12}|^2 = 0.31$ and $|S_{13}|^2 = 0.41$. Then, using one of the unitarity conditions $|S_{11}|^2 + |S_{12}|^2 + |S_{13}|^2 = 1$, we find $|S_{11}|^2 = 0.28$. In the figure we show the data for a wide range of E_p, from 400 to 800 Mev. It can be seen from the graph that all three curves have the tendency to go through the same point at a proton energy of $E_p = 616$ Mev, which has the feature that the total energy of two colliding protons[4] in the center-of-mass system is equal to the resonance energy for meson-nucleon scattering, when account is taken of the π-meson rest mass.

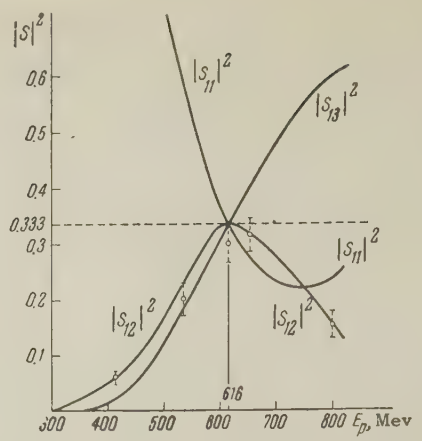

Dependence of the squares of S-matrix elements on proton energy. o – results of reference 1.

If we assume that this, in fact, occurs, then the remaining two unitarity relations give

$$|S_{22}|^2 = |S_{33}|^2; \quad |S_{22}|^2 + |S_{23}|^2 = {}^2/_3.$$

These results can be used in carrying out phase-shift analyses of p-p scattering and scattering π^+ mesons on deuterons.

The author would like to express his gratitude to R. M. Ryndin for valuable advice.

[1] M. G. Meshcheriakov and B. S. Neganov, Dokl. Akad. Nauk SSSR **100**, 677 (1955).

[2] Akimov, Savchenko and Soroko, J. Exptl. Theoret. Phys. **35**, 89 (1958), (this issue, p. 69).

[3] S. Mandelstam, Proc. Roy. Soc. **A244**, 491 (1958).

[4] Meshcheriakov, Neganov, Soroko and Vzorov, Dokl. Akad. Nauk SSSR **99**, 959 (1954).

Translated by G. E. Brown
38

AN ESTIMATE OF THE ENERGY OF SHOWER-PRODUCING PARTICLES WITH ALLOWANCE FOR THEIR ENERGY SPECTRUM

Zh. S. TAKIBAEV

Institute of Nuclear Physics, Academy of Sciences, Kazakh S.S.R.

Submitted to JETP editor January 23, 1958

J. Exptl. Theoret. Phys. (U.S.S.R.) **35**, 277-279 (July, 1958)

THE importance of accounting for the energy spectrum of shower-producing particles in estimating their energy from the angular distribution of the secondary particles has been stressed in a number of discussions.* One can account for the spectrum without recourse to any theory of multiple-meson production.

Let θ^* and θ represent the angle of π meson emission in the c.m. and laboratory systems respectively. We have then

$$\gamma_c \tan\theta_i = \sin\theta^*/(\cos\theta^* + \beta_c/\beta^*),$$

where β_c/β^* is the ratio of the velocity of the c.m.s. to the velocity of the meson in that system, and $\gamma_c = (1-\beta_c)^{-1/2}$. Calculating hence $\gamma + 1 = 2\gamma_c^2$, taking the logarithm and summing over all shower particles, we obtain

$$\ln(\gamma+1) = \frac{1}{n_s}\sum_{i=1}^{n_s} \ln\frac{2}{\tan^2\theta_i} + \frac{1}{n_s}\sum_{i=1}^{n_s} \ln\left[\frac{\sin\theta_i^*}{\cos\theta_i^* + \beta_c/\beta_i^*}\right]^2$$

Let us introduce the notation

$$x_i = \ln\frac{2}{\tan^2\theta_i}, \qquad \mu = \ln(\gamma+1),$$
$$U_i = -\ln\left[\frac{\sin\theta_i^*}{\cos\theta_i^* + \beta_c/\beta_i^*}\right]^2.$$

Let us assume further that, corresponding to the assumptions of Castagnoli et al.,[1] the U_i are random quantities. We then have

$$U_i = x_i - \mu = \ln(2/\tan^2\theta_i) - \ln(\gamma+1).$$

Let us first assume, for the sake of simplicity, that $\beta_c/\beta = 1$. Let us assume, besides, that the mesons are emitted symmetrically in the c.m.s. This means that the angle θ^* occurs as often as does $\pi - \theta^*$. We have then $\gamma + 1 = 2$ and the average of U_i equals zero, i.e., the random U_i are distributed uniformly about a zero mean value.

We have investigated, furthermore, the distribution of the experimentally measured values $V_i = x_i - \bar{x}$ for a number of showers. The analysis shows that in a number of cases the distribution law of random V_i coincides to a satisfactory degree with the normal distribution law

$$\varphi(x) = \frac{1}{\sqrt{2\pi}\sigma}\exp\left\{-\frac{(x-\bar{x})^2}{2\sigma^2}\right\},$$

where σ^2 is determined for each shower from the measurements of the angles of the shower particles with respect to the direction of the primary particle. Basically, a normal distribution of the V_i is not a necessary condition. If we assume that $\bar{x} \approx \mu$, then $V_i \equiv U_i$, which fully corresponds to the physical sense of U_i.

The quantity $\bar{x}$ is itself random and subject to statistical fluctuations; in other words, it varies as the n measurements, on which it is based, are repeated. According to the theory of probability, $\bar{x}$ has a normal distribution for all n, with a mean value μ and a standard deviation $\sigma' = \sigma/\sqrt{n}$. We shall call the quantity

$$\varphi(\bar{x}) = \frac{1}{\sqrt{2\pi}\sigma'}\exp\left\{-\frac{[\bar{x}-\mu(\gamma)]^2}{2\sigma'^2}\right\}$$

the probability $P(\bar{x}/\gamma)$ that an event $\bar{x}$ takes place after the event $\mu(\gamma)$. In other words, it represents the probability of observing $\bar{x}$ for a given value γ of the energy of a shower-producing particle.

On the other hand, the spectrum of shower-producing particles is given by the expression $P(5) = A\gamma^{-2.7}$. We calculate

$$P(\gamma/\bar{x}) = P(\gamma)\,P(\bar{x}/\gamma)/\int P(\gamma)\,P(\bar{x}/\gamma)\,d\gamma,$$

and obtain from the condition $\partial P(\gamma/\bar{x})\,\partial\gamma = 0$

$$2.7\sigma'^2(\gamma+1) = \gamma[\bar{x} - \ln(\gamma+1)]$$
$$\text{or} \quad \ln(\gamma+1) \approx \bar{x} - 2.7\sigma'^2.$$

This means, for example, that the energy of a shower-producing particle, found equal to 5500 Bev without accounting for the spectrum, must be reduced to 4500 Bev if $\sigma^2 \approx 1$.

We have assumed, in the above, that $\beta_c/\beta = 1$. It can be easily seen that this assumption is unnecessary. It has been shown by several authors[2,3] that the introduction of the energy spectrum leads to a change of $\ln(\gamma+1) = \ln B^2 + \bar{x}$. In consequence, in all previous formulae, one has to substitute $\bar{x}$ for $\bar{x} + \ln B^2$. The energy of the primary particle is then found from the relation

$$\ln(\gamma+1) = \bar{x} + \ln B^2 - 2.7\,\sigma^2/n_s;$$

the value of σ^2 is determined experimentally from the usual formula $\sigma^2 = \frac{1}{n_s}\sum(x-\bar{x})^2$. It is

then immaterial whether the distribution of x is normal or not. Such an estimate accounts for the energy spectrum $E_0^{2.7}$ of shower-producing particles, and for the energy spectrum of secondary shower particles (through the factor B). The factor B depends also on the angular distribution of shower particles. (cf. references 2 and 3).

More detailed data on actual energies of primary particles for individual showers and fluctuation curves will be given in a work devoted to the study of showers detected in emulsions at high altitudes.

*The necessity of this has been demonstrated by N. L. Grigorov. A number of important observations has been made by G. P. Zhdanov.

[1] Castagnoli, Cortini, Franzinetti, Manfredini, and Moreno, Nuovo cimento 10, 1939 (1953).

[2] W. Heisenberg, Kosmische Strahlung, Berlin-Göttingen-Heidelberg (1953).pp. 563-564.

[3] L. v. Lindern, Z. Naturforsch IIa, 5, 340 (1956).

Translated by H. Kasha
39

CONTRIBUTION TO THE THEORY OF THE POMERANCHUK EFFECT IN He^3

D. G. SANIKIDZE

Khar'kov State University

Submitted to JETP editor February 8, 1958

J. Exptl. Theoret. Phys. (U.S.S.R.) 35, 279-280 (July, 1958)

POMERANCHUK[1] predicted that the melting curve of He^3 would have a minimum on the p-T diagram, and that below this minimum the heat of melting would be negative. Since this effect has been observed experimentally,[2] it is interesting to examine this problem by using the thermodynamic functions calculated on the basis of the Fermi-liquid model, as proposed by Landau.[3] Our purpose is to reconstruct the left branch of the melting curve from the experimentally-known portion of the curve above the minimum.

The equation relating the two melting temperatures, for equal pressure, is of the form

$$\Phi^{I}(p, T_1) - \Phi^{I}(p, T_2(p)) = \Phi^{II}(p, T_1) - \Phi^{II}(p, T_2(p)), \quad (1)$$

where $\Phi^{I}(p, T_1)$ and $\Phi^{II}(p, T_1)$ are the thermodynamic potentials below the minimum point for the liquid and solid phases respectively, and $\Phi^{I}(p, T_2(p))$ and $\Phi^{II}(p, T_2(p))$ are the corresponding quantities above the minimum point.

It is known that above 0.5°K the entropy of liquid He^3 is essentially of spin origin. On the other hand, the spin entropy should increase with increasing pressure, owing to the increase in the exchange interaction that contributes to the parallel orientation of the spins[3,4] and competes with the Fermi tendency towards the anti-parallel spin arrangement. From the equality $(\partial S/\partial p)_T = -(\partial V/\partial T)_p$ we see that the coefficient of expansion is negative in that region of temperatures, in which $(\partial S/\partial p)_T > 0$. Consequently, the density of liquid He^3 should have a maximum, as indeed was observed experimentally[5] (the temperature of the maximum is $T_0 \approx 0.4$°K). In view of the fact that the density of liquid He^3 has a maximum near the minimum point of the pT diagram, it is easy to show that the effect of the change in volume can be neglected. Assuming that the coefficient of expansion of solid He^3 is of the same order of magnitude as that of He^4, the change in volume can also be neglected in the solid phase. Equation (1) can then be replaced by

$$F^{I}(T_1, V) - F^{I}(T_2, (p), V) = F^{II}(T_1, V) - F^{II}(T_2(p), V), \quad (2)$$

where F(T, V) is the free energy.

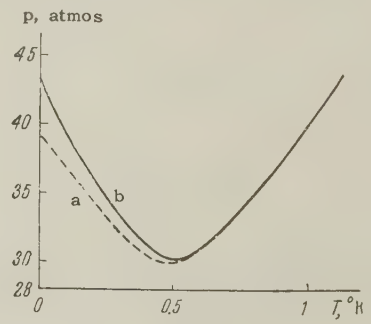

FIG. 1

Using the results of Khalatnikov and Abrikosov,[4] it is possible to calculate the free energy of liquid He^3 for two possible forms of the spectrum

$$\varepsilon(p) = p^2/2m, \quad (3a)$$

$$\varepsilon(p) = (p - p_0)^2/2m. \quad (3b)$$

The calculations yield, respectively

$$F^{I} = RT\{-2I_{3/2}/3I_{1/2} + \ln A\}, \quad (4a)$$

$$F^{I} = RT\{-2I_{1/2}/I_{-1/2} + \ln A\}, \quad (4b)$$

where

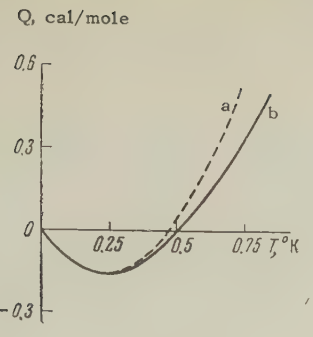

FIG. 2

$$I_\alpha = \int_0^\infty \frac{x^\alpha}{e^x/A + 1}\, dx, \quad A = e^{\mu/kT}.$$

In the solid phase, according to references 1 and 2, the spin orientation begins at temperatures considerably below those of the liquid phase. Consequently, we can write for the free energy $F^{II} = -RT \ln 2$. The thermal portion of the free energy, proportional to $RT(T/\Theta)^3$, we neglect since $T \ll \Theta$.

Solving (2) graphically, we find the connection between T_1 and $T_2(p)$. Knowing $T_2(p)$ from experiment,[6] it is possible to plot the p-T diagram (Fig. 1). In view of the fact that the entropy and specific heat of liquid He^3 are in better agreement with experiment for the spectrum (3b), the corresponding curve should fit better the transition from the liquid phase into the solid phase. As can be seen from Fig. 1, where the letters a and b correspond to spectra (3a) and (3b) respectively, the p-T diagram should have a minimum at $T \approx 0.5°K$ and $p \approx 30$ atmos.

The heat of melting is computed as $Q = T(S_l - S_S)$. Below 0.5°K the heat of melting is negative and reaches a maximum value at $T \approx 0.25°K$ (Fig. 2).*

In conclusion the author considers it his pleasant duty to thank Professor I. M. Lifshitz for suggesting the problem and for valuable advice.

*In the calculation of Q, no account was taken of the dependence of the entropy on the pressure.

[1] Ia. Pomeranchuk, J. Exptl. Theoret. Phys. (U.S.S.R.) **20**, 919 (1950).

[2] G. Walters and W. Fairbank, Bull. Amer. Phys. Soc. **2**, 183 (1957).

[3] L. D. Landau, J. Exptl. Theoret. Phys. (U.S.S.R.) **30**, 1058 (1956), Soviet Phys. JETP **3**, 920 (1956).

[4] I. M. Khaltnikov and A. A. Abrikosov, J. Exptl. Theoret. Phys. (U.S.S.R.) **32**, 915 (1957), Soviet Phys. JETP **5**, 745 (1957).

[5] D. M. Lee and H. A. Fairbank. The Fifth International Conference on Low Temperature Physics and Chemistry, U. of Wis., Madison, 1957.

[6] Weinstock, Abraham, and Osborne, Phys. Rev. **85**, 158 (1952).

Translated by J. G. Adashko
40

DISCRETE ENERGY LOSSES OF ELECTRONS IN SOLIDS AND YIELD OF SECONDARY ELECTRONS

N. B. GORNYI

Leningrad Electrotechnical Institute for Communication

Submitted to JETP editor March 8, 1958

J. Exptl. Theoret. Phys. (U.S.S.R.) **35**, 281-283 (July, 1958)

THE yield of secondary electrons in metals is small. This is explained by the interaction between the secondary electrons that move in the substance and the conduction electrons. As a result of this interaction, many secondary electrons reach the surface with an energy less than the work function in vacuum. The loss of secondary electrons in dielectrics and semiconductors should obviously be due to a different mechanism. As early as in 1939, Bruining and deBoer proposed that substances with high and low values of the secondary-emission coefficient δ have different arrangements of the energy bands.[1]

The electrons reflected after interaction in media, like the incident electrons, participate apparently in the formation of secondary electrons. If it is assumed that secondary electrons are produced by the incident and reflected electrons via the same mechanism, then investigations on the energy losses of the reflected electrons can be generalized to include the incident electrons.

Many investigations[2-6] have led to the conclusion that the discrete energy losses of the low-energy electrons incident on matter are due to the electron excitation by the crystal lattice and to their transition from the filled band to one of the allowed free bands located above the potential of vacuum. Such a loss mechanism is accompanied by the appearance of electrons with increased energies in media. Under favorable conditions, if the energy of an electron reaching the surface of the substance is greater than the work function, it can escape into the vacuum as a secondary electron.

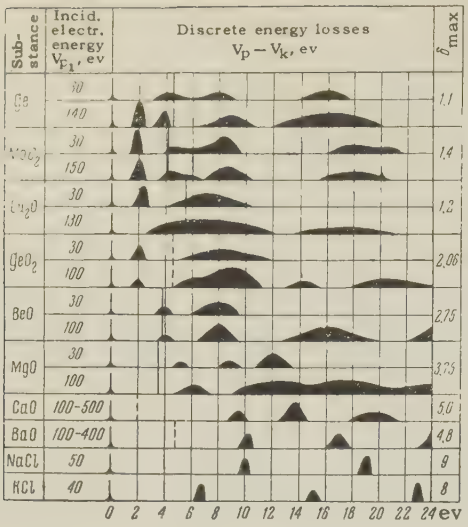

It is interesting to compare the values of the discrete energy losses $V_p - V_k$ with the values of the work function $e\varphi$ and with the maximum value of the secondary-emission coefficient δ_{max} for a given substance. The table shows schematically the discrete energy losses of the incident electrons, obtained in our laboratory for many substances,[2,4-6] and also the value of $e\varphi$.[7] The last column shows the values of δ_{max} obtained with the same targets as used to determine the discrete energy losses. In the case of insulators, δ was measured with a balanced pulse curcuit developed in our laboratory.* The table includes also data on the discrete energy losses for CaO and BaO, taken from the work of Rudberg,[8] and for NaCl and KCl, taken from the work of Shul'man and Fridrikhov.[9] The work functions are represented by lines. In the absence of reliable data on the work function, the line is shown dotted. By comparing the relation between the values of $V_p - V_k$ and $e\varphi$ with the value of δ_{max} for various substances given in the table, we can separate these substances in three groups.

1. Substances for which all values of the discrete-loss energies are greater than $e\varphi$ have a large secondary-electron yield. These include MgO, CaO, BaO, NaCl, and KCl.

2. Substances for which the most intense discrete energy losses have values less than $e\varphi$. These have a low yield of secondary electrons and include Ge and MoO_2.

3. An intermediate group is characterized by the fact that, in addition to discrete losses with energy values greater than $e\varphi$, there exists also a more or less intense loss with an energy value less than $e\varphi$, occurring principally at low values of V_p. If the relative intensity of the discrete losses with energies less than $e\varphi$ is considerable, then δ_{max} is small (Cu_2O). If the indicated intensity is insignificant compared with the intensity of the discrete losses with energies greater than $e\varphi$, then δ_{max} can be comparatively large (GeO_2 and BeO).

The dependence of the yield of secondary electrons on the ratio of the values of $V_p - V_k$ and $e\varphi$, found for the above substances, can be explained as follows. The secondary electrons produced inside the substance can lose energy to excitation of the valence-band electrons only if their energy is not less than the minimum energy of the discrete losses. At lower values of the secondary-electron energy, the electrons can lose their energy only to interaction with the lattice vibrations, giving up very small batches of energy, on the order of kT, in each collision.

The secondary electrons produced in the substances of the first group can cover a relatively large distance before their energy is reduced by phonon losses to a value less than $e\varphi$. The secondary-electron yield will therefore be greater for substances of this group and δ_{max} occurs at large values of $V_{p\,(max)}$.

In substances of the second group, the secondary emission is produced only because electrons in the valence bands receive from the primary electrons energies $V_p - V_k$ greater than $e\varphi$. Since the intensity of such discrete losses is small, the number of corresponding secondary electrons is also small. In addition, the only electrons in this group capable of escape to the vacuum are those which have not had time to reduce their energy to a value of less than $e\varphi$ and which obviously occur only relatively close to the surface of the target. Therefore δ_{max} is small and $V_{p\,(max)}$ should be less than for the first group of substances.

Everything said above concerning the second group of substances is correct also for the intermediate group. The only difference is that the number of secondary electrons occurring in the substance and having energies $V_p - V_k > e\varphi$ will be greater, and the probability of their losing energy to the excitation of electrons from the valence band will be less. Consequently, the values of δ_{max} can be greater for substances in the intermediate group than for substances in the second group.

We can thus conclude from the above comparison of the experimental data that the inter-band transitions play a substantial role in secondary

emission in insulators and semiconductors, and determine essentially the value of δ.

*A. Iu. Reitsakas, Diploma Thesis, 1957.

[1] H. Bruining and J. H. de Boer, Physica **6**, 834 (1939).

[2] N. B. Gornyi, J. Exptl. Theoret. Phys. (U.S.S.R.) **27**, 649 (1954).

[3] A. R. Shul'man and I. I. Farbshtein, Dokl. Akad. Nauk SSSR **104**, 56 (1955).

[4] N. B. Gornyi, J. Exptl. Theoret. Phys. (U.S.S.R.) **31**, 132 (1956), Soviet Phys. JETP **4**, 131 (1957).

[5] N. B. Gornyi and A. Iu. Reitsakas, J. Exptl. Theoret. Phys. (U.S.S.R.) **33**, 571 (1957), Soviet Phys. JETP **6**, 443 (1958).

[6] N. B. Gornyi, Izv. Akad. Nauk SSSR, Ser. Fiz. (in press).

[7] B. N. Tsarev, Контактная разность потенциалов (Contact Potential Difference) GITTL, M. 1955.

[8] E. Rudberg, Proc. Roy. Soc. **A127**, 111 (1930).

[9] A. R. Shul'man and S. A. Fridrikhov, J. Tech. Phys. (U.S.S.R.) **25**, 1344 (1955).

Translated by J. G. Adashko
41

ON THE DAMPING OF ELECTROMAGNETIC WAVES IN A PLASMA SITUATED IN A MAGNETIC FIELD

K. N. STEPANOV

Physico-Technical Institute, Academy of Sciences, Ukrainian S.S.R.

Submitted to JETP editor April 11, 1958

J. Exptl. Theoret. Phys. (U.S.S.R.) 35, 283-284 (July, 1958)

THE damping of high frequency electromagnetic waves in a completely ionized plasma is usually determined by the frequency of collisions between electrons and ions[1] $\nu_{eff} = 2\sqrt{2\pi}\, e^4 n_0 L / m_e^{1/2} T^{3/2}$, where e is the charge, m_e the mass, n_0 the electron density, T the plasma temperature, and L the Coulomb logarithm. For high temperatures and low plasma densities, ν_{eff} is small. Under these conditions it may turn out that the damping of electromagnetic waves γ due to the existence of thermal motion of electrons is significant (this damping is similar to the well known[2] damping of longitudinal plasma oscillations. γ increases sharply when the frequency of the wave ω becomes close to the Larmor frequency ω_H of the electron or to a multiple of it ($\omega_H = eH_0/m_e c$, H_0 is the intensity of the external magnetic field).

Using the expressions obtained by Silenko and Stepanov[3] for the components of the dielectric permittivity tensor, we obtain for the damping coefficient $\gamma = \gamma_m$ for $\omega \approx m\omega_H$, $m = 1, 2, 3, \ldots$ the following expression:

$$\frac{\gamma_m}{\omega} = \varkappa_m [\sin^2\theta n^4 - (1-v)(1+\cos^2\theta) n^2 + 2\left(1 - \frac{v}{1-u} + \frac{v\sqrt{u}}{1-u}\right)(1 - v - \sin^2\theta n^2)] \times [(2 - 3u - 3v + 4uv\cos^2\theta) n^4 + (4u + 8v - 2 - 6v^2 - 3uv - 3uv\cos^2\theta) n^2 - u - v(3 - 6v + 3v^2 - 2u)]^{-1}, \quad (1)$$

$$\varkappa_m = \frac{\sqrt{\pi}\, m^{2m-2} \sin^{2m-2}\theta (u-1)\Omega^2}{2^{m+3/2} m! |\cos\theta| \omega_H^2} (\beta n)^{2m-3} e^{-z_m^2},$$

$$z_m = \frac{1 - m\omega_H/\omega}{\sqrt{2}\beta n \cos\theta},$$

where $n = kc/\omega$, $\mathbf{k}$ is the propagation vector, θ is the angle between $\mathbf{k}$ and $\mathbf{H}_0$,

$$u = (\omega_H/\omega)^2, \quad v = (\Omega/\omega)^2, \quad \Omega = (4\pi e^2 n_0/m_e)^{1/2},$$
$$\beta = v_T/c, \quad v_T = (T/m_e)^{1/2}.$$

In deriving expression (1) it was assumed that

$$kv_T \ll \omega_H, \quad \gamma_m \ll kv_T |\cos\theta|, \quad |z_{1,2}| \gg 1.$$

The frequency ω is found from the equation

$$(1 - u - v + uv\cos^2\theta) n^4 - [2(1-v)^2 + u(v-2) + uv\cos^2\theta] n^2 + (1-v)[(1-v)^2 - u] = 0. \quad (2)$$

If it follows from (2) that $\omega \approx \omega_H, 2\omega_H$, with $|z_{1,2}| \sim 1$, then formula (1) is not valid for $\gamma_{1,2}$. In this case $\gamma_{1,2}/\omega \sim \beta n$ for values of θ which are not close to zero. However, the exact value of $\gamma_{1,2}$ for $|z_{1,2}| \sim 1$ may only be obtained numerically. For the case $\theta = 0$, the resonance $\omega = \omega_H$ which occurs for the extraordinary wave has been investigated by Silin.[4]

The damping (1) is determined by the interaction with the electromagnetic wave of those electrons, whose thermal velocity in the direction of H_0 is close to $(\omega - m\omega_H)/k\cos\theta$. For $n \gg 1$ formula (1) gives for γ_m the result obtained by Sitenko and Stepanov.[3]

For large T and small n_0, γ_m may be considerably larger than ν_{eff}. For example, let $n_0 \sim 10^8\,cm^{-3}$, $H_0 \sim 20$ gausses, $n \sim 1$, then $\gamma_{1,2}/\nu_{eff} \sim 10^6$ for $T \sim 10^{6\circ}K$. Far from resonance, γ is exponentially small and is usually much less than ν_{eff}.

In conclusion, I wish to express my sincere

gratitude to A. I. Akhiezer and Ia. B. Fainberg for discussing the results of this work.

[1] Al'pert, Ginzburg, and Feinberg, Распространение радиоволн (Propagation of Radio Waves), GTTI, Moscow, 1943.

[2] L. D. Landau, J. Exptl. Theoret. Phys. (U.S.S.R.) **16**, 574 (1946).

[3] A. G. Sitenko and K. N. Stepanov, J. Exptl. Theoret. Phys. (U.S.S.R.) **31**, 642 (1956), Soviet Phys. JETP **4**, 512 (1957).

[4] V. P. Silin, Труды ФИАН СССР (Trans. Phys. Inst. Acad. Sci. U.S.S.R.) **6**, 199 (1955).

Translated by G. Volkoff
42

NUCLEAR ISOMERISM AND ATOMIC SPECTRA

R. WEINER

Physics Institute, Academy of Sciences, Romanian Peoples Republic

Submitted to JETP editor March 13, 1958

J. Exptl. Theoret. Phys. (U.S.S.R.) **35**, 284-286 (July, 1958)

In two earlier works[1] we predicted a shift of the atomic spectrum of In^{115} III as the result of nuclear isomerism.

This result can be generalized to include all odd nuclei, subject to the following assumptions: (1) In accordance with the shell model, the nuclear transitions are single-particle transitions. (2) In nuclei with optical protons, the shift is connected with the Coulomb interaction. In nuclei with optical neutrons the shift is due to the electron-neutron interaction. (3) In the first approximation, the effect is expressed in terms of perturbation theory in the Rosental-Breit form.[2] The "unperturbed" wave functions of the electron are calculated for uniform charge distribution over the nuclear volume.

It can be shown that the absolute value of the shift is determined only by the difference in the nucleon distributions in the nucleus. Since the nuclear excitation is connected only with the change in the state of the optical nucleon, the effect is expressed, in the final analysis, by the difference between the mean-squared radii of the optical nucleons. This is an important property of the phenomenon and determines its significance; it can yield new information on the outer shell of the nucleus and on the mechanism of nuclear excitation.

The sign of the shift depends, on one hand, on the entire nuclear configuration and, on the other, on the quantum numbers of the two corresponding nuclear states. For a given configuration, the sign, in the case of the potential of a harmonic oscillator, is determined by the sign of the difference $N - N'$, where N and N' are the principal quantum numbers of the ground and excited states respectively. An analogous result is obtained for the quantum orbital number l in the case of a well with infinite walls. Incidentally, in the latter case the shift is proportional to the difference in the orbital momenta of the corresponding nuclear states and, thus, the measurement of the shift consists in principle of measuring these momenta.

The theoretical value of the shift ΔE was calculated for two transitions, $1g_{9/2} - 2p_{1/2}$ and $2d_{3/2} - 1h_{11/2}$ (these transitions are characteristic of a large number of isomers with an optical proton). The shape of the well was found to have little effect on the result of the calculation, carried out with the aid of four potentials independent of the velocity (harmonic oscillator, rectangular well with infinite walls, and diffuse well of two types, given in references 3* and 4).

For these transitions, in nuclei with odd Z and even N, the shift ΔE was found to be greater than 10^{-2} cm^{-1} for s electrons. This can apparently be observed experimentally. The Nilsson nonspherical potential leads in our case to practically the same results as the harmonic oscillator. This is due to the degeneracy of the eigenfunctions of the harmonic oscillator, which were assumed in reference 5 as the basis vectors.

In nuclei with even Z and odd N, the isomer excitation causes a change in the neutron distribution, which in turn leads to a change in the energy of interaction between the electron and the neutron. Although here the theoretical order of magnitude of the shift is at the experimental limits of observation (in Hg^{197} II, for example, $\Delta E \approx 10^{-4}$ cm^{-1} for the transition $3p_{1/2} - 1i_{13/2}$), it would be particularly important to be able to observe this effect. Actually, we deal here in principle with a pure electron-neutron interaction (if we neglect the possible exchange effect), even in those particular conditions when the neutron is bound.† In those conditions, the effective mass of the nucleon in the nucleus is less than the mass of the free nucleon and the magnetic moment of the nucleon can also be expected to have another (greater) value

in the nucleus than in the free state.[6] However, inasmuch as the magnetic moment of the neutron is due essentially to its interaction with the electron,[7] the attraction between the electron and neutron will be stronger in the case of a bound neutron (let us note that this can increase the theoretical value of the shift, which we have calculated for the free neutron).

An experimental observation of the isomer shift can lead to a new method of investigating the nuclear structure and will permit checking assumptions 1 and 2. At the present time, F. Bitter (private communication) is attempting to observe the isomer shift in Hg^{197} by means of double magnetic and optical resonance.

The author is grateful to Academicians S. Titeica, H. Jussim and D. Bogdan for many valuable remarks and to Academician E. Bedereu and Professor Ia. A. Smorodinskii for interest in this work.

*I am grateful to R. L. Lawson who was kind enough to supply me with the corresponding wave functions, calculated on the Berkeley differential analyzer (some of the functions were calculated specially for our problem).

†In the case of an isotopic shift, this effect is masked by the Coulomb interaction.

[1] R. Weiner, Nuovo cimento, Ser. X, **4**, 1587 (1956); Studii si Cercetari de Fizica **7**, 596 (1956).

[2] J. Rosental and G. Breit, Phys. Rev. **41**, 459 (1932).

[3] Ross, Mark, and Lawson, Phys. Rev. **104**, 1613 (1956).

[4] A. Green, Phys. Rev. **104**, 1617 (1956).

[5] S. Nilsson, Kongl. Danske Vidensk. Seleska Mat.-Fys., Medd., **29**, No 16, (1955).

[6] Bell, Eden, and Skyrme, Nucl. Phys. **2**, 586 (1956-7). J. Bell, Nucl. Phys. **4**, 295 (1957).

[7] L. Foldy, Phys. Rev. **87**, 693 (1952).

Translated by J. G. Adashko
43

SOUND ABSORPTION IN FERROMAGNETIC DIELECTRICS IN A MAGNETIC FIELD AT LOW TEMPERATURES

L. A. SHISHKIN

Kharkov State University

Submitted to JETP editor March 29, 1958

J. Exptl. Theoret. Phys. (U.S.S.R.) **35**, 286-287 (July, 1958)

IT was shown by Akhiezer and the author[1] that the sound absorption in ferromagnetic dielectrics, which is associated with the internal friction in a system of elementary excitations, phonons and spin waves, is, at low temperatures, principally determined by the spin waves and does not depend on the temperature. An external magnetic field changes the relaxation time in such a system and leads to a change in the temperature dependence of the sound-absorption coefficient.

The relaxation times of spin waves and phonons are determined from the expressions

$$1/\tau_k = 1/\tau_k^{(1)} + 1/\tau_k^{(2)},\quad 1/\tau_f = 1/\tau_f^{(1)} + 1/\tau_f^{(2)},$$

where $\tau_k^{(1)}$ is the relaxation time of the spin waves and is connected with the interaction of the spin waves with spin waves; $\tau_k^{(2)}$ is the relaxation time of the spin waves connected with phonon interaction; $\tau_f^{(1)}$ is the relaxation time of the phonons relative to phonon interaction, while $\tau_f^{(2)}$ is the relaxation time of the phonons relative to the spin-wave interaction.

As was shown by Akhiezer,[2] the following elementary processes are of the greatest importance: the conversion of two spin waves into a single spin wave, the conversion of two phonons into a single phonon, and the scattering of spin waves by phonons.

In the presence of an external magnetic field, the energy of the spin wave depends on the field and has the value $\epsilon_0 + 2\beta H$, where ϵ_0 is the energy of the spin wave in the absence of a magnetic field, H is the intensity of the magnetic field, β is the Bohr magneton. This dependence leads to a dependence of the relaxation times of phonons and spin waves on the magnetic field. Carrying out the calculation gone through in detail in reference 2, we can determine the relaxation time in the presence of the field. In such a case, it is shown that the relaxation time has a different form relative to the spin-spin interaction for the cases of large and small value of $2\beta H/\kappa T$ (κ is Boltzmann's constant, $2\beta/\kappa \sim 10^{-4}$):

$$\tau_k^{(1)} \approx \frac{\Theta_c \hbar}{w^2}\left(\frac{\Theta_c}{T}\right)^{1/2} \ln^2 \frac{w + 2\beta H}{T},\quad \frac{H}{T} \ll 10^4,\quad T \ll \frac{\Theta^2}{\Theta_c},$$

$$\tau_k^{(2)} \approx \frac{\Theta_c \hbar}{w^2}\left(\frac{\Theta_c}{T}\right)^{1/2} \exp\left\{\frac{2\beta H}{T}\right\},\quad \frac{H}{T} \gg 10^4,\quad T \ll \frac{\Theta^2}{\Theta_c}.$$

Here $w = \beta^2/a^2$ is the energy of the magnetic interaction of two atoms, and a is the lattice constant.

The relaxation times of the spin waves and phonons relative to interaction among the spin waves and among phonons do not change in the presence of an external magnetic field and have the form

$$\tau_k^{(2)} \approx \frac{\rho}{\hbar}\left(\frac{a\Theta_c}{\Theta}\right)^5\left(\frac{\Theta^2}{\Theta_c T}\right)^{3/2}\exp\left\{\frac{\Theta^2}{4\Theta_c T}\right\};\quad T \ll \frac{\Theta^2}{\Theta_c},$$

$$\tau_f^{(2)} \approx \frac{\rho}{\hbar}\left(\frac{a\Theta_c}{\Theta}\right)^5\frac{\Theta^2}{\Theta_c T}\exp\left\{\frac{\Theta^2}{4\Theta_c T}\right\};\quad T \ll \frac{\Theta^2}{\Theta_c},$$

$$\tau_f^{(1)} \approx \frac{\rho}{\hbar}\left(\frac{a\Theta_c}{\Theta}\right)^5\left(\frac{\Theta^2}{\Theta_c T}\right)^5;\quad T \ll \Theta;$$

where ρ is the density of the material.

As a result, it follows that for $H/T \ll 10^4$ and $T \ll \Theta^2/\Theta_c$, the dissipation function and the sound absorption coefficient Γ are determined by the relaxation time $\tau^{(1)}$:

$$\Gamma = C\omega^2(\lambda_{ij}\dot{u}_{ij})\ln^2\frac{w+2\beta H}{T},$$

where $\dot{u}_{ij}$ is the change in the deformation tensor of the crystal, λ_{ij} is some tensor, C is a constant, and ω is the sound frequency. In this case, the magnetic field increases the sound absorption.

For $H/T \gg 10^4$ and $T \ll \Theta^2/\Theta_c$, the spin-spin interaction has a small probability, and the principal contribution to the distribution function is made by the interaction of the spin waves with the phonons. The absorption coefficient in this case is determined by the time $\tau_k^{(2)}$ and has the form

$$\Gamma = C'\omega^2(\lambda_{ij}\dot{u}_{ij})\exp\{\Theta^2/4\Theta_c T\}.$$

In a sufficiently large magnetic field, the sound absorption depends exponentially on the temperature and not on the field.

In both cases, we can show that $\tau_f \ll \tau_k$ for $T \ll \Theta^2/\Theta_c$, and, consequently, the phonons play a small role in the sound absorption.

The author thanks Prof. A. I. Akhiezer for discussion of the problem.

[1] A. I. Akhiezer and L. A. Shishkin, J. Exptl. Theoret. Phys. (U.S.S.R.) **35**, Soviet Phys. JETP **8** (in press).

[2] A. I. Akhiezer, J. Phys. (U.S.S.R.) **10**, 217 (1946).

Translated by R. T. Beyer
44

INFLUENCE OF ACOUSTIC VIBRATIONS ON THE PARAMETERS OF THE BANDS OF IMPURITY ABSORPTION IN CRYSTALS

V. L. VINETSKII and M. F. DEIGEN

Physics Institute, Academy of Sciences, Ukrainian S.S.R.

Submitted to JETP editor April 1, 1958

J. Exptl. Theoret. Phys. (U.S.S.R.) **35**, 287-289 (July, 1958)

In a previous paper[1] the authors considered a system of an ionic crystal and an F-center in a macroscopic approximation and obtained expressions for the energies of the ground and excited states of the system and for the parameters of the corresponding absorption bands. These expressions depend, according to reference 1, on the sums $q_1 = \Sigma\cos^2\theta_\alpha/f_\alpha^2$ and $q_2 = \Sigma\cos^2\theta_\alpha/f_\alpha$, where θ is the angle between the displacement vector of the medium u and the wave vector κ for the α-th branch of the elastic vibrations of the crystal ($\alpha = 1, 2, 3$); f_α determines the angular dependence in the dispersion law for the frequencies of the elastic vibrations $\omega_{\kappa\alpha}$: $f_\alpha = \omega_{\kappa\alpha}/|\kappa|$.

In reference 1 we used for the evaluation of the sums q_1 and q_2 the results of a paper by Tolpygo[2] where the consideration was based on a microscopic approximation. It turned out, however, that it was possible to perform, in general form, a consistent macroscopic consideration for a large group of crystals for which the anisotropy was not too large (for crystals which did not satisfy this condition it was necessary to resort to numerical calculations).

The quantities f_α are, as is well known, the solutions of the characteristic determinant

$$n_1^2/(n_1^2-\gamma_1) + n_2^2/(n_2^2-\gamma_2) + n_3^2/(n_3^2-\gamma_3) = 1, \qquad (1)$$

where

$$\gamma_i = (A-C)n_i^2 + C - x;\quad A = \lambda_{1111}/(\lambda_{1122}+\lambda_{1212});$$
$$C = \lambda_{1212}/(\lambda_{1122}+\lambda_{1212});$$
$$x = \rho f_\alpha^2/(\lambda_{1122}+\lambda_{1212});$$

λ_{iklm} are the elasticity moduli of a cubic crystal; n_i a unit vector in the direction κ, and ρ the crystal density. It is convenient to rewrite Eq. (1) in the form

$$x^3 + bx^2 + cx + d = 0, \tag{2}$$

where

$$b = -(1 + 3C + \eta); \quad c = C(2 + 3C) + 2\eta(C + L_0) + L_0\eta^2;$$
$$d = -[C^2(C + 1) + \eta(C^2 + 2CL_0) + \eta^2(CL_0 + 3L_1) + \eta^3 L_1]; \tag{2a}$$
$$L_0 = n_1^2n_2^2 + n_1^2n_3^2 + n_2^2n_3^2; \quad L_1 = n_1^2n_2^2n_3^2.$$

The quantity $\eta = A - C - 1$ can be considered to be the "anisotropy parameter" (in the isotropic case $\eta \to 0$). Approximate solutions of Eq. (2) can be written as series in powers of η. For many crystals retaining terms of the first order in η is already a good approximation:

	AgBr	NaBr	NaCl	Ge	Si	MgO	LiF
$\eta =$	0.22	−0.27	0.35	−0.46	−0.46	−0.46	−0.48.

In zeroth approximation the roots of Eq. (2) are

$$x_{1,2}^0 = C; \quad x_3^0 = C + 1. \tag{3}$$

Looking for corrections in the first and the second approximation, we get

$$x_{1,2} = C + L_0\left(1 \pm \sqrt{1 - \frac{3L_1}{L_0^2}}\right)\eta + \frac{(4L_0^3 - L_0^2 - 3L_0L_1)\sqrt{1 - 3L_1L_0^{-2}} \pm (4L_0^3 - L_0^2 - 9L_0L_1 + 2L_1)}{2L_0\sqrt{1 - 3L_1L_0^{-2}}}\eta^2 + \ldots \tag{4}$$

$$x_3 = C + 1 + (1 - 2L_0)\eta + (L_0 - 4L_0^2 + 3L_1)\eta^2 + \ldots.$$

Using the equations of motion for the elastic vibrations of the lattice we get easily the expressions

$$\cos^{-2}\theta_x = n_1^2/(n_1^2 - \gamma_1)^2 + n_2^2/(n_2^2 - \gamma_2)^2 + n_3^2/(n_3^2 - \gamma_3)^2. \tag{5}$$

Substitution of (4) into (5) enables us to get final expressions for $\cos^2\theta_\alpha$ and after that to evaluate the sums q_1 and q_2. Restricting ourselves to linear terms in η we get

$$q_1 = \frac{\rho}{(\lambda_{1122} + \lambda_{1212})(C + 1)}\left(1 - \frac{1 - 2L_0}{C + 1}\eta\right),$$
$$q_2 = \left[\frac{\rho}{(\lambda_{1122} + \lambda_{1212})(C + 1)}\right]^{1/2}\left[1 - \frac{1 - 2L_0}{2(C + 1)}\eta\right]. \tag{6}$$

Use of (6) leads to final expressions for the quantities J_0, J_1, σ_1, σ_2, with the aid of which the required energy levels are determined according to reference 1 and also the frequency of the corresponding absorption band and its half-width (in the limiting cases of high and low temperatures).

$$J_0[\alpha_0] = \frac{1}{14}\left\{3\frac{\hbar^2}{\mu_0}\alpha_0^2 - 3\frac{e^2}{\varepsilon}(3z + \varepsilon c)\alpha_0 - \frac{\alpha_0^3}{\mu_0 g_0 e^2}\right\};$$
$$g_0 = \frac{2^8 \cdot 7\pi(C + 1)^2(\lambda_{1122} + \lambda_{1212})}{437a^2\mu_0e^2(C + 1 - 0.6\eta)};$$
$$J_1[\beta] = \frac{1}{2}\left\{\frac{\hbar^2}{\mu_0}\beta^2 - \frac{e^2}{\varepsilon}(z + 0.3914\varepsilon c)\beta - \frac{\beta^3}{3e^2g_1\mu_0}\right\}; \tag{7}$$
$$g_1 = \frac{2^8\pi(C + 1)^2(\lambda_{1122} + \lambda_{1212})}{3a^2\mu_0e^2[9(C + 1) - 41\eta/7]};$$

$$\sigma_1 = \frac{\alpha_0^3}{\hbar}\left\{\frac{1}{2\mu_0e^2}\left(\frac{1}{7g_0} + \frac{1}{3v^3g_1}\right) - \frac{a^2(27v^2 + 14v + 2)}{14\pi(1 + v)^7}\frac{1 - 0.6\eta/(C + 1)}{(C + 1)(\lambda_{1122} + \lambda_{1212})}\right\};$$

$$\sigma_2 = \frac{a^2\alpha_0^4}{\hbar\sqrt{\rho(C + 1)(\lambda_{1122} + \lambda_{1212})}}\left\{\frac{183}{7^3 \cdot 10\pi^2}\left(1 - \frac{0.3\eta}{C + 1}\right) + \frac{1}{70\pi^2v^4}\left(\frac{73}{15} - \frac{23}{14}\frac{\eta}{C + 1}\right) - \frac{4}{7\pi^2}\left(1 - 0.3\frac{\eta}{C + 1}\right)\right.$$
$$\left.\times\left[\frac{-7v^8 - 480v^6 - 930v^4 - 32v^2 + 9}{6(v^2 - 1)^6} + 2\frac{v^2\ln v}{(v^2 - 1)^7}(27v^6 + 141v^4 + 77v^2 - 5)\right]\right\}.$$

We have used in these formulae the notation of reference 1.

The approximation used above can also be used to consider the behavior of an electron of an impurity center in homopolar crystals.

[1] M. F. Deigen and V. L. Vinetskii, J. Exptl. Theoret. Phys. (U.S.S.R.) 32, 1382 (1957), Soviet Phys. JETP 5, 1125 (1957).

[2] K. B. Tolpygo, Тр. Ин-та физики АН УССР (Trans. Phys. Inst. Acad. Sci. Ukrainian S.S.R.) 6, 102 (1955).

Translated by D. ter Haar
45

THE π-MESONIC ATOM AND CORRECTIONS TO THE DISPERSION RELATIONS

V. A. MESHCHERIAKOV

Moscow State University

Submitted to JETP editor April 3, 1958

J. Exptl. Theoret. Phys. (U.S.S.R.) **35**, 290 (July, 1958)

RECENTLY there appeared a series of papers[1] devoted to various corrections to the dispersion relations. All those effects due to the mass difference between the neutral and the charged mesons and to the electromagnetic interaction proved to be too small to explain the Puppi-Stanghellini puzzle.[2] This consists in the fact that the dispersion relations for the process $\pi^- + p \to \pi^- + p$ agree with experiment with the choice of $f^2 = 0.04$ for the coupling constant of the nucleon-meson interaction up to the resonance, whereas $f^2 = 0.08$ after the resonance. Such a marked energy dependence of f^2 contradicts the results of other methods for the determination of f^2, which give the value $f^2 = 0.08$ for the above energy region. The aim of this paper is to estimate the magnitude of the corrections due to the π mesonic atom.

The appearance of a state with only a nucleon and a photon in the expansion of the antihermitian part of the scattering amplitude in terms of a complete system of functions does not fully account for the electromagnetic interaction. In the case of π^--p scattering we have to consider the π mesonic atom. For this purpose the forward scattering amplitude $f_-(\omega)$ for the process $\pi^- + p \to \pi^- + p$ has to be investigated more carefully. It can be represented as the sum of three terms: (1) the Rutherford amplitude, (2) a purely nuclear term, and (3) an interference term of the preceding two. The last term is small for energies of some 10 Mev, since it is proportional to α/η (α is the fine-structure constant, $\eta = p/m_\pi c$). But in the dispersion relations it is important to know the scattering amplitude for small $\omega - m_\pi > 0$, in which case the interference term is not small. We note that the dispersion relations are strictly proven[3] only for the nuclear part of the scattering amplitude. Therefore we have to regard the interference term as a correction to the usual dispersion relations for the processes $\pi^\pm + p \to \pi^\pm + p$.

The interference term contains poles corresponding to the bound states of the system π^-, p. The correction to the dispersion relations due to these states is equal to

$$\Delta\left(\frac{D_\mp^b}{r_0}\right) = \pm \frac{\eta\eta^b}{\omega - 1}\left[\frac{8\pi^2\alpha}{9}(4a_1^2 + a_3^2 + 4a_1a_3) \times \sum \frac{(-1)^n}{n!\,(n+1)!} + O(\alpha)\right],$$

where $D_\pm = \mathrm{Re}\, f_\pm(\omega)$, $r_0 = \hbar/m_\pi c$, and the index b implies taking the value in the center-of-mass system. The sum arises from the inclusion of all bound states. These states are considered stable, the finite level width effecting only the terms $0(\alpha)$. The quantities a_1, a_2 are equal to α_1/η, α_3/η and are taken from the paper of Orear.[4] Numerical calculations show that the correction coming from the π mesonic atom is a small effect and accounts for only 4% of the deviation of the coupling constant f^2 in the region of 120 Mev.

In conclusion I express my gratitude to D. V. Shirkov for helpful discussions and interest in this work.

[1] A. Agodi and M. Cini, Nuovo cimento **5**, 1256 (1957); **6**, 686 (1957). Agodi, Cini, and Vitale, Phys. Rev. **107**, 630 (1957). V. K. Fedianin, J. Exptl. Theoret. Phys. (U.S.S.R.) **33**, 1301 (1957); Soviet Phys. JETP **6**, 1001 (1958).

[2] G. Puppi and A. Stanghellini, Nuovo cimento **5**, 1305 (1957).

[3] N. N. Bogoliubov and D. V. Shirkov, Введение в теорию квантованных полей (Introduction into the Quantum Theory of Fields), Gostekhizdat, M. 1957.

[4] J. Orear, Phys. Rev. **96**, 176 (1954).

Translated by R. Lipperheide
46

EFFECT OF UNIAXIAL ELASTIC DEFORMATIONS ON THE MAGNETIC PROPERTIES OF ZINC CRYSTALS AT LOW TEMPERATURES

B. I. VERKIN and I. M. DMITRENKO

Physico-Technical Institute, Academy of Sciences, Ukrainian S.S.R.

Submitted to JETP editor April 4, 1958

J. Exptl. Theoret. Phys. (U.S.S.R.) **35**, 291-293 (July, 1958)

UNIFORM compression of zinc crystal at an approximate pressure of 700 kg/cm^2 increases the period of oscillations of its magnetic susceptibility by 40 to 50%, and reduces correspondingly the

number of mobile charge carriers in the anomalously small group by more than 40%.[1] Thanks to the anisotropy of the compressibility of the zinc crystal, uniform compression leads to a reduction in the ratio c/a of the crystal axis and thus makes its lattice structure closer to that corresponding to hexagonal dense sphere packing.

We considered it important to investigate the influence of uniform elastic deformations of the lattice on the de Haas — van Alphen effect in zinc crystals, in order to establish above all the connection between the change in the number of charges in the anomalously small group and the sign of variation of c/a.

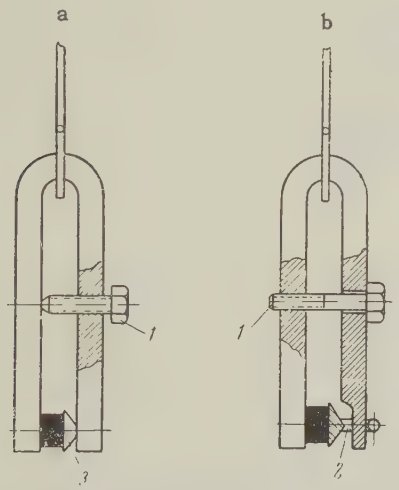

FIG. 1. Clamping springs for the investigation of the anisotropy of magnetic properties of uniaxially elastically-deformed crystals.

Figure 1 shows an instrument that produces elastic uniaxial compression or tension in zinc crystals at low temperatures. Special springs made of very pure beryllium bronze were calibrated at low temperature. Having determined the elastic constant of such a spring it became possible to establish by means of screw 1, the fixed value of spring tension or compression required to apply a specified load to the crystal. Crystals of the required size were pricked out of a large cylindrical zinc crystal, freely grown in a vessel of pyrophyllite on a plate in which a temperature gradient was produced. One spallation surface of one specimen investigated was glued to the smooth arm of the clamp spring, and the second surface was glued either to a small thimble 2 (for uniaxial tension of the crystal — Fig. 1b) or to a knife edge 3 with a polished base (for uniaxial compression of the crystal — Fig. 1a). The clamping spring was attached together with the crystal to the suspension system of the usual instrument used to investigate the anisotropy of magnetic properties.[2]

TABLE I

Uniaxial compression			Uniaxial tension		
θ°	$T \cdot 10^4$, Oe^{-1}		θ	$T \cdot 10^4$, Oe^{-1}	
	$p = 0$	$p \approx 100$ kg/cm^2		$p = 0$	$p \approx 20$ kg/cm^2
20	0.492	0.520	20	0.506	0.494
30	0.455	0.478	30	0.465	0.454

We first investigated the anisotropy of the magnetic properties of the unloaded zinc crystal. The prestressed spring was then unloaded by rotating screw 1 and the zinc crystal was subjected respectively to either uniaxial compression or uniaxial tension along the hexagonal axis c. We then investigated, at the same crystal orientation in the field, the anisotropy of the magnetic properties of the uniaxially deformed zinc.

During the investigation the orientation of the zinc crystals in the field was such that the axis of suspension of the spring and of the specimen was perpendicular to the hexagonal and binary axes of the crystal. The load does not exceed 100 kg/cm^2 in uniaxial compression or 20 kg/cm^2 in uniaxial tension.

The results of the measurement (the periods T of the oscillations of the susceptibility due to the small group of charges) are given in Table I (θ is the angle between the field vector H and

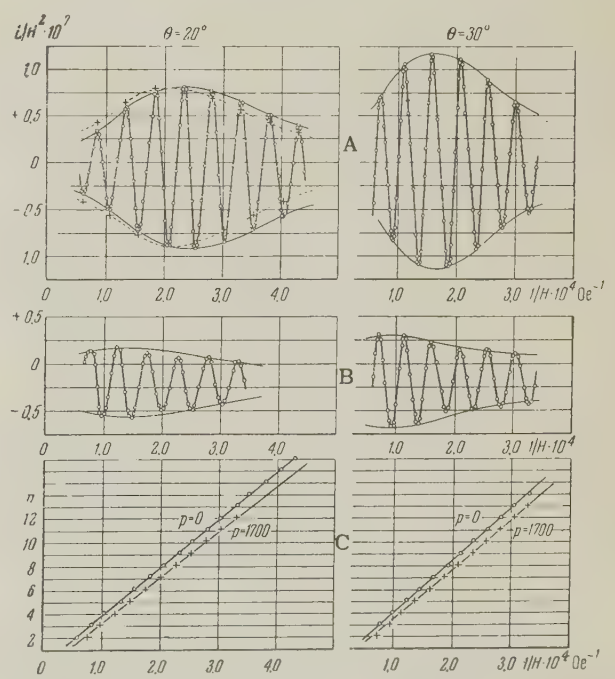

FIG. 2. Curves of L_y/H^2 (which is proportional to $\Delta\chi = \chi_3 - \chi_2$) vs. 1/H for free and uniaxially-compressed zinc crystals; T = 4.2°K; A — free crystal (p = 0); o — prior to loading, + — after removal of load; B — uniaxially-compressed crystal (p ~ 100 kg/cm^2); C — n(1/H) for free and uniaxially-compressed crystal at θ = 20 and 30 degrees.

the principal axis of the crystal).

In the graphs of Fig. 2, the influence of uniaxial elastic compression of the zinc crystals is illustrated by the shapes of the curves $\Delta\chi(1/H)$. The same figure shows the straight line $n(1/H)$, which determine the period of oscillation of susceptibility of a free and compressed crystal at $\theta = 20$ and 30°.

The uniform compression of zinc crystals in the region $\theta \leq 30°$ increases the period of susceptibility oscillations by 4 to 5%. With increasing θ, the oscillation period increases less, at $\theta = 70°$ it stays unchanged, and at $\theta = 80°$ the period of oscillation even diminishes somewhat ($\Delta T/T \sim 1\%$).

Uniaxial tension of zinc crystals in the region $\theta \leq 30°$ decreases the period of the susceptibility oscillations by 2 or 3%. The amplitude of the susceptibility oscillations diminishes several-fold in uniaxial elastic deformation of the crystal. After removing the load the period and the amplitude of the oscillations return to their initial values.

The investigations performed have thus shown that reducing c/a for elastic deformation of the crystal leads to an increase in the periods of the susceptibility oscillations, leading in turn to an increase in the number of charges in the anomalous group. On the contrary, an increase in c/a causes a reduction in the oscillation periods and a corresponding increase in the number of charges in this group.

[1] Dmitrenko, Verkin, and Lazarev, J. Exptl. Theoret. Phys. (U.S.S.R.) **33**, 287 (1957), Soviet Phys. JETP **6**, 223 (1958).

[2] D. Shenberg, J. Exptl. Theoret. Phys. (U.S.S.R.) **8**, 1271 (1938).

Translated by J. G. Adashko
47

INFLUENCE OF MULTIPLE SCATTERING ON THE DEVELOPMENT OF HIGH-ENERGY ELECTRON-PHOTON CASCADES IN LEAD

T. G. VOLKONSKAIA, I. P. IVANENKO, and G. A. TIMOFEEV

Moscow State University

Submitted to JETP editor April 8, 1958

J. Exptl. Theoret. Phys. (U.S.S.R.) **35**, 293-294 (July, 1958)

THE influence of the multiple scattering of electrons on atomic nuclei on the processes of bremsstrahlung and pair production was investigated in recent years by several authors.[1-4] It was found that the cross-sections for the above processes for particle energies $> 10^{11}$ ev are considerably different from the Bethe-Heitler cross sections.[5] For an experimental test of the theoretical predictions, it is necessary to recalculate the development of cascade showers using the new values of the cross-sections for the basic processes in the early stages of development.

We carried out calculations of the longitudinal development, for two cascade units, of 154 showers initiated by 10^{12} ev electrons, and of 40 showers initiated by an electron or a photon in lead, for four cascade units. The calculations were carried out by the Monte-Carlo method using the "Strela" electronic computer. The cross sections for bremsstrahlung and pair production were taken from reference 4, accounting for the fact that the refraction index of the medium is different from unity. Ionization losses were neglected.

The circles in the figure represent the mean energy spectrum of electrons at the depth of 0.5,

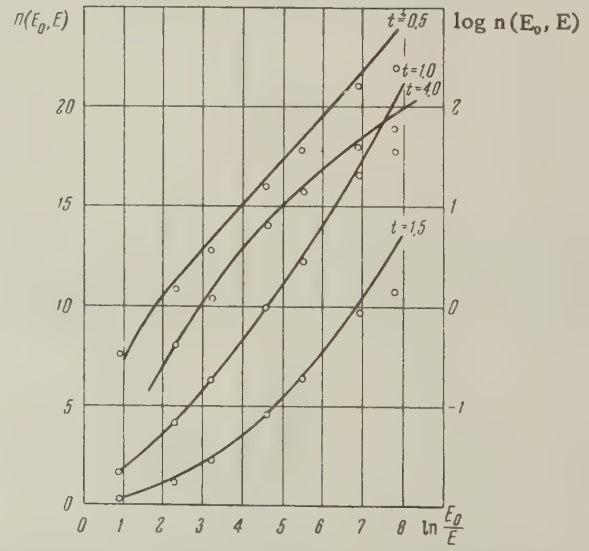

Mean energy spectra of electrons at various depths. Solid curves are taken from reference 5; circles represent calculations of the authors. The scale indicated refers to the curves for t = 0.5, 1.0, and 1.5. In order to obtain numerical values the ordinate of the first curve should be multiplied by 10^{-1}, of the second – by 3×10^{-1}, and of the third – by 1. The curve for t = 4 is represented in a logarithmic scale. The latter curve is calculated according to reference 5, since that given in reference 4 is subject to a ~ 30 % error.

Number of showers having N electrons with energy > E at depth t

$t = 0.5$					$t = 1.5$				
N	E, ev				N	E, ev			
	10^{10}	$4\cdot10^{9}$	10^{9}	$4\cdot10^{8}$		10^{10}	$4\cdot10^{9}$	10^{9}	$4\cdot10^{8}$
0	1	0	0	0	0—5	103	76	46	41
1	102	94	84	83	6—10	45	57	49	44
2	24	23	14	9	11—15	4	18	35	29
3	16	24	38	41	16—20	1	2	14	21
4	7	6	4	6	21—25	0	1	6	14
5	4	5	9	8	26—30	0	0	3	0
6	0	2	0	2	31—35	0	0	0	3
7	0	0	4	4	36—40	0	0	1	1
8	0	0	1	0					
9	0	0	0	0					
10	0	0	0	1					

1.0, 1.5, and 4 cascade units, and the solid curves represent the spectra calculated using the usual values of the cross-sections.[6] It is evident that the energy spectrum calculated accounting for multiple scattering is different: there are more high-energy particles and less low-energy particles ($< 10^9$ ev) present than in the usual spectrum.

The distribution of showers with respect to the number of particles with energy > E at two depths is given in the table. It can be seen that the fluctuations of $\overline{N}(>E)$, of the order of $\pm 0.7\,\overline{N}(>E)$, occur in about 30% of all cases at the depth of one cascade unit. Fluctuations of $\overline{N}(>E)$ in showers calculated using the usual values of the cross sections are, evidently, of similar magnitude. Great statistical accuracy is, therefore, needed for a confirmation of the effects predicted in references 1 to 4 by a measurement of the energy spectrum of electrons with energies 4×10^8 ev in showers initiated by 10^{12}-ev particles.

The authors thank V. Ia. Pivkin for help in the reduction of data.

[1] L. D. Landau and I. Ia. Pomeranchuk, Dokl. Akad. Nauk SSSR **92**, 535 (1953).

[2] L. D. Landau and I. Ia. Pomeranchuk, Dokl. Akad. Nauk SSSR **92**, 735 (1953).

[3] M. L. Ter-Mikhaelian, Dokl. Akad. Nauk SSSR **94**, 1033 (1954).

[4] A. B. Migdal, J. Exptl. Theoret. Phys. (U.S.S.R.) **32**, 633 (1957), Soviet Phys. JETP **5**, 527 (1957).

[5] S. Z. Belen'kii, Лавинные процессы в космических лучах (Cascade Processes in Cosmic Rays) Gostekhizdat, 1948.

[6] N. Arley, Proc. Roy. Soc. **A168**, 519 (1938).

Translated by H. Kasha
48

INCREASE OF THE BAROMETRIC EFFECT WITH THE ENERGY OF EXTENSIVE AIR SHOWERS

D. D. KRASIL' NIKOV

Yakutsk Branch, Academy of Sciences, U.S.S.R.

Submitted to JETP editor April 9, 1958

J. Exptl. Theoret. Phys. (U.S.S.R.) **35**, 295-296 (July, 1958)

TWO series of observations of the time variations of extensive air showers frequency were carried out in 1954 through 1956 in Yakutsk, latitude 62° N, longitude 129° E, elevation 100 m. The measurements covered a range of mean shower densities and arrays of self-quenching Geiger-Müller counters were used.

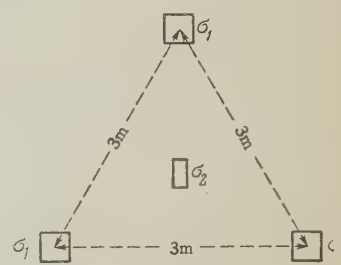

FIG. 1. Diagram of the position of counter trays under 60 g/cm² of matter. Effective counter tray area: $\sigma_1 = 0.1$ m², $\sigma_2 = 0.033$ m².

In the first series (Fig. 1), triple coincidences of counter trays of area σ_1 and fourfold coincidences C_3 and C_4 were recorded under 60 g/cm² of matter. In the second series (Fig. 2), the thickness was reduced to 2.5 g/cm² of a light substance. Six-fold coincidences C_6 of counter trays of area σ_1, eight-fold coincidences C_8 and, independently, coincidences C_3 not accompanied by a six-fold coincidence were recorded in the second series besides the coincidences C_3 and C_4 in the two independent arrays.

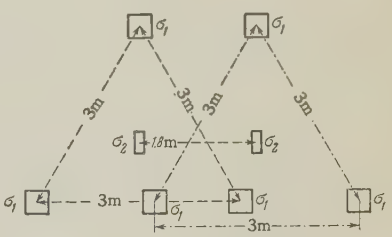

FIG. 2. Diagram of the position of counter trays under 2.5 g/cm² of matter. Effective counter tray area: $\sigma_1 = 0.1$ m², $\sigma_2 = 0.033$ m².

A statistical analysis of the variation of the mean daily number of showers, correlated with the variations of the mean daily values of the temperature and pressure at the point of observation, revealed a marked increase of the barometric coefficient with increasing mean particle

flux density $\bar{\rho}$ in the showers. The measured partial coefficients of the barometric effect, in percent per millibar of pressure variation, are given below for different densities $\bar{\rho}$ (particles/m^2).

	$\bar{\rho}$	Under 60 g/cm²	Under 2.5 g/cm²
$A_3 = C_3 - C_6$	15		-0.55 ± 0.05
C_3	26	-0.68 ± 0.07	-0.58 ± 0.04
C_4	50	-0.76 ± 0.11	
C_6	53		-0.70 ± 0.05
C_8	100		-0.73 ± 0.07

Assuming that $\bar{\rho}$ equals the particle flux density in recorded showers at a certain distance from shower axis, and using the energy estimate given by Greisen,[1] it is possible to estimate the mean energy of the primary particles initiating the showers. We found that the energies are 1×10 and 2×10^{15} ev for coincidences C_3 and C_6 respectively.

The observed increase of the barometric effect with energy can be explained on the lines of the theory proposed recently by Nikol'skii, Vavilov, and Batov.[2]

The author would like to thank S. I. Nikol'skii for a discussion of the work and to N. N. Efimov, N. P. Emel'ianov, and T. F. Panfilova for help in reducing the data.

[1] K. Greisen, Progr. in Cosmic Ray Physics **3**, 1-141 (1956).

[2] Nikol'skii, Vavilov, and Batov, Dokl. Akad. Nauk. SSSR 111, **71** (1956), Soviet Phys. "Doklady" **1**, 625 (1956).

Translated by H. Kasha
49

A CONTRIBUTION TO NEUTRINO THEORY

V. V. CHAVCHANIDZE and M. E. PEREL' MAN

Submitted to JETP editor December 24, 1957

J. Exptl. Theoret. Phys. (U.S.S.R.) **35**, 296-297 (July, 1958)

WE show in the present article that all the experimental results which can be explained by a two-component neutrino theory[1] can also be explained without introducing a longitudinal (asymmetric) neutrino. We suggest replacing this longitudinal-neutrino assumption by the assumption that in β, μ, and π decays there is emitted a quantum mechanical mixture of two light neutral Dirac particles of opposite parity, each being the antiparticle of the other, and for this purpose we introduce a possible new particle-antiparticle conjugation rule.

We shall, for simplicity, consider only β decay, given by a Hamiltonian of the form

$$H = \sum_{i=1}^{5} c_i (\bar{\psi}_n O_i \psi_p)(\bar{\psi}_e O_i \Phi). \tag{1}$$

Before the work of Lee and Yang[2] the symbol Φ stood either for ψ_ν or $\psi_{\bar{\nu}}$, which is equivalent to postulating the possibility of experimentally differentiating between ν and $\bar{\nu}$. The possibility that a quantum mixture $\nu \pm \bar{\nu}$ may be emitted was not considered, i.e., the number of leptons assumed to be conserved. In the two-component theory, however, we write

$$\Phi \to \Phi^{(\pm)} = (1 \mp \gamma_5)\psi_\nu/\sqrt{2} = (\psi_\nu \mp \gamma_5 \psi_\nu)/\sqrt{2}. \tag{2}$$

Let us write, to be specific, $\psi_\nu = \psi_{+\uparrow}$ (the explicit form for the solutions to the Dirac equation are given by Schiff;[3] we write everywhere $E = E_+ = -E_-$). Then

$$\gamma_5 \psi_{+\uparrow} = \begin{pmatrix} 0 & 0 & -1 & 0 \\ 0 & 0 & 0 & -1 \\ -1 & 0 & 0 & 0 \\ 0 & -1 & 0 & 0 \end{pmatrix} \begin{pmatrix} -p_z/E \\ -(p_x + ip_y)/E \\ 1 \\ 0 \end{pmatrix} e^{i(\mathbf{pr}-Et)}$$

$$= \begin{pmatrix} -1 \\ 0 \\ p_z/E \\ (p_x + ip_y)/E \end{pmatrix} e^{i(pr-Et)} = -\psi_{-\downarrow}(-E).$$

Our hypothesis is equivalent to the assumption that

$$\psi_{\bar{\nu}}(E) = \psi_-(-E) = -\gamma_5 \psi_+(E) \tag{3}$$

behaves like the wave function of $\bar{\nu}$, while $\psi_\nu = \psi_+(E)$ is the wave function of ν.

Usually the wave function of a particle and an antiparticle (such as, for instance, the electron and positron) are related by

$$\psi_n = C\bar{\psi}^*_-(-\mathbf{p}). \tag{4}$$

This relation is necessary, and is the only possible one because in the negative-frequency equation

$$[\boldsymbol{\alpha} \cdot (\mathbf{p} - e\mathbf{A}) + \beta m + eA_0 + E]\psi_- = 0$$

it is necessary, on going over to the antiparticle equation

$$[\boldsymbol{\alpha} \cdot (\mathbf{p} + e\mathbf{A}) + \beta m - eA_0 - E]\psi_n = 0,$$

to change the sign of both the energy and the charge.

Because of its zero mass, however, the neutrino does not participate in electromagnetic interactions, and therefore the transition from $[\boldsymbol{\alpha}\cdot\mathbf{p}+E]\,\psi_-(E)=0$ to the anti-particle equation $[\boldsymbol{\alpha}\cdot\mathbf{p}-E]\,\psi_{\overline{\nu}}(E)=0$ is possible only with the aid of (3).

It is not evident that (3) must be true also for the neutrino (see Gell-Mann and Pais[4]). In particular, the C matrix is necessary to interchange the large and small components of a bispinor so that the wave function of a real antiparticle will be different from zero even in the nonrelativistic limit. For a neutrino, however, such a matrix is not necessary.

Thus assuming (3), we find that a Hamiltonian of the form of (1), where

$$\Phi^{(\pm)}=(\psi_\nu\pm\psi_{\overline{\nu}})/\sqrt{2}$$

[which is equivalent, from the analytic point of view, to (2)] gives the same cross sections for decay as does the two-component theory. In this way, the reason for the asymmetry in decay is not assumed due the properties of one of the particles, but to nonconservation of the lepton charge nonconserving in the interaction itself. At the same time it is seen that only mixtures of the form $\nu+\overline{\nu}$ or $\nu-\overline{\nu}$ have a definite type of interaction* (which means that it is just these which are emitted in β, μ, and π decays). The selectivity of the interaction lies in the choice of the phase factor of the emitted mixture.

We note that with our approach it is possible, though less preferable, to take mixtures of ν and $\overline{\nu}$ with different statistical weights in the form

$$\Phi=a\psi_\nu+b\psi_{\overline{\nu}}, \tag{6}$$

which would correspond to the more general assumption[2] that

$$\Phi=(1+\lambda\gamma_5)\,\psi_\nu. \tag{7}$$

It should be noted that the difference between the analytical expressions obtained from our approach and from the two-component theory will become evident if one finds "analyzers" (nuclei or particles) capable of absorbing from a mixture those Dirac particles which in themselves conserve parity (compare with Pontecorvo[5]). According to Landau[1] such "analyzers" cannot exist, since the longitudinal neutrino will not reduce to any particle with other properties.

In conclusion the authors consider it their duty to thank Professor V. I. Mamasakhlisov for valuable discussion and interest in the work.

*The situation is then similar to that for neutral K mesons.[4]

[1] L. D. Landau, J. Exptl. Theoret. Phys. (U.S.S.R.) **32**, 405 (1957), Soviet Phys. JETP **5**, 336 (1957); T. D. Lee and C. N. Yang, Phys. Rev. **105**, 1671 (1957); A. Salam, Nuovo cimento **5**, 299 (1957).

[2] T. D. Lee and C. N. Yang, Phys. Rev. **104**, 254 (1956).

[3] L. Schiff, Quantum Mechanics, McGraw-Hill, N. Y., 1955, p. 315.

[4] M. Gell-Mann and A. Pais, Phys. Rev. **97**, 1387 (1955).

[5] B. M. Pontecorvo, J. Exptl. Theoret. Phys. (U.S.S.R.) **34**, 247 (1958), Soviet Phys. JETP **7**, 172 (1958).

Translated by E. J. Saletan
50

THE STATISTICAL WEIGHTS OF K^+ AND K^- MESONS PRODUCED IN PION-NUCLEON COLLISIONS

E. K. MIKHUL

Joint Institute for Nuclear Research

Submitted to JETP editor April 8, 1958

J. Exptl. Theoret. Phys. (U.S.S.R.) **35**, 298-299 (July, 1958)

BY projecting the isotopic space of the initial pion-nucleon system in the subspaces of the individual strange particles, we find the probability of production of one or more strange particles of particular signs of charge. For the statistical weight of the particles produced, independent of the charge, we have used the data of reference 1.

We furthermore take into account the fact that a number of pions may be produced together with the strange particles,[2] and also that isobaric states may exist.[3]

In this way we have calculated the statistical weights on two sets of assumptions: those of Schwinger and Gell-Mann[4] about a global interaction of pions with baryons, which we denote by W_1; and that in which it is assumed that the interaction of pions with K, Λ, Σ, and Ξ particles is much smaller than that with nucleons, which we denote by W_2.

In particular, for pions of energy 5 Bev we find the following values for the statistical weights on

the hypotheses stated; we compare these results with the experimental data:

Experiment	W_1 (theoretical)	W_2 (theoretical)
K^+ 2.8 ± 1.2%	3.341%	0.399%
K^- 1.2 ± 0.6%	0.655%	0.741%

Since K^- (or $\tilde{K}^+$) occurs only in the group $K\tilde{K}$, for which there is no essential difference between the hypotheses stated above, we cannot expect any difference between the corresponding values. For K^+, however, which occurs also in the group $K\Sigma$, we get a marked difference, since in this case there is a decided difference between the two hypotheses.

As can be seen from the data given above, the hypothesis of Schwinger and Gell-Mann is in better agreement with experiment.

The writer thanks V. S. Barashenkov for his constant interest in this work.

[1] V. S. Barashenkov and V. M. Maltsev, Acta Phys. Polon. **17**, 177 (1958).

[2] Y. Yeivin and A. de Shalit, Nuovo cimento **1**, 1146 (1955).

[3] V. S. Barashenkov and V. M. Barbashov, Suppl. Nuovo cimento **7**, 19 (1958).

[4] M. Gell-Mann, Phys. Rev. **106**, 1296 (1957).

[5] Besson, Crussard, Fouche, Hennessy, Kayas, Parikh, and Trilling, Nuovo cimento **6**, 1168 (1957).

Translated by W. H. Furry
51

REFLECTION OF ELECTRONS FROM A HIGH-FREQUENCY POTENTIAL BARRIER

M. A. MILLER

Gor'kiy State University

Submitted to JETP editor April 9, 1958

J. Exptl. Theoret. Phys. (U.S.S.R.) **35**, 299-300 (July, 1958)

In the works of Gaponov and the author[1,2] it was shown that the nonrelativistic motion of a charged particle in a high-frequency electromagnetic field is determined by the time-averaged distribution of the high-frequency potential $\Phi = (\eta/2\omega)^2 |\mathbf{E}|^2$, where η is the charge-to-mass ratio, $\mathbf{E}$ the field strength, and ω the angular frequency of the field. In particular, the average trajectory of the motion is found directly from the energy integral

$$\tfrac{1}{2}\dot{\mathbf{r}}^2 + \Phi(\mathbf{r}) = \text{const.} \qquad (1)$$

The simplest experimental test of these conclusions involves studying the reflection of particles from high-frequency potential barriers. Let the barrier be given by the function $\Phi(z)$, which has a maximum at the point $z = z_1$. Then a particle flying toward the barrier with a speed $\dot{z}$ ($v=\sqrt{2|\eta|V}$) will, as can be seen from (1), be reflected from it if the condition

$$|E|_{z=z_1} > 2\omega\sqrt{V/|\eta|}. \qquad (2)$$

is fulfilled.

The experiment was conducted with a continuously evacuated electron tube comprising a rectangular resonator ($2.9 \times 1.3 \times 10$ cm), excited through a narrow inductive "window" and tuned to resonance by a special vacuum piston (wave mode TE_{105}, resonant frequency $\omega = 5.8 \times 10^{10}$ sec.$^{-1}$). Cylindrical pipes (0.97 cm in diameter) were soldered from the outside into the two wide walls of the resonator in such a way that their axis would go through the antinode of the field $\mathbf{E}$. Since only exponentially decreasing waves were excited inside the cylinders, the distribution of the potential Φ along their axis had the shape of a potential barrier with a maximum in the center of the resonator and zero points deep inside the cylindrical pipes. In one of the pipes we placed a two-electrode electron gun, and in the second a disc-shaped collector. To prevent dispersion of the electrons, a weak-focusing magnetic field (on the order of 40 oersteds) was superimposed. The absence of high frequency fields near the surface of the electrodes eliminated the detected current due to phase sorting of the electrons.

The resonator was excited by high-frequency pulses of 10^{-6} sec duration. The height of the barrier was measured by the value of the positive compensating voltage pulse applied to the electron-gun anode, i.e., by the value of the minimal speed of electrons necessary to overcome the barrier. The results are presented in the figure. The power P (in kilowatts) fed into the resonator is plotted on the abscissa and the height of the barrier V (in volts) is plotted on the ordinate. The dotted line in the same figure is calculated from formula (2), taking into account the configuration of the fields in the resonator and its Q factor. The discrepancies do not exceed the error limits of the measurements.

The experiment was conducted at relatively low power levels, although, in principle, peak powers up to 10^6 w may be fed into such systems,

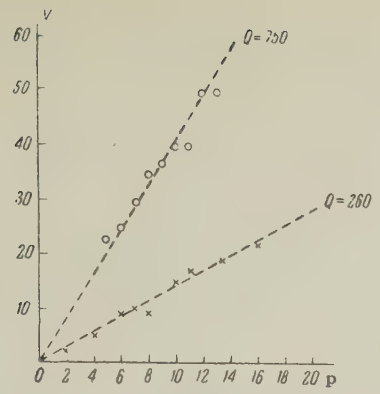

FIG. 1

i.e. barriers up to 10^4 v may be realized. However, in experiments with reflection of fast particles, it should be taken into account that the time of motion of the particles along the slope of the barrier should comprise a sufficiently large number of high-frequency cycles, or else the potential picture itself would lose its sense and the particle could jump the barrier at favorable phases (some kind of "tunnel effect") even though its velocity satisfies condition (2).

Boot and Harvie[3] described an experiment to demonstrate the presence of a potential barrier in a multicavity magnetron. The electrons that appear close to the anode block as a result of ionization (high-frequency discharge) roll down the slope of the barrier to the cold cathode. This effect was detected by the appearance of current in the external circuit and by cathode heating caused by electron bombardment. Experiments with magnetrons conducted by us previously have shown that for unambiguous interpretation of the effect it is necessary to remove the electrodes from the high frequency field, i.e., to avoid a sharp slope of the potential distribution in the whole interaction space.

The author is very grateful to B. G. Eremin, E. V. Zagriadski, V. A. Lopyrev, S. B. Mochenev and V. A. Fliagin who took part in the construction of the tubes and in the experiment.

[1] A. V. Gaponov and M. A. Miller, J. Exptl. Theoret. Phys. (U.S.S.R.) **34**, 242 (1958), Soviet Phys. JETP 7, 168 (1958).

[2] M. A. Miller, Изв. Высш. школы Мин-ва высш. образов., Радиофизика (Bull. Higher School of Ministr. of Higher Educ., Radiophysics)(in press).

[3] H. Boot and R. Harvie, Nature No. 4596, 1187 (1957).

Translated by Z. Scheidlinger
52

NUCLEAR MAGNETIC RESONANCE SHIFT IN MOLYBDENUM

S. I. AKSENOV

P. N. Lebedev Physics Institute, Academy of Sciences, U.S.S.R.

Submitted to JETP editor April 14, 1958

J. Exptl. Theoret. Phys. (U.S.S.R.) **35**, 300-301 (July, 1958)

We have investigated the shift of the nuclear magnetic resonance, due to the paramagnetism of the conduction electrons (Knight shift)[1] in metallic molybdenum. The spectrometer was similar to the one used before.[2] An electromagnet with a pole diameter of 300 mm and a gap of 42 mm made possible work in fields up to 14,000 gausses, stabilized with deuteron resonance as reference. The frequency was measured with a type 528 wavemeter.

In order to avoid the influence of skin-effect on the resonance line,[3] we worked with a powder prepared by filing a molybdenum sheet and sifting the filings through a sieve of 150 mesh. The molybdenum content in the sheet was not less than 99.9%, and the paramagnetic impurities not more than 0.008%. To relieve the internal stresses, the powder was annealed at 1250°C for two hours in a vacuum of 10^{-4} Hg.

Resonance caused by both odd isotopes of molybdenum was observed in the powder thus obtained. The amplitude ratio of the resonance lines of Mo^{95} and Mo^{97} was 3:1, whereas the isotope-content ratio was only 1.5:1. An even bigger difference was obtained in the unannealed metal, where the Mo^{97} line was not observed at all, although the Mo^{95} resonance exceeded the noise level by 5 to 6 times. The Mo^{95} signal in the powder immediately after filing was nearly one order lower than in the annealed one. All this points to a strong effect of the interaction between the nuclear quadrupole moments and the gradient of the electrical field, an interaction due to the disturbance of the lattice structure. The quadrupole interaction was noticed to be greater for Mo^{97}. This agrees with the data of W. G. Proctor F. C. Yu on nuclear magnetic resonance of molybdenum in an aqueous solution of K_2MoO_4.[4]

Bloembergen and Rowland[5] showed that a shift of the resonance lines becomes possible at a quadrupole interaction big enough for second-order quadrupole effects to appear. The shifted line should be asymmetrical. For molybdenum,

comparison of the amplitudes of the resonance lines of Mo^{95} and Mo^{97} with the ones expected, taking into account the sensitivity of the measuring apparatus, shows that, at least for Mo^{97}, the weakening of the line is caused to a considerable extent by second-order quadrupole effects. At the same time, both resonances in the annealed molybdenum are symmetrical and, in spite of a noticeably different influence of the quadrupole interaction, they have approximately the same width. This brings us to the conclusion that the observed part of the resonances corresponds to nuclei weakly exposed to the influence of quadrupole effects. Because of the sharp dependence of second-order quadrupole effects on the distance, the resonance caused by other nuclei closer to points of structural disturbances becomes so blurred as to be unobservable.[5] The effect of quadrupole interaction on the shift in molybdenum can thus be neglected.

The Knight shift was measured relative to the resonances of Mo^{95} and Mo^{97} in an aqueous solution of K_2MoO_4, i.e., with an accuracy up to the value of the chemical shift in this compound. From a series of successive measurements with metallic and nonmetallic samples in a field of 12600 gausses, we obtained the following values of the shift

$$\frac{\Delta H}{H}(Mo^{95}) = (0.582 \pm 0.005)\%,$$

$$\frac{\Delta H}{H}(Mo^{97}) = (0.586 \pm 0.005)\%.$$

Analogous results were obtained in a field of 8300 gausses.

The fact that the same shift was obtained for both isotopes at two values of the field also proves the assumption that the influence of the quadrupole interaction upon the shift can be neglected.

[1] W. D. Knight, Solid State Physics, II, N. Y. (1956) p 93-136.

[2] S. I. Aksenov and K. V. Vladimirskii, Dokl. Akad. Nauk SSSR **96**, 37 (1954).

[3] N. Bloembergen, J. Appl. Phys., **23**, 1383 (1952). A. C. Chapman et al., Proc. Phys. Soc., **B70**, 345, 448 (1957).

[4] W. G. Proctor and F. C. Yu, Phys. Rev., **81**, 20 (1951).

[5] N. Bloembergen and T. J. Rowland, Acta Metallurgica, **1**, 731 (1953). N. Bloembergen, Report of the Conference on Defects in Crystalline Solids, Bristol (1954) p 1-32.

Translated by Z. Scheidlinger
53

STIMULATED R.F. AMPLIFIER WORKING ON HYPERFINE LEVELS OF PARAMAGNETIC ATOMS

K. A. VALIEV and Sh. Sh. BASHKIROV

Kazan' Pedagogical Institute

Submitted to JETP editor April 15, 1958

J. Exptl. Theoret. Phys. (U.S.S.R.) **35**, 302-303 (July, 1958)

THE idea of using a paramagnetic crystal as an active element (substance) in stimulated microwave amplifiers was expressed by Bloembergen.[1] Such an amplifier was realized with crystals of salts containing Gd^{3+} ions, by using the dipole transitions between the energy levels of the electron spins of paramagnetic Gd^{3+} ions.[2] In the work of Itoh[3] it was shown that diamagnetic crystals, containing atoms with substantial quadrupole splitting of nuclear spin levels, can be employed in amplifiers at low frequencies (10^6 cps). Abragam and others[4] have pointed out the possibility of the appearance of a stimulated radiation in transitions between the energy levels of proton spins in liquid solutions of paramagnetic ions. We would like to call attention to the possibility of obtaining amplification of signals in the frequency range of 10^8 to 10^9 cps by employing transitions between hyperfine levels of paramagnetic ions.

As an example let us consider crystals of salts containing bivalent ions of the Cu^{64} isotope (ground state ^2D, $S = \frac{1}{2}$, $I = 1$) (obviously, the conclusions reached here are applicable to other paramagnetic atoms). The scheme of the spin levels of Cu^{++} ions in a strong magnetic field is shown in the figure. The relaxation transition probabilities, the ratio of which determines the possibility of creating negative differences of populations between adjacent hyperfine levels at temperatures of liquid helium and fields of about 5000 oe, have the following values: $W_{a'a} = 10^3$ to 10^4 sec^{-1} (for electron transitions) and $W_{a'b'} = 0.1$ to 1 sec^{-1} (for nuclear transitions). The stationary populations of hyperfine levels that appear upon saturation of the electron transitions, were calculated in our work[5] devoted to the polarization of Cu^{64} nuclei.

Thus, upon saturation of the electron transition $a \rightarrow a'$, the populations of the hyperfine levels are characterized by the following relations:[5]

$$a'/b' = 1 + 3\Delta/2,\ b'/c' = 1,\ c/b = 1,$$

$$b/a = 1 + \Delta/2,\quad \Delta = g_e\beta H_0/2kT.$$

We see that the upper of the two adjacent levels a'b' (or a,b) is much more populated than the

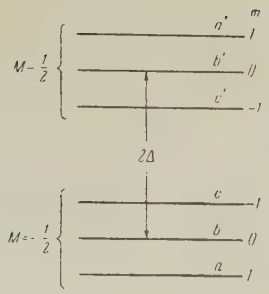

FIG. 1

lower one. Because of that, a signal of frequency $\nu_{a'b'}$ (or ν_{ab}) acting on the crystal should bring about stimulated atomic radiation (emission) at the same frequency. The above-mentioned frequencies will be of the order of 10^8 cps for ions of the iron group and approximately 10^9 cps for rare-earth ions. At $H_0 = 5000$ oe, $T = 2$ to 4°K, and $N = 10^{19}$ (number of paramagnetic ions), the stored energy for one pair of hyperfine levels (e.g., a', b') will be on the order of 1 to 2 ergs. When pulsing with pulse durations of 10^{-4} sec, the output power may reach 10^{-3} w.

Negative differences between the populations of lower and higher adjacent hyperfine levels appear also upon saturation of "forbidden" electron transitions $(M, m) \rightarrow (M+1, m-1)$ (cf. references 5 and 6).

In conclusion, the authors would like to thank A. S. Altschuler for helpful discussions of the results.

[1] N. Bloembergen, Phys. Rev. **104**, 324 (1956).
[2] Scovil, Feher and Seidel, Phys. Rev. **105**, 762 (1957).
[3] J. Itoh, J. Phys. Soc. Japan, **12**, 1053 (1957).
[4] A. Abragam et al., Compt. rend., **245**, 157 (1957).
[5] Sh. Sh. Bashkirov and K. A. Valiev, J. Exptl. Theoret. Phys. (U.S.S.R.) **35**, 678 (1958), Soviet Phys. JETP **8**, (in press).
[6] G. Feher, Phys. Rev., **103**, 500 (1956).

Translated by Z. Scheidlinger
54

A STUDY OF FAST DEUTERONS AT 3200 m ABOVE SEA LEVEL

G. V. BADALIAN

Physics Institute, Academy of Sciences, Armenian S.S.R.

Submitted to JETP editor April 15, 1958

J. Exptl. Theoret. Phys. (U.S.S.R.) **35**, 303-305 (July, 1958)

A study of cosmic ray deuterons was carried out at 3200 m above sea level (Mt. Aragats) using new and improved apparatus — a magnetic spectrometer used in conjunction with two multiplate cloud chambers.[1]

The deuterons were identified by their momentum as measured in the magnetic spectrometer, and by their ionization range in the lower cloud chamber. The new apparatus was different from all previous magnetic mass spectrometers in that it permitted, first, to distinguish properly between particles stopped ionization losses and those stopped by nuclear collisions and, second, to follow the paths of the particles in the upper chamber and to observe the events of local particle production in the matter of the chamber. The total equivalent of the chamber, including the top and the bottom, amounted to ~ 87.5 g/cm^2 Pb.

In all, ~242 deuterons with range in the lower chamber between 1.2 and 5.4 cm Pb were registered. Of these, 81 entered the chamber from the air, 104 were produced in nuclear processes in the matter of the top chamber, and the remaining 57 deuterons could not be traced in the upper chamber for various reasons (the tracks were invisible due to incidence upon non-illuminated region of the chamber, etc.). Simultaneously with these deuterons, ~3200 protons were detected.

The fraction of deuterons which came from the air, traversed the top chamber, and were stopped in the lower chamber within the stated range interval, amounts to 0.063 ± 0.0072 of the analogous number of protons, in agreement with references 2 and 3 (taking into account corrections for the optical aperture and nuclear absorption). If one considers the fraction of air deuterons compared with the number of protons of the same momentum range (1.2 to 1.39 Bev/c), the result, 0.086 ± 0.010, coincides with the data of Aivazian.[4]

An analysis fo the produced particles revealed that the number of deuterons produced by primary neutrons is (2.64 ± 0.62) times the number of

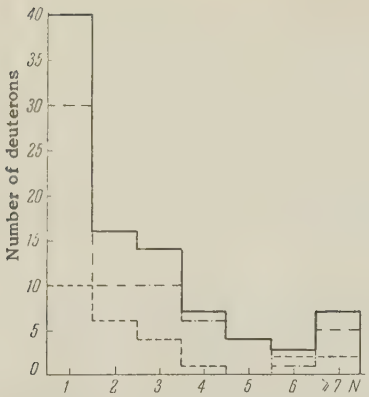

FIG. 1. Distribution of produced deuterons with respect to the number of prongs in the star (N). The dotted lines represent production by charged particles, dot-dash – by neutral particles, solid – total production.

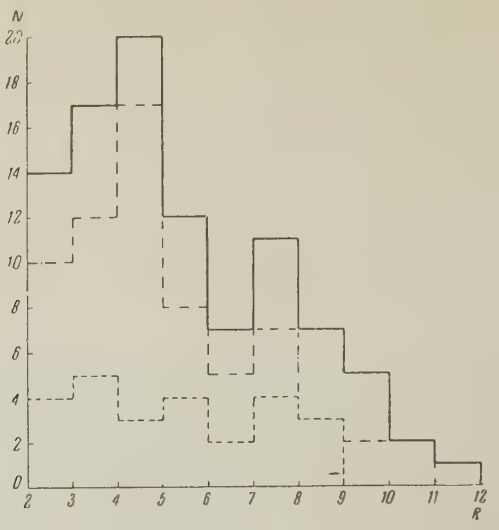

FIG. 2. Distribution of produced deuterons with respect to the total range R (cm Pb). Dotted line represents production by charged particles, dot-dash – by neutral particles, solid – total production.

proton produced deuterons. This is due to the fact that the deuterons are mainly produced in low-energy stars, for which the number of primary neutrons is larger than that of primary protons.

It follows from Figs. 1 and 2 that the number of produced deuterons decreases sharply with increasing number of prongs (energy) of the star, or with the total range of the deuteron itself. The ratio of deuterons produced by neutrons to deuterons produced by charged particles decreases also.

The momentum spectrum of deuterons produced in 1 g/cm^2 of matter, calculated by us with allowances for all the necessary corrections, is shown in Fig. 3. For $p \gtrsim 1$ Bev/c, the spectrum can be approximated by the expression

$$n(p)\,dp = (7.85 \pm 1.48) \cdot 10^{-7} \cdot p^{-3.14 \pm 0.44}\,dp \text{ particles/g-sec-sterad}$$

i.e., it is clearly somethat steeper than the spectrum of the primary producing particles.

An estimate of the cross section for the production of deuterons with momentum between 0.785 and 1.38 Bev/c in lead by cosmic ray nucleons with $E \gtrsim 200$ Mev, based on our data, yields the value $\sigma = 38 \pm 4.3$ millibarns. This is lower than that obtained in reference 5, where the primary particles possessed an energy of ≈ 90 Mev. The results obtained are in agreement with the conception of the direct or indirect "pickup" production of fast deuterons,[6,7] according to which the probability of deuteron production decreases with increasing energy of the incident nucleons.

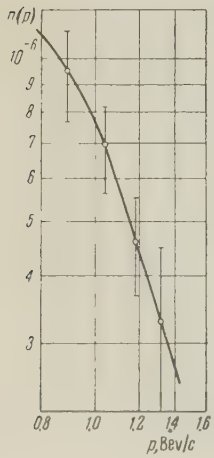

FIG. 3. Differential momentum spectrum of deuteron production.

A full presentation of the work will be given in Bulletin (Izvestria) of the Academy of Sciences, Armenian S.S.R.

The author wishes to express his deep gratitude to Prof. A. I. Alikhanian for his constant interest in the work and to Prof. N. M. Kocharian for discussion of results.

[1] Alikhanian, Shostakovich, Dadaian, Fedorov, and Deriagin, J. Exptl. Theoret. Phys. (U.S.S.R.) **31**, 955 (1956), Soviet Phys. JETP **4**, 817 (1957).

[2] G. A. Marikian, Dissertation, Erevan (1954).

[3] M. I. Daion, Dokl. Akad. Nauk. SSSR **101**, 5 (1955).

[4] M. T. Aivaizian, Izv. Akad. Nauk Arm. SSR, Ser. FMET Nauk, **9**, 91 (1956).

[5] J. Hadley and H. F. York, Phys. Rev. **80**, 345 (1950).

[6] W. N. Ness and B. J. Moyer, Phys. Rev. **101**, 337 (1956).

[7] K. Kikuchi, Progr. Theor. Phys. **18**, 503 (1957).

Translated by H. Kasha
55

ON THE INFLUENCE OF DOMAIN STRUCTURE ON THE ELECTRICAL RESISTIVITY OF IRON AT LOW TEMPERATURES

A. M. SUDOVTSOV and E. E. SEMENENKO

Institute for Technical Physics, Academy of Sciences, Ukrainian S.S.R.

Submitted to JETP editor April 21, 1958

J. Exptl. Theoret. Phys. (U.S.S.R.) **35**, 305-307 (July, 1958)

THE electrical resistivity of a ferromagnet can be written in the form $R = R_0 + R_1 + R_2 + R_3$, where R_0 is the residual resistance, R_1 the phonon part, R_2 the ferromagnon part of the resistivity,[1] and R_3 the resistivity caused by the scattering of the conduction electrons at the domain boundaries. The R_3 part of the resistivity will show up when the other components are small, i.e., for pure specimens and at low temperatures when the mean free path approaches or becomes larger than the domain dimensions. It was possible to show up R_3 by measuring the electrical resistivity of a metal by enlarging the domain structure in a magnetic field.

A measurement was carried out of the electrical resistivity of iron in its dependence on the magnitude of the longitudinal and transverse magnetic fields at temperatures from room temperature down to liquid helium temperatures. At these temperatures the magnetization curves were obtained.

For our investigation we took a sample of very pure iron grown in the form of a needle by distillation in vacuo. The sample had transverse dimensions of 0.1 mm, and a length of 38 mm. The grain size was approximately equal to the sample diameter.

In the demagnetized state in such a thin specimen the domains are oriented mainly perpendicularly to the longitudinal axis; their width is $\sim 10^{-3}$ cm.[2,3] The mean free path at room temperature in iron $\lambda \sim 10^{-5}$ to 10^{-6} cm; the domain boundaries will therefore not influence the electrical resistivity. If the temperature is lowered, the mean free path will increase and approach the domain dimensions, and scattering by domain boundaries begins to be important for the magnitude of the electrical resistivity.

The results of the measurements are given in Figs. 1 and 2 in the form of graphs of the dependence of the change in relative electrical resistivity $\Delta R/R$ (along the ordinate axis) on the external magnetic field (along the abscissa axis), where $\Delta R = R_H - R$; R is the value of the electrical resistivity without a field, and R_H the resistivity in the magnetic field. The earth field was compensated within an accuracy of 0.5%.

In a longitudinal magnetic field of ~ 10 Oe

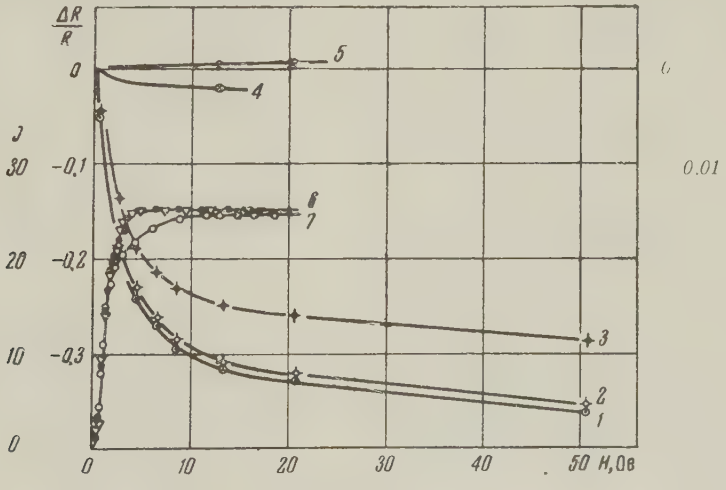

FIG. 1

(Fig. 1) at a temperature of 300°K (curve 5) when the mean free path is appreciably less than the domain size, an increase in the electrical resistivity (of $\sim 0.02\%$), which is characteristic for ferromagnets[4-6] is observed, but already at 77°K (curve 4) a decrease in the electrical resistivity of $\sim 0.2\%$ takes place, reaching a value of $\sim 23\%$ at 20.4°K (curve 3) and of $\sim 30\%$ at helium temperatures (curve 1 refers to measurements at 1.3°K, curve 2 at 4.2°K). Curves 4 and 5 are drawn to a larger scale along the ordinate (scale on the right). In this graph we have drawn to an arbitrary scale the magnetization curves. Curve 7 refers to measurements at 300°K, curve 6 to meas-

urements at a temperature of 20.4°K (triangles) and of 4.2°K (black points). The basic effect of a decrease in the electrical resistivity is observed in the region of the technical magnetization of the specimen. This can be explained by two circumstances: mainly by an extension of the domain structure in the magnetization process, i.e., by a decrease in the number of boundaries and, apart from that, by a rotation of the magnetic moment of the region in the direction of the external magnetic field.[6]

From the magnitude of the decrease in electrical resistivity of ~30% at helium temperature in a longitudinal magnetic field, and from the theoretical work on the determination of the influence of the specimen size on the electrical resistivity,[7] we can determine the magnitude of the mean free path, $\lambda \sim 10^{-3}$ cm. This value coincides with the estimate of the domain width for the given sample in the demagnetized state.

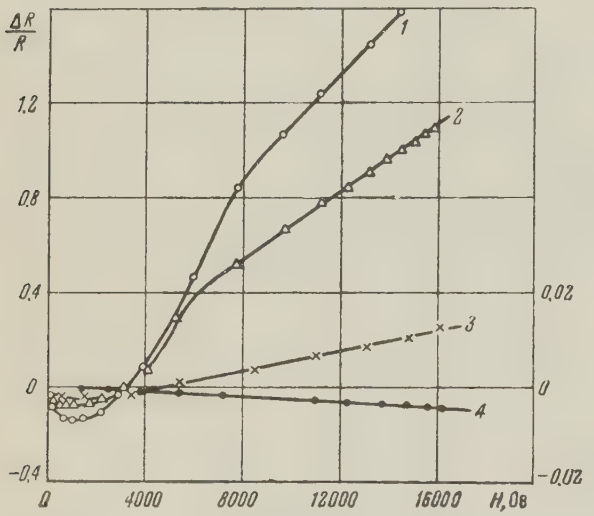

FIG. 2

In a transverse magnetic field (Fig. 2) two effects take place: an extension of the domain structure (decrease of the electrical resistivity in weak fields) and the ordinary galvanomagnetic effect which dominates in high fields.[8] The curves 1, 2, 3, and 4 refer to measurements at temperatures of 4.2, 20.4, 77, and 300°K, respectively. The scale on the right refers to curves 4 and 5 [sic!].

An influence of the measuring current on the magnitude of the electrical resistivity was detected. An increase by 20% in the resistivity was observed when the measuring current increased from 0.1 to 1000 ma. Unfortunately the literature contains no data at all considering domain structure in the field of a current. Apparently, the measuring current leads to a decreased domain structure, since it produces in the sample an inhomogeneity in the magnitude and direction of the magnetic field.

We must still remark that to determine the residual resistivity of a ferromagnet as a criterion for the purity it is necessary to take into account the dependence of the electrical resistivity on the measuring current and the magnetic field. For the specimen under investigation the relative residual resistivity was 4×10^{-3} if the influence of the domain structure was not taken into account and 3×10^{-3} if it was taken into account.

In conclusion the authors express their gratitude to B. G. Lazarev, S. V. Vonsovskii, and M. I. Kaganov for discussing the results and showing an interest in this work.

[1] A. I. Sudovtsov and E. E. Semenenko, J. Exptl. Theoret. Phys. (U.S.S.R.) **31**, 525 (1956), Soviet Phys. JETP **4**, 592 (1957).

[2] E. M. Lifshitz, J. Exptl. Theoret. Phys. (U.S.S.R.) **15**, 97 (1945); J. Phys. (U.S.S.R.) **8**, 337 (1944).

[3] W. C. Elmore, Phys. Rev. **62**, 486 (1942).

[4] W. L. Webster, Proc. Roy. Soc. (London) **A113**, 196 (1926); **A114**, 611 (1927).

[5] S. V. Vonovskii and Ia. S. Shur, Ферромагнетизм (Ferromagnetism), M.—L., 1948.

[6] M. I. Kaganov, Тр. Совещания по микроструктуре ферромагнетиков, Красноярск (Proceedings of the Conference on the Microstructure of Ferromagnetics, Krasnoiarsk) 1958 (in press).

[7] R. B. Dingle, Proc. Roy. Soc. (London), **A201**, 545 (1950).

[8] P. Kapitza, Proc. Roy. Soc. (London) **A123**, 292 (1929).

Translated by D. ter Haar
56

ANGULAR CORRELATION OF CIRCULARLY POLARIZED GAMMA QUANTA ON THE μ-MESONIC ATOM

V. A. DZHRBASHIAN

Physics Institute, Academy of Sciences, Armenian S.S.R.

Submitted to JETP editor April 23, 1958

J. Exptl. Theoret. Phys. (U.S.S.R.) **35**, 307-308 (July, 1958)

THE μ-mesonic atom, produced as a result of capture of a polarized μ^- meson on the external

orbit, will radiate circularly-polarized gamma quanta. As a consequence of the spin-orbit interaction, which leads to depolarization of the μ^- meson on the orbit, the angular distribution and the angular correlation of these quanta depend on the degree of polarization of the μ^- meson.

Comparison of theory with experiment can yield information on the magnitude of the degree of polarization ($|P|$) and the direction of depolarization (sign of P) of μ^- mesons produced in decay of negative pions.

In the case of lead, according to Wheeler,[1] the energies of the gamma quanta radiated during the cascade transition 2s-2p-1s are respectively equal to 1.33 and 4.42 Mev.*

To obtain the correlation functions it is possible to employ the formula obtained in our preceding work,[3] neglecting the interaction at the first level. It is also necessary to take it into account that for the case of circularly-polarized quanta the formula changes somewhat. A factor† $(-\tau_1)^{\nu_1}(\tau_2)^{\nu_2}$ appears under the summation sign, where ν_1 and ν_2 are the orders of the spherical functions, which (together with the order of the degree of orientation k) can assume also odd values. Inserting the values of the spin of the μ meson ($s = 1/2$) and considering a nucleus of spin $I = 0$, we obtain for the cascade $0(1)\ 1(1)\ 0$

$$W = 1 - \frac{7}{6}\tau_1\tau_2\cos\theta + \frac{4}{9}\tau_2 P\cos\theta_2 + \frac{1}{12}(3\cos^2\theta - 1) \quad (1)$$
$$- \frac{1}{6}\tau_1 P[\cos\theta_1(3\cos^2\theta_2 - 1) + 3\cos\theta_2(\cos\theta - \cos\theta_1\cos\theta_2)]$$
$$- \frac{1}{18}\tau_2 P[\cos\theta_2(3\cos^2\theta_1 - 1) + 3\cos\theta_1(\cos\theta - \cos\theta_1\cos\theta_2)].$$

Here θ_i is the angle between the direction of the i-th quantum ($i = 1, 2$) and that of the incident negative muon, and θ is the angle between the two quanta. A value $P > 0$ corresponds to a predominant spin alignment with the direction of the incident negative muon.

If the direction of the first quantum is assumed the same as that of the incident negative muons, then

$$W = 1 + \left(-\frac{7}{6}\tau_1\tau_2 + \frac{1}{3}\tau_2 P\right)\cos\theta$$
$$- \frac{1}{6}\tau_1 P(3\cos^2\theta - 1) + \frac{1}{12}(3\cos^2\theta - 1). \quad (2)$$

When $\theta = 24°39'$ we have $W_{++} = 0.077(1 + 0.9P)$, along with the ratio

$$(W_{++} - W_{--})/(W_{++} + W_{--}) = 0.9P. \quad (3)$$

Here $W_{++}(W_{--})$ denotes the value of W for $\tau_1 = \tau_2 = 1$ ($\tau_1 = \tau_2 = -1$). When $\theta \to 0$ the multiplier of P in Eq. (3) tends to unity, but at the same time $W \to 0$.

Integrating (1) over $d\Omega_1$ we get the angular distribution for the transition $2p \to 1s$

$$W = 1 + {}^4/_9\tau_2 P\cos\theta_2,$$

i.e.,

$$[W(0°) - W(180°)]/W(90°) = {}^8/_9\tau_2 P. \quad (4)$$

We take this opportunity to express our deep gratitude to V. V. Vladimirskii for the interest displayed, and to K. A. Ter-Martirosian for valuable discussions.

*According to data by Fitch and Rainwater,[2] gamma quanta of energy 6.02 Mev are emitted in the transition $2p \to 1s$.

†$\tau = +1$ ($\tau = -1$) for right-hand (left-hand) circularly polarized gamma quantum.

[1] J. A. Wheeler, Revs. Modern Phys. **21**, 133 (1949).

[2] V. L. Fitch and J. Rainwater, Phys. Rev. **92**, 789 (1953).

[3] V. A. Dzhrbashian, J. Exptl. Theoret. Phys. (U.S.S.R.) **34**, 260 (1958), Soviet Phys. JETP **7**, 181 (1958).

Translated by J. G. Adashko
57

BREMSSTRAHLUNG AND PAIR PRODUCTION FROM PROTONS WITH ALLOWANCE FOR FORM FACTOR

I. ZLATEV and P. S. ISAEV

Joint Institute for Nuclear Research

Submitted to JETP editor April 23, 1958

J. Exptl. Theoret. Phys. (U.S.S.R.) **35**, 309-310 (July, 1958)

ACCORDING to the present view, a nucleon consists of a "core" surrounded by a cloud of virtual mesons. The distribution of nucleonic charge and magnetic moment has been studied in detail by Hofstadter in the scattering of high-energy electrons from protons and neutrons. In this connection it is of interest to investigate the influence of the form factor on the related reactions e.g., bremsstrahlung and pair production on nucleons.

We have calculated these processes on protons in the lowest order of perturbation theory (third order in e). Graphs a and b were computed for bremsstrahlung and graphs c and d for pair production. An additional contribution is due to

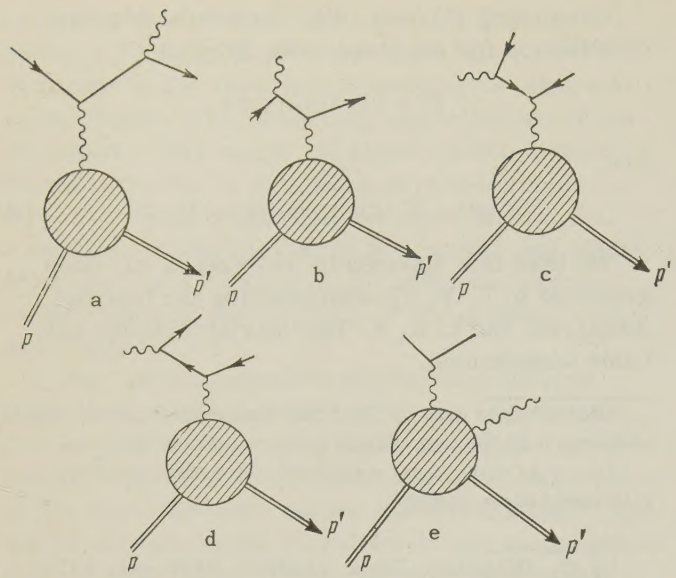

the meson "jacket" (graph e). However, its evaluation is much more complicated than that of the graphs a, b, c, and d. In this note we shall therefore give only some indications of its contribution. In the graphs a double line denotes a proton, a single line an electron and a wavy line a photon. The proton vertex is described not by $e\gamma_\alpha$, but by the factor[1]

$$e\gamma_\alpha F_1(|p-p'|^2) + (\mu/2M)\,F_2(|p-p'|^2)(\sigma_{\alpha\beta}(p-p')_\beta),$$

$$\sigma_{\alpha\beta} = {}^1/_2(\gamma_\alpha\gamma_\beta - \gamma_\beta\gamma_\alpha),$$

where μ is the anomalous proton magnetic moment, M the proton mass, and F_1 and F_2 form factors that depend on the proton recoil. The computations were performed by the Feynman method.

The formulae obtained are rather lengthy and will not be given here. In the special case where $M \to \infty$ (recoil equals zero; energy conservation is expressed by $\epsilon = k' + \epsilon'$ where ϵ, k' and ϵ' are the energies of the incident electron, the created photon, and the scattered electron respectively) the formulae go over into the Bethe-Heitler expressions[2] for bremsstrahlung and pair production.

In their measurement of bremsstrahlung from 500 and 550 Mev electrons on hydrogen, Bernstein and Panofsky[3] found that the Bethe-Heitler cross sections are true to a high degree of accuracy, at least for small photon emission angles θ_0 (not exceeding 7 to 10°).

One thus can surmise that if deviations from the Bethe-Heitler formulae are observed at all, it will be at large angles θ_0 or at very large electron energies ($\gg$ 500 Mev). It therefore follows that if there is a difference between our expressions and the Bethe-Heitler formula, this will indicate not only the influence of the recoil and of the form factor on the cross section of the particular process, but a possible contribution to this cross section from the meson jacket.

We have compared the expressions for the differential cross section for the case where the incoming electron has an energy of 500 Mev. The form factors $F_1(|p-p'|^2)$ and $F_2(|p-p'|^2)$ were taken from Hofstadters experiments[4] on the scattering of electrons of energy ~500 Mev on protons (exponential model, $F_1 = F_2$). As an example we list a few members concerning the special case where the momenta of the photon

$\theta_0 = 30°$. Photon energy = 235 Mev

θ	Differential cross section according to the Bethe-Heitler formula ($d\sigma_{B\text{-}H}$)	Differential cross section with allowances for recoil and form factor ($d\sigma_{F\text{-}F}$)	$\frac{d\sigma_{F\text{-}F}}{d\sigma_{B\text{-}H}}$	Differential cross section without allowance for form factor
30°	31332	27434	0.875	29880
60°	3137	2686	0.855	2780
90°	739	480	0.650	600
120°	127.5	56.4	0.442	92.5
150°	27.85	11.33	0.405	22.3

Note. The differential cross section is given in arbitrary units. θ_0 and θ are the angles between the photon momentum and the momenta of the incident and scattered electron respectively.

and of the electron before and after scattering are complanar.

At different values of the angles θ and θ_0, as well as in the noncomplanar case, we obtain results which differ from the Bethe-Heitler formulae by approximately the same amount as the tabulated values. From the comparison of the cross sections it is clear that even for not too large angles ($\theta_0 \approx 30°$) the difference reaches appreciable values (~15%). This obviously points to a small but perceptible contribution of the meson "jacket" to the bremsstrahlung cross section. At present we are engaged in a calculation of this contribution, upon the completion of which we shall be able to answer this question.

In conclusion the authors express their deep

gratitude to A. A. Logunov and A. N. Tavkhelidze for their valuable discussion of the results obtained.

[1] Yennie, Lévy and Ravenhall, Revs. Modern Phys. **29**, 144 (1957).

[2] W. Heitler, The Quantum Theory of Radiation, Oxford, 1953.

[3] D. Bernstein and W. K. H. Panofsky, Phys. Rev. **102**, 522 (1956).

[4] R. Hofstadter, Revs. Modern Phys. **28**, 214 (1956), Russian translation Usp. Fiz. Nauk **63**, 693 (1957).

Translated by M. Danos
58

DIFFRACTION SCATTERING OF FAST PARTICLES

D. I. BLOKHINTSEV, V. S. BARASHENKOV and V. G. GRISHIN

Joint Institute for Nuclear Research

Submitted to JETP editor April 23, 1958

J. Exptl. Theoret. Phys. (U.S.S.R.) **35**, 311-312 (July, 1958)

THE structure of elementary particles can be determined by studying the elastic scattering of some type of beam by these particles. In the application to nuclei and nucleons, the only example of such a beam up to present is the well known work of the group of Hofstadter with electron scattering, which makes it possible to determine the form factors of the electric charge and of the magnetic moment.[1] However, analysis of the elastic scattering of other types of particles also makes it possible to obtain valuable information about the structure of nucleons and of the nucleus.* By way of example, we consider the scattering of π^- mesons by nucleons.[3,4]

For simplicity, we disregard the spin-dependence of the interaction and neglect the process of charge exchange. We assume also that the real part of the phase shift, Re $\eta_l = 0$, which is in good agreement with experiment for energies $E_\pi \geq 1$ Bev.[2,5] A rigorous solution of the problem will be published later.

In Fig. 1 the solid lines show the quantity

$$\operatorname{Im}\eta_l = -\frac{1}{2}\ln\left\{1 - \lambda^{-1}\int_0^\pi \sqrt{(d\sigma_d(\theta)/d\Omega)}\,P_l(\cos\theta)\sin\theta\,d\theta\right\}$$

for the case of scattering of 1.3-Bev π^- mesons.

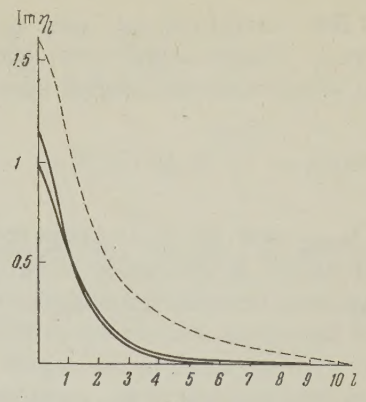

FIG. 1

In order to calculate these functions, curves of least and greatest curvature were constructed between the limits of the experimental values of the differential cross section for elastic scattering ($\sigma_d \approx \sigma_{el}$) from reference 3. The curves in Fig. 1 were drawn through the centers of the rectangles of the corresponding histograms. The dashed line in Fig. 1 gives the values of Im η_l calculated from the mean experimental data from reference 4 for the scattering of 5-Bev π^- mesons.

At high energies, where the wavelength $\lambda\!\!\!^{-}$ becomes substantially smaller than the dimensions of the scattering system, and the relative change in the absorption coefficient K over a wavelength $\lambda\!\!\!^{-}$ is small, the quasi-classical approximation can be employed with a high accuracy. Taking Im η_l from Fig. 1, we obtain from well-known formulas[6] the values: $\sigma_{in} = (25.5 \pm 1.5)$mb, $\sigma_d = 7.4 \pm 0.1$)mb for E = 1.3 Bev and $\sigma_{in} \approx 23$ mb, $\sigma_d \approx 5$ mb for E = 5 Bev. The good agreement of these quantities, as well as that of the angular distribution we calculated for the elastically scattered particles, with the data of references 3 and 4 is one of the justifications of the following applications of the quasi-classical approximation.

In Fig. 2 we give the values K = K(r) (where r is the distance from the center of the nucleon)

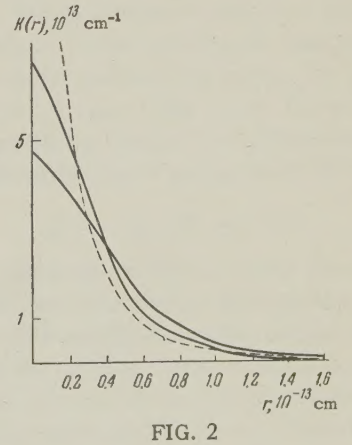

FIG. 2

for E = 1.3 Bev (solid curves) and E = 5 Bev (dotted curve). These values were obtained from a numerical solution of the integral equation

$$2 \operatorname{Im} \eta_l = \int_0^{\sqrt{L^2-l^2}} K(\sqrt{l^2+s^2})\, ds,$$

where $L = l_{max}$ and Im η_l is taken from Fig. 1.

Values of K(r) in the region of small r are not unambiguously determined and depend on the way in which the cross section for diffraction scattering is approximated in the region of large angles. As a consequence of the large experimental errors in reference 4, the rise in the values of K(r) upon going from E = 1.3 Bev to E = 5 Bev in the region $r \sim 0$ is also not completely reliable.

The mean square 'pion' radius of the nucleon calculated from the curves of K(r) in Fig. 2 is equal to $(0.82 \pm 0.06) \times 10^{-13}$ cm, and its value at E = 5 Bev is, within the limits of experimental error, the same.

The example considered is a particular case of the solution of the so-called inverse problem of scattering: given the scattered wave, determine completely the interaction potential.

It is our pleasant duty to thank K. Danilov for help in the numerical calculations.

*The work of reference 2 is devoted to a detailed consideration of this problem.

[1] R. Hofstadter, Revs. Modern Phys. **28**, 214 (1956).

[2] Blokhintsev, Barashenkov, and Grishin, Nuovo cimento **9**, 249 (1958).

[3] M. Chretien et al., Phys. Rev. **108**, 383 (1957).

[4] G. Maenchen et al., Phys. Rev. **108**, 850 (1957).

[5] Grishin, Saitov, and Chuvilo, J. Exptl. Theoret. Phys. (U.S.S.R.) **34**, 1221 (1958), Soviet Phys. JETP **7**, 844 (1958).

[6] Fernbach, Serber, and Taylor, Phys. Rev. **75**, 1352 (1949).

Translated by G. E. Brown
59